

JOURNAL OF

Ultrastructure Research

Editors

FRITIOF S. SJÖSTRAND *Editor-in-Chief*

ARNE ENGSTRÖM

Editorial Board

F. B. BANG • W. BERNHARD • A. CLAUDE • V. E. COSSLETT

A. J. DALTON • J. FARRANT • A. FREY-WYSSLING • A. J. HODGE • H. E. HUXLEY

D. C. PEASE • J. B. LE POOLE • J. T. RANDALL • E. RUSKA

W. J. SCHMIDT • H. THEORELL • A. TISELIUS

R. W. G. WYCKOFF

Volume 1 • 1957/1958



ACADEMIC PRESS INC., PUBLISHERS, NEW YORK 3, NEW YORK

All Rights Reserved

*No part of this book may be reproduced in any form by
photostat, microfilm, or any other means without
written permission from the publishers,*

ACADEMIC PRESS INC.

NEW YORK 3, NEW YORK

Printed in Sweden

Almqvist & Wiksells

B O K T R Y C K E R I A B

U P P S A L A 1 9 5 8

Table of Contents

NUMBER 1, NOVEMBER 1957

| | |
|--|----|
| ROUILLER, CH. et FAURÉ-FREMIET, E., Ultrastructure réticulée d'une fibre squelettique chez un Cilié | 1 |
| FERREIRA, DAVID, L'ultrastructure des cellules du pancréas endocrine chez l'embryon et le rat nouveau-né | 14 |
| EKHOLM, R., Some Observations on the Ultrastructure of the Mouse Parathyroid Gland | 26 |
| FREY-WYSSLING, A. and MÜLLER, H. R., Submicroscopic Differentiation of Plasmodesmata and Sieve Plates in <i>Cucurbita</i> | 38 |
| MENEFFEE, MAX G., Some Fine Structure Changes Occurring in the Epidermis of Embryo Mice during Differentiation | 49 |
| KUFF, EDWARD L. and DALTON, ALBERT J., Identification of Molecular Ferritin in Homogenates and Sections of Rat Liver | 62 |
| SJÖSTRAND, F. S. and ANDERSSON-CEDERGREN, EBBA, The Ultrastructure of the Skeletal Muscle Myofilaments at Various States of Shortening | 74 |

NUMBER 2, DECEMBER 1957

| | |
|--|-----|
| MÜLLER, H. R., Gefriertrocknung als Fixierungsmethode an Pflanzenzellen | 109 |
| BANG, B. G. and BANG, F. B., Graphic Reconstruction of the Third Dimension from Serial Electron Microphotographs | 138 |
| ENGSTRÖM, A., LINDBERG, B. and BERGENDAHL, GUDRUN, High Resolution Microradiography with Ultrasoft X-Rays | 147 |
| MANNWEILER, KL. et BERNHARD, W., Recherches ultrastructurales sur une tumeur rénale expérimentale du Hamster | 158 |
| NILSSON, O., Observations on a Type of Cilia in the Rat Oviduct | 170 |
| EKHOLM, R. and SJÖSTRAND, F. S., The Ultrastructural Organization of the Mouse Thyroid Gland | 178 |

NUMBER 3, APRIL 1958

| | |
|--|-----|
| WISCHNITZER, S., An Electron Microscope Study of the Nuclear Envelope of Amphibian Oocytes | 201 |
|--|-----|

| | |
|---|-----|
| ROTH, L. E., A Filamentous Component of Protozoan Fibrillar Systems | 223 |
| LEVER, J. D., A Comment on the Fine Structure of the Parathyroid Gland | 235 |
| EKHOLM, R., Remark on J. D. Lever's Note "A Comment on the Fine Structure of the Parathyroid Gland" | 238 |
| SJÖSTRAND, F. S. and BAKER, R. F., Fixation by Freezing-Drying for Electron Microscopy of Tissue Cells | 239 |
| KREGER, D. R., X-Ray Diffraction of Stopper Cork | 247 |
| YASUZUMI, G. and DEGUCHI, N., Submicroscopic Structure of the Compound Eye as Revealed by Electron Microscopy | 259 |
| SJÖSTRAND, F. S., ANDERSSON-CEDERGREN, EBBA and DEWEY, M. M., The Ultrastructure of the Intercalated Discs of Frog, Mouse and Guinea Pig Cardiac Muscle | 271 |

NUMBER 4, AUGUST 1958

| | |
|---|-----|
| ROUILLER, CH. et FAURÉ-FREMIET, E., Ultrastructure des cinétosomes à l'état de repos et à l'état cilière chez un Cilié péritriche | 289 |
| YASUZUMI, G., TEZUKA, O. and IKEDA, T., The Submicroscopic Structure of the Inner Segments of the Rods and Cones in the Retina of <i>Uroloncha Striata</i> var. <i>Domestica</i> Flower | 295 |
| DEUTSCH, K. and DUNN, A. E. G., A Method for Preparing Individual Cells for Electron Microscopy | 307 |
| BENEDETTI, E. L. et BERNHARD, W., Recherches ultrastrurales sur le virus de la leucémie érythroblastique du poulet | 309 |
| MOSLEY, V. M. and WYCKOFF, R. W. G., Microradiography for Absorption Analysis | 337 |
| GILËV, V. P., The Use of Gelatin for Embedding Biological Specimens in Preparation of Ultrathin Sections for Electron Microscopy | 349 |
| YAMADA, E., The Fine Structure of the Tapetum of the Kitten Eye as Revealed by the Electron Microscope | 359 |
| SJÖSTRAND, F. S. and POLSON, A., Macrocrystalline Patterns of Closely Packed Poliovirus Particles in Ultrathin Sections | 365 |
| NILSSON, O., Ultrastructure of Mouse Uterine Surface Epithelium under Different Estrogenic Influences. 1. Spayed Animals and Oestrous Animals | 375 |
| FREY-WYSSLING, A. and KREUTZER, EMILIA, The Submicroscopic Development of <i>Capsicum annum</i> L | 397 |

| | |
|---|-----|
| THORSSON, K. G. and WEIBULL, C., Studies on the Structure of Bacterial L Forms, Protoplasts and Protoplast-like Bodies | 412 |
| ELFVIN, L.-G., The Ultrastructure of Unmyelinated Fibers in the Splenic Nerve of the Cat | 428 |



Digitized by the Internet Archive
in 2024

Ultrastructure réticulée d'une fibre squelettique chez un Cilié

CH. ROUILLER et E. FAURÉ-FREMIET

*Laboratoires de Médecine expérimentale
et d'Embryologie expérimentale du Collège de France*

Reçu le 11 février 1957

Le tube infundibulaire d'un Cilié péritriche, *Campanella umbellaria*, est maintenu béant par une fibre squelettique spiralée qui accompagne les rangées ciliaires adorales. La substance protéique constituant cette fibre présente une structure réticulaire à mailles hexagonales contrastant avec la structure fibrillaire, non moins régulièrement ordonnée, montrée chez d'autres Ciliés par des fibres de soutien analogues. La structure réticulaire de la fibre de *Campanella* se retrouve, peut-être, chez quelques autres Péritriches; elle répond néanmoins à un type extrêmement particulier, dont le seul équivalent connu jusqu'ici est donné par une lame collagène de l'œil des Vertébrés (membrane de Descemet). Le réseau protéique constituant la fibre de *Campanella* paraît s'organiser au contact de l'infrciliature adoral sous forme de « racines ciliaires » portant des condensations périodiques. La comparaison de cette structure réticulée avec certains aspects décrits au cours de la précipitation des collagènes solubles doit être examinée.

L'ARMATURE INFUNDIBULAIRE DES CILIÉS PÉRITRICHES

La bouche proprement dite, ou cytostome, s'ouvre chez les Ciliés péritriches à l'extrémité centrale d'un canal profondément enfoncé dans l'endoplasme à partir de la gouttière péristomienne, sur le côté ventral de laquelle il prend naissance. Ce canal, qui sera désigné ici sous le nom d'infundibulum¹, est maintenu béant par une armature rigide et élastique constituée, outre l'infrciliature des deux membranes vibratiles adorales, par une ou plusieurs fibres scléroprotéiques (3, 6, 8).

Chez *Trichodinopsis paradoxa* (6) ces fibres infundibulaires apparaissent au microscope électronique comme autant de faisceaux de très fines fibrilles parallèles; une telle structure se retrouve, au niveau du pharynx, chez beaucoup d'autres Ciliés (12) où la densité de l'assemblage fibrillaire, comme sa disposition plus ou moins ordonnée, peuvent varier d'un cas à l'autre.

¹ Il nous a semblé nécessaire (6) dans le cas des Péritriches d'ajouter ce terme à la nomenclature des structures buccales proposée par Corliss (2).

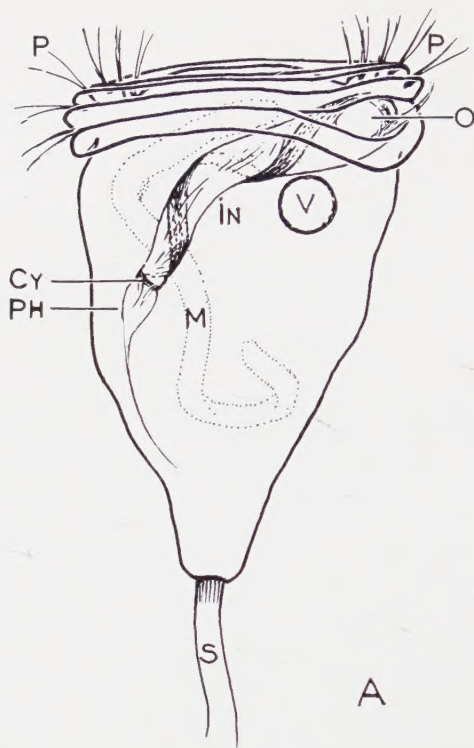


FIG. A.—*Campanella umbellaria*. Aspect d'un individu à l'état vivant (semi schématique). *P, P*, coupe optique des rangées ciliaires péristomiennes dessinant une double spirale autour du disque apical. *O*, ouverture buccale; *IN*, infundibulum, montrant un ruban spiralé constitué par les deux membranes vibratiles adorales bordées par les deux fibres myoïdes et squelettiques; *Cy*, cytostome (bouche proprement dite); *Ph*, pharynx; *V*, vacuole contractile; *M*, macronucleus; *S*, style.

Chez *Campanella umbellaria* (3) et quelques autres Pérित्रiches coloniaux il existe deux fibres infundibulaires, bien visibles chez l'Infusoire vivant (fig. A) et mieux encore sur les coupes colorées par les techniques cytologiques courantes (fig. B). L'une de ces fibres, assez fine, paraît être contractile, et les micrographies électroniques lui montrent une structure feuilletée rappelant les myoïdes ectoplasmiques des Hétérotriches (5, 7). L'autre, épaisse de près de 2μ , et moins fortement colorable, est une fibre de soutien, résistante et élastique; bien que ses caractères physiques et microchimiques soient insuffisamment connus, il s'agit très probablement d'une fibre scléroprotéique. Les micrographies électroniques montrent que cette fibre présente une ultrastructure réticulée tout à fait particulière et assez surprenante, car la seule image comparable qui nous soit actuellement connue est offerte par une lame collagène appartenant à l'œil des Vertébrés (11).

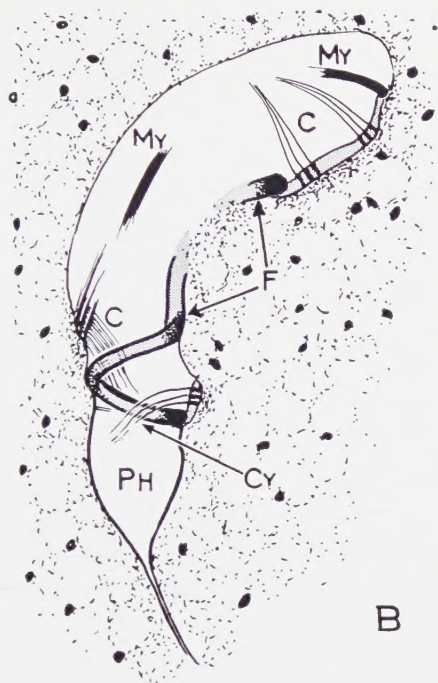


FIG. B.—Aspect semi schématique d'une coupe passant par l'extrémité centrale de l'infundibulum. Cy, cytostome; Ph, pharynx; C, les deux membranes vibratiles adoraes constituées, à ce niveau, par trois rangées ciliaires; My, fibre supposée myoïde; F, fibre infundibulaire squelettique.

MATERIEL ET TECHNIQUE

Les colonies de *Campanella umbellaria* ont été fixées soit dans un mélange de tétroxyde d'osmium (12) et de bichromate de potassium (pH 7,9), soit dans une solution de tétroxyde d'osmium à 1% (pH 7,9) tamponnée par du véronal sodique.

Au cours de la déshydratation, le contraste des préparations a été augmenté en incorporant à l'alcool à 70° 1% d'acide phosphotungstique.

Le matériel a été enrobé dans le méthacrylate de butyle et les sections, obtenues à l'aide du microtome Servall de Porter et Blum, examinées au microscope électronique RCA, type EMU 3B.

LA FIBRE INFUNDIBULAIRE DE *CAMPANELLA*

La fibre infundibulaire dont la largeur atteint près de 2μ , apparaît sur nombre de sections, coupée sous des incidences diverses; dans tous les cas, sa masse montre l'aspect d'un réseau à mailles hexagonales centrées, de structure remarquablement régulière (fig. 2 et 3).



FIG. 1.—*Campanella umbellaria*. Section transversale de l'infundibulum *I* montrant les rangées ciliaires adorales *C* coupées à différents niveaux. La fibre infundibulaire *F* est coupée obliquement. Les corpuscules nodaux se disposent à la périphérie de la fibre en rangées parallèles *P*. *MA* : macro-nucleus. 16.000 \times .

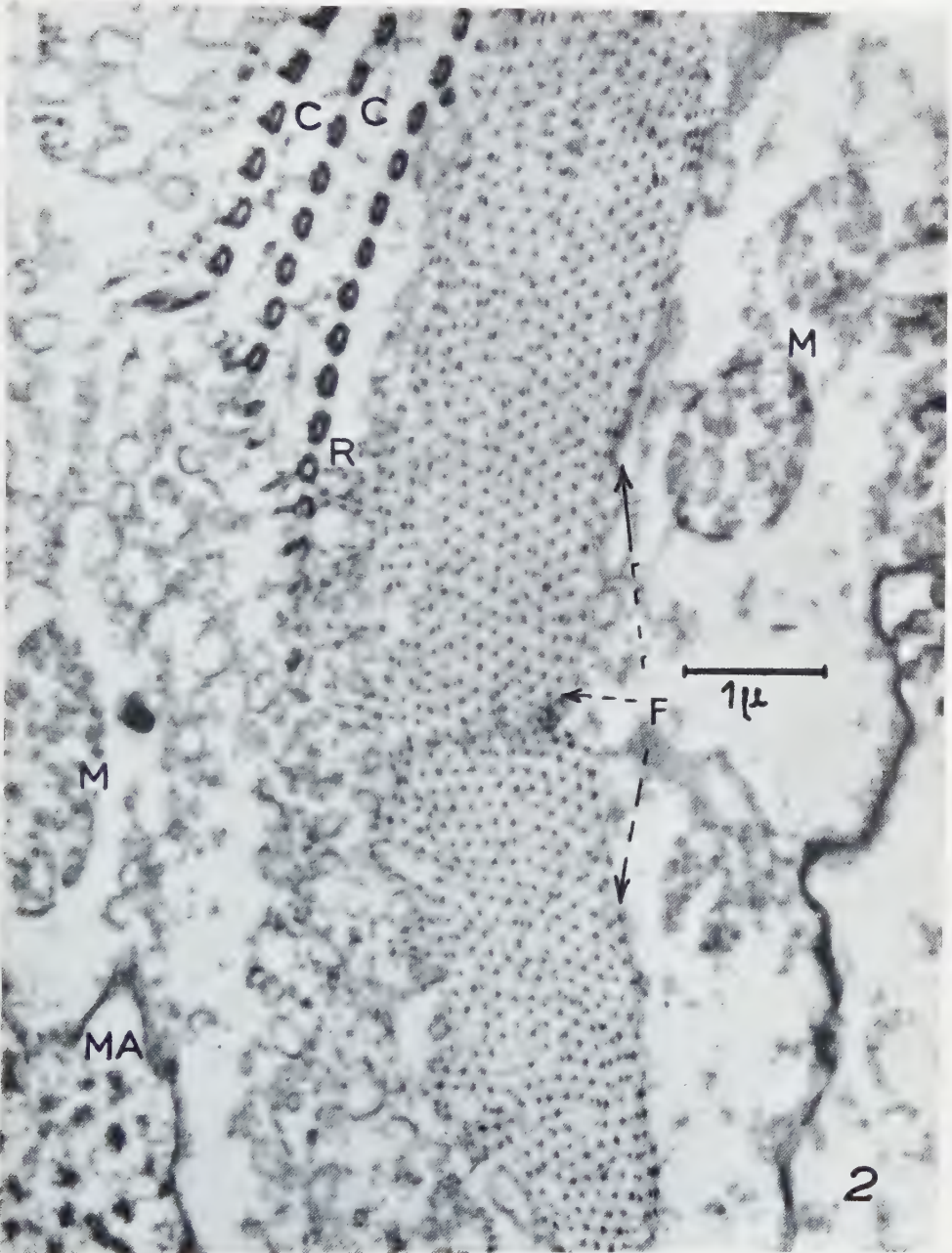


FIG. 2.—Section longitudinale de la fibre infundibulaire *F*, montrant la distribution des corpuscules sur les nœuds d'un réseau hexagonal à mailles centrées. *C* : rangées de corpuscules ciliaires; *R* : racines ciliaires en continuité avec le réseau (voir fig. 3, 4 et 5). *M* : mitochondries; *MA* : macronucleus. 19.000 ×.

Les nœuds du réseau sont occupés par des corpuscules mesurant 30 à 40 $m\mu$; autour de chaque corpuscule nodal rayonnent six bras ténus, composés de deux ou trois lamelles ou fibrilles parallèles, larges de 10 à 20 Å, qui le relient à six autres corpuscules (fig. 3 et 6). Ce réseau paraît tridimensionnel, son aspect restant à peu près le même quelle que soit l'incidence de la section, sauf toutefois à la périphérie de la fibre, comme on le verra plus loin; cet aspect pourrait être dû à la superposition de plusieurs grilles réticulaires à mailles hexagonales, légèrement et régulièrement décalées les unes sur les autres.

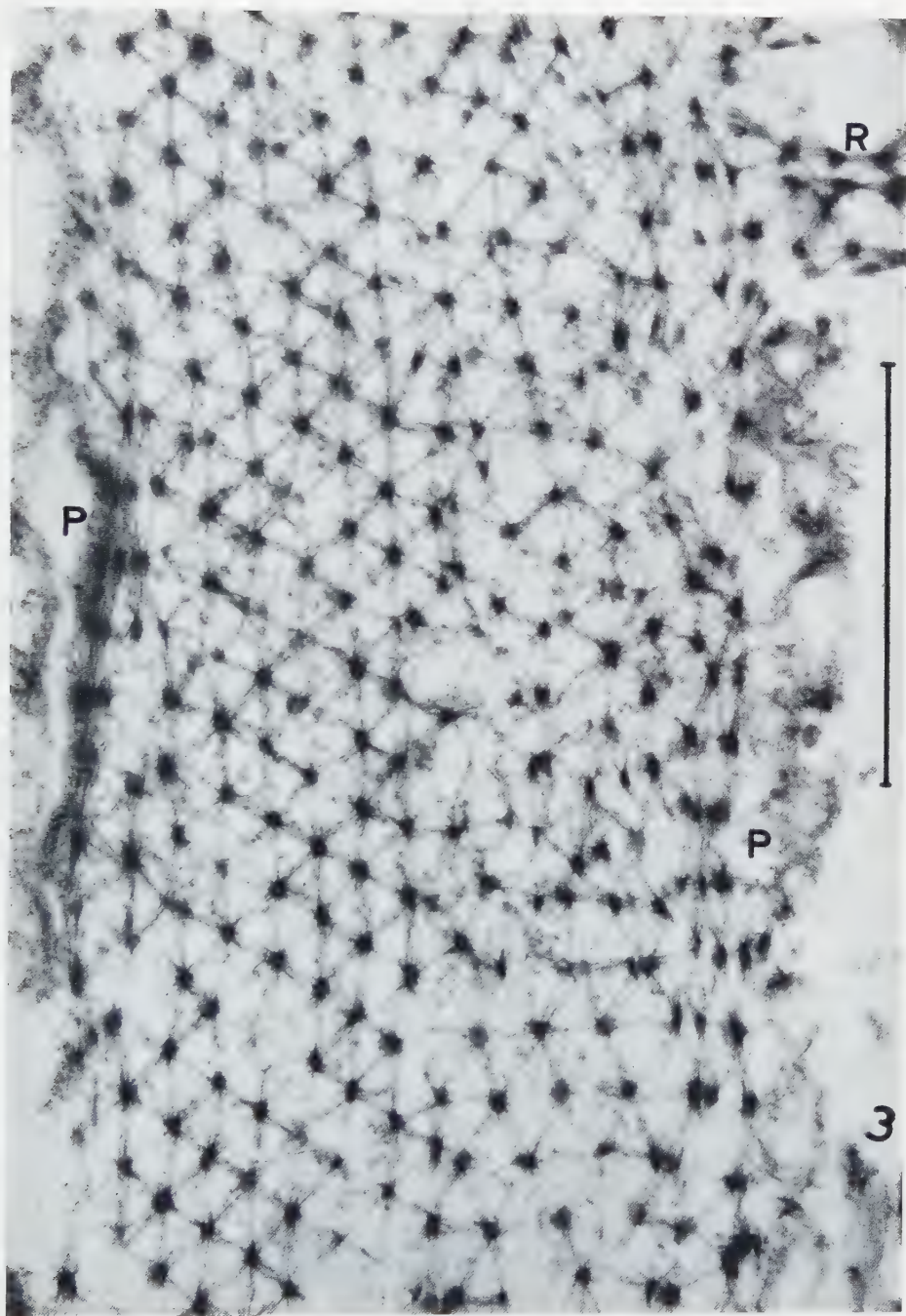
Les distances réticulaires, comptées d'un centre nodal à l'autre, sont comprises entre 120 et 170 $m\mu$; des différences de cet ordre paraissent être en général systématiquement distribuées, et l'on peut admettre qu'elles mesurent les déformations subies par la trame réticulaire soit au cours des manipulations aboutissant à la confection des coupes, soit peut-être chez l'infusoire vivant soumis à des contractions et à des distorsions d'ordre physiologique.

COMPARAISON AVEC LE COLLAGÈNE RÉTICULÉ

Avant de décrire certains aspects particuliers de cette trame réticulaire, il faut noter qu'une structure étroitement comparable vient d'être décrite par Jakus (11) dans le feuillet conjonctif apparemment homogène constituant la membrane de Descemet de l'œil des Vertébrés. Résumant ses observations Jakus écrit : « ... tangential sections showed a two-dimensional array of dark nodes and thin internodal filaments which connected each node with the six others around it to form a hexagonal figure. The average distance between nodes, and between the dark bands in transverse sections, was about 1070 Å; the width of the nodes was about 270 Å; and the width of the connecting filaments was less than 100 Å. This pattern has been found in all species of Descemet's membrane so far examined, although it appeared to be better developed in some forms than in others. So far as known, it has not been observed in any other type of tissue. »

On doit noter 1° que le réseau à mailles hexagonales décrit par Jakus est à deux dimensions et que la membrane de Descemet est formée par la superposition d'une série de grilles, tandis que le réseau de la fibre infundibulaire de *Campanella* paraît s'étendre dans trois dimensions; 2° que les dimensions mesurées dans l'un et l'autre cas accusent de légères différences tout en restant du même ordre de grandeur; soit pour les distances réticulaires, 900 à 1300 Å dans la membrane de Descemet contre

FIG. 3.—Même section que fig. 2 fortement grossie montrant le réseau hexagonal particulièrement régulier sur le côté gauche avec tassement périphérique, *P*, des mailles et des nœuds. *R*, jonction (racines ciliaires) avec les cinétosomes. 57.000 \times .



1200 à 1700 Å dans la fibre infundibulaire; et pour la diamètre des corpuscules nodaux ~ 270 Å dans le premier cas contre ~ 350 Å dans le second.

La nature collagène de la membrane de Descemet étant démontrée par l'ensemble de ses propriétés physiques et microchimiques, Jakus cherche dans les propriétés des particules élémentaires de collagène étudiées par Schmitt, Gross et Highberger (13, 14) et dans leur mode d'agrégation, une interprétation de la structure réticulaire observée. Gross (9) discute les divers modes d'association des particules de tropo-collagène; examinant au microscope électronique, après coloration phosphotungstique, différents stades de précipitations obtenues par dialyse des solutions de collagène, il observe des amas de particules denses disposées suivant un ordre approximativement hexagonal et distantes les unes des autres de 1500 à 2500 Å. Des condensations se produisent bientôt dans ce système et l'on voit apparaître, au bord des amas particuliers, des tactoïdes présentant la « fibrous long spacing » période de ~ 2400 Å. Gross écrit : « the beautifully organized three dimensional network of collagen in Descemet's membrane described in this volume by Jakus suggests that two and three dimensionally ordered collagen is not just an interesting *in vitro* artefact. It is worthy of note that this structure is not enterely dissimilar to the clouds of collagen observed in the formation of FLS (fibrous long spacing). »

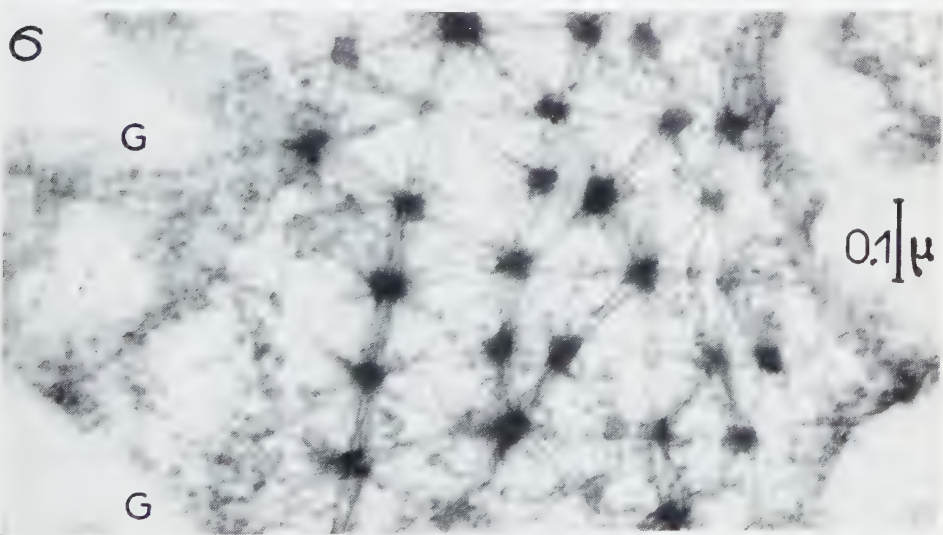
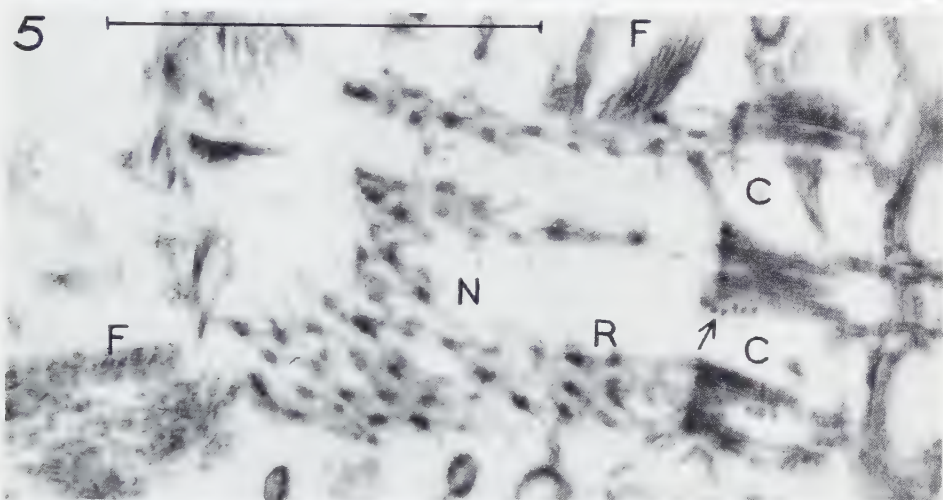
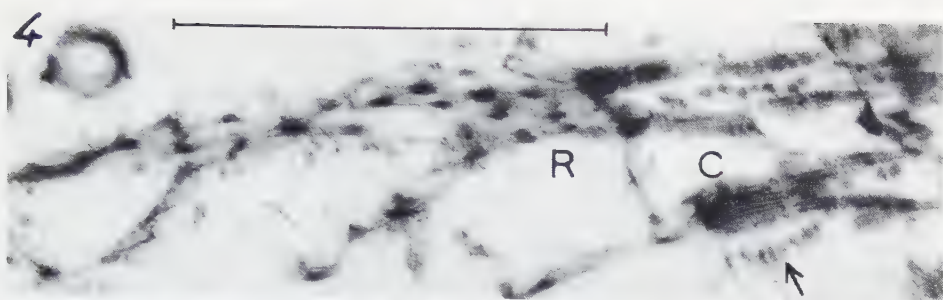
RAPPORTS DE LA FIBRE INFUNDIBULAIRE AVEC L'INFRACILIATURE ADORALE

Ces remarques suggèrent la possibilité d'interpréter certaines structures observées à la périphérie du réseau constituant la fibre infundibulaire.

Diverses sections de cette fibre montrent dans la substance réticulée un ordonnancement moins régulièrement hexagonal des corpuscules nodaux, et leur tassement sur une série de rangées parallèles occupant transversalement une zone corticale (fig. 1, P); d'autres sections coupent des épaisissements corticaux régulièrement mais largement espacés (fig. 7, P); d'autres encore sont tangentes à une sorte d'écorce comportant une série d'épaisissements transversaux de forte densité (fig. 8) dont l'espace-

FIG. 4 et 5.—Corpuscules ciliaires (cinetosomes) C, en liaison par les travées réticulaires formant les racines ciliaires R, avec la substance réticulée de la fibre infundibulaire. Remarquer dans la paroi des cinétosomes C les fibres ciliaires périphériques, et sur leur côté (flèches) la présence de fines granulations ou de prolongements fibreux. Les racines ciliaires R montrent un réseau à mailles allongées, les nœuds étant rapprochés en rangées parallèles courtes. F : masses fibrillaires denses. 56.000 \times .

FIG. 6.—Détail de la structure réticulée, montrant les nœuds denses, de forme stellaire et les connectifs; l'image est prise à la périphérie de la fibre infundibulaire; le réseau est moins régulièrement hexagonal; il se continue avec des amas ou des rangées de très petits granules, G, dont la signification est inconnue. 110.000 \times .



ment moyen est de l'ordre de 2000 Å. On peut se demander si ces différents aspects ne correspondraient pas à ceux obtenus *in vitro* par Gross (9) et montrant au bord des amas particuliers de collagène en cours de précipitation, l'apparition de tactoïdes à structure périodique large.

Un autre problème de morphogénèse est posé par les relations de la substance réticulée avec les corps ciliaires basaux ou cinétosomes.

Les images topographiques à faible grossissement (fig. 2, *R*) montrent que l'un des bords de la fibre infundibulaire est en contact avec l'infaciliature adorale. Les cinétosomes apparaissent sur les micrographies à fort grossissement (fig. 4 et 5) sous l'aspect habituel d'un organite tubulaire long de 0,5 à 0,7 μ , dans la paroi duquel se continuent les 9 fibrilles périphériques du cil, et dont la base est plus ou moins épaissie. Mais on remarque de plus qu'un important système fibreux rayonne à partir de ces corps infraciliaires.

Autour de leurs surfaces latérales et perpendiculairement à celles-ci de fins tractus, portant de très petits granules inférieurs à 100 Å, semblent relier les cinétosomes les uns aux autres (fig. 6, *G*). Mais les structures les plus remarquables sont constituées par les importants faisceaux trabéculaires qui partent de la base des cinétosomes et s'enfoncent dans l'endoplasme sur une longueur de 1 à 1,5 μ avant de se dilater et de se confondre dans la masse réticulée de la fibre infundibulaire (fig. 4 et 5).

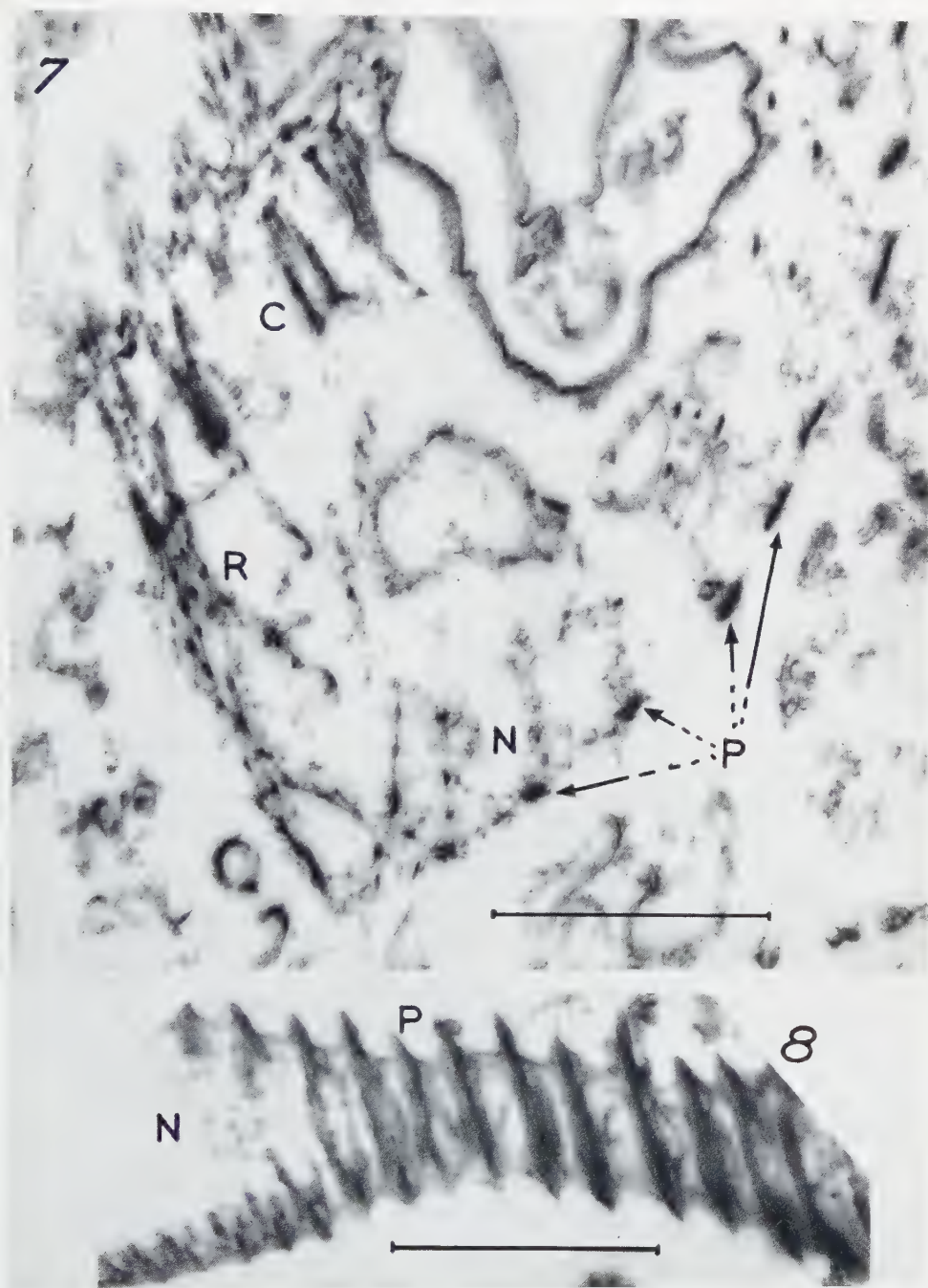
D'après leur position, ces faisceaux devraient être considérés comme des racines ciliaires; ils diffèrent cependant de celles observées chez les *Stentor* p. ex. (5) par leur structure réticulée à mailles allongées et la présence de corpuscules nodaux identiques à ceux déjà décrits dans le corps de la fibre. Les figures 3, *R*, 6 et 7 montrent comment les faisceaux radiculaires se dilatent et se fusionnent en formant le réseau continu à mailles hexagonales déjà décrit. On observe de place en place, sur le côté des faisceaux radiculaires, des masses d'aspect finement fibreux dont la nature comme les connexions restent indéterminées.

La formation de structures protéiques fibreuses orientées au contact des cinétosomes ciliaires évoque les images de centrioles tubulaires obtenues par Bernhard et De Harven (1, 10) montrant à leur contact des condensations fibrillaires de nature fusoriale.

INTERPRÉTATION ET DISCUSSION

La fibre infundibulaire de *Campanella* est constituée par une protéine probablement voisine des collagènes; sa structure si particulière représente peut-être un état

FIG. 7.—Section à travers la paroi infundibulaire montrant les rangées ciliaires (voir 4 et 5) prolongées par le réseau *N* de la fibre; noter les condensations périphériques périodiques *P*. 38.000 \times .
 FIG. 8.—Section tangente à l'écorce de la fibre infundibulaire montrant le réseau sous-jacent *N* et les condensations transversales périphériques *P*. 37.000 \times .



d'agrégation macromoléculaire qui, dans ce cas comme dans celui de la membrane de Descemet, serait stable et permanent.

Malgré les intéressants schémas proposés par Gross et par Jakus, il semble prématuré d'interpréter la structure réticulée de la fibre infundibulaire en fonction des propriétés macromoléculaires des tropocollagènes. On notera que les filaments connectifs sont formés par un assemblage de travées lamellaires ou fibrillaires, bien dessinées par la « coloration » phosphotungstique, mais dont l'épaisseur ne saurait dépasser 10 à 20 Å; cet ordre de grandeur limite singulièrement le nombre des chaînes protéiques associées dans ces fines structures. La question se pose de savoir quelles relations existent entre ces éléments connectifs presque macromoléculaires et les corpuscules nodaux qu'ils relient.

Les corpuscules nodaux présentent toujours une forme irrégulièrement stellaire, comme si la masse dense qui les constitue s'étirait sur la base des connectifs; d'autre part, nombre d'images laissent supposer que les constituants lamellaires ou fibrillaires des connectifs traversent toute la masse d'un corpuscule nodal. Il est donc bien difficile de décider si les uns et les autres représentent deux états d'agrégation d'une même protéine ou deux substances protéiques différentes.

D'autre part certaines constatations touchant l'ordonnement des corpuscules doivent être retenues. On se souvient que sur les travées qui partent de la base des cinétosomes, les corpuscules nodaux se trouvent serrés les uns contre les autres sur une série de niveaux (fig. 5, *R*) comme s'ils résultaient de la condensation périodique d'une substance protéique. Plus loin, dans la masse de la fibre, ces corpuscules s'écartent les uns des autres en dessinant le réseau à mailles hexagonales régulières comme si un effet de gonflement était intervenu. Mais à la périphérie de la masse réticulée les nodules se condensent à nouveau en rangées parallèles, créant ainsi une structure périodique superficielle qui précède, peut être, la formation des crêtes parallèles denses représentées à la fig. 8.

BIBLIOGRAPHIE

1. BERNHARD, W. et DE HARVEN, ET., *Compt. rend.* **242**, 288 (1956).
2. CORLISS, J. O., *J. Protozoology* **2** (Suppl.), 12 (1955).
3. FAURÉ-FREMIET, E., *Compt. rend. soc. biol.* **58**, 215 (1905).
4. FAURÉ-FREMIET, E., *Bull. soc. zool.* **81**, 9 (1956).
5. FAURÉ-FREMIET, E. et ROUILLER, CH., *Compt. rend.* **241**, 678 (1955).
6. FAURÉ-FREMIET, E., ROUILLER, CH. et GAUCHERY, M., *Bull. soc. zool.* **81**, 77 (1956).
7. — *Arch. d'anat. microsc. morphol. exp.* **45** 139 (1956).
8. FAURÉ-FREMIET, E. et THAUREAUX, J., *Bull. biol. France et Belg.* **78**, 143 (1944).
9. GROSS, J., *J. Biophys. Biochem. Cytol.* **2**, 261 (1956).
10. DE HARVEN, ET. et BERNHARD, W., *Z. Zellforsch. u. mikroskop. Anat.* **45**, 378 (1956).

11. JAKUS, M. A., *J. Biophys. Biochem. Cytol.* **2**, 241 (1956).
12. ROUILLER, CH., FAURÉ-FREMIET, E. et GAUCHERY, M., *Electron Microscopy. Proc. Stockholm Conference*, 216-218, *Stockholm*, 1956.
13. SCHMITT, F. O., GROSS, J. et HIGHBERGER, J. H., *IX Symposium Soc. Exp. Biology "Fibrous Proteins and Their Biological Significance"* 1955, 148.
14. ——— *Exptl. Cell Research, Suppl.*, **3**, 326 (1955).

L'ultrastructure des cellules du pancréas endocrine chez l'embryon et le rat nouveau-né

DAVID FERREIRA¹

Laboratoire de Microscopie Electronique de l'Institut de Recherches sur le Cancer, Villejuif (Seine). Directeur : Prof. Ch. Oberling

Reçu le 11 février 1957

Cette étude porte sur l'examen au Microscope Electronique de coupes ultra-fines de pancréas endocrine d'embryon et de rat nouveau-né.

Les îlots de Langerhans sont entièrement constitués par des cellules β . L'analyse de l'ultrastructure de ces éléments révèle, en dehors des organites cellulaires bien communs la présence de grains sphériques, d'un diamètre moyen de 150 m μ , répondant aux granulations β .

On observe tous les stades intermédiaires entre cette granulation et les microvésicules de l'appareil de Golgi, généralement hypertrophié. L'auteur attribue un rôle essentiel à cette organite cellulaire dans l'élaboration des granules de sécrétion.

Les cellules endocrines sont séparées des capillaires sanguins par un espace péricapillaire ou subendothélial. Au niveau de la membrane des cellules endothéliales, qui délimite cet espace, on note l'existence de pores et de petites protrusions. Le mécanisme du transport du produit de sécrétion vers la lumière capillaire est discuté.

La découverte de Langerhans qui, en 1869 (22), a signalé dans le pancréas les îlots qui portent son nom, a ouvert dans les études biologiques un chapitre nouveau dont l'importance n'a été comprise que 50 ans plus tard, à l'occasion de la découverte de l'insuline.

Bien que cet auteur ait été le premier à signaler l'existence des groupes cellulaires auxquels, plus tard, on a attribué la sécrétion endocrine du pancréas, c'est à Laguesse (19, 20) et Tschassownikow (33) que revient le mérite d'avoir précisé la description cytologique des îlots pancréatiques et en particulier d'avoir signalé leurs granulations caractéristiques.

En 1907, Lane (21) a reconnu dans les îlots de Langerhans deux types cellulaires différents : les cellules α dont les granulations résistent aux fixateurs alcooliques et les cellules β dont les granulations sont dissoutes par ces mêmes fixateurs, mais conservées

¹ Assistant à l'Institut d'Histologie et d'Embryologie de la Faculté de Médecine de Lisbonne. Boursier de l'Instituto para a Alta Cultura.

après l'emploi de fixateurs aqueux. Ces observations ont pu être confirmées, en 1911, par Bensley (1) qui a mis au point des colorations spécifiques permettant l'identification des différents types cellulaires. Enfin, l'emploi de ces méthodes à l'étude des espèces animales les plus variées et l'introduction de nouveaux procédés de coloration, parmi lesquels ceux de Gomori (13, 14) occupent une place très particulière, ont permis l'identification dans cet organe, d'autres types cellulaires appelés C et D. Chez le rat adulte, en particulier, les îlots de Langerhans sont constitués par trois types cellulaires: α , β et D. De nombreux travaux ont établi le rôle fondamental que jouent les cellules β dans la sécrétion de l'insuline, d'où l'importance de leur étude cytologique et physiologique. Le but de notre travail est d'éclaircir l'organisation ultrastructurale de ces éléments à l'aide du microscope électronique. Dalton (8) ainsi que Robertson (30) rapportent déjà l'observation de tissu endocrine à l'occasion de leur étude sur le pancréas exocrine d'animaux adultes. Ces auteurs n'ont remarqué qu'un seul type de cellules sans avoir précisé leur nature.

On pourrait s'imaginer que les différences histochimiques permettant la classification de ces cellules au microscope optique seraient accompagnées de différences ultrastructurales suffisantes pour permettre leur distinction au microscope électronique. Malheureusement les coupes ultra-fines du pancréas de rat adulte n'intéressent que rarement la partie endocrine et de ce fait, l'étude de la structure fine des îlots de Langerhans est rendue assez difficile.

Pour faciliter l'investigation de ce tissu, il est utile de se servir de matériel embryonnaire, et ceci pour deux raisons: d'une part, les îlots occupent une portion plus importante du pancréas, et sont donc plus facilement accessibles, d'autre part, ils sont constitués d'un seul type cellulaire. En effet, selon les travaux de Hard (17) confirmés par Nereimberg (26) les cellules β sont les premières à se différencier dans le pancréas endocrine de l'embryon de rat vers le 18^e jour de la vie intra-utérine, et jusqu'au second jour après leur naissance, ces mêmes cellules sont le constituant exclusif des îlots.

MATERIEL ET METHODES

Les tissus faisant l'objet de cette étude proviennent du pancréas de 15 embryons de rats du 18^e au 20^e jour de la gestation, ainsi que de 8 rats nouveaux-nés (1 à 2 jours).

L'extraction des embryons a été pratiquée sur des femelles préalablement anesthésiées à l'éther. Tout de suite après, la cavité abdominale du fœtus est ouverte et quelques gouttes de fixateur sont versées sur le pancréas. Celui-ci est ensuite isolé et coupé en petits morceaux d'un millimètre cube à l'aide d'une lame de rasoir. Les animaux nouveaux-nés, après décapitation ont subi le même traitement.

Après fixation d'une à deux heures à l'acide osmique à 1% tamponné selon Palade (— 3°C), les fragments ont été déshydratés dans l'appareil de Bernhard (2) et inclus au *n*-butylméthacrylate selon la technique courante. Les coupes faites avec l'ultramicrotome de Porter-Blum ont été observées au microscope RCA EMU 2E.

RESULTATS

L'ultrastructure de la cellule β .—A un faible grossissement, les cellules présentent une région basale, en partie occupée par le noyau et une zone apicale (pôle vasculaire) en rapport avec un capillaire sanguin.

Dans le cytoplasme, outre les éléments communs à d'autres types cellulaires : le chondriome, l'appareil de Golgi et l'ergastoplasme, on observe des granulations frappantes par leur forte osmiophilie. (fig. 1.)

Le *noyau* à structure granuleuse est, comme d'habitude, limité par une double membrane où l'on peut observer des pores. Il n'est pas rare de voir un nucléole toujours relativement petit par rapport au volume total du noyau. Quelquefois, il présente l'aspect filamenteux ou réticulé décrit au microscope électronique dans d'autres cellules animales (3, 4, 5).

Le *chondriome* très polymorphe est constitué par des mitochondries ovalaires ou allongées, aspects résultant de différentes incidences de coupe.

L'*ergastoplasme* est représenté par des sacs ou des vésicules; sur leur membrane adhèrent les particules ribonucléoprotéiques décrites par Palade (28). Ceux-ci se trouvent également isolés et dispersés dans tout le cytoplasme.

L'*appareil de Golgi* paraît hypertrophié (fig. 2 à 4). En accord avec les descriptions de Dalton et Felix (8), Sjöstrand et Hanzon (32), Haguenau et Bernhard (16) on peut y reconnaître ces trois constituants habituels :

- 1° Les grandes vacuoles limitées par des membranes sans granules, quelquefois allongées avec l'aspect de canaux sinueux.
- 2° Les microvésicules ou granules limités par une membrane très nettement dessinée. De contenu très dense, ils sont surtout nombreux à la périphérie des grandes vacuoles.
- 3° Les faisceaux de doubles membranes lisses.

Ces trois éléments se situent dans une zone de la cellule dont la substance fondamentale plus dense est quelquefois parcourue par des fibrilles très minces (30 Å) qui s'entrecroisent (fig. 3).

Les *granulations β* , qu'on peut observer dans tout le cytoplasme sont plus nombreuses dans la zone située entre l'appareil de Golgi et le pôle vasculaire. Sphériques ou légèrement ovalaires (effet de compression de la coupe par le rasoir), elles possèdent un centre très osmiophile séparé du cytoplasme par une zone moins dense. Cette zone est séparée du corps central par une membrane interne, et du cytoplasme par une membrane externe. Le corps central est homogène dans la plupart des granulations, mais il peut présenter des zones de condensation. Le diamètre des granulations a été mesuré séparément chez les embryons et les nouveaux-nés. La différence des deux moyennes obtenues n'est pas significative.

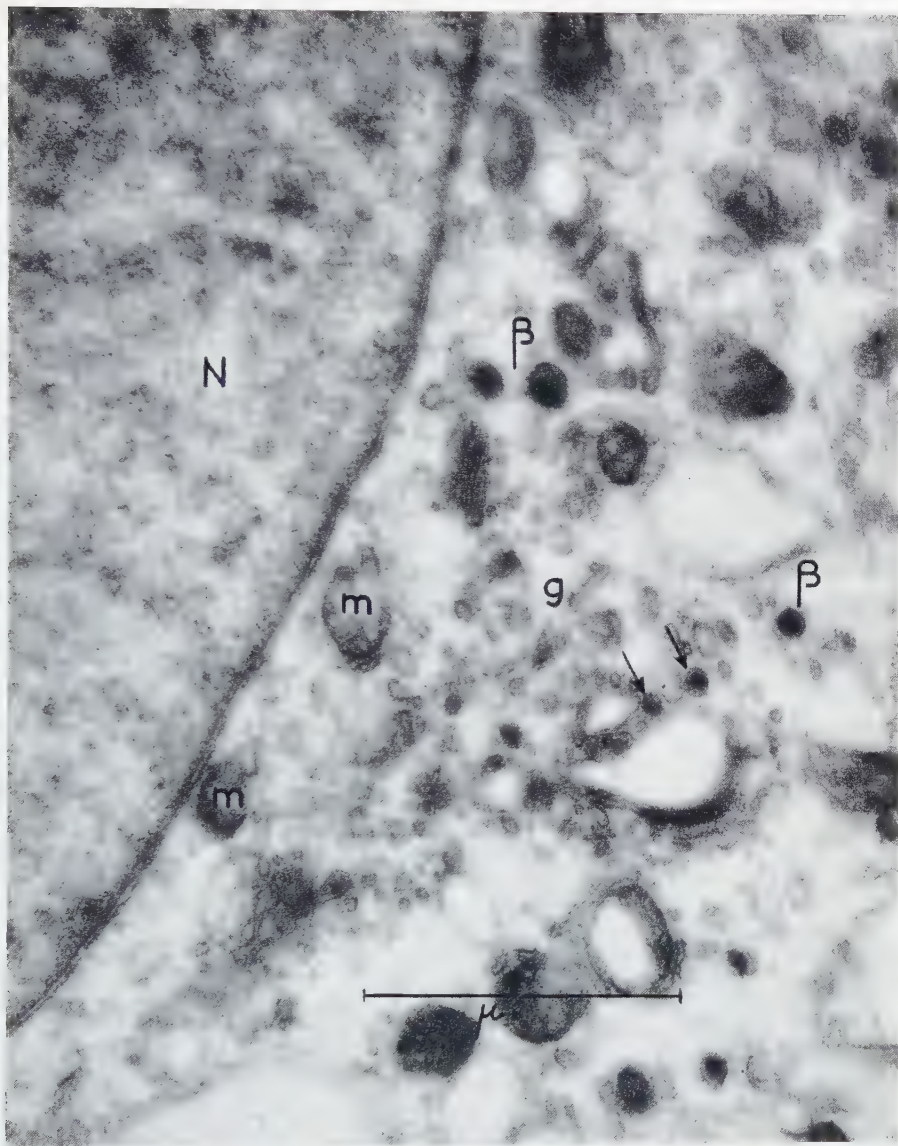


FIG. 1.—Cellule endocrine d'un îlot de Langerhans d'un rat âgé de 2 jours. Portion cellulaire avec noyau (*N*), Appareil de Golgi (*g*), mitochondries (*m*) et granulations β . Les flèches (\rightarrow) indiquent des ébauches de ces granules dans les microvésicules golgiennes. 42.000 \times .

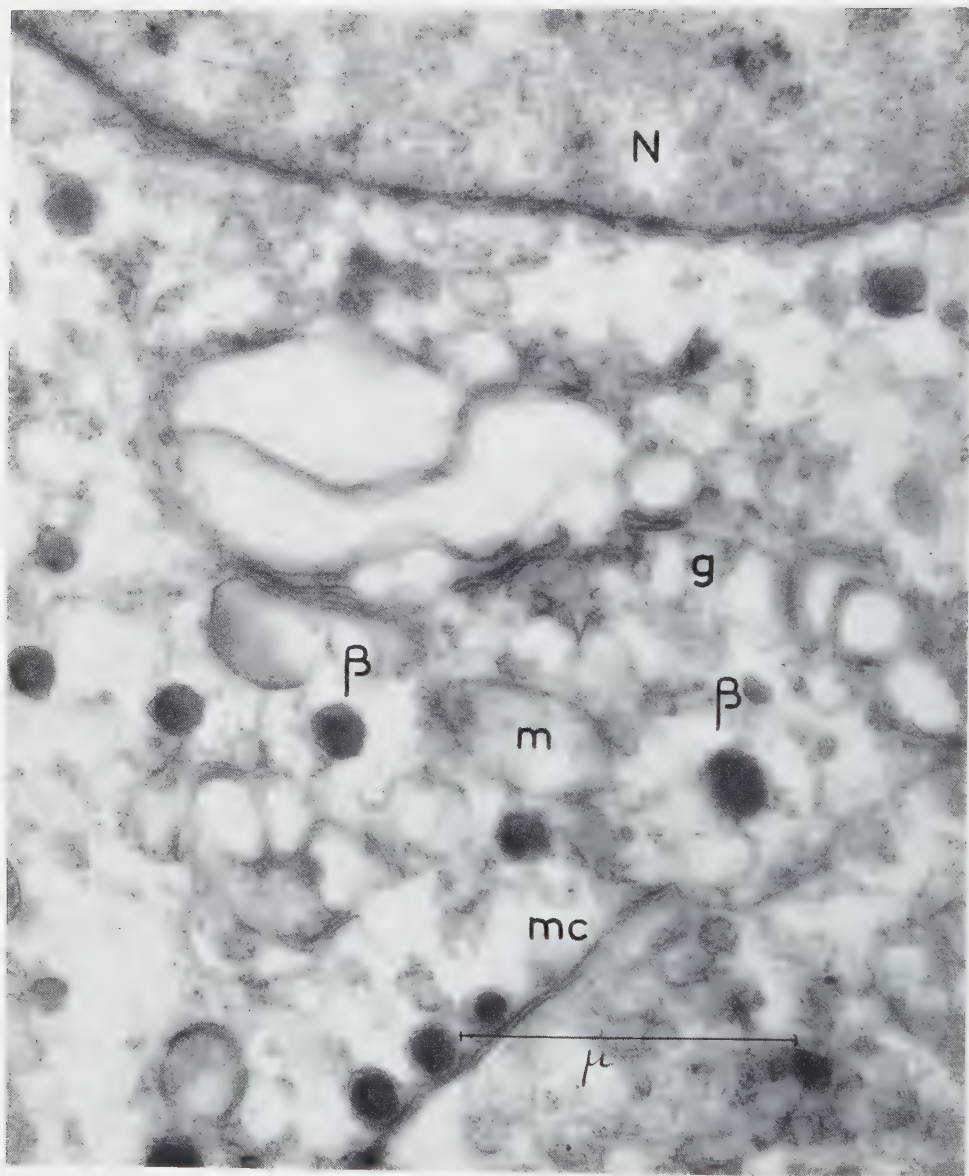


FIG. 2.—Cellule insulaire d'un embryon de rat de 20 jours, montrant l'appareil de Golgi (*g*) et dans son voisinage des granulations β . *N* = Noyau. *mc* = Membrane cellulaire. 44.000 \times .

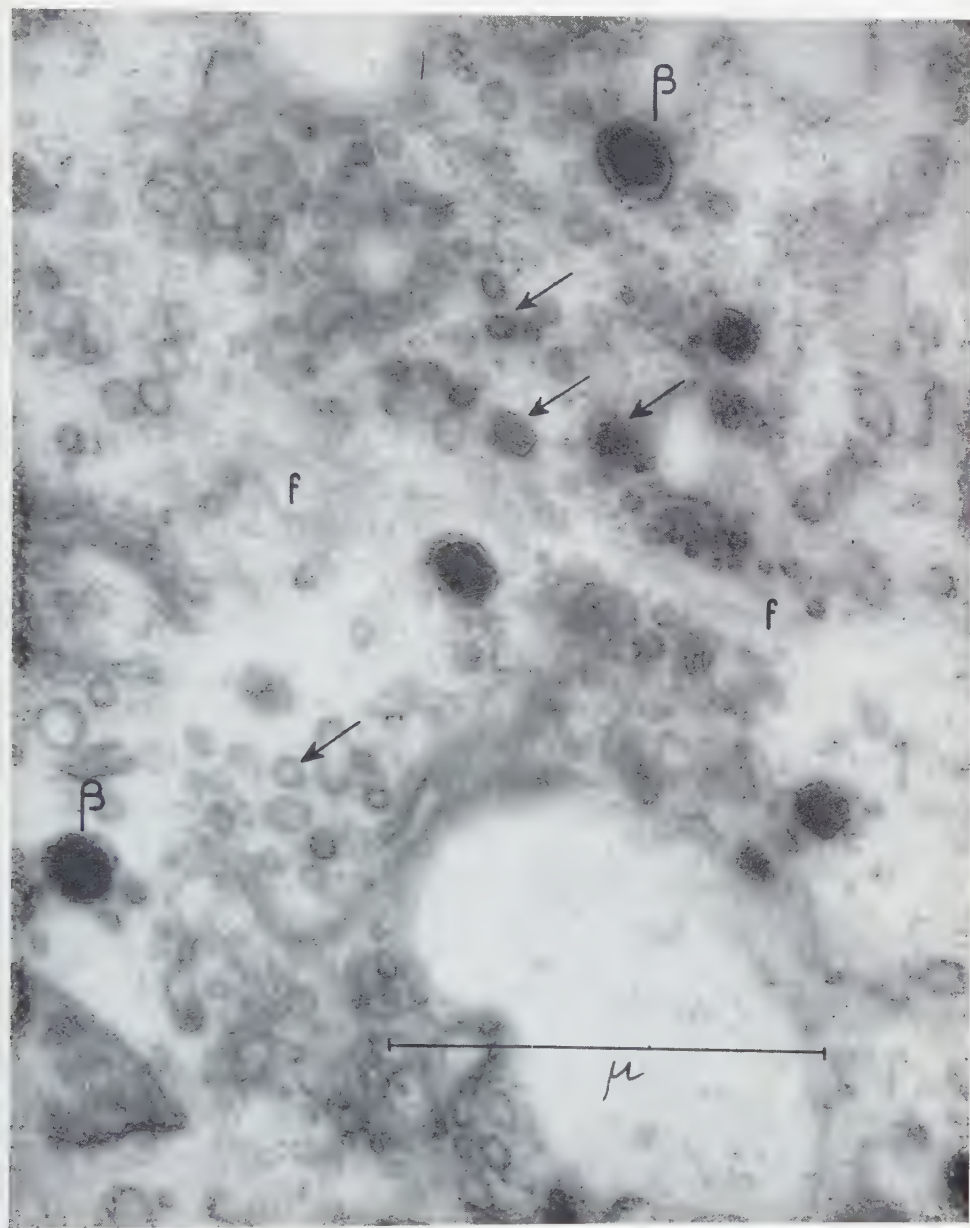


FIG. 3.—Îlot de Langerhans, rat de 2 jours. Portion d'une cellule avec un appareil de Golgi très développé au sein duquel on remarque des granules de transition () entre les microvésicules Golgiennes et la granulation β . Présence de fines fibrilles (*f*) dans la substance fondamentale. 59.000 \times .

L'ensemble des mesures considérées comme échantillons d'une seule population donne un diamètre moyen de 150 m μ environ.

Rapport entre l'appareil de Golgi et les granulations β .—Les microvésicules et les granules de l'appareil de Golgi ne sont pas homogènes (fig. 1). Leur différence de taille et de densité frappe l'observateur. En dehors des petites vésicules ou granules à parois simples qui sont les plus fréquentes, il en existe d'autres, plus grandes, à parois doubles et à contenu plus dense (fig. 3). Plus rarement, on observe des granules avec une zone centrale bien contrastée et très osmophile. Ainsi, entre les vésicules et granules de l'appareil de Golgi et les granulations tous les aspects intermédiaires peuvent être observés. Cette succession d'images suggère l'origine de ces granulations. Ces observations sont en accord avec celles rapportées pour deux autres types cellulaires : d'une part Sjöstrand et Hanzon (32) ont décrit dans le pancréas exocrine de la souris des rapports semblables entre les granules de l'appareil de Golgi et les grains de zymogènes; d'autre part, Haguenau et Bernhard (16) ont signalé une participation probable de l'appareil de Golgi dans la formation des granulations spécifiques des cellules du lobe antérieur de l'hypophyse.

Rapport entre les cellules et les capillaires sanguins.—Dans les cellules endothéliales qui constituent la paroi des capillaires du pancréas endocrine, on observe, à l'exception de l'appareil de Golgi tous les organites cellulaires habituels.

La surface endothéliale peut présenter des encoches pénétrant profondément dans le cytoplasme (fig. 5). Les capillaires et les cellules du parenchyme endocrine sont séparés par un *espace péri-capillaire ou sous-endothélial* (fig. 5), délimité d'une part par la membrane cellulaire de l'endothèle, d'autre part par la paroi du pôle vasculaire des cellules endocrines. Cet espace présente un écartement moyen d'environ 80 m μ . On y trouve une substance amorphe de faible contraste électronique, adjacente aux deux membranes. L'ensemble de cette formation correspond à la basale des auteurs classiques. Fait important : la membrane endothéliale paraît fréquemment interrompue par des pores de 300 Å de diamètre environ. En coupe perpendiculaire, ceux-ci se présentent sous forme de petites protrusions vésiculaires dans le cytoplasme endothélial (fig. 5). Par ailleurs, les granulations β situées dans le pôle vasculaire de la cellule sont souvent en contact par l'intermédiaire de leur membrane avec l'espace péri-capillaire (fig. 5).

DISCUSSION

Grâce à un matériel particulièrement favorable, ces observations nous ont permis en premier lieu d'identifier la structure des cellules et granulations β . Il est probable que la comparaison entre les cellules ici décrites et les îlots de Langerhans d'animaux adultes permettra également de reconnaître les autres types cellulaires. En second

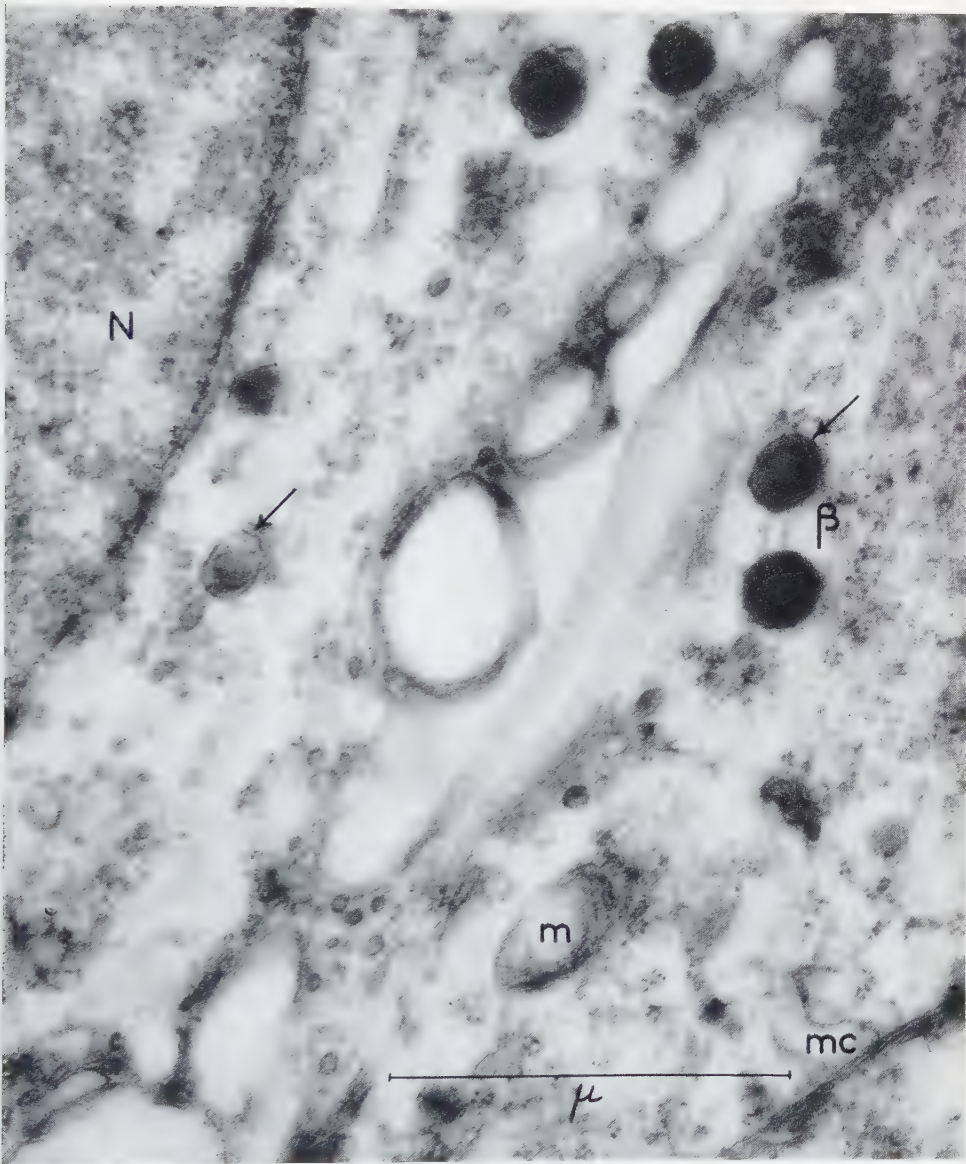


FIG. 4.—Îlots de Langerhans, embryon de 20 jours. Portion d'une cellule β avec quelques granulations spécifiques dont l'ultrastructure est bien visible (\rightarrow). *mc* = Membrane cellulaire. 53.000 \times .

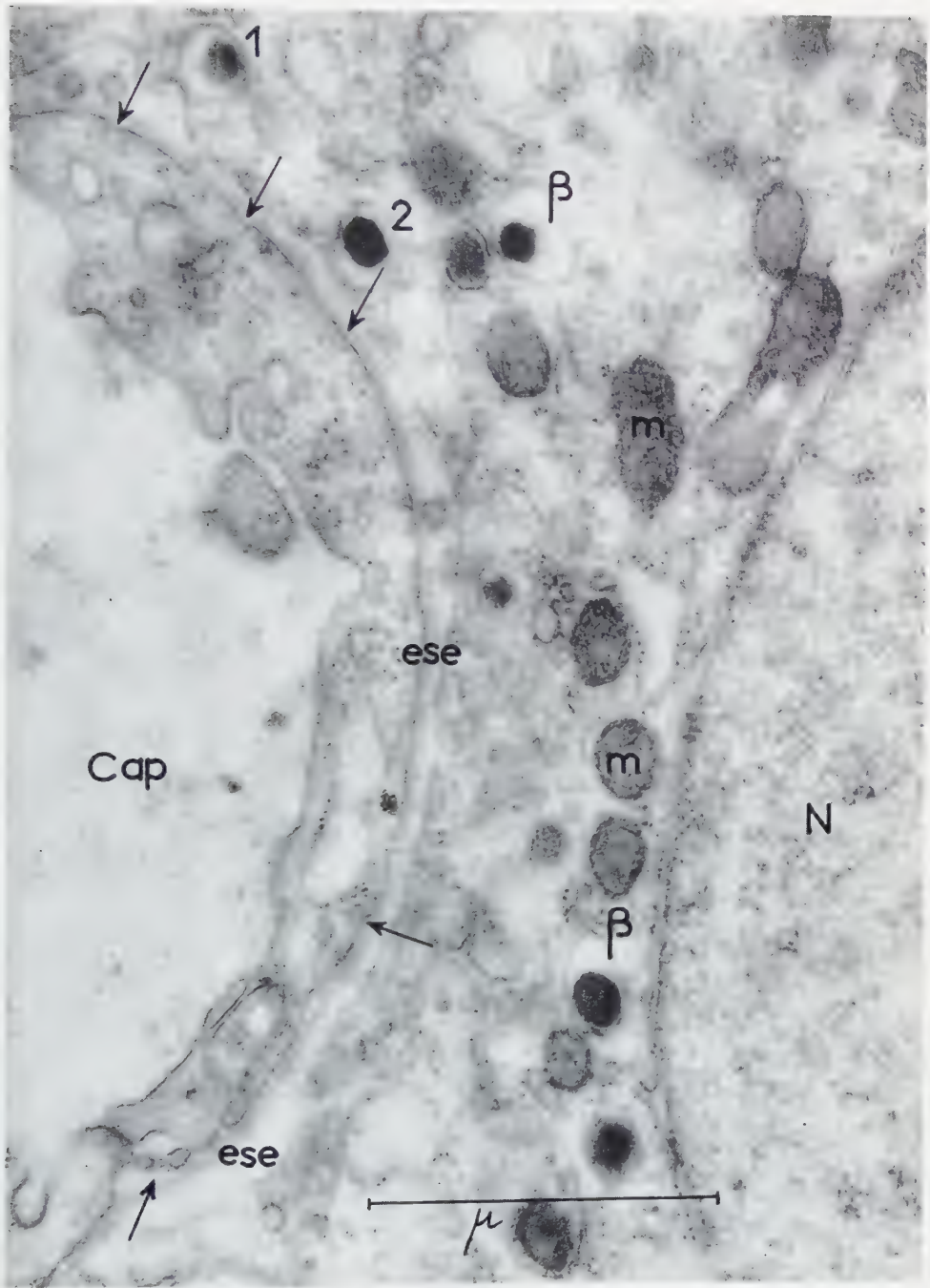
lieu, cette étude jette une lumière sur la genèse d'une granulation spécifique d'une glande endocrine. Etant donné que les granulations β contiennent les précurseurs de l'insuline, il est d'un grand intérêt de savoir quel organite cellulaire les élabore et quelle structure elles présentent au microscope électronique. En 3^e lieu, il a paru utile de préciser les rapports entre ces cellules et les capillaires afin de savoir si le mécanisme du passage d'un produit de sécrétion endocrine peut être éclairci par la morphologie ultrastructurale.

La *genèse des granulations* au sein de l'appareil de Golgi s'accorde bien avec certaines hypothèses classiques, notamment avec celle de Cajal (6), qui a déjà admis en 1914 que les produits de sécrétion des glandes salivaires et du pancréas exocrine seraient dus à l'activité de l'appareil de Golgi. Après cet auteur beaucoup d'autres ont essayé d'établir le même rapport, tant dans les cellules glandulaires exocrines que dans les cellules endocrines. La relation entre l'appareil de Golgi et le sens de l'excrétion signalée par Cajal (6) est largement rapportée par la littérature classique. Entre autres, plusieurs hypothèses ont essayé d'expliquer en détail sa participation dans l'élaboration des grains sécrétoires (voir 18), mais les ressources de la microscopie optique n'ont pas permis de les vérifier. Ce n'est qu'après la première mise en évidence, des structures golgiennes au microscope électronique par Dalton et Felix (8) que l'étude de ce mécanisme obscur pouvait être abordé. Ainsi, Sjöstrand et Hanzon (32) sont arrivés à admettre la participation de l'appareil de Golgi dans la formation des grains de zymogène dans les cellules du pancréas exocrine. Deux observations servent de base à leur conclusion: la localisation des granules de zymogène en rapport avec l'appareil de Golgi d'une part, et les images de transition entre les granules Golgiens et les granules de sécrétion de l'autre. Le rôle élaborateur de l'appareil de Golgi a aussi été admis, bien qu'avec réserves, par Haguenau et Bernhard (16) pour les granulations des cellules basophiles de la préhypophyse.

Nos observations sont analogues à celles de ces auteurs : la localisation topographique des grains rassemblés en plus grand nombre dans la zone comprise entre l'appareil de Golgi et le pôle sécrétoire de la cellule et les images de transition très frappantes entre les grains golgiens et les grains de sécrétion sont caractéristiques.

D'autre part, il n'a pas été possible de trouver de rapport entre les grains de sécrétion et les autres organites cellulaires. L'hypothèse de leur origine aux dépens du chondriome ne peut plus être admise. On se souvient que cette théorie a eu beaucoup de partisans parmi les histologistes classiques, et plus récemment encore le travail

FIG. 5.—Îlots de Langerhans, Rat de 2 jours. Cellule et Capillaire (Cap.) séparés par l'espace subendothélial (e.s.e.) (« Membrane basale » au microscope optique). Dans cet espace, présence d'une substance amorphe condensée le long des membranes cellulaires. Les flèches (-) indiquent la portion des pores et protrusions de la membrane endothéliale. (1) et (2) Granulations β en contact avec l'espace subendothélial. 48.000 \times .



de Challice et Lacy (7) tend à démontrer l'élaboration des grains de zymogène par les mitochondries. Cependant la documentation apportée pour ces auteurs ne nous paraît pas suffisamment démonstrative.

Quant au rapport existant entre les cellules insulaires et les capillaires sanguins, il convient de comparer nos observations à celles déjà signalées pour d'autres organes. L'espace subendothélial ou péricapillaire a été déjà mis en évidence dans des tissus endocriniens. Il est d'autre part comparable à l'espace situé entre les cellules endothéliales et les cellules du foie décrites par Disse (10) et dont l'existence réelle a pu être démontrée au microscope électronique (12, 31).

Farquhar et Rinehart (11) l'ont décrit dans le lobe antérieur de l'hypophyse, Dempsey et Petterson (9) dans la thyroïde et Lever (25) dans la surrénale et parathyroïde. Nous n'avons pas observé dans cet espace des fibrilles collagènes comme le signalent ces auteurs. Dans le lobe antérieur de l'hypophyse, Green et van Bremen (15) y ont observé des granules de sécrétion, contrairement à ces auteurs, aucune formation identifiable aux granulations n'a pu être reconnue entre les deux membranes limitant l'espace péricapillaire.

Rinehart et Farquhar (29) ont décrit dans cet espace au niveau du lobe antérieur de l'hypophyse des masses cytoplasmiques contenant des granulations.

Selon ces auteurs, les granulations y seraient solubilisées et passeraient ainsi sous la forme diffuse dans la circulation. Le travail de Lever (24) pourrait être cité à l'appui de cette hypothèse. Etudiant après stimulation la médullaire et le cortex surrénal, cet auteur signale l'existence d'une masse diffuse dans l'espace sub-endothélial qu'il interprète comme produit de sécrétion. Mais, il ne s'agit probablement que de cette substance amorphe signalée ci-dessus, et constamment présente dans cet espace.

L'interprétation de nos propres images ne peut définitivement trancher la question. S'il paraît acquis que les granulations β se forment au niveau de l'appareil de Golgi s'accroissent ensuite à la membrane cellulaire pour entrer en contact intime avec l'espace péricapillaire, le mécanisme de leur passage reste à être élucidé. Les granules pourraient en effet se solubiliser et leur contenu passer à travers les différentes barrières membraneuses sur une forme invisible au microscope électronique. Mais, tenu compte de l'existence des pores et des protrusions au niveau de la membrane endothéliale basale, il est fort probable que le produit de sécrétion traverse par petits paquets la membrane selon un mécanisme déjà suggéré par Palade (28).

En conclusion, ce travail ne donne que les premiers éléments d'une étude des îlots de Langerhans au microscope électronique. On peut cependant facilement prévoir de nouvelles recherches qui, s'attaquant surtout à l'étude des variations fonctionnelles et des états pathologiques de ces glandes, pourront fournir d'autres renseignements du plus haut intérêt sur leur structure fine.

Nous exprimons notre profonde reconnaissance au D^r Bernhard qui nous a guidé de ses précieux conseils tout au long de ce travail. Nous remercions très vivement M^{lle} Karin Lindmark et M. Halpern pour leur très utile collaboration technique.

BIBLIOGRAPHIE

1. BENSLEY, R. R., *Am. J. Anat.* 12, 297 (1911).
2. BERNHARD, W., *Exptl. Cell Research* 8, 248 (1955).
3. BERNHARD, W., BAUER, A., GROPP, A., HAGUENAU, F. et OBERLING, CH., *Exptl. Cell Research* 9, 88 (1955).
4. BERNHARD, W., HAGUENAU, F. et OBERLING, CH., *Experientia* 8, 58 (1952).
5. BORYSKO, E. et BANG, F., *Bull. Johns Hopkins Hosp.* 89, 468 (1951).
6. CAJAL, S. R., *Trab. lab. inv. bio.* 12, 127 (1914).
7. CHALLICE, C. E. et LACY, D., *Nature* 174, 1150 (1954).
8. DALTON, A. J., *Am. J. Anat.* 89, 109 (1951).
9. DEMPSEY, E. W. et PETERSON, R. R., *Endocrinology* 56, 46 (1955).
10. DISSE, J., cité d'après FAWCETT, D. W., *J. Appl. Phys.* 24, 1424 (1953).
11. FARQUHAR, M. G. et RINEHART, J. F., *Endocrinology* 55, 857 (1954).
12. FAWCETT, D. W., *J. Natl. Cancer Inst.* 15, 1475 (1955).
13. GOMORI, G., *Anat. Record* 74, 439 (1939).
14. ——— *Am. J. Pathol.* 15, 497 (1939).
15. GREEN, J. D. et VAN BREMEN, V. L., *Am. J. Anat.* 97, 177 (1955).
16. HAGUENAU, F. et BERNHARD, W., *Arch. anat. micr. morph. exp.* 44, 27 (1955).
17. HARD, W., *Am. J. Anat.* 75, 369 (1944).
18. HIRSCH, G. C., *Form und Stoffwechsel der Golgi-Körper*, Edit. BORNTÄGER. Berlin, 1939.
19. LAGUESSE, E., *Compt. rend. soc. biol.* 45, 819 (1893).
20. ——— Rapport au 16^e Congr. intern. Médec. Budapest, 1909.
21. LANE, M. A., *Am. J. Anat.* 7, 409 (1907).
22. LANGERHANS, cité d'après WARREN, S. et LE COMPTE, P., *The Pathology of Diabetes Mellitus*, Lea & Febiger, Philadelphia, 1952.
23. LEVER, J. D., *Am. J. Anat.* 97, 409 (1955).
24. ——— *Endocrinology* 57, 621 (1955).
25. ——— *J. Biophys. Biochem. Cytol.* 2, Suppl. 1956.
26. NEREMBERG, S. T., *A.M.A. Arch. Pathol.* 58, 236 (1954).
27. OPIE, E. L., *Cytology of the Pancreas in Special Cytology*. Ed. by E. COWDRY. New York, 1932.
28. PALADE, G. E., *J. Biophys. Biochem. Cytol.* 2, Suppl. 1956.
29. RINEHART, J. F. et FARQUHAR, M. G., *Anat. Record* 121, 207 (1955).
30. ROBERTSON, J. S., *Australian J. Exptl. Biol. Med. Sci.* 32, 229 (1954).
31. ROULLER, CH., *Compt. rend. soc. biol.* 148, 2008 (1954).
32. SJÖSTRAND, F. S. et HANZON, V., *Exptl. Cell Research* 7, 415 (1954).
33. TSCHASSOWNIKOW, S., cité d'après WARREN, S. et LE COMPTE, P., *The Pathology of Diabetes Mellitus*. Lea & Febiger, Philadelphia, 1952.

Some Observations on the Ultrastructure of the Mouse Parathyroid Gland

R. EKHOLM

Department of Anatomy, University of Gothenburg

Received April 2, 1957

Only one type of cells is identified in the mouse parathyroid in the present study. The most important observations on the organization and structure of these cells are as follows.

The cells are bounded by a sharply outlined plasma membrane. Adjacent cells are separated by an intercellular space of varying width containing two basement membranes and an intervening zone of very low density. These basement membranes are continuous with the epithelial basement membrane of the periendothelial space. This space is also triple-layered in a way similar to the intercellular one.

The mitochondria are large and oval and distributed throughout the cytoplasm. They are bordered by a triple-layered outer membrane and contain triple-layered inner membranes usually arranged at a right angle to the long axis of the mitochondria. The inner membranes are sometimes observed to be continuous with the inner layer of the outer membranes. The Golgi zone contains parallel membranes, vacuoles and vesicles. Round globules filled with a homogeneous osmium-impregnated material or rounded spaces with a varying amount of an osmiophilic matter are observed in most cells. In the ground cytoplasm minute dense granules and small vesicles are generally observed.

The parathyroid glands of the mouse are very small and, therefore, very difficult to study in isolated state. However, during an investigation of the ultrastructure of the mouse thyroid I have met with parathyroid tissue in a rather large percentage of the sections. The present paper is the result of a study performed on these sections.

Hitherto only one paper on the ultrastructure of the parathyroid has appeared, an investigation on the rat parathyroid recently published by Lever (9). However, at least some of the pictures in this paper seem to be derived from the thyroid gland and the description given by Lever is in many respects more applicable to the thyroid than to the parathyroid.

A large number of light microscopical studies on the parathyroid from different species have been published. The results obtained concerning the cytological differentiation have earlier been considerably at variance. However, in recent years

most authors have agreed that in the parathyroid from most mammals only two chief groups of cells are to be distinguished, viz. principal cells and oxyphil cells. Both these groups contain, however, several types of cells.

The mouse parathyroid does not seem to have been subjected to light microscopical cytological investigation. However, several authors have studied the rat parathyroid, among others Hoskins (8), Rosof (14), De Robertis (13), Baker (1), Rucart (15) and Sandritter *et al.* (16). They all state that the rat parathyroid contains exclusively or chiefly principal cells.

MATERIAL AND METHODS

The present study was carried out on tissues of white mice primarily intended for a study of the thyroid. In the sections from nine of these animals parathyroid tissue was found. All the animals were male and adult and they were kept in normal laboratory conditions.

The specimens were fixed at $+2^{\circ}\text{C}$ for one hour in a solution of 1% OsO_4 buffered with veronal-acetate to pH 7.2 (11) and with an osmolality of about 0.3. The embedding of the specimens was carried out in methacrylate, in the main according to Newman *et al.* (10). The sectioning was performed partly in a Sjöstrand ultramicrotome (17), and partly in a microtome designed by Ekholm and Zelander (6). In both cases stainless steel knives were used (4).

The microscopy was carried out in an RCA EMU-2b and in an RCA EMU-3b electron microscope.

RESULTS

In the mouse the parathyroid tissue lies in close relationship to the thyroid. Very often the two glands are separated only by a narrow space containing no defined structures, in other cases small bundles of fibrils and/or blood capillaries are seen to be interposed between the two tissues (Fig. 1).

Only one type of cells has been distinguished in the mouse parathyroid in this study. As will be seen below, the cells were observed to differ in one respect. However, this difference is not judged to be of such significance to justify a differentiation into separate cell types.

The parathyroid cells are bounded by a sharply outlined continuous *plasma membrane*, about 60 Å thick. Adjacent cells are separated by an *intercellular space* of irregular width, in this study varying between 200 and 800 Å. This space as a rule contains three layers. Two of these have a moderate density and a homogeneous structure and are localized close to the plasma membrane. The third one is of very low density and is interposed between the two dense layers. (Figs. 2-3.)

Those parts of the plasma membrane that are facing the blood capillaries are

separated from the endothelium by a *periendothelial space* of varying width. This is usually observed to be composed of three layers similar to those in the intercellular space. One of the dense layers is applied close to the plasma membrane of the epithelium (the epithelial basement membrane) and the other close to the endothelium (the endothelial basement membrane). The third one is interposed between the two dense layers and is of very low density. All the three layers appear homogeneous.

In many places the periendothelial space is widened and here it is sometimes observed to contain a lamellated or stratified structure of moderate density. Within these areas the triple-layered organization is obscured but the basement membranes are usually still discernible (Fig. 4).

When an intercellular space reaches the periendothelial one the epithelial basement membranes of this space are seen to be continuous with the dense layers of the intercellular space. Hence, it seems appropriate to designate the dense layers of the intercellular space as basement membranes (Fig. 5).

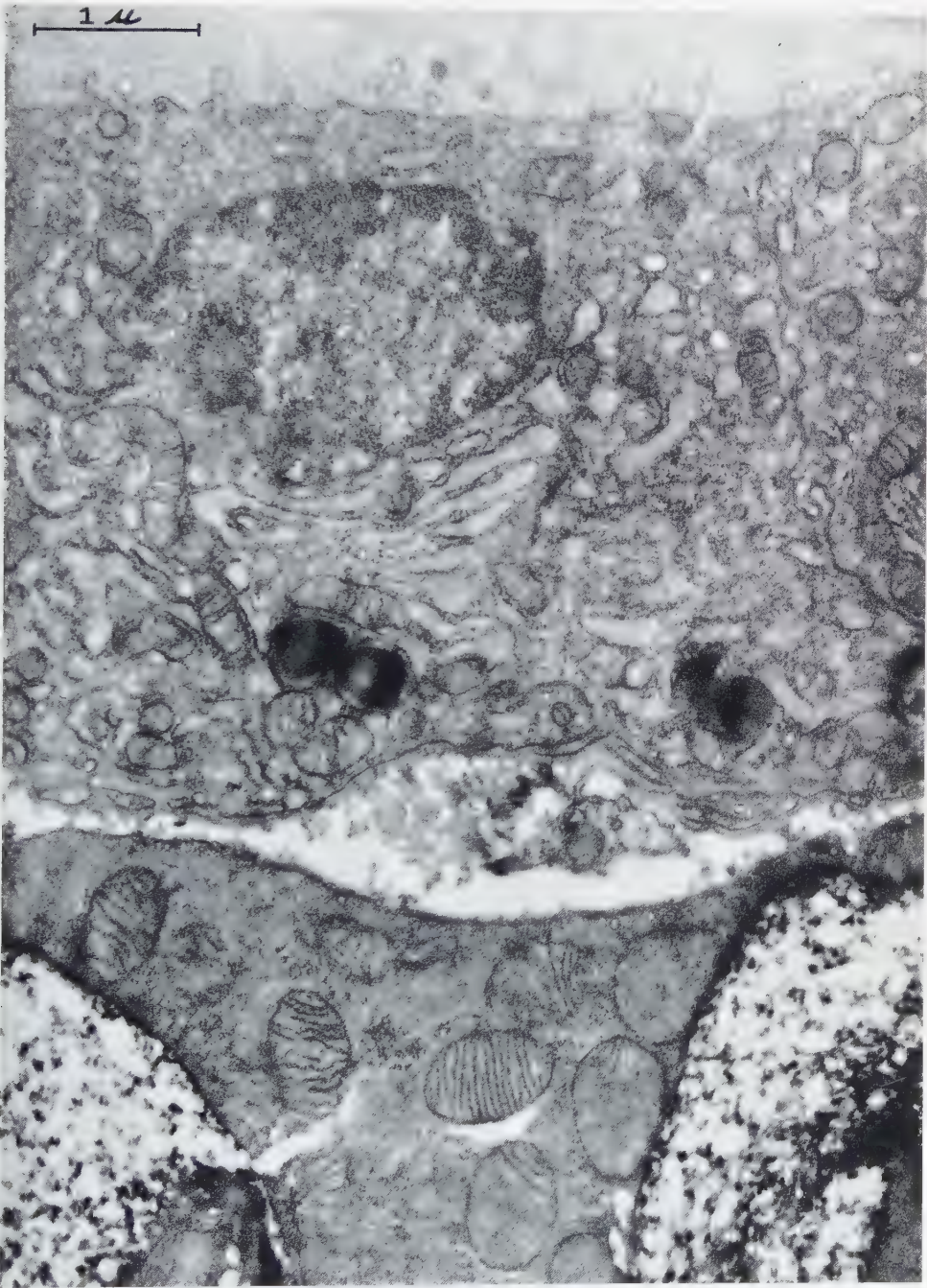
The *endothelium* of the blood capillaries is of varying thickness but the major part is very thin. Within the thin parts discontinuities of the endothelial cytoplasm are observed. However, these discontinuities are not complete interruptions of the endothelial wall since the cytoplasm is replaced here by a more or less distinct membranous structure. Furthermore, the endothelial basement membrane shows no interruptions at the discontinuities.

Among the intracellular elements the *mitochondria* are outstanding owing to their large number and even distribution throughout the cytoplasm. They have a rather uniform appearance, most of them being oval and relatively large. They are bordered by a triple-layered outer membrane consisting of two dense layers with a less opaque space in between. In the interior of the mitochondria there is a system of triple-layered membranes built up in principle in the same way as the outer membrane and usually orientated at a right angle to the long axis of the mitochondrion. Almost without exception the inner membranes are seen to bridge the whole width of the mitochondrion. In some places the outer dense layers of the inner membranes are observed to be continuous with the inner dense layer of the outer membranes (Fig. 6).

The total thickness of the outer mitochondria membranes is $160 \pm 5 \text{ \AA}$ and of the inner membranes $195 \pm 5 \text{ \AA}$. The inner membranes are situated at a distance of about 400 \AA from each other.

The *Golgi zone* is situated close to the nucleus. It has a rather large extension and contains membranes in parallel arrangement, vacuoles of varying size and shape,

FIG. 1.—Survey picture showing a mouse thyroid cell at the top and part of a parathyroid cell at the bottom. $\times 22,000$.



and small round vesicles. The vesicles are bordered by a distinct membrane but the vacuoles have only partially a marked surface membrane (Fig. 7).

In some cells *round globules* are observed filled with a homogeneous, intensely osmium-impregnated material. These globules are found in all parts of the cell and are of varying size, measuring from about $0.2\ \mu$ to about $1\ \mu$. They are demarcated by an osmiophilic layer of membranous character (Fig. 2).

In other cells round or oval spaces are found which contain varying amounts of a homogeneous osmium-impregnated material. Sometimes these spaces are nearly filled with the dense matter but there are also spaces which only contain grains and minute strands of the osmiophilic material. Between these extremes all transitions exist. In each individual cell all the spaces show about the same degree of filling. It is further observed that, as a rule, the larger the spaces are the emptier they appear.

The size of the spaces varies, the smallest ones being of the same order of magnitude as the globules just described and the largest ones having about the same size as the nucleus. The large spaces are sometimes seen to occupy the major part of the cell, the cytoplasm being reduced to narrow strands between the spaces (Fig. 4a).

The spaces are demarcated by an osmiophilic layer of membranous character. To the inside of this layer small aggregates of the osmiophilic content are often attached, giving the membranous structure a somewhat irregular appearance.

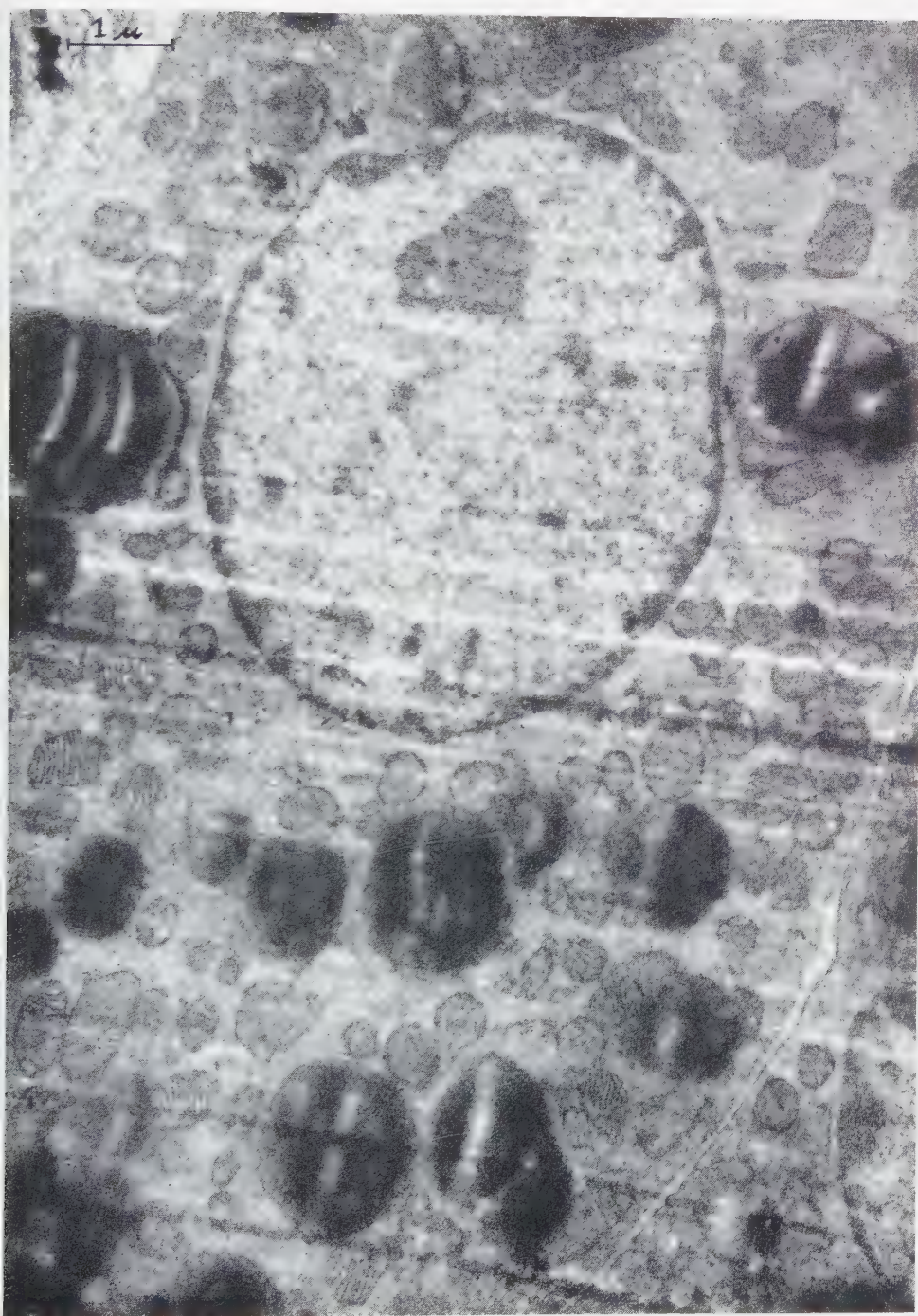
In the *ground cytoplasm* two distinct structures are regularly observed, viz. minute dense granules and small vesicles.

The granules, having a diameter of about $160\ \text{\AA}$, are usually accumulated in small clusters, which can be found in all parts of the cells (Fig. 8).

Occasionally short membranes are observed to which small granules are attached at one side. These granules seem to be of about the same size as the free granules described above. However, the membranes are so short and so rare that it is impossible to draw any conclusions about the interrelation between the free and attached granules.

The vesicles are round, fairly uniform in size ($550 \pm 30\ \text{\AA}$) and have a content of low electron density. They are bordered by a surface membrane about $50\ \text{\AA}$ thick. The vesicles are observed throughout the cytoplasm but they are found in great number only in the most peripheral zones of the cells. They are most abundant along those parts of the plasma membrane that border on a capillary. The surface membranes of the vesicles seem to be intimately related to the plasma membranes, and observations have been made which indicate that the vesicle membranes can be

FIG. 2.—Survey picture of a parathyroid cell with an oval nucleus, several round globules with osmiophilic content and numerous oval mitochondria. To the right an irregular intercellular space. In the upper left corner part of a thyroid cell. $\times 14,000$.



continuous with the plasma membranes. In a few cases that part of the vesicle membrane which faces the plasma membrane seems to be lost so that the vesicle opens on the surface of the cell (Figs. 4–5).

The nucleus of the parathyroid cell is usually found to be round or slightly oval. It has a fine granular content, the granules being accumulated in dense zones immediately inside the nucleus membrane and, in one or two masses, in the central part of the nucleus. The nuclear membrane is triple-layered with two dense layers and a less opaque space in between (Figs. 2 and 7).

DISCUSSION

It must be emphasized that it is not difficult to distinguish between thyroid and parathyroid tissue in the electron microscope. The organization of the thyroid in regular follicles and the internal structure of the cells with their well-developed systems of intracellular membranes are very typical (5) and fundamentally diverges from the electron microscopic picture of the parathyroid.

Among the observations made in this study the organization of the intercellular and periendothelial spaces seems to be of special interest. As described above these two spaces are organized in a very similar way. They are composed of two basement membranes and an intervening zone of minute density. However, this zone is considerably wider in the periendothelial space than in the intercellular one and in the former space it often contains a lamellated structure. The epithelial basement membrane of the periendothelial space is continuous with the basement membranes of the intercellular space.

This organization differs essentially from the electron microscopic pattern usually observed in other organs. According to this pattern the intercellular space usually appears as a bright zone of uniform width, 110–130 Å (18) and the basement membrane of the epithelium cells generally passes straight and uninterrupted over the cell boundaries without showing any tendency to curve into the intercellular space. This organization pattern is observed even in endocrine glands as the thyroid (3, 5).

The periendothelial space must be of great importance for the transport between the epithelium and the capillaries, especially in an endocrine organ. Therefore, one may suppose that this space is organized with regard to this function. Since the intercellular spaces of the parathyroid are organized in essentially the same way as the periendothelial space, it seems justified to assume that the intercellular space serves as a space for transport.

In this connection the small vesicles found predominantly in the peripheral zones of the cytoplasm are of interest. As described above they are intimately related

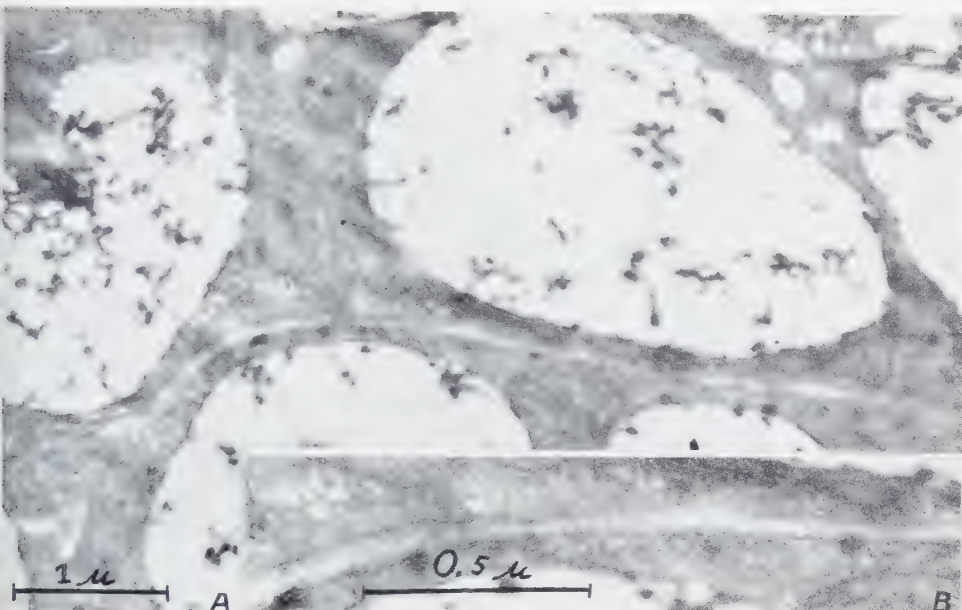


FIG. 3.—(a) Parts of two parathyroid cells with large, almost empty spaces. The cells are separated by an irregular intercellular space. $\times 20,000$. (b) The intercellular space of (a) at higher magnification showing its composition of three layers (the basement membranes and an intervening zone of minute density). $\times 61,000$.

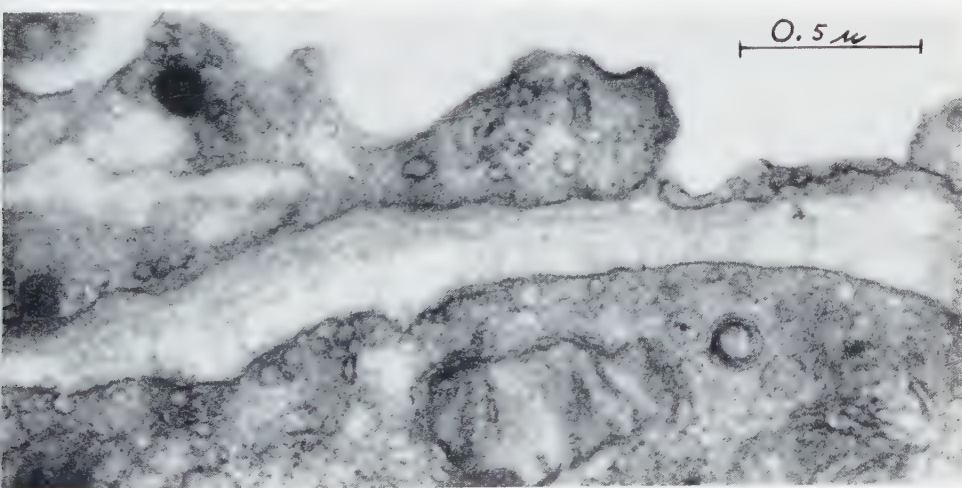


FIG. 4.—A periendothelial space showing a lamellated structure. In the cytoplasm of the parathyroid cell (at the bottom) several small vesicles are seen some of which are closely related to the plasma membrane. $\times 48,000$.

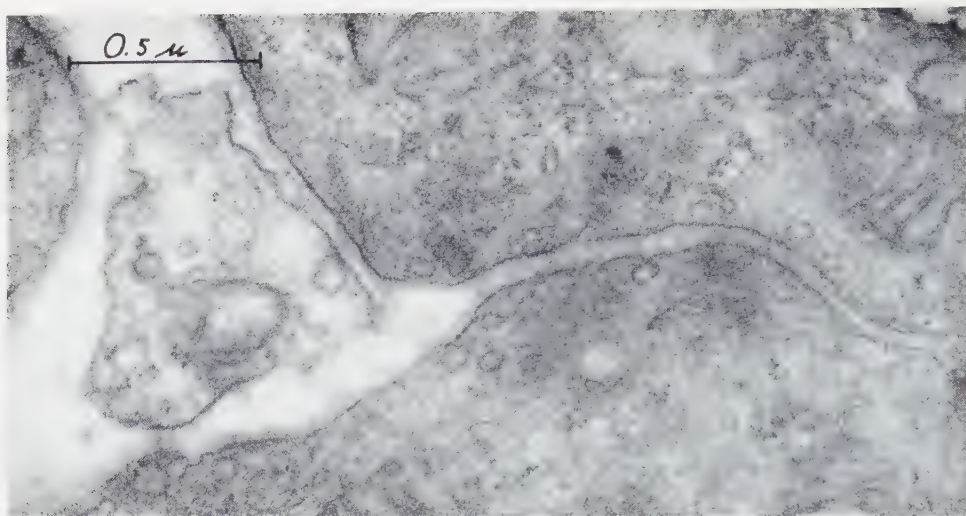


FIG. 5.—A periendothelial space (to the left) joining an intercellular space. The epithelial basement membranes of the periendothelial space are seen to be continuous with those of the intercellular space. $\times 51,000$.

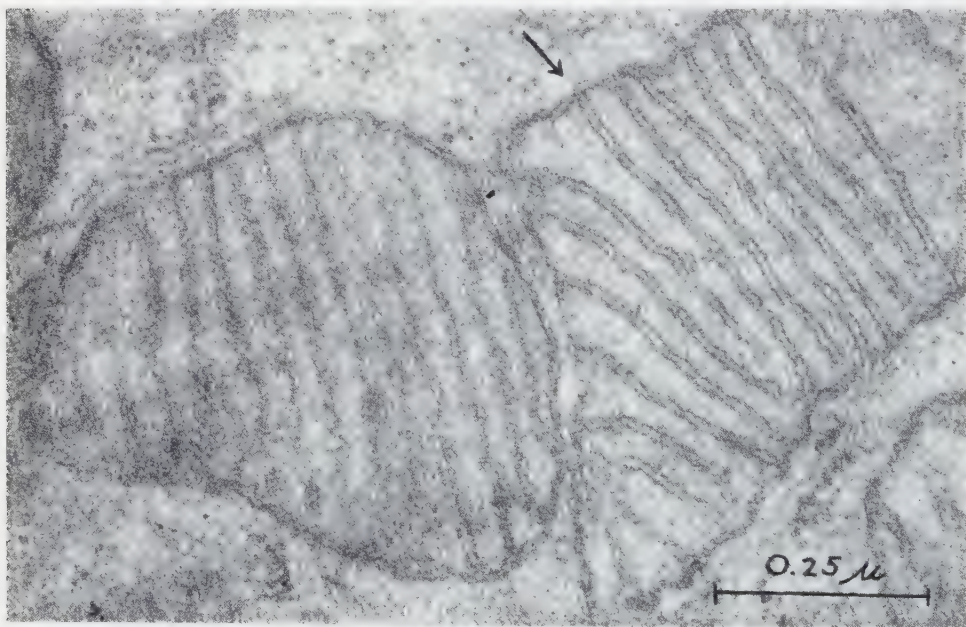


FIG. 6.—Some of the mitochondria from Fig. 6 at a higher magnification showing the triple-layered outer and inner membranes. At the arrow the dense layers of an inner membrane are seen to be continuous with the inner layer of the outer membrane. $\times 98,000$.

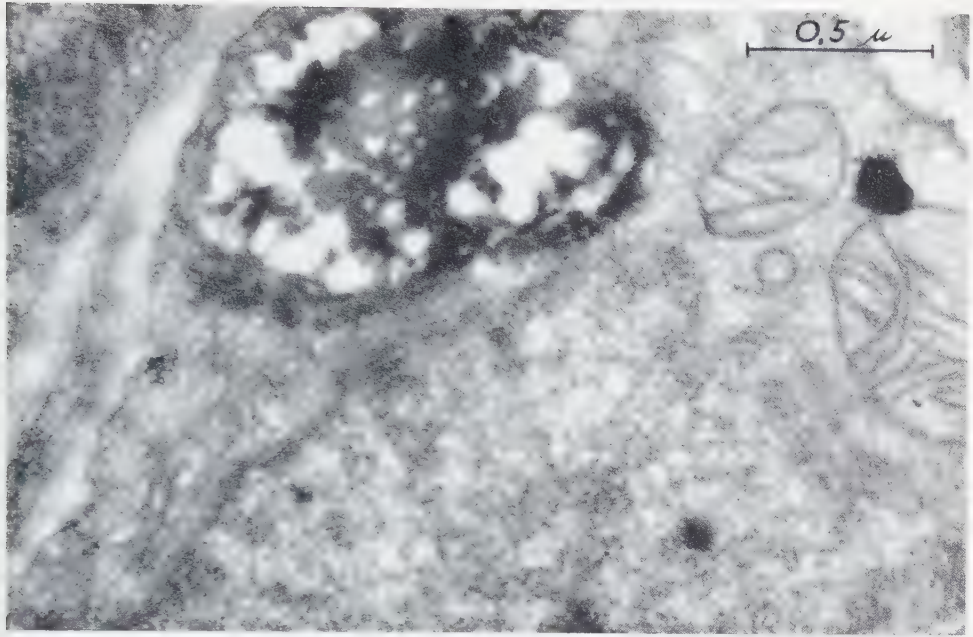


FIG. 7.—Part of a parathyroid cell showing part of the nucleus (at the bottom) with triple-layered nuclear membrane. To the left and above the nucleus the Golgi zone containing membranes in parallel arrangement, vacuoles and vesicles. In the Golgi zone a rounded space partly filled with an osmophilic material. $\times 49,000$.

to the plasma membrane and sometimes they give the impression of being open to the cell surface. It does not seem unlikely that this picture represents a transportation mechanism between the cells and the periendothelial and intercellular spaces.

Similar vesicles have earlier been observed in endothelial cells by Palade (12), who supposed that they represent a transportation mechanism of water through these cells.

Cytoplasmic discontinuities of the capillary endothelium of the type observed in this study have earlier been described in the mouse thyroid (3, 5). In the sections of the present study it has often been observed that a capillary borders with one side on a thyroid cell and with the other on a parathyroid cell. Therefore, it is not surprising that the same observation is made in both glands. Similar discontinuities are also reported in the mouse adrenal cortex (20).

It is difficult to preclude the possibility that the discontinuities observed represent artefacts due to improper preparation. However, since the structures observed have

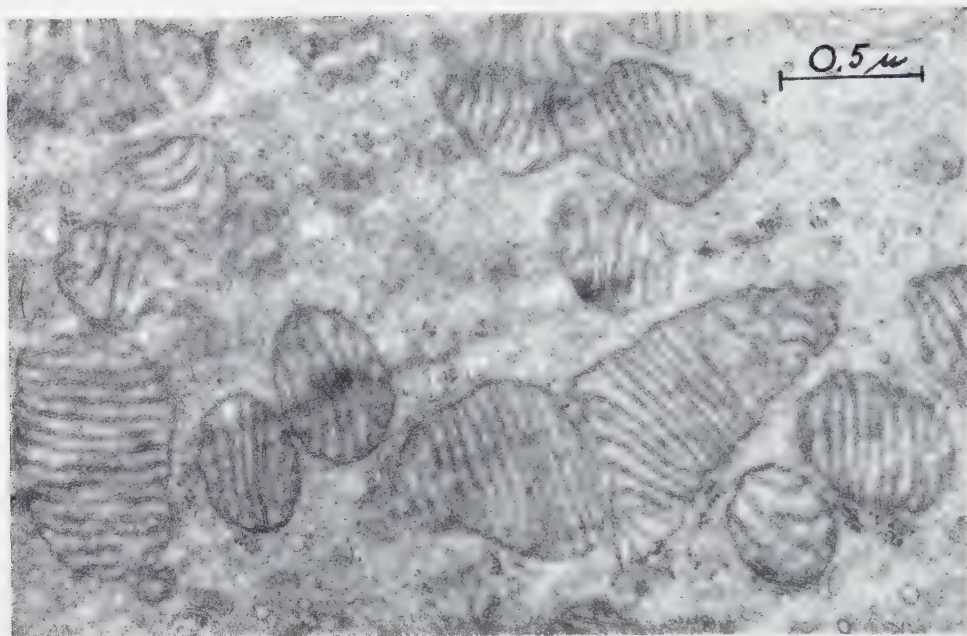


FIG. 8.—Survey picture showing numerous mitochondria and heaps of small dense granules in the ground cytoplasm. $\times 39,000$.

a uniform appearance in a very large material of thyroid glands the cytoplasmic structures of which are very well preserved, an artefact theory does not seem justified.

As stated above some parathyroid cells contain round globules filled with a homogeneous osmium-impregnated material. In other cells rounded spaces are observed containing varying amounts of an osmiophilic material. All transitions from completely filled globules to almost empty sacs are encountered. No modifications of the other cytoplasmic constituents are observed in connection with the varying appearance of the globules and spaces. For this reason and because of the even transition from completely filled globules to almost empty spaces it seems justified to assume that the globules and spaces are of similar nature and that the cells containing these different structures are of the same kind.

It seems impossible to determine from the electron micrographs the nature of the osmiophilic material and the reason for the great fluctuations of the amount of this matter. Owing to its affinity to osmic acid one might feel tempted to assume that the material is of lipid nature. Such an assumption seems to be supported by some light microscopical studies (2, 7, 15) in which large lipid granules, sometimes of the same magnitude as the nucleus, are reported as normal cell constituents.

Also, it is easy to explain the variation of the amount of osmium-impregnated material on the basis of variations in the loss of this material during the preparation procedures. On the other hand, in several light microscopical investigations no lipids have been found in the parathyroid cells (16).

Apart from the small vesicles discussed above only minute granules are generally found in the ground cytoplasm of the parathyroid cells. Intracellular membranes of the type termed α -cytomembranes by Sjöstrand (18) are observed only exceptionally. This seems rather remarkable since the α -cytomembranes are as a rule very well developed in secretory cells as the exocrine cells of the pancreas (19) and the epithelium of the thyroid gland (5).

REFERENCES

1. BAKER, B. L., *Anat. Record* **93**, 125 (1945).
2. BERGSTRAND, H., *Acta Med. Scand.* **52**, 791 (1920).
3. EKHOLM, R., *Z. Zellforsch.* **46**, 139 (1957).
4. EKHOLM, R., HALLÉN, O. and ZELANDER, T., *Experientia* **11**, 361 (1955).
5. EKHOLM, R. and SJÖSTRAND, F. S., Electron Microscopy, Proc. Stockholm Conf. 1956, p. 171. Almqvist & Wiksell, Stockholm, 1957.
6. EKHOLM, R. and ZELANDER, T., *Experientia* **12**, 195 (1956).
7. GILMOUR, A. L., *Endocrinology* **26**, 857 (1940).
8. HOSKINS, M. M., *Endocrinology* **8**, 777 (1924).
9. LEVER, J. O., *J. Anat.* **91**, 73 (1957).
10. NEWMAN, S. B., BORYSKO, E. and SWERDLOW, M., *J. Research Natl. Bur. Standards* **4**, 183 (1949).
11. PALADE, G. E., *J. Exptl. Med.* **95**, 285 (1952).
12. ——— *J. Appl. Phys.* **24**, 1424 (1953).
13. DE ROBERTIS, E., *Anat. Record* **78**, 473 (1940).
14. ROSOF, J. A., *J. Exptl. Zool.* **68**, 121 (1934).
15. RUCART, G., *Arch. d'anat. micr.* **38**, 1 (1949).
16. SANDRITTER, W., FEDERLIN, K. and GERATZ, D., *Frankfurt. Z. Pathol.* **66**, 290 (1955).
17. SJÖSTRAND, F. S., *Experientia* **9**, 114 (1953).
18. ——— Physical Techniques in Biological Research. Vol. III, p. 241. Academic Press Inc., New York, 1956.
19. SJÖSTRAND, F. S. and HANZON, V., *Exptl. Cell Research* **7**, 393 (1954).
20. ZELANDER, T., *Z. Zellforsch.* (in press).

Submicroscopic Differentiation of Plasmodesmata and Sieve Plates in *Cucurbita*¹

A. FREY-WYSSLING and H. R. MÜLLER

*Department of General Botany,
Swiss Federal Institute of Technology, Zürich*

Received April 13, 1957

In the skeletal network of the youngest partition walls in parenchyma cells no plasmodesmata are visible (Fig. 2). These differentiate only later when the production of microfibrils, which is a continuous process, progresses (Figs. 3-5). Sometimes initiated plasmodesmata are covered and closed by the proceeding deposition of microfibrils (Fig. 6). Pits originate in that the development of the secondary wall is prevented on top of a local cluster of numerous plasmodesmata (Fig. 7).

The formation of pores between sieve tubes is caused by an early discontinuation of fibril deposition in local fields of the transverse wall, while bars of tangential fibrillar strands are secreted between those localities (Figs. 8-10). Subsequently the bars are narrowed by active growth of a cytoplasmic plug which covers the area of the future pore (Figs. 10-12). If two adjacent cells differentiate sieve pores, the original network of the field will disappear so that open pores result (Figs. 12, 13). This is not the case if one-sided sieve plates are formed in contact with companion cells (Figs. 14-17).

With the aim of elucidating the formation of sieve plates in the electron microscope, we have investigated the youngest internodes below the apex of *Cucurbita* shoots, where sieve tubes are differentiated in the phloem.

METHODS

The preparation of young sieve plates has been performed along two lines. The first was the maceration method of Mühlethaler (5) which consists in boiling the tissue alternatively in acids and alkali. For our purpose glacial acetic acid (conc.) plus hydrogen peroxide (35%) was used for 30 minutes in a reflux condenser, followed by washing with aq. dest. and boiling for 80-90 minutes in sodium bisulfite. Then the material was carefully washed and boiled for 20 minutes in 2% potassium hydroxide. As a result the tissues disintegrated into individual cells on washing and shaking or, if necessary, agitating in a mixer.

¹ This investigation has been performed with funds granted by the Swiss National Research Council (Forschungsrat des Schweizerischen Nationalfonds).



FIG. 1.—Shadowing of sections $2\ \mu$ thick. α = angle of shadowing = $40-50^\circ$.

By this treatment, which destroys the whole cell content and dissolves the pectic ground-mass of the cell walls, beautiful ghosts of their cellulosic skeleton are obtained which are dried on a carrier net and shadowed with chromium. The disadvantage of this procedure is that the macerated cells collapse. As a consequence two superposed walls are observed so that it is difficult to ascertain whether existing pores are really open or closed by a film of microfibrils.

Therefore, sections were cut across the internodes in a second assay. Before embedding in methacrylate, the internodes were macerated without the alkali treatment to such an extent that the coherence of the cells was weakened but not broken, so that the disintegration of the tissue was just prevented. Since the sieve plates are partition cell walls with considerable distances between them, it was useless to try fine sectioning which would have yielded chiefly sections without sieve plates. For that reason sections of about $2\ \mu$ were cut which guaranteed the possibility to find sieve plates on the sections at least sporadically.

The methacrylate was removed from the sections with amyl alcohol and amyl acetate, followed by shadowing with chromium. The shadow angle had to be rather steep in order to get at least parts of the partition wall shadowed (Fig. 1). These sections had the advantage that the diaphragms were not covered by other cell walls and that the presence of primary xylem elements permitted to locate and identify the different cells on the section with certainty, which is not the case in preparations of fully macerated tissues.

PLASMODESMATA IN PARTITION WALLS

Since sieve tubes are elongated cells, we observed many more transverse cell walls of parenchyma cells than sieve plates. These partition walls permit the differentiation of plasmodesmata to be studied (Figs. 2-7). In our macerated preparations "plasmodesmata" mean pores whose content has been removed.

The youngest parenchyma walls display a uniformly dispersed network of cellulosic microfibrils (Fig. 2). It is not easy to deduce from this picture how the contact between adjacent cells is maintained across such a wall. If we assume the interfibrillar material

to be in a metabolizing living state, there would be no difficulty; but if we assume an inert, pectic groundmass, a metabolically passive sheet (middle lamella + primary wall) would separate the two cells. The first alternative seems more probable since the thickening of the primary wall by the formation of additional microfibrils is prevented in numerous polygonal spots (Fig. 3). Soon after this stage, these spots appear as foramina whose circumference is formed by tangentially disposed microfibrils (Fig. 4). The deposition of microfibrils continues so that a canal is kept open (Fig. 5). Such ducts have diameters of the order of $0.1-0.2\mu$, i.e. their size falls within the border range between microscopic and submicroscopic dimensions. As clearly seen in Fig. 5, neighbouring cells must spare these ducts at the same place, so that open pores result. This morphological analysis leaves no doubt that they contain the classical plasmatic connections across the cell walls. It is generally admitted that, in growing cell walls, these strands represent living cytoplasm, whilst they consist of some kind of denatured protein stainable by mordant dyes in cells with passive functions.

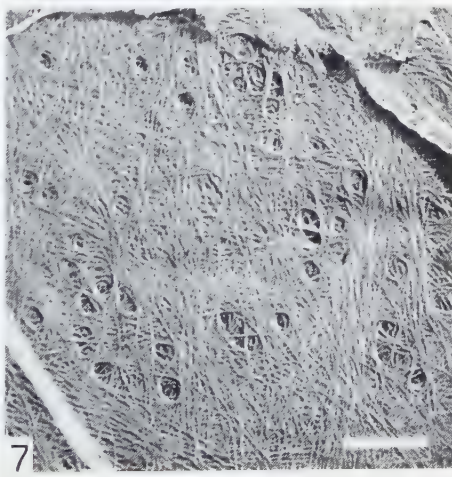
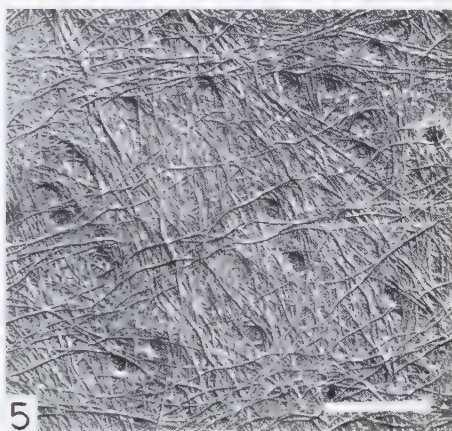
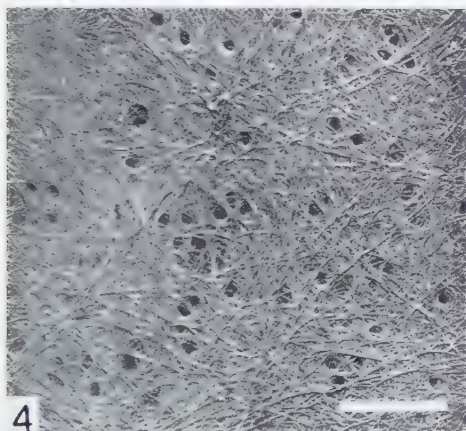
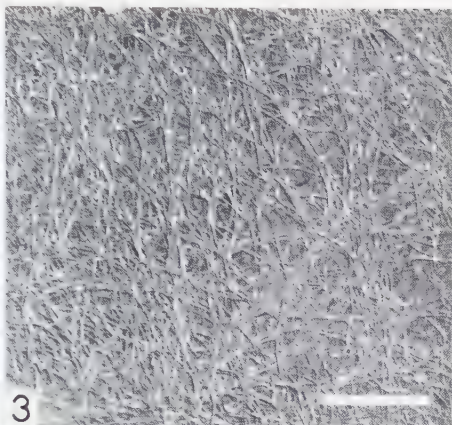
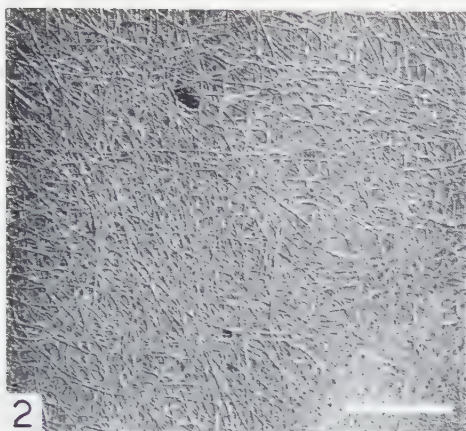
Fig. 5 shows the transient phase, when the primary wall with its loosely interwoven dispersed texture is followed by the formation of a much denser secondary wall with parallel textured coarser strands of parallelized microfibrils.

In the secondary wall of partition membranes the development of the plasmodesmata follows different lines. The dispersed submicroscopic pores may persist as in the transverse walls of the staminal hairs of *Tradescantia* (6), or they may be partly covered and closed by the deposition of new microfibrils so that only sporadic plasmodesmata are left over (Fig. 6). In xylem parenchyma, however, a third type is found, where the plasmodesmata of the primary wall are grouped in clusters (Fig. 7). Later on, the thickening of the secondary wall proceeds around these clusters producing a simple pit whose pit membrane is perforated by the plasmodesmata of the primary wall.

TRANSVERSE SIEVE PLATES

The youngest sieve plates in our preparations found directly under the vegetation cone are already considerably differentiated (Figs. 8, 9). It is important to state that in this stage the future sieve pores are closed by a loose network of microfibrils. Those are the first fibrils laid down in the primary wall of these elements, when it

FIGS. 2-7.—Partition walls of parenchyma cells. 2: Equally dispersed microfibrils (the black spot is a hole in the carrier film). 3: Formation of angular plasmodesmata. 4: Differentiation of plasmodesmata. 5: Full-grown plasmodesmata. 6: Elimination of superfluous plasmodesmata. 7: Cluster of plasmodesmata at the base of a differentiating pit.



still showed a uniform dispersed texture. But very early the production of microfibrils is discontinued in the places where pores have to be differentiated.

This statement is proved by Fig. 10, which shows the development of a sieve plate in the phloem of the second internode. As every cell wall, the sieve plates are double sheets of the coats of two adjacent cells. In Fig. 10 the two lamellae have been separated by our pretreatment of partial maceration and they have been mutually shifted to some extent. This picture shows that the two contiguous sieve tubes have reached quite different levels of differentiation. The riper tube has already produced neatly delimited pores, whilst the other cell is found in a still very early state of differentiation; there are no pores yet but only places with a loose network surrounded by broad and diffuse strands of more or less parallelized microfibrils. Obviously, the differentiation process goes on individually in each cell. Probably it is very fast, because pictures like Fig. 10 are found very rarely. It demonstrates that the differentiation of the pores consists (*a*) in a removal of the sparse fibrils which fill the future opening, and (*b*) in a narrowing of the future bars between the pores. This can be explained by the following assumption: First a diffuse plug of plasma gel prevents the further synthesis of microfibrils at the location of future pores. Between these plugs the production of fibrils goes on. Then the plugs grow in diameter striving for a definite shape and delimitation. Hereby the peripheral microfibrils are pushed aside and gathered in dense strands tangential to the pores (Figs. 12, 13). After this widening the pores appear to be open (cf. 3, 7). It is difficult to decide whether the microfibrils which close the pore (Figs. 8, 9) are pushed away or torn into pieces; there is as yet no indication that they are dissolved by cellulase. Simultaneously with the removal of microfibrils from the future bore of the pore, new fibrils are produced between the plasmatic plugs reinforcing the rim of these large pores (Fig. 11).

In general the membranogen cytoplasm forms straight microfibrils. But in the formation of the bars they are clearly curved (Figs. 10, 11) by an active deviation process. The tendency to form straight fibrils is shown in Fig. 12, where uninterrupted microfibrils run right across the stellate fields between the pores from one bar to the next. That one and the same thread is involved in the delimitation of several pores is demonstrated by some isolated loose and straight microfibrils which were probably just formed before the specimen was prepared so that they were not yet correctly incorporated into the texture of the sieve plate.

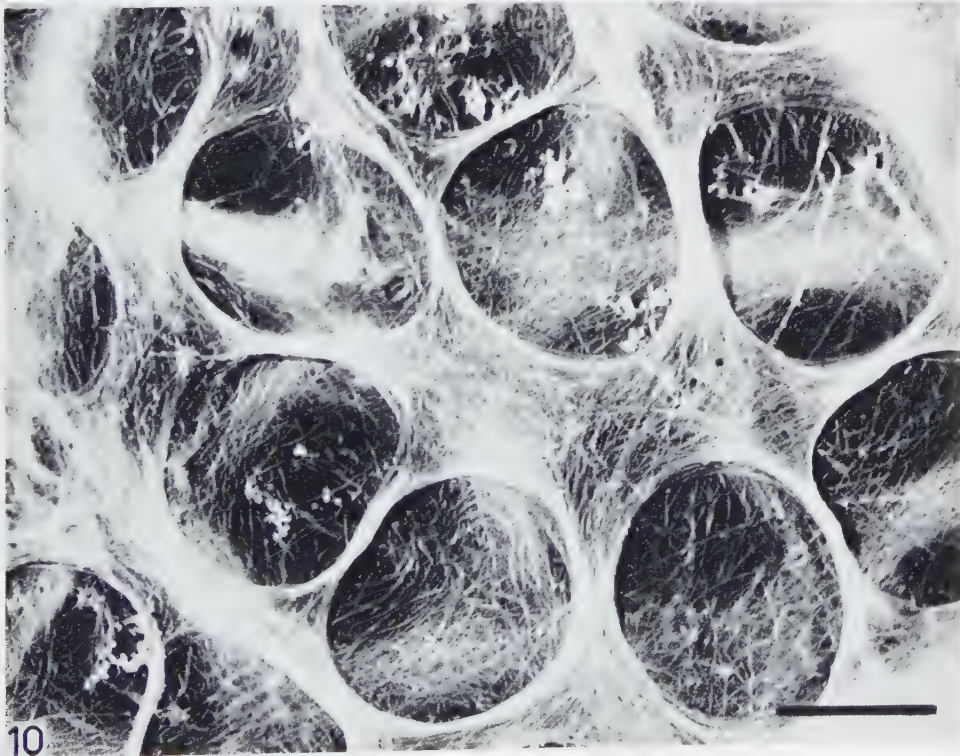
FIGS. 8-13 (Figs. 11-13 on next plate).—Transverse sieve plates. 8: From vegetation cone, future pores already visible. 9: From first internode. 10: From second internode. The degree of differentiation in two adjacent sieve tubes differs considerably; the two plates are somewhat displaced by the preliminary maceration (see text). 11: Broad fibrillar bars between the future pores. 12: Narrow bars between the open pores. *l*, longitudinal wall folded onto the sieve plate; *f*, loose microfibrils showing their straight feature. 13: Ripe sieve plate, open pores.



8



9



10

In the fully differentiated sieve plate the rest of the cell wall between the pores is reduced to a minimum (Fig. 13). Owing to our method of preparation no signs of callose are visible (*I*, p. 269).

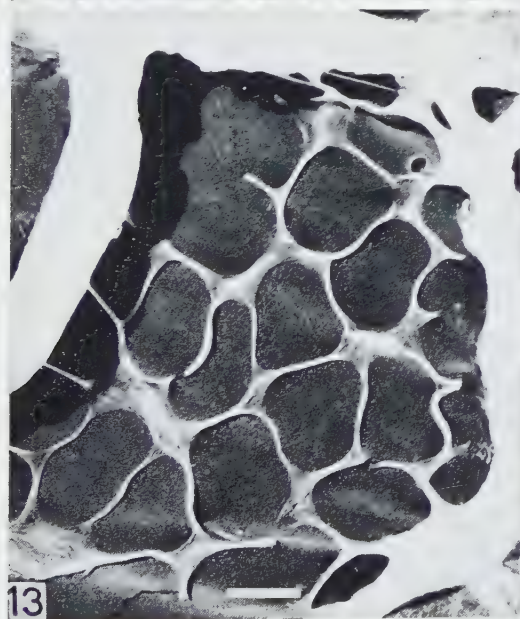
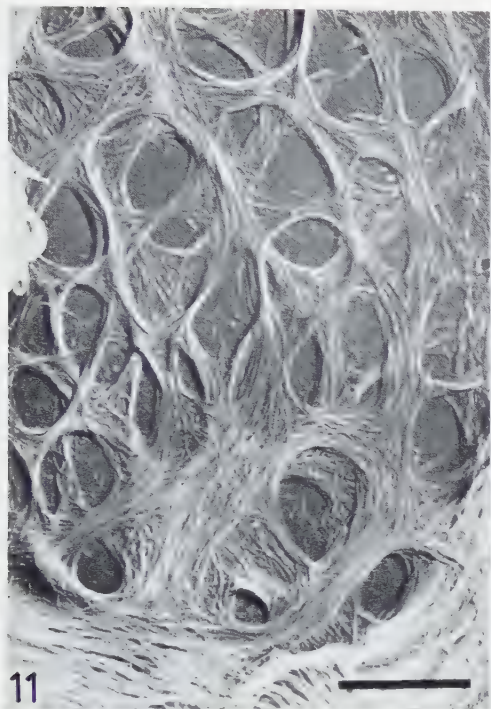
SIEVE PLATES OF THE LONGITUDINAL WALL

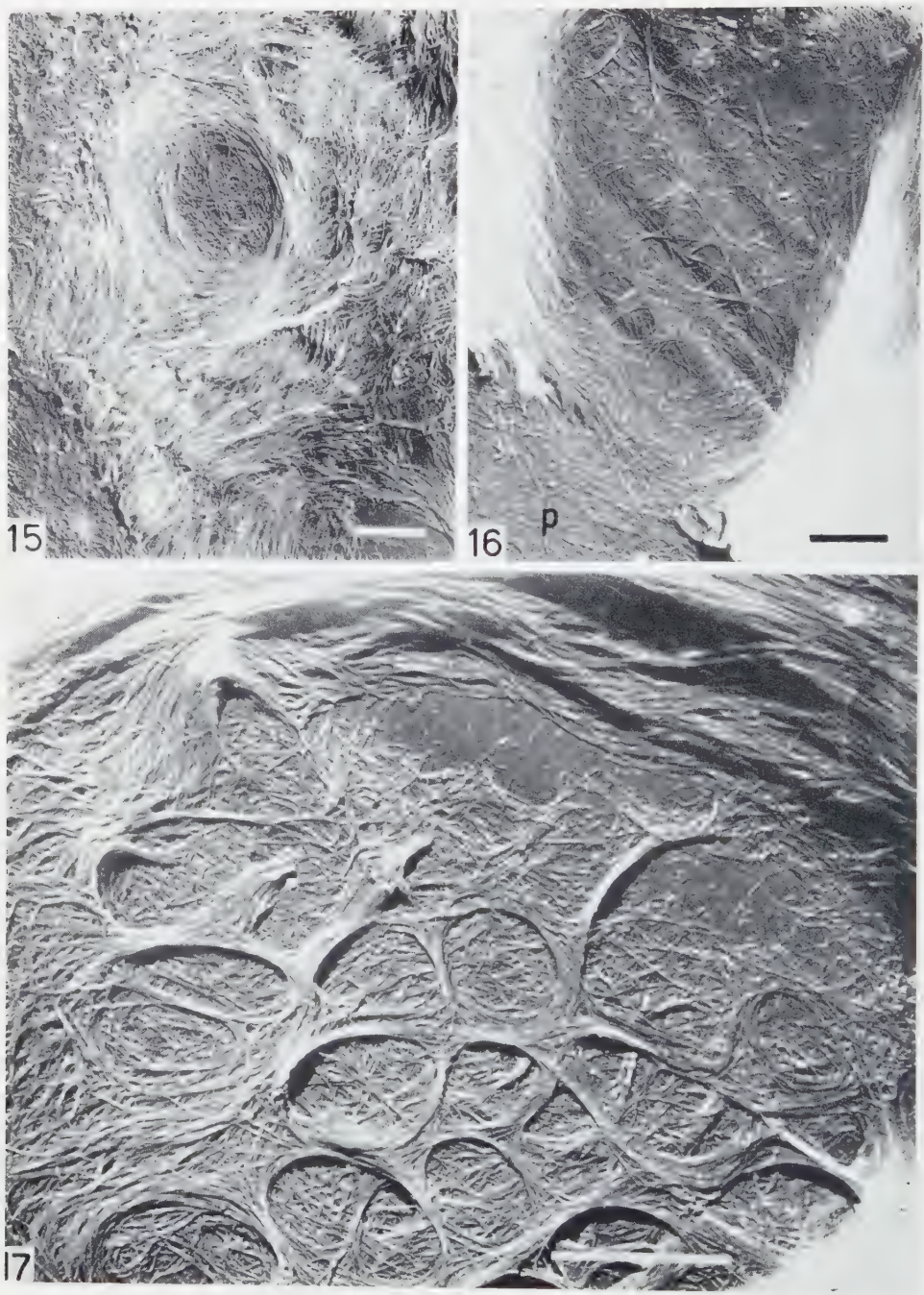
In a very early stage, the longitudinal walls of the sieve tubes thicken rapidly and assume a strikingly dense texture of parallelized microfibrils (Figs. 12, 14, 15). Therefore, they display a typical secondary texture, coated by a lamella of dispersed primary texture (Fig. 16), while the walls of the neighbouring parenchyma cells still persist in the primary stage. As a consequence, young sieve tubes can fairly easily be identified under the electron microscope. The density of their texture causes the special pearly luster of the walls of sieve tubes (nacr  wall; *I*, p. 276) in the light microscope.

In these longitudinal walls, sieve plates are differentiated for connection with the companion cells. The activity of the postulated plasmatic plug is especially conspicuous in this case. In an almost dramatic fashion it "defends" the sieve area against the formation of the secondary wall which is deposited like a whirl around the future sieve plate (Figs. 14, 15). Otherwise the differentiation of the pores follows the same line as described for transverse sieve plates. But there is a remarkable difference in that the adjoining companion cell, which does not thicken its walls (*I*, p. 278), does not develop pores but only—at this stage angular—plasmodesmata (Fig. 17). This again shows how every cell proceeds individually in the differentiation of a field of contact with its neighbors. As a result we find that there are only open sieve pores between sieve tubes but no such open connections with the companion cells, which do not cooperate in the differentiation of the pores, so that only a one-sided sieve plate results (cf. one-sided bordered pits in the contact of tracheary elements with xylem parenchyma). This establishment of open and closed sieve pores is certainly of interest for the interpretation of the physiological activity of sieve tubes and companion cells.

DISCUSSION

Our study of the differentiation of the skeletal component in plasmodesmata and sieve pores shows that the formation of cellulose microfibrils in the growing cell wall is a continuous process. In the early stages very few microfibrils are produced, they lie far apart from one another and display a dispersed orientation (primary wall); later they become so numerous that they touch mutually and hinder their





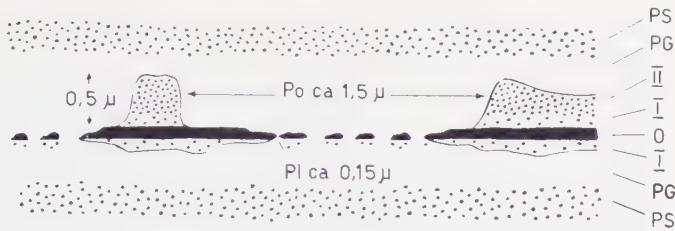


FIG. 18.—Diagram of plasmatic plugs forming a one-sided sieve plate. O, middle lamella of the cell wall; I, primary lamella of the cell wall; II, secondary lamella of the cell wall. Po, pore in the cell wall; Pl, plasmodesmata in the cell wall; PG, plasma gel of the cytoplasm; PS, plasma sol of the cytoplasm.

free development, which must be one of the causes of their parallel arrangement (secondary wall). There is no interruption between the formation of the primary and the secondary wall but uninterrupted production of skeletal material goes on so that transition stages with an incomplete parallelism of the microfibrils are visible.

If plasmodesmata, sieve pores or pits have to be spared as spaces free of microfibrils, local areas of the cytoplasmic surface must discontinue the production of microfibrils, while their deposition continues around these localities. As a result, processes or plugs of cytoplasm are enclosed by the thickening membrane. In this way the young cell wall assumes a characteristic mosaic structure. The plugs prevent growth locally, while the cell wall grows between the plugs in both thickness and surface (2, 8). Besides, in the case of the sieve pores the plugs help to widen their diameter by active narrowing of the microfibrillar bars between the pores.

In very young stages, the place of future plasmodesmata and pores is always covered by a loose network of dispersed microfibrils. In pores between sieve tubes it disappears completely by mechanical means. Whether it persists in plasmodesmata is difficult to decide. As a matter of fact it is so loosely woven that it cannot be a hindrance for the contact of vicinal protoplasts.

An important fact is the finding that every cell organizes the texture of its cell wall individually according to the differentiation plan inherited by its cytoplasm. The future function decides whether neighboring cells cooperate to produce coincident plasmodesmata (partition wall of parenchyma cells) or pores (adjacent sieve

FIGS. 14-17 (Fig. 14 on preceding plate).—Sieve plates on longitudinal walls. 14: Secondary texture of longitudinal wall. 15: The primary wall with its dispersed texture is visible below the secondary wall. 16: *p*, primary wall of the adjacent companion cell. 17: The pores stay closed by the wall of the companion cell.

tubes) or whether each of them follows its own line, so that unilateral pores (companion cells) or one-sided pits originate.

Since there is streaming plasma in the differentiating cells, the question arises whether this flow interferes with the formation of the cell wall (4). We are of opinion that this is only indirectly the case. The plasmic plugs of future pores (Fig. 18, *Po*) and of plasmodesmata (Fig. 18, *Pl*) must be stable, and we imagine that they, as well as the membranogenous surface layer of the cytoplasm, represent a kind of plasma gel (Fig. 18, *PG*) which soaks and penetrates into a certain depth of the growing wall. The fluid plasma sol (Fig. 18, *PS*), which carries and distributes the necessary assimilates as construction material, must flow over this stationary layer. The differentiation into a gelated exoplasm and a fluid endoplasm, as observed in many algae and protozoa, fulfills this requirement.

REFERENCES

1. ESAU, K., *Plant Anatomy*. Wiley & Sons, New York, 1953.
2. FREY-WYSSLING, A., *Macromolecules in Cell Structure*. Harvard University Press, Cambridge (Mass.), 1957.
3. HEPTON, C. E. L., PRESTON, R. D. and RIPLEY, G. W., *Nature* **176**, 868 (1955).
4. ITERSON, G. VAN, *Chem. Weekblad (Amsterdam)* **24**, 181 (1927).
5. MÜHLETHALER, K., *Ber. schweiz. botan. Ges.* **60**, 614 (1950).
6. ROELOFSEN, P. W. and HOUWINK, A. L., *Protoplasma* **40**, 1 (1951).
7. VOLZ, G., *Z. wiss. Mikroskop.* **7**, 251 (1952).
8. WARDROP, A. B., *Australian J. Botan.* **3**, 137 (1955).

Some Fine Structure Changes Occurring in the Epidermis of Embryo Mice during Differentiation¹

MAX G. MENEFFEE^{2,3}

Washington University School of Medicine, St. Louis, Missouri

Received May 13, 1957

It was shown that tonofilaments are 40 Å in diameter and have alternating densities along their length which suggest granularity. The majority of the contents of the cornified cell consists of 40 Å granules. There appears to be a direct relation of the mitochondria to keratinization in that the tonofilaments are often in direct continuity with the mitochondrion. This relationship is retained even after the mitochondria degenerate and enter into the formation of "keratohyaline granules".

A possible explanation for the paucity of Golgi material was presented, based upon its osmoregulatory function.

The continuity of reticular fibers of the dermis with the basement membrane was observed.

The problem of the mode of formation of keratin is of long standing and has been well covered by Montagna (25). In addition to this, the fine structure of keratin from many sources has been intensively studied since Astbury and Woods presented their classic work using X-ray diffraction (3). Both large and small angle X-ray diffraction, infra-red spectroscopy, electron microscopy, analytical chemistry, and histochemistry have all been applied to the problem. Polarization microscopy was used before 1934 and has been used since to study keratin structure. A representative sample of the findings obtained by physical methods other than direct visualization *in situ* by electron microscopy can be found in the references (3, 5, 7, 15, 17, 18, 19, 20, 21, 23, 24, 30). Recently, the electron microscope has been applied to visualization of keratin *in situ* (1, 2, 4, 28, 29, 31, 35).

Tonofibrils have been considered to contain keratin for many years and more recently the tonofibrils have been shown to be made up of smaller fibrillar units called tonofilaments (31). Keratinization has been thought to involve several stages, with tonofibrils being one of the earliest forms in which keratin appears (2, 15, 17,

¹ This investigation was supported in part by a grant-in-aid from the National Institutes of Health (C-2174).

² Fellow of the Arthritis and Rheumatism Foundation.

³ Present address: National Cancer Institute, Bethesda 14, Maryland.

18, 19, 20, 21, 22, 24, 25, 26). By the use of small angle X-ray diffraction, Bear and Rugo (7) derived a model of keratin having a basic net structure. They found a large period of 95 Å and deduced that this represents either two or four particles along the axis. In anticipation of the results reported in the present paper, it may be noted that two particles of 47.5 Å would fit the periodic dimensions of their model and that the net could be made up of these in a close packed array.

The present study was undertaken to determine the changes in epidermal fine structure which occur as differentiation proceeds in the mouse embryo so that some further knowledge of the mechanism of keratin formation might be obtained. Some additional observations are reported on structure of dermis and on changes in epidermal fine structure which are not necessarily correlated with the production of keratin.

MATERIALS AND METHODS

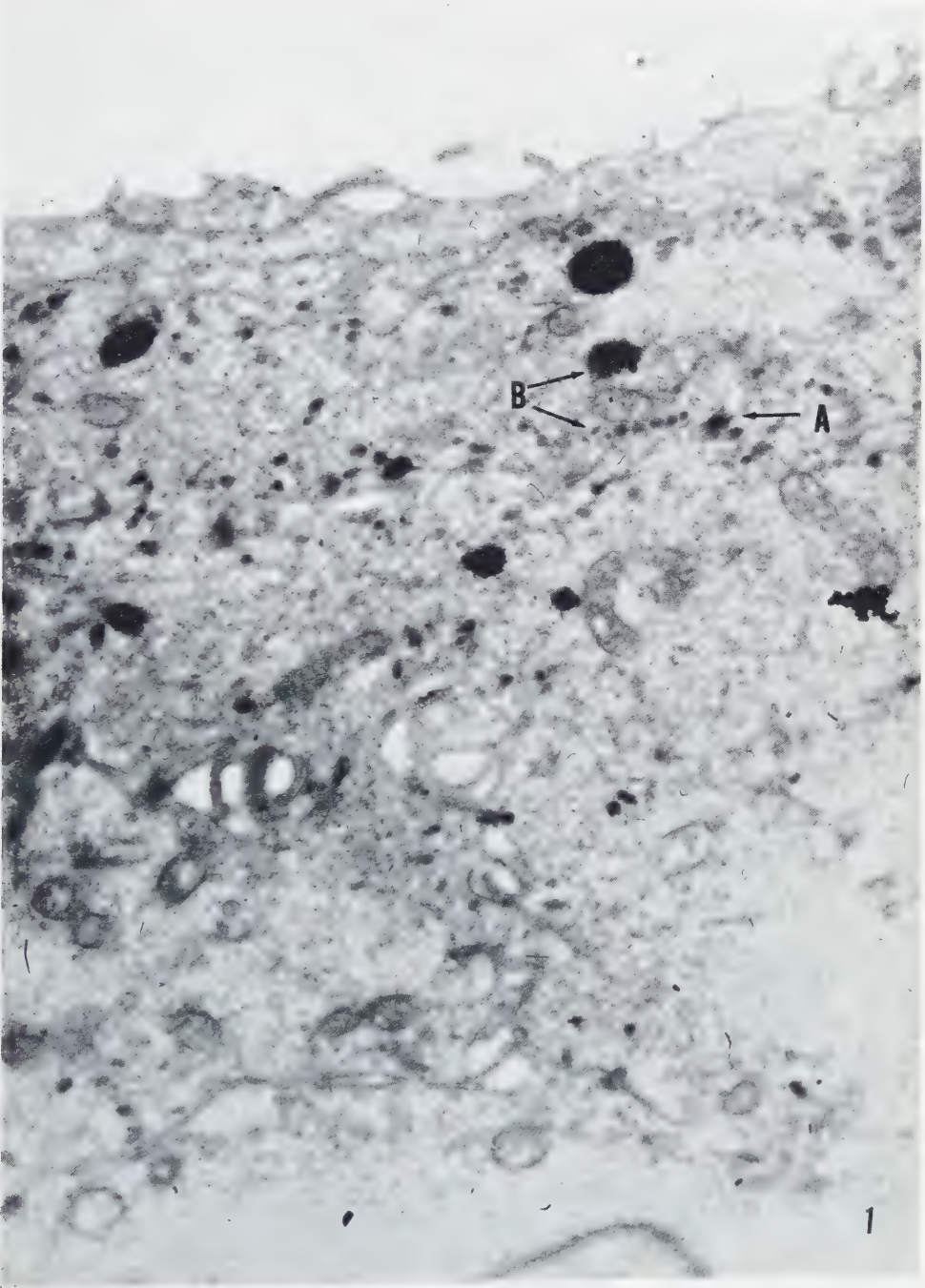
Timed embryos from Swiss Albino mice were taken at 14, 15, 16, 18, and 20 days of gestation and at birth. Small pieces of skin were cut off, mounted by applying the dermis side to pieces of paper, and fixed by immersion for 10 to 30 minutes in Dalton's fixative (10) at pH 7.4 with the youngest embryos receiving the shortest time. Washing was done in running tap water for 15 minutes. Dehydration was by a graded series of ethanol solutions starting with 10% alcohol and proceeding by 10% increases to absolute. Imbedding was carried out in a partially polymerized mixture of 3 parts butyl to one part methyl methacrylate to which a small amount of benzoyl peroxide had been added. Polymerization was allowed to proceed at 60 C. Sections were cut at 200 to 300 Å on the International microtome equipped with the improved glass knife holder (13) or on the Porter-Blum microtome. Photographs were made on an EMU-2C electron microscope.

OBSERVATIONS

Description of the skin of the very young embryo

The fourteen- or fifteen-day embryo epidermis is stratified in a manner very similar to the adult except that the stratum corneum is not present (Fig. 1). The basement membrane makes up the most superficial part of the dermis and acts as a support of the epidermis. It has essentially the same structure in the fourteen-day embryo that it has in the new born animal. The basement membrane consists of a continuous

FIG. 1.—Fifteen-day embryo mouse epidermis. Membrane thickenings opposite each other are indicated at *A*. Arrows at *B* point to a large granular body above and to a row of small granular bodies below; a normal mitochondrion is between the two. Cytoplasmic processes extending from the surface can be seen. $\times 18,000$.



homogeneous layer which follows the contours of the cell membranes of the basal cells and is separated from the cells by a constant space which is filled with a material of electron density somewhat less than that of the basement membrane itself (Figs. 2 and 5). Fine fibers of the dermis are continuous with the basement membrane. Most of these fibers are surrounded by a less dense material which appears the same as that between the basement membrane and the basal cell membranes. This material decreases in density at a distance from the fiber so that it has no discrete boundary. Reasoning from its location it probably corresponds to the polysaccharide or glycoprotein which Bear (6) describes as being associated with reticular fibers.

The internal structure of both the stratum germinativum and stratum spinosum is essentially the same. The major distinguishing feature is the more vertically elongate shape of the basal cells as compared to the more equally dimensioned spinous cells. The mitochondria are small in these cells but structurally are ordinary in their appearance (Fig. 1). Cytoplasmic processes are frequent and extensive in all cells of the epidermis at this age, and there is much intertwining of these processes so that in a section the cell membranes have a very convoluted appearance.

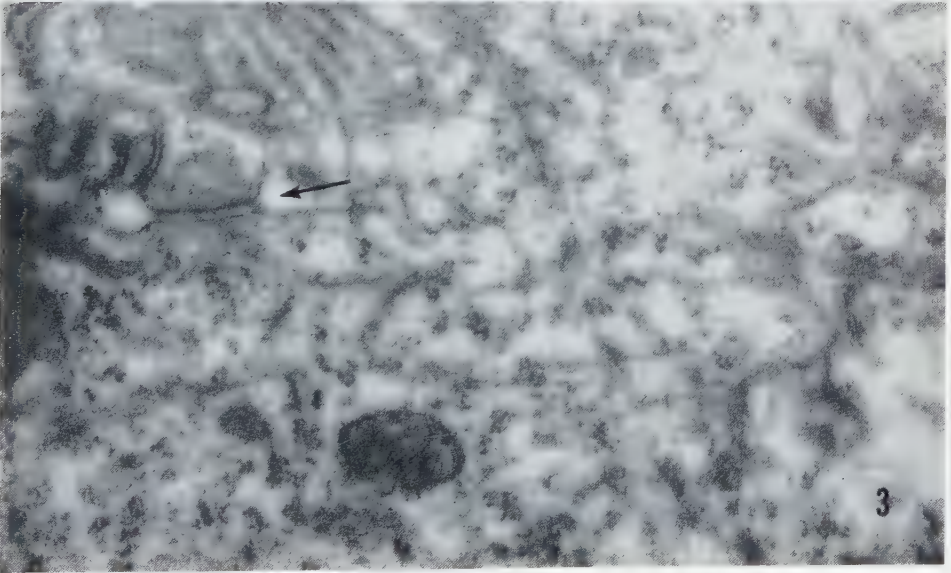
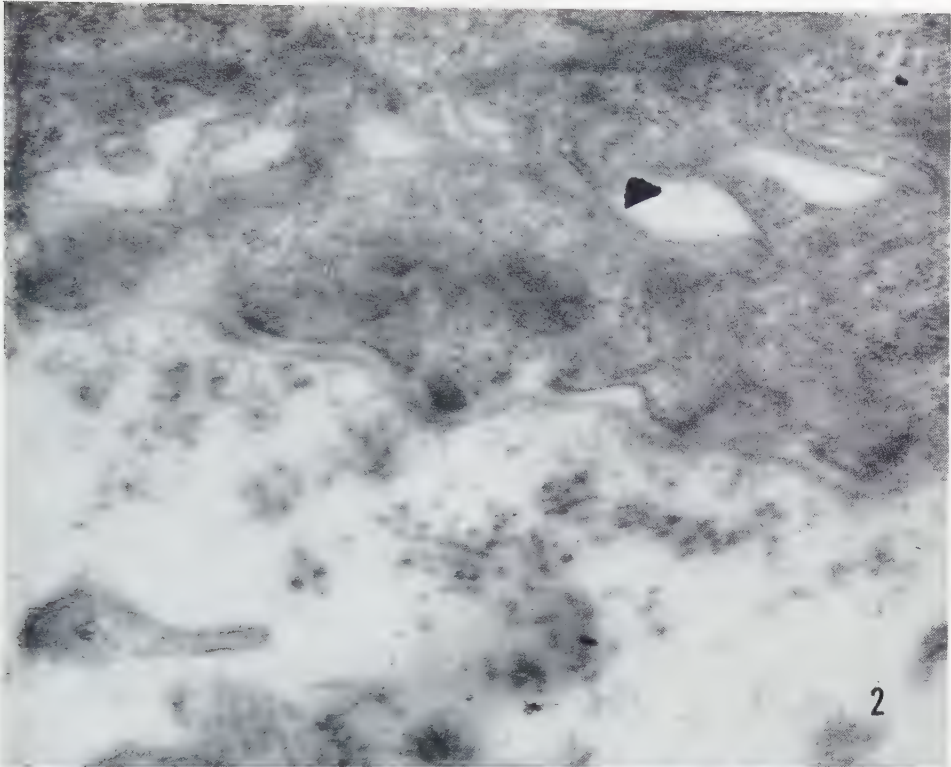
A few fine filaments (tonofilaments of Selby, 31) are found in the fifteen-day embryo (Figs. 1 and 6). They are about 40 Å in diameter, are sometimes seen to have a granularity along their length, and are usually aggregated into bundles which would correspond to classic tonofibrils. At this and later stages there is a frequent association of the tonofilaments with mitochondria (Figs. 5 and 6). In many instances this association can be seen to involve a direct contact of the end of a tonofilament with the mitochondrial membrane (Fig. 5).

Membrane thickenings occur at many places throughout the epidermis in the fifteen-day embryo. These thickenings are generally associated with a granular structure which projects into the surrounding cytoplasm and they universally occur on membranes exactly adjacent to a similar structure on the cell membrane of a neighboring cell (Fig. 1). The cell membranes next to the basement membrane have the same kind of thickening although they obviously have no neighboring cell membranes to match. These membrane thickenings will be described in more detail when changes in the older embryos are presented.

There is a paucity of Golgi material in the fifteen-day embryo. This is also true of the older animals as noted by Selby (31). However, there are some double membrane structures present in the cytoplasm which defy identification with any other organelle and which most closely resemble the Golgi double membranes (Fig. 4). Since this

FIG. 2.—Basement membrane adjacent to the germinal layer of the epidermis in a newborn mouse. Reticular fibers can be seen to be continuous with the basement membrane. $\times 34,000$.

FIG. 3.—Newborn mouse epidermis. The membrane thickenings can be seen opposite each other (arrow) and the tonofilaments can be seen in continuity with them. $\times 43,000$.



identification is by no means certain, it must be concluded here, as in Selby's work, that the Golgi body is vestigial if it exists at all in the epidermis. The more superficial layers of the stratum spinosum in the fifteen-day embryo contain electron dense granular bodies of varying size, with the smallest being about 500 Å diameter. These granular bodies can be seen to be made up of smaller granules about 60 to 80 Å diameter. In the stratum granulosum the smaller granular bodies are gradually replaced by larger ones which range up to the size of mitochondria near the surface of the epidermis (Figs. 1, 8, 9).

In the region of transition between the stratum spinosum and stratum granulosum in the fifteen-day embryo there is a gradual decrease in the number of mitochondria, and this decrease appears to be of approximate inverse relation to the increase in number and size of the granular bodies mentioned above. The membrane thickenings are found in the stratum granulosum just as they are in the deeper layers.

The extensively intertwined cytoplasmic processes found in the deeper strata of the fifteen-day embryo are also present in the stratum granulosum. In addition, the cytoplasmic processes project from the surface cells so that the appearance of microvilli is presented (Fig. 1).

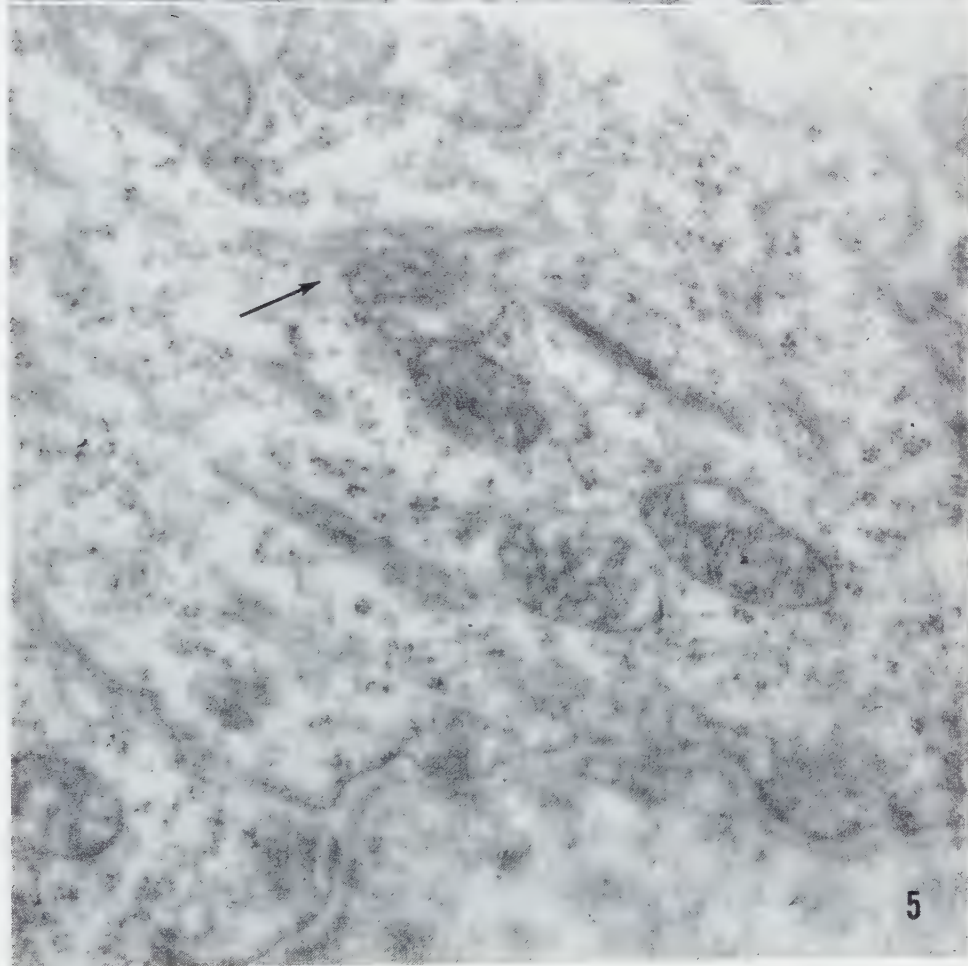
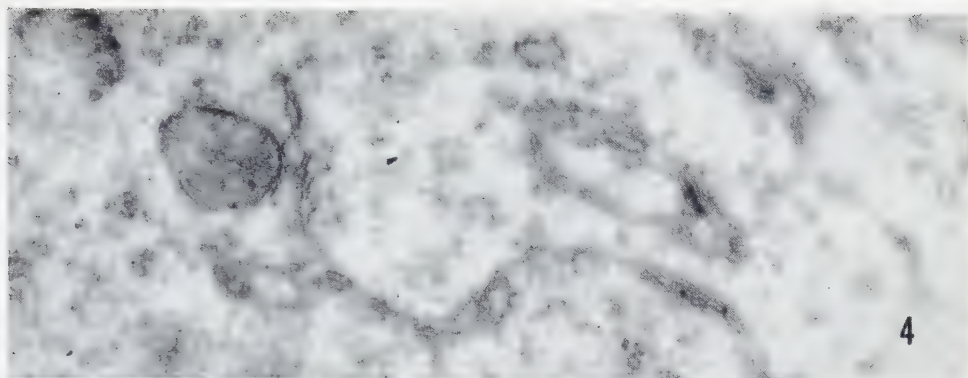
Developmental changes from the fifteenth embryonic day to birth

There is no change in the basement membrane during this period so that the description of the earlier embryo can also be applied to the newborn animal.

The tonofilaments increase greatly in number in the stratum germinativum and stratum spinosum. They gain attachment to the membrane thickenings in many places (Fig. 7) and still maintain their relationship to the mitochondria (Fig. 5). The membrane thickenings are electron dense and in favorable sections (Fig. 7) it can be seen that they are separated by a distance greater than that separating the plasma membranes in other places. The material between these thickenings is more dense than the material between the membranes elsewhere. The density of this material is about the same as that described for the material between the basement and the basal cells. At the resolutions possible, it appears that the tonofilaments attach to the membrane thickenings simply by becoming continuous with them. Tonofilaments attach to membrane thickenings on the cell membranes adjacent to the basement membrane in the same manner.

FIG. 4.—Fifteen-day embryo mouse epidermis. A mitochondrion plus some double membrane structures which are not definitely identifiable but which may bear some relation to Golgi double membranes are visible. $\times 43,000$.

FIG. 5.—Germinal layer of epidermis in newborn mouse. Basement membrane is at bottom of picture. Note the apparent continuity of the fibrils with the mitochondrion in the middle of the field. $\times 43,000$.



There appear to be fewer of the double membrane structures, which are possibly related to the Golgi complex, in the older embryos than in the fifteen-day embryos. Conversely, there appears to be an increase in the number of mitochondria in the lower strata of the epidermis.

The cell processes of the stratum geminativum and stratum spinosum cells do not change in character as the epithelium develops, but they become less attenuated in the more superficial parts of the stratum granulosum and are no longer present in the most superficial cell layer of the granulosum in the newborn mouse (Fig. 9).

The internal structure of the granular bodies of the stratum granulosum does not change with differentiation of the epidermis, but attachment of the tonofilaments to the surface of the granular bodies becomes generalized (Fig. 8).

The most superficial cells of the stratum granulosum rather abruptly change in structure to give rise to the deep layer of the stratum corneum. The differences between these two cell types can be seen in Fig. 9. By the time the superficial layers of the stratum granulosum are reached, there are not many intact tonofibrils remaining in the cytoplasm. When the cells in the granulosum are transformed into cornified cells, there are no tonofibrils or tonofilaments remaining as such in the cytoplasm; however, the greater part of the cytoplasm of the stratum corneum cells appears to be filled with granules of about 40 Å diameter. Clumps of larger granules, about 60 to 80 Å diameter, are aggregated within the general mass of 40 Å granules (Fig. 9). These clumps of larger granules appear to be all that remains of the "keratohyaline granules" in the cells of the stratum corneum. There are no membrane thickenings in the stratum corneum although the cell membranes themselves remain intact in this layer.

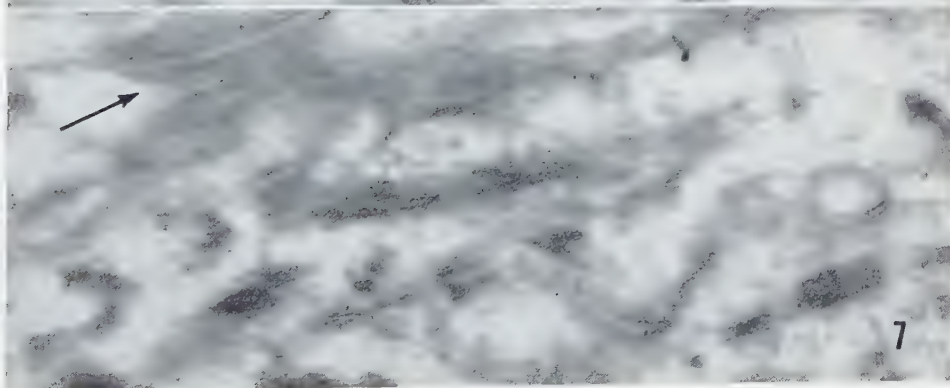
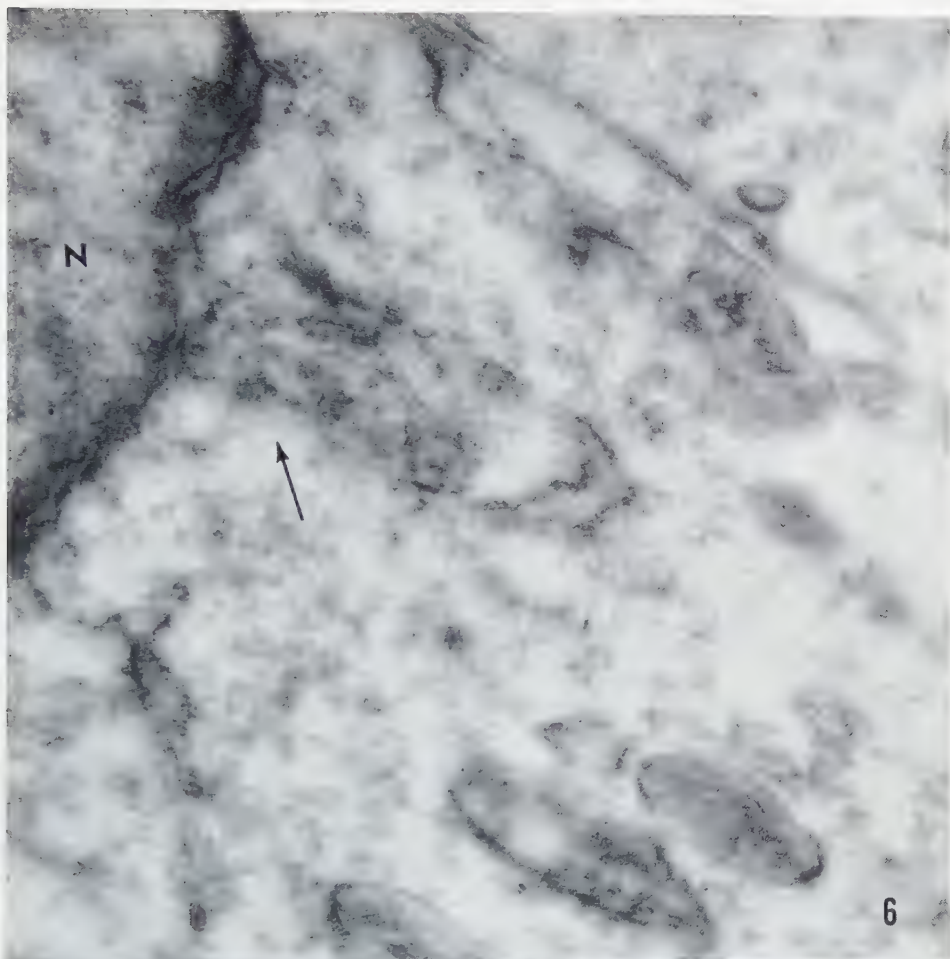
DISCUSSION

The first visible manifestations of keratin formation, i.e. tonofilaments, appear to have a spatial relationship to mitochondria. It may be conjectured that this spatial relationship reflects a stage of keratin formation in which mitochondria may participate in a more or less active fashion. There are several considerations, other than the direct observation of tonofilament-mitochondrial relation, which lead to the concept of an active role of mitochondria in keratin synthesis. Some of these will be given below.

The observation reported here that tonofilaments are attached to the granular

FIG. 6.—Fifteen-day embryo mouse epidermis. Relation between an incomplete mitochondrion and tonofilaments at the arrow near the nucleus (N). $\times 54,250$.

FIG. 7.—Plantar epidermis of a newborn mouse. Arrow points to the attachment of tonofilaments to a membrane thickening. $\times 54,250$.



bodies (keratohyaline granules) would be expected if the granular bodies were derived from mitochondria. In that case the attachment would be considered as simply a continuation of a previously existing relationship between the two. Sheldon and Zetterqvist (32) showed that mitochondria are indeed transformed to "keratohyaline granules" in the cornea when a vitamin A deficiency is induced. Bern and others (8) showed that "keratohyaline granules" contain phospholipoprotein and RNA which would suggest that they are derived from mitochondria and ergastoplasm.

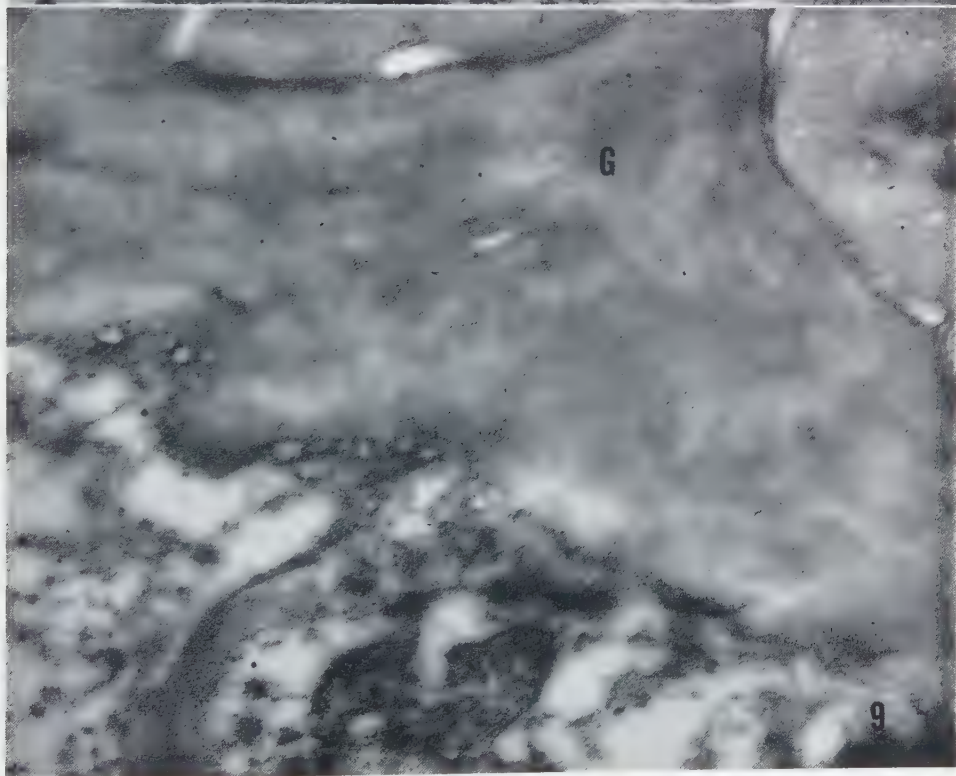
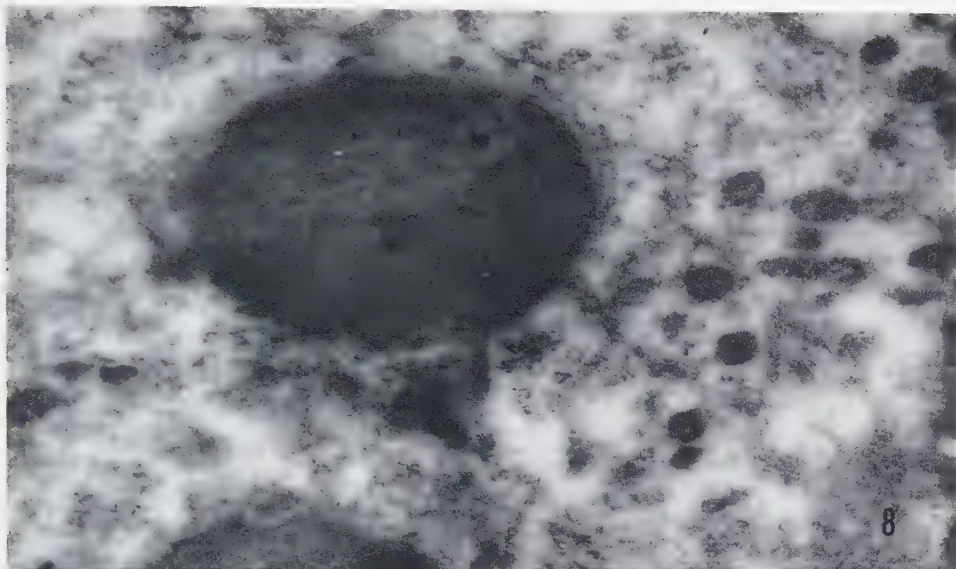
The concept of Ludford (22) that "keratinization is mainly a function of the ground cytoplasm" might well be restated in terms of current knowledge to implicate ergastoplasm or cytoplasmic RNA. Recent work (16) led to the conclusion that both mitochondria and ergastoplasm participate in protein synthesis. This conclusion was based upon the fact that if the adrenal gland is stimulated with ACTH, there is an increase in cytoplasmic RNA followed or accompanied by an increase in amount of cytoplasmic nucleoprotein and number of mitochondria. These changes are followed later by an increase in nuclear RNA, an increase in total cytoplasm and finally by cell division. The authors believe that the mitochondria and "chromidia" are interdependent and interact by a "circular mechanism", or in other words a cyclical relationship exists. It would appear from the present work that keratin sub-units could be synthesized in the ergastoplasmic system or elsewhere in the cell while mitochondria might be involved in a later stage of polymerization into visible tonofilaments.

It is quite possible that the 40 Å granules of the cornified cell represent some modified form of the material which makes up the tonofilaments which are also 40 Å in diameter and are granular. This would be in accord with the keratin model derived by Bear and Rugo (7). That some kind of net structure is present in the stratum corneum can be seen in Fig. 9. The dense regions having 60 to 80 Å sub-granules in the cornified cell could well correspond to the aggregates of degeneration products seen in the granular bodies of the stratum granulosum. That such non-keratin products are commonly present in fully cornified structures was pointed out by Bollinger and Gross (9) who found inorganic salts, non-keratin proteins, lipids, and other material in human toenails.

The "desmosome" region described by light microscopists includes the membrane thickenings of two adjacent cells and whatever material is between them plus the terminations of tonofilaments as they attach to the membrane. Wislocki (36) found

FIG. 8.—Newborn mouse epidermis. Relation of tonofilaments to the granular bodies of the stratum granulosum. $\times 43,000$.

FIG. 9.—Newborn mouse epidermis. A mitochondrion, which appears to have several tonofilaments attached to it, is seen in the stratum granulosum. This is unusual because the mitochondria have almost always degenerated before reaching this level. The stratum corneum is distinguished by its much more homogeneous appearance. Cell membranes separating cornified cells may be seen in the upper and upper right part of the picture. Typical remnant of a granular body is at G. $\times 38,200$.



that this region is rich in phospholipid and it would seem that the membrane thickening is the most likely locus of this material.

Some additional observations which are not obviously related to the keratinization process will be briefly discussed. The paucity of Golgi material in the epidermis when viewed by electron microscopy has been observed previously by Selby (31). It will be noted that this is not in agreement with some of the results of classical silver staining methods which do show that a "Golgi net" is present in epidermal cells (25). One possible explanation of this apparent discrepancy is that the double membranes described above may give a silver reaction which results in the appearance of the Golgi body by light microscopy even though the usual three component structure observed by electron microscopy (11) may not be present. Dalton and Felix (12) studied the Golgi complex in several tissues from several different species and observed that it is most highly developed in those instances when large amounts of water must be removed from the cytoplasm, and conversely is least developed when such an osmoregulatory function is not demanded. Since epidermal cells are in an osmotic environment and a functional state neither of which requires the cells to dispose of any excess water, the observed scarcity of Golgi material would be expected. Described in another way, the Golgi apparatus would be at the lower limit of the "condensation-expansion scale" of Elftman (14).

The basement membrane reported here has all of the features of basement membranes found in other tissues (27, 33, 34). For this reason it would seem better to retain the term basement membrane rather than coin any new terms such as Selby (31) suggested when she proposed "dermal membrane" to describe it.

I should like to express my appreciation for the interest and encouragement of Dr. E. W. Dempsey during the work reported here.

REFERENCES

1. ADOLPH, W. E., BAKER, R. F. and LEIBY, G. M., *Science* **113**, 685 (1951).
2. ALBERTINE, A., *J. Natl. Cancer Inst.* **13**, 1473 (1953).
3. ASTBURY, W. T. and WOODS, H. J., *Trans. Roy. Soc. London A* **173**, 333 (1934).
4. BAHR, G. F. and MOBERGER, G., *Exptl. Cell Research* **6**, 506 (1954).
5. BARNETT, R. and SELIGMAN, A., *J. Natl. Cancer Inst.* **14**, 769 (1954).
6. BEAR, R. S., *Advances in Protein Chem.* **7**, 69 (1952).
7. BEAR, R. S. and RUGO, H. J., *Ann. N.Y. Acad. Sci.* **53**, 627 (1951).
8. BERN, H. A., ELIAS, J., PICKETT, P., POWERS, T. and HARKNESS, M., *Am. J. Anat.* **96**, 419 (1955).
9. BOLLIGER, A. and GROSS, R., *Australian J. Exptl. Biol. Med. Sci.* **31**, 127 (1953).
10. DALTON, A. J., *Anat. Record* **121**, 281 (1955).
11. DALTON, A. J. and FELIX, M. D., *Am. J. Anat.* **94**, 171 (1954).

12. ——— *J. Biophys. Biochem. Cytol.* **2**, 79 (1956).
13. DEMPSEY, E. W. and LANSING, A. I., *Proc. Soc. Exptl. Biol. Med.* **82**, 253 (1953).
14. ELFTMAN, H., *Anat. Record* **118**, 147 (1954).
15. FARRANT, J. L., REES, A. L. G., and MERCER, E. H., *Nature* **159**, 535 (1947).
16. FIALA, S., SPROUL, E. and FIALA, A., *J. Biophys. Biochem. Cytol.* **2**, 115 (1956).
17. FRASER, R. D. B., *Nature* **172**, 675 (1953).
18. GIROUD, A. and LEBLOND, C. P., *Annals N.Y. Acad. Sci.* **53**, 613 (1951).
19. HAPPEY, F., MACRAE, T. P. and WESTON, G. J., *Nature* **172**, 673 (1953).
20. KING, L., *J. Natl. Cancer Inst.* **10**, 689 (1949).
21. LEBLOND, C. P., *Ann. N.Y. Acad. Sci.* **53**, 464 (1951).
22. LUDFORD, R. J., *Quart. J. Microscop. Sci.* **69**, 27 (1924).
23. MENEFEE, M. G., *Anat. Record* **122**, 181 (1955).
24. MERCER, E. H., *Biochim. et Biophys. Acta* **3**, 161 (1949).
25. MONTAGNA, W., *Intern. Rev. Cytol.* **1**, 265 (1952).
26. ——— The Structure and Function of Skin. Academic Press Inc., New York. 356 pp. (1956).
27. OTTOSON, D., SJÖSTRAND, G., STENSTRÖM, S. and SVAETICHIN, G., *Acta Physiol. Scand.* **29**, 611 (1953).
28. PEASE, D. C., *Am. J. Anat.* **89**, 469 (1951).
29. PORTER, K. R., *Anat. Record* **118**, 433 (1954).
30. RUDALL, K. M., *Advances in Protein Chem.* **7**, 253 (1952).
31. SELBY, C. C., *J. Biophys. Biochem. Cytol.* **1**, 429 (1955).
32. SHELDON, H. and ZETTERQVIST, H., *Exptl. Cell Research* **10**, 225 (1956).
33. SJÖSTRAND, F. S. and RODIN, J., *Exptl. Cell Research* **4**, 426 (1953).
34. WEISS, P. and FERRIS, W., *Proc. Natl. Acad. Sci. U.S.* **40**, 528 (1954).
35. ——— *Exptl. Cell Research* **6**, 546 (1954).
36. WISLOCKI, G. B., *Anat. Record* **109**, 388 (1951).

Identification of Molecular Ferritin in Homogenates and Sections of Rat Liver

EDWARD L. KUFF and ALBERT J. DALTON

*National Cancer Institute, National Institutes of Health,
United States Public Health Service, Bethesda, Maryland*

Received May 20, 1957

Dense particles, approximately 55 Å in diameter, were observed in fractions isolated by high-speed centrifugation from rat liver homogenates. These were identified as the iron-containing micelles of ferritin. Similar particles were observed in thin sections of intact liver cells. They increased greatly in number following the administration of iron to the animals.

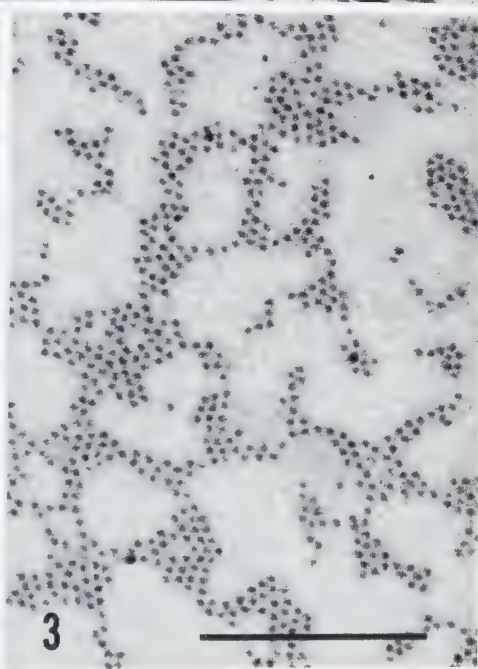
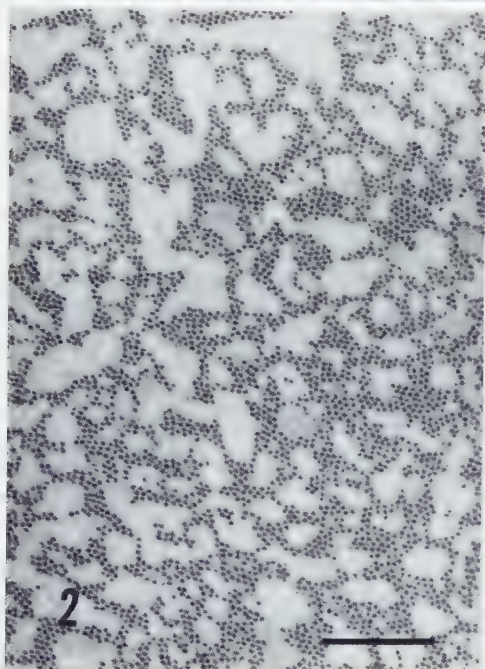
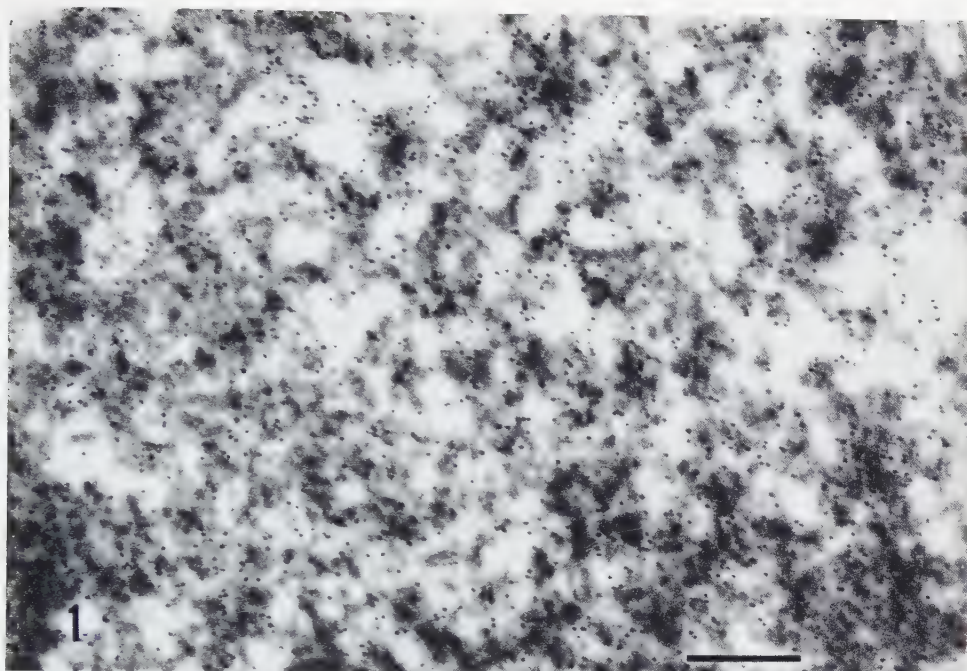
The physical properties of the iron-protein complex, ferritin, have been studied most thoroughly in the case of material derived from horse spleen (5). Here, Farrant (2) has demonstrated by electron microscopy that most of the iron, which constitutes approximately 20% of the dry weight of crystalline preparations, is localized in the form of micelles within the interiors of the apoferritin molecules. The over-all molecular diameter was found to be 94 Å; when fully developed, the micelles averaged 55 Å in diameter and consisted of symmetrical arrangements of 4 sub-units approximately 27 Å in size. The relationships between the molecular structure of ferritin and its physiological properties have been recently reviewed (11, 24).

During a study of tissue fractions isolated by high-speed centrifugation from homogenates of rat liver, dense particles about 55 Å in size were observed by electron microscopy in some of the preparations. These particles were found to represent the central iron-containing micelles of ferritin molecules. Similar particles were observed in sections of intact liver cells, where they increased greatly in number following the administration of iron to the animals.

FIG. 1.—Electron micrograph of a thin section of a fixed pellet of Fraction IV (see text). A diffusely granular material composes the main bulk of the fraction. Numerous very dense particles approximately 55 Å in diameter are also present. The line in this and the succeeding figures represents 0.2 μ. × 75,000.

FIG. 2.—Electron micrographs of rat liver ferritin plated from dilute aqueous solution onto formvar film and examined without fixation. The small dense particles, which represent the iron-containing micelles of ferritin molecules, are similar in appearance to those seen in Fig. 1. × 75,000.

FIG. 3.—Electron micrograph of the same preparation shown in Fig. 2, at a higher magnification, showing the highly regular arrays formed in certain areas during drying of the ferritin solution on the film. The sub-structure of the micelles is not resolved. × 150,000.



MATERIALS AND METHODS

Female Sprague-Dawley rats, weighing 150 to 200 g. were studied. In fractionation experiments, homogenates of perfused livers were prepared in 0.25 *M* sucrose (22) and the centrifugations carried out at 0° unless otherwise noted. Total nitrogen was determined by nesslerization of acid digests (25), ribonucleic acid phosphorus (RNA-P) by the procedure of Schneider (21), and, after acid digestion, total phosphorus by the method of Fiske and Subbarow (4) and iron by the method of Schade *et al.* (20). The iron content of solutions of purified ferritin could be estimated quite accurately from their light absorption at 310 m μ , using an extinction coefficient of 45.1 per mg ferritin iron per ml per cm (18).

For electron microscopy, tissue fractions isolated by centrifugation were fixed as pellets in cold 1.0% osmium tetroxide containing 0.25 *M* sucrose. The fixative was decanted after one hour and the pellets sliced into small pieces which were dehydrated and embedded as previously described (8). Thin slices of whole liver were fixed in a chrome-osmic mixture (1), and similarly embedded. Sections were cut on a Porter-Blum microtome (17) set to cut at 250 Å. Solutions of purified ferritin were diluted with distilled water to an iron content of 0.3 μ g per ml or less and plated directly on formvar-covered specimen grids. After drying, the grids were generally washed with water to remove traces of salt. Some preparations were lightly double-shadowed with chromium as described by Kahler and Lloyd (7).¹ Most of the electron micrographs were taken with an RCA model EMU2C electron microscope. The chromium-shadowed ferritin was also studied with a Siemens Elmiskop I instrument.²

RESULTS

Typical distributions of total nitrogen, RNA-P, and iron among fractions isolated from liver homogenates at progressively increasing speeds and times of centrifugation are shown in Table I. Biochemical and electron microscopic evidence, to be presented elsewhere, revealed that fractions I and II possessed an enzyme complement characteristic of the "microsome" fraction of liver (6) and were composed of both rough- and smooth-surfaced membranous elements (8, 15). Fractions III and IV, designated "post-microsome" fractions, were distinctly yellow in color when resuspended in sucrose. They contained greatly elevated concentrations of iron relative to the whole homogenate (Table I). Fig. 1 illustrates the appearance of a thin section through a fixed pellet of fraction IV, and shows that the predominant visible component was a rather dense granular material composed chiefly of particles ranging from 100 to

¹ The shadowing was kindly performed by Mr. B. J. Lloyd.

² This instrument was made available by Dr. Keith R. Porter, of the Rockefeller Institute.

FIG. 4. Electron micrograph of plated ferritin that has been lightly double-shadowed with chromium at an angle of 11° in the axis indicated by the lower arrow. The individual molecules are outlined by the chromium, which appears particulate. The dense centrally located micelles are, in most instances, seen to be composite in nature. The upper arrow indicates a ferritin molecule in which four sub-units can be distinguished within the central region. $\times 195,000$.

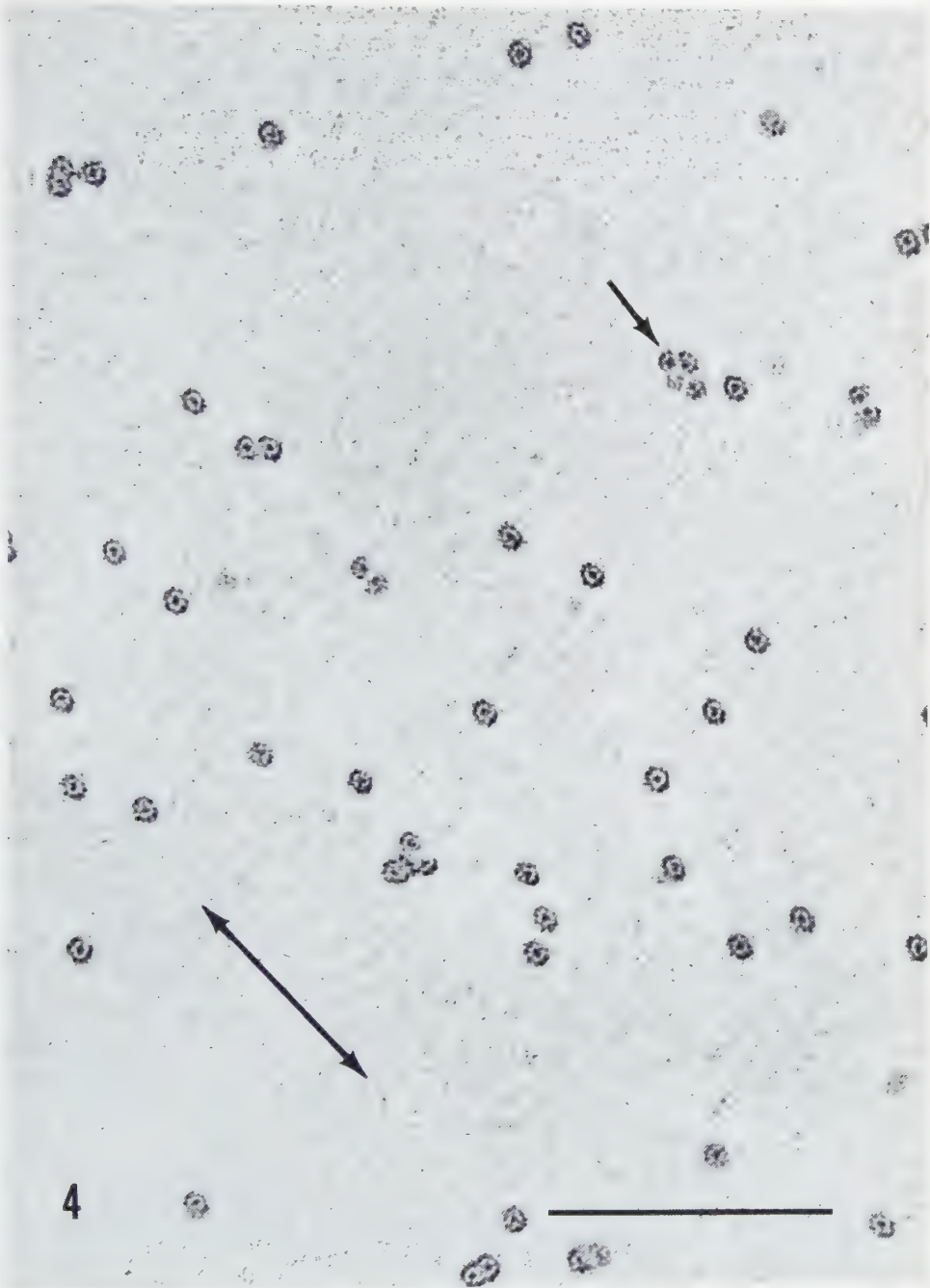


TABLE I

THE DISTRIBUTION OF RNA-P, IRON, AND TOTAL NITROGEN AMONG FRACTIONS ISOLATED FROM RAT LIVER HOMOGENATE BY DIFFERENTIAL CENTRIFUGATION

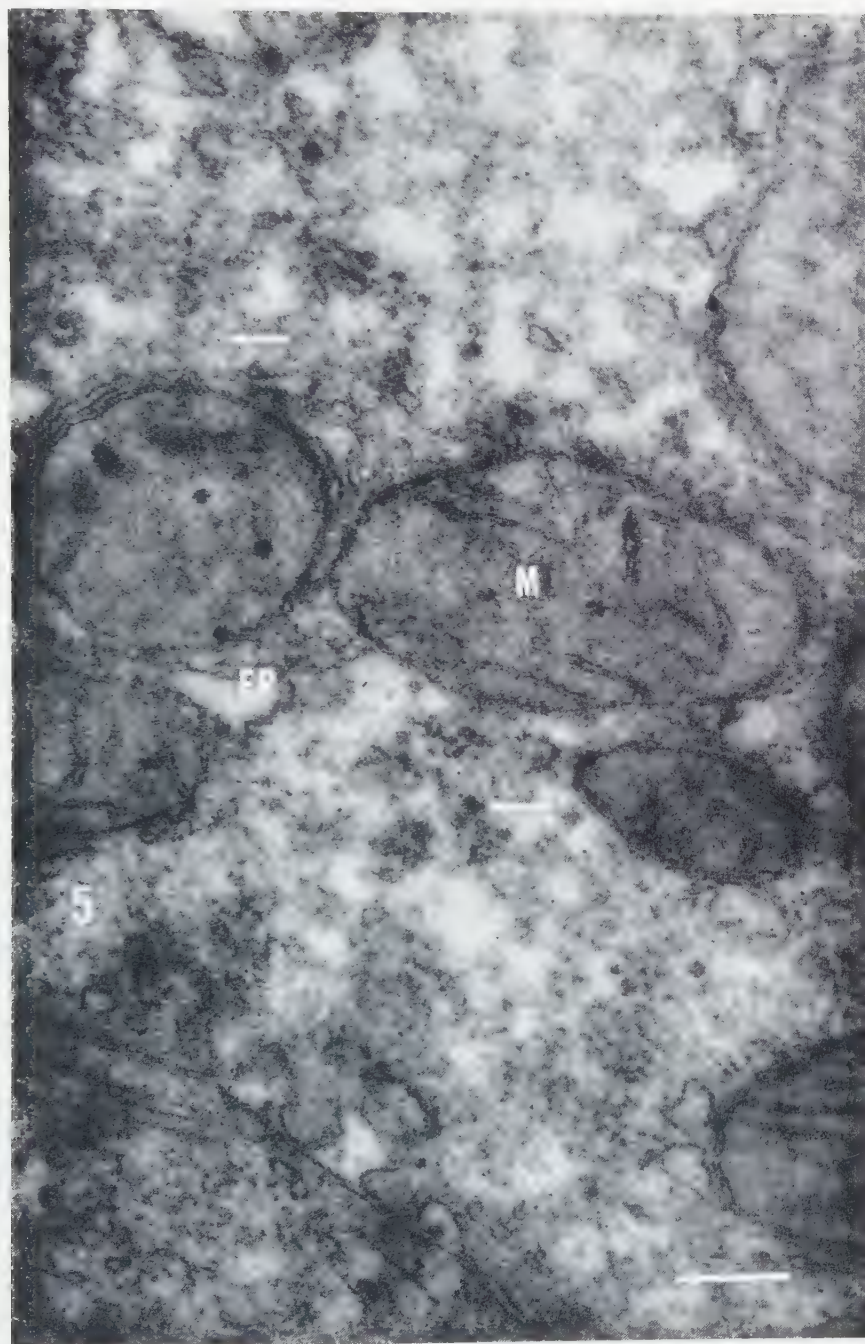
H represents a 12.5 percent homogenate of perfused liver in 0.25 *M* sucrose; S₁, the supernatant fluid obtained by centrifugation of H for 10 minutes at 18,000 *g*; fractions I-IV, the sediments obtained by serial centrifugation of S₁ at the specified times and forces (SW-29 rotor, Spinco model E ultracentrifuge); and S₂, the final supernatant fluid.

| Fraction (time and speed of centrifugation) | Total N | | RNA-P | | | Iron | | |
|---|-------------|---------------|------------------|---------------|------------------|------------------|---------------|------------------|
| | mg per ml H | Per cent of H | μ g per ml H | Per cent of H | μ g per mg N | μ g per ml H | Per cent of H | μ g per mg N |
| H | 3.64 | (100) | 100 | (100) | 27 | 8.3 | (100) | 2.3 |
| S ₁ | | | | | | | | |
| (10 min., 18,000 <i>g</i>) | 1.67 | 46 | 53 | 53 | 32 | 6.5 | 78 | 3.9 |
| Fraction I (15 min., 70,000 <i>g</i>) | 0.300 | 8.2 | 17 | 17 | 57 | 0.69 | 8.3 | 2.3 |
| Fraction II (17 min., 125,000 <i>g</i>) | 0.131 | 3.6 | 9.5 | 9.5 | 72 | 0.78 | 9.3 | 5.9 |
| Fraction III (40 min., 125,000 <i>g</i>) | 0.077 | 2.1 | 8.4 | 8.4 | 109 | 1.2 | 15 | 16 |
| Fraction IV (90 min., 125,000 <i>g</i>) | 0.072 | 2.0 | 6.5 | 6.5 | 90 | 1.9 | 23 | 26 |
| S ₂ | 1.09 | 30 | 11 | 11 | 10 | 1.9 | 23 | 1.7 |
| Total, fractions I-IV and S ₂ (compare with S ₁) | 1.67 | | 52.4 | | | 6.47 | | |

250 Å in diameter. Similar particles were concentrated in fraction III (not shown). Their size and density to the electron beam, when taken in conjunction with the elevated concentrations of RNA-P in fractions III and IV, suggest that these particles represented a ribonucleoprotein component of the liver cytoplasm (10, 14, 15).

Abundantly interspersed in the granular material of fraction IV were other small, very dense, particles approximately 55 Å in diameter (Fig. 1). They were less numerous in fraction III and were infrequently observed in fractions I and II. Parallel variations

FIG. 5.—Electron micrograph of rat liver fixed in osmium tetroxide buffered at pH 7.2. The junction of two parenchymal cells runs obliquely across the lower left corner of the picture. Dispersed throughout the ground substance of the cytoplasm are numerous small dense particles (see arrows) similar to those seen in Figs. 1 and 2. Note that they do not appear in particular association with the mitochondria (*M*) or the membranes of the endoplasmic reticulum (*ER*). $\times 75,000$.



in the iron content of the fractions (Table I) suggested that the 55 Å particles might represent the iron-containing micelles of ferritin molecules. Accordingly, attempts were made to isolate ferritin from the post-microsome fractions.

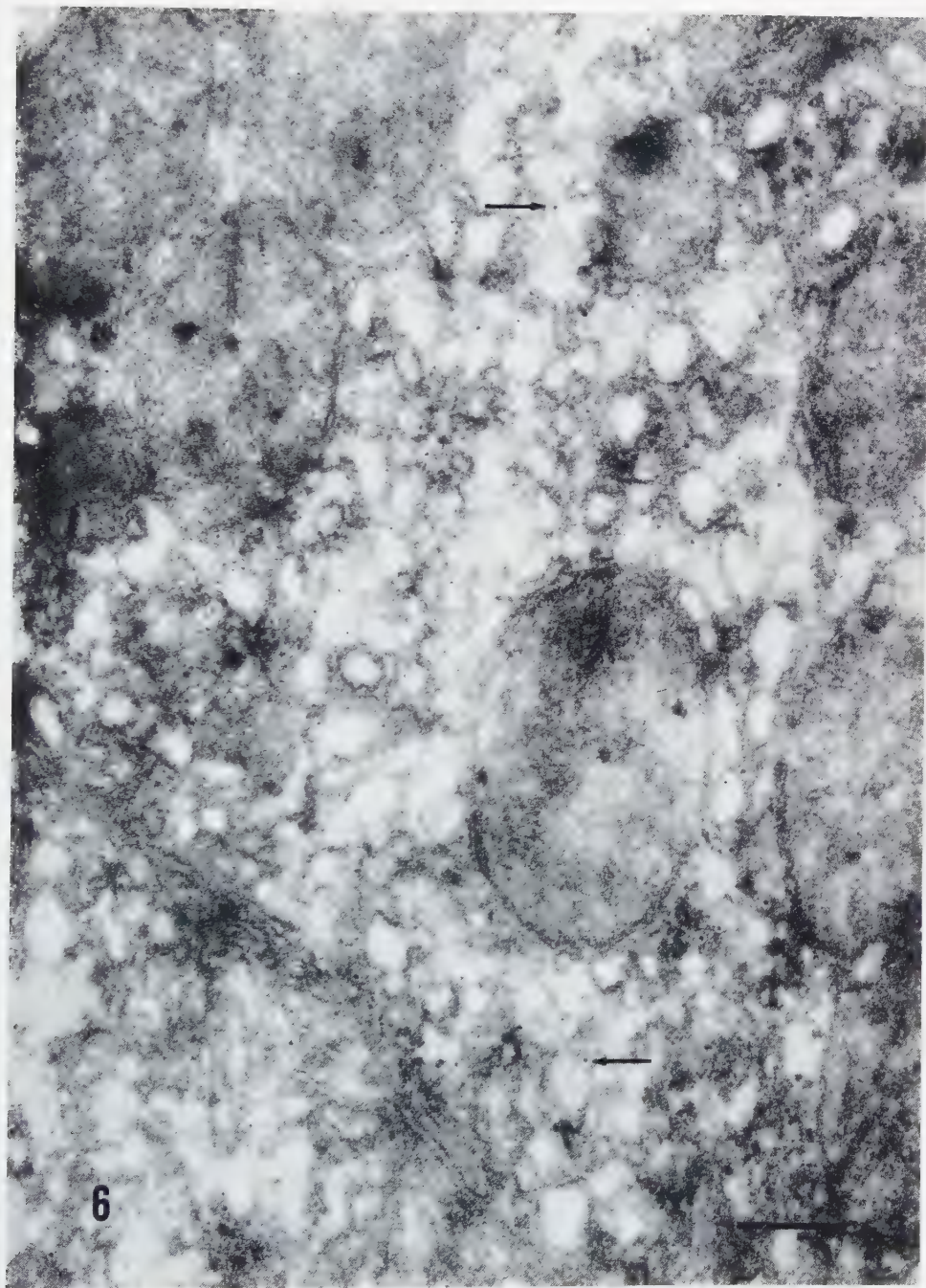
Combined fractions III and IV were prepared from liver (Table I), resuspended in a small volume of 0.05 *M* sodium chloride, and heated in a water bath at 75° for five minutes (9). The bulky light tan precipitate that formed was removed by low-speed centrifugation. The brown supernatant fluid, after standing overnight at 0°, was further clarified by centrifugation at 76,000 *g* (average) for 20 minutes at room temperature. Finally, the solution was centrifuged for 90 minutes at 137,000 *g*, yielding an almost colorless supernatant fluid and a dark brown sediment which readily dissolved in dilute saline and constituted the isolated ferritin.

Three such preparations exhibited iron: nitrogen ratios between 2.5 and 2.7 and absorption spectra typical of ferritin (5). Iron:phosphorus ratios of 33 and 21 were observed in two instances. The formation of brown octahedral crystals occurred promptly in systems containing one mg of ferritin nitrogen per ml and 2.5 to 5% cadmium sulfate (5, 9). In the optical ultracentrifuge (solvent 0.05 *M* sodium chloride, ferritin nitrogen 1.3 per ml) the major boundary was fairly broad but symmetrical, with an $s_{20,w}$ of 60 S. Values of 63 and 65 S have been observed for rat liver (16) and horse spleen (19) ferritin, respectively. Approximately 20% of the total refractive increment was included in a very rapidly spreading boundary preceding the main peak. No other components were seen. Yields of ferritin corresponding to 44 to 58 µg of iron per gram of perfused liver were obtained by the above method of isolation.

Dilute ferritin solutions, when dried on formvar films, presented the appearance shown in Fig. 2. The dense iron-containing micelles of the ferritin molecules corresponded in size (55 Å) to the small particles seen in the postmicrosome fractions. The protein portions of the molecules were not visualized in unshadowed preparations; however, their dimensions could be estimated from the spacing of the micelles. Thus, it was calculated that the particularly regular arrays observed in certain areas (Fig. 3) could have been formed by the close packing in two dimensions of elliptical particles with axes of 95 and 115 Å.

High resolution photomicrographs of double-shadowed preparations of ferritin were obtained with the Siemens microscope (Fig. 4). The dense centrally located micelles were now seen to be composite in nature; frequently two or three, and occasionally as many as four, sub-units were resolved. Their structure was thus entirely similar to that observed in the case of horse spleen ferritin (2). The over-all

FIG. 6.—Electron micrograph of a section of mouse liver comparable to that shown in Fig. 5. The arrows again indicate some of the small dense particles in the cytoplasmic ground substance. 75,000.



molecular diameter, as measured from the inner edges of the shadowing material, was approximately 105 Å. A similar value (110 Å) was obtained as the minimum distance of approach between the centers of particles in pairs of larger groups.

Examination of electron micrographs of thin sections of livers of normally fed mice and rats revealed in hepatic parenchymal cells the presence of particles having approximately the same dimensions and electron density as those identified as ferritin in the centrifuged material. These particles were not found in nuclei, mitochondria, nor within the areas enclosed by the membranes of the ergastoplasm (endoplasmic reticulum). They tended to be concentrated near plasma membranes and in the interstices between groups of mitochondria (Fig. 5). They were found to be most readily resolved in areas of the cytoplasm free of ergastoplasm, areas considered to contain particulate glycogen (Figs. 6 and 7).

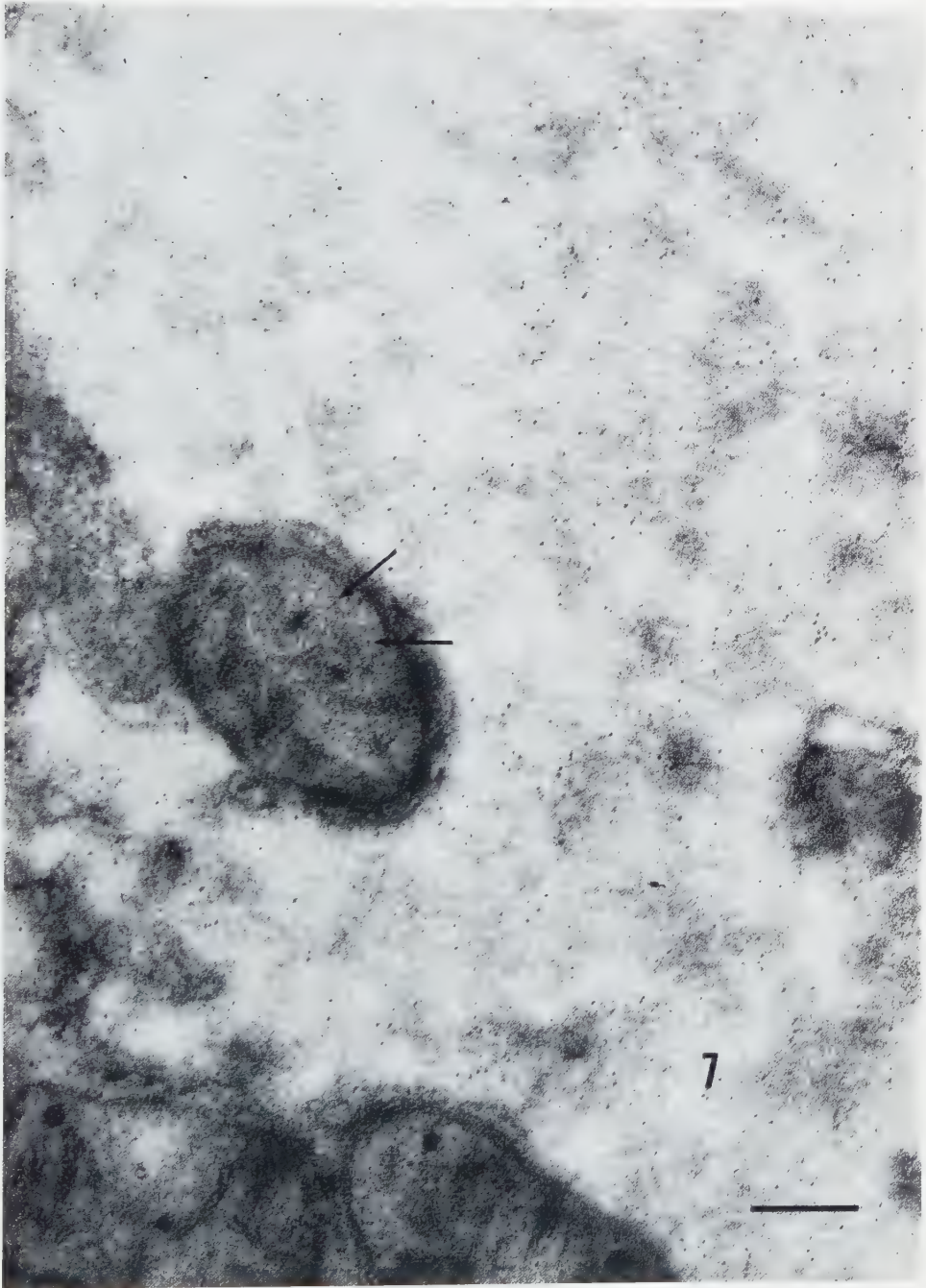
It is known that parenteral administration of ferric iron induces a rapid synthesis of ferritin in the liver (3, 23). Single doses of saccharated iron oxide ("Feojectin", Smith, Kline and French) containing 10 mg of iron were injected intravenously into 200 g rats. Nine days later, the iron contents of both the whole livers and the combined post-microsome fractions isolated therefrom were approximately 10 times greater than those of uninjected rats. Electron micrographs of such ferritin-rich livers revealed greatly increased numbers of the small dense particles (Fig. 7). Under these conditions there was some evidence of their presence in the matrix of mitochondria.

DISCUSSION

Resolution of a characteristic substructure in the 55 Å particles was not achieved in micrographs of the isolated tissue fractions or of the intact liver. Identification of the particles as the iron-containing micelles of ferritin rested, in the case of the fractions, upon (1) correlation between the iron contents of the fractions and the frequency with which the particles were observed therein; (2) the actual isolation of ferritin from the fractions; and (3) the similarity in appearance between the particles and the micelles of known ferritin. In sections of normal liver, size and density to the electron beam were of necessity the criteria for identification. The striking increase in the number of dense 55 Å particles observed after the administration of iron was strong confirmatory evidence that the particles represented ferritin.

Larger aggregates of iron-rich protein (e.g., hemosiderin granules (5)), have not

FIG. 7.—Electron micrograph of a portion of the cytoplasm of a parenchymal liver cell from a rat injected 9 days previously with saccharated ferric oxide. A great number of dense particles are observed which resemble those seen in the normal livers. The arrows indicate particles that appear to lie within the matrix of mitochondria. $\times 75,000$.



been considered in the present study. It might be mentioned in this regard that membrane-enclosed structures containing dense particles that resembled ferritin have been described in thin sections and homogenates of rat liver (13, 15). Such structures appeared to be rare in the livers of the rats employed in the present experiments.

Ferritin obtained from horse spleen by the usual method of crystallization with cadmium sulfate contains 20 to 25% iron-free apoferritin with an $S_{20,w}$ of approximately 17 S (19). As might be expected, ferritin isolated by a centrifugal method appears to contain little or none of the iron-free protein. The purity of the present preparations has not been critically determined. However, the iron:nitrogen ratios and the absorption spectra compared favorably with those of highly purified ferritin (5, 12). The electron microscopic appearance of plated material also suggests the absence of gross contamination. The spreading boundary preceding the main ferritin peak in the optical ultracentrifuge may well have represented aggregates of two or more ferritin molecules (cf. (19)) such as were visualized in the shadowed preparations. A centrifugal method for the isolation of ferritin may be useful under circumstances where the presence of cadmium in the final preparation is to be avoided.

REFERENCES

1. DALTON, A. J. and FELIX, M. D., in *Fine Structure of Cells, Symposium, VIIIth Intern. Congr. Cell Biol., Leiden, 1954*, p. 274. P. Noordhoff Ltd., Groningen, 1955.
2. FARRANT, J. L., *Biochim. et Biophys. Acta* **13**, 569 (1954).
3. FINEBERG, R. A. and GREENBERG, D. M., *J. Biol. Chem.* **214**, 91 (1955).
4. FISKE, C. H. and SUBBAROW, Y., *J. Biol. Chem.* **66**, 375 (1925).
5. GRANICK, S., *Chem. Revs.* **38**, 379 (1946).
6. HOGEBOM, G. H. and SCHNEIDER, W. C., in CHARGAFF, E. and DAVIDSON, J. N., *The Nucleic Acids*, Vol. II, p. 199. Academic Press Inc., New York, 1955.
7. KAHLER, H. and LLOYD, B. J., *J. Appl. Phys.* **21**, 699 (1950).
8. KUFF, E. L., HOGEBOM, G. H. and DALTON, A. J., *J. Biophys. Biochem. Cytol.* **2**, 33 (1956).
9. LAUFBERGER, V., *Bull. soc. chim. biol.* **19**, 1575 (1937).
10. LITTLEFIELD, J. W., KELLER, E. B., GROSS, J. and ZAMECNIK, P. C., *J. Biol. Chem.* **217**, 111 (1955).
11. MAZUR, A., in GRAFF, S., *Essays in Biochemistry*, p. 198. John Wiley and Sons Inc., New York, 1955.
12. MAZUR, A., LITT, I. and SHORR, E., *J. Biol. Chem.* **187**, 473 (1950).
13. NOVIKOFF, A. B., BEAUFAY, H. and DUVE, C. DE, *J. Biophys. Biochem. Cytol.* **2** (Suppl.), 179 (1956).
14. PALADE, G. E., *J. Biophys. Biochem. Cytol.* **1**, 59 (1955).
15. PALADE, G. E. and SIEKEVITZ, P., *J. Biophys. Biochem. Cytol.* **2**, 171 (1956).
16. PETERMANN, M. L. and HAMILTON, M. G., *J. Biol. Chem.* **224**, 725 (1957).
17. PORTER, K. R. and BLUM, J., *Anat. Record* **121**, 281 (1955).

18. PRICE, V. E. and GREENFIELD, R., personal communication.
19. ROTHEN, A., *J. Biol. Chem.* **152**, 679 (1944).
20. SCHADE, A. L., OYOMA, J., REINHART, R. W. and MILLER, J. R., *Proc. Soc. Exptl. Biol. Med.* **87**, 443 (1954).
21. SCHNEIDER, W. C., *J. Biol. Chem.* **161**, 293 (1945).
22. SCHNEIDER, W. C. and HOGEBOM, G. H., *J. Biol. Chem.* **195**, 161 (1952).
23. SHODEN, A., GABRIO, B. W. and FINCH, C. A., *J. Biol. Chem.* **204**, 823 (1953).
24. SHORR, E., *Harvey Lectures* **50**, 112 (1954-1955).
25. UMBREIT, W. W., BURRIS, R. H. and STAUFFER, J. F., *Manometric Techniques and Tissue Metabolism*, p. 191. Burgess Publishing Co., Minneapolis, 1949.

The Ultrastructure of the Skeletal Muscle Myofilaments at Various States of Shortening

F. S. SJÖSTRAND and EBBA ANDERSSON-CEDERGREN

*Laboratory for Biological Ultrastructure Research
Department of Anatomy, Karolinska Institutet, Stockholm*

Received August 2, 1957

The ultrastructure of the myofilaments of skeletal muscle has been studied at various degrees of shortening and stretch of the muscle fibers. The material consisted of frog and mouse muscle.

The relation of the A- and I-band widths to the sarcomere length is fundamentally different when examining sarcomere lengths above and below the resting length. The increase of the sarcomere length when stretching above resting length is associated with a corresponding increase of the I-band width, the A-band width remaining fairly constant. Shortening below resting length is associated with a decrease of the A-band as well as the I-band width.

The mean diameter of the myofilaments within the different bands varies with the degree of shortening. The difference between stretched and shortened sarcomeres was 2.5-3 times (from 50-60 Å to 150 Å within the H-band). Within the H- and M-bands the mean diameter is proportional to the A-band width.

In the opaque part of the A-band extending between the H-band and the I-band the myofilaments can be split into several branches.

A substructure in the myofilaments has been observed. It appears as about 20 Å thick and about 100 Å long rodlets which seem to form parts of subfilaments arranged in a helical fashion.

When shortening the orientation of the substructural components changes from a roughly longitudinal to a transversal.

An interpretation of the observations is presented according to which the shortening is due to a folding of the subfilaments representing cables of supercoiled α -helices.

The biochemistry of muscle contraction has presented an impressive collection of descriptive data regarding the proteins of the muscle machine. Experiments on various models have clearly shown that a reaction more or less closely imitating or corresponding to that of the contracting living muscle may be provoked at various levels of structural organization. These experiments show that we are dealing with a labile

system of proteins. We are, however, lacking information as to the factors which are directly involved in the drastic reaction of these proteins when forced to contract. The ATP may transfer the energy necessary for the reaction, but what is the nature of the changes produced by this energy transfer?

We also lack a more precise knowledge regarding the molecular morphology of the contractile mechanism. There seems to be no reason to doubt that such a knowledge would give important hints as to the mechanism ultimately involved in contraction.

This investigation aims at an analysis of the molecular morphology of the contractile mechanism through a direct study by means of electron microscopy. The labile system that is studied and the crudeness of the techniques make such an analysis difficult and may well explain that conflicting results may be achieved by different investigators.

Our analysis deals primarily with the morphology of the individual myofilaments at various states of shortening of the muscle fibers. The results do not agree with those reported from studies on the organization of the myofilaments within the myofibrils and of the variations of A- and I-band width of the sarcomere (6, 7, 11, 12, 13).

MATERIAL AND METHODS

Frog leg muscles and frog abdominal muscles as well as the intercostal and abdominal muscles of the mouse have been fixed *in situ*. In order to reduce spontaneous shortening produced during the fixation, the frogs had been cooled down before fixation to a body temperature of about 0°C by keeping the animals in a cold room at -5°C. The mice were cooled down in the same way to a body temperature of about +20°C before the preparation started. For fixation an osmium tetroxide solution was used buffered to pH 7.2 by means of Michaeli's veronal acetate buffer and made isotonic by adding NaCl, KCl and CaCl₂. In a number of experiments fixation in 10% neutral formalin was also applied, followed by treatment in an osmium tetroxide solution for electron staining. The times in the OsO₄ solution have varied from 30 minutes to four hours. The prefixation in formalin for 15 minutes was followed by osmium tetroxide treatment for four hours.

In order to achieve rapid fixation of leg muscles the fascia was opened, and a part of the muscle fibers removed through careful dissection with glass instruments. The abdominal muscles of the frog and the mouse were fixed *in situ* by attaching a small glass collar to the abdominal wall with the skin removed and filling the glass collar with osmium tetroxide solution. The mice were kept under narcosis, the frogs were decapitated before the application of the osmium solution. Osmium tetroxide solution was also injected intraperitoneally inside the region where the fixative was applied externally. Shortening of the muscle fibers was attained by direct electric stimulation to tetanic contraction during the first 10 minutes of the fixation at about 0°C for frogs and about 20°C for mice.

After fixation the tissue was washed in Ringer's solution and dehydrated in a graded series of alcohol concentrations. Ethyl as well as isopropyl alcohol or acetone were used. Electron staining with phosphotungstic acid (PTA) was applied by adding 1% phosphotungstic acid to the alcohol used for dehydration.

The tissue was embedded in a mixture of n-butyl- and methyl methacrylate according to Newman, Borysko, and Swerdlow (15). The whole muscle portion that had been fixed *in situ* was cut out before or after the dehydration. The muscle tissue was divided into pieces of a suitable size when the embedding in plastic had been finished.

Sections were cut on Sjöstrand ultramicrotomes (16, 17) using either metal or glass knives. When cutting longitudinal sections the direction of the movement of the tissue block in relation to the knife edge was transversal with respect to the orientation of the myofilaments. Only sections which show dark grey reflections when floating in the liquid surface are sufficiently thin for a more detailed study. Silvery sections are too thick. The sections were collected on copper grids covered either with conventional formvar films or metallized formvar nets (18, 20).

The sections were examined in a modified RCA EMU 3a electron microscope* at 100 kV. A 50 μ objective aperture was used. The specimen holder was lengthened to allow an electron optical magnification of over 36,000 times.

RESULTS

The following description refers primarily to the morphology of the frog skeletal muscle. Apart from differences regarding details similar observations have been made on mouse muscle.

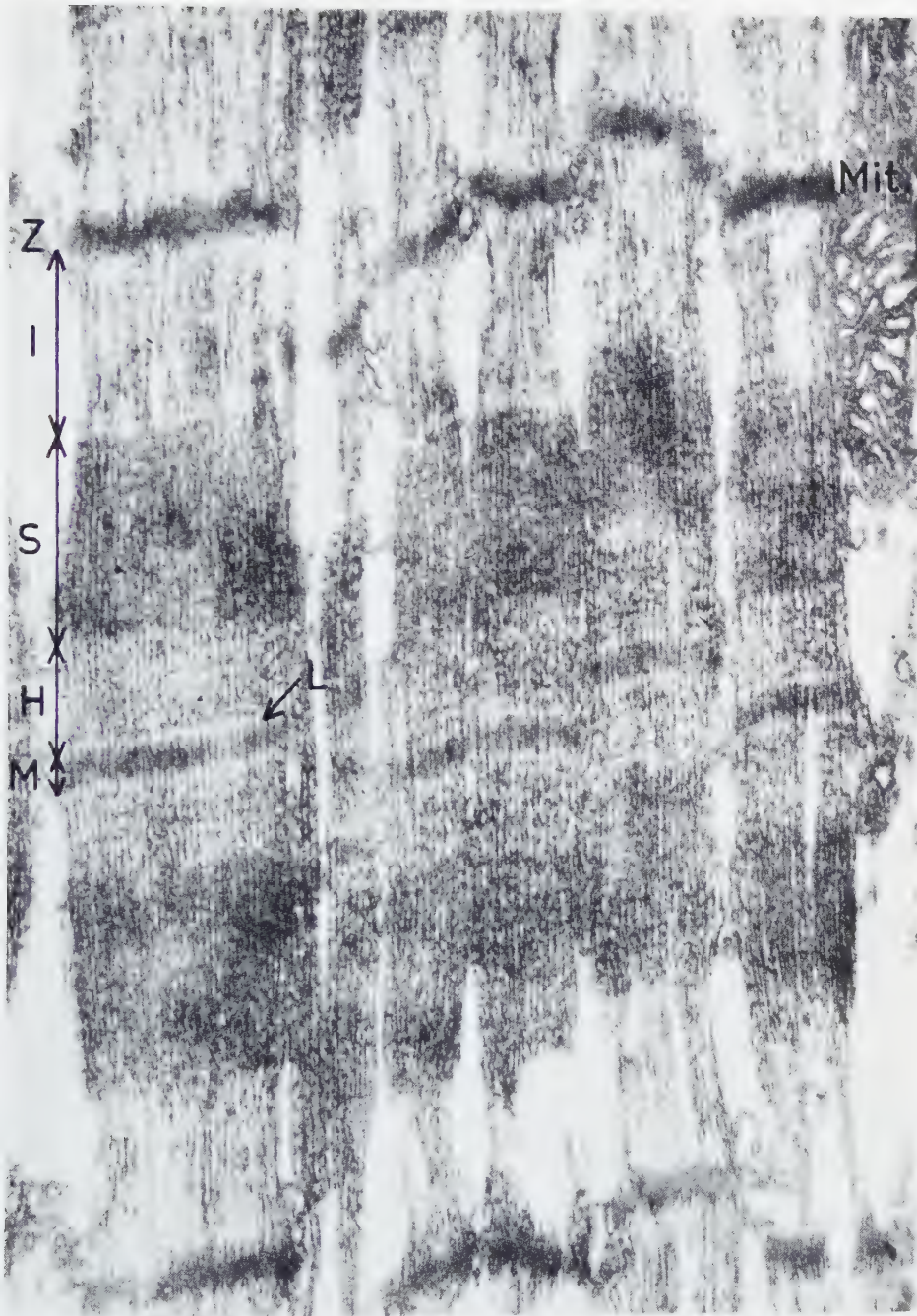
The sarcomere

The I- and the A-bands are easily distinguished through their great difference in opacity (Fig. 1). The M-band in the middle of the A-band is especially opaque. The H-zone extending symmetrically on both sides of the M-band may be more or less well differentiated. It is characterized by being slightly less opaque than the rest of the A-band. A narrow zone on both sides of the M-band appears lighter than the rest of the M-band. This zone will here be referred to as the light zone or the L-zone of the H-band.

The lengths of the sarcomeres may vary in different muscle fibers of the same specimen. By cooling the muscle tissue of frog to 0°C and of mouse to 20°C, the chances increase considerably for obtaining muscle fibers fixed at resting length without glycerination. However, there still occur shortened muscle fibers mixed with muscle fibers obviously fixed at resting length. During the dissection of the frog semitendinosus muscle a part of the muscle was completely removed and discarded. Another part was detached from its insertion and therefore could shorten under conditions that can be considered as roughly isotonic with a rather low load. Those contracting

* This microscope has been modified by Mr. Holmes Halma, R. C. A.

FIG. 1.—Survey picture of sarcomeres at resting length (2.3 μ) showing I-, N-, A-, H- and M-bands and Z-, S- and L-zones. *Mit.* = mitochondrion. $\times 62,000$.



muscle fibers which were left with intact relations to their tendons, on the other hand, contracted isometrically as the leg was kept firmly fixed in an almost extended position. Electrical stimulation of the frog muscle tissue cooled to 0°C results in a contraction which, however, not necessarily include all muscle fibers. It is therefore frequently possible to analyze shortened and presumably relaxed muscle fibers in the same specimen. Fixation of glycerinated muscles *in situ* is not accompanied by shortening of the sarcomeres.

The banding of the sarcomere varies with the length of the sarcomere. The most complete banding includes the M-band, the H-band and the L-zones of the A-band and the Z- and N-zones of the I-band. The M-zone is constant but, under certain conditions, no H-zone may be distinguished. These differences may be correlated with the length of the sarcomere and with the treatment of the muscle tissue prior to fixation. These relationships will be discussed further below.

It has been considered useful to distinguish the part of the A-band that extends between the H-zone and the I-band as the S-zone of the A-band. This zone has frequently been referred to as the dense or opaque zone of the A-band. When no H-zone appears to be present when examining the cross banding in a crude way, the reason is in fact not that the H-zone is lacking but that the S-zone is rather minute or lacking. As will be seen below the cross banding of the sarcomere is primarily due to differences regarding the morphology of the myofilaments.

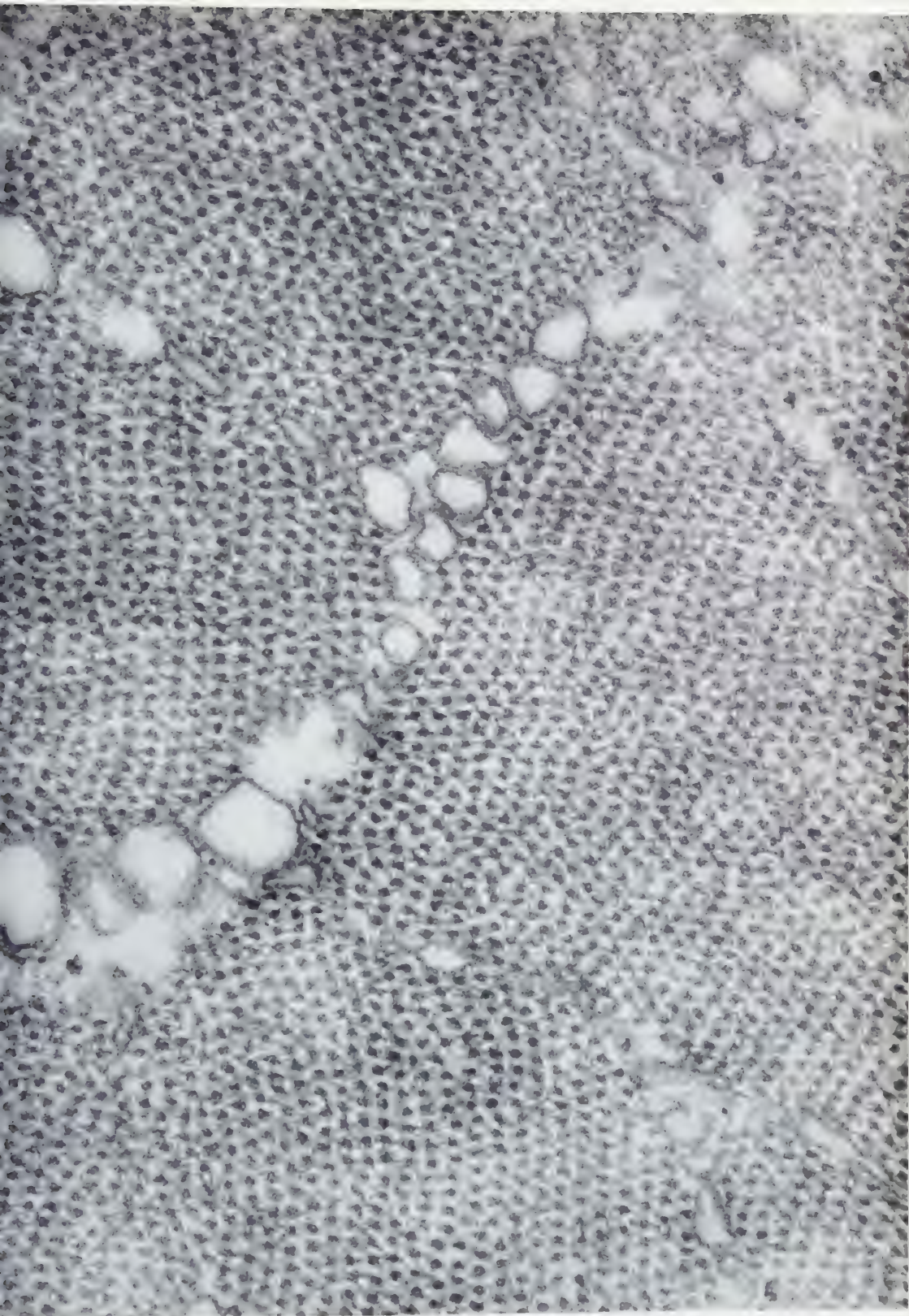
The myofibrils

The myofibrils are fairly irregularly outlined and appear as anastomosing regions of densely packed myofilaments and separated by irregularly arranged interspaces containing the sarcoplasmic components. Some of these components, for instance, the sarcotubules may be present in the central portion of what may be distinguished as a myofibril (1).

In the myofibrils, the myofilaments are arranged in a hexagonal array as is clearly shown in cross sections through the A-band (Fig. 2). In the I-band the arrangement of the myofilaments is more irregular. At the Z-zone, however, the hexagonal array is obvious.

At the Z-zone, the myofilaments stain heavily with PTA. They are mutually connected through bridges or branches. The filaments and the bridges form a very dense

FIG. 2.—Transversal section through frog semitendinosus muscle in isometric contraction. (Fig. 6 is a picture from a longitudinal section through the same piece of muscle tissue.) The cross sections of the myofilaments are arranged in a hexagonal array. The main part of the area represents the A-band. In the upper right corner the section is passing through an I-band region. Notice that only one type of myofilaments is present in the A-band region. Between the myofibrils the sarcotubules are seen. $\times 166,000$.



network (Fig. 3). These details can only be observed on very thin sections. On slightly thicker sections the Z-zone appears uniformly opaque and strongly stained due to superposition effects. The myofilaments then appear as glued together through some opaque interfilamentous material.

From the thinnest sections, which allow a detailed analysis, it is possible to conclude that no continuous membranous structure exists at the Z-zone. There is a Z-network of interwoven myofilaments, the meshes of which are more or less elongated and stretched parallel to the long axis of the myofilaments in sarcomeres at resting length. In shortened sarcomeres, the meshes are stretched in a transversal direction (Fig. 4). Therefore, the Z-zone appears thinner in shortened sarcomeres than in those at resting length.

Between the myofibrils, however, a membranous structure connects the adjacent Z-zones (2). This membranous structure appears as a flattened vesicle or a double membrane bounding a closed interspace. This structure seems to be rather labile, and when the myofibrils have been forced to slide in relation to each other the double membrane or vesicle is deranged. This structure will be referred to as the Z-membrane although no definite proofs have been presented whether we are dealing with a fenestrated membrane through the holes of which the myofibrils pass, or with a system of flattened vesicles or tubules.

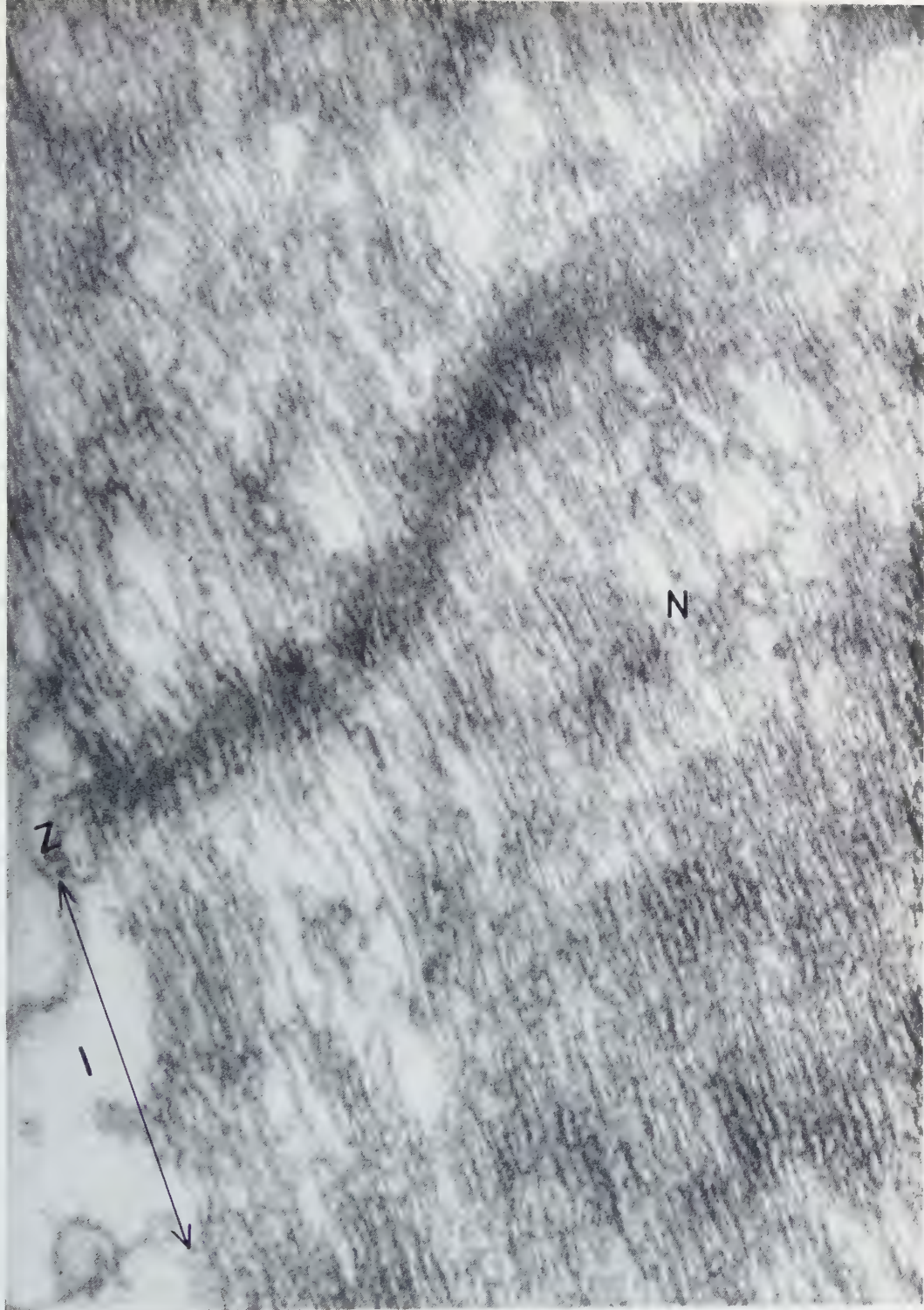
The system of sarcotubules in adjacent sarcomeres reach the Z-membrane structure, and the part of the sarcotubules closest to the Z-membrane structure is more or less widened. As has been described by Andersson-Cedergren (2) the sarcotubules do not seem to pass through the Z-membrane.

The transition between A- and I-bands is fairly abrupt. In shortened sarcomeres a narrow transition zone can, however, be observed in which the diameter of the myofilaments gradually decreases in the A-I direction.

The myofilaments

The myofilaments extend along the whole length of the sarcomere and pass through the Z-zone. The great difference in opacity of the various bands in the sarcomere, which is so obvious already at a low magnification, is mainly due to a variation of the thickness and arrangement of the myofilaments. In addition the interfilamentous material, represented mainly by transversally arranged bridges connecting adjacent myofilaments, contributes to this differentiation of the opacity.

FIG. 3.—Longitudinal section through the I-band of a muscle fiber at about resting length. Z-line appears as a dense network due to numerous branches connecting adjacent myofilaments. Notice the transition between A-band and I-band parts of the myofilaments. Within the I-band there are areas in which the I-band parts of the myofilaments form dense networks. These areas can be aligned in such a way that a transversal band is formed within the I-band. This band is interpreted as the N-band. $\times 155,000$.



We may distinguish between different parts of the myofilaments. The M-part is the thickest part. This part is characterized by very broad interfilamentous connections that appear as a homogeneous interfilamentous substance extending across the M-band region along its whole width. The H-part is somewhat thinner than the M-part. The bridges connecting adjacent myofilaments within the H- and S-zones are distinct and narrow. The light zone of the H-band (the L-zone) is characterized by a complete lack of cross-bridges. The absence of cross-bridges gives this zone its lesser opacity than the rest of the A-band.

In the zone which extends from the H-band to the I-band, and which here is called the S-zone, there are frequently more filamentous components present per unit area of a cross section than in the H- and M-bands. This fact can easily be established both in longitudinal and transversal sections. However, in many cases, as will be described below, no such difference in the number of filaments can be observed. The filamentous components in the S-zone can be identical as to their diameters, or the diameters can be different. These filamentous components of the S-zone can represent two different size classes, one with a diameter close to that of the H-band filaments and the other definitely thinner.

As branching of the myofilaments has been observed at the H-S-transition zone, the greater number of filamentous components in the S-zone has been interpreted as due to a splitting up or branching of the myofilaments. All these branches seem to continue into the I-band as I-band filaments of the regular I-band type.

The I-band zone of the myofilaments is characterized primarily by the rather uniform thickness of the myofilaments from the I-A-band transition zone to the Z-zone (Fig. 3). The I-band parts of the myofilaments are mutually connected to form a network with the meshes drawn out parallel to the length of the myofilaments. The interconnections are especially abundant in a narrow zone of the I-band. This zone seems to represent the N-band (Figs. 3 and 10). The myofilaments appear to stain less intensely in the I-band. This contributes with the smaller number of cross-bridges to the lower opacity of this zone.

The different parts of the myofilaments will here be referred to as their M-, H-, S-, and I-parts. The S-part is frequently lacking. In those cases the H-part directly continues into the I-part.

The cross striations of the myofibrils at various lengths of the sarcomere

The pattern of cross striations of the sarcomeres varies considerably with the degree of shortening or stretch (Figs. 1, 4-7). First two types of "contraction" patterns may be

FIG. 4. Survey picture of sarcomeres in a shortened muscle fiber. Length of the sarcomeres $1\ \mu$. 83,000.



distinguished. They can be considered as due to morphologically fundamentally different reactions of the contractile material.

The one pattern is characterized by a disorganization of the I-band structure with a random aggregation of I-band material at the Z-zone. This pattern corresponds to what usually is described as "contraction" bands. This pattern is frequently observed in connection with heavy electrical stimulation during the fixation.

The other "contraction" pattern, on the other hand, shows striking changes in the A-band associated with a reduction of the I-band width. Only this latter "contraction" pattern will be considered in more detail in this paper.

The width of the various bands within the sarcomere has been measured, and in Diagram 1 the band widths are presented as functions of the sarcomere length. These values were obtained from the material which has been used for the measurements of the diameters of the myofilaments. A similar result has been obtained by Andersson-Cedergren on an extensive material (unpublished). The diagram shows that the width of the I-bands as well as that of the A-bands decreases with the length of the sarcomeres within a range extending from about $2\ \mu$ down to below $1\ \mu$. At sarcomere lengths above about $2\ \mu$, the I-band width increases in direct proportion to the sarcomere length, and the A-band width remains roughly constant. The small decrease shown in Diagram 1 might well be accidental. Furthermore, the length of the S-part of the A-band decreases slightly with decreasing length of the sarcomere from about $2\ \mu$ to the minimum values for the sarcomere length which have been measured in this study. Above about $2.2\ \mu$ no indications, or only very weak indications of an S-part were observed. Glycerinated muscles represented exceptions from this latter observation. The S-part of the A-band can be absent or only indicated in shortened sarcomeres. It has not been observed in what has been interpreted as isometrically shortened sarcomeres. The points indicated by arrows in the diagram represent sarcomeres that presumably have shortened isometrically. In these cases the values for A- and I-band widths fall far off the respective curves. The A-band width is reduced, and the I-band width increased as compared to the values at resting length.

The form of the curves gains more interest when it is realized that the turning points of all the three curves are located at that length of the sarcomeres which closely corresponds to the resting length of the muscle.

The myofilaments at various degrees of shortening of the sarcomeres

The mean diameter of the myofilaments has been measured on high resolution electron micrographs of very thin longitudinal sections. These electron micrographs were taken at an electron optical magnification of over 36,000 times, and all micrographs were obtained under identical electron optical conditions. The myofilaments were measured on photographic prints representing a magnification of over 150,000

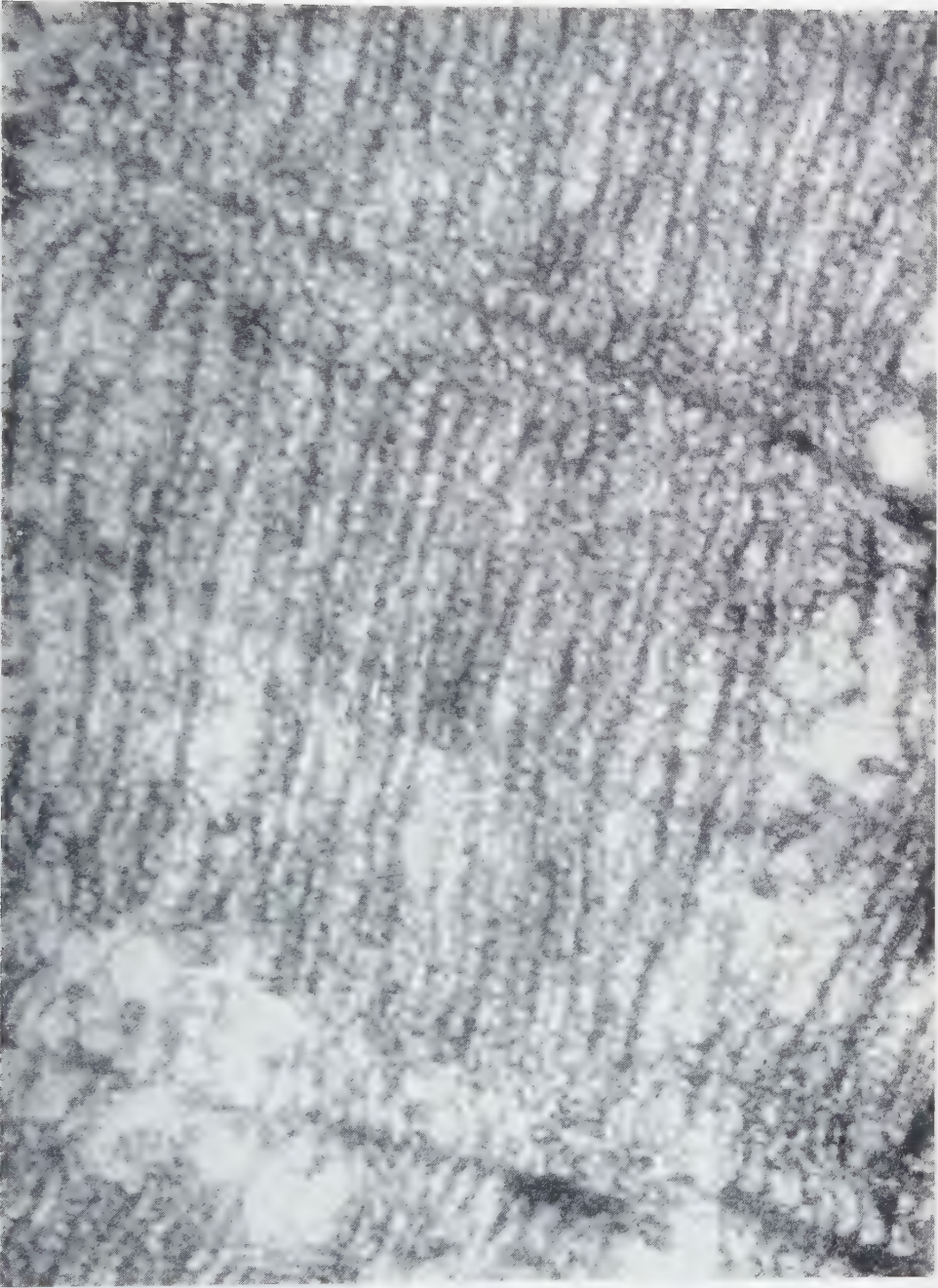


FIG. 5.—Extensively shortened sarcomere. The I-band filaments form a coarse network. Sarcomere length about 0.7μ . In spite of the high degree of shortening the A-band parts of the myofilaments do not reach in contact with the Z-line $\times 152,000$.

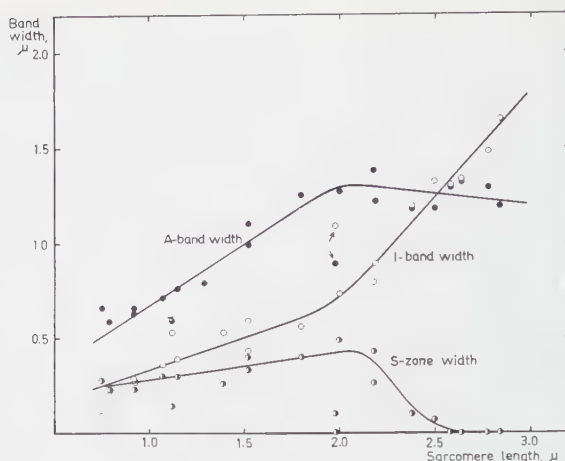


DIAGRAM 1.—The relation between A-band, I-band and S-zone width and the length of the sarcomere.

times. A magnifying (8 times) lupe with a scale divided into tenths of a millimeter was used. To secure a random selection of measuring points, lines were drawn on the prints across the myofibrils at random within the various bands. Each mean value is based on measurements on 25 myofilaments which appeared with sufficiently good contrast at the place where the lines crossed the myofilament to make a measurement possible.

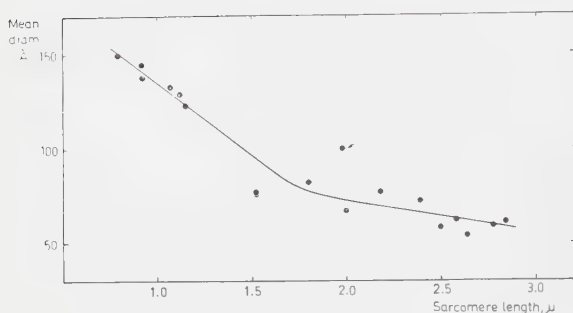
In order to check the reliability of the method for measuring the diameters of the myofilaments, double estimations were made on two different electron micrographs of the same sarcomere. The difference of the two mean values so obtained was 2–3 per cent.

The accuracy of these mean values varies somewhat with the dimension of the myofilaments. The values obtained for the thinnest myofilaments are probably too large as there are chances for the very thinnest filaments to escape observation due to their low contrast.

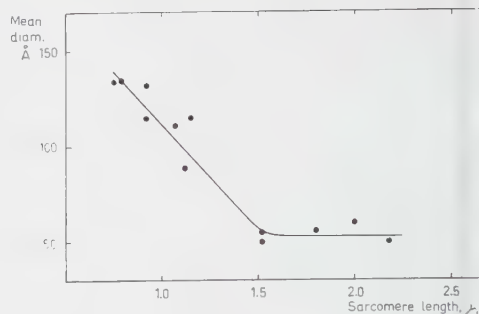
It is less reliable to measure the diameter of the myofilaments on cross sections because the form of the myofilaments is irregular. In a microtome section through a muscle fiber, about 100 Å thick and transversally oriented, the value for the diameter of the myofilaments will be represented by that at their thickest parts and, therefore,

FIG. 6.—Sarcomere in a muscle fiber which presumably has contracted isometrically. The I-bands are wide, the A-band width is reduced and the diameter of the myofilaments within the A-band is increased and corresponds in comparison with that formed at resting length to that of shortened sarcomeres with the same A-band width. Only one type of filaments is seen in the A-band corresponding to the information presented by Fig. 2. $\times 83,000$.

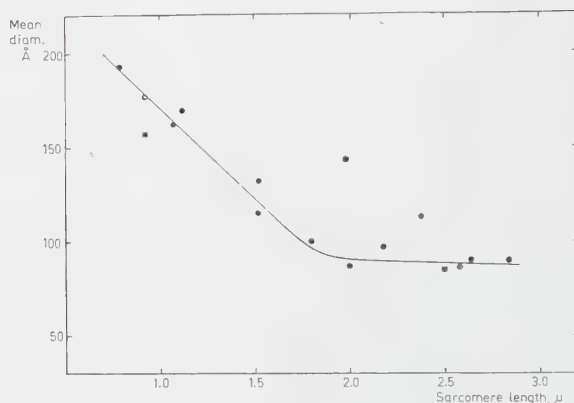




2.



3.



4.

DIAGRAMS 2-4.—The relation between the mean diameter of the myofilaments and the length of the sarcomere. Each point represents the mean value for 25 measurements. The arrow in Diagram 2 points to the value obtained from the same sarcomere as is indicated by arrows in Diagram 1. *Diagram 2*, H-band; *Diagram 3*, S-zone; *Diagram 4*, M-band.

it will not represent the average diameter. Furthermore, a certain evaporation of the methacrylate in the electron beam will make the ends of the myofilaments protrude over the surface of the methacrylate. These parts will be deformed due to surface tension forces and will flatten down towards the new level of the methacrylate surface.

The measurements of the diameters of the myofilaments require high resolution pictures taken very close to focus where the general background granularity due to

FIG. 7.—Sarcomeres in a muscle fiber in veratrin rigor. The I-bands are wide and the A-band width is reduced. The diameter of the myofilaments within the A-band is increased. Only one type of myofilaments could be observed in this specimen irrespective of the thickness of the sections. $\times 51,000$.





FIG. 8.—Myofilaments in a sarcomere which has been extended by stretch prior to fixation. Length of the sarcomere $2.9\ \mu$. Notice the small diameter of the individual myofilaments. $\times 148,000$.

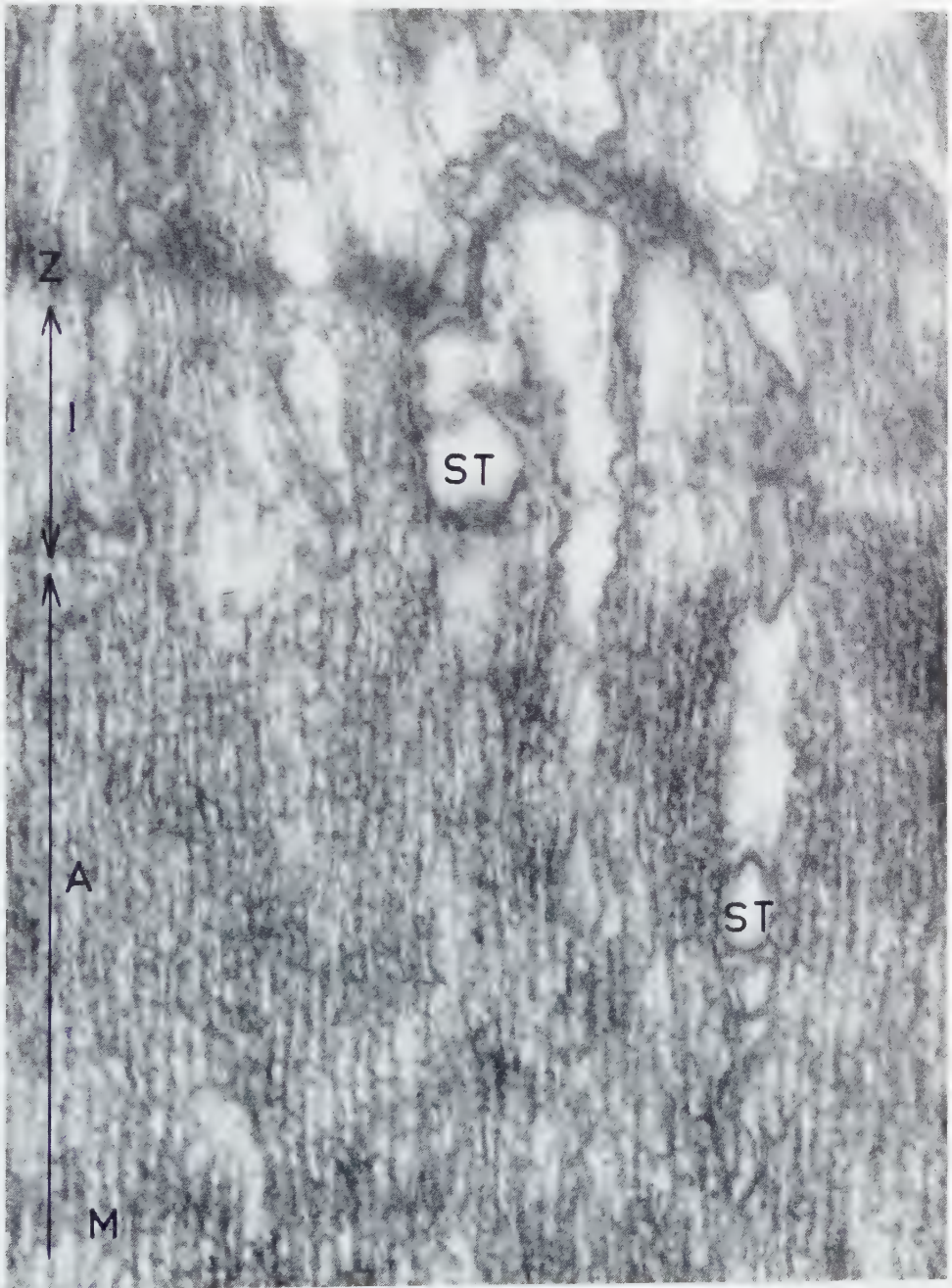
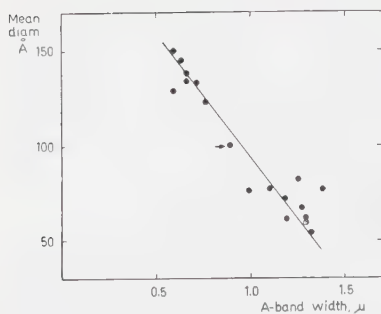
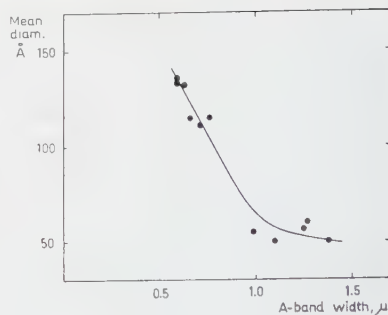


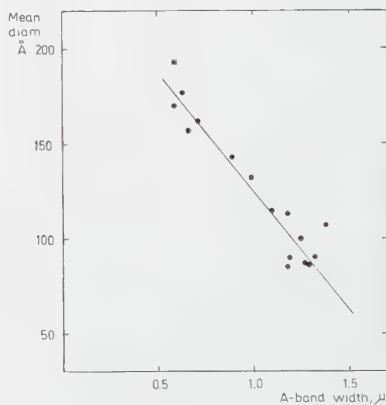
FIG. 9.—Myofilaments in a sarcomere at about 80% of average resting length. Notice the small diameter of the myofilaments. ST = sarcotubule. $\times 155,000$.



5.



6.



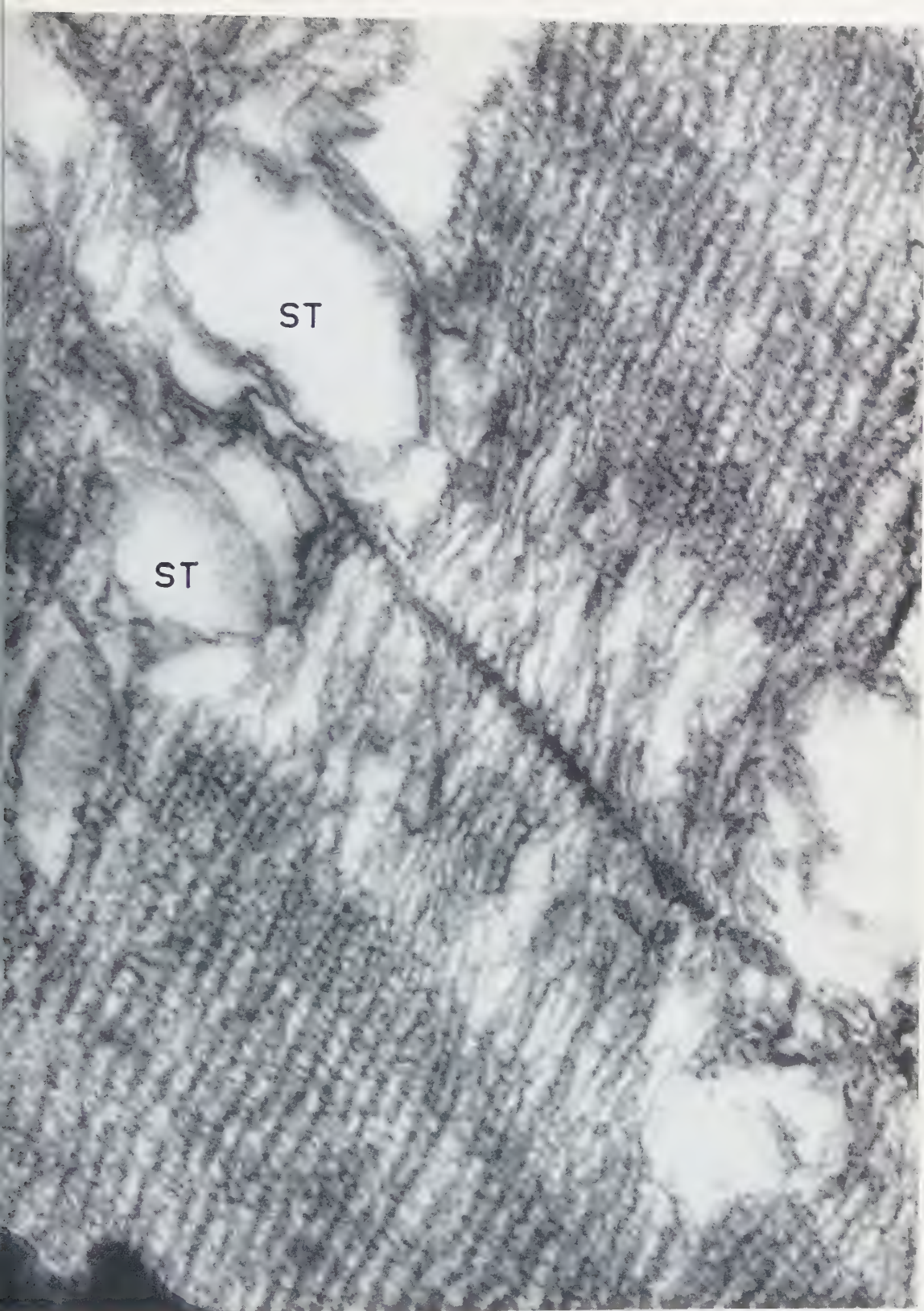
7.

DIAGRAMS 5-7. The relation between the mean diameter of the myofilaments and the A-band width. The arrow in Diagram 5 points to the value for the the same sarcomere as is represented in Diagrams 1 and 2 by arrows, the sarcomere that presumably has been fixed during isometric contraction. Diagram 5, H-band; Diagram 6, S-zone; Diagram 7, M-band.

phase contrast effects does not distort the contours. In order to obtain high resolution pictures which allow measurements where errors introduced by superposition effects are small, it is necessary to prepare very thin sections, that is, about 100 Å thick.

High resolution pictures of thin longitudinal sections of muscle fibers at various degrees of shortening show that the mean width of the myofilaments varies with the length of the sarcomeres (Figs. 8-12). In Diagrams 2-4 the mean diameters of the

FIG. 10.—Myofilaments in shortened sarcomeres. Sarcomere length 1.1 μ. Notice the diameter of the myofilaments in the A-band, the transversal orientation of opaque regions in the myofilaments and the numerous cross-bridges. ST = sarcotubule. $\times 152,000$.



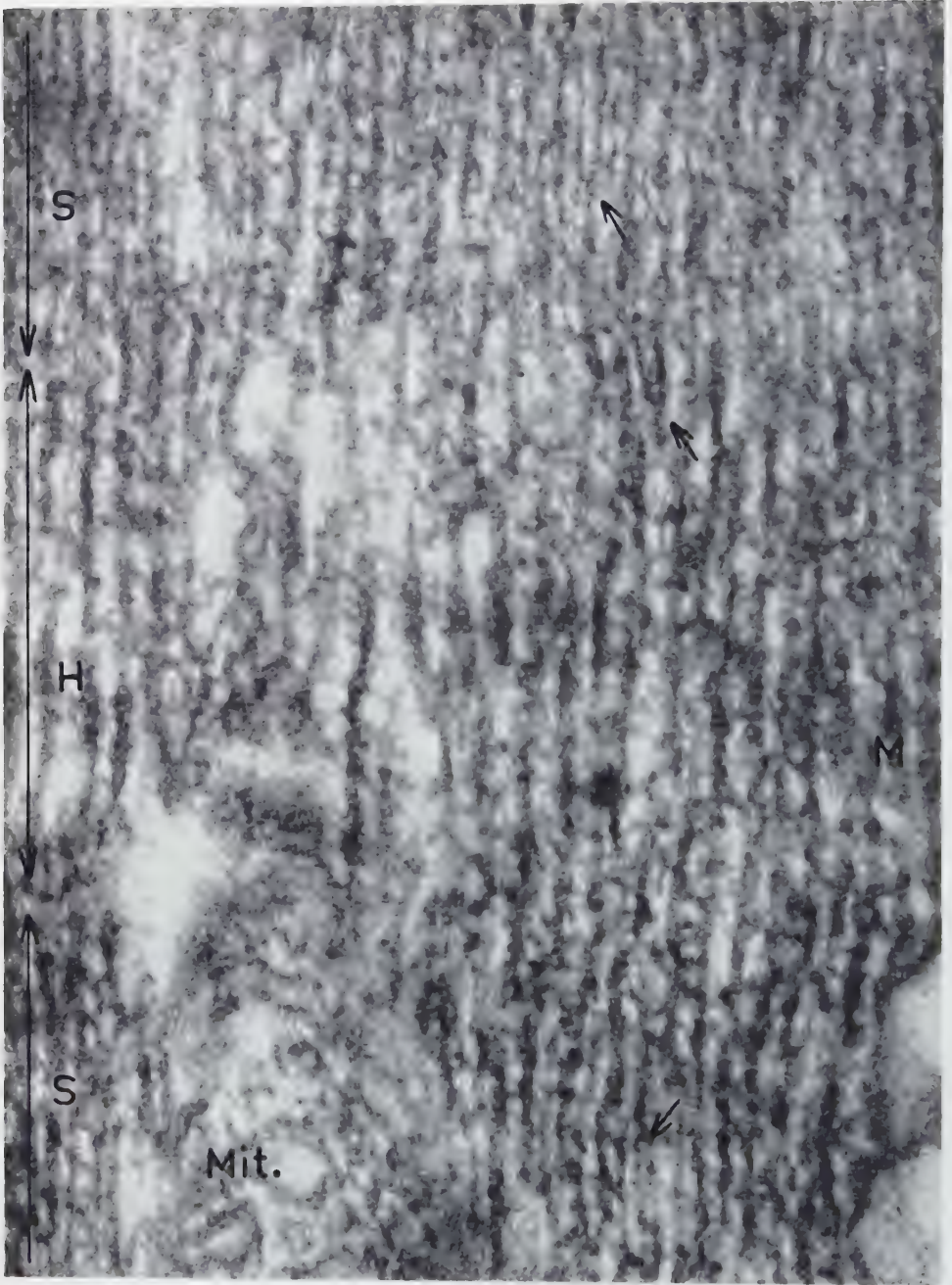


FIG. 11.—Myofilaments in the A-band of a slightly shortened sarcomere. The diameter of the myofilaments is larger in the H-band than in the S-zone. The filamentous components are more numerous in the S-zone. Branchings of the myofilaments can be observed (indicated by arrows). *Mit.* = mitochondrion. $\times 260,000$.

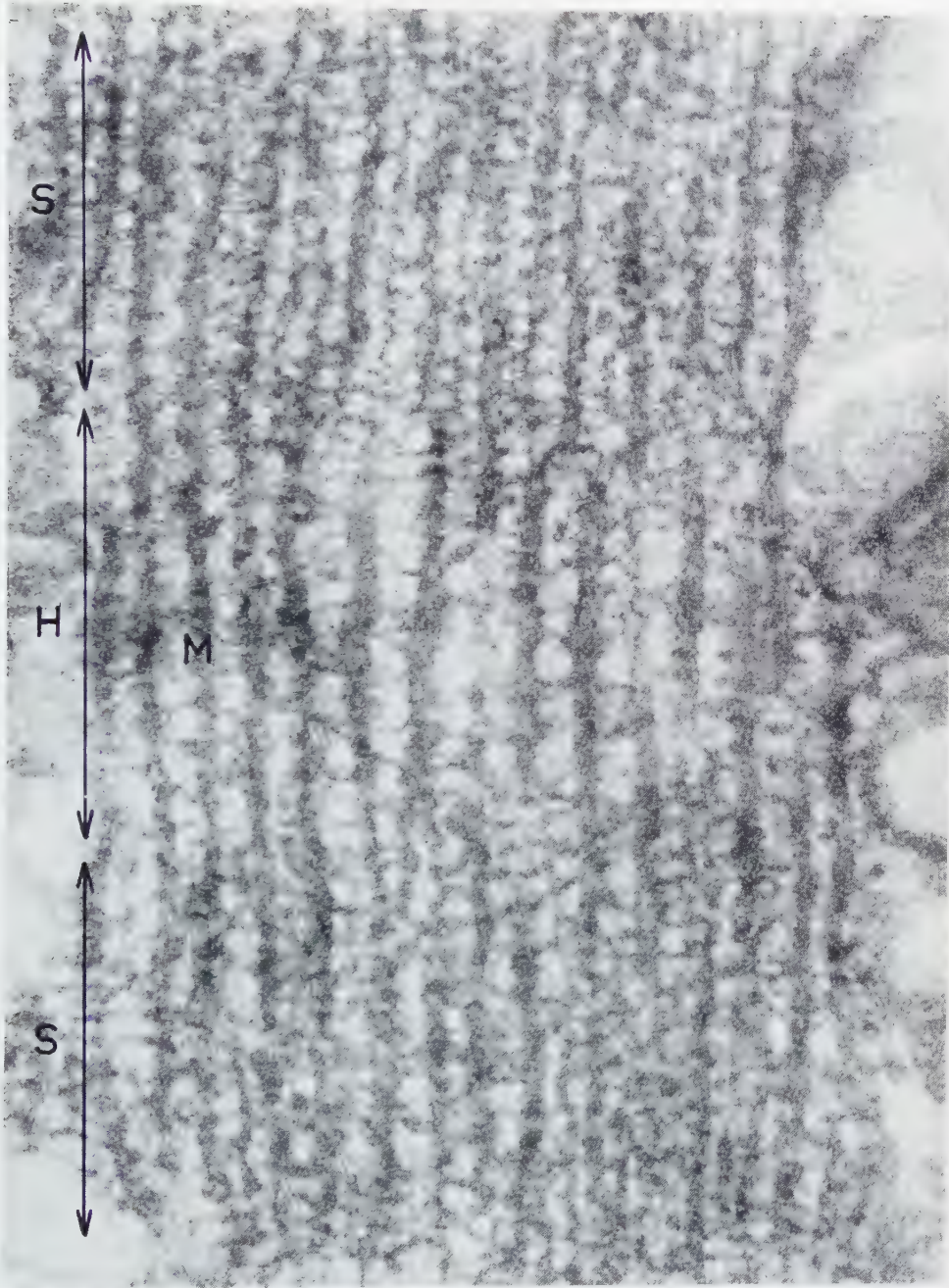


FIG. 12.—A region of a sarcomere corresponding to that of Fig. 11 but from a sarcomere that has shortened to about 50% of resting length. The diameter of the myofilaments is much larger than in Fig. 11 and there is an extensive variation of the diameter along each individual myofilament. Notice the transversal orientation of opaque regions in the myofilaments and the numerous cross-bridges. $\times 260,000$.

myofilaments in the H-, S-, and M-bands are plotted against the sarcomere length. Within the H-, S-, and M-bands the mean diameter of the myofilaments increases with decreasing length of the sarcomeres. The curve for the H-band shows a rather gentle slope between sarcomere lengths of 3 to below $2\ \mu$ but turns to a steeper course at the interval between $2\text{--}1.5\ \mu$. The minimum mean values represented by stretched muscle fibers are about $50\text{--}60\ \text{\AA}$, and the maximum values about $150\ \text{\AA}$, that is, a difference of 2.5–3 times.

The diameters of the myoflamentous components in the S-zone show a similar relationship with the exception that they seem to attain a certain minimum value of $50\text{--}60\ \text{\AA}$ which—as far as the present measurements show—is rather constant in the range from $1.5\ \mu$ to $2.2\ \mu$.

The M-part is the thickest part of the myofilaments. The diameter of this part also varies with the length of the sarcomeres as is obvious from Diagram 4. The mean thickness varies from $170\text{--}190\ \text{\AA}$ at a sarcomere length of $0.9\ \mu$ to $80\text{--}90\ \text{\AA}$ at a length of the sarcomeres of $2.5\text{--}3\ \mu$.

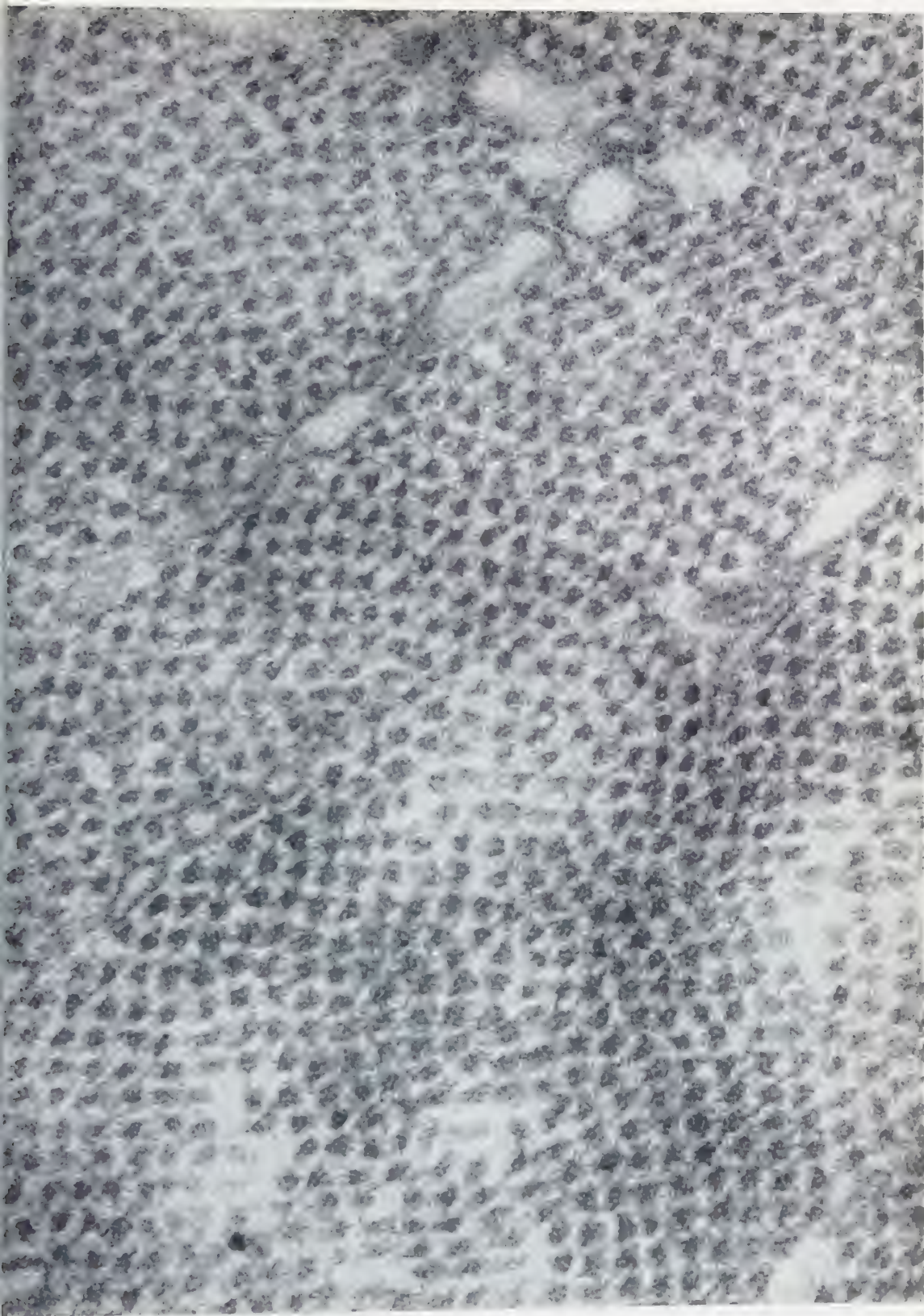
In Diagrams 5–7 the mean diameters of the myofilaments have been plotted as functions of the A-band width. The diameters of the myofilaments in the H- and M-bands are inversely proportional to the A-band width. The mean diameters of the myofilaments in the S-zone also increase with decreasing A-band width from $1\ \mu$ down, but at A-band widths of $1\ \mu$ to over $1.5\ \mu$ their diameters seem to be rather constant, $50\text{--}60\ \text{\AA}$.

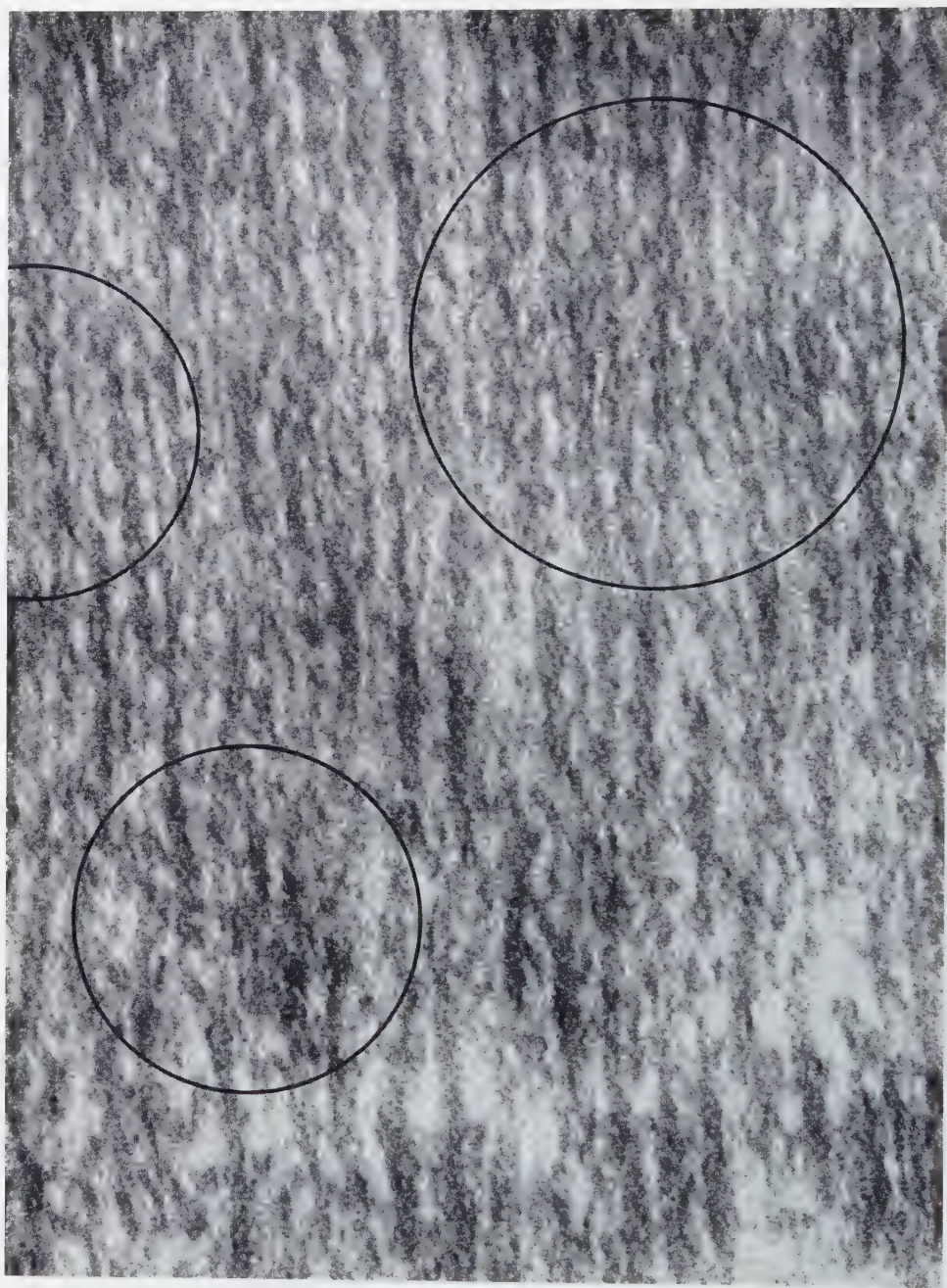
The form of the myofilaments in the A-band shows striking differences when comparing shortened and extended sarcomeres. In the shortened sarcomeres (Figs. 10 and 12), the diameter of the individual myofilaments varies considerably along their course. These variations may be as large as from 50 to $200\ \text{\AA}$. In the extended sarcomeres (Fig. 8) with their thinner myofilaments, the diameter is more uniform along the individual myofilaments with a variation of only about 100 %.

Due to the great variations of the diameter along the individual myofilaments the contours of the A-band parts of the myofilaments in the shortened sarcomeres are rather irregular, but there is a strikingly high frequency of protrusions showing an angular shape and pointing laterally. The contours can resemble the edge of a saw blade.

The myofilaments are mutually connected with thin cross-bridges. The thinnest bridges measure only about $20\ \text{\AA}$ in diameter. The bridges are more numerous in the S-zone. They appear to be more densely spaced in shortened than in extended sarcomeres. This assumption needs to be checked by quantitative estimations. The cross-bridges are lacking in the L-zone of sarcomeres at resting length.

FIG. 13.—Transversal section through the A-band. Notice the great number of triangular cross sections. $\times 260,000$.







FIGS. 14-15.—Myofilaments in a sarcomere at about resting length. The individual myofilaments show a complicated pattern due to differential staining of minute rod-shaped elements and of sub-filaments. The diameter of these elements is about 20 Å. $\times 300,000$ and $360,000$ respectively.

The cross sections of the A-band part of the myofilaments are angularly shaped with a strikingly high frequency of triangular forms (Fig. 13).

The I-band part of the myofilaments measures 30–40 Å in diameter.

The subunits of the myofilaments

In previous papers (19, 21, 22) the shortening of the myofilaments has been assumed to be due to a folding of subunits of the myofilaments. The complex form of the shortened myofilaments and the irregular arrangement of alternating regions of high and low opacity of these filaments seemed to make such an interpretation justifiable. Direct indications of the existence of such subunits were also found but in rather few cases.

It has now been possible to observe this substructure of the myofilaments more clearly (Figs. 14–16). The subunits are thin filaments or rodlets measuring 20 Å or less in diameter. The true value for the diameter might well be below 20 Å, but the specimen resolution of the present micrographs (slightly better than 20 Å) does not allow reliable measurements of finer dimensions.

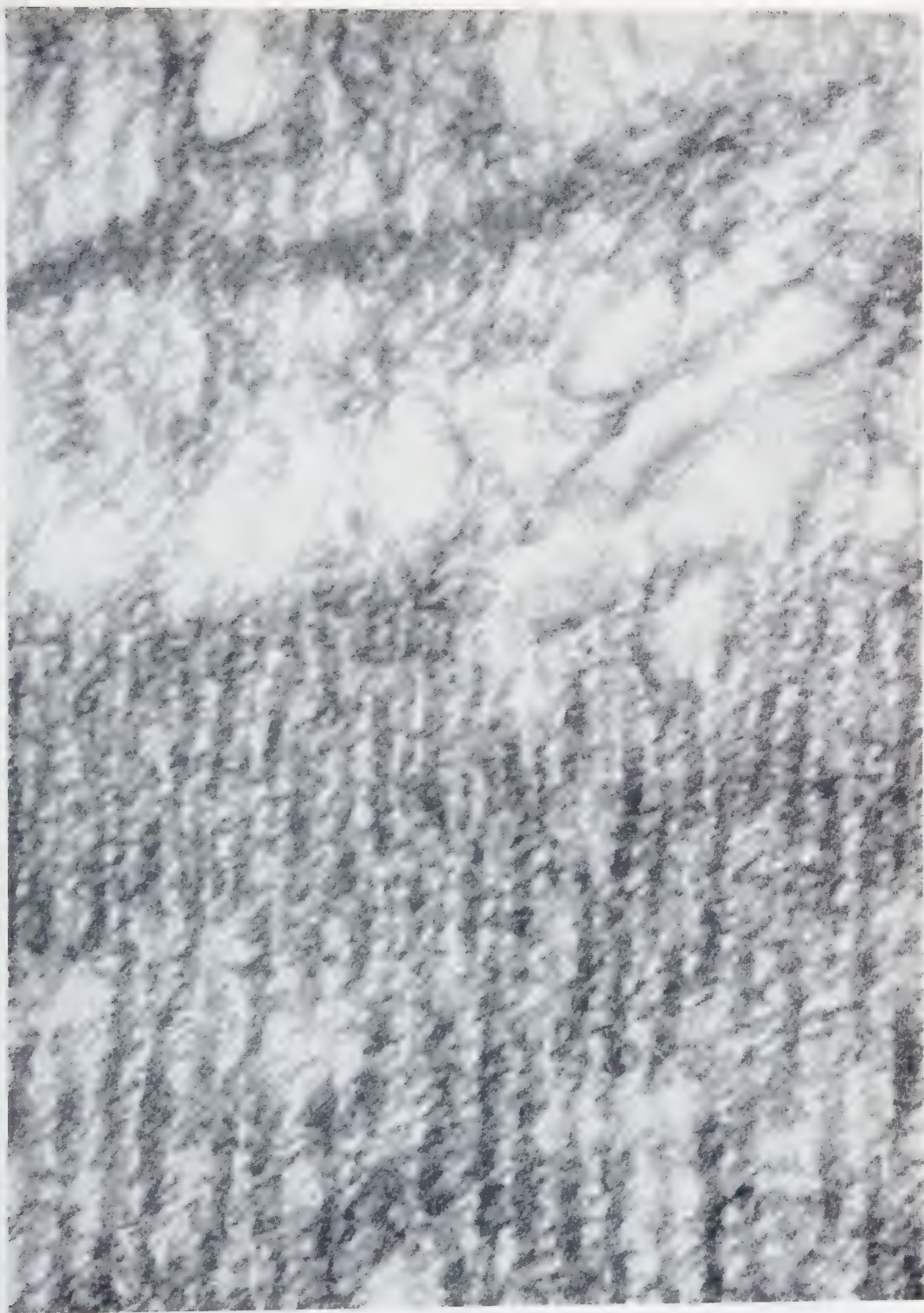
The mean length of the rodlets has been estimated in a crude way to be about 100 Å. They are mostly oriented obliquely to the axis of the myofilaments. Adjacent rodlets are oriented at different directions in such a way that they form angles. The angles pointing radially are obtuse and those pointing axially are acute in myofilaments of sarcomeres at resting length.

In muscle fibers at resting length these rodlets are frequently lined up in such a way that they appear as parts of a filamentous subunit. The diameter of the myofilaments varies along its length frequently in a fairly regular way. The mean distance between the narrower regions along the myofilament is about 200 Å.

The arrangement of the rodlets and the variation of the diameter of the myofilaments may be interpreted to reflect a helical arrangement of a few loosely twisted subfilaments with the axis of the helix corresponding to the axis of the myofilament. The spacing between the narrow regions along the myofilaments would then represent half the pitch of the helix.

In shortened sarcomeres the myofilaments show a complicated structure. The myofilaments are subdivided by transversally oriented, rather opaque cross-bands separated by less opaque regions (Fig. 16). Frequently the opaque cross-bands are very distinctly outlined, and they may appear as transversally oriented rodlets

FIG. 16. Myofilaments in a shortened sarcomere. The individual myofilaments in the A-band show a complicated pattern of transversally oriented frequently very narrow opaque regions. When looking at the A-band the picture appears as if the specimen had drifted during the exposure but a look at the I-band region shows no indication of such a drift. This reflects the dominance for transversally oriented substructures in the myofilaments in the A-band and the numerous cross-bridges. $\times 260,000$.



sometimes arranged in pairs like a sign of equality. The transversal orientation of the opaque bands can be so consistent that the image of the A-band region appears to have drifted in a transversal direction. A look at the structural details in the sarcomplasmic regions and in the I-band region on the same picture is then necessary to make sure that such an image defect has not produced a spurious cross-banding. The thickness of the opaque cross-bands varies, but the most distinctly outlined and most opaque cross-bands measure about 20 Å in thickness.

DISCUSSION

This study of the contractile elements of the skeletal muscle has been performed on muscle tissue fixed *in situ*, partially *in vivo* (mice), and partially immediately after decapitation (frogs). It seemed important to choose such experimental conditions that would involve as conservative a treatment of the tissue as the present technique permits. Therefore, extraction with glycerin has been applied only in certain cases as a first attempt gradually to remove structural components.

It has not been considered appropriate to use the property of reacting with a mechanical response, which more or less truly imitates that of living muscle tissue, as a criterion for an intact structural organization. The reason is that such a reaction has been demonstrated at various levels of organization of the muscle proteins. These levels are represented by the intact muscle fiber, the glycerinated muscle fiber, the artificial actomyosin threads with varying concentrations of proteins and by actomyosin gels. The conclusion that seems justifiable is that shortening and development of tension are not sufficient criteria for intact structural organization, but reflect some reactions in these protein systems that are rather independent of structural organization, with the exception that the imitation becomes more similar to muscle contraction the more the components are oriented in one main direction. The basic chemical events may well be identical in all cases. However, in intact muscle a system is present, which shows very high degrees of autonomy and of reversibility. These properties, it may be assumed, should be reflected in the structural organization characteristic for the intact muscle fiber and there are great chances that these structural characteristics are lost to a greater or lesser extent in the various models.

For a study of the behavior of the myofilaments at various degrees of shortening of a muscle fiber, it has been considered important to choose the myofilament itself as the object for an analysis instead of the cross-banding of myofibrils analyzed by means of light or interference microscopy. This means, however, that we are restricted to a study of fixed material. A very extensive experience from various kinds of tissues has shown that the most drastic effects on structural organization are produced by changing the normal milieu for cell components when these components still are in a

reactive state. The fixation seems to prevent these structural changes by drastically changing the reactivity, for instance, the enzymatic activities of the structural components. Against the artifacts introduced by fixation, we have to balance the drastic artifacts due to changes of the physiological milieu or to *post mortem* conditions in unfixed material. As to fixation artifacts, it seems justifiable to assume that they become less striking the higher the organization of the structural components because a high degree of organization means that numerous bonds are involved that stabilize, for instance, the supramolecular structural units. The artifacts mainly result in a randomness of the structural organization. That such an effect is present in the material described here is rather probable. However, x-ray studies of small angle diffraction of muscle have shown that the structural pattern in muscle has no very high degree of geometrical regularity.

The present study has dealt with the widths of the various cross-bands of the sarcomere as reflecting the differentiation of the myofilaments into a series of segments, and with the dimensions of the myofilaments at these various segments. All quantitative data have been correlated to the length of the actual sarcomere as an index of the degree of shortening. Only one type of shortening pattern has been considered, namely that characterized by a pronounced reduction of the I-band width with the structural organization within the remaining I-band unchanged.

The main results show that, under isotonic contraction, the I-band width as well as the A-band width decrease linearly with the sarcomere length within a range extending from resting length to about 30 per cent of the resting length. When the sarcomere has been stretched over resting length the increase in length of the sarcomere is due to a lengthening of the I-band.

The dense part of the A-band, which extends between the H-band and the I-band—in this study referred to as the S-zone of the A-band—decreases with shortening below the resting length. This zone may be completely absent or only indicated as a narrow transition zone at the A–I-boundary when the sarcomere has been stretched over resting length. It can also be absent in shortened sarcomeres, and was absent in isometrically contracted sarcomeres.

In the S-zone the number of filamentous elements can be greater than in the H-band. This difference has been interpreted as due to a branching of the myofilaments at the H–S-boundary. When no S-zone can be observed no such branching is present. The myofilaments then extend uniformly from the M-band, where their diameter is larger, to the A–I-boundary. The possibility that this variation in appearance is due to differences regarding the orientation of the sections with respect to the array of the myofilaments is easily excluded by the fact that a great number of sections have been examined all of which exhibit the same pattern. The possibility that the thickness of the sections would be responsible for these observations is also excluded because

sections of quite different thickness have been examined down to a thickness where only parts of the myofilaments have been chipped off. Furthermore, the transversally oriented sections of the same muscle fibers do not show but one type of cross sectioned myofilaments in these cases.

In the cases where a branching of the myofilaments has been observed and where the branches have represented two classes as to the dimension of their diameters, these two classes have also been observed in transversally oriented microtome sections. A pattern identical to that originally described by H. E. Huxley is then observed. This pattern Huxley interpreted as indicating the existence of two different sets of myofilaments. According to Huxley only the thin components were continuous with the I-band filaments. This assumption finds no support in the present analysis where it has been observed repeatedly that the thick component are likewise continuous with the I-band filaments. Spiro (23) has observed that the number of filamentous components is identical in the opaque zone of the A-band and in the Z-zone. He therefore concludes that all filaments in the A-band are continuous with the I-band filaments.

The behavior of the A- and I-band widths as observed here agrees, as far as a comparison is possible, fairly well with the results reported by Knappeis and Carlsen (14), (compare Fig. 1 in the latter paper). Their results are, however, not comparable at sarcomere lengths below resting length as they were studying contracted sarcomeres with I-band contractions. With their experimental technique, the estimations of the I-band width in sarcomeres that had shortened below resting length were unreliable (the length of the I-band was assumed identical to the width of the Z-line of the sarcomere at resting length).

Villafranca (24) studied the band widths of stretched rabbit psoas fibers and found no appreciable effect on the A-band width. The dense zone of the A-band, here called the S-zone, decreased with stretch. These results are confirmed by the present study with the exception that the S-zone in the latter case was more drastically reduced in connection with stretch. However, according to our observations this seems not to be the case if the muscle fibers have been glycerinated before fixation as was the material of Villafranca.

The present results do not agree with those of Hanson and H. E. Huxley (7, 13) on isolated and glycerinated rabbit psoas myofibrils which were contracted through ATP. Nor do they agree with those of A. F. Huxley and Niedergerke (11) on surviving frog fibers. The explanation for these discrepancies seems to be that these authors have studied mainly muscle fibers or myofibrils above resting length, and they have observed the states of shortening below resting length of the sarcomeres only to a rather limited extent.

A. F. Huxley and Niedergerke in fact report on a definite decrease of the A-band width in connection with a shortening below a sarcomere length of 2.5μ .

It is also obvious from the data of Hanson and H. E. Huxley that a reduction of the A-band width is noticeable at the shortest sarcomere lengths that were measured in spite of these lengths being only slightly below the length of the unstretched sarcomere, 2.4μ (only a small group of values for sarcomeres belonging to the shortest group, $1.7\text{--}2.0 \mu$).

The present results are in good agreement with those of Engelmann (5) who studied the change of band width at various states of contraction by means of polarization optical analysis of living and fixed muscle fibers.

That the A-band width decreases during isometric shortening was demonstrated by Buchthal *et al.* (4) and by Buchthal and Knappeis (3) on living isolated frog muscle fibers. Their experiments on isotonic contractions they evaluated as less reliable since the actual resistance to shortening could not be defined. These experiments did not show any appreciable effect on the I-band width. This result might reflect that the conditions for contraction, in fact, were not strictly isotonic.

No obvious changes of the structure of the individual myofilaments have been observed earlier in connection with a shortening of the muscle fibers. Wide angle x-ray data have not revealed any changes of intramolecular spacings indicating folding of the peptide chains within the physiological range of shortening.

In the present study, a change with shortening of the mean diameter of the myofilaments within the A-band has been observed. There is an inverse linear relationship between the A-band width and the mean diameter of the myofilaments. The diameter of the myofilaments in sarcomeres shortened to 30–50 % of resting length is about three times as large as that of moderately stretched myofilaments.

The curve illustrating the relationship between the diameter of the myofilaments and the sarcomere length shows a knick at sarcomere lengths between 2.0 and 1.5μ . The curves illustrating the I- and A-band widths as a function of sarcomere length also show knicks at about the same values for the sarcomere length. The resting length of the sarcomeres after fixation we estimate to $2.0\text{--}2.4 \mu$ from the fact that longer sarcomeres were observed only in stretched muscles. Knappeis and Carlsen (14) estimate the resting length to 2.2μ for frog semitendinosus muscle. The present observations seem to indicate that the shortening down to somewhere slightly below resting length is mainly due to a transformation of the I-band part of the myofilaments to the structural pattern characteristic for the S-zone of the A-band part. The part added to the A-band does not result in any more pronounced increase of the A-band width due to a shortening of the A-band part of the myofilaments. At small degrees this shortening masks the adding of material from the I-band. More extensive short-

ening is associated with a pronounced shortening of the A-band parts of the myofilaments and a rapid increase of the diameter of these parts. With shortening the width of the S-zone of the A-band decreases to about 50 % of that at resting length, and in some cases no S-zone was observed in shortened sarcomeres.

Another possible explanation for the lengthening of the I-band at stretch might be that the N-zone of the I-band is stretched. This zone represents a rather dense network at resting length and can contain 20 Å thick rodlets similar to those of the myofilamentous subunits within the A-band.

The following interpretation of the structural changes during shortening may be proposed. The myofilaments represent continuous structural elements extending through the whole sarcomere and through the Z-zone. The cross striations reflect different reversible states regarding the structural organization of the myofilaments. Each myofilament consists presumably of three filamentous subunits. These subunits consist of rows of rodlets which stain well with PTA and measure 20 Å or less in diameter and about 100 Å in length. The subunits are assumed to represent cables of supercoiled α -helices. The arrangement of these subunits varies in the different states of the myofilaments. In the I-band part of the myofilaments, the subunits are stretched and closely packed. In the H-band part of the myofilaments, the helically wounded subunits form a fairly loose supercable. The pitch of the helix is estimated to roughly 400 Å. A full turn of each filamentous subunit involves four about 100 Å long rodlets. In the S-zone of the A-band the supercable can be split. When shortening, the subunits fold within the A-band part of the myofilaments and the close packing of the subunits in the I-band part is lockered as a preparation for shortening through folding. The folding appears to be due to a rearrangement of the cables of α -helices without changing the basic α -pattern of the individual helices. This is in agreement with the x-ray data showing no change in the α -configuration of the muscle proteins at this range of sarcomere lengths. The changes of the structural arrangement take place in a three dimensional network. It seems justifiable to assume that the subunits correspond to the myosin. However, preliminary experiments on the structural changes produced by extracting the muscle proteins with various standard solvents have given results that are rather difficult to interpret for the time being and therefore experimental evidence for this assumption is lacking.

When assuming that the structural arrangement of subunits within the myofilaments differs in different parts along the myofilament, it seems possible to explain differences in the solubility of these various parts without presuming that there is any fundamental difference in chemical composition. Thus, the experiments on extraction of myosin with microscopical observation of the effect on the various cross-bands (7) do not necessarily prove that the I-band parts of the myofilaments have a chemical composition that basically differs from that of the A-band parts. It is,

however, not impossible that the structural difference of the I-band parts of the myofilament as compared with the A-band parts can be due to a high actin and low myosin concentration in the I-band parts.

The results reported in this study are in obvious conflict to what would be expected from the hypothesis of Hanson and H. E. Huxley (7, 13) and of A. F. Huxley (10). This hypothesis was mainly based on an analysis of the band widths at various degrees of stretch. It supposes that two kinds of myofilaments would exist, the actin filaments extending through the I-band and the S-zone of the A-band, and the thicker myosin filaments confined to the A-band. During shortening the actin filaments would move between the myosin filaments towards the M-band. This mechanism would not involve any change of the diameter of the myofilaments; it would mean an increase of the width of the S-zone with shortening, the formation of a contraction band at the M-band due to a folding up of the central ends of the actin filaments, and a formation of a contraction band at the Z-zone due to an accumulation of the myosin.

In this study a striking variation of the thickness of the myofilaments with the sarcomere length has been observed; the S-zone *decreases* with shortening, and no contraction bands have been observed at the M-band or the Z-zone at degrees of shortening down to about 30 % of resting length. The contraction bands that under certain conditions can occur at the Z-band are due to an aggregation of the I-band part of the myofilaments and not to an aggregation of the A-band part.

Filamentous components with different thickness, sometimes representing two size classes, can occur in the S-zone. These filamentous components have here been interpreted as branches of the myofilaments. That the thicker components are continuous with I-band filaments as well as the thinner components has been observed. According to Hodge (8, 9) analyzing dipteran flight muscle, only one type of myofilaments would exist and these myofilaments were continuous through the A- and I-bands.

Furthermore, the myofilaments are interconnected by a great number of cross-bridges as demonstrated by Hodge in dipteran flight muscle. These cross-bridges are abundant in the S-zone. The rather dense network so formed seems difficult to consider consistent with the sliding mechanism of Hanson and H. E. Huxley, and of A. F. Huxley.

This study has demonstrated that a change in the length of the sarcomeres in this material was accompanied with a change in the organization of the individual myofilaments. It is impossible to tell what relation this kind of shortening has to the physiological contraction of the muscle fiber. However, the present results clearly show that in the muscle fiber there exist definite conditions for shortening through a mechanism involving a structural change of the individual myofilaments.

REFERENCES

1. ANDERSSON, EBBA, *Proc. Stockholm Conf. Electron Microscopy*, 1956, p. 208. Almqvist & Wiksell, Stockholm, 1957.
2. ANDERSSON-CEDERGREN, EBBA, *J. Ultrastructure Research* **1**, in press.
3. BUCHTHAL, F. and KNAPPEIS, G. G., *Skand. Arch. Physiol.* **78**, 97 (1938).
4. BUCHTHAL, F., KNAPPEIS, G. G. and LINDHARD, J., *Skand. Arch. Physiol.* **73**, 163 (1936).
5. ENGELMANN, TH. W., in *Pflügers Arch. ges. Physiol.* **18**, 1 (1878).
6. HANSON, JEAN and HUXLEY, H. E., *Nature* **172**, 530 (1953).
7. ——— *Symposia Soc. Exptl. Biol.* **9**, 228 (1955).
8. HODGE, A. J., *J. Biophys. and Biochem. Cytol.* **1**, 361 (1955).
9. ——— *Proc. 3rd Internatl. Conf. Electron Microscopy, London*, 1954, p. 572. Royal Microscopical Society, London, 1956.
10. HUXLEY, A. F., *Progr. Biophys. and Biophys. Chem.* **7**, 257 (1957).
11. HUXLEY, A. F. and NIEDERGERKE, R., *Nature* **173**, 971 (1954).
12. HUXLEY, H. E., *Biochim. et Biophys. Acta* **12**, 387 (1953).
13. HUXLEY, H. E. and HANSON, JEAN, *Nature* **173**, 973 (1954).
14. KNAPPEIS, G. G. and CARLSEN, F., *J. Biophys. Biochem. Cytol.* **2**, 201 (1956).
15. NEWMAN, S. B., BORYSKO, E. and SWERDLOW, M., *J. Research Natl. Bur. Standards* **43**, 183 (1949).
16. SJÖSTRAND, F. S., *Experientia* **9**, 114 (1953).
17. ——— *Physical Techniques in Biological Research*. Vol. III, p. 241. Academic Press, New York, 1956.
18. ——— *Exptl. Cell Research* **10**, 657 (1956).
19. ——— *Klin. Wochschr.* **35**, 237 (1957).
20. ——— *Proc. Stockholm Conf. Electron Microscopy*, 1956, p. 120. Almqvist & Wiksell, Stockholm, 1957.
21. SJÖSTRAND, F. S. and ANDERSSON, EBBA, *Exptl. Cell Research* **11**, 493 (1956).
22. ——— *Proc. Stockholm Conf. Electron Microscopy*, 1956, p. 204. Almqvist & Wiksell, Stockholm, 1957.
23. SPIRO, D., *Exptl. Cell Research* **10**, 562 (1956).
24. VILLAFRANCA, G. W., *Exptl. Cell Research* **12**, 410 (1957).

NOTICE TO AUTHORS

Journal of Ultrastructure Research publishes papers dealing with the ultrastructural organization of biologic material as analyzed by means of electron microscopy, X-ray diffraction techniques, X-ray microscopy, and polarization optical analysis. Papers dealing with techniques and instruments which are of importance for the development of this field will also be accepted. The field covered by the journal extends from the structure of molecules which are of biologic interest to the level of cell and tissue organization at the limit of the range of light microscopy.

Address: The author's complete address should be placed on the manuscript.

Manuscript: Manuscripts should be sent to the Editorial Office, Department of Anatomy, Karolinska Institutet, Stockholm 60, Sweden. Manuscripts in English, French or German are accepted. The manuscripts should be typed double-spaced on one side of the paper only. Footnotes should be avoided, but if used they must be numbered consecutively and placed on a separate sheet at the end of the manuscript. Authors are requested to conclude their manuscripts with a brief summary not exceeding 150 words, and to indicate an *abbreviated running title* on the title page. Descriptions of technique and sections of minor importance will be printed in small type.

Manuscripts should be submitted in complete and final form for publication. The policy of the editors will be as prompt a publication as is possible. Papers will be published within three to six months after the date of receipt of the manuscripts by the Editors. Galley proofs will be sent to the authors who are requested to return them together with proofs of the figures immediately by air-mail to the Editorial Office. The point of insertion of each figure should be indicated.

Tables and Figures: The dimensions of the printed page, 5" × 7" or 125 × 175 mm, should be kept in mind in preparing figures and tables for publication. Each table should be typewritten on a separate sheet and all figures and tables should be identified with the author's name. Figure legends should be typed in sequence on a separate sheet. Graphs and diagrams should be carefully drawn in black ink on white paper or blue coordinate paper, and all drawings should be so prepared and lettered that they can stand a reduction of 50 per cent. No illustrations in color will be accepted unless the author is prepared to cover the cost of reproduction.

Literature cited: Papers referred to in the manuscript should be listed on a separate page and headed "References". The journal, volume, page number, and year of publication should be indicated. The system of abbreviation given in "List of Periodicals" in *Chemical Abstracts*, 45, No. 24, Part II (1951), should be followed. The references should be arranged in alphabetical order according to the (first) author's surname. They should also be numbered so that each may be referred to in the text by number only. Please follow carefully the following style for punctuation and order of listing:

1. LACY, D., *Nature* **173**, 1235 (1955).
2. PRICE, G. R. and SCHWARTZ, S., *Physical Techniques in Biological Research*, Vol. III, p. 91. Academic Press, New York, 1956.
3. SZENT-GYÖRGYI, A. G., MAZIA, D. and SZENT-GYÖRGYI A., *Biochim. et Biophys. Acta* **16**, 339 (1955).

Reprints: Authors will be furnished, free of charge, with fifty reprints without covers. Additional reprints may be obtained at cost. Order forms will be submitted with the galley proofs. These should be filled in, indicating shipping and billing instructions, and returned with the proofs.

Abstracts: Authors are requested to provide an abstract for *Biological Abstracts* on a special form which is submitted with the galley proofs.

Now complete

PHYSICAL TECHNIQUES IN BIOLOGICAL RESEARCH

Edited by GERALD OSTER, Polytechnic Institute of Brooklyn
and ARTHUR W. POLLISTER, Columbia University

VOLUME 3 Cells and Tissues

1956, 728 pp., illus., \$16.50

CONTENTS:

- | | |
|---|--|
| Freeze-Drying. <i>By L. G. E. Bell</i> | Microphotometry with Visible Light. <i>By</i> <i>Hewson Swift and Ellen Rasch</i> |
| Phase Contrast and Interference Microscopy in Cytology. <i>By R. Barer</i> | Ultraviolet Absorption Techniques. <i>By Peter</i> <i>M. B. Walker</i> |
| Fluorescence Microscopy. <i>By George R. Price</i> <i>and Samuel Schwartz</i> | Historadiography. <i>By Arne Engström</i> |
| Birefringence and Dichroism of Cells and Tissues. <i>By Fritz Ruch</i> | Autoradiography at the Cellular Level. <i>By</i> <i>J. Herbert Taylor</i> |
| Electron Microscopy of Microorganisms. <i>By</i> <i>Thomas F. Anderson</i> | Manometric Techniques for Single Cells. <i>By</i> <i>H. Holter, K. Linderström-Lang, and E.</i> <i>Zeuthen</i> |
| Electron Microscopy of Cells and Tissues. <i>By Fritiof S. Sjöstrand</i> | Microtomy. <i>By Mark E. Gettner and Leo-</i> <i>nard Ornstein</i> |
| Techniques for the Mass Isolation of Cellular Components. <i>By Norman G. Anderson</i> | AUTHOR INDEX—SUBJECT INDEX. |

Previously published:

VOLUME 1 **Optical Techniques**. 1955, 564 pp., illus., \$13.50

VOLUME 2 **Physical Chemical Techniques**. 1956, 502 pp., illus., \$12.80



ACADEMIC PRESS INC., Publishers

111 Fifth Avenue, New York 3, New York, U.S.A.

British Office: ACADEMIC BOOKS LTD., 129, Queensway, London W. 2

German Agent: MINERVA, G.M.B.H., Holbeinstrasse 25-27, Frankfurt am Main

Indian Agent: ASIA PUBLISHING HOUSE, Nicol Road, Ballard Estate, Bombay 1

Just published

INTERNATIONAL REVIEW OF CYTOLOGY

Prepared under the Auspices of the International Society for Cell Biology

Edited by G. H. BOURNE and J. F. DANIELLI

VOLUME VI

September 1957, 566 pp., illus., \$12.00

CONTENTS:

G. H. Beale, The Antigen System of *Paramecium aurelia*

Sajiro Makino, The Chromosome Cytology of the Ascites Tumors of Rats, with Special Reference to the Concept of the Stemline Cell

Arthur W. Pollister and *Priscilla F. Pollister*, The Structure of the Golgi Apparatus

A. Monroy, An Analysis of the Process of Fertilization and Activation of the Egg

Robley C. Williams, The Role of the Electron Microscope in Virus Research

Arthur J. Hale, The Histochemistry of Polysaccharides

J. Gross, The Dynamic Cytology of the Thyroid Gland

Elio Borghese, Recent Histochemical Results of Studies on Embryos of Some Birds and Mammals

R. J. O'Connor, Carbohydrate Metabolism and Embryonic Determination

G. Siebert and *R. M. S. Smellie*, Enzymatic and Metabolic Studies on Isolated Nuclei

George H. Hogeboom, *Edward L. Kuff*, and *Walter C. Schneider*, Recent Approaches to the Cytochemical Study of Mammalian Tissues

Freda Bowyer, The Kinetics of the Penetration of Nonelectrolytes into the Mammalian Erythrocyte

AUTHOR INDEX—SUBJECT INDEX.

CUMULATIVE SUBJECT INDEX FOR VOLUMES I-V.

Previously published:

VOLUME I, 1952, 368 pp., illus., \$ 9.50

VOLUME II, 1953, 545 pp., illus., \$11.00

VOLUME III, 1954, 530 pp., illus., \$ 9.50

VOLUME IV, 1955, 419 pp., illus., \$ 9.00

VOLUME V, 1956, 570 pp., illus., \$11.50.



ACADEMIC PRESS INC., Publishers

111 Fifth Avenue, New York 3, New York, U.S.A.

Gefriertrocknung als Fixierungsmethode an Pflanzenzellen¹

H. R. MÜLLER

*Institut für Allgemeine Botanik der Eidgenössischen Technischen
Hochschule, Zürich*

Eingegangen am 29. Juli 1957

Wir haben Pollenmutterzellen von *Tradescantia virginiana* und Chloroplasten von *Eucharis grandiflora* durch Gefriertrocknung fixiert und diese mit den lebenden oder chemisch fixierten Objekten verglichen.

Die Gewebe wurden in Propan bei -185°C eingefroren und unter Hochvakuum bei Temperaturen von -40° bis -70°C entwässert. Die Trocknungsanlage ist mit einem Stickstoffring und mit einer Öldiffusionspumpe ausgerüstet. Sie eignet sich besonders für tiefe Trocknungstemperaturen.

Genaue Restwasserbestimmungen in Blattgeweben ermöglichten uns schliesslich eine Einbettung der Objekte in Methacrylat. Diese wird mit einer speziellen Einrichtung bei geringem Vakuum vorgenommen. Die Objekte werden beim Einbetten und bei der Polymerisierung des Methacrylates gekühlt. Damit lassen sich Lösungseffekte im Gewebe vermeiden. Die Härtung wird in $2\frac{1}{2}$ –3 Stunden mit ultraviolettem Licht eines Quecksilberhochdruckbrenners vorgenommen.

Diese Fixierungs- und Präparationstechnik gestattete uns, an Dünnschnitten die submikroskopische Lamellenstruktur der Chloroplasten ohne chemische Fixation im Elektronenmikroskop darzustellen. Die Resultate sind in licht- und elektronenmikroskopischen Bildern zusammengestellt (Tafeln I–V).

Durch die Verfahren der histologischen Fixation will man das instabile lebende System im Gewebe durch besondere Kunstgriffe beim Abtöten festigen. Im Präparat soll ein naturgetreues Bild der Lebensstruktur erhalten bleiben, und weitere Präparationsvorgänge dürfen keine neuen Veränderungen herbeiführen.

Am ehesten sind Gewebelemente beständig, welche aus wenig elastischen Gelen bestehen. Die weniger zähen oder halbflüssigen Gele, die echten Sole und ihre zahlreichen Zwischenstufen sind unbeständige Formbestandteile. Zeiger (52) unterscheidet daher zwischen fixationsstabilen und fixationslabilen Feinstrukturen. Oft

¹ Die vorliegende Arbeit wurde am Institut für Allgemeine Botanik der Eidgenössischen Technischen Hochschule in Zürich ausgeführt. Meinem verehrten Lehrer, Herrn Prof. Dr. A. Frey-Wyssling, möchte ich für seine Unterstützung meinen besten Dank aussprechen. Herrn Prof. Dr. K. Mühlethaler und Herrn Prof. Dr. F. Ruch danke ich für viele praktische Hinweise beim Bau der neuen Trocknungsanlage und bei der Präparation für die licht- und elektronenmikroskopischen Untersuchungen. Ebenso bin ich Herrn Dr. A. Vogel für viele Anregungen zu besonderem Dank verpflichtet.

treten während der Fixation Strukturbilder auf an Orten, die im Leben lichtmikroskopisch homogen erscheinen. Diese können im lebenden Gewebe schon in irgend einer Form vorhanden sein. Ihres starken Hydratationszustandes wegen sind sie aber maskiert und daher im gewöhnlichen Licht nicht zu sehen.

Das Hydratationswasser macht im Pflanzengewebe 70–90 % seines Frischgewichtes aus. Mit jeder Fixierung will man diesen labilen Anteil entfernen. Bei der chemischen Fixation können dabei je nach der Struktur des Gewebes und nach den verwendeten Fixationsgemischen neben diesem Wasser bis 60 % der Trockensubstanz durch Auswaschen verlorengehen (45). Gewöhnlich werden die besonders reaktionsfähigen Seitengruppen der Moleküle von den chemischen Mitteln besetzt. Bei der Osmiumsäurefixierung werden die Zellbestandteile zudem von Reduktionsprodukten angefärbt. Die Präparate sind daher für cytochemische Untersuchungen — vor allem für Absorptionsmessungen im Ultraviolettmikroskop — ungeeignet.

Die Gefriertrocknungsmethode nach Altmann und Gersh kann hier in der Fixierungstechnik eine Lücke schliessen. Sie wurde denn auch in den letzten Jahren immer mehr für cytochemische Untersuchungen angewandt (2, 32, 36, 45). Einige Autoren haben diese Technik auch für die Darstellung von Viren, Bakterien (41, 49, 51) und verschiedenen tierischen Geweben (5, 39) im Elektronenmikroskop herangezogen.

In der vorliegenden Arbeit soll untersucht werden, wie weit die Gefriertrocknung zur Fixierung von Pflanzengewebe in Frage kommt. Die Gewebe sollten cytochemisch und morphologisch unverändert bleiben. Dazu ist eine leistungsfähige Trocknungsanlage notwendig, welche eine Sublimation des Eises bei Temperaturen von -50°C bis -80°C ermöglicht. Auf diese Weise würde eine Rekristallisation während der Trocknung weitgehend vermieden, und die Gewebe könnten auch elektronenmikroskopisch geprüft werden.

Die gefriergetrockneten Objekte sollen in licht- und elektronenmikroskopischen Aufnahmen mit den lebenden und chemisch fixierten verglichen werden.

APPARATUREN UND METHODEN

EINFRIEREN DER GEWEBE

Eiskristallbildung

Entscheidend für den Erfolg einer Fixierung in morphologischer Hinsicht ist die Geschwindigkeit, mit der die Stabilisierung des lebenden Zustandes erfolgt. Die Gefriertrocknung müsste darnach eine ideale Fixierungsmethode darstellen. In kleinen Objekten erstarrt das Gewebswasser beim Einfrieren schon in einem Bruchteil einer Sekunde. Infolge der schlechten Wärmeleitfähigkeit kann aber nach Luyet (23) in biologischen Objekten eine Eiskristallbildung nicht vollständig vermieden werden. Dazu wären Kühlgeschwindigkeiten von einigen hundert Graden in der Sekunde notwendig.

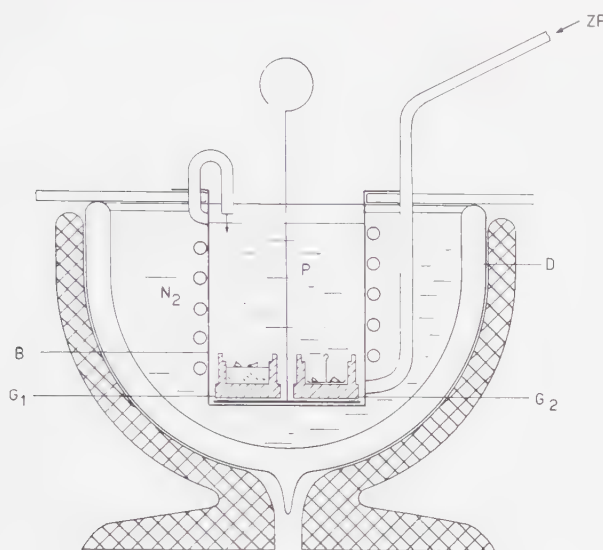


FIG. 1.

| | | | |
|----------------|----------------------|----------------|---------------------------------------|
| B | Aluminiumbecher | ZP | Zuleitung für das Propangas |
| D | Deward-Gefäss | G ₁ | Objektbehälter mit Einbettungsmittel |
| N ₂ | Stickstoff (flüssig) | G ₂ | Objektbehälter ohne Einbettungsmittel |
| P | Propan (flüssig) | | |

Die Kristallgrösse ist umgekehrt proportional zur Dichte der Kristallpopulation und zur Gefriereschwindigkeit. Sie wird wesentlich bestimmt durch die thermischen Eigenschaften der Gewebe, durch ihre Form und den Wassergehalt und durch die Eigenschaften der Grenzschicht zwischen der Gewebeoberfläche und der Kühlflüssigkeit (12, 27). Gegen die inneren Zellschichten nimmt die Gefriereschwindigkeit ab, was eine Zunahme der Kristallgrösse zur Folge hat. Es ist daher für das Einfrieren eine grosse Wärmeleitfähigkeit der Kühlflüssigkeit und ein steiles Temperaturgefälle anzustreben. Diese Forderungen haben wir erfüllt, indem wir nur sehr kleine oder wenigstens doch sehr dünne Gewebestücke fixierten.

Wird zu langsam eingefroren, so tritt nach den Arbeiten von Meryman und Hale (28), eine Kristallisation zuerst vorwiegend extrazellulär auf. Die zwischen den Zellen gelagerten Kristallisationskeime sind osmotisch wirksam und entziehen den Zellen Wasser. Als Folge davon treten Diffusionsströmungen auf, welche zu Substanzverlagerungen führen können. In den Zellen steigt zugleich die Salzkonzentration und der Gefrierpunkt wird herabgesetzt. Dadurch erstarrt der Zellinhalt erst später. Als Schäden treten im Gewebe Risse und starke Schrumpfungen auf.

Methode für das Einfrieren der Gewebe

Als Gefriermedien werden heute gewöhnlich nur noch Isopentan und flüssiges Propan verwendet. Beide weisen verglichen mit flüssiger Luft eine grosse Wärmeleitfähigkeit auf. Isopentan wird aber schon bei -150°C hochviskos und erstarrt bei -160°C . Wir haben

deshalb für unsere Versuche flüssiges Propan als Kontaktmittel vorgezogen. Dieses Gas hat einen Siedepunkt von $-44,5^{\circ}\text{C}$ und wird erst bei -190°C fest. Wenn wir nach der Trocknung die Gewebe in Paraffin, Carbowax oder Glycerin einbetten, wird das Einbettungsmittel zuerst im Objektbehälter G_1 (Fig. 1) eingefroren. Für die elektronenmikroskopische Präparation haben wir Methacrylat verwendet. Dieses verdampft im Vakuum und kann daher erst nach der Trocknung in den Objektbehälter eingefüllt werden (G_2).

Ist das Gefrierbad P durchgehend gleichmässig auf -185°C abgekühlt, werden die Objekte an feinen Nadelspitzen in die Objektbehälter G gebracht. Durch das sehr schnelle Eintauchen gelangen die $50\text{--}100\ \mu$ dicken Gewebeschnitte immer in Kontakt mit frischem Propan und sind bis sie den Objektbehälter erreichen vollständig eingefroren. Die Schnitte bleiben einige Minuten im Gefrierbad und werden dann auf dem kürzesten Weg in den Trocknungstubus übertragen, der auf -70° bis -80°C vorgekühlt worden ist (Fig. 3).

TROCKNEN DER GEWEBE

Trocknungstemperatur und Trocknungszeit

Die grösste Trocknungsgeschwindigkeit erreicht man im Bereiche möglichst hoher Sättigungsdampfdrucke, d.h. knapp unter dem Gefrierpunkt. Die empfindlichen biologischen Objekte müssen aber bei bedeutend tieferen Temperaturen getrocknet werden. Seit Scott (38) ist allgemein bekannt, dass die Vorteile der Gefriertrocknung hinsichtlich der Erhaltung der Struktur und der vitalen Verteilung chemischer Bestandteile der Zellen nur dann bestehen bleiben, wenn die Trocknungstemperatur tiefer liegt, als die Temperatur des tiefsten eutektischen Punktes der Gewebesalze. Beim einfachen Zweistoffsystem $\text{CaCl}_2\text{--Wasser}$ liegt der eutektische Punkt bei $-54,9^{\circ}\text{C}$. Bei ternären, quaternären oder komplizierteren Systemen, wie sie in biologischen Objekten auftreten, muss diese kritische Temperatur noch tiefer liegen. Trotzdem wird von den meisten Histologen zwischen -30°C und -40°C getrocknet (2, 10, 19). Dies geschieht wohl deshalb, weil mit den gebräuchlichsten Apparaturen eine Trocknungstemperatur unter -55°C die Trocknungszeit sehr stark verlängert. Neumann (32) ist der Ansicht, dass für Zwecke der reinen Morphologie eine Trocknungstemperatur von -40°C ausreicht, dass aber für histochemische und elektronenmikroskopische Untersuchungen unterhalb von -55°C gearbeitet werden muss. Williams (48, 49) hat Viren, Bakterien und Bakteriophagen nach Gefriertrocknung im Elektronenmikroskop untersucht. Die Temperatur hielt er während der Trocknungszeit von 15–20 Minuten bei -45°C . Kulenkampf (21) hat verschiedene tierische Gewebe bei einer Temperatur von -80°C mindestens 3 Tage lang getrocknet.

Diese Angaben bestätigen in erster Linie die physikalische Tatsache, dass die Trocknungszeit mit sinkender Temperatur stark anwächst. Neben der Temperatur hängt die Trocknungsdauer wesentlich vom strukturellen Aufbau des Gewebes und von der Leistung der Trocknungsapparatur (13) ab. Bei fortschreitender Trocknung bildet sich im Gewebe eine eindeutige Grenze zwischen schon dehydriertem und noch wasserhaltigem Anteil (Fig. 2). Diese Zone verlagert sich allmählich immer weiter von der Oberfläche gegen die inneren Gewebezonen. Die Wassermoleküle, die von dieser Grenzschicht wegdampfen, müssen sich, ehe sie freien Weg zur Kondensationsfläche oder Pumpe bekommen, zuvor durch die bereits getrocknete äussere Schicht hindurchbewegen. Die Verzögerung, die sie dadurch erleiden, verlangsamt die Trocknungsgeschwindigkeit. Für Gewebe mit gleichem strukturellem Aufbau liess sich zeigen, dass die Trocknungszeit sich umgekehrt proportional zu ihrer Schichtdicke verhält (12).

Rekristallisation

Nach Luyet und Gehenio (24) kann man beim Einfrieren von biologischen Geweben Kristallbildungen nicht ganz verhindern. Bei langen Trocknungszeiten kann es daher zu einer Rekristallisierung kommen. Man versteht darunter ein bevorzugtes Wachstum von grossen Kristallen auf Kosten von kleinern. Diese Erscheinung ist bedingt durch Oberflächenenergiedifferenzen zwischen grossen und kleinen Kristallen und durch Unterschiede in der freien Energie, die durch innere Spannungen verursacht werden.

Verunreinigungen oder viskose Lösungen zwischen den Kristallen können die Rekristallisation fördern. Daneben ist sie aber wesentlich von der Temperatur abhängig. In der Nähe des Gefrierpunktes haben die Moleküle genug Beweglichkeit, um sich in ein Kristallgitter einzuordnen. Die Rekristallisierung ist daher hier am grössten. Mit sinkender Temperatur nimmt sie dagegen ab.

Eine eindeutige Rekristallisierungstemperatur lässt sich in pflanzlichen und tierischen Geweben nur sehr schwer bestimmen, weil die strukturellen Unterschiede eine entscheidende Rolle spielen. Wir haben an Pollenmutterzellen von *Tradescantia virginiana* festgestellt (Tafel I, Abb. 1–4), dass bei -40°C Trocknungstemperatur Eiskristalle in den Chromosomen bis zu einer Grösse von $1\ \mu$ im Durchmesser auswachsen können. Wenn die Gewebe unter -50°C getrocknet wurden, blieben diese Artefakte aus.

Trocknungsapparatur

Die Trocknungsgeschwindigkeit ist neben der Grösse und der Struktur des Gewebes ganz besonders von der Leistung der Trocknungsapparatur abhängig, Gersh und Stephenson (12) haben diese in folgende einfache Beziehung zum Wasserdampfdruck gebracht:

$$L = 1 - P_a / P_g.$$

L ist die Leistung der Trocknungsapparatur, P_g der gesättigte Dampfdruck des Eises an der oben erwähnten Grenzfläche und P_a der Dampfdruck an der Oberfläche des Gewebes.

Für kurze Trocknungszeiten muss P_a möglichst klein und das Druckgefälle zwischen P_g und P_k , dem Dampfdruck an der Kondensationsfläche (Fig. 2), möglichst gross sein.

Dies wird durch ein gutes Vakuum im Tubus und durch eine wirksame Kondensation der Wassermoleküle in einer Kühlfalle erreicht. P_a sollte nicht grösser als $P_g/100$ sein. Die

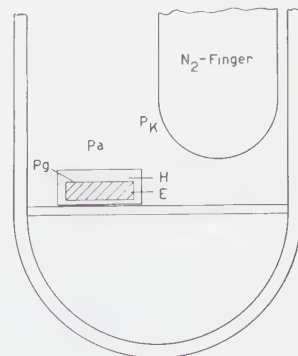


FIG. 2.— H trockene Schicht des Gewebes, E gefrorene Schicht im Innern des Gewebes.

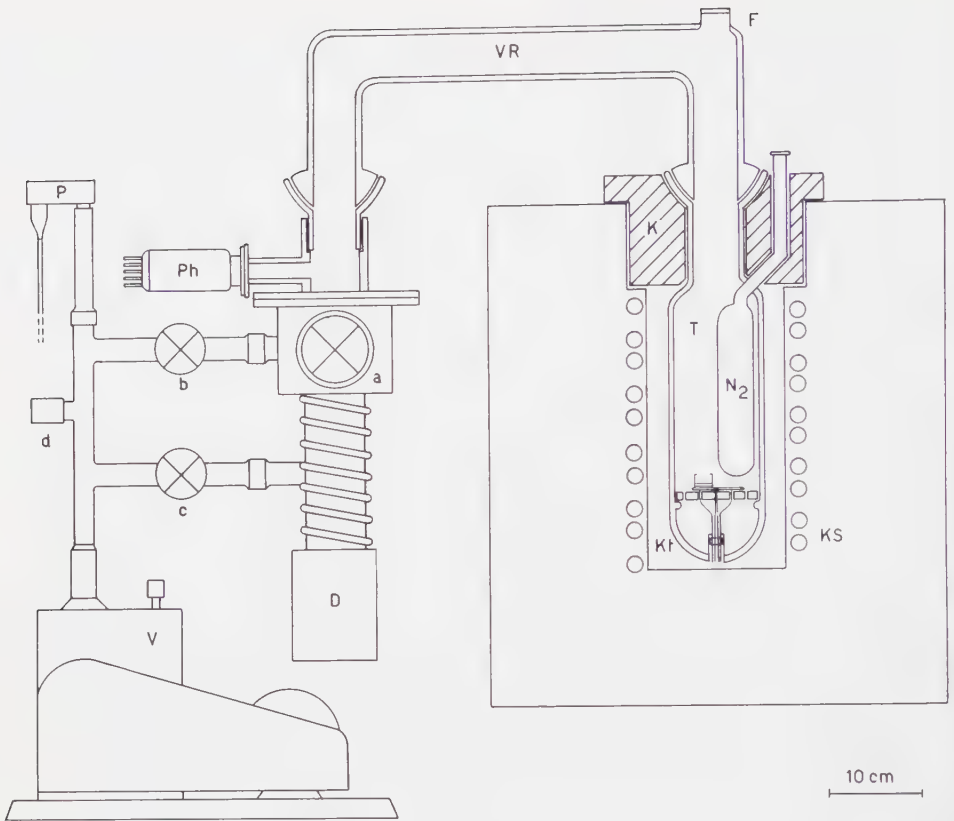


FIG. 3.—Trocknungsapparat

| | | | |
|----------------------|------------------|-------------|---------------------|
| <i>V</i> | Vorvakuumpumpe | <i>T</i> | Trocknungstubus |
| <i>D</i> | Diffusionspumpe | <i>K</i> | Korkdeckel |
| <i>P</i> | Pirani-Messröhre | <i>F</i> | Beobachtungsfenster |
| <i>Ph</i> | Ionisationsröhre | <i>KS</i> | Kühlschlangen |
| <i>VR</i> | Verbindungsrohr | <i>a</i> | Baffle-Hahn |
| <i>Kt</i> | Kühltruhe | <i>b, c</i> | Vakuumhähne |
| <i>N₂</i> | Stickstoffinger | <i>d</i> | Flutventil |

Erfahrung zeigt, dass mit einem P_a von 10^{-3} mm Hg noch bei einer Temperatur von -30°C rationell getrocknet werden kann. Für tiefere Trocknungstemperaturen ist ein Vakuum von mindestens 10^{-4} mm Hg notwendig (12).

In Fig. 3 ist die von uns verwendete Trocknungsapparat dargestellt. Die Anlage wurde so gebaut, dass sie während einigen Tagen ohne spezielle Wartung arbeiten kann. Normalerweise werden zwei Vakuumumpen hintereinander geschaltet: Eine Ölrotationspumpe für das Vorvakuum und eine Diffusionspumpe für das Hochvakuum. Die Leistung der Diffusionspumpe beträgt 50 l/sec bei einem Endvakuum von $5 \cdot 10^{-6}$ mm Hg. Wird nur ein Vakuum von 10^{-2} mm Hg benötigt, kann die Diffusionspumpe durch die Hähne *a* und *c*

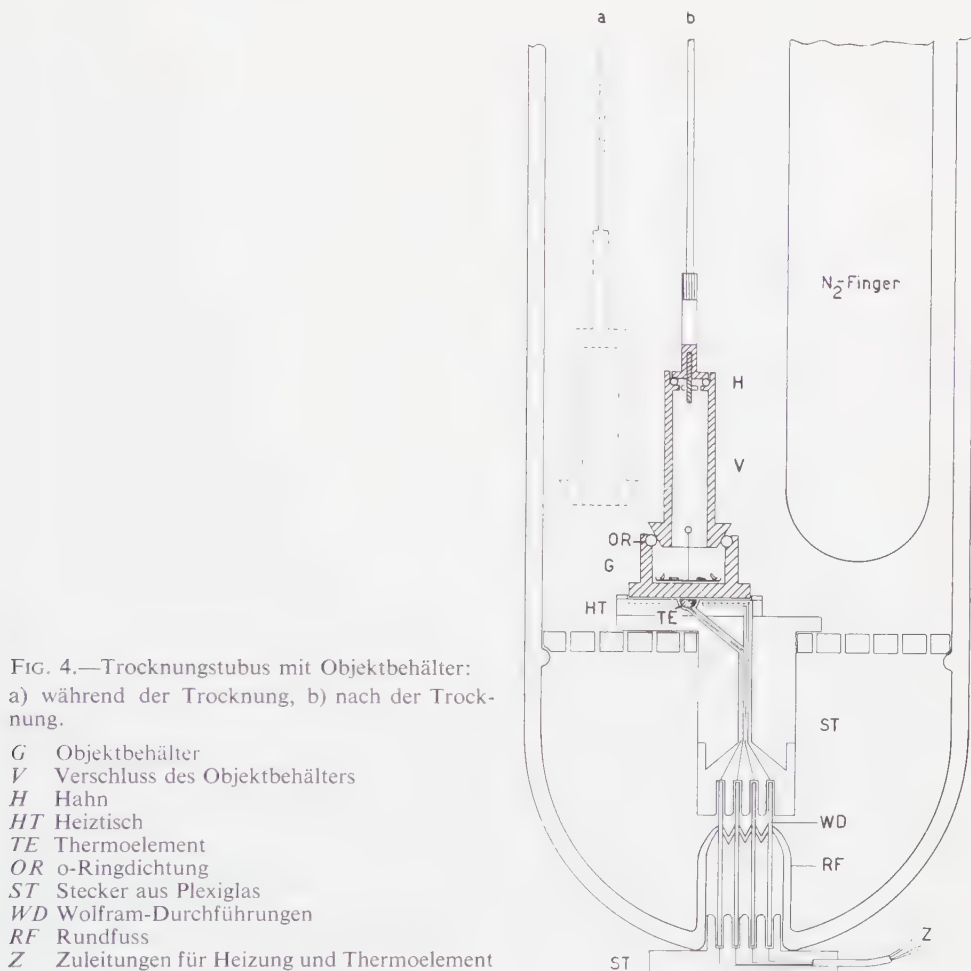


FIG. 4.—Trocknungstubus mit Objektbehälter:
a) während der Trocknung, b) nach der Trocknung.

- G* Objektbehälter
V Verschluss des Objektbehälters
H Hahn
HT Heiztisch
TE Thermoelement
OR o-Ringdichtung
ST Stecker aus Plexiglas
WD Wolfram-Durchführungen
RF Rundfuss
Z Zuleitungen für Heizung und Thermoelement

abgeschlossen werden. Die Vorvakuumpumpe arbeitet dann direkt über Hahn *b* am Trocknungstubus. Zur Messung des Vakuums dient ein Edwards Philani-Gerät mit einer Pirani-Messröhre *P* für das Vorvakuum und einer Philips-Ionisationsröhre *Ph* für das Hochvakuum.

Der Trocknungstubus *T* und das Verbindungsrohr *VR* zum Flanschsaufsatz der Diffusionspumpe bestehen aus 4 mm starkem Pyrexglas. Die Verbindung unter den Glasteilen wird durch zwei Kugelschliffe hergestellt. Die innere Weite des Glasrohres beträgt 60 mm. Damit haben wir eine Beeinträchtigung der Pumpleistung durch allzu enge Vakuumleitungen ausgeschlossen. Der Trocknungstubus *T* ist in eine Kühltruhe *Kt* eingetaucht, welche durch einen 12 cm dicken Korkdeckel *K* abgeschlossen wird. Die Kühlung dieser Truhe erfolgt durch ein dreistufiges Kühlaggregat.

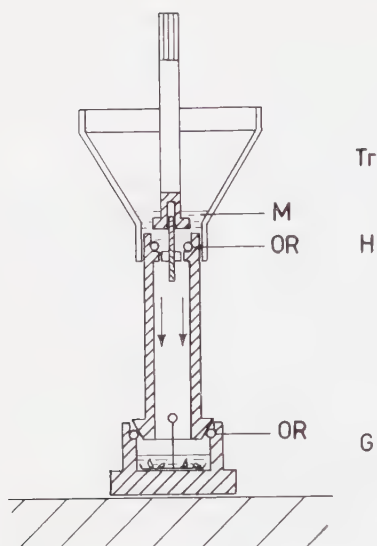


FIG. 5.

| | | | |
|----------|----------------|-----------|----------------|
| <i>G</i> | Objektbehälter | <i>Tr</i> | Trichter |
| <i>H</i> | Hahn | <i>OR</i> | o-Ringdichtung |
| <i>M</i> | Methacrylat | | |

Im Trocknungstubus ist ein Glasfinger N_2 eingesetzt, der von aussen her mit flüssigem Stickstoff gefüllt wird. Damit können wir die Kondensationsfläche für den Wasserdampf in unmittelbarer Nähe des Gewebes auf -190°C abkühlen (Fig. 4). Die Zuleitungen für die Heizung und das Thermoelement *TE* werden über Wolframdurchführungen *WD*, welche in einem Rundfuss *RF* eingeschmolzen sind, und über zwei Plexiglasstecker in den Tubus geführt.

EINBETTEN DER GEWEBE

Für histologische Untersuchungen sind wir auf dünne Gewebeschnitte angewiesen. Über den Einfluss bestimmter Einbettungsmittel auf das Gewebe soll in einem späteren Kapitel die Rede sein. Wir beschränken uns hier auf die Einbettungsmethode.

Die Gewebe können nach der Trocknung in Glycerin, Carbowax oder Paraffin direkt im Trocknungstubus unter Vakuum eingebettet werden (2, 11, 21). Der Objektbehälter *G*₁ (Fig. 1) wird dazu vorsichtig erwärmt, bis das Einbettungsmittel schmilzt. Durch ein Planglas *F* (Fig. 3) im Verbindungsrohr kann dieser Vorgang beobachtet werden. Sind die Objekte eingesunken, lässt man das Einbettungsmittel erstarren. Dann wird das Flutventil *d* geöffnet und getrocknete Luft in den Tubus gebracht. Das Verbindungsrohr *VR* kann nun vom Tubus entfernt werden.

Schwieriger sind die Verhältnisse, wenn in Methacrylat eingebettet werden soll, da dieses im Vakuum verdampft und hydrophobe Eigenschaften zeigt. Die Gewebe sind nach der Trocknung stark hygroskopisch und nehmen sofort Luftfeuchtigkeit auf. Um dies zu vermeiden, haben wir den Objektbehälter *G* mit einem Verschluss *V* versehen (Fig. 4). Wenn Luft in den Trocknungstubus einströmt, wird dieser durch den äusseren Luftdruck auf die o-Ringdichtung gepresst. Dadurch werden die Objekte unter Vakuum im Behälter eingeschlossen. Die Einbettung in Methacrylat wird ausserhalb des Trocknungstubus vorge-

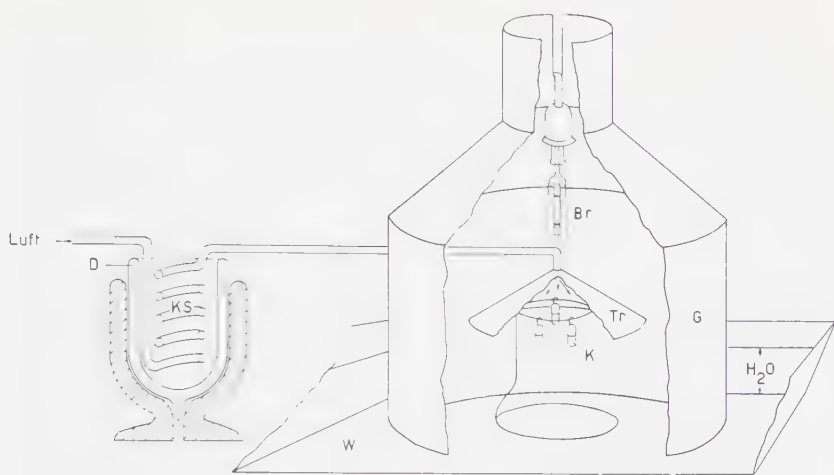


Fig. 6.—UV-Polymerisation des Methacrylates.

| | | | |
|----------|------------------|-----------|---------------------------------------|
| <i>D</i> | Dewardgefäß | <i>Br</i> | Brenner einer Quecksilberdampfampe |
| <i>G</i> | Gehäuse | <i>Tr</i> | Abschirmung gegen direkte Bestrahlung |
| <i>K</i> | Gelatine kapseln | <i>KS</i> | Kühlschlangen |
| <i>W</i> | Wanne | | |

nommen. Dazu wird dem Verschluss ein Trichter *Tr* (Fig. 5) aufgesteckt und in diesen das Einbettungsmittel *M* eingefüllt. Dann wird Hahn *H* geöffnet und das Methacrylat in den Behälter eingesogen. Bevor Luft nachströmen kann schliessen wir den Hahn wieder ab. Nach wenigen Minuten ist die Einbettung abgeschlossen und der Objektbehälter kann geöffnet werden. Für die Polymerisierung des Methacrylates werden die Gewebestücke in Gelatine kapseln übertragen.

POLYMERISATION DES METHACRYLATES

Eine Polymerisation des Methacrylates im Wärmeschrank bei 48–50°C ist an gefriergetrocknetem Gewebe nicht möglich, weil grosse Schäden in den Zellen auftreten. Wir haben daher die Härtung mit ultraviolettem Licht nach der Methode von Massey (25) und Weinreb (47) durchgeführt. Es wurde dazu die Einrichtung von Vogel (46) verwendet. Als Lichtquelle dient ein Quecksilber-Hochdruckbrenner mit einer Leistung von 75 Watt (Fig. 6). Das Gehäuse *G* und die Wanne *W* sind mit Aluminiumfolien ausgekleidet. Ein kegelförmiges Dach *Tr* schützt die Kapseln *K* mit den eingebetteten Objekten vor einer direkten Bestrahlung. Während der Polymerisierung wird die Aussentemperatur durch tiefgekühlte Luft unter 10°C gehalten. Wir brauchen dazu Pressluft, die wir zuerst in einem Dewardgefäß *D* mit Kohlensäureschnee abkühlen und die dann durch ein gut isoliertes Rohr in den Trichter gelangt, wo sie sich regelmässig über den Kapseln verteilt. Für die Bestrahlung der Kapseln wird das Licht verwendet, das vom Boden der Wanne reflektiert wird. Die Infrarotstrahlen werden durch eine 10 cm tiefe Schicht von fließendem Wasser absorbiert.

RESULTATE

UNTERSUCHUNGSOBJEKTE

Unter den Objekten, welche nach der Fixierung mit der Gefriertrocknungsmethode histologisch, cytologisch und histochemisch untersucht wurden, nehmen die pflanzlichen Gewebe gegenüber den tierischen in der Literatur einen äusserst bescheidenen Raum ein. Dies ist darauf zurückzuführen, dass das Pflanzengewebe durch seine zellulosischen Membranen beim Einfrieren und Trocknen mehr Schwierigkeiten bereitet als das tierische. Tierische Gewebeschnitte können in wenigen Stunden trocken sein, während man für pflanzliches Material unter gleichen Bedingungen einige Tage braucht.

Goodspeed, Uber und Avery (14) haben als erste mit dieser Fixierung an Zellkernen aus den Antheren von *Lilium longiflorum* gute Resultate erzielt. Jensen (19, 20), hat eine neue Trocknungseinrichtung gebaut, mit der er vergleichende Untersuchungen an verschiedenen Pflanzengeweben anstellte. Er hat dabei grössere Unterschiede in den Trocknungszeiten zwischen verschiedenen Geweben als zwischen gleichem Gewebe verschiedener Pflanzen gefunden. An unserem Institut konnten mit einem Edwards „Tissue Dryer“ für lichtmikroskopische Untersuchungen gute Resultate erzielt werden (37). Wir haben diese Versuche mit der neuen Gefriertrocknungsanlage fortgesetzt. Als Untersuchungsobjekte haben wir Pollenmutterzellen von *Tradescantia virginiana* und Chloroplasten von *Eucharis grandiflora* und *Aspidistra elatior* ausgewählt.

EINFLUSS VERSCHIEDENER EINBETTUNGSMITTEL AUF DAS GEWEBE NACH GEFRIERTROCKNUNG

Bei der Gefriertrocknung tritt im Gewebe keine nennenswerte Denaturierung der Proteine ein (3, 10, 18). Sämtliche chemischen Bestandteile, wie auch die kolloide Dispersität sollen in der Zelle erhalten bleiben. Die Gefriertrocknung muss aus diesem Grunde gegenüber den üblichen chemischen Fixierungen für viele histo- und cytochemische Untersuchungen bedeutende Vorteile bieten (2, 45).

Für die morphologischen Untersuchungen sind wir auf dünne Gewebeschnitte angewiesen. Die auf die Trocknung folgende Behandlung des Materials stellt aber einige Probleme, welche noch sehr wenig bekannt sind. Wir müssen annehmen, dass durch die Einbettung je nach dem chemischen Verhalten des Gewebes verschiedene strukturelle Veränderungen auftreten. Bei hohen Einbettungstemperaturen werden die Lipide herausgelöst, und durch starke Volumveränderungen beim Erstarren des Einbettungsmittels zeigen sich Quellungs- und Schrumpfungseffekte. Schliesslich gehen bei der Behandlung von Paraffinschnitten mit Alkohol, Xylol oder Benzol feste Zellanteile in Lösung oder werden denaturiert. Für manche Untersuchungen an gefriergetrockneten Objekten ist daher eine vorausgehende Fixierung durch Alko-

hol oder Hitze im Vakuum vorzuziehen. Allerdings macht auch eine solche Denaturierung die Gewebseiseweisse nicht absolut unlöslich. Sylvén (45) konnte nachweisen, dass nach 24stündiger chemischer Fixierung 40–60 % der Trockensubstanz durch Auswaschen und durch die letzten Schritte der Präparation verloren gehen. Neben Kohlehydraten und anorganischen Ionen wurden besonders Lipide, Proteine und Nukleotide herausgelöst. Wolken (50) stellte fest, dass sich an OsO_4 -fixiertem Material von *Euglena gracilis* beim Entwässern mit Alkohol 2–10 % der Pigmente lösen. Dauert diese Behandlung mehrere Tage, schwinden sogar 15–40 % der Farbstoffe. Auch Strügger (43) hat beobachtet, dass die Granen der Chloroplasten nach der Osmiumsäurefixierung weder gegen eine längere Alkohol- und Xylolbehandlung noch gegen eine Temperatur von 60°C im Wärmeschränk resistent sind.

Wenn solche Schäden schon an chemisch fixiertem Gewebe auftreten, muss diesen vor allem bei der Gefriertrocknung besondere Beachtung geschenkt werden. Dies umso mehr, als die Chloroplasten schon bei Temperaturen von 33°–45°C irreversibel ausbleichen (35). Wir fanden diese Ergebnisse auch in den von uns verwendeten Einbettungen bestätigt.

Einbettungen für lichtmikroskopische Untersuchungen

Am besten liess sich das Gewebe nach Gefriertrocknung in wasserfreiem Glycerin mit dem lebenden Objekt vergleichen (Tafel I und II). Dieses Einbettungsmittel kann sich im Gewebe mit dem restlichen Konstitutionswasser vermischen, ohne dass im mikroskopischen Bild Strukturveränderungen zu sehen sind. Man kann daher auch mit relativ kurzen Trocknungszeiten bei einer Trocknungstemperatur von –60°C gute Resultate erzielen.

Anders sind die Verhältnisse bei der üblichen Paraffineinbettung. Für diese soll das Gewebe nicht mehr als 2 % Restfeuchtigkeit enthalten. Wir haben Flächenschnitte aus dem Blatt von *Eucharis grandiflora* nach dem Einfrieren 45 Stunden lang bei –50°C getrocknet und unter Vakuum in Weichparaffin (Smp. 43°C) eingebettet. Aus 2–3 μ dicken Mikrotomschnitten lösten wir mit Chloroform während 15 Minuten das Einbettungsmittel heraus. Darauf wurden sie in absolutem Alkohol kurz gespült und schliesslich in einem Tropfen Glycerin unter dem Phasenkontrastmikroskop mit Ölimmersion untersucht. Wenn die Einbettung innerhalb weniger Minuten bei 45°C vorgenommen wird, bleibt die Granenstruktur in den Chloroplasten erhalten (Tafel II, Abb. 8). Bei 50°C und einer Einbettungsdauer von 30 Minuten dagegen verschwinden die Granen (Abb. 7). Wir müssen annehmen, dass durch zu starke Erwärmung die Lipide schmelzen und als Folge davon die submikroskopische Lamellenstruktur in den Chloroplasten aufgelöst wird. Dadurch kommt eine homogene Verteilung der Granenmasse über den ganzen Chloroplasten zustande.

Für Untersuchungen an Lipoiden eignet sich daher die Paraffineinbettung nicht. Gersh (11) hat dazu Polyäthylenglykol (Carbowax) als Einbettungsmittel verwendet. Carbowax ist in Wasser und Alkohol löslich und greift die Lipide nicht an.

Einbettung für elektronenmikroskopische Untersuchungen

Bretschneider und Elbers (5) haben für elektronenmikroskopische Untersuchungen verschiedene tierische Gewebe nach Gefriertrocknung in eine Mischung von Bienenwachs und Paraffin eingebettet. Auch bei der sehr hohen Schmelztemperatur von 70 C sollen dabei keine zusätzlichen Artefakte in den Schnitten auftreten. Aus den oben erwähnten Gründen kam aber für pflanzliche Objekte ein Einbettungsmittel mit so hohem Schmelzpunkt nicht in Frage. Wir haben deshalb für unsere Versuche Methacrylat verwendet. Die Einbettung wurde mit der vorher (S. 116) beschriebenen Vorrichtung bei geringem Vakuum durchgeführt.

In einer ersten Versuchsreihe haben wir das Methacrylat im Wärmeschrank bei 50°C während 12 Stunden polymerisiert. Das Einbettungsmittel setzte sich zusammen aus n-Butylmethacrylat und Methylmethacrylat im Verhältnis von 10 : 1 mit einem Zusatz von 1 % 2,4-Dichlorbenzoyl-Peroxyd als Beschleuniger. Die Objekte wurden zuerst mit monomerem Methacrylat durchtränkt und dann in vorpolymerisiertes Einbettungsmittel übertragen.

Methacrylat extrahiert bei Zimmertemperatur in wenigen Minuten die Pigmente aus dem Gewebe. Im Kühlschrank (-5 C) behalten die eingebetteten Blattstücke ihre grüne Farbe während einigen Tagen. Nach der darauffolgenden Polymerisation in der Wärme werden sie aber vollständig ausgebleicht. Die Chloroplasten verquellen und ihre Innenstruktur wird aufgelöst (Tafel V, Abb. 15). Die Geldrollenstruktur der Granen kann dargestellt werden, wenn das Gewebe nach der Trocknung 90 Minuten lang mit OsO_4 -Dampf nachfixiert wird (Abb. 16). Nach dieser Behandlung treten aber immer noch deutliche Artefakte auf. Die Chloroplasten sind auch hier verquollen und die Lamellen oft untereinander verklebt. Dies kann entweder durch eine mangelhafte Trocknung vor der Einbettung oder durch die Aufnahme von Feuchtigkeit während der OsO_4 -Dampfbehandlung bedingt sein.

Die Tatsache, dass bei tiefen Temperaturen die gefriergetrockneten Mesophyllschnitte auch nach längerer Zeit im monomeren Methacrylat nicht ausbleichen, brachte uns auf die Idee, eine beschleunigte Polymerisation mit ultravioletem Licht durchzuführen. Als Einbettungsmittel verwendeten wir dazu n-Butylmethacrylat, in welchem wir 0,5 % Benzoin als Beschleuniger auflösten. Die Objekte wurden schon beim Einbetten in der in Fig. 5 dargestellten Vorrichtung auf mindestens -10 C gekühlt, dann in die Gelatine kapseln übertragen, welche ebenfalls mit vorgekühltem Methacrylat gefüllt sind. Während der ganzen Polymerisation wird die Aussen-

temperatur um die Kapseln durch kohlensäureschnee-gekühlte Pressluft unter 10°C gehalten.

Die meisten Autoren, welche mit ultraviolettem Licht polymerisierten (25, 47), verwendeten Gemische von Methyl- und Butylmethacrylat ohne Katalysatoren. Ihre Präparate waren in 6–12 Stunden gehärtet. Wird aber wie in unseren Versuchen Benzoin dazugegeben, ist die Polymerisierung nach $2\frac{1}{2}$ –3 Stunden abgeschlossen. Da die Präparate von der Unterseite her bestrahlt werden, beginnt die Härtung am Kapselgrund und erfasst daher das Objekt sehr früh. Nur so ist es möglich, eine Extraktion der Pigmente zu vermeiden. Die Blattschnitte behalten daher ihre ursprüngliche grüne Farbe.

BESTIMMUNG DES RESTWASSERGEHALTES IM GEWEBE NACH GEFRIERTROCKNUNG

Methacrylat zeigt stark hydrophobe Eigenschaften. Eine gute Einbettung ist deshalb nur nach einer zuverlässigen Dehydrierung des Gewebes möglich. In der gewöhnlichen Technik werden die Objekte nach dem Auswaschen der Fixierlösungen durch Alkohol entwässert und dann in ein Gemisch von absolutem Alkohol und monomerem Methacrylat (1 : 1) gebracht. Erst in einem weiteren Schritt können sie in reines Methacrylat übertragen werden.

Nach der Gefriertrocknung haben wir eine zusätzliche Behandlung mit Alkohol absichtlich vermieden, weil dadurch die Eiweiße denaturiert würden. Wir haben dafür in Reihenversuchen experimentell abgeklärt, wie weit das Gewebe nach verschiedenen Trocknungszeiten in unserer Anlage dehydriert werden kann.

Methode

Da zuverlässige Vergleichsmessungen nur an gleichem Gewebe ausgeführt werden können, haben wir ausschliesslich Blattstücke von *Eucharis grandiflora* dazu verwendet. Zuerst wurde die Epidermis an der Blattunterseite entfernt und ca. 20 mm² grosse Blattstücke geschnitten. Etwa 200 mg von diesen werden bei –180°C in Propan eingefroren und in dem Trocknungstube in ein Wägegglas mit Schliffdeckel übertragen. Nach einer bestimmten Trocknungszeit wird das Glas, wie dies in Fig. 4 dargestellt ist, geschlossen und darauf in einen Exikkator über Silicagel gebracht, bis sich Glas und Objekte der Aussentemperatur angleichen. Dann wird die erste Wägung durchgeführt. Über Nacht werden die Blattschnitte im Wärmeschrank bei 105°C nachgetrocknet und darauf von neuem gewogen. Aus dieser zweiten Messung erhalten wir das effektive Trockengewicht und aus der Differenz zur ersten den Restwassergehalt des Gewebes nach Gefriertrocknung.

TABELLE I

RESTWASSERGEHALT IN GEFRIERGETROCKNETEN BLATTSTÜCKEN VON *Eucharis grandiflora* IN PROZENTEN BEZOGEN AUF DAS TROCKENGEWICHT

t Trocknungszeit in Stunden.

| <i>t</i> | Trocknungstemperaturen | | | | | |
|----------|---|--------------------------|-------|-------|-------|-------|
| | A, über P ₂ O ₅ + 20°C | B, nach Gefriertrocknung | | | | |
| | | -20°C | -30°C | -40°C | -50°C | -60°C |
| 1 | | | | | | |
| 2 | 145,0 | | | | | |
| 3 | 33,0 | | | | | |
| 4 | 8,0 | 25,0 | 54,0 | | | |
| 5 | | | | 189,0 | | |
| 6 | 5,0 | 17,0 | | | 393,0 | |
| 7 | | | 26,0 | | | |
| 8 | 4,5 | | | 92,0 | 293,0 | 461,0 |
| 9 | | 8,5 | | | | |
| 10 | | | | 52,0 | 191,0 | |
| 12 | 3,5 | 5,5 | 11,0 | 28,5 | 129,0 | 308,0 |
| 15 | | | 8,0 | 17,0 | 73,0 | 220,0 |
| 20 | | | 5,5 | 8,0 | 33,0 | 130,0 |
| 25 | 3,0 | | 5,0 | 5,5 | 18,5 | 80,0 |
| 30 | | | | | 13,0 | 54,0 |
| 40 | | | | | 9,5 | 29,5 |
| 50 | 3,0 | | | | | 18,0 |
| 80 | | | | | | 10,0 |

Resultate

Wir haben nach dieser Methode 50 Restwasserbestimmungen bei verschiedenen Trocknungstemperaturen durchgeführt. Die Resultate sind in der Tabelle I und in den Figuren 7 und 8 dargestellt. Als Vergleichswert unter den einzelnen Versuchen diente der Restwassergehalt nach Gefriertrocknung in Prozenten bezogen auf das Trockengewicht des Gewebes. Dieser Wert ist bedeutend konstanter als der des Frischgewichtes. Bei einzelnen Zahlen wurde der Mittelwert aus zwei oder drei Versuchen eingesetzt.

Zur Kontrolle haben wir gleiches Gewebe bei 20°C und normalem Luftdruck über Phosphorpentoxyd getrocknet (Tabelle I, Kolonne A). Die Kurve in Fig. 7 zeigt, dass in den ersten vier Stunden der Hauptanteil des Hydratationswassers verdampft. Nach 25 Stunden ist das Gewebe getrocknet. Auch nach weiterer Trocknung während einiger Tage tritt keine Gewichtsveränderung mehr auf. Beim Nachtrocknen im Wärmeschrank (105°C) gehen aber nochmals 3 % des Gewichtes verloren. Das effektive Trockengewicht beträgt darnach bei diesem Blattmaterial im Durchschnitt 11 % des Frischgewichtes.

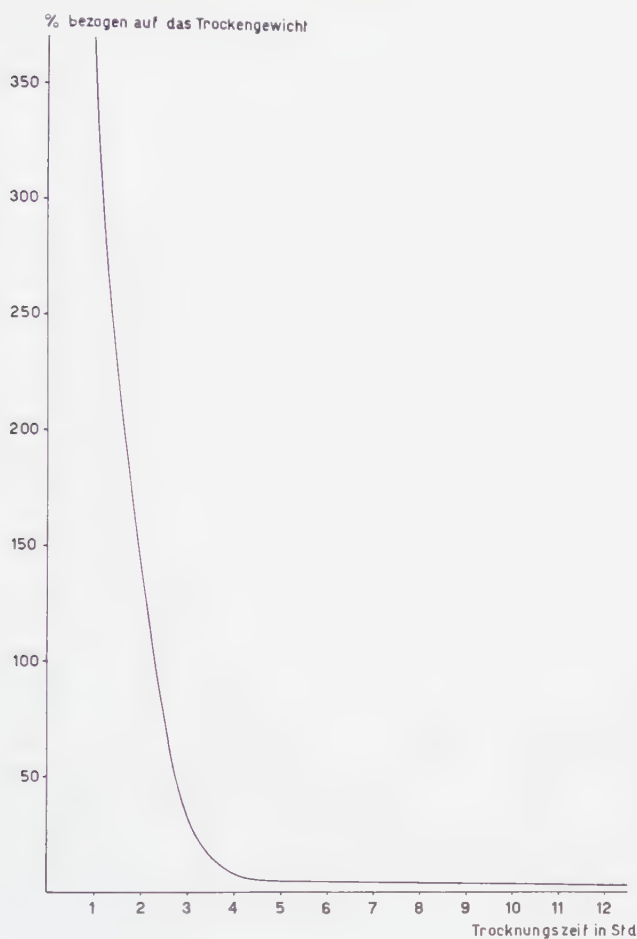


FIG. 7.—Wassergehalt in pflanzlichem Gewebe während der Trocknung über P_2O_5 bei $20^\circ C$.

Die Restwasserbestimmungen nach Gefriertrocknung ergaben ähnliche Kurven (Fig. 8). Mit sinkender Temperatur steigt die Trocknungszeit stark an. Das Kurvenbild wird dadurch immer flacher. Die Endwerte, die wir erreichten, zeigen, wie schwierig eine restlose Entfernung des Wassers aus dem pflanzlichen Gewebe sein kann. Nach 80 Stunden langer Trocknung bei $-60^\circ C$ bleiben im Gewebe immer noch 10 % Wasser bezogen auf das Trockengewicht zurück. Dieses Wasser muss irgendwie chemisch oder physikalisch stärker ans Gewebe gebunden sein. Obwohl wir für unsere morphologischen Untersuchungen bedeutend weniger Blattmaterial und auch viel kleinere Gewebestücke einfroren, hielten wir uns weitgehend an diese

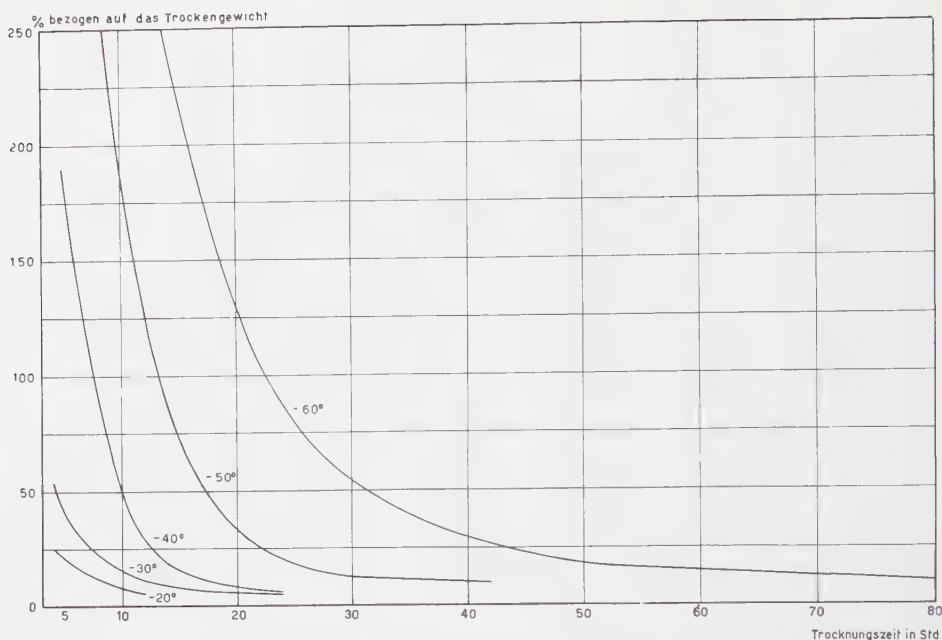


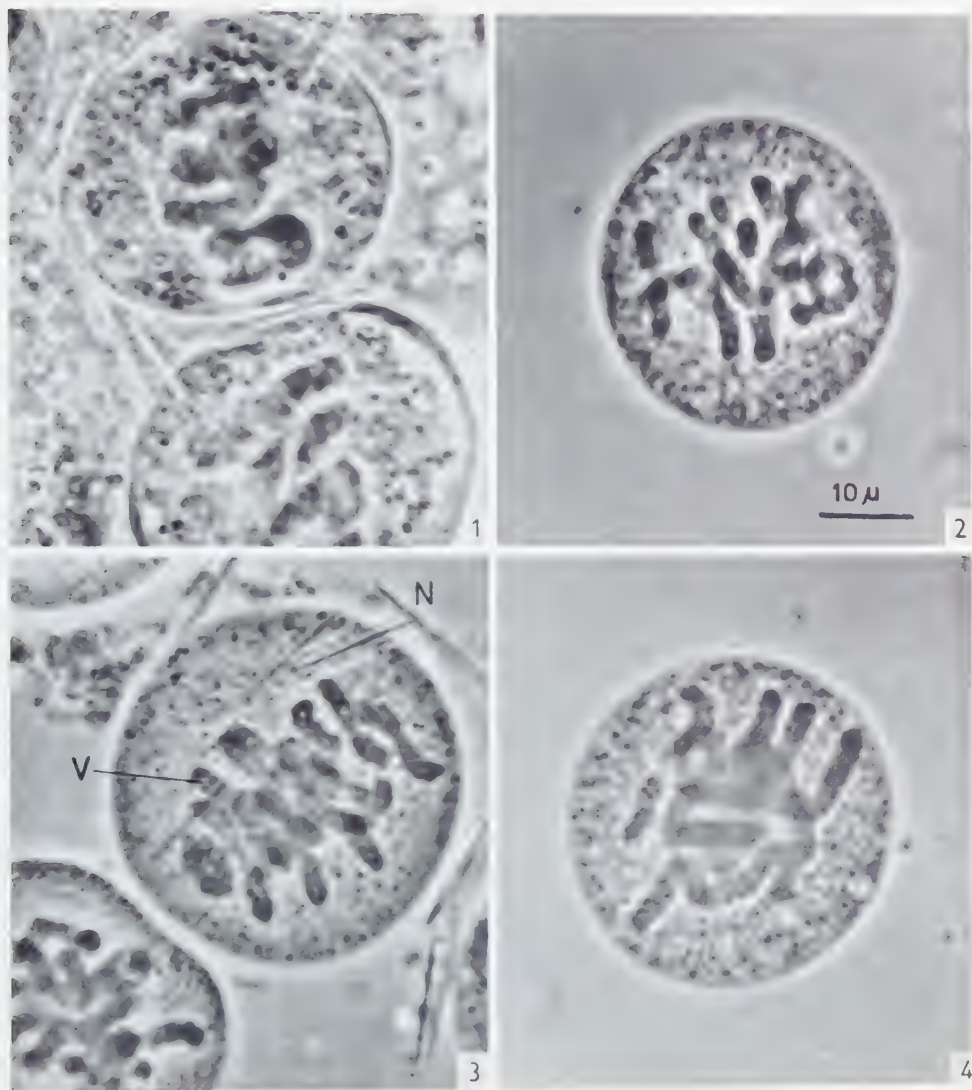
FIG. 8.—Restwassergehalt in pflanzlichem Gewebe nach der Trocknung bei tiefen Temperaturen.

Trocknungszeiten. Um einen noch besseren Dehydrierungsgrad zu erreichen, trockneten wir in den letzten zehn oder zwanzig Stunden bei höheren Temperaturen (bis gegen 0°C). Damit wurden die letzten Reste des Wassers entfernt und das Gewebe konnte gut eingebettet werden.

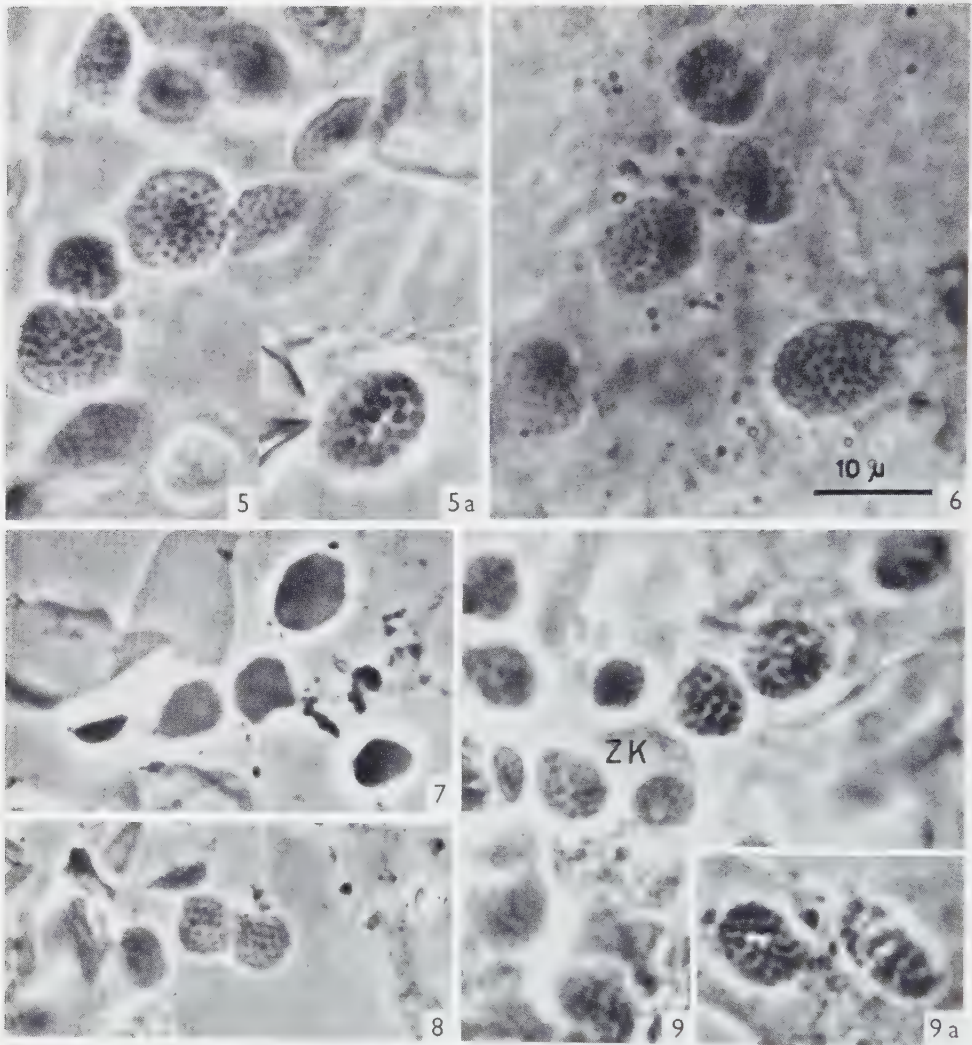
MORPHOLOGISCHE AUSWERTUNG

Pollenmutterzellen

Wir haben die Antheren von *Tradescantia virginiana* an feinen Nadelspitzen in flüssigem Propan auf -185°C abgeschreckt und bei -40° und -55°C im Hochvakuum 70 Stunden lang getrocknet. Darauf wurden sie unter Vorvakuum in wasserfreies Glycerin eingebettet. Schliesslich haben wir die Pollenmutterzellen aus den aufgeschlitzten Antheren herausgespült und in einem Tropfen Glycerin unter dem Mikroskop geprüft. Sämtliche mikroskopischen Aufnahmen machten wir mit einem Phasenkontrastmikroskop von Zeiss mit 90-fachem Objektiv und Ölimmersion. Für den morphologischen Vergleich wurden Pollenmutterzellen in der Metaphase ihrer ersten Reifeteilung ausgewählt. Diese stellen ein ausgeglichenes Testobjekt dar, in welchem die Chromosomenstruktur sich besonders schön vom umgebenden Plasma abhebt (Tafel I, Abb. 1–4).



TAFEL I.—Pollenmutterzellen von *Tradescantia virginiana*. 1190 \times . 1: lebende Pollenmutterzellen, Metaphase, in Paraffinöl. 2: nach Gefriertrocknung (Trocknungstemperatur -40°C , Trocknungszeit 70 h, in wasserfreiem Glycerin). 3: nach Gefriertrocknung (Trocknungstemperatur -40°C , Trocknungszeit 70 h, in wasserfreiem Glycerin; Vakuolen (V) entstanden durch Rekristallisation, N Kristallnadeln (Calciumoxalat). 4: nach Gefriertrocknung (Trocknungstemperatur -55°C , Trocknungszeit 70 h, in wasserfreiem Glycerin). Gute Fixation.



TAFEL II.—Chloroplasten von *Eucharis grandiflora*. 1540 \times . 5: Chloroplasten lebend in 0,15 molarer Rohrzuckerlösung. 6: mit gepufferter Osmiumsäure fixierte Chloroplasten. 7: nach Gefriertrocknung eingebettet in Weichparaffin bei 50 C, Granenstruktur zerstört. 8: nach Gefriertrocknung eingebettet in Weichparaffin bei 45 C, Granenstruktur erhalten. 9: nach Gefriertrocknung in wasserfreiem Glycerin, Trocknungstemperatur 55 C, Trocknungszeit 8 h. Granenstruktur gut erhalten, Chloroplasten leicht geschrumpft. In der Seitenansicht Geldrollenstruktur der Granen sichtbar (9a).

Die gefriergetrockneten Pollenmutterzellen weisen in ihrem mikroskopischen Bild verglichen mit den lebenden keine wesentlichen Artefakte auf (Abb. 1, 4). Bei einer Trocknungstemperatur von -40°C können aber in den Chromosomen $1-1,5\ \mu$ grosse Vakuolen V auftreten (Abb. 3). Sowohl in lebenden Zellen wie auch nach der Trocknung unter -50°C haben wir diese nie gefunden (Abb. 4). Sie müssen als Ergebnis einer erhöhten Rekristallisierung des Eises bei -40°C gedeutet werden.

Chloroplasten

Präparation: Wir haben an ausgewachsenen aber noch jungen, durch ihre hellgrüne Farbe gekennzeichneten Blättern von *Eucharis grandiflora* aus dem Schwammparenchym ca. $50\ \mu$ dicke Flächenschnitte hergestellt. Diese wurden entweder in einer 0,15 molaren Rohrzuckerlösung lebend unter dem Phasenkontrastmikroskop untersucht oder teils mit Osmiumsäure, teils durch Gefriertrocknung fixiert.

Das Osmiumsäuregemisch besteht aus einer 1 % OsO_4 -Lösung, welche mit Veronalacetat auf einen pH-Wert von 7,2 gepuffert wird (30, 33, 34). Nach einer Fixationsdauer von 4–5 Stunden werden die Schnitte in Tyrodelösung (40) gewaschen, in Äthylalkohol getrocknet und in Butylmethacrylat mit 0,5 % Benzoin eingebettet.

Die Flächenschnitte, welche wir mit der Gefriertrocknungsmethode fixierten, wurden bei -50° , -60° und -70°C getrocknet. Für den lichtmikroskopischen Vergleich haben wir sie in Glyzerin oder in Weichparaffin eingebettet (Abb. 7–9). Für die elektronenmikroskopische Präparation wurde dazu Methacrylat (s. oben) verwendet. Die Polymerisierung erfolgte sowohl nach Osmiumsäurefixierung als auch nach Gefriertrocknung mit ultraviolettem Licht (Abb. 10–14, 17). Daneben haben wir diese Methode verglichen mit der gewöhnlichen Methacrylateinbettung. Einige Gewebeschnitte wurden deshalb nach der Trocknung in einem Gemisch von Methyl- und Butylmethacrylat (1 : 10) mit 1 % 2,4-Dichlorbenzoyl-Peroxyd als Beschleuniger eingebettet und dieses bei 50°C polymerisiert (Tafel V, Abb. 15, 16).

Die Dünnschnitte wurden an einem LKB-Mikrotom nach Sjöstrand oder mit demjenigen von Porter und Blum hergestellt. Wir haben sie ohne das Einbettungsmittel zu entfernen im Philips-Elektronenmikroskop bei 60 kV Strahlspannung untersucht.

Ergebnisse: Die Chloroplasten aus den Blättern von *Eucharis grandiflora* zeigen in ihrem mikroskopischen Bild eine feine, regelmässige Granulierung (Tafel II, Abb. 5). Ihre mittlere Grösse beträgt $3-8\ \mu$ im Durchmesser. Unter dem Phasenkontrastmikroskop heben sich vom helleren Stroma die dunklen, runden Granenscheiben ab. Diese variieren in ihren Ausmassen ziemlich stark. Die grössten haben einen Durchmesser von $1\ \mu$ (Abb. 5a), während die kleinsten unter dem Mikroskop kaum mehr aufgelöst werden können. Heitz (16) stellte fest, dass die Granengrösse art- und gewebespezifisch ist und dass grosse jahreszeitliche Unterschiede auftreten.

In vielen Geweben nimmt ihre Grösse von aussen nach innen zu. Auch in unseren Flächenschnitten durch Schwammparenchym und Palisadengewebe haben wir grosse Unterschiede festgestellt. Trotzdem lassen sich die gefriergetrockneten Chloroplasten (Abb. 9, 9a) gut mit den lebenden vergleichen (Abb. 5, 5a). Die Granenstruktur wird durch die Gefriertrocknung kaum verändert, obwohl sich in den Chloroplasten leichte Schrumpfungen nachweisen lassen.

Es ist uns mit der hier beschriebenen Methode zum ersten Male gelungen, die submikroskopische Feinstruktur dieser Zellpartikel auch ohne chemische Fixierung im Elektronenmikroskop darzustellen.

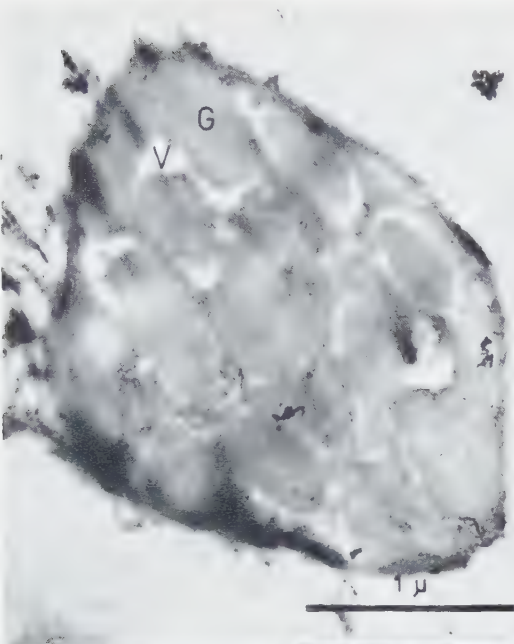
In Abb. 11 (Tafel III) ist eine Gruppe von mediangeschnittenen Chloroplasten getroffen. Sie zeigen eine deutliche Lamellierung aber noch keine Granenbezirke. Hodge, McLean und Mercer (17) haben solche granenlose Chloroplasten in den Parenchymzellen der Leitbündelscheide von *Zea Mays* gefunden. In unserem Objekt sind die Lamellen dichter aneinander gelagert und können kaum mehr einzeln aufgelöst werden. Sie sind hie und da unterbrochen von 0,35–0,5 μ grossen Vakuolen *V*.

In Abb. 12 ist ein junger Chloroplast mit einer durchgehenden Lamellierung des Stromas festgehalten, in welchem sich einzelne Granenbezirke *G* abzeichnen. Es handelt sich dabei nach dem Entwicklungsschema von Mühlethaler (31) um einen Jungchloroplasten. Werden die Plastiden horizontal geschnitten, heben sich die Granen als runde Scheiben mit Durchmessern von 0,25–0,5 μ vom Stroma ab. Ovale Formen wie in Abb. 10 treten dann auf, wenn die Granenreihen schräg angeschnitten werden.

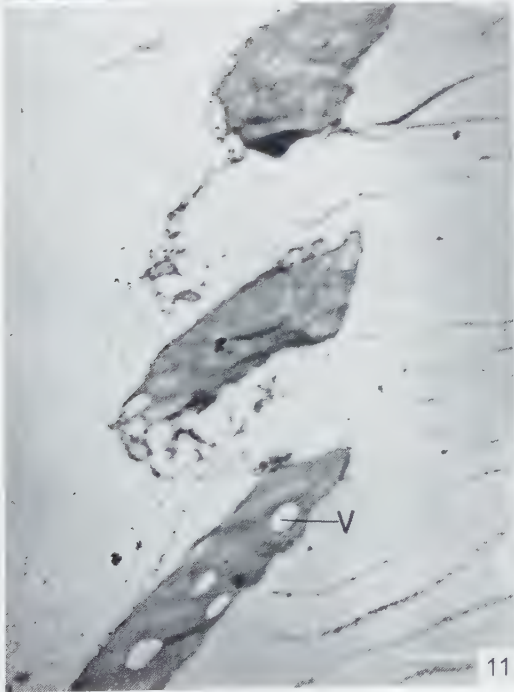
Nach der Fixierung mit Osmiumsäure erreichten wir bedeutend kontrastreichere Bilder als nach Gefriertrocknung (Tafel IV, Abb. 13). Dies ist darauf zurückzuführen, dass sich OsO_4 an ungesättigten Fettsäuren (34) und vor allem an den Doppelbindungen der Zystein-, Histidin- und Tryptophanseitenketten der Proteine anlagern kann (1, 6). Die eindeutige Wechselwirkung zwischen dichten, osmophilen Schichten und ihren hellen Zwischenzonen kann damit aber noch nicht erklärt werden.

Mit der Gefriertrocknung ist es nun möglich nach der Polymerisierung des Einbettungsmittels mit ultravioletttem Licht, Vergleichsbilder ohne chemische Veränderungen zu erhalten. So haben wir nach dieser Fixierung in den Plastiden ebenfalls eine eindeutige Lamellenstruktur gefunden (Abb. 12, 14). Dickenunterschiede zwischen gefriergetrockneten und osmiumsäurefixierten Lamellen können aber erst in einem Elektronenmikroskop mit besserem Auflösungsvermögen gemessen werden.

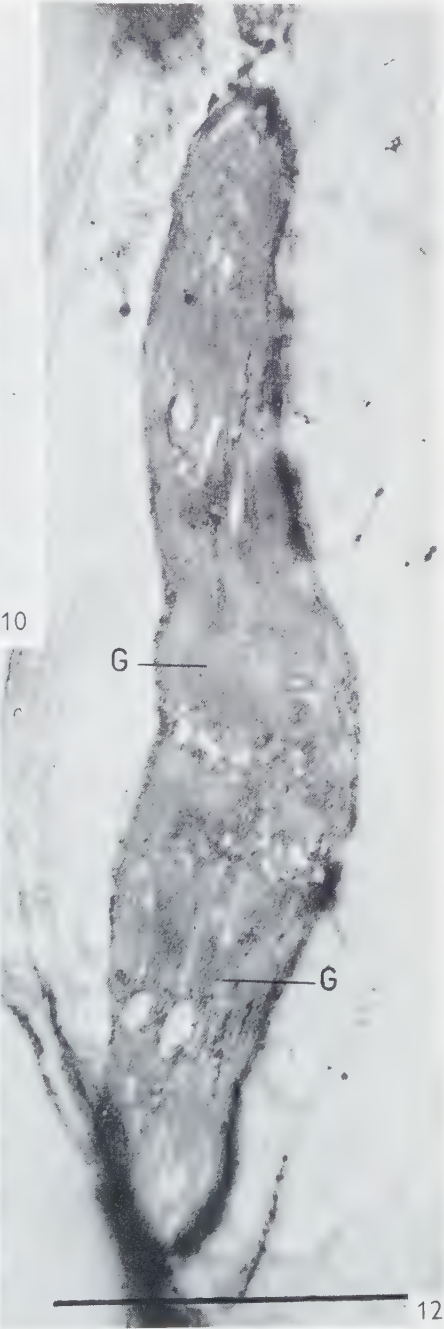
TAFEL III.—Chloroplasten von *Eucharis grandiflora*. Dünnschnittpräparate nach Gefriertrocknung: Verschiedene Trocknungstemperaturen: -50°C (11), -60°C (12), -70°C (10). 10: Flächenschnitt durch einen Chloroplasten, Granen *G* in der Aufsicht. *V* Vakuolen. 26800 \times . 11: Granenlose Chloroplasten mit Stärkevakuolen *V*. 9400 \times . 12: Median geschnittener Jungchloroplast mit einzelnen Granenbezirken *G*. 46000 \times .



10



11



12

TABELLE II

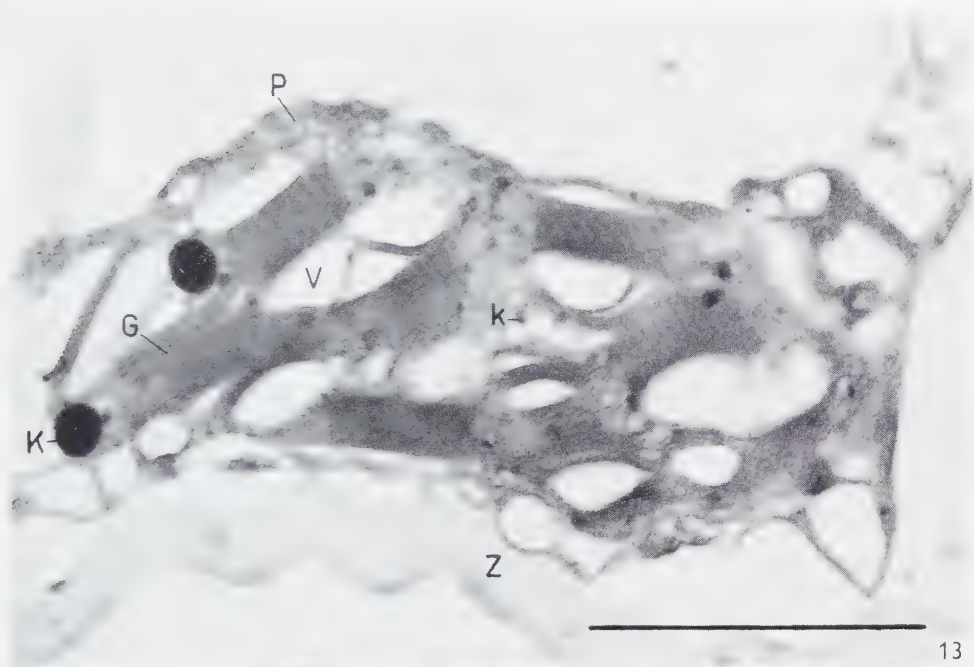
MESSWERTE AUS EINEM CHLOROPLASTEN VON *Eucharis grandiflora* NACH OSMIUMSÄURE-FIXIERUNG (TAFEL IV, ABB. 13)

| | |
|---|------------|
| Chloroplastendurchmesser | 2,7 μ |
| Grösste Dicke des Chloroplasten | 1,0 μ |
| Grösste Dicke des Peristromiums | 0,1 μ |
| Dicke des Granenbereiches <i>G</i> | 0,28 μ |
| Granendurchmesser (Durchschnitt) | 0,41 μ |
| Dicke der Stromalamellen | 85–90 Å |
| Dicke der osmophilen Schicht im Granenbereich | 50–55 Å |
| Dicke der hellen Zwischenzone | 60–65 Å |
| Anzahl Stromalamellen im Granenbereich <i>G</i> | 13–15 |
| Anzahl der osmophilen Schichten im Granenbereich <i>G</i> | 26–28 |

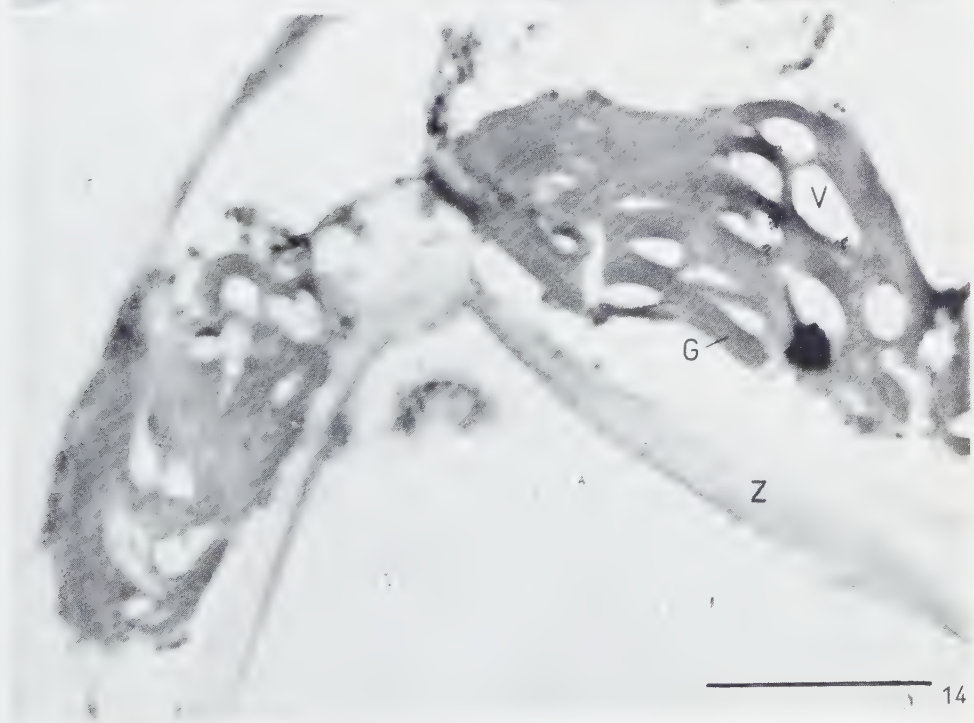
In den Granenbereichen werden die Stromalamellen in dicht ineinandergepackte Doppellamellen aufgeteilt (Abb. 13). Diese Aufspaltung in zwei dünnere osmophile Schichten entspricht in morphologischer Hinsicht dem in Mais-Chloroplasten vorgefundenen Typ (17). Das Zahlenverhältnis zwischen den Lamellen im Stroma und denjenigen im entsprechenden Granenbereich beträgt 1 : 2. Dies stimmt wiederum mit den Resultaten von Hodge, McLean und Mercer (17) überein. Doppelte Trägerlamellen, wie sie Steinmann und Sjöstrand (42) an *Aspidistra*-Chloroplasten darstellten, konnten wir nicht nachweisen. Die Ausmasse der Lamellen weichen aber von den bis heute beschriebenen Chloroplasten ab (Tabelle II). Strugger (44) hat an *Chlorophytum comosum* 240–290 Å dicke Stromalamellen gefunden. In *Zea Mays* (17) sind sie 125 Å und in *Aspidistra elatior* nur 30 Å dick. In *Eucharis grandiflora* haben wir für diese Lamellen eine Dicke von 85–90 Å gemessen. Auch die osmophile Schicht im Granenbereich ist mit 50–55 Å etwas weniger dick als in den Chloroplasten von *Aspidistra* (65 Å). Dagegen stimmen die Werte der hellen Zwischenzonen mit 60–65 Å eher mit diesem Objekt überein.

Die lamellierte Zone ist in den Chloroplasten häufig durch eine fein granulierte äussere Stromaschicht *P* (Abb. 13) eingeschlossen. Diese Schicht wird von Mühlethaler (29) und Strugger (44) als das nach der Theorie von Senn geforderte Peristromium bezeichnet. Nach der Fixierung mit Osmiumsäure treten gewöhnlich ausserhalb der Granen stark osmophile, kugelige Körperchen *K* auf, welche einen Durchmesser von ca. 0,2 μ aufweisen. Man hat diese auch in den Chloroplasten von *Aspi-*

TAFEL IV.—Chloroplasten von *Eucharis grandiflora*. *G* Granenreihen, *K*, *k* osmophile Körperchen, *P* Peristromium, *V* Vakuole, *Z* Zellwand. 13: In Osmiumsäure fixierter Chloroplast, Polymerisation mit ultraviolettem Licht. 44300 \times . 14: Chloroplasten nach Gefriertrocknung, Polymerisation mit ultraviolettem Licht. 29500 \times .



13



14

distra, *Agapanthus* und *Zea Mays* vorgefunden (17, 22, 29, 42). Daneben sind im Stroma ähnliche Gebilde *k* zu sehen, die aber bedeutend weniger dicht sind und einen Durchmesser von nur 400 Å besitzen. In gefriergetrockneten Chloroplasten liessen sich solche Erscheinungen nie nachweisen.

DISKUSSION

ARTEFAKTPROBLEM

Die Artefakte, die bei jeder chemischen Fixation auftreten, sind das Resultat tiefgreifender, irreversibler Störungen im submikroskopischen Gefüge eines Gewebes. Sie treten als Ergebnis von Schrumpfungen oder Quellungen oder von Verflüssigungs-, Koagulations- und Entmischungsvorgängen auf. Sie verursachen Veränderungen im kolloiden und chemischen Bestand des Plasmas und in seiner mikroskopischen Erscheinung. Daher muss man für die Beurteilung einer Fixation chemische und morphologische Gesichtspunkte trennen.

Für histochemische Untersuchungen ist die Erhaltung des chemischen Vitalbestandes oder doch bestimmter Substanzen ausschlaggebend. Wenn möglich soll auch eine Denaturierung vermieden werden. Das Ausmass der strukturellen Veränderungen spielt dabei keine grosse Rolle. Diesen kommt dagegen für morphologische Probleme eine grosse Bedeutung zu. Das denaturierte Plasma weist je nach dem verwendeten Fixationsmittel eine spezifische Struktur auf (4, 15, 34). Nach Osmiumsäure-, Sublimat- oder Formolfixierung erscheinen die plasmatischen Strukturen im mikroskopischen Bild verfeinert, regelmässiger, oft unscheinbar oder ganz ausgelöscht. Wendet man dagegen Chromsäure, Pikrinsäure, Alkohol oder Eisessig an, werden die Strukturen gröber, schwammig oder vakuolisiert. Durch verschiedene Gemische der einzelnen Komponenten und durch Zusatz von Pufferlösungen in die sauren Fixationsmittel versucht man, die ursprüngliche Struktur zu erhalten.

Für elektronenmikroskopische Untersuchungen werden die pflanzlichen und tierischen Gewebe heute vorwiegend mit gepufferter Osmiumsäure fixiert. Diese Fixierung und die Dünnschnittechnik haben in den letzten Jahren zur Aufklärung der submikroskopischen Lamellen in den Chloroplasten verschiedener Pflanzen geführt (17, 22, 42, 44). Dadurch wurde die früher schon polarisationsoptisch nachgewiesene Schichtenmischkörperstruktur (7, 9, 26) bestätigt. Nach Frey-Wyssling (8) stellen die Lamellen in den Chloroplasten Lipoproteinkomplexe dar, in welchen die Pigmente und Lipoide in monomolekularen Schichten eingelagert sind. Es ist heute noch sehr unklar, wie weit durch die Fixierung mit OsO_4 die Form und Dichte der submikroskopischen Strukturen beeinflusst werden. Die Gefriertrocknungsmethode gibt uns die Möglichkeit, Vergleichsbilder von chemisch unveränderten Zellbestandteilen

herzustellen. Dies ist aber nur dann möglich, wenn die chemisch äusserst labilen, fermentaktiven Gewebe nach der Trocknung keine strukturellen Veränderungen mehr erfahren. Die Vorteile dieser Methode liegen vor allem darin, dass die Fixierung sehr schnell erfolgt und keine Denaturierung der Eiweisse auftritt.

Die Gefriertrocknung wurde denn auch mit Erfolg zur Untersuchung von Viren und Bakterien durchgeführt (49, 51). Die Mikroorganismen werden nach der Trocknung im Vakuum schräg mit Chrom bedampft und entweder direkt oder an einem Kohleabdruck nach dem Replica-Verfahren im Elektronenmikroskop abgebildet (41). Mit dieser Präparationsmethode erhält man Aufschluss über die Form und die Oberflächenstrukturen von biologischen Objekten. Zur Aufklärung der Innenstruktur sind wir auf Dünnschnitte angewiesen. Die Präparation von gefriergetrocknetem Gewebe zur Herstellung von solchen Schnitten ist aber mit Schwierigkeiten verbunden, weil die Objekte nach der Trocknung sehr hygroskopisch, chemisch labil und — besonders die lipoidreichen Bestandteile — äusserst empfindlich auf hohe Temperaturen sind.

ARTEFAKTE AN GEFRIERGETROCKNETEM GEWEBE

Beim Einfrieren von grossen Gewebestücken kommt es im Plasma und im Zellkern zur Bildung von Eiskristallen. Nach Bretschneider und Elbers (5) können diese im getrockneten Gewebe bis $1\ \mu$ grosse Vakuolen hinterlassen. Aus Abb. 17 (Tafel V) sieht man, dass jeder Zellbestandteil eine typische Vakuolengrösse aufweist. Der Zellkern *ZK* zeigt in seinem Innern — eingeschlossen von einer deutlich sichtbaren Membran — zwei verschieden dichte Massenanteile. Beide sind von feinen Vakuolen durchsetzt. Im dichteren Teil erreichen diese eine Grösse von $500\ \text{\AA}$ und in den helleren Bereichen eine solche von $750\ \text{\AA}$ im Durchmesser. Auch im Plasmabelag *Pl*, welcher Kern und Plastiden einfasst, liegen ähnliche Verhältnisse vor. Im dichteren Plasma *Pl*₁ haben wir eine bedeutend geringere Vakuolisierung als im wesentlich dünneren *Pl*₂, welches durch eine typische Schaumstruktur charakterisiert wird. Es ist denkbar, dass die grossen Vakuolen nicht allein durch die beim Einfrieren verursachte Eiskristallbildung hervorgerufen werden, sondern dass sie ebensogut Trocknungsartefakte darstellen können. Je nach dem Wassergehalt der Zellbestandteile weisen sie daher so starke Grössenunterschiede auf.

Wir haben für unsere Untersuchungen nur kleine und sehr dünne Flächenschnitte eingefroren. Damit konnten wir wenigstens in den Chloroplasten, welche, verglichen mit dem Grundcytoplasma, wenig Wasser enthalten, eine Eiskristallbildung vermeiden. Die Vakuolen, die trotzdem in den Plastiden zu finden sind, müssen mit einer bestimmten physiologischen Funktion dieser Zellorgane in Beziehung gebracht werden, da sie auch in chemisch fixiertem Gewebe in gleicher Grösse auftreten

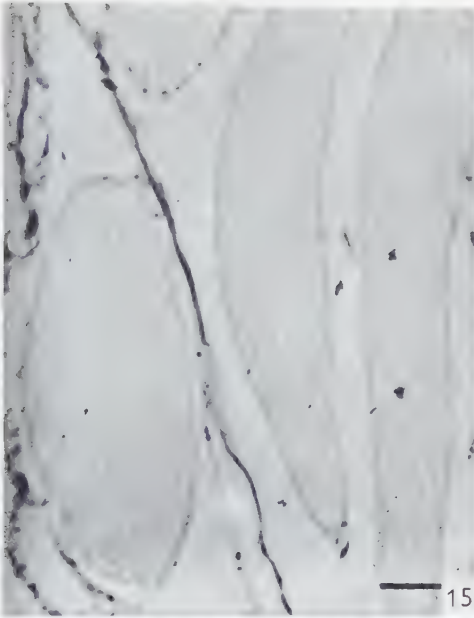
(Abb. 13). In Chloroplasten von *Aspidistra elatior* und *Zea Mays* wurden in diesen Hohlräumen Stärkekörner gefunden (17, 22). Wir konnten solche Körner mit Durchmessern bis zu $3\ \mu$ auch in ausgewachsenen Chloroplasten von Blättern nachweisen, welche 30 Stunden lang belichtet wurden. Sie sind zwischen die Granen eingelagert und lassen sich unter dem Mikroskop mit der Jodprobe eindeutig als Stärke bestimmen. In dunkel adaptierten Blättern konnten wir sie nicht mehr finden. Es muss sich um transitorische Stärke handeln, welche über Nacht abgebaut wird. Weil wir unsere Schnitte am Morgen zwischen 9 und 10 Uhr fixierten, fehlt die Stärke in den Vakuolen.

Die typischen Artefakte, die man an gefriergetrockneten Gewebeschnitten beobachtet, sind neben der Eiskristallbildung beim Einfrieren besonders auf die Wirkung bestimmter Einbettungsmittel und auf zu hohe Temperaturen bei der Einbettung zurückzuführen. Dabei verquellen die Chloroplasten und die Pigmente und Lipide werden aus den Lipoproteinkomplexen herausgelöst (Tafel V, Abb. 15). Eine auffallende Verquellung tritt auch dann auf, wenn das Gewebe nach der Gefriertrocknung mit OsO_4 -Dampf nachfixiert wird (Abb. 16). Diese kann oft so weit gehen, dass die Grenzmembranen der Plastiden aufspringen. Durch schnellere Polymerisierung mit ultraviolettem Licht bei tiefen Temperaturen kann diese als „Popcorn“-Effekt bekannte Erscheinung eindeutig vermieden werden (25, 46). Ebenso unterbleibt ein Herauslösen der Pigmente. Die Blattschnitte behalten daher im festen Methacrylat ihre grüne Farbe.

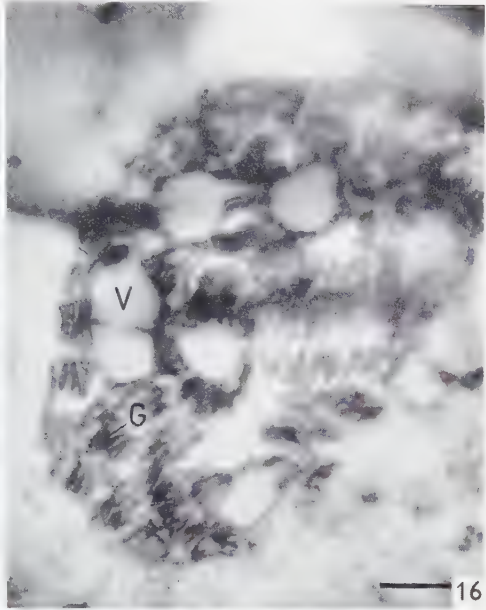
Schwierigkeiten, die etwa beim Schneiden auftreten, gehen gewöhnlich auf eine mangelhafte Trocknung der Gewebe zurück. Das Objekt wird dann vom Methacrylat nicht vollständig durchdrungen und daher beim Schneiden aus dem Blockchen herausgerissen.

An Chloroplasten, welche bei verschiedenen Trocknungstemperaturen von -50° bis 70°C entwässert wurden, konnten wir keine strukturellen Unterschiede nachweisen. Vor allem fanden wir keine störenden Vakuolen, die auf eine Rekristallisierung oder auf eine Eiskristallbildung beim Einfrieren hindeuten würden. Sind diese aber einmal ausgeschaltet, kann uns die Gefriertrocknungsmethode bei vorsichtiger Präparation neue Möglichkeiten für die elektronenmikroskopische Auswertung nichtdenaturierter Gewebe erschliessen.

TAFEL V.—Artefakte. 15: Chloroplasten von *Eucharis grandiflora* nach Gefriertrocknung. Polymerisation des Methacrylates im Wärmeschrank bei 50°C . Chloroplasten verquollen, Innenstrukturen durch Herauslösen der Pigmente und Lipide vollständig zerstört. 7700 \times . 16: Chloroplast von *Eucharis grandiflora* nach Gefriertrocknung mit OsO_4 -Dampf nachfixiert. Polymerisation des Methacrylates im Wärmeschrank. Chloroplast verquollen, Granenstruktur *G* erhalten. *V* Vakuolen. 9300 \times . 17: Dünnschnitt aus dem Mesophyll von *Aspidistra elatior* mit Eiskristall- und Trocknungsartefakten, nach Gefriertrocknung und UV-Polymerisation des Methacrylates. ZK Zellkern, *P* Plastiden, *Pl*₁ dichter Plasmabelag, *Pl*₂ dünner Plasmabelag. 12200 \times .



15



16



17

LITERATUR

1. BAHR, G. F., *Exptl. Cell Research* **7**, 443 (1954).
2. BELL, L. G. E., in „Freezing and Drying“, S. 35. *Symp., London*, 1951.
3. BENSLEY, R. R. und GERSH, I., *Anat. Record* **57**, 217 (1933).
4. BRETSCHNEIDER, L. H., *Proc. Koninkl. Ned. Akad. Wetenschap.* **53**, 1476 (1950).
5. BRETSCHNEIDER, L. H. und ELBERS, P. F., *Proc. Koninkl. Ned. Akad. Wetenschap.* **55**, 675 (1952).
6. FINEAN, J. B., *Exptl. Cell Research* **6**, 283 (1954).
7. FREY-WYSSLING, A., *Protoplasma* **29**, 279 (1937).
8. ——— *Discussions Faraday Soc.* **6**, 130 (1949).
9. FREY-WYSSLING, A. und STEINMANN, E., *Biochim. et Biophys. Acta* **2**, 254 (1948).
10. GERSH, I., *Anat. Record* **53**, 309 (1932).
11. ——— in „Freezing and Drying“, S. 165. *Symp., London*, 1951.
12. GERSH, I., und STEPHENSON, J. L., in HARRIS, R. J. C. (Ed.), *Biological Applications of Freezing and Drying*, S. 329. Academic Press Inc., New York, 1954.
13. GLICK, D. und BLOOM, D., *Exptl. Cell Research* **10**, 687 (1956).
14. GOODSPEED, T. H., UBER, F. M. und AVERY, P., *Univ. Calif. Publ. Botany* **18**, 33 (1935).
15. HAGUENAU, F. und BERNARD, W., *Exptl. Cell Research* **3**, 629 (1952).
16. HEITZ, E., *Planta* **26**, 134 (1936).
17. HODGE, A. J., MC LEAN, J. D. und MERCER, F. V., *J. Biophys. Biochem. Cytol.* **1**, 605 (1955).
18. HOERR, N. L., *Anat. Record* **65**, 66 (1936).
19. JENSEN, W. A., *Stain Technol.* **29**, 3 (1954).
20. JENSEN, W. A. und KAVALJIAN, L. G., *Stain Technol.* **32**, 33 (1957).
21. KULENKAMPE, H., *Z. wiss. Mikroskop.* **62**, 7 (1955).
22. LEYON, H., *Exptl. Cell Research* **7**, 609 (1954).
23. LUYET, B. J., in „Freezing and Drying“, S. 77. *Symp., London*, 1951.
24. LUYET, B. J. und GEHENIO, P. M., *Biodynamica* **3**, 33 (1940).
25. MASSEY, B. W., *Stain Technol.* **28**, 19 (1953).
26. MENKE, W., *Kolloid-Z.* **85**, 256 (1938).
27. MERYMAN, H. T., *Science* **124**, 515 (1956).
28. MERYMAN, H. T. und HALE, W. T., Naval Med. Research Inst. Rept. Bethesda, 1955.
29. MÜHLETHALER, K., *Internat. Rev. Cytol.* **4**, 197 (1955).
30. ——— *Protoplasma* **45**, 264 (1955).
31. ——— *Naturwissenschaften* **7**, 204 (1957).
32. NEUMANN, K. H., *Grundriss der Gefriertrocknung*. „Musterschmidt“, Wissenschaftl. Verlag, Göttingen, 1952.
33. PALADE, G. E., *J. Exptl. Med.* **95**, 285 (1952).
34. PORTER, K. R. und KALLMANN, F., *Exptl. Cell Research* **4**, 127 (1953).
35. PRINGSHEIM, E. G. und PRINGSHEIM, O., *New Phytologist* **51**, 65 (1952).
36. RUCH, F., Vortrag Botanikertagung in Hann.-Münden, 1956.
37. SAXER, G., Zellfixierung durch Gefriertrocknung. Diplomarbeit, Zürich, 1953.
38. SCOTT, G. H., *Protoplasma* **20**, 131 (1933).
39. SJÖSTRAND, F., in „Freezing and Drying“, S. 177. *Symp., London*, 1951.
40. ——— *J. Cellular Comp. Physiol.* **42**, 15 (1953).

41. STEERE, R. L., *J. Biophys. Biochem. Cytol.* **3**, 45 (1957).
42. STEINMANN, E., und SjöSTRAND, F. S., *Exptl. Cell Research* **8**, 15 (1955).
43. STRUGGER, S., *Ber. deut. bot. Ges.* **64**, 69 (1951).
44. — *ibid.*, **69**, 177 (1956).
45. SYLVÉN, B., in „Freezing and drying“, S. 169. *Symp., London*, 1951.
46. VOGEL, A., *Experientia* (im Druck).
47. WEINREB, ST., *Science* **121**, 774 (1955).
48. WILLIAMS, R. C., *Exptl. Cell Research* **4**, 188 (1953).
49. — in HARRIS, R. J. C. (Ed.), *Biological Applications of Freezing and Drying*, S. 303. Academic Press Inc., New York, 1954.
50. WOLKEN, J. J., *J. Protozool.* **3**, 211 (1956).
51. WYCKOFF, R. W. G., *Science* **104**, 36 (1946).
52. ZEIGER, K., *Physikochemische Grundlagen der histologischen Methodik*. Steinkopf Verlag, Dresden und Leipzig, 1938.

Graphic Reconstruction of the Third Dimension from Serial Electron Microphotographs¹

B. G. BANG and F. B. BANG

Department of Pathobiology, The Johns Hopkins University, School of Hygiene and Public Health, Baltimore, Md.

Received June 24, 1957

The third dimension may be reconstructed from a series of electron microphotographs (1) by a linear method which has been used by anatomists and embryologists since 1886 (4) and probably before. The usefulness and refinements of the method as applied to electron microscopy will increase in proportion to improvements in techniques of sectioning, but it already gives a clearer concept of some intracellular structures than may be realized from a single section. The same basic method may be used in building plastic models (3) of the structures but we are concerned at present with a graphic medium that may be inexpensively reproduced in print.

The partial reconstruction shown in Figs. 1 and 2 represents a slice about $\frac{1}{4}$ micron thick (inset), of the free surface of a ferret nasal epithelial cell (2) and was built from eleven serial sections. These sections (#10-21) were selected from a longer series because they showed minimal successive deviation due to the process of sectioning. Taking #21 as the most proximal and #10 the most distal in the series, the images in #21 (Fig. 1) were carefully traced in outline on a sheet of soft transparent flexible acetate plastic. On the same sheet, using these traced images as focal points, the outlines of those in #20 were traced with a hardlead color pencil, then those in #19 with another color. The drawing in Fig. 1 shows these three proximal superimposed tracings in ink, of course, instead of color. Tracings were then continued distally on the same sheet, using a different color for each successive section so that a permanent key to the positions in depth was available. The outlines of the combined superimposed eleven tracings are shown, in ink, in Fig. 2a.

Fig. 2b is a halftone rendering of the same tracings showing #21 as a cut surface. Since this includes only a thin slice of one portion of the cell, the forms and interrelations of the whole complement of mitochondria is not known. Fig. 3a shows the

¹ Supported by a Grant-in-Aid from the National Microbiological Institute (E-135) of the U.S. Public Health Service and Lasdon Foundation.



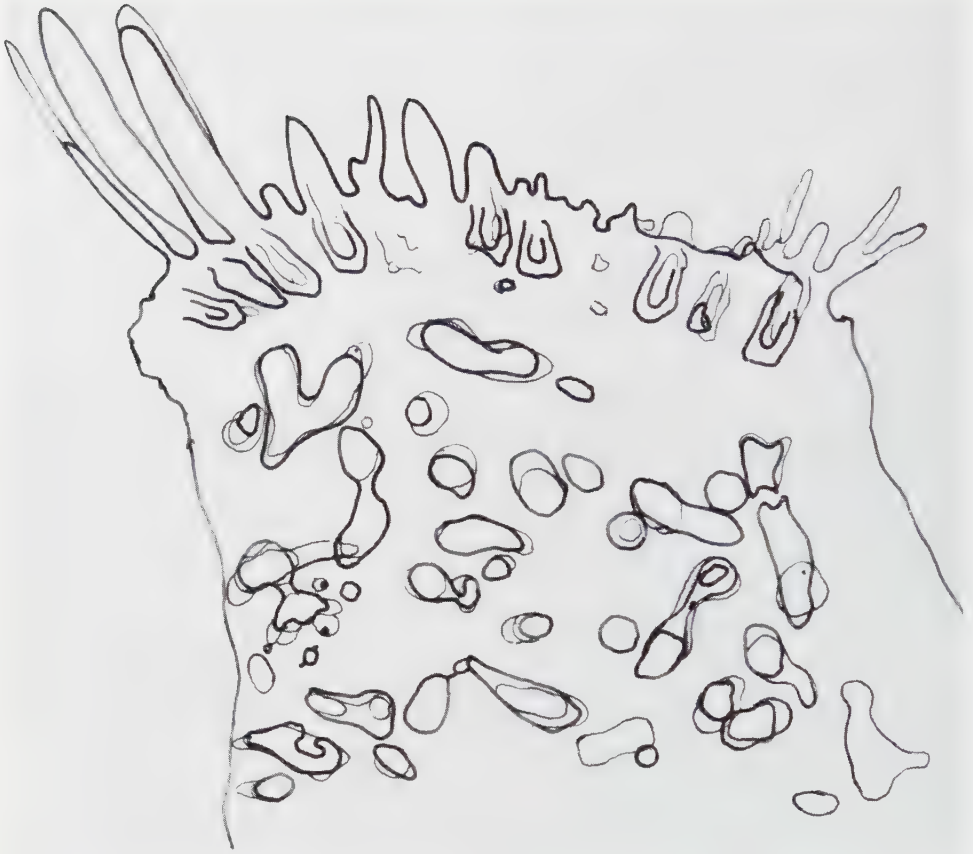
portions of mitochondria which are unequivocally conjoined within this slice. Artifacts and equivocal shadows were not traced.

Enlarged photographs of some of the individual components of an electron microphotographic series may also be used for reconstructions so that one basal body or one nucleolus, for example, can be rebuilt. Fig. 3*d* is a reconstruction of five enlarged serial photographs of mitochondrial fragments which seem to meet or to be within two adjoining normal human liver cells. *b* and *c* show the proximal two photographs in the series. A convenient way of presenting the dimension gained by serial sections so that a stereoscopic effect is seen is one which adapts the method of Vosmaer (5) to electron microscopic material. Oriented tracings in which structures of serial significance are filled in with translucent colored ink may be stacked at equal distances apart and then transilluminated from the distal end. Stiff, completely transparent plastic sheets are used and are kept equidistant by cardboard frames.

It should be emphasized that present sectioning techniques do not allow for serially perfect orientation of an entire photographic field so that single components may be compressed or may otherwise vary slightly in shape or position from one section to the succeeding one. The reconstruction, model or stereoscopic demonstration must therefore develop from serial tracings of each individual component and the final orientation of these components is their mean position within consistent fixed points.

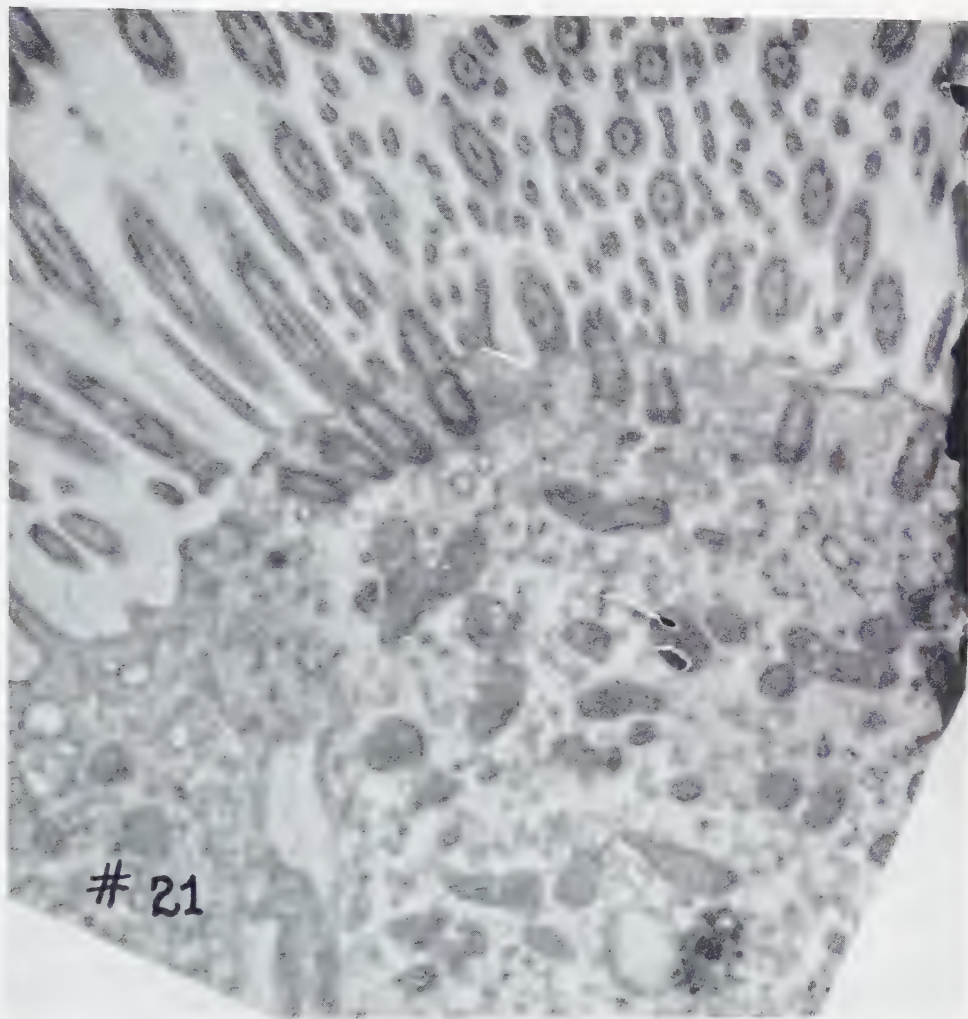
REFERENCES

1. BORYSKO, E., personal communication.
2. HOTZ, G. and BANG, F. B., *Bull. Johns Hopkins Hosp.* **101**, 175 (1957).
3. LEE, BOLLES, *The Microtomists Vade-Mecum*, 11th ed., p. 473. P. Blakiston's Son & Co., Philadelphia, 1950.
4. STRASSER, H., *Z. wiss. Mikroskop.* **3**, 179 (1886).
5. VOSMAER, G. C. J., *Anat. Anz.* **16**, 269 (1889).

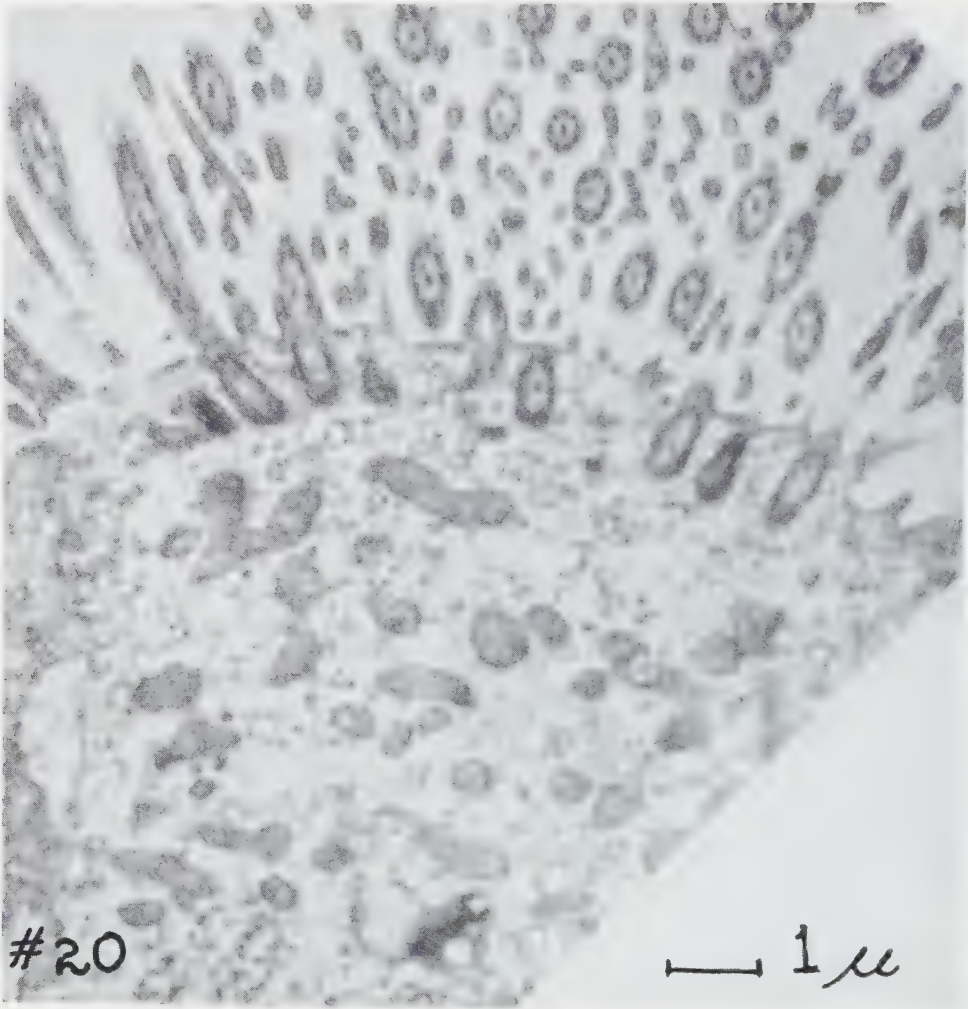


1 a.

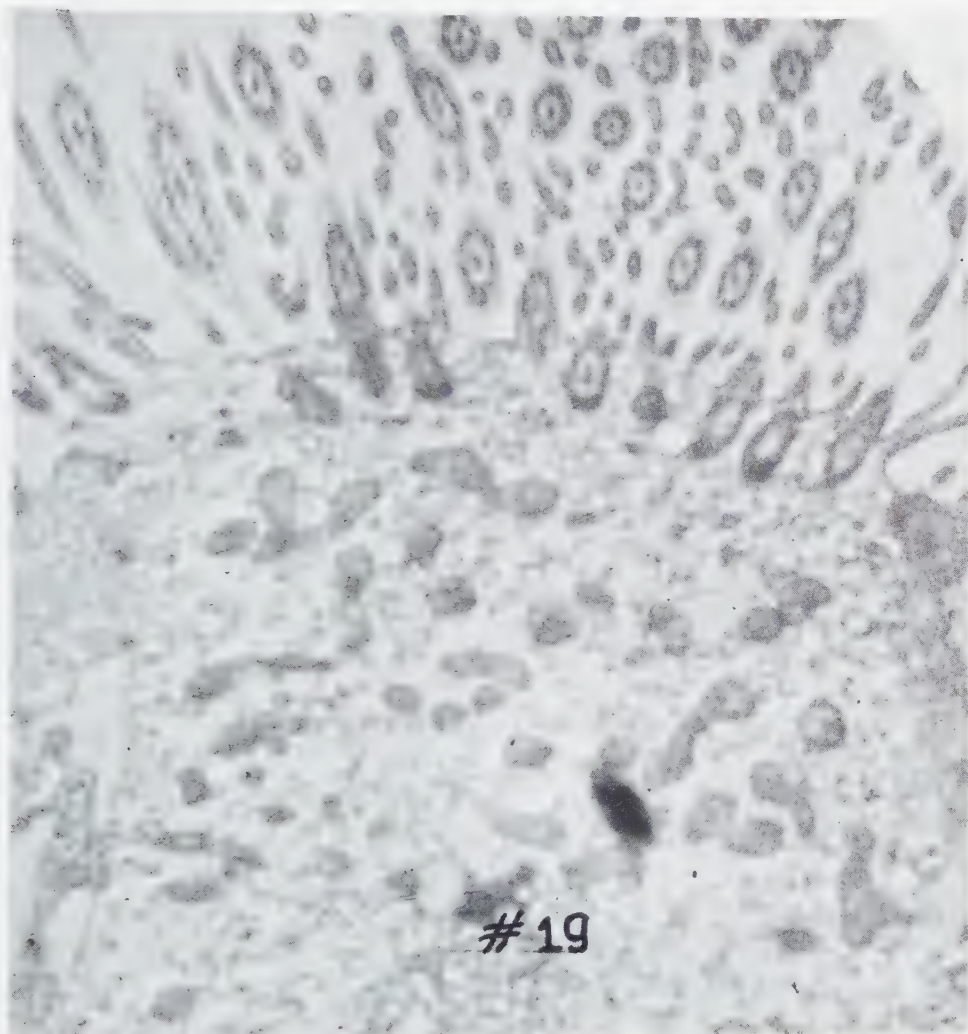
FIG. 1 *a-d*.—The line drawing shows ink tracings of mitochondrial fragments in the proximal three (#21, 20, 19) of eleven serial sections through the surface area of a ferret nasal ciliated epithelial cell, cut at right angles to the surface and photographed in the electron microscope. The tracings are superimposed, with the most proximal (#21) in slightly heavier lines.



1 b.



1 c.



1 d.



FIG. 2a.—The superimposed tracings of the mitochondrial fragments in all eleven serial electron microphotographs, with #21 again in the proximal position.

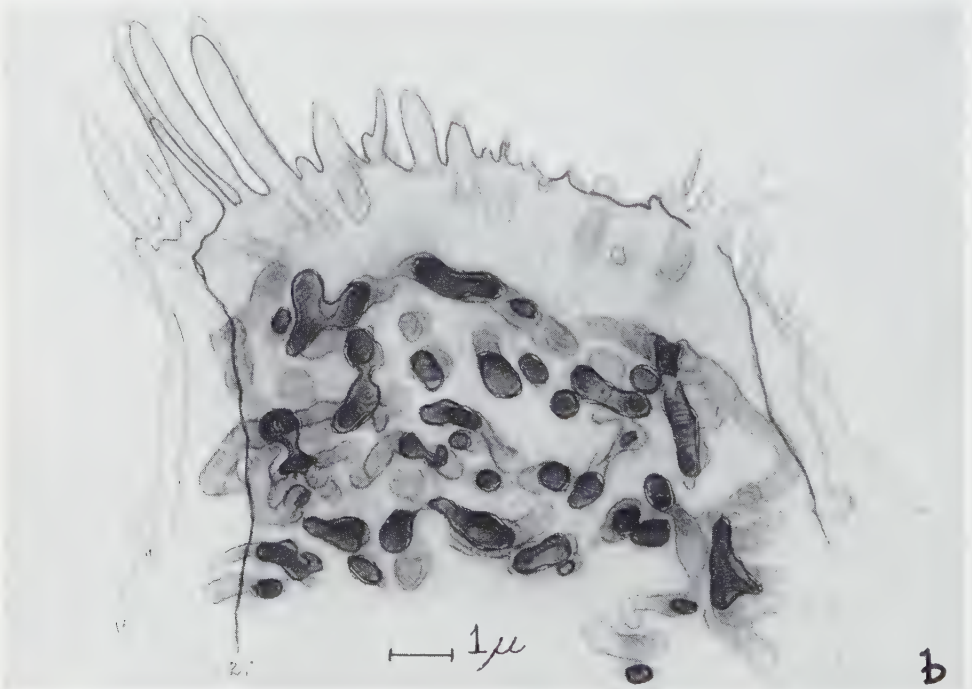


FIG. 2b.—A three dimensional reconstruction made from the serial tracings shown in ink in Fig. 2a. The original tracings were made in eleven different colors in order to have a key to each relative position in depth. #21 is shown as a cut surface.

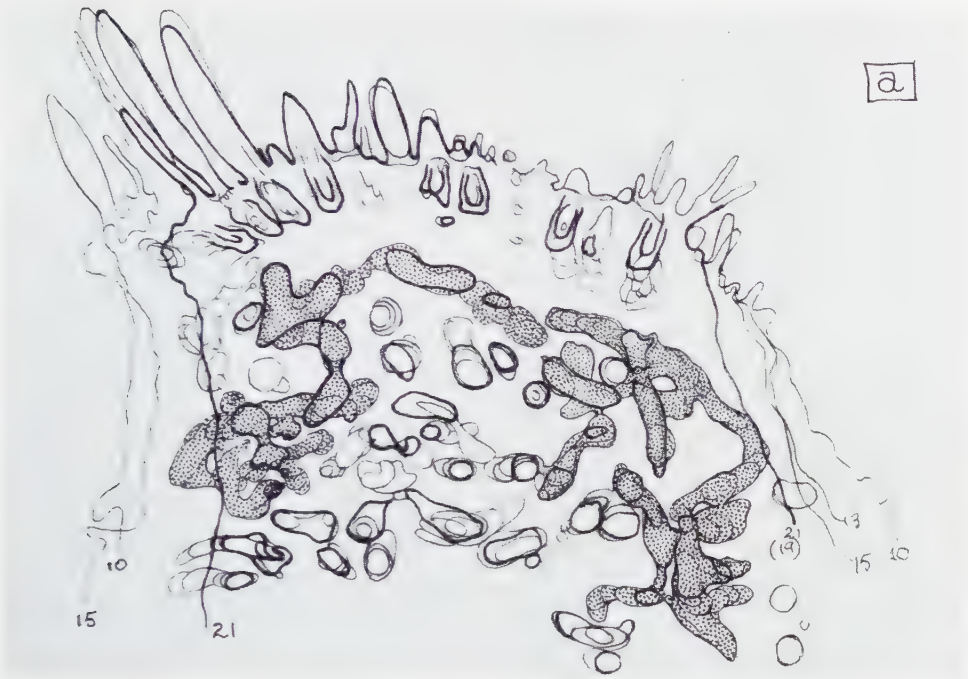


FIG. 3a.—The figure shows the portions of the mitochondrial fragments represented in Fig. 2b, which in this $\frac{1}{4} \mu$ slice, were joined together.

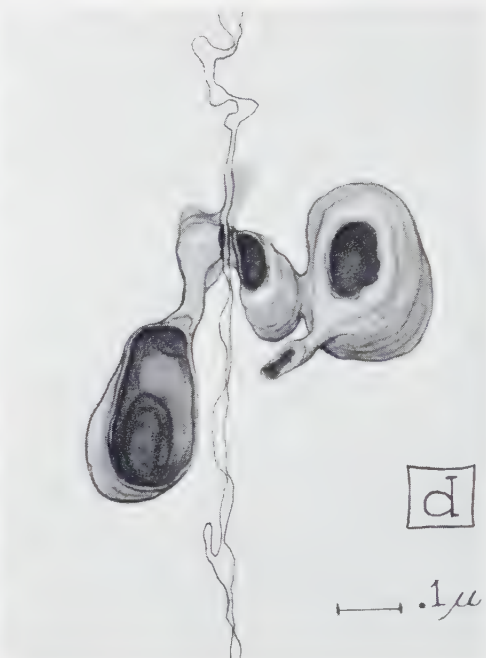
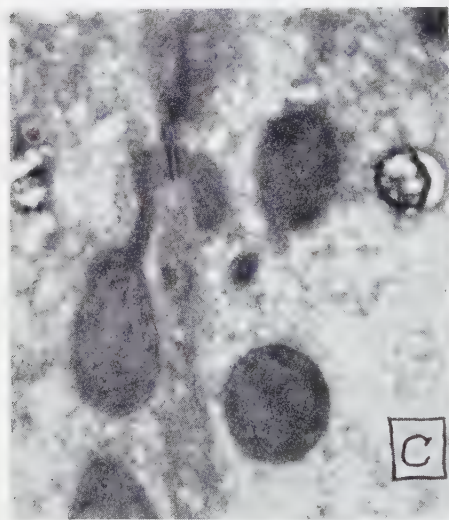
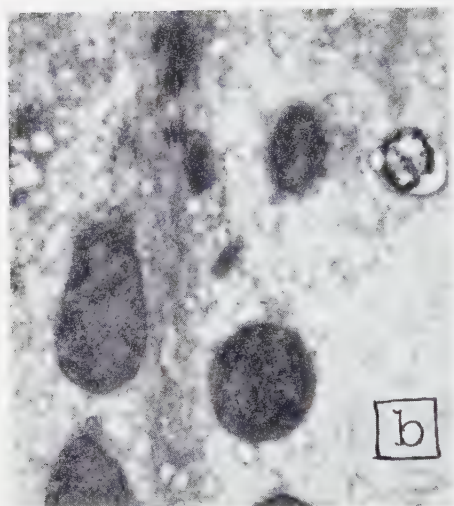


FIG. 3*b-d*.—*b* and *c* show the proximal two of five serial electron microphotographs of mitochondrial fragments at the border area between two normal human liver cells; *d* is a reconstruction of five serial sections through this area, with *b* as the proximal section shown as a cut surface.

High Resolution Microradiography with Ultrasoft X-Rays¹

A. ENGSTRÖM, B. LUNDBERG and GUDRUN BERGENDAHL

*Department for Medical Physics, Karolinska Institutet,
Stockholm*

Received August 27, 1957

A small compact microradiographic unit for microradiography with ultrasoft X-ray has been developed. The equipment is simple in operation and yields microradiograms with a linear resolution of about $\frac{1}{4}$ of a micron. The microradiograms recorded with soft and ultrasoft X-rays will show the distribution of dry weight in soft biological material, and also the distribution of water. The procedure of quantitative microradiography gives the possibility of obtaining accurate information about the parameters mentioned, and with an analytical error of only a few to ten per cent.

Various modifications of X-ray microscopy are continuously finding applications to several research fields, ranging from metallurgy and mineralogy to biology and medicine. Among the techniques of X-ray microscopy the microradiographic technique offers the most convenient technical procedure, and up till now this method gives the best linear resolution of biological specimens.

In recent years the technique for microradiography of extremely thin biological specimens has considerably advanced (1, 4-6). The value of X-ray microscopy is the combined structural and chemical information which is contained in the X-ray microscopic absorption image. Thus it is possible by X-ray microscopy to determine cytochemically the amount of certain elements (for survey see (4)), and the distribution of mineral salts in calcified tissues (for survey see (1)). The dry weight or mass of biological objects as well as the water content of cells and tissues can also be determined (2-4, 7). The chemical information contained in the microradiogram is obtained through measuring the X-ray attenuation within a microscopic structure of the specimen either by direct recording techniques or via photometry of the microradiographic image. Both procedures have recently been developed to a good precision, and the X-ray absorption can be determined with an error of only one to two per cent (7). Thus under favourable conditions of transmission the amount of substance can be determined with an error of only a few per cent.

¹ This investigation has been supported by grants from Statens Medicinska Forskningsråd, Riksföreningen för kräftsjukdomarnas bekämpande, SPP:s fond för cirkulationsforskning, and European Office Air Research and Development Command, contract AF 61(514)-861, through its European office in Brussels.

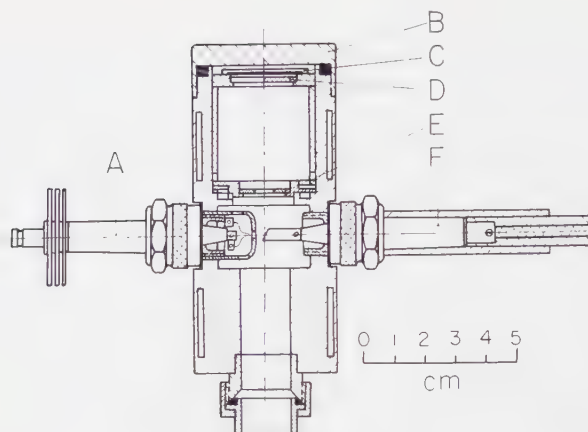


FIG. 1.—Cross-section of the small X-ray tube. *A*, cathode; *B*, removable lid; *C*, sample, mounted on the photographic emulsion; *D*, aperture containing a slit for the reference system; *E*, window, 1000 Å Al; *F*, anode, exchangeable.

In the following contribution some newly developed equipment for microradiography of biological materials utilizing ultrasoft X-rays will be described and a few applications given. X-rays with wavelengths between 1 and 10 Å are called soft and between 10 and 100 Å ultrasoft.

EQUIPMENT

The small X-ray tube earlier described (5) has been modified to ensure an easy operation. Fig. 1 shows a cross-section of the tube. The light from the filament is screened by a 1000 Å thick aluminium window and this window is thin enough to secure a high transmission of X-rays up to 50 Å, but thick enough to absorb the light from the hot filament, and also thick enough to stop all electrons scattered from the cathode. The emission of X-rays from the window is negligible. The sample and the film are placed in close contact with each other at a distance of about 20 mm from the focal spot. The holder containing the thin aluminium window has several channels so that the air can pass freely from the upper to the lower compartment during the evacuation of the tube. This arrangement is necessary as the 1000 Å thick window otherwise easily breaks during the evacuation procedure. The tube is continuously evacuated and has a by-pass valve system, so that when the sample is changed it takes not more than about one minute to have the tube for renewed operation. Good focusing of the electrons is obtained at about 1 mA current. Fig. 2 shows a photograph of the equipment, and the X-ray tube, the high vacuum diffusion pump (Distillation Products, Type VMF-20), the high voltage set and the vacuum meter are built together into a compact unit. The tube can be energized with voltages up to 5 kV from the high voltage generator which consists of a generator modified from a Philips CMR-5 unit (Fig. 3). After being in operation for some time the thin aluminium window becomes covered with a thin tungsten coating from the filament and hence has to be replaced. Therefore a small vacuum coating unit has been constructed which can be inserted on the place of the tube and run from the same unit. Fig. 4 shows a cross-section of the evaporation

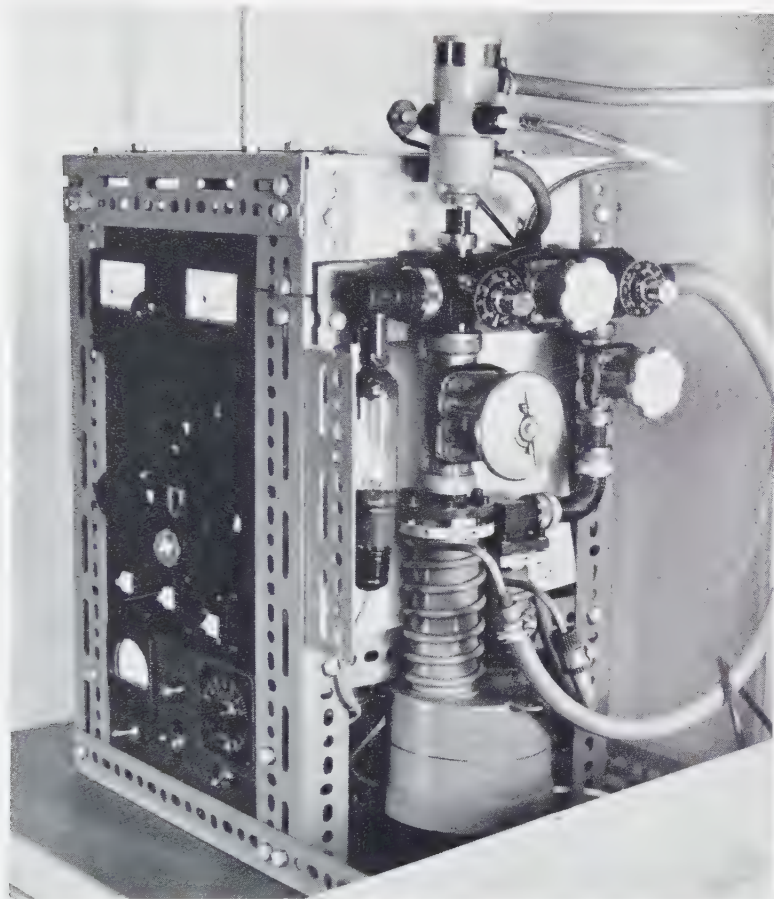


FIG. 2.—Photograph of the X-ray tube mounted on high vacuum diffusion pump and with the high voltage generator, exchangeable.

chamber and Fig. 5 its arrangement on a microradiographic unit. The equipment in Fig. 5 is similar to the one shown in Fig. 2 except that the high voltage set and the X-ray tube in this unit are separated. The thickness of the evaporated metal film is sufficient when the filament is barely visible through the evaporated layer.

The output of the X-ray tube was determined for several voltages and Fig. 6 gives the density per milliamperere-minute as a function of voltage. It is seen that for voltages of 1 kV or below the exposure times necessary to obtain a satisfactory density are in the order of

10 to 100 minutes. As a first approximation the voltage should be $V \approx 1.5 \cdot 10^4 \sqrt[3]{\rho t}$, where t is the thickness in cm, ρ the density of dried tissue in $\text{g} \cdot \text{cm}^{-3}$ and V the voltage in volts. The value of ρ for a dried tissue with its original spatial relationships is about 0.3.

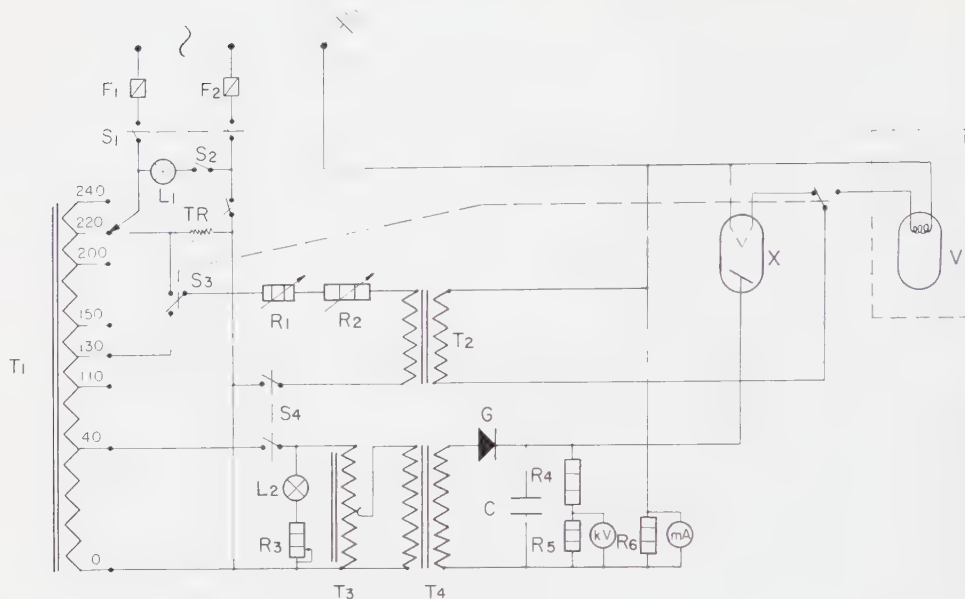


FIG. 3.—Wiring diagram for the electrical circuit.

- | | |
|---|---|
| <i>F1</i> Fuse 2 Amp. | <i>R4</i> $12 \times 820 \text{ kohm} + 220 \text{ kohm}$; 1 W |
| <i>F2</i> Fuse 2 Amp. | <i>R5</i> $2 \times 150 \text{ ohm} + 2 \times 100 \text{ ohm}$; 1 W |
| <i>S1</i> Main switch | <i>R6</i> 43 kohm 1 W |
| <i>S2</i> Light switch | <i>TR</i> Time relay 0–60 min. |
| <i>S3</i> X-ray and “vacuum coating” switch | <i>L1</i> Pilot light for instrument |
| <i>S4</i> High tension and filament switch | <i>L2</i> Pilot lights for high tension and filament |
| <i>T1</i> Main transformer | 6, 5 V 0, 1 A |
| <i>T2</i> Filament transformer 220 V/5 V, 10 A | <i>G</i> Rectifiers. Siemens $2 \times \text{E 3000 CS}$ |
| <i>T3</i> Variac 120 VA 40 V/0–40 | <i>C</i> Condensor 6000 V 0.25 μF |
| <i>T4</i> High tension transformer 40 V/6000 V 8 mA | mA 5 mA 8 mV |
| <i>R1</i> 50 ohm 50 W, potentiometer. | kV 100 μA 2500 ohm |
| <i>R2</i> 300 ohm 100 W, potentiometer. | <i>X</i> Midget X-ray tube |
| <i>R3</i> 400 ohm 8 W | <i>V</i> Vacuum coating unit |

PREPARATION OF SPECIMEN AND PHOTOGRAPHIC EMULSION

High resolution photographic emulsions are now commercially available; in this work Eastman Kodak Spectroscopic Plate type 649 and Kodak Maximum Resolution Plate have been used. Under suitable exposure conditions these plates have a resolution which is considerably better than 1000 lines per mm. It should be mentioned that the resolution of the plates seems to increase with decreasing energy of the X-rays, probably depending upon the lower energy of the various transforms of the X-rays created in the sample and emulsion. In the original X-ray weighing technique (2, 3) a microtome section or a smear of the tissue was placed on a thin collodion foil stretched over a hole in a metal holder. This set was then placed in contact with the fine-grained photographic emulsion and exposed to the soft or ultrasoft X-rays (2, 3, 7). In order to secure a better resolution, however, the specimen

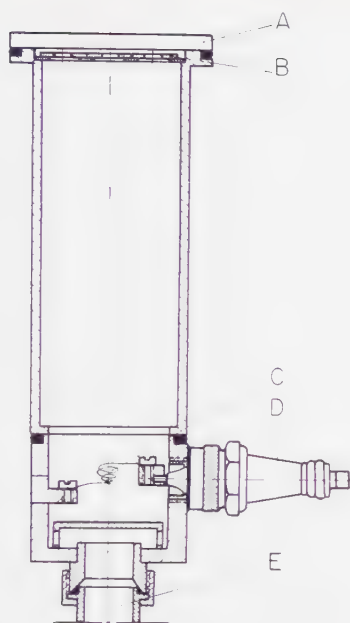


FIG. 4.—Simple vacuum coating chamber. *A*, removable lid of glass; *B*, holder for the specimens; *C*, heating foil; *D*, current inlet; *E*, connection to the vacuum system.

has to be mounted directly on the photographic emulsion and this procedure naturally must be performed under the safe light in the dark room (6). Pieces about 1 cm^3 in area are cut from the fine-grained photographic emulsion and these pieces are dipped for a short moment in a 1 % collodion solution and allowed to dry in the darkness in a vertical position. The collodion used for this very thin coating must be carefully filtered and kept in a dry atmosphere. Approximately, the coating of the photographic emulsion is only a few 100 \AA thick. The microtome sections of the tissue are floated onto the coated photographic plate and allowed to dry, and the section is subsequently deparaffinized in benzene or clean gasoline. Smears of cells and tissues can be made directly on the coated film. The film with the smear or the deparaffinized microtome section is exposed in the microradiographic camera, and after exposure the collodion is dissolved away in an alcohol-ether mixture. After washing, the plate is developed in the standard manner and after fixing and drying it is mounted with canada balsam on a glass slide with a cover slip to protect the small microradiographic image from scratching. The microradiogram is inspected in the light microscope and enlargements from it are obtained by photomicrography.

In order to permit quantitative measurements, the aperture in front of the photographic film has a small slit, and on this slit is mounted a small reference system built up of extremely thin collodion foils. This reference system has the form of a step wedge, thus situated a few tenths of a millimeter from the photographic emulsion. The individual steps are about 0.5 mm wide, and the small blurring caused by the separation of the reference system from the photographic emulsion does not influence the measurements of the X-ray absorption in each step. This arrangement also has the advantage that the same step wedge can be used

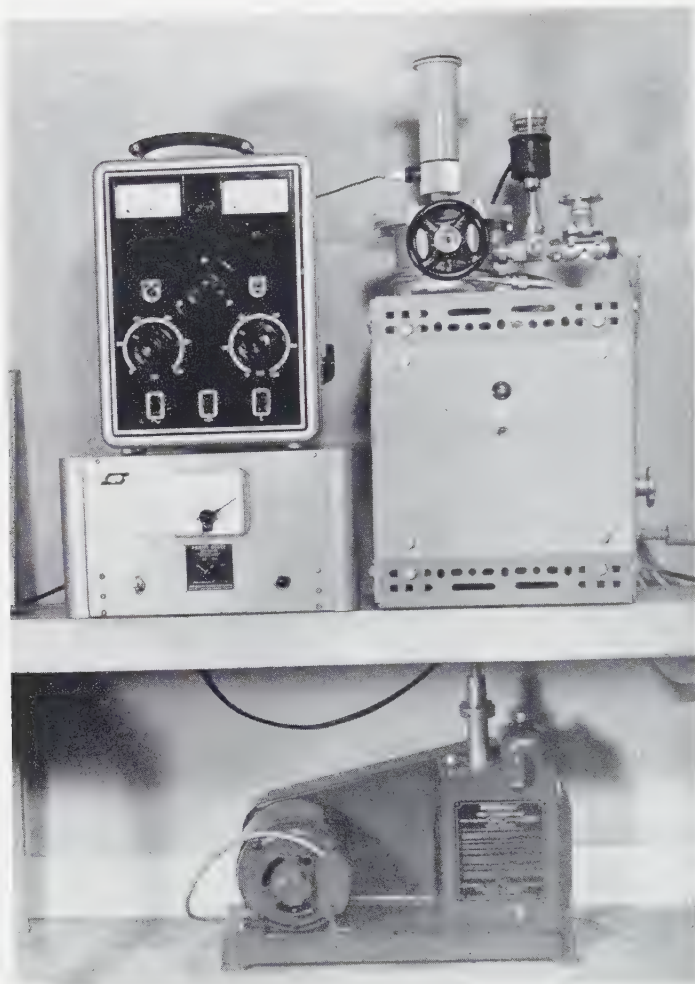


FIG. 5.—Photograph of the vacuum coating chamber inserted on the place of the X-ray tube. This equipment differs somewhat from the one shown in Fig. 2, the high voltage set and X-ray tube with pumps being separated.

for a great number of measurements, and the different biological structures can always be compared with the same reference system. The biological sample, however, must, as indicated above, always be in extreme contact with the photographic emulsion.

In general it is advisable to record two microradiograms, one heavily exposed and which is intended for visual inspection, and one less exposed which is to be used for the subsequent microdensitometry.

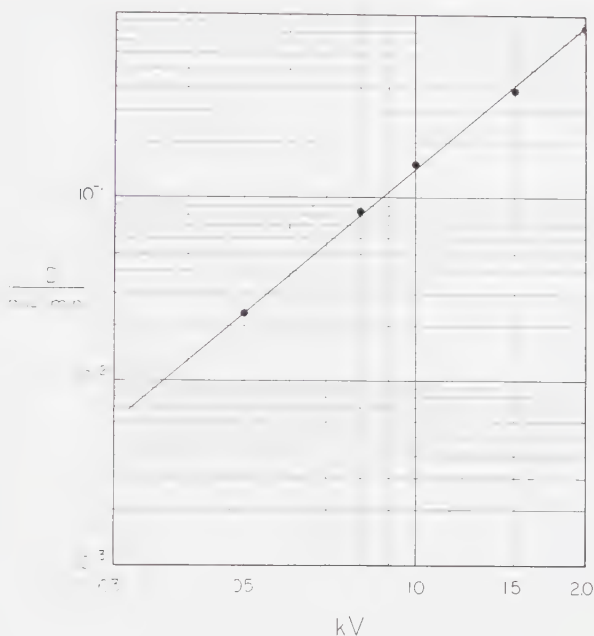


FIG. 6.—The performance of the X-ray tube. The density per milliampere minute as function of voltage.

PERFORMANCE OF THE MICRORADIOGRAPHIC UNIT

The following set of illustrations (Figs. 7-12) shows the resolution which can be obtained with this modification of the microradiographic technique. In the best microradiograms a resolution as good as a quarter of a micron has been observed, and we have the feeling that in many cases more resolution is contained in the microradiographic image than what can be taken out by the optical microscope. Besides the structural information these microradiographic images give a map of the distribution of dry mass within the biological specimen. Thus in the microradiogram of the muscle fiber it appears that the anisotropic bands have considerably higher mass than the isotropic ones. In the section of the aorta it is clearly seen that the elastica interna has a high dry weight as compared with the rest of the aortic wall.

DISCUSSION

It has been emphasized earlier that X-ray microscopy, of which microradiography is one technique, has the unique advantage of giving both structural and chemical information. In order to obtain as much information as possible from the specimen, the wavelengths of the X-ray used must naturally be properly chosen. Thus for elementary analyses, strictly monochromatic X-rays are necessary, but in

order to measure the dry weight of the specimen, X-rays containing more wavelengths can be used. The only requirement is that the radiation has a wavelength longer than about 6 Å, i.e. wavelengths longer than the K-absorption edge of phosphorus. In the wavelength region from 6 to 23 Å, dry weight determinations can be accurately performed. At about 23 Å oxygen has its K-absorption edge and if the wavelength of this is exceeded, the X-ray image will no longer indicate the true distribution of dry mass. From the point of view of weighing, therefore, the wavelength region between 23 and 50 Å is of less value as the K-edges of O, N and C are situated in this region. However, a simple calculation indicates that for maximum contrast in a microradiographic image of a sample a few microns thick, the suitable wavelength region is situated between 10 and 20 Å, corresponding to 1-0.5 kV X-rays. In addition to the data about the distribution of dry weight a microradiogram gives information about the water content of various structures. Thus a single microradiogram, provided the thickness is known, gives both the percentages of dry weight and water in the various structures under examination.

When evaluating the X-ray absorption in the microradiographic image by densitometry, naturally, factors like the inhomogeneous distribution of absorbing material, and the influence of stray light in the optical system used must be properly controlled. To overcome these difficulties microphotometric systems utilizing scanning principles are preferably used, but the discussion of the actual procedures of the quantitative measurements of the density distribution in the microradiograms will be given in a later communication.

REFERENCES

1. ENGSTRÖM, A., BJÖRNERSTEDT, R., CLEMEDSON, C-J. and NELSON, A., Bone and Radiostrontium. Almqvist & Wiksell, Stockholm, 1957.
2. ENGSTRÖM, A. and LINDSTRÖM, B., *Nature* **163**, 563 (1949).
3. ——— *Biochim. et Biophys. Acta* **4**, 351 (1951).
4. ——— in DANIELLI, J. F. (Ed.), *Standard Cytochemical Techniques*. Academic Press, New York, 1958 (in press).
5. ENGSTRÖM, A. and LUNDBERG, B., *Exptl. Cell Research* **12**, 198 (1957).
6. GREULICH, R. C. and ENGSTRÖM, A., *Exptl. Cell Research* **10**, 251 (1956).
7. LINDSTRÖM, B., *Acta Radiol.*, Suppl. 125. Stockholm, 1955.

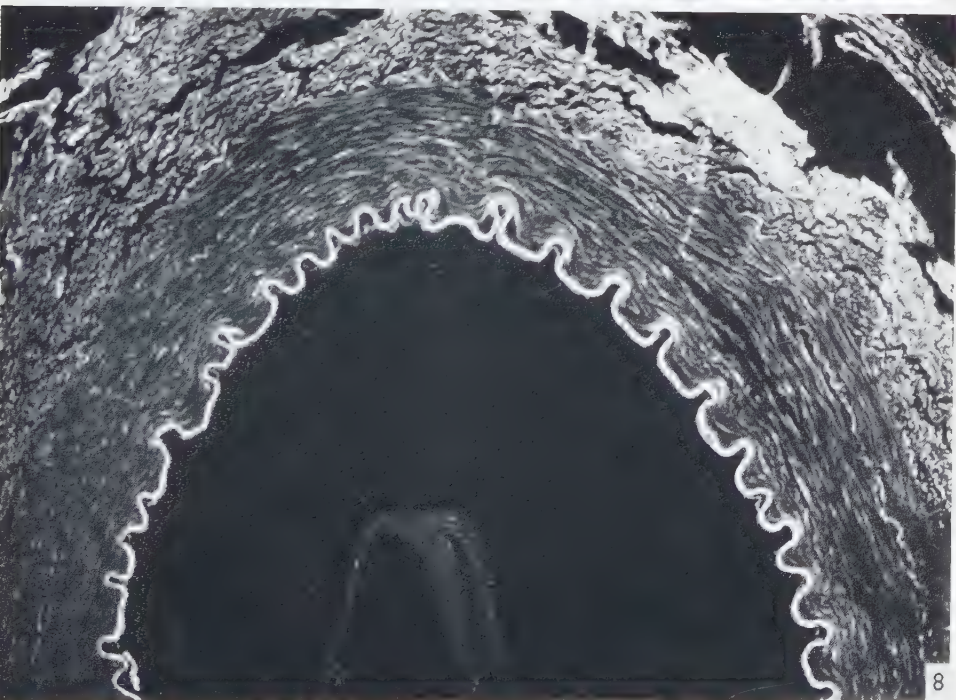


FIG. 7.—Microtome section of cartilage from fish showing the distribution of dry weight. $\times 280$.
FIG. 8.—Cross-section through the aorta from a dog showing high dry weight in the internal elastic lamellae. $\times 135$.

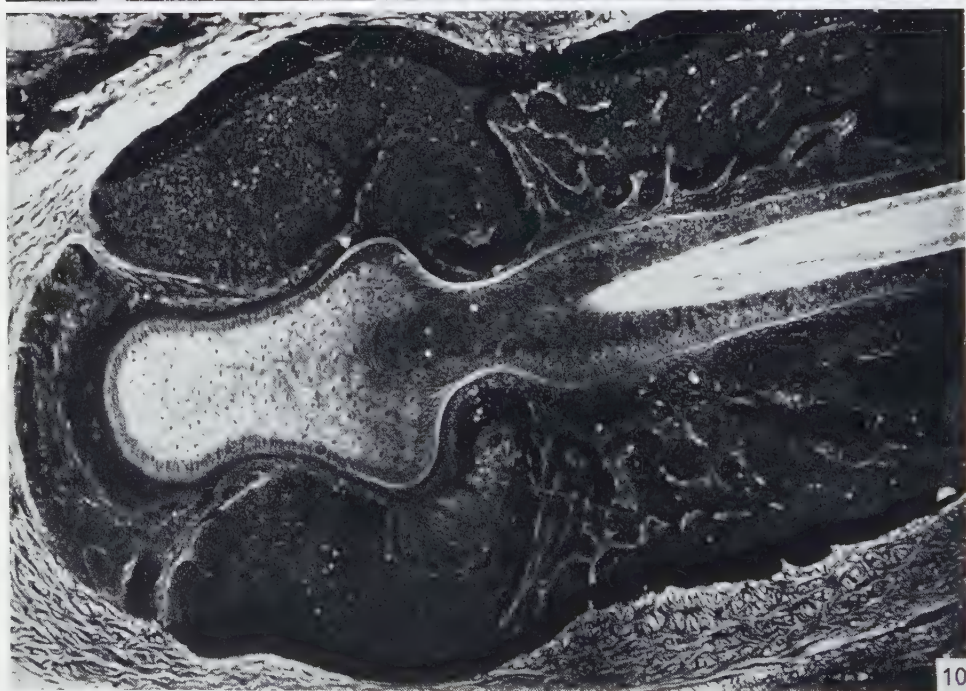
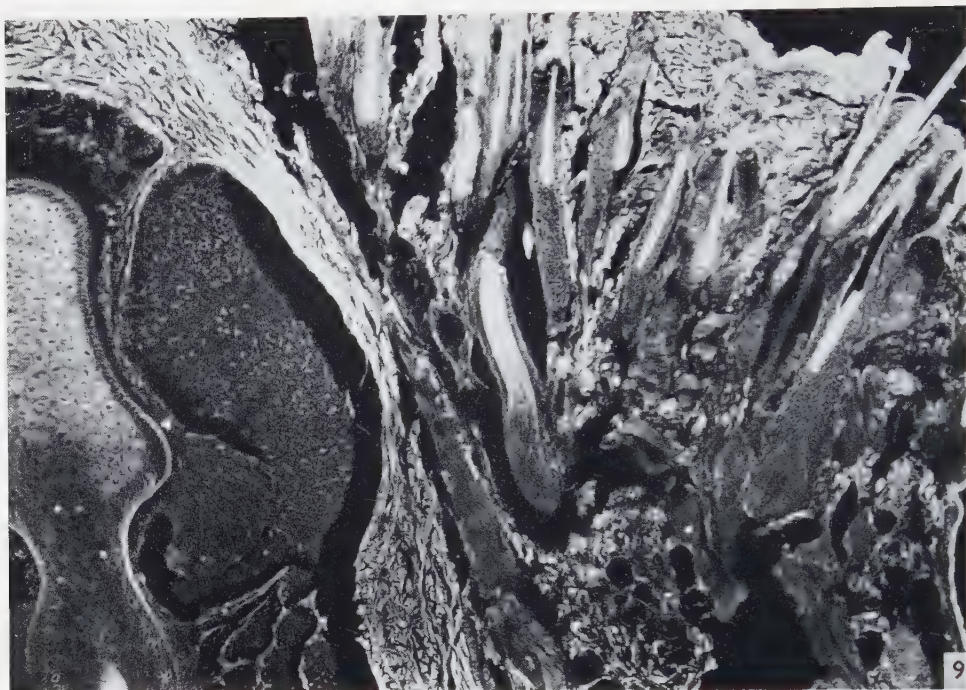


FIG. 9.—Section through the pelt of a rat showing distribution of dry weight within the hair follicles. $\times 144$.

FIG. 10.—Section through a large follicle showing mass distribution in the different structures. $\times 144$.

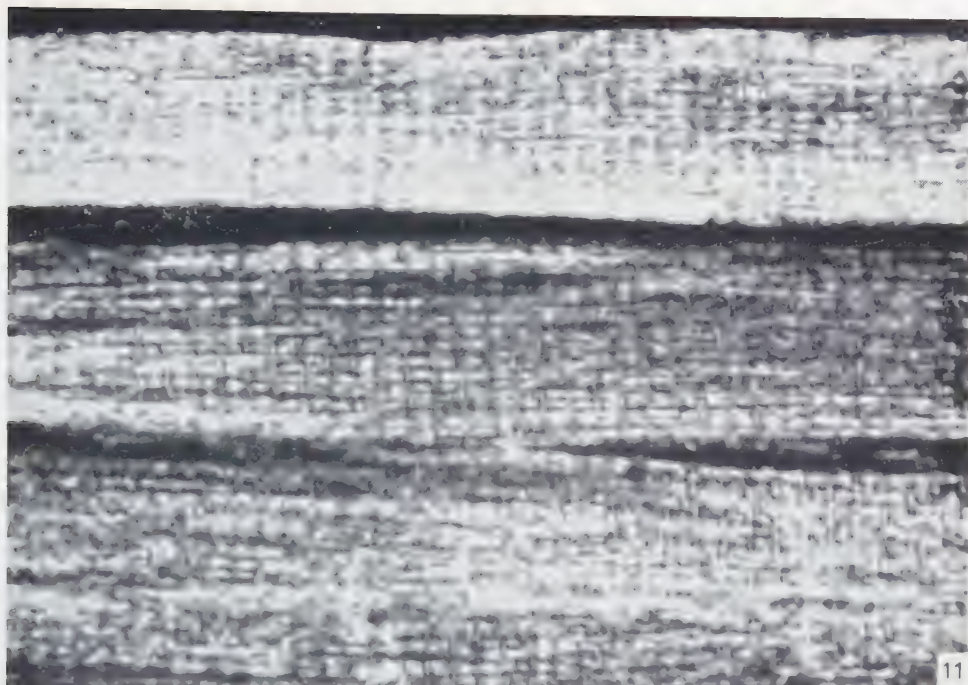


FIG. 11.—Section of striated muscle from rat indicating the different density of the various bands. The A bands have a high density. $\times 1750$.

FIG. 12.—Smear of ram sperm showing the resolution of the microradiographic technique. This microradiogram was recorded on a relatively coarse-grained emulsion, hence the graininess. $\times 750$.

Recherches ultrastructurales sur une tumeur rénale expérimentale du Hamster¹

KL. MANNWEILER et W. BERNHARD

Institut de Recherches sur le Cancer, Villejuif (Seine)

Reçu le 18 août 1957

Cette étude porte sur l'examen au microscope électronique de six tumeurs rénales, provoquées chez le hamster mâle par l'implantation de propionate de diéthylstilbestrol. De plus, les reins normaux de six hamsters adultes mâles et femelles et de sept hamsters nouveaux-nés ont été examinés. Il en résulte que les cellules tumorales offrent l'image de dédifférenciation structurale à des degrés variables et des phénomènes de nécrobiose. Par ailleurs, elles possèdent fréquemment une bordure ciliée hautement différenciée qui n'a pas été trouvée dans les reins des contrôles du hamster ou chez d'autres mammifères. L'ultrastructure des cils est identique à celle décrite par plusieurs auteurs chez des protozoaires et dans les épithéliums ciliés d'espèces variées. La signification de cette observation inhabituelle est discutée.

La dédifférenciation ou l'anaplasie cellulaire qui accompagne le processus de la cancérisation est un fait connu depuis longtemps en microscopie optique. La microscopie électronique a pu montrer ce phénomène au niveau de l'ultrastructure cytoplasmique des cellules tumorales (4, 5, 9). La disparition progressive des structures cellulaires hautement organisées peut être considérée comme une règle générale, mais il existe des exceptions où les cellules cancéreuses maintiennent parfois à un degré étonnant la fonction des cellules normales dont elles dérivent et, par conséquent, leur ultrastructure cellulaire. La présente observation entre également dans ce cadre en montrant la formation d'organites hautement spécialisés n'existant même pas dans les cellules du tissu d'origine. Il s'agit d'un carcinome rénal du hamster, dont beaucoup de cellules sont pourvues d'une bordure ciliée présentant l'ultrastructure complexe des cils décrits dans de nombreux tissus normaux (1, 2, 6, 10, 24, 31, 32, 34, 36, 37). D'autre part, elles peuvent être cloisonnées par un système de doubles membranes intracytoplasmiques, caractérisant les cellules des tubes conournés et collecteurs du rein normal (1, 7, 8, 27-30, 33, 35).

¹ Cette étude a pu être entreprise grâce à l'aide généreuse de la Mutuelle de l'Education Nationale à laquelle nous exprimons toute notre gratitude. Nous remercions également le Dr. Benedetti pour son aide précieuse et ses remarques critiques.

Ce néoplasme, objet de la présente étude, se comporte cliniquement comme une tumeur maligne et se développe dans la région corticale du parenchyme rénal chez le hamster mâle, mais non chez les femelles ni chez les autres rongeurs. Sa croissance est due à l'action prolongée d'un œstrogène de synthèse, implanté chez des hamsters mâles. Matthews, Kirkman et Bacon (22, 23) ont découvert ces tumeurs et en ont donné une première description. Horning et Whittick (20) se sont en particulier occupés de l'histogénèse assez obscure de ce cancer, appelé dépendant ou *conditionné* puisque la croissance de la tumeur initiale ou celle des greffes sous-cutanées s'arrête aussitôt que la stimulation hormonale cesse. Les questions de la pathogénèse de ce cancer qui sont du plus grand intérêt pour la cancérologie expérimentale sont discutées ailleurs (17-19). Nos recherches concernent exclusivement l'ultrastructure de cette tumeur.

MATERIEL ET METHODE

Le tissu cancéreux ayant servi à cette étude provient de six hamsters mâles¹ (*Cricetus auratus*) ayant reçu à six mois d'intervalle deux implantations de 20 mg de propionate de diéthylstilboestrol. Les tumeurs rénales ainsi provoquées et leurs métastases furent prélevées vers le neuvième mois de l'expérience. De plus, les reins normaux de trois mâles et de trois femelles adultes ainsi que les reins de sept hamsters nouveaux-nés, âgés de 12 à 80 heures, ont servi de contrôles.

Les tissus furent fixés à l'acide osmique 2 % tamponné selon Palade (25), déshydratés dans l'appareil de déshydratation continue (3) et inclus dans le méthacrylate de butyle selon la méthode courante. Les coupes furent effectuées à l'ultramicrotome Servall et ensuite examinées aux microscopes électroniques RCA EMU 2E et Elmiscope I Siemens.

Des coupes plus épaisses (0.8-1.2 μ) des mêmes blocs furent colorées au PAS et à l'hématéine-éosine selon la méthode de De Harven (15) et examinées au microscope optique.

RESULTATS

L'étude au *microscope optique* de toutes ces tumeurs originaires du cortex rénal révèle la structure d'un épithélioma à forme trabéculaire avec formation d'images tubuleuses ou micro-kystiques, les cavités étant, dans ce dernier cas, tapissées par une ou plusieurs couches cellulaires. Dans certains cas, surtout dans les tumeurs jeunes, l'aspect trabéculaire est pur; les tumeurs plus évoluées sont, en général, plus polymorphes. Les cellules sont le plus souvent acidophiles et peuvent contenir de grosses gouttes hyalines comme on les voit dans les cellules des tubes contournés, dans certaines néphroses. Ça et là, aussi, on voit des cavités tubuleuses dont les cellules présentent un revêtement cilié. Certains éléments semblent infiltrés de graisse et présentent un aspect spumeux; d'autres, montrent un cytoplasme

¹ Nous tenons à exprimer notre gratitude au Dr. J. Harel, du Service de Médecine Expérimentale, qui a bien voulu mettre à notre disposition son matériel d'expérience.

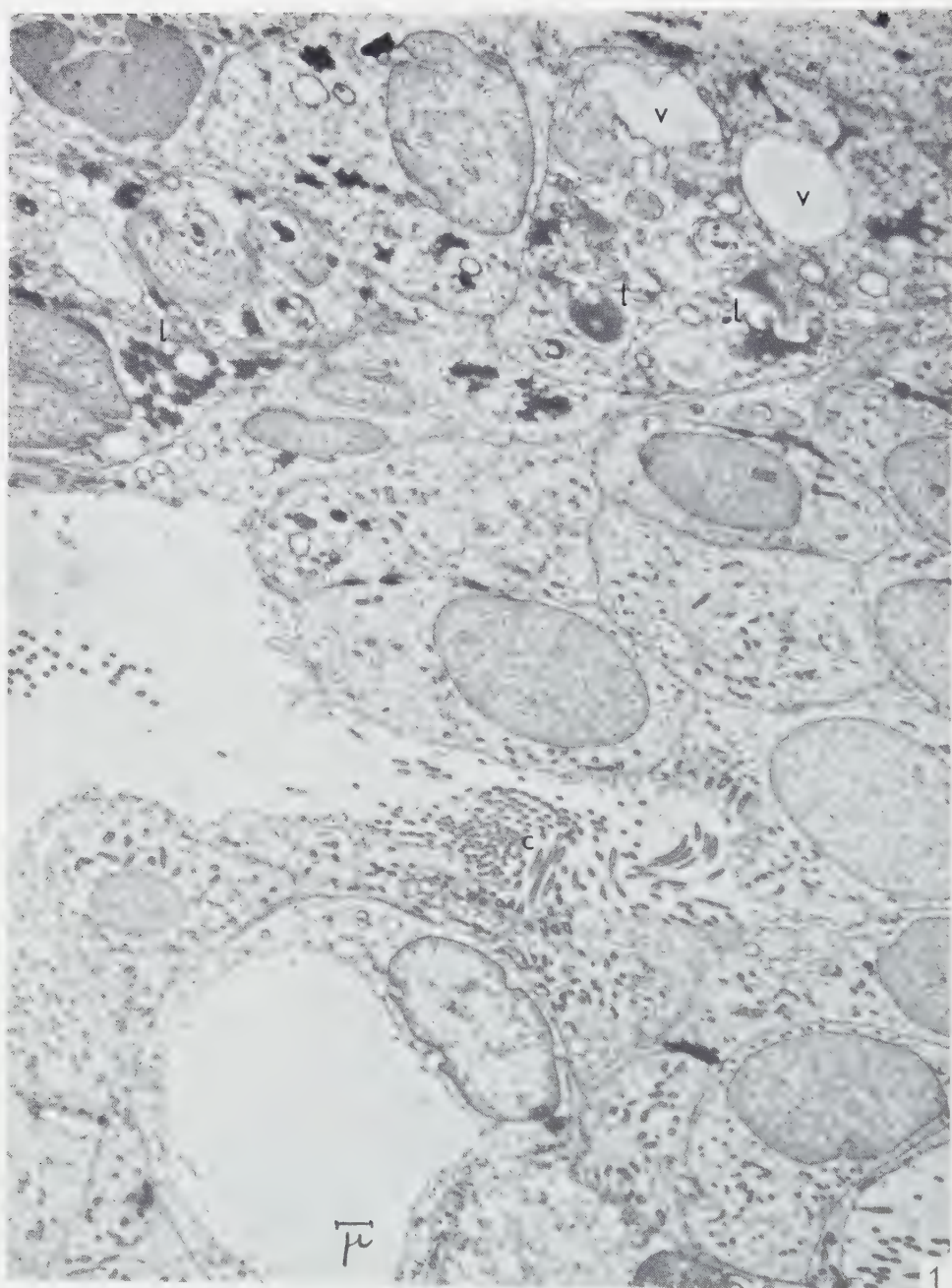


FIG. 1.—Vue d'ensemble d'un groupe de cellules tumorales, rangées autour d'une cavité. Aspect dédifférencié de la plupart des éléments. Altérations dégénératives en haut de l'image. Inclusions lipidiques (*l*). Vacuoles (*v*). Bordure ciliée (*c*). 4400 \times .

entièrement clair comme il est classique de le rencontrer dans certaines tumeurs rénales. Les zones nécrotiques ou nécrobiotiques sont fréquentes.

Le *microscope électronique* permet de montrer des cellules tumorales de taille et d'aspect relativement homogènes : les noyaux sont ronds ou ovalaires, plus rarement polylobés avec des encoches profondes, et leur cytoplasme, comparé à celui des cellules des tubes contournés normaux, se révèle assez différencié. Dans l'ensemble, ces cellules présentent un aspect plus embryonnaire (7), (fig. 1). Il y a relativement peu de *mitochondries*. Elles sont de petite taille, très denses (fig. 2), ou bien, gonflées, présentent l'image de la tuméfaction trouble (fig. 3), phénomène souvent observé dans les cellules cancéreuses les plus diverses (5). L'*Appareil de Golgi* est de taille variable (11), mais à peine hypertrophié, contrairement à l'observation de Haguenau et Lacour (12) dans les adénomes chromophobes de l'hypophyse du rat, obtenus après injections répétées d'œstrogène. L'*ergastoplasme* sous sa forme organisée est fort peu développé; on trouve par contre des grains ribonucléoprotéiques (26) disséminés dans tout le cytoplasme; cette répartition embryonnaire de la basophilie caractérise beaucoup de néoplasmes (4, 5, 9).

Des indices de *nécrobiose* sont fréquents. Le cytoplasme peut être vacuolaire ou contenir des inclusions lipidiques opaques ou stratifiées (fig. 1). On note également la présence de masses opaques à formes allongées, principalement au niveau de la zone périphérique du tissu tumoral. Il peut s'agir dans ce cas de lambeaux de membranes basales détruites par la croissance excessive des cellules malignes.

Les structures les plus inattendues et les plus intéressantes dans cette tumeur sont sans doute les *cils* bordant la surface de nombreuses cellules et pénétrant dans la lumière de formations pseudo-tubulaires ou kystiques (fig. 4 à 7). Ils furent trouvés en nombre variable non seulement dans toutes les six tumeurs d'origine mais aussi dans une métastase péritonéale. Suivant l'incidence de la coupe, les cils peuvent être uniques ou rangés parallèlement par petits groupes. Ils sont répartis sporadiquement dans certains endroits du tissu tumoral, ou bien, ils forment une bordure aussi dense et régulière que par exemple, l'épithélium cylindrique des bronches (31). Ils semblent parfois être situés à l'intérieur du cytoplasme d'une seule cellule, très semblables aux « Flimmerblasen » de Hamperl (13), décrites par cet auteur comme stades évolutifs d'une bordure ciliée dans des polypes utérins. Mais il peut aussi s'agir de coupes tangentielles d'une encoche de la membrane cellulaire (fig. 4). Sur des coupes épaisses de contrôle, colorées selon la réaction de PAS, ces régions ciliées ne prennent pas le colorant.

L'*ultrastructure* de ces cils est identique à celle montrée pour des épithéliums cylindriques de plusieurs espèces de vertébrés par Fawcett et Porter (10), pour certains protozoaires par Sedar et Porter (34), pour la partie proximale des tubes contournés (col. Halsstück) du rein de *Xenopus laevis* par Bargmann et Coll. (1) et,

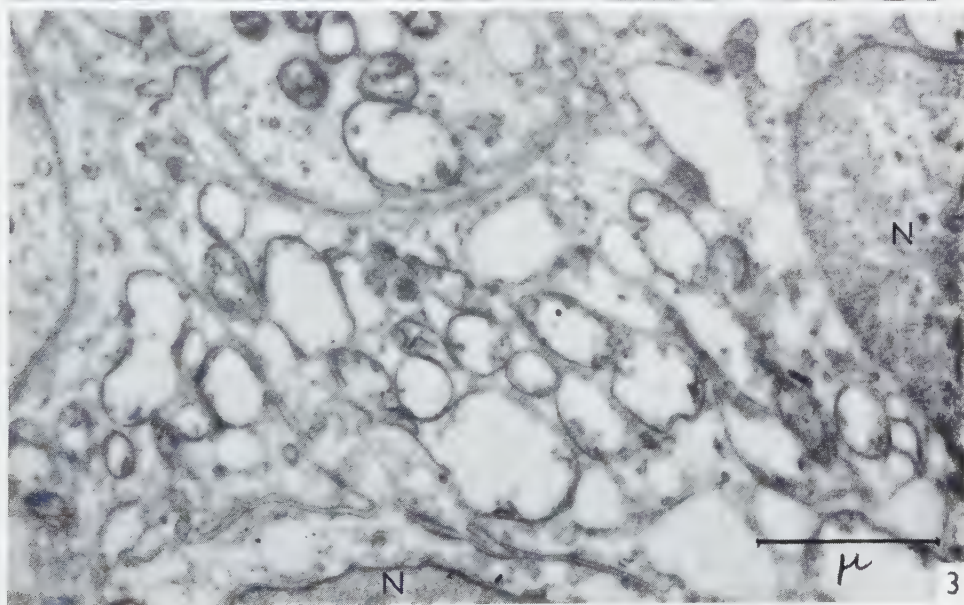
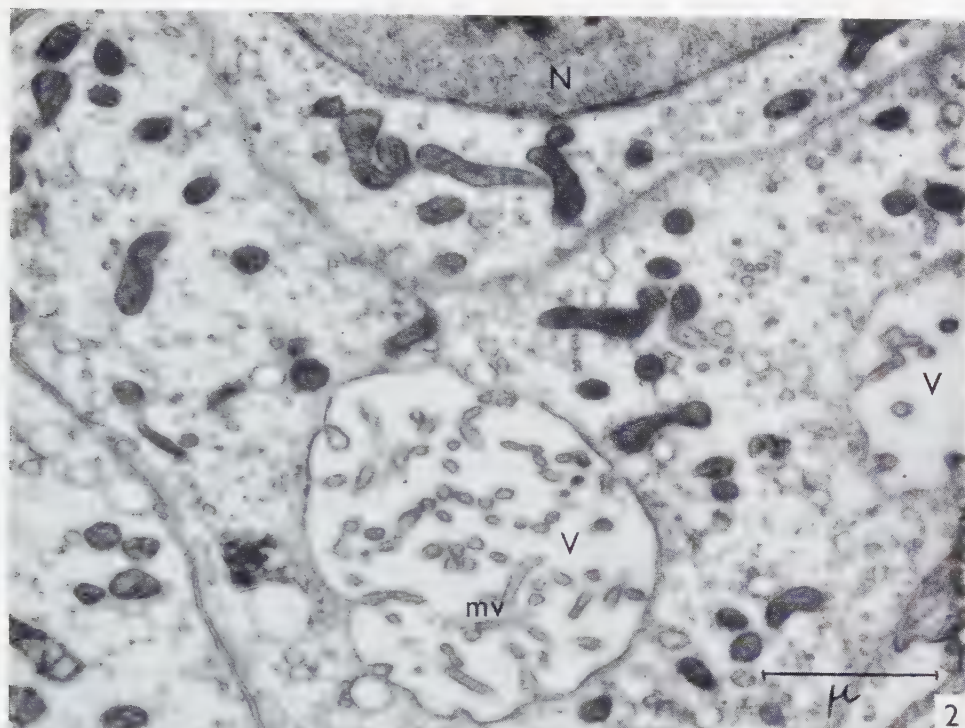
pour le ductus deferens du hamster, par Burgos (6). La structure fine de ces formations a été étudiée plus en détail pour l'épithélium bronchique du rat par Rhodin et Dalhamn (31) et chez *Euplotes patella* par Roth (32).

En coupe *transversale* (fig. 5), les cils offrent un profil parfaitement arrondi, d'un diamètre de 230 $m\mu$. Ils sont cernés d'une membrane extérieure par endroits dédoublée. Sousjacentes à cette membrane et disposées à intervalles réguliers sous forme d'un cercle, se trouvent neuf formations d'aspect vésiculaire, très osmiophiles, ayant un diamètre moyen de 25 $m\mu$. Certaines d'entre elles sont nettement doubles et probablement le sont-elles toutes; cependant les grossissements employés ici ne permettent pas de l'affirmer. Au centre du tronc ciliaire enfin, se trouvent deux autres formations du même type structural. Les coupes *longitudinales* (fig. 6) montrent que chacune de ces structures à contour circulaire correspond à un mince filament d'apparence creuse allant en continuité directe de l'insertion cytoplasmique jusqu'à l'extrémité des cils et mesurant jusqu'à 4 μ de longueur. Toutes ces structures filamenteuses ou canaliculaires sont enrobées dans une masse homogène faiblement contrastée, remplissant l'intérieur de chaque cil.

Il est intéressant de noter les rapports de ceux-ci avec le cytoplasme. Tandis que leur membrane extérieure rejoint la membrane cellulaire et ne représente qu'une excroissance de celle-ci, les structures canaliculaires sousjacentes à la membrane ciliaire pénètrent dans le cytoplasme périphérique et y sont ancrées dans les corpuscules basaux suivant un mode schématisé par Fawcett et Porter (10) et par Rhodin et Dalhamn (31). Ces corpuscules basaux ont une ultrastructure très semblable à celle du centriole décrit dans des tissus variés par De Harven et Bernhard (16). Il est curieux que ces cellules ciliées puissent même se trouver, bien que moins fréquemment que dans les tumeurs primitives, dans les métastases dont l'aspect général témoigne d'une dédifférenciation beaucoup plus poussée (fig. 7).

Une autre observation est importante et mérite d'être signalée. Certaines des cellules tumorales faisant partie des formations trabéculaires ou pseudo-tubulaires sont implantées sur une membrane basale comme le sont les cellules des tubes contournés normaux. Comme chez celles-ci, leur cytoplasme peut alors être compartimenté par l'invagination de doubles membranes lisses qui s'insèrent sur la face interne de la basale (fig. 8). Ce système membraneux est typique pour certaines classes de cellules épithéliales normales très différenciées dont la fonction est essentiellement le transport de liquide (29). Jusqu'ici on n'a pas signalé l'existence de ces membranes dans des cellules tumorales. Ce fait semble bien prouver l'origine de la tumeur, à

FIG. 2.—Cytoplasme de cellules tumorales avec de nombreuses petites mitochondries très denses. *V*, vacuole ou invagination de la surface cellulaire, bordée de microvillosités (*mv*); *N*, noyau. 23.500 \times .
FIG. 3.—Portion cytoplasmique d'une autre région. Toutes les mitochondries sont gonflées et montrent l'aspect de la tuméfaction trouble. *N*, noyau. 23.500 \times .



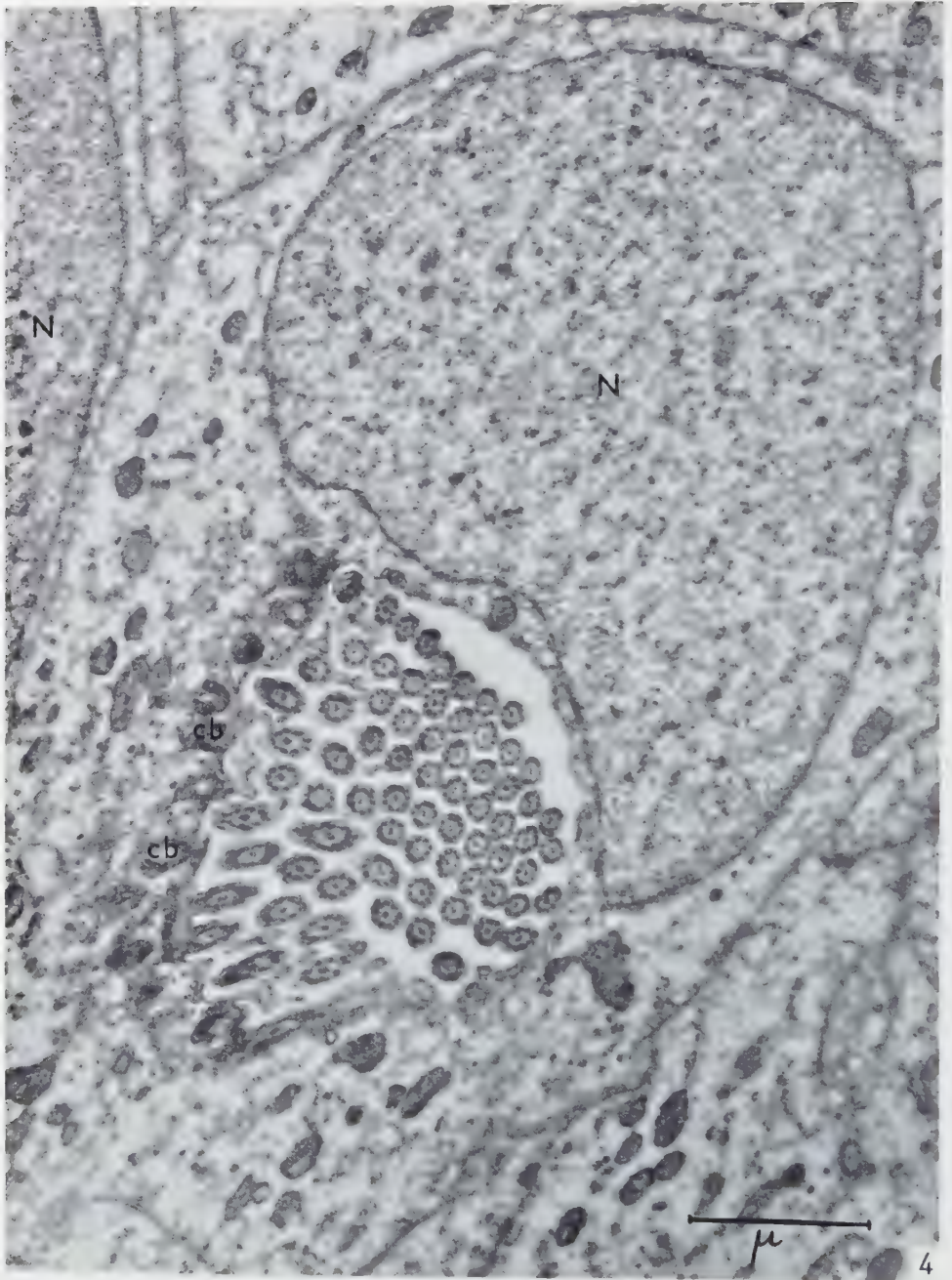


FIG. 4.—Cellule tumorale avec de nombreux cils coupés transversalement. Les formations semblent se trouver à l'intérieur d'une vacuole cytoplasmique, mais il s'agit peut-être d'une en coque de la surface, coupée tangentiellement. *N*, noyau; *cb*, région des corpuscules basaux. 23.500 \times .

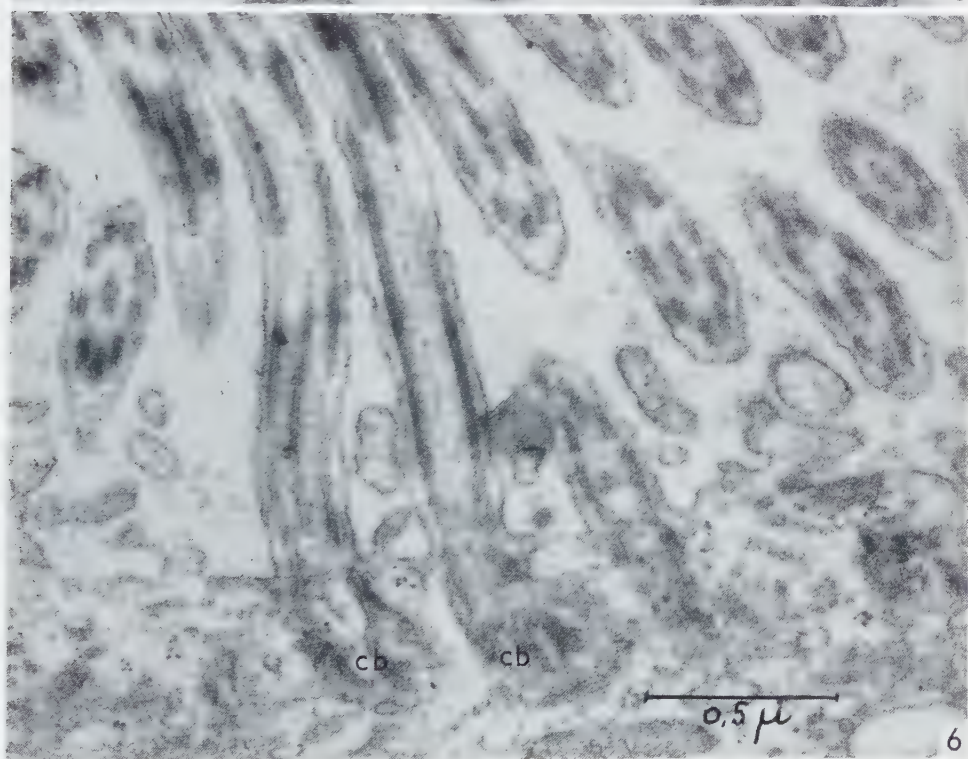
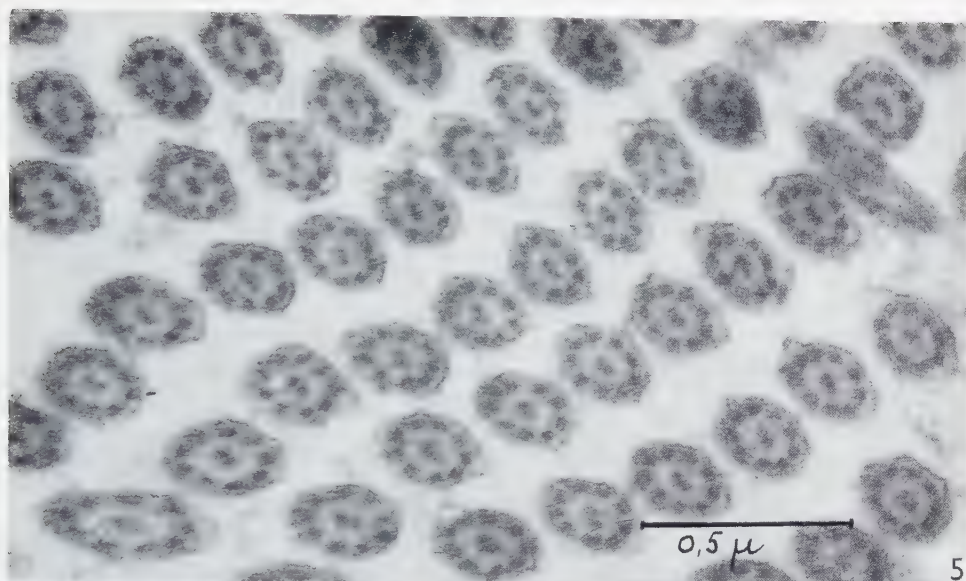


FIG. 5 et 6.—Coupes transversale et longitudinale des cils, permettant de voir l'ultrastructure du cylindre ciliaire. Chaque cil contient neuf filaments ou neuf paires de filaments périphériques rangés en cercle et une paire de filaments axiaux nettement visibles au centre. *cb*, région des corpuscules basaux. Fig. 5 : 54.400 \times . Fig. 6 : 48.800 \times .

savoir l'épithélium rénal des tubes contournés. On pourrait évidemment penser que les cellules contenant ces formations seraient les vestiges du tissu normal infiltré par la tumeur et ne seraient donc pas cancéreuses. Cependant l'aspect de leurs noyaux, souvent monstrueux, et du cytoplasme est atypique et ne peut être qualifié de normal.

Notons encore qu'aucune des tumeurs examinées ici n'avait un aspect sarcomateux. Les cellules tumorales étaient exclusivement de nature épithéliale et aucune de nos observations ne soutiennent la thèse de Kirkman (21) suivant laquelle le mésenchyme interstitiel jouerait un rôle important dans la genèse de la tumeur.

DISCUSSION

Cette étude ajoute aux nombreuses questions biologiques posées par la tumeur rénale du hamster des problèmes morphologiques. L'existence de structures aussi complexes que les cils dans des cellules tumorales qui ont, par leur comportement biologique, toutes les caractéristiques de cellules malignes, est déjà étonnant en soi. La mise en évidence de cils dans une métastase formée par des cellules dédifférenciées d'avantage que celles de la tumeur primitive est à retenir plus particulièrement. C'est la première fois que le microscope électronique révèle de tels organites dans des cellules cancéreuses qui sont en général caractérisées par un degré d'organisation structurale plus simple. Un autre problème concerne l'origine de ces cils. La seule description au microscope électronique de pareilles structures au niveau du rein a été donnée par Bargmann et Coll. (1). Ces auteurs ont trouvé des cils dans la partie proximale (col) du tube contourné chez des amphibiens (*Xenopus laevis*). Ils n'ont jamais été vus jusqu'ici dans les reins de mammifères (7, 8, 27, 28, 30, 35). Cependant, Zimmermann (38) a décrit chez le lapin dans la partie descendante de l'anse de Henlé, et chez le lapin et l'homme dans les tubes contournés II, un « appareil central », flagelle unique du type blépharoblaste, ancré dans le cytoplasme des cellules par un corpuscule basal. Cette observation est intéressante et mériterait d'être refaite au microscope électronique. Ces « flagelles » révéleraient sans doute une architecture identique ou semblable aux formations que nous venons de signaler.

De pareilles structures n'ont été vues ni chez trois hamsters mâles ni chez trois femelles adultes de contrôle. Le revêtement de l'épithélium du néphron adulte du hamster est toujours représenté soit par une bordure en brosse, soit par des microvillosités suivant le secteur des tubules. Si les cellules tumorales forment également des villosités, elles ne sont par contre jamais revêtues de bordure en brosse; mais, s'approchant de l'état embryonnaire de l'organe, elles refont peut-être des structures qui ont caractérisé un stade évolutif antérieur de celui-ci; il pourrait donc s'agir d'une régression ontogénétique. Cependant, les reins de sept hamsters nouveaux-nés n'ont pas permis de déceler des cils. Les reins de souris nouveaux-nés ne les contiennent

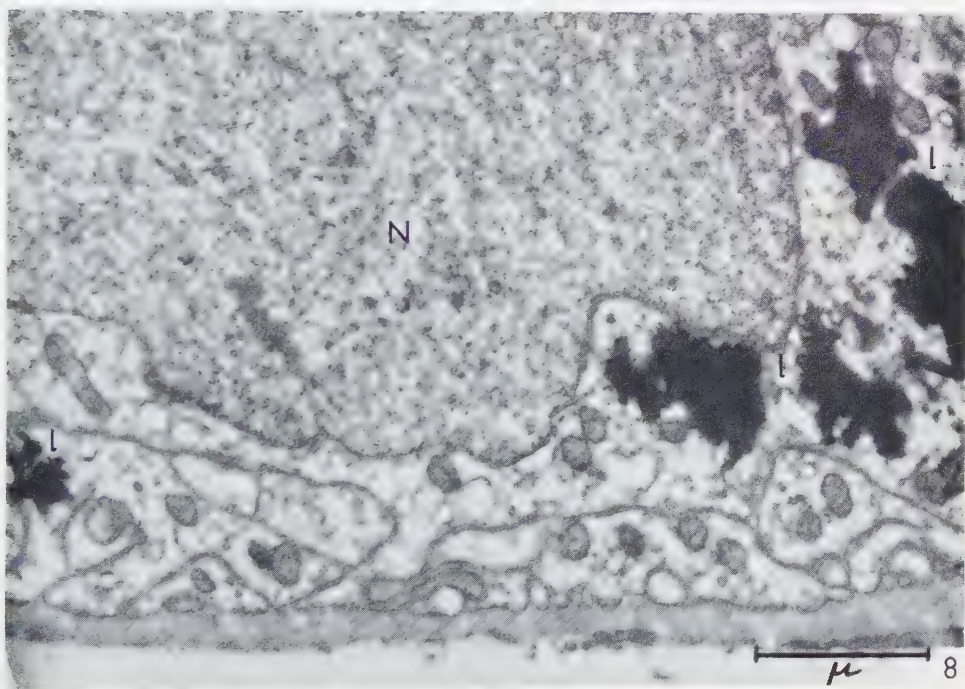
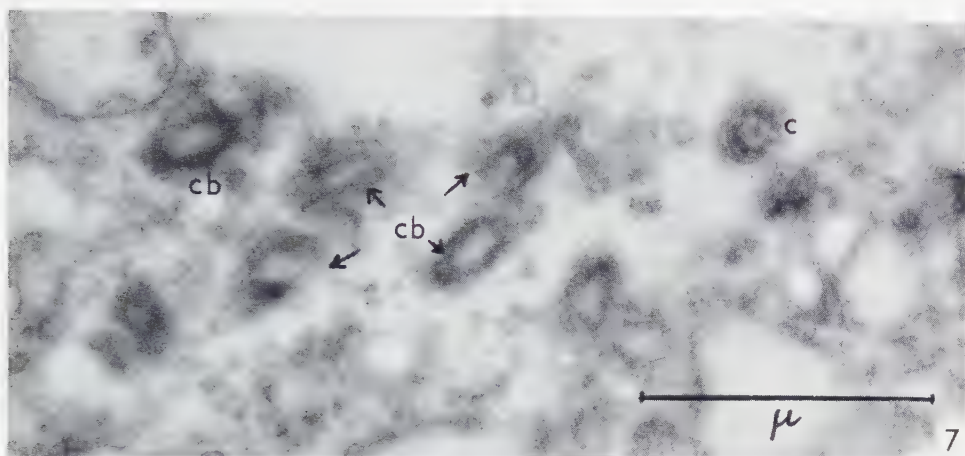


FIG. 7.—Métastase mésentérique. Présence des mêmes cils dans une cellule tumorale coupée tangentielle. *c*, corps ciliaire extracytoplasmique; *cb*, corpuscules basaux. 38.000 \times .

FIG. 8.—Portion d'une cellule assise sur une membrane basale prélevée en plein tissu tumoral. Présence de doubles membranes lisses insérées dans la basale et cloisonnant le cytoplasme du pôle basal de la cellule. *N*, noyau; *l*, inclusions lipidiques. 22.200 \times .

pas non plus (7). Il serait évidemment du plus grand intérêt de connaître l'ultrastructure de reins de stades embryonnaires plus précoces, mais cette étude n'a pas encore été entreprise.

Par ailleurs les pathologistes savent que certaines tumeurs peuvent se différencier en formant des structures (par exemple un épithélium pavimenteux stratifié ou des cellules mucipares) qui manquent totalement au tissu d'origine mais que l'on rencontre dans des tissus embryonnaires d'autres organes ayant une proche parenté ontogénétique (14).

L'hypothèse que les tumeurs rénales du hamster mâle en raison de leur structure trabéculaire dérivent de cellules glandulaires endocrines différentes du parenchyme rénal et qui commenceraient à proliférer sous l'action d'œstrogènes n'est soutenue par aucun argument morphologique. L'ultrastructure de toutes les cellules normales ou pathologiques n'en a jamais révélé la moindre trace. Il est d'ailleurs intéressant de remarquer dans ce contexte que les mitochondries de ces tumeurs n'ont pas la structure des mitochondries tubuleuses habituellement rencontrées dans la cortico-surrénale.

Le fait qu'on observe dans le tissu tumoral un système de doubles membranes cytoplasmiques caractérisant la région basale des tubes contournés et collecteurs, ne semble laisser aucun doute sur son origine. Mais la présence dans une tumeur d'organites cellulaires qui ne se trouvent pas dans le tissu d'où elle dérive, pose un problème qui n'est pas encore résolu.

SUMMARY

This study is concerned with the examination by electron microscopy of six kidney tumours of male golden hamsters. They were obtained by implantation of diethylstilboestrol dipropionate. In addition, the normal kidneys of six grown hamsters of both sexes and of seven newborn hamsters were examined. The tumour cells demonstrate structural dedifferentiation in various degrees, and necrobiotic phenomena. In addition, a highly differentiated ciliated border is formed, which has not been observed in kidneys of the control hamsters nor in other mammals. The ultrastructure of the cilium is identical with that of protozoa and of ciliated epithelial cells in different species. The significance of this unusual observation is discussed.

BIBLIOGRAPHIE

1. BARGMANN, W., KNOOP, A. et SCHIEBLER, TH., *Z. Zellforsch. u. mikroskop. Anat.* **42**, 386 (1955).
2. BEAMS, H. W., TAHMISIAN, T. N. et DEVINE, R., *Abstr. Anat. Record* **127**, 460 (1957).
3. BERNHARD, W., *Exptl. Cell Research* **8**, 248 (1955).
4. — *Klin. Wochschr.* **35**, 251 (1957).

5. BERNHARD, W. et OBERLING, CH., Electron microscopy of the malignant cell with special references to viruses, *11th Canadian Conference on Cancer*. Academic Press, 1957.
6. BURGOS, M. H., Abstr. *Anat. Record* **127**, 401 (1957).
7. CLARK, S. L., *J. Biophys. Biochem. Cytol.* **3**, 349 (1957).
8. DALTON, A. J., *J. Natl. Cancer Inst.* **11**, 1163 (1951).
9. DALTON, A. J. et FELIX, M. D., *N.Y. Acad. Sci.* **63**, 1117 (1956).
10. FAWCETT, D. W. et PORTER, K. R., *J. Morphol.* **94**, 221 (1954).
11. HAGUENAU, F. et BERNHARD, W., *Arch. Anat. Micr. Morph. Exp.* **44**, 27 (1955).
12. HAGUENAU, F. et LACOUR, F., *Compt. rend. 8^e congrès intern. biol. cell., Leyden*, 1954. Fine Structure of Cells, p. 316. Noordhoff Ltd., Groningen, 1955.
13. HAMPERL, H., *Virchow Arch.* **319**, 256 (1950).
14. —, *dans* Handbuch der allgemeinen Pathologie, Bd. VI, Teil 3, Geschwülste. Springer, 1956.
15. DE HARVEN, E., *Compt. rend. soc. biol.* **CL**, 63 (1956).
16. DE HARVEN, E. et BERNHARD, W., *Z. Zellforsch. u. mikroskop. Anat.* **45**, 378 (1956).
17. HORNING, E. S., *Brit. J. Cancer* **8**, 627 (1954).
18. — *Z. Krebsforsch.* **61**, 1 (1956).
19. — *Brit. J. Cancer* **10**, 678 (1956).
20. HORNING, E. S. et WHITTICK, J. W., *Brit. J. Cancer* **8**, 451 (1954).
21. KIRKMAN, H., Abstr. *Anat. Record* **109**, 311 (1951).
22. KIRKMAN, H. et BACON, R. L., *Anat. Record* **103**, 475 (1949).
23. MATTHEWS, V. S., KIRKMAN, H. et BACON, R. L., *Proc. Exptl. Biol. N.Y.* **66**, 195 (1947).
24. ODOR, L. D., Abstr. *Anat. Record* **115**, 434 (1953).
25. PALADE, G. E., *J. Exptl. Med.* **95**, 285 (1952).
26. — *J. Biophys. Biochem. Cytol.* **1**, 59 (1955).
27. PEASE, D. C., *J. Histochem. Cytochem.* **3**, 295 (1955).
28. — *Anat. Record.* **121**, 723 (1955).
29. — *J. Biophys. Biochem. Cytol.* **2**, No. 4, Suppl., 203 (1956).
30. RHODIN, J., Correlation of Ultrastructural Organization and Function in Normal and Experimentally Changed Proximal Convoluted Tubule Cells of the Mouse Kidney. Stockholm, 1954.
31. RHODIN, J. et DALHAMN, T., *Z. Zellforsch. u. mikroskop. Anat.* **44**, 345 (1956).
32. ROTH, L. E., *J. Biophys. Biochem. Cytol.* **2**, No. 4, Suppl., 235 (1956).
33. RUSKA, H., MOORE, D. H. et WEINSTOCK, J., *J. Biophys. Biochem. Cytol.* **3**, 249 (1957).
34. SEDAR, A. W. et PORTER, K. R., *J. Biophys. Biochem. Cytol.* **1**, 583 (1955).
35. SJÖSTRAND, F. S. et RHODIN, J., *Exptl. Cell Research* **4**, 426 (1953).
36. YOSHIHIDE, T., *J. Electron Microscopy (Jap.)* **5**, 43 (1957).
37. WORLEY, L. G., FISCHBEIN, E. et SHAPIRO, J. E., *J. Morphol.* **92**, 545 (1953).
38. ZIMMERMANN, K. W., cité d'après v. MOELLENDORF, W., Handbuch der mikroskopischen Anatomie des Menschen, Bd. VII, 1930, Harn und Geschlechtsapparat, Teil I. Springer, 1930.

Observations on a Type of Cilia in the Rat Oviduct

O. NILSSON

*Department of Histology and Laboratory for Biological Ultrastructure Research,
Department of Anatomy, Karolinska Institutet, Stockholm*

Received July 1, 1957

The processes that extend from the surface of the secretory cells of the rat oviduct are classified as stereocilia. They are about $3-5\ \mu$ long, have a diameter of $500-600\ \text{\AA}$, and appear sometimes to ramify. Their limiting membrane is composed of two osmiophilic layers. The interior of the cilia contains an osmiophilic structure, which is found either in the form of a central ring or as about six filaments lying apart more peripherally. No filaments can be traced into the cytoplasm of the cell.

An electron microscopical investigation of the mucosa of the rat oviduct was made by Odor (10). She described two types of epithelial cells: cells with kinocilia and cells carrying long protoplasmic processes. The latter processes were found to be shorter and thinner than kinocilia, and lacked longitudinal fibrils and basal granules. It was shown by Nilsson *et al.* (9) that these processes extended from the surface of cells of the secretory type. Fawcett and Porter (5) studied the mouse oviduct with reference to the kinocilia.

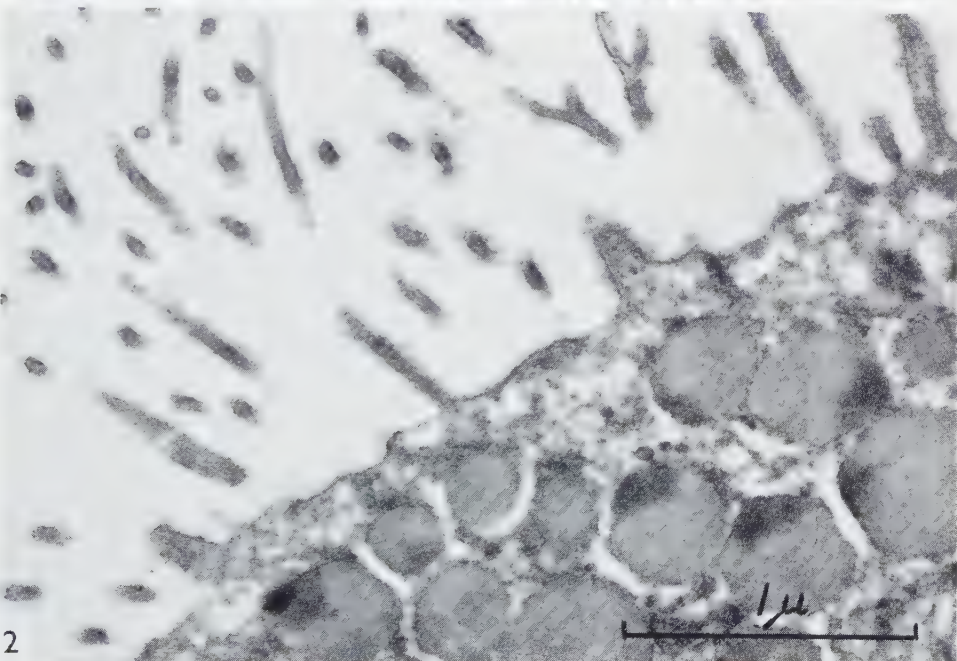
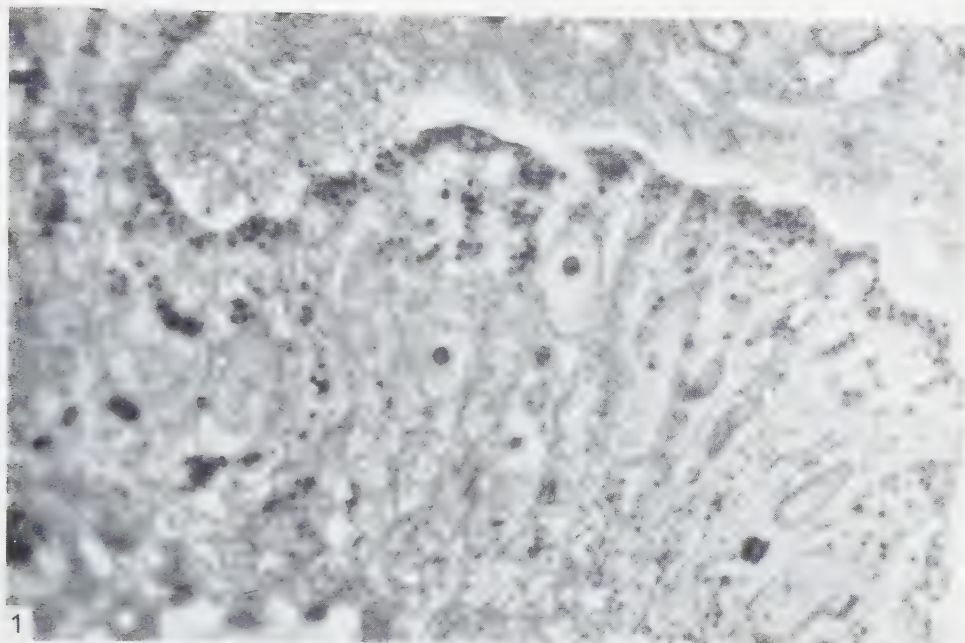
The present investigation was undertaken in order to study the internal structure of the cilia from the secretory cells of the rat oviduct.

MATERIAL AND METHODS

White rats in oestrus were used. With the animal in ether narcosis the uterine tubes were exposed, and a buffered isotonic solution of 1 % osmium tetroxide (11, 14) was injected into the tubes from the uterine cavity. The oviducts were dissected free, cut into small pieces, and fixed for 3 hours. After dehydration in ethyl alcohol the pieces were

FIG. 1.—Secretory cells of tubal epithelium from rat in oestrus. A number of cytoplasmic processes are seen extending from the upper cell surfaces. Secretory granules are visible in the supra nuclear part of the cells. The basement membrane is found in the lower part of the picture (fixed in osmium solution, embedded in plastic, cut with the Spencer microtome, observed with phase-contrast photomicrography). $\times 1500$.

FIG. 2.—Part of secretory cell of tubal epithelium from rat in oestrus. Two stereocilia show ramifications. Secretory granules are found under the cell surface. $\times 38,000$.



embedded in *n*-butyl methacrylate (7), catalyzed by 0.1 % benzoyl peroxide, and polymerized at 45°.

Sections were cut with the ultramicrotome designed by Sjöstrand (15), and were examined in an RCA EMU 2c electron microscope.

RESULTS

The secretory cells of the rat Fallopian tube lie singly or in groups interposed among cells carrying motile cilia. They possess on their upper surface fine cytoplasmic processes numbering 10–15 per square micron (Figs. 1 and 2).

These cilia are 3–5 μ long, and have a diameter of 500–600 Å. They sometimes appear to ramify (Figs. 2 and 3).

Their limiting membrane is composed of two osmiophilic layers about 70 Å apart as measured from the centres of the layers (Figs. 5, 6, 8, and 9). The interior of the processes is composed of a homogeneous ground substance, in which an osmiophilic structure is found.

This osmiophilic structure is found in transverse sections either in the form of a central ring (Fig. 7) or as about six filaments lying apart more peripherally (Fig. 8). Longitudinal sections show in the central parts of the processes osmiophilic strands, which sometimes appear as two filaments running parallel about 70 Å apart (Figs. 4–6). The appearance of the osmiophilic structure at the ramification of the cilia is not known.

The membrane that covers the cilia is continuous with the membrane that forms the upper cell surface, and there is a direct continuity between the ground substance of the cilia and the cytoplasm. An indication of an incipient filamentous structure is often found at the base of the processes but no filaments can be followed down into the cytoplasm of the cell (Fig. 2).

Fragments of living mucosa of the rat oviduct in Tyrode solution were studied by phase contrast microscopy at +37°C. The cytoplasmic processes of the secretory cells exhibited a wavy motion of varying intensity, but this motility appeared to be passive.

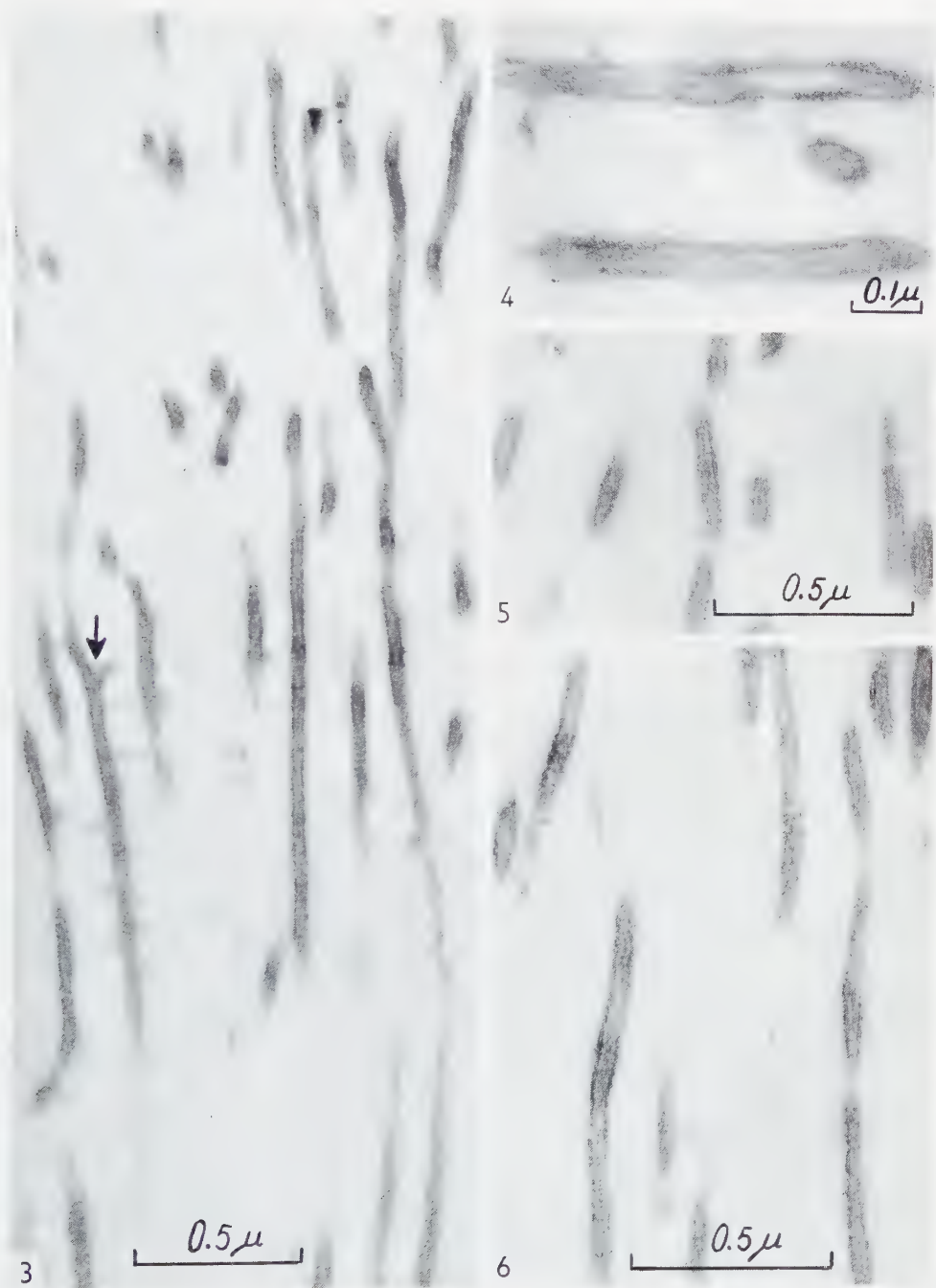
DISCUSSION

“The term cilium used in its broadest sense includes all vibratile and non-vibratile homogeneous, thread-like, protoplasmic structures which arise from the free surface of the cell. The term cilium in a restricted sense refers to a fine vibratile process which occurs usually in large numbers on a cell surface” (6). “In various epithelia there are

FIG. 3.—Stereocilia of rat oviduct. The arrow points to a ramification. $\times 45,000$.

FIG. 4.—Stereocilia of rat oviduct. $\times 98,000$.

FIGS. 5 and 6.—Stereocilia of rat oviduct. $\times 55,000$.



appendices similar in shape to cilia, but immobile and called stereocilia. Examples are the prolongations of the epithelial cells of the epididymis which seem to intervene in the elimination of the cellular secretion, or the rigid filaments of the cells of the macula and crista in the internal ear, which serve as receptors for stimuli and transmit them to the cells" (13).

The internal structure of some mammalian cilia have been studied by electron microscopy and similarities in their structure and in the ultrastructure of the cilia of the secretory cells are discernible.

The vibratile cilia or kinocilia, are mostly found on special cells in ciliated epithelia (1, 3-5, 9, 12, and others). They have a length of about $5\ \mu$ and a diameter of about $0.2\ \mu$. They are bordered by a membrane consisting of two osmiophilic layers. The internal filaments are arranged as a central pair surrounded by nine doubled filaments. The filaments continue down into the cytoplasm under the cell surface and take part in the formation of the basal corpuscle.

The processes of the secretory cells of the rat oviduct have the length of kinocilia but only a fourth of their thickness. Their bordering membrane is also double layered. The arrangements of the filaments in the processes sometimes appear similar to the patterns of the filaments of kinocilia.

The processes are very thin and are visualized in the *in vitro* studies as diffuse clusters. The observed motility of these cilia was very irregular as compared to the regular beating of the kinocilia. It was probably due to the movement in the fluid medium induced by the neighbouring vibratile cilia. It cannot be excluded that the Tyrode solution had an unfavourable effect on the motility of the processes, but this is not likely as the kinocilia seemed to be unaffected. As this investigation failed to reveal any active motility of the cilia of the secretory cells, they should be classified as stereocilia.

The internal structure of the different forms of non-motile cilia is not so well known. The ultrastructure of the stereocilia of the epithelium of the cristae ampullares of the guinea pig has been studied by Wersäll (16). These hairs were found to have the dimensions of kinocilia, and showed an axial fibril continuing down into the cuticle. Dalton *et al.* (2) studied the stereocilia of the epithelium of the rat epididymis and found that they were about one third of the width of kinocilia, and about one half their length. No association with filamentous structures in the cytoplasm below the free cell surface were found.

The processes of the secretory cells of the rat oviduct are of about the same width as the stereocilia of the epididymis but are longer. Moreover they possess internal

FIG. 7.—Transverse section of stereocilia of rat oviduct. $\times 60,000$.

FIG. 8.—Transverse section of stereocilia and kinocilia of rat oviduct. The arrows show the stereocilia in which the internal filaments are best visible. $\times 59,000$.

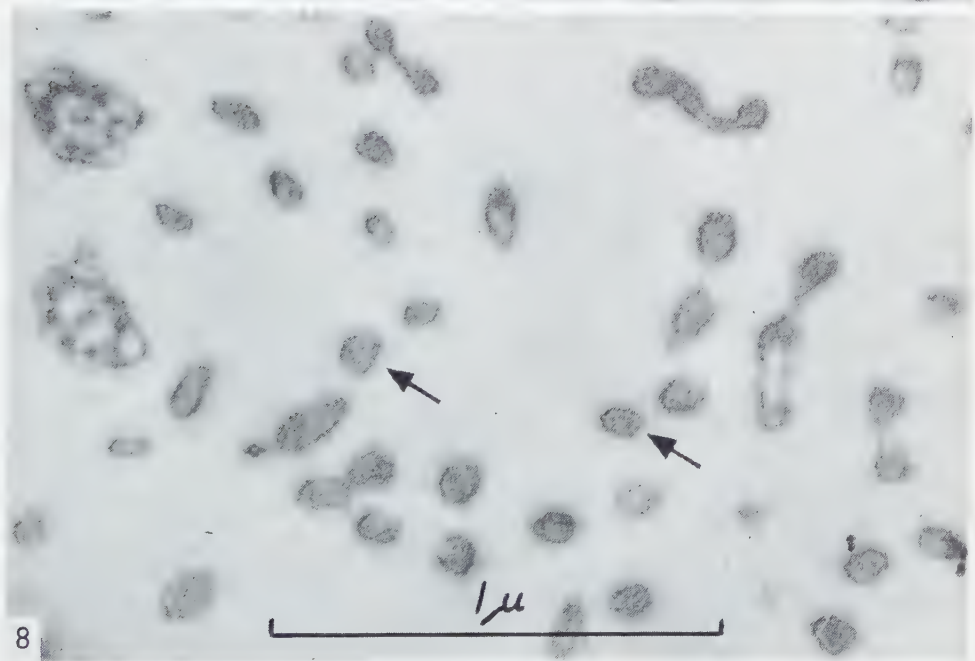
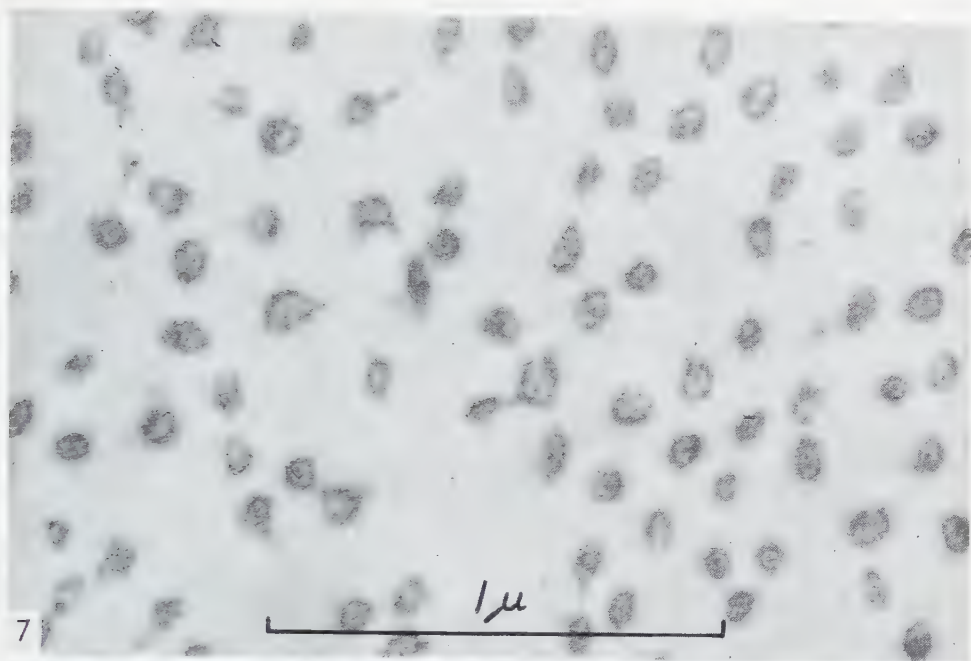




FIG. 9.—Stereocilia of rat oviduct. 102,000.

filaments, but these cannot be followed down into the cytoplasm of the cell as is the case of the sensory hairs. Thus the stereocilia of the rat oviduct do not correspond in structure to any of the described processes.

The secretion mechanism of the rat oviduct is not yet known and the role of the stereocilia of the secretory cells in this process is still uncertain. But the secretory granules, as visualized in the sections (Fig. 2), do not seem to be able to leave the cell through the cilia. This, however, does not exclude their ability to take part in secretion of other products of the cell.

The secretory cells of the rabbit Fallopian tube do not show cilia but short filiform projections (1, 8). A possible reason for the numerous stereocilia in the rat Fallopian tube could be the anatomical differences between rabbit and rat oviducts. The rabbit oviduct has a slightly wavy course, but the rat oviduct has a very tortuous course. The enormous mass of tiny cilia gives the lumen a firm, waving carpet that perhaps facilitates the transport of mucus and egg cells through the winding uterine tube.

REFERENCES

1. BORELL, U., NILSSON, O., WERSÄLL, J. and WESTMAN, A., *Acta Obstet. Gynecol. Scand.* **35**, 35 (1956).
2. DALTON, A. J., KAHLER, H. and LLOYD, B. J., *Anat. Record* **111**, 67 (1951).
3. ENGSTRÖM, H., *Acta Oto-Laryngol.* **39**, 364 (1951).
4. ENGSTRÖM, H. and WERSÄLL, J., *Ann. Otol. Rhinol. & Laryngol.* **61**, 1027 (1952).
5. FAWCETT, D. W. and PORTER, K. R., *J. Morphol.* **94**, 221 (1954).
6. LUCAS, A. M., in COWDRY, E. V. (Ed.), *Special Cytology*, p. 407. Paul B. Hoeber, 1932.
7. NEWMAN, S. B., BORYSKO, E. and SWERDLOW, M. J., *J. Research Nat. Bur. Standards* **43**, 183 (1949).
8. NILSSON, O., *Exptl. Cell Research* (in press).
9. NILSSON, O., BORELL, U., GUSTAVSON, C.-H. and WESTMAN, A., *Acta Obstet. Gynecol. Scand.* (in press).
10. ODOR, D. L., *Anat. Record* **115**, 434 (1953).
11. PALADE, G. E., *J. Exptl. Med.* **95**, 285 (1952).
12. RHODIN, J. and DALHAMN, T., *Z. Zellforsch. u. mikroskop. Anat.* **44**, 345 (1956).
13. DE ROBERTIS, E. D. P., NOWINSKI, W. W. and SACZ, F. A., *General Cytology*, 2nd ed. W. B. Saunders Company, Philadelphia, 1954.
14. SJÖSTRAND, F. S., *J. Cellular Comp. Physiol.* **42**, 15 (1953).
15. ——— *Experientia* **9**, 114 (1953).
16. WERSÄLL, J., *Acta Oto-Laryngol.*, Suppl. 126 (1956).

The Ultrastructural Organization of the Mouse Thyroid Gland¹

R. EKHOLM and F. S. SJÖSTRAND

Department of Anatomy, University of Gothenburg, and Laboratory for Biological Ultrastructure Research, Department of Anatomy, Karolinska Institutet, Stockholm

Received July 29, 1957

The thyroid cells are bounded by a plasma membrane that appears as a single dark line about 80 Å thick. In those areas where two cells lie close together these lines are separated by a space of fairly constant width, about 145 Å. That part of the plasma membrane which bounds the cell from the colloid forms microvilli, which have a maximum length of about 0.44 μ and a maximum width of about 0.14 μ .

The endothelial lining of the capillaries exhibits cytoplasmic discontinuities, the cytoplasm being replaced by a thin (50 Å) membranous structure. The width of the discontinuities is about 400 Å.

The thyroid mitochondria are mostly rod-shaped. They are bordered by a triple-layered membrane consisting of two opaque layers with a less opaque layer interposed. In the interior of the mitochondria there is a large number of similarly triple-layered membranes. The mean thickness of the outer membranes is 165 Å and of the inner membranes 180 Å.

The Golgi zone contains pairs of membranes, vacuolar spaces and small vesicles.

In the cytoplasm there is a well developed system of membranes (α -cytomembranes). These consist of basic membranes, 55 Å thick, to one side of which dense particles with a diameter of about 145 Å are attached. The membranes bound more or less wide spaces which contain a homogeneous material of low opacity.

Two types of big granules are observed delimited by a single membrane, about 50 Å thick. One type has a homogeneous, rather dense content and a regular rounded shape. The granules of the other kind are filled with an inhomogeneous matter and their outline is somewhat wavy.

The nuclear membrane appears as a double membrane consisting of two opaque layers separated by a less opaque interspace. The outer opaque layer seems to belong to the α -cytomembrane system.

We have earlier published a study on the ultrastructure of the mouse thyroid (14) but, owing to limitations of space, this previous paper was very sparing in both text and illustrations. We therefore consider it justified to present an additional report which is both more detailed and more completely elucidated by electron micrographs.

¹ This investigation has been supported by grants from the Swedish Cancer Society.

Like the previous report the present one is founded on the results obtained by studying animals kept in normal laboratory conditions. However, the present study also contains some observations made on animals subjected to cold exposure.

The rat and guinea-pig thyroid has earlier been studied with the aid of the electron microscope by several investigators. Monroe (16) seems to have been the first to publish such an investigation and was then followed by Braunsteiner, Fellingner and Pakesch (7) and Dempsey and Peterson (11). The observations made by these authors are in general accord. Thus, they all give an account of the existence of microvilli on the follicular surface of the thyroid cells and a "lamellar" or "canalicular" structure in the cytoplasm. Dempsey and Peterson describe in addition a system of dense granules associated with this structure. However, as regards the structure of the capillaries the opinions are at variance. Monroe believes that the endothelium lining the capillaries is discontinuous, but Dempsey and Peterson are of the opinion that close examination always reveals a continuous capillary wall.

MATERIAL AND METHODS

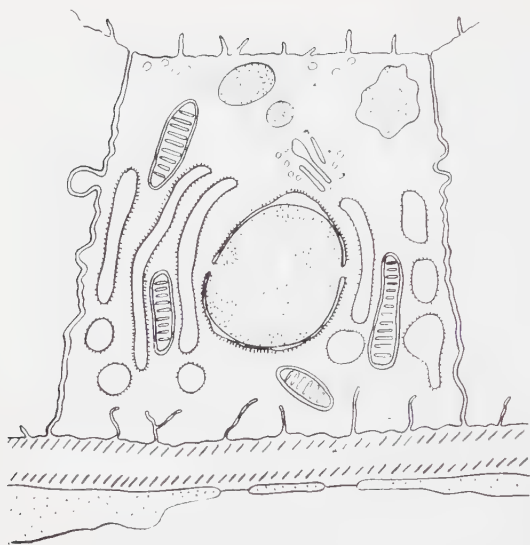
The thyroid glands of 50 adult male white mice have been examined, forty of which were kept in normal laboratory conditions. Ten animals lived at a room temperature of about $+2^{\circ}\text{C}$ the last five days before they were killed. All the animals were killed by decapitation at a room temperature of about $+2^{\circ}\text{C}$. In order to avoid post-mortem changes, the upper part of the trachea, the larynx and the thyroid were excised in one piece and put into the fixating-fluid within 1–2 min. This was kept at -2°C and consisted of a blood-isotonic 1% osmium tetroxide solution, buffered at pH 7.2 with veronal-acetate, a modification of the osmium solution of Palade (18). After fixation for 1.5–2 hours the tissue was washed in physiological saline for one hour, and dehydrated in alcohol, slowly brought to room temperature. In the alcohol the thyroid was isolated under the microscope from the other tissues of the specimen and divided into its two lobes. The lobes were separately embedded in a mixture of *n*-butyl and *n*-methyl methacrylate mainly according to Newman, Borysko and Swerdlow (17) or, in the later part of the investigation, according to Borysko (5).

The ultrathin sectioning was performed partly with the microtome designed by Sjöstrand (24), partly with an instrument described by Ekholm and Zelander (15). For both microtomes steel knives were used, sharpened according to Ekholm *et al.* (12, 13).

The sections were examined partly in an RCA EMU 2b electron microscope, partly in an RCA EMU 3b microscope. The objective lenses of the microscopes were kept carefully compensated, and each of them was equipped with an aperture having a bore of $70\ \mu$ and $50\ \mu$ respectively.

RESULTS

The appearance of the mouse thyroid in the electron microscope is very regular both in the interrelationship between the different constituents of the gland and in the ultrastructural organization of the individual cells. In survey pictures (Figs. 1, 2)



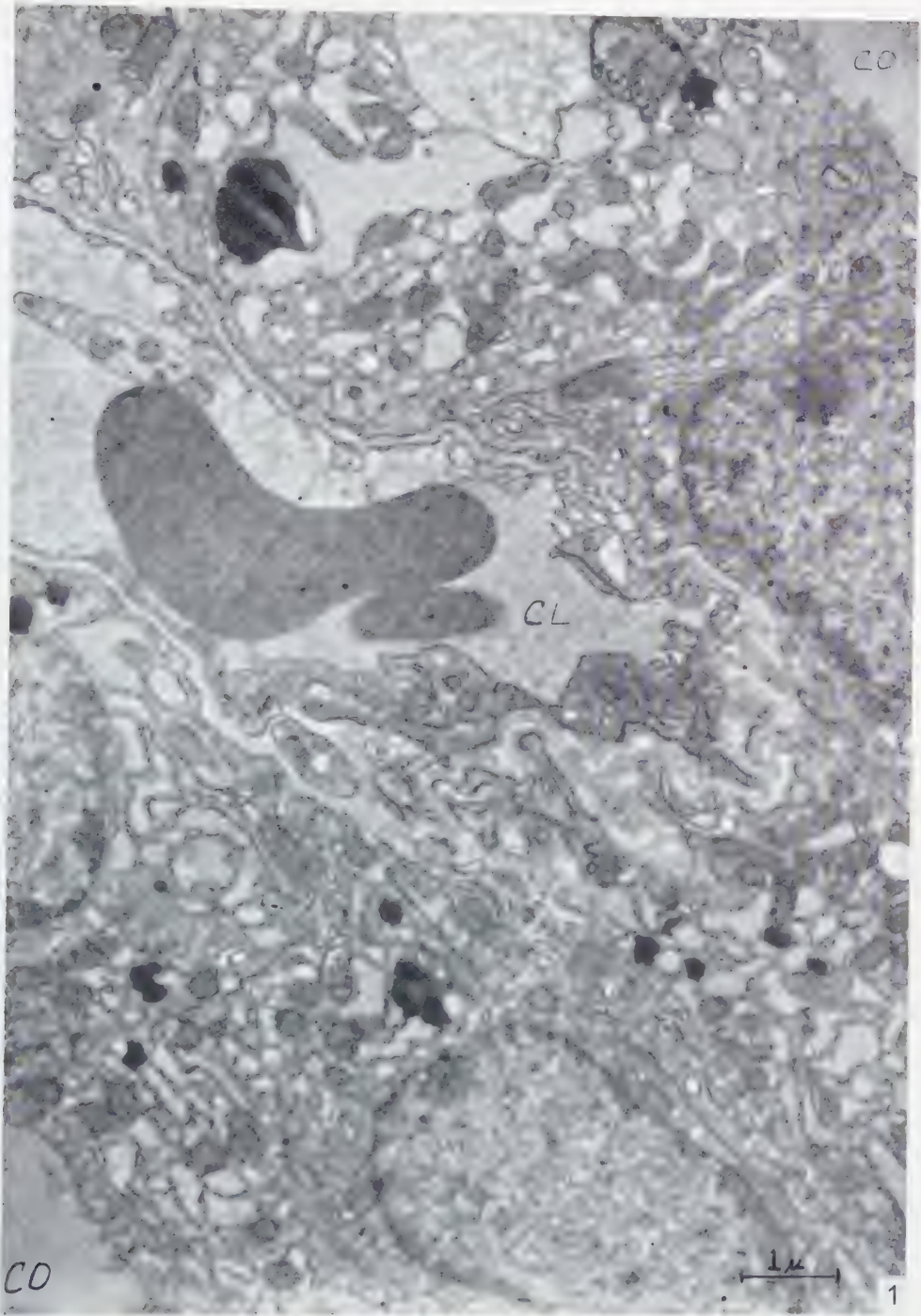
Schematic drawing showing a thyroid cell with the nucleus, a number of mitochondria, α -cytomembranes and two kinds of big granules. The cell is facing the colloid with the apical surface and is bordering on a capillary with its base.

the gland cells are seen to bound the colloid with their apical surfaces and to border on a blood capillary with their bases. There is no or only minute bundles of connective tissue seen between adjacent follicular units. The cells forming the follicles lie close together separated only by thin plasma membranes and a narrow space of low density between these membranes. At the surface facing the colloid the plasma membrane is seen to protrude as a lesser or greater number of microvilli. In the centre of the cell, or somewhat eccentrically in the basal direction, the cell nucleus, which has a granular appearance, is observed. A large number of mitochondria, mostly rod-shaped, are evenly distributed throughout the cells. The apical zone of the cells contains granules of varying number, size and density. In all parts of the cells more or less regular systems of membranes are seen.

The thyroid cells are bounded by a *plasma membrane* that, in its major course, appears as a single dark line. In those areas where two cells lie close together these dense membranes are separated by a space of low density and of a fairly constant width ($145 \pm 7 \text{ \AA}$). The course of two adjacent plasma membranes is rather straight for long distances but shows, at intervals, horseshoe-like bulges or more complicated irregularities (Fig. 6).

In the neighbourhood of the free cell surface it is observed that the plasma membranes of two adjacent cells within a short distance are surrounded by an area of

FIG. 1.—Survey picture of some mouse thyroid cells. The cells belong to two neighbouring follicles which are separated only by a blood capillary. CO, colloid; CL, capillary lumen. $\times 13,000$.



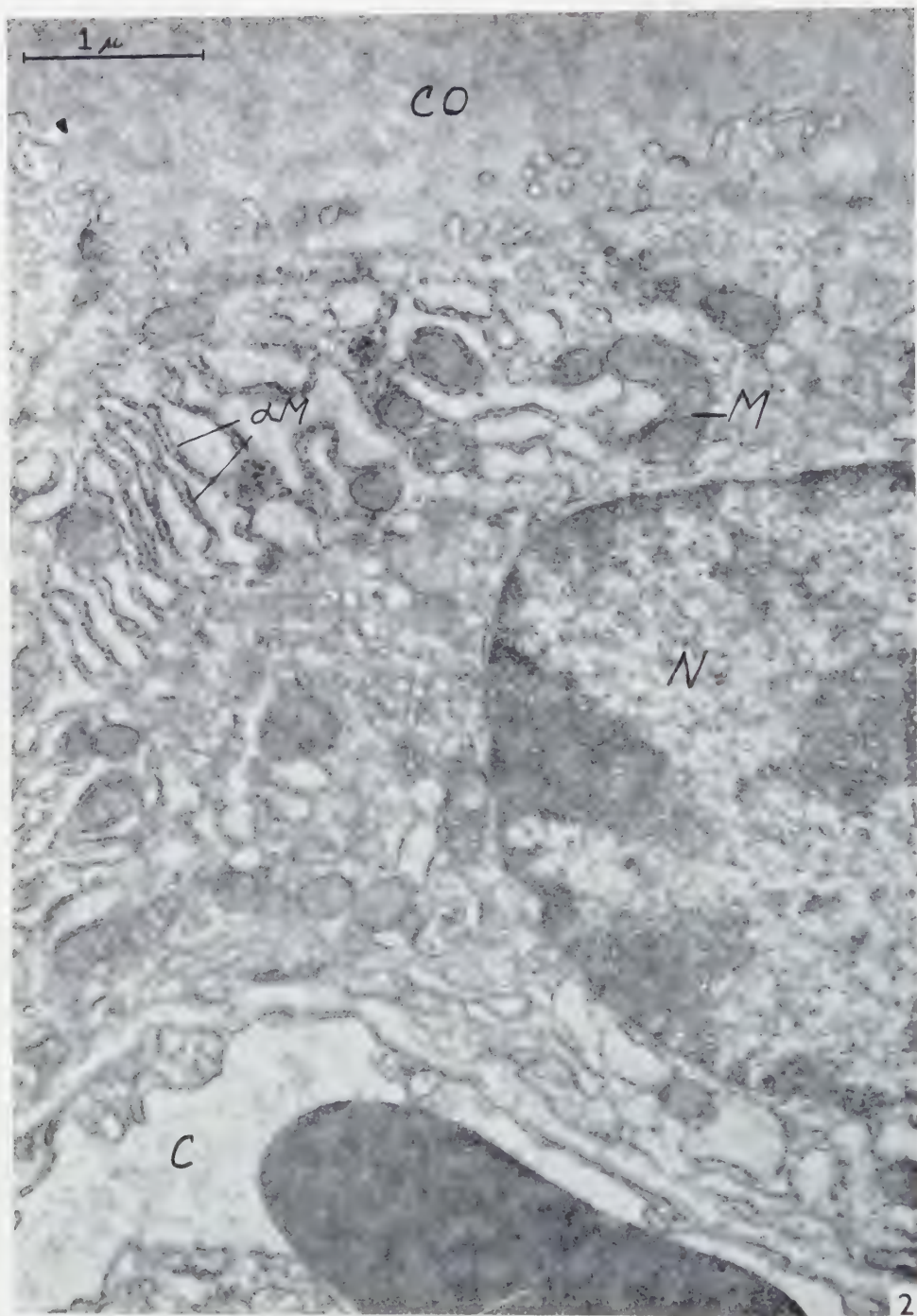


FIG. 2.—Survey picture of a mouse thyroid cell with its top surface facing the colloid (CO) and with its base bordering on a capillary (C). In the interior of the cell mitochondria (M), α -cytomembranes (αM) and the nucleus (N) are seen. $\times 24,000$.



FIG. 3.—Longitudinal section through microvilli protruding from the apical surface of the thyroid cells. At the arrows the plasma membrane is seen to be triple-layered. $\times 220,000$.

high density. Within these regions the intercellular space is slightly widened and each plasma membrane is split into two dark lines separated by a layer of low density (Fig. 5). A similar structure is described by Zetterquist (29) in the columnar absorbing cells of the mouse jejunum and is assumed by him to correspond to the "terminal bars" of the light microscopy. In an apical direction from these areas the interspace between the two plasma membranes seems to be somewhat narrower than the main part of the intercellular space.

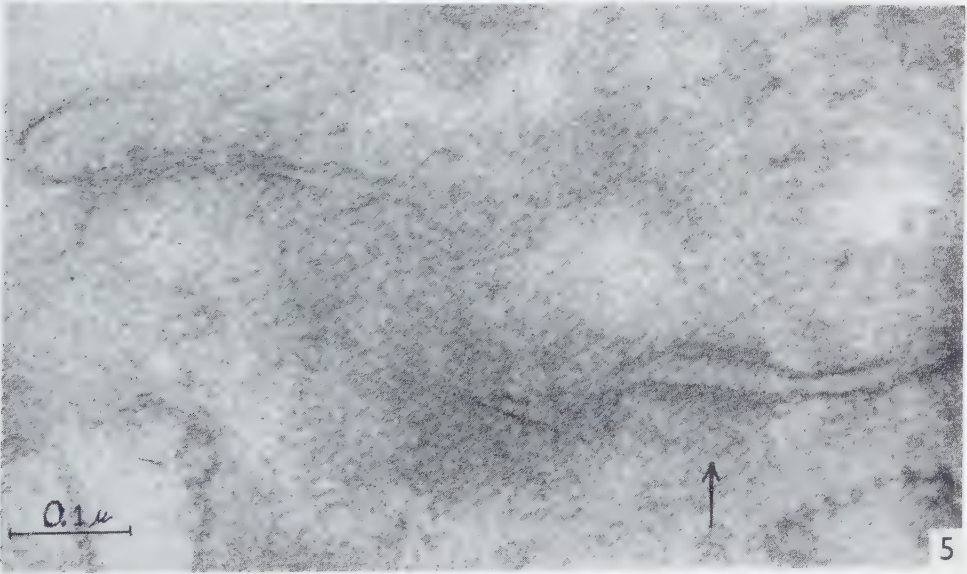
From the apical surface of the cells microvilli protrude into the colloid. These microvilli appear as pure cytoplasmic projections and do not contain any fibrillar or otherwise specialized structure. Their number is widely varying; sometimes only two or three villi are observed in a longitudinal section through a whole cell, but in other cases they stand only a villus' width apart. The shape of the villi varies from slender finger-like projections to short blunt bulges. (The max. length of the villi is measured to be 0.44μ and the max. width to 0.10μ .) The plasma membrane covering the villi and bounding the cell between the bases of the villi appears triple-layered, being composed of two dense layers separated by a less dense space (Figs. 3, 4). This apical part of the plasma membrane is only $60 \pm 5 \text{ \AA}$ thick and seems, consequently, somewhat thinner than the intercellular part of the membrane which is measured to be $80 \pm 3 \text{ \AA}$.

At the base of the cell the plasma membrane is irregularly folded in such a way that the basal cell zone is divided into a number of compartments of varying size and shape (Fig. 7). Those parts of the plasma membrane that dive into the cytoplasm lie close together, separated only by a space of about the same width as the intercellular one.

In almost all sections comprising the basal parts of the cells these are seen to lie in close vicinity to a *blood capillary* (Figs. 1, 2). Between the capillary endothelium and the plasma membrane of the epithelial cells there is a periendothelial space (Fig. 7). This space, usually having a width of $0.15\text{--}0.2 \mu$, is regularly composed of three layers. Two of these layers are of moderate density and situated close to the plasma membranes of the epithelium and endothelium respectively. The third layer, interposed between the two dense ones, is of very low density and varying width. The dense layer close to the epithelium, the epithelial basement membrane, runs uninterrupted over the cell boundaries and over the foldings of the plasma membrane and it never shows any tendency to dive into the intercellular spaces. The dense layer

FIG. 4.—Transverse section through microvilli showing the triple-layered nature of the plasma membrane. $\times 220,000$.

FIG. 5.—Longitudinal cell section showing the plasma membranes of two adjacent thyroid cells near the apical surface. The plasma membranes are surrounded by a dense area and exhibit (at the arrow) a triple-layered structure. $\times 150,000$.



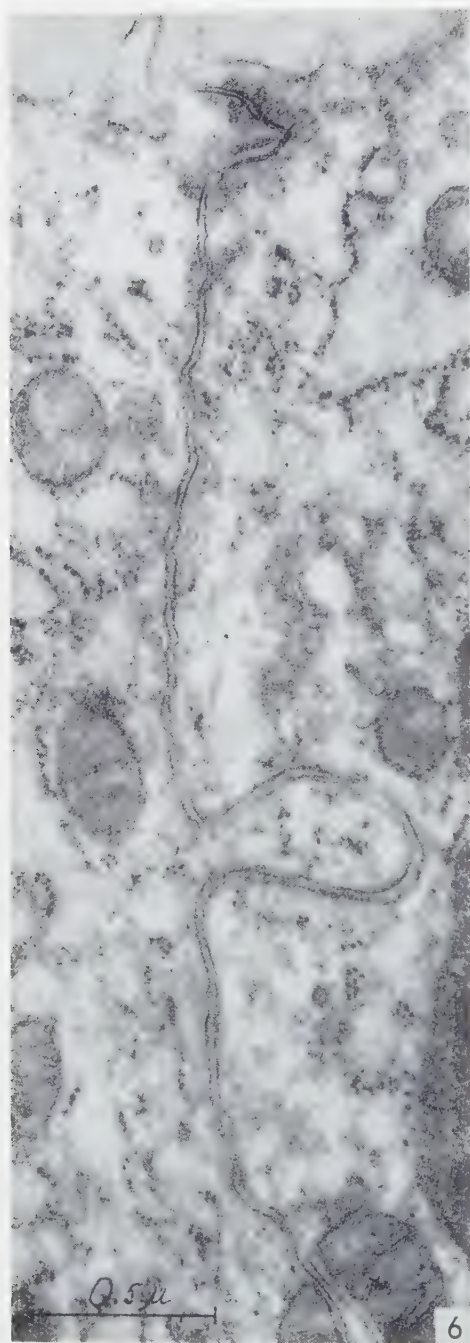


FIG. 6.—Longitudinal cell section showing a typical course of the plasma membranes of two adjacent thyroid cells. $\times 48,000$.



FIG. 7.—Section through the basal part of a thyroid cell and part of capillary wall. Note the folded course of the plasma membrane of the thyroid cell. *END*, endothelium; *BM*, basement membranes in the pericapillary space. At the arrows, discontinuities of the endothelium. $\times 67,000$.

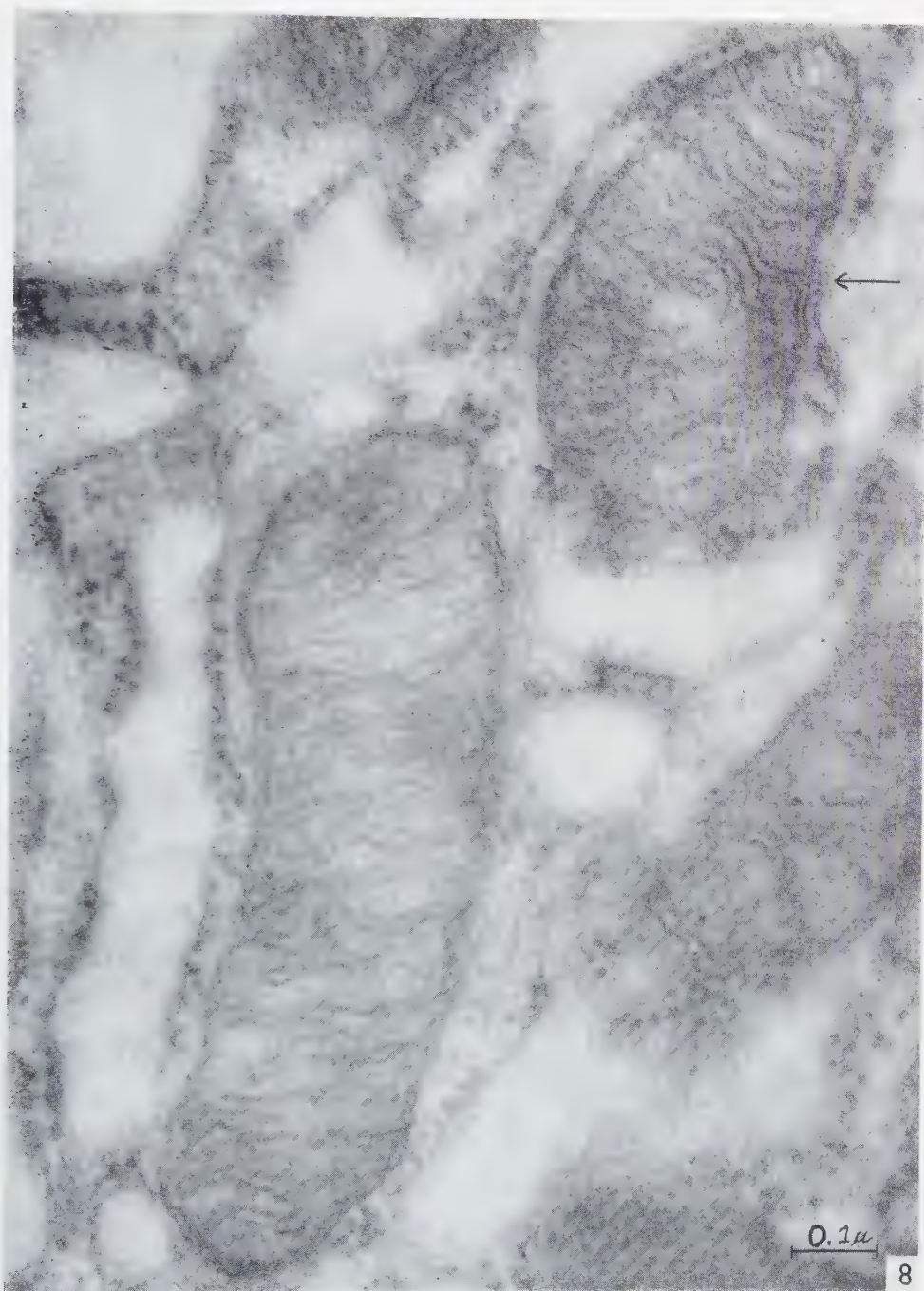


FIG. 8.—A number of thyroid mitochondria showing the triple-layered outer and interior membranes. At the arrow the inner dense layer of the outer mitochondrion membrane is seen to be continuous with the dense layers of an interior membrane. $\times 114,000$.

closely applied to the endothelium, the endothelial basement membrane, runs likewise uninterrupted over the endothelial cell boundaries. The thickness of the epithelial basement membrane is measured to $490 \pm 13 \text{ \AA}$ and the corresponding figure for the endothelial one is $420 \pm 12 \text{ \AA}$.

The thickness of the capillary endothelium differs very much from place to place but the major part of the endothelium is very thin (200–600 \AA). Within these thin parts a type of incomplete interruption of the endothelial wall is regularly observed (Fig. 7). These interruptions appear as cytoplasmic discontinuities, the cytoplasm of the endothelium being replaced by a thin membranous structure about 50 \AA thick. At the margins of the discontinuities the plasma membranes of the outer and inner surfaces of the endothelium are seen to join. The endothelial basement membrane runs uninterrupted over the discontinuities. The width of the discontinuities is about 400 \AA ($395 \pm 10 \text{ \AA}$).

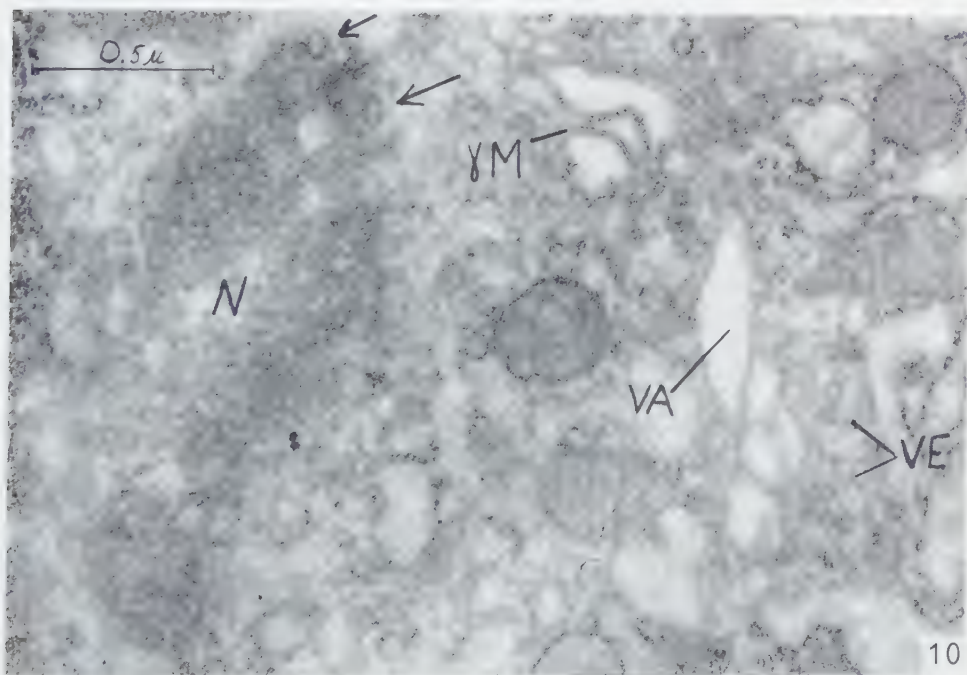
Among the intracellular elements of the thyroid cell the *mitochondria* are conspicuous owing to their large number and regular structure. They are scattered throughout the cytoplasm at random. Most of the mitochondria are rod-shaped, of varying length but of fairly constant width ($0.25 \pm 0.016 \mu$).

The ultrastructure of the thyroid mitochondria is similar to that which is well known from a large number of other epithelial cells. Thus they are bordered by a triple-layered membrane consisting of two opaque layers with a less opaque layer interposed. In the interior of the mitochondria systems of similarly triple-layered membranes are observed, most of which are oriented perpendicularly to the long axis of the mitochondria. Usually the inner membranes bridge over the whole width of the mitochondrion but sometimes only one end of an inner membrane reaches the outer one, the other end being free. In some places the inner opaque layer of the outer membrane is seen to be continuous with the opaque layers of an inner membrane. Usually, however, the central light layers of the outer and inner membranes are separated at the place of contact by an opaque layer (Fig. 8).

The ground substance of the mitochondria is finely granular, the granules being of moderate opacity. The total thickness of the outer mitochondrial membranes is measured to $165 \pm 4 \text{ \AA}$ and of the inner membranes to $180 \pm 3 \text{ \AA}$. The distance between the centres of the opaque layers of the outer membranes is found to be $110 \pm 3 \text{ \AA}$ and the corresponding distance for the inner membranes $125 \pm 4 \text{ \AA}$. Hence, the width of each opaque layer of the outer membrane is calculated to be 55 \AA and of the less

FIG. 9.—A Golgi apparatus showing some short membranes ($\gamma'M$), vacuoles (VA) and small vesicles (VE). $\times 68,000$.

FIG. 10.—A Golgi apparatus close to a tangentially cut nucleus (N). The Golgi zone contains γ -cytomembranes ($\gamma'M$), vacuolar spaces (VA) and small vesicles (VE). At the arrows, ring-shaped structures probably corresponding to nuclear "pores". $\times 44,000$.



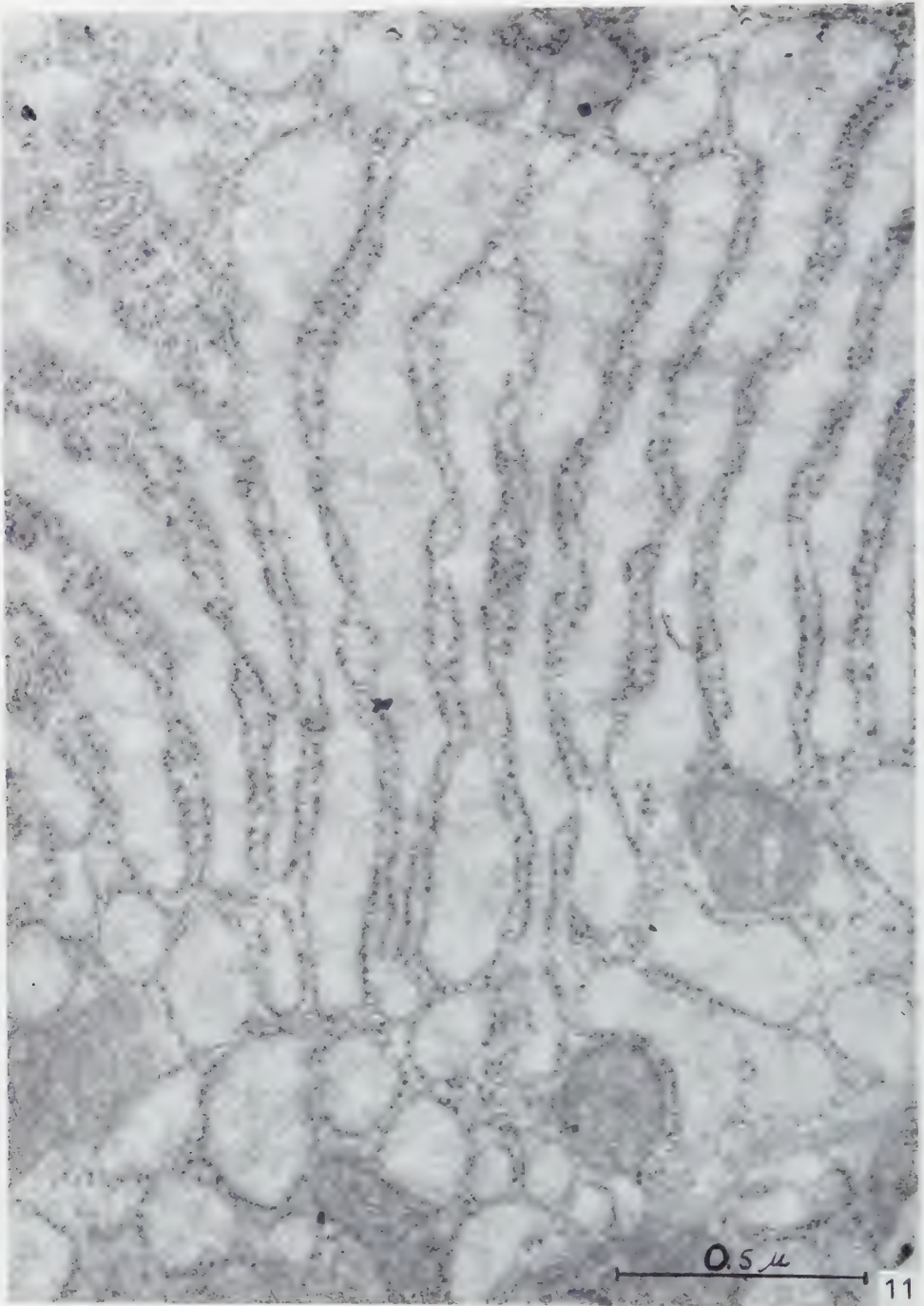


FIG. 11.— α -Cytomembranes with a fairly regular parallel arrangement. In the upper left part, rows of dense particles without any visible contact with membranes. $\times 67,000$.



FIG. 12.—A number of mitochondria and α -cytomembranes in irregular arrangement. Note that the α -cytomembranes in some places are void of dense particles. $\times 55,000$.

opaque central layer to 55 Å. The corresponding figures for the inner membranes are 55 and 80 Å respectively. The distance between the inner membranes (measured between the centres of the membranes) varies from 250 to 800 Å.

The *Golgi zone* (Figs. 9, 10) is usually found in the neighbourhood of the nucleus. It consists of a few pairs of membranes in more or less parallel arrangement and usually with somewhat wavy course (γ -cytomembranes according to Sjöstrand, 25). In association with these membranes a number of vacuolar spaces of varying size are found. The third component of the Golgi zone is a large number of small vesicles which surround the membranes and vacuoles. These vesicles have a distinct surface membrane and a fairly constant size (400–800 Å).

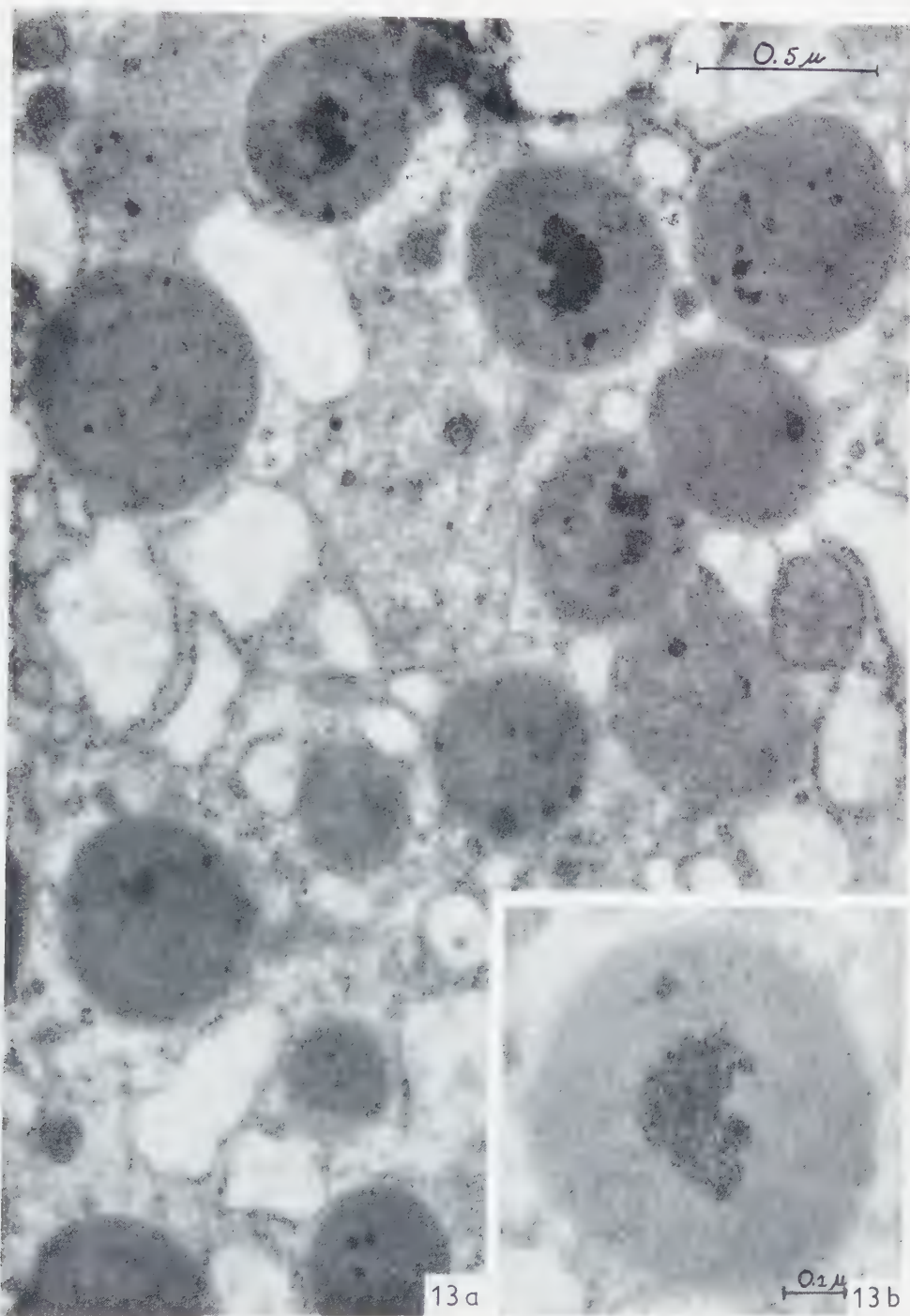
In the thyroid cells there is a well developed system of intracellular membranes of the type that by Sjöstrand (25) is named α -cytomembranes (Figs. 11, 12). These membranes appear as a thin basic membrane to which at one side small opaque particles are attached. These particles have a varying shape—irregularly rounded, rectangular or triangular—but are in general fairly regularly interspaced (150–350 Å) along the basic membrane. However, within short distances the membranes are completely free from particles. On the other hand, rows and clusters of particles of the size and shape described, but without contact with any basic membrane, are frequently observed. The mean diameter of the particles is 145 ± 9 Å and the mean thickness of the basic membranes is 55 ± 3 Å.

The α -cytomembranes are observed in all parts of the cytoplasm but are usually most numerous in the middle and basal parts of the cells. The general arrangement of the membranes varies. Within restricted areas they show a fairly regular arrangement, being disposed in pairs in such a way that two adjacent membranes face each other with the particle-covered side, the distance between the two components of each pair being rather constant (about 500 Å). The smooth sides of the membranes are in these areas separated by a wider and more irregular space. If the membranes are followed for a distance, it is seen that the two nearest membranes from two adjacent pairs join and so close the space which is bounded by the smooth sides of the membranes.

In other regions the regular arrangement of the membranes just described is not obvious because the spaces lined by the smooth sides, as well as those lined by the particle-covered ones, are irregular or rounded and vary more widely in size.

The spaces lined by the smooth sides of the α -cytomembranes contain a homogeneous matter of low electron density. On the other hand, the spaces bounded by

FIG. 13.—(a) A number of big granules with a dense and fairly homogeneous content. In the upper right part of the picture a granule with a distinct surface membrane. In the centre a granule with an unhomogeneous content. $\times 48,000$. (b) A "homogeneous" granule at higher magnification showing an aggregate of very dense small particles. $\times 83,000$.



the particle-covered sides have a most varying content, for these spaces lodge all the defined cytoplasmic structures—the mitochondria, the granules and the Golgi zone.

The number and sizes of the *granules* vary greatly, apparently depending on the functional state of the cell. In cold-exposed animals the granules are generally more numerous and larger than in animals kept in ordinary laboratory conditions. But also in cold-stimulated gland, cells with few and small granules are common. Most of the granules are found in the apical zone of the cells.

At least two types of big granules can be distinguished. The first type has a regularly circular shape and a relatively dense homogeneous content and is surrounded by distinctly outlined single-surface membrane, about 50 Å thick (Fig. 13a). In a rather large percentage the granules of this type contain small aggregates of rounded, very dense particles about 70 Å in diameter (Fig. 13b). The size of the granules varies; usually the diameter lies between 0.15 and 0.8 μ .

The big granules of the second type are fundamentally rounded or oval, but have as a rule a somewhat wavy outline (Fig. 14). They have an unhomogeneous content consisting of irregular aggregates of a moderately dense material. The granules are bordered by a distinct single membrane, about 50 Å thick. The size of this type of granules varies within wide limits, the largest observed having a diameter of about 2.2 μ and the smallest only 0.15 μ . Both types of the granules described appear simultaneously in the same cell.

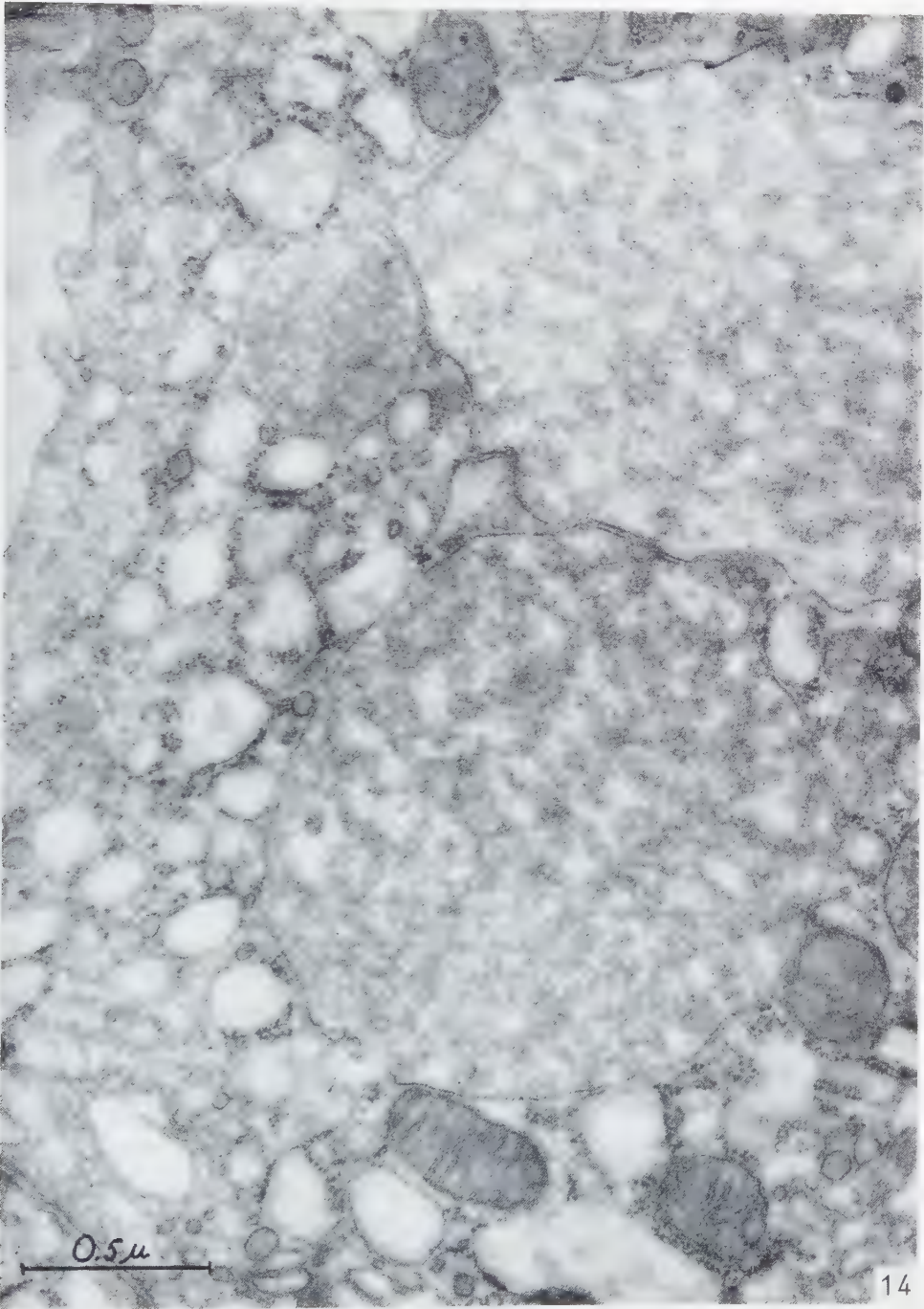
In addition to these well defined big granules there are in every cell, predominantly in the apical zone, a varying number of small granules or vesicles. Most of these have a rounded shape, a homogeneous content or moderate opacity and a distinct surface membrane. Their size varies between 400 and 1000 Å.

In a large percentage of the thyroid cells heavily *osmium-impregnated globules* are found. They have a rounded or irregular form and lack a delimiting surface membrane. The globules are observed anywhere in the cells but always in those areas of the cytoplasm that are bordered by the particle covered side of the α -cytomembranes.

The *cell nucleus* has a content of rounded or irregularly shaped osmiophilic particles of fairly constant size (about 130 Å). The particles are densely accumulated at the nuclear membrane and in some areas in the interior of the nucleus (Figs. 2, 15, 16). Throughout the remainder of the nucleus only a few particles are scattered, giving a rather low opacity to these parts.

In sections cut at right angles to the nuclear surface the nuclear envelope appears within rather long distances as a double membrane consisting of two opaque layers (each about 50 Å thick) separated by a less opaque interspace (80–250 Å wide). On

FIG. 14.—Some big granules with an unhomogeneous content and a distinct and wavy surface membrane. In the upper left part, the apical cell surface. $\times 50,000$.



close inspection the outer opaque layer seems to be of the α -cytomembrane type (Figs. 15, 16). As a rule these α -cytomembranes close to the nucleus are almost devoid of their characteristic particles. However, the nature of these membranes can usually be established by the fact that—when followed for a certain distance—they are seen to recede from the nucleus and to continue as a typical particle-covered α -cytomembrane.

In sections perpendicular to the surface of the nucleus the outer and inner nuclear membranes seem to join at intervals, which results in a gap that is closed by an osmiophilic membrane (Figs. 15, 16). The dimension of these gaps is about 400 Å. In sections cut tangentially to the nuclear surface ring-shaped structures are observed which probably correspond to these gaps (Fig. 10).

DISCUSSION

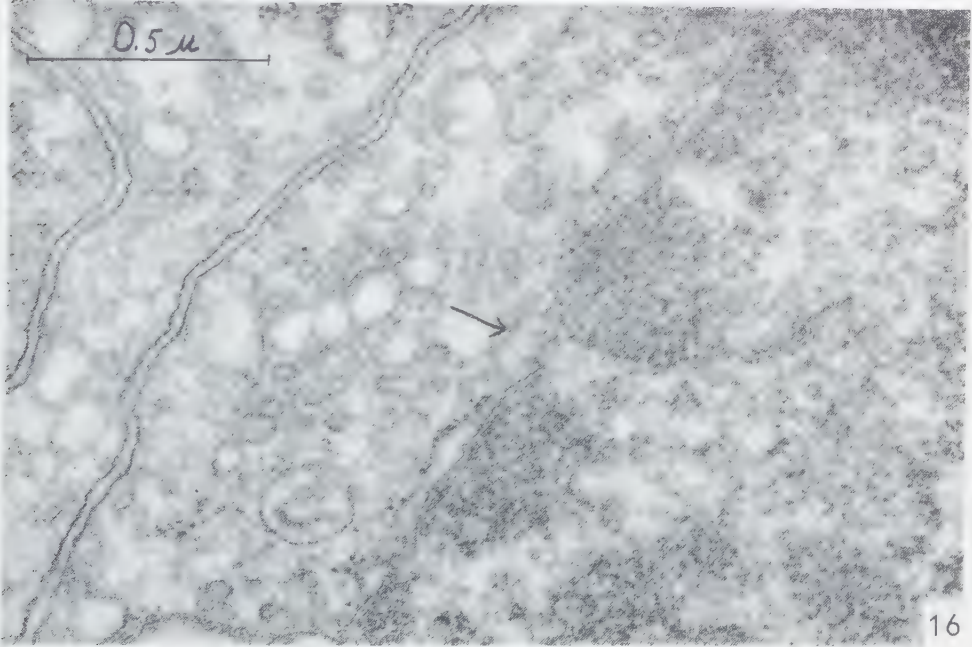
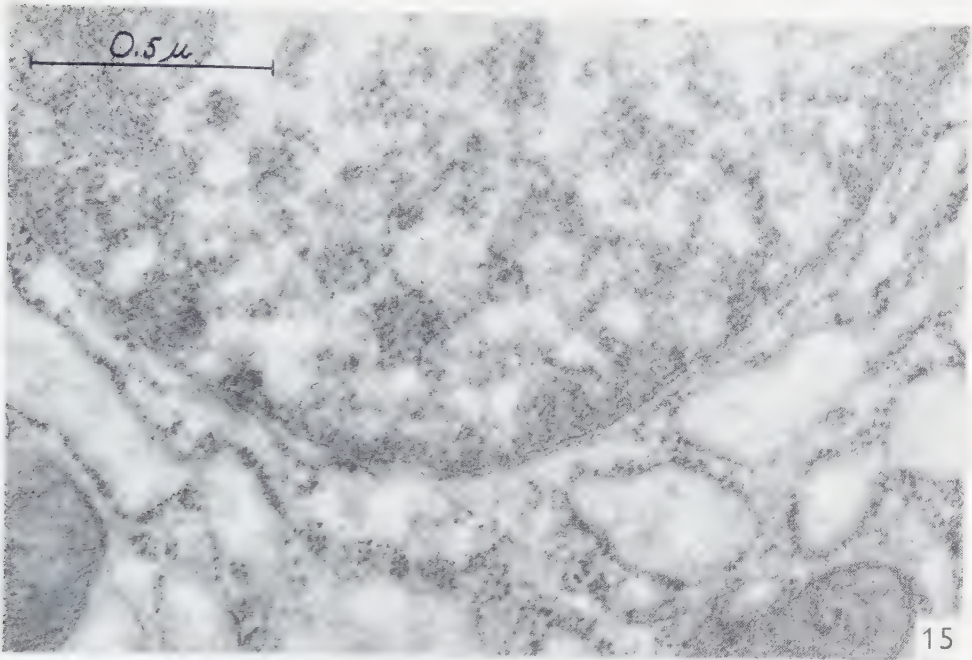
In the endocrine organs the ultrastructure of the blood capillary wall as well as the interrelation between the capillaries and the epithelium seems to be of special interest with regard to the transportation of secretion products between the epithelium and the blood. Concerning the capillary wall in the thyroid Monroe (16) suggested, as mentioned above, that the endothelium is discontinuous, while Dempsey and Peterson (11) considered such pictures as artefacts. In the present study cytoplasmic discontinuities of the endothelial lining of the blood capillaries are constant findings. However, these discontinuities are not complete interruptions of the wall, as an osmiophilic membrane bridges the gap in the cytoplasmic layer. The same kind of cytoplasmic discontinuities are observed in some other endocrine glands, for instance, the mouse adrenal cortex (28). Apparently it is very difficult to determine with certainty whether these cytoplasmic discontinuities are artefacts or true formations.

The organization of the intercellular space in the thyroid is identical with that generally observed in epithelial tissues. It has been assumed (Sjöstrand, 26) that the light space between the dense plasma membranes corresponds to an organized layer of material, possibly lipids, and that this layer represents a part of the plasma membranes.

As described above the thyroid cells contain a well developed system of intracellular membranes of the type that is called α -cytomembranes by Sjöstrand (25).

FIG. 15.—Section at a right angle to the nuclear surface showing α -cytomembranes in close relation to the nuclear membrane. \times 61,000.

FIG. 16.—Part of a nucleus cut perpendicularly to the nuclear surface. The nuclear membrane is seen to join with two α -cytomembranes, resulting in a gap without a distinct nuclear membrane (at the arrow). \times 61,000.



The membranes observed correspond undoubtedly to the linings of the "lamellar" or "canalicular" structures earlier observed in thyroid cells (7, 11, 16).

The appearance of these membranous systems varies considerably from gland to gland and from cell to cell in the same gland. This applies especially to the size of the spaces bounded by the membranes. Apparently the quality of the fixation plays an important role in this connection, the spaces showing a tendency to widen when the preservation is not perfect. On the other hand, there is no doubt that appreciable variations in the α -cytomembranous spaces exist independently of the type of fixation. It seems very probable that these variations are related to alterations in the functional state of the cells.

Particles of the same size and density as those attached to the basic membranes of the α -cytomembranes are also observed free in the cytoplasm in the spaces bordered by the particle-covered sides of the membranes. Sometimes these free particles are arranged in regular rows and, therefore, it seems possible that their isolated appearance is due to oblique sectioning. On the other hand it is not impossible that some of the particles are really free.

α -Cytomembranes are described in a variety of cells and seem generally to be especially abundant in secretory cells as in the exocrine cells of the pancreas (27). The α -cytomembranes are now included by several authors in a system called the "endoplasmic reticulum", a name originally presented by Porter and Kallman (23). This "endoplasmic reticulum" has been studied in a large number of cell types (especially by Porter and Palade; cf. Palade, 19) and is assumed by Palade (19) to be present in all animal cells. It must be pointed out, however, that the "endoplasmic reticulum" which includes almost anything bounded by a membrane is a much wider concept than the α -cytomembranes. It refers, to a great extent, to membranous and vesicular structures which morphologically are not conclusively related to the α -cytomembranes.

According to several authors (3, 4, 10, 22) the "endoplasmic reticulum" corresponds to those areas of the cytoplasm which in light microscopy exhibit basophilia. Furthermore, it has been demonstrated that there is an intimate connection between cytoplasmic basophilia and the presence of ribonucleic acid (6, 8). It is also of interest in this connection that the microsome fraction of homogenized liver, which contains about 50 % ribonucleic acid (1, 2, 9, 21) is found to consist of membranous and vesicular structures associated with small particles (20).

Above are described two types of big granules in the thyroid cells. As both kinds sometimes appear simultaneously in the same cell, the consideration that the structural differences are due to variations in the preparation can be excluded. The granules are usually localized to the apical part of the cells and always to those spaces which are bordered by the particle-covered sides of the α -cytomembranes.

Otherwise no local relation to other cytoplasmic structures is observed. The granules increase in size and number in connection with cold stimulation and therefore it can be assumed that their occurrence is related to the functional state of the cell. However, nothing can be said at the present about the nature of the granules.

REFERENCES

1. BAHR, G. F., *Acta Radiol.*, Suppl. 147 (1957).
2. BARNUM, C. P. and HUSEBY, R. A., *Arch. Biochem.* **19**, 17 (1948).
3. BERNHARD, W., GAUTIER, A. and OBERLING, C., *Compt. rend. soc. biol.* **145**, 566 (1951).
4. BERNHARD, W., HAGUENAU, F., GAUTIER, A. and OBERLING, C., *Z. Zellforsch. u. mikroskop. Anat.* **37**, 281 (1952).
5. BORYSKO, E., *J. Biophys. Biochem. Cytol.* **2**, No. 4, Suppl. 3 (1956).
6. BRACHET, J., *Le rôle des acides nucléiques dans la vie de la cellule et de l'embryon*. Masson, Paris and Desoer, Liège, 1952.
7. BRAUNSTEINER, H., FELLINGER, K. and PAKESCH, F., *Endocrinology* **53**, 123 (1953).
8. CASPERSSON, T. and SCHULTZ, J., *Proc. Natl. Acad. Sci. U.S.* **26**, 507 (1940).
9. CHANTRENNE, H., *Biochim. et Biophys. Acta* **1**, 437 (1947).
10. DALTON, A. J., *Am. J. Anat.* **89**, 109 (1951).
11. DEMPSEY, E. W. and PETERSON, R. R., *Endocrinology* **36**, 46 (1955).
12. EKHOLM, R., HALLEN, O. and ZELANDER, T., *Experientia* **11**, 361 (1955).
13. ——— *Proc. 3rd Internat. Conf. Electron Microscopy, London, 1954*, p. 114. Royal Microscopical Society, London, 1956.
14. EKHOLM, R. and SJÖSTRAND, F. S., *Proc. Stockholm Conf. Electron Microscopy, 1956*, p. 171. Almqvist & Wiksell, Stockholm, 1957.
15. EKHOLM, R. and ZELANDER, T., *Experientia* **12**, 195 (1956).
16. MONROE, B. G., *Anat. Record* **116**, 345 (1953).
17. NEWMAN, S. B., BORYSKO, E. and SWERDLOW, M., *J. Research Natl. Bur. Standards* **4**, 183 (1949).
18. PALADE, G. E., *J. Exptl. Med.* **95**, 285 (1952).
19. ——— *J. Biophys. Biochem. Cytol.* **2**, No. 4, Suppl., 85 (1956).
20. PALADE, G. E. and SIEKEVITZ, P., *Federation Proc.* **14**, 262 (1955).
21. PETERMANN, M. L., MIZEN, N. A. and HAMILTON, M. G., *Cancer Research* **13**, 372 (1953).
22. PORTER, K. R., *J. Exptl. Med.* **97**, 727 (1953).
23. PORTER, K. R. and KALLMAN, F. L., *Ann. N.Y. Acad. Sci.* **54**, 882 (1952).
24. SJÖSTRAND, F. S., *Experientia* **9**, 114 (1953).
25. ——— *Physical Techniques in Biological Research*, Vol. III, p. 241. Academic Press Inc., New York, 1956.
26. ——— *Intern. Rev. Cytol.*, Vol. V, p. 455. Academic Press Inc., New York, 1956.
27. SJÖSTRAND, F. S. and HANZON, V., *Exptl. Cell Research* **7**, 393 (1954).
28. ZELANDER, T., *Z. Zellforsch. u. mikroskop. Anat.* (in press).
29. ZETTERQUIST, H., *The Ultrastructural Organization of the Columnar Absorbing Cells of the Mouse Jejunum*. Stockholm, 1956.

NOTICE TO AUTHORS

Journal of Ultrastructure Research publishes papers dealing with the ultrastructural organization of biologic material as analyzed by means of electron microscopy, X-ray diffraction techniques, X-ray microscopy, and polarization optical analysis. Papers dealing with techniques and instruments which are of importance for the development of this field will also be accepted. The field covered by the journal extends from the structure of molecules which are of biologic interest to the level of cell and tissue organization at the limit of the range of light microscopy.

Address: The author's complete address should be placed on the manuscript.

Manuscript: Manuscripts should be sent to the Editorial Office, Department of Anatomy, Karolinska Institutet, Stockholm 60, Sweden. Manuscripts in English, French or German are accepted. The manuscripts should be typed double-spaced on one side of the paper only. Footnotes should be avoided, but if used they must be numbered consecutively and placed on a separate sheet at the end of the manuscript. Authors are requested to conclude their manuscripts with a brief summary not exceeding 150 words, and to indicate an *abbreviated running title* on the title page. Descriptions of technique and sections of minor importance will be printed in small type.

Manuscripts should be submitted in complete and final form for publication. The policy of the editors will be as prompt a publication as is possible. Papers will be published within three to six months after the date of receipt of the manuscripts by the Editors. Galley proofs will be sent to the authors who are requested to return them together with proofs of the figures immediately by air-mail to the Editorial Office. The point of insertion of each figure should be indicated.

Tables and Figures: The dimensions of the printed page, 5" × 7" or 125 × 175 mm, should be kept in mind in preparing figures and tables for publication. Each table should be typewritten on a separate sheet and all figures and tables should be identified with the author's name. Figure legends should be typed in sequence on a separate sheet. Graphs and diagrams should be carefully drawn in black ink on white paper or blue coordinate paper, and all drawings should be so prepared and lettered that they can stand a reduction of 50 per cent. No illustrations in color will be accepted unless the author is prepared to cover the cost of reproduction. Photographs, whether "figures" or "plates", should be numbered consecutively as Fig. 1, Fig. 2, etc. Other illustrations, such as diagrams, should be called Chart 1, Chart 2, etc. Tables should be numbered with roman numerals.

Literature cited: Papers referred to in the manuscript should be listed on a separate page and headed "References". The journal, volume, page number, and year of publication should be indicated. The system of abbreviation given in "List of Periodicals" in *Chemical Abstracts*, 45, No. 24, Part II (1951), should be followed. The references should be arranged in alphabetical order according to the (first) author's surname. They should also be numbered so that each may be referred to in the text by number only. Please follow carefully the following style for punctuation and order of listing:

1. LACY, D., *Nature* **173**, 1235 (1955).
2. PRICE, G. R. and SCHWARTZ, S., *Physical Techniques in Biological Research*, Vol. III, p. 91. Academic Press, Inc., New York, 1956.
3. SZENT-GYÖRGYI, A. G., MAZIA, D. and SZENT-GYÖRGYI A., *Biochim. et Biophys. Acta* **16**, 339 (1955).

Reprints: Authors will be furnished, free of charge, with fifty reprints without covers. Additional reprints may be obtained at cost. Order forms will be submitted with the galley proofs. These should be filled in, indicating shipping and billing instructions, and returned with the proofs.

Abstracts: Authors are requested to provide an abstract for *Biological Abstracts* on a special form which is submitted with the galley proofs.

An Electron Microscope Study of the Nuclear Envelope of Amphibian Oocytes¹

S. WISCHNITZER²

*Division of Biological and Medical Research,
Argonne National Laboratory, Lemont, Illinois*

Received September 28, 1957

Immature oocytes from *Triturus viridescens* of two stages, both prior to yolk formation, were studied by electron microscopy. In the transition from the first to the second of these stages, two nuclear transformations, namely, undulation of the nuclear envelope and nucleolar shredding, apparently take place simultaneously. The nuclear outpocketings are usually bulbous. Infrequently, invaginations of the nuclear envelope occur.

The nuclear envelope is composed of two membranes, each about 75 Å thick, which are separated by a perinuclear space which is 150 Å in width. The envelope is interrupted by small circular discontinuities, 800-1000 Å in diameter, which result from the union of the two membranes at regular intervals.

It has been established that there are tubes within the discontinuities which are probably not interrupted by the nuclear envelope. Each tube is about 1000 Å in diameter and has a total height of 1500 Å. The annuli seen in tangential sections are considered to represent cross-sections of the tubes. Within or making up the tube walls are about 8 microcylinders which are seen in cross-section as subannuli. Many of the annuli were seen to contain a central granule about 150 Å in diameter. The nucleoli, which increase in size during the transition from one stage to another, are made up of granules about 150 Å in diameter.

A new approach to the geometric interpretation of structures has been presented. X-rays of lucite models embedded in paraffin have been studied in order to determine that the conclusions regarding the structural relationships seen in electron micrographs were not optical illusions.

It is generally believed that the nucleus is responsible for the long term direction and continued maintenance of the synthetic and morphogenetic activities of the cell (22, 40). However, the exact method by which the nucleus influences the cytoplasm remains as yet unclarified. Investigations even before the turn of the century (cited in Wilson (60)), as well as some very recent studies (13, 20) have suggested that in oocytes at least, nucleocytoplasmic interchange takes place by means of nucleolar extrusion. This hypothesis was based upon observations made principally upon fixed and sectioned material studied by light microscopy. It would appear to require

¹ This work performed under the auspices of the U.S. Atomic Energy Commission, while the author was a Postdoctoral Resident Research Associate at Argonne National Laboratory.

² Present address: Department of Anatomy, New York Medical College, New York City.

modification, since the presence of nucleoli in the cytoplasm may be an artifact produced by the dragging effect of the microtome blade (24). Also, in sea urchin oocytes, the cytoplasmic bodies have different staining and solubility properties than the nucleoli from which they supposedly originate (2). Since it is generally believed that nucleocytoplasmic interchange takes place directly rather than by long range forces, and by means of macromolecules (6), it is felt that electron microscopy should be helpful in gaining a better understanding of this process. A number of investigators using this technique have recently presented both indirect (28, 57) and direct (5) evidence on this subject.

The direct interchange of material between the nucleus and cytoplasm is governed by the permeability of the nuclear envelope which in large measure is determined by its ultrastructure. Flemming, as early as 1883, described a clearly visible double-layered nuclear envelope around the germinal vesicle of eggs (cited in Henneguy (32)). This description was confirmed in 1926 by Scarth (54) using micromanipulative techniques and in 1950 by Callan and Tomlin (11) with the electron microscope. Working with amphibian oocyte nuclei, and using isolated nuclear envelopes which were placed on grids, fixed, and then shadow cast, they described a double membrane of which the outer one contained discontinuities. Watson (59), who has reviewed all the subsequent studies on this subject, has shown that discontinuities in the nuclear envelope result from the union of its two membranes and that there is an intimate relationship between the annuli and these discontinuities.

The present paper describes the ultrastructure of the nuclear envelope in amphibian oocytes. Nucleocytoplasmic relationships prior to the onset of yolk formation are discussed in terms of observations of an increase in the nuclear envelope surface and simultaneously, a shredding of the periphery of the nucleolus.

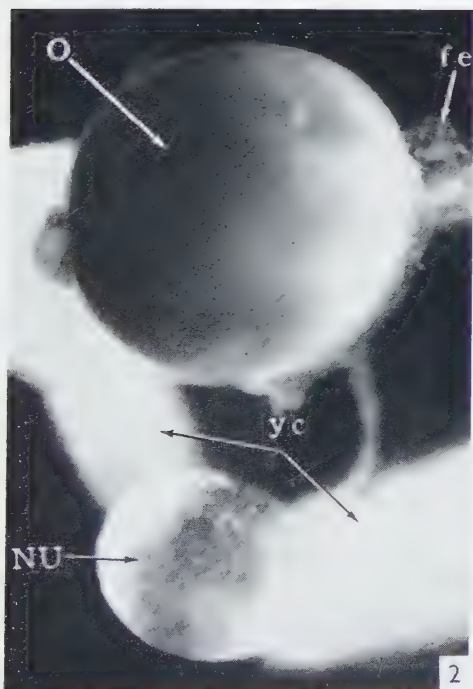
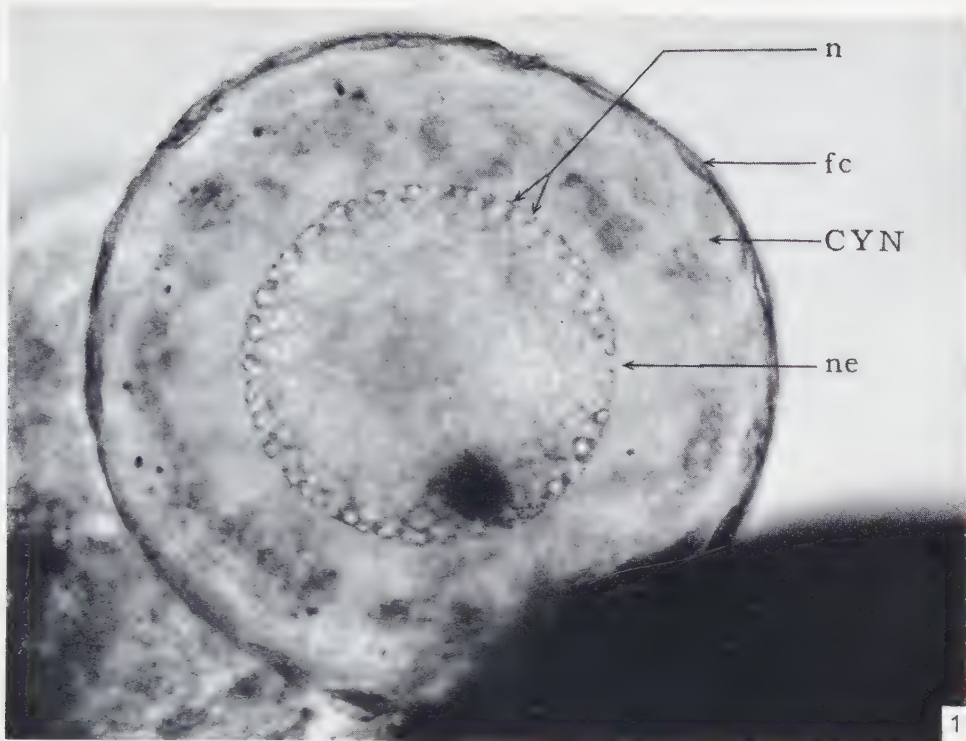
MATERIALS AND METHODS

Ovaries from decapitated *Triturus viridescens* were excised and placed in 0.1 M sodium chloride (24). Under a binocular dissecting microscope, and with the aid of McClure scissors and jeweler's forceps, small clusters of immature, yolk-free, i.e., transparent, oocytes, still enclosed in their follicular epithelium, were dissected out of the ovary. These were immediately placed in the fixative, which consisted of 1% OsO_4 in 0.7% sodium chloride, adjusted to pH 7.4 (45) with McIlvaine's standard buffer solution (0.05 M).

FIG. 1. An immature, yolk-free oocyte from *Triturus viridescens*. The oocyte is still enclosed within its follicular epithelium within which lie the spindle-shaped follicle cells (*fe*). The nuclear envelope (*ne*) and the nucleoli (*n*) are seen distinctly in these transparent oocytes. *CYN*, cytoplasm $\times 775$.

FIG. 2. The method of isolating nuclei from yolk-filled oocytes is illustrated in this photograph. By puncturing and putting a little pressure on a yolk-filled oocyte (*O*), the nucleus (*NU*) emerges as a "swelling" in the ribbon of yolky cytoplasm (*yc*). *fe*, follicular epithelium. $\times 35$.

FIG. 3. A nucleus containing a multitude of nucleoli, isolated by the method shown in Fig. 2. Almost all of the adhering yolk granules have been removed. $\times 90$.



After fixation for $1\frac{3}{4}$ to $2\frac{1}{2}$ hours the material was dehydrated by passage through a graded ethanol series followed by impregnation with three changes of 4 parts ethyl to 6 parts *n*-butyl methacrylate (44). The oocytes were then embedded in the methacrylate mixture to which 1%, lupercol CDB (a preparation of 2,4-dichlorobenzoyl peroxide) had been added, and polymerization was accomplished by maintaining at 60°C in an oven for 24 hours.

Sections, averaging 300 Å in thickness, were cut with a glass knife (38) using a Porter-Blum microtome (52). After spreading, the sections were mounted on grids coated only by carbon films as a result of the removal of the parlodion membranes (58). Both RCA EMU-2A and EMU-3A (100 kv. beam) microscopes were used for observation and photography.

The X-ray of the plastic model was taken at 300 ma, 30 kv. for $\frac{3}{20}$ second with the specimen 6 inches from the source with no filtration.

NOMENCLATURE

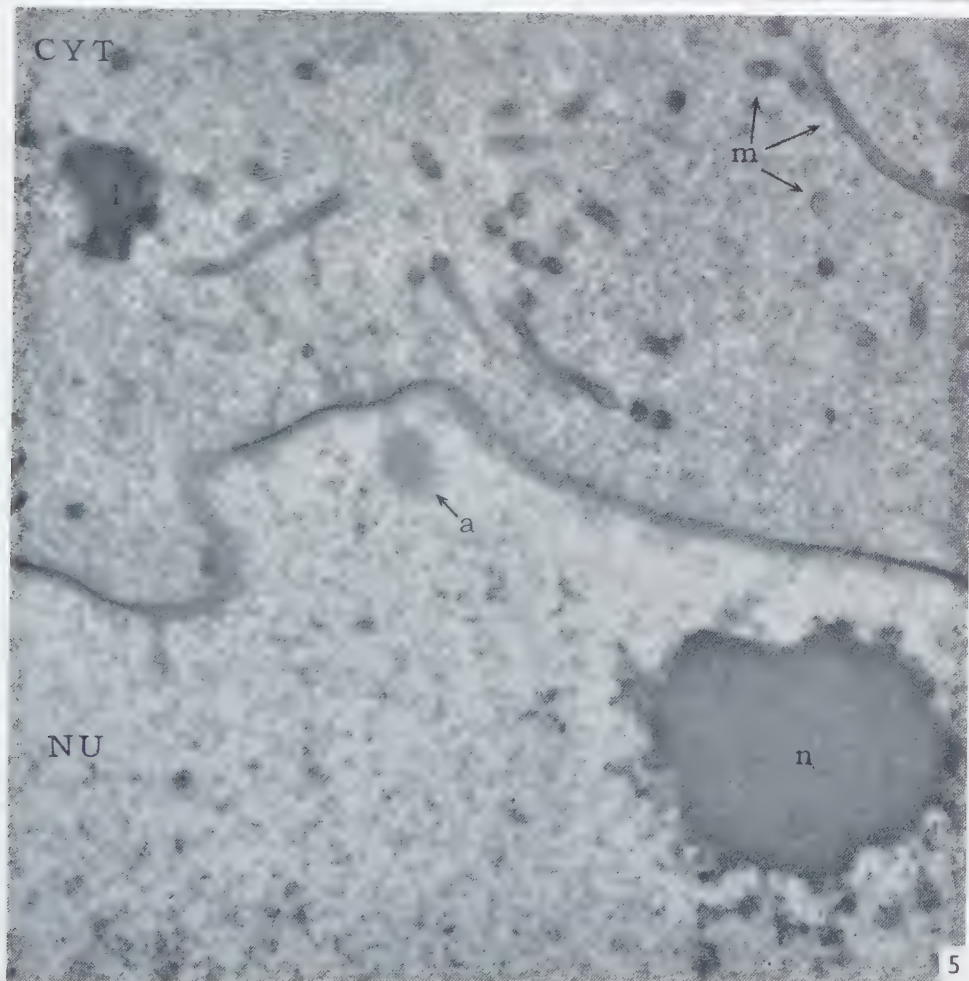
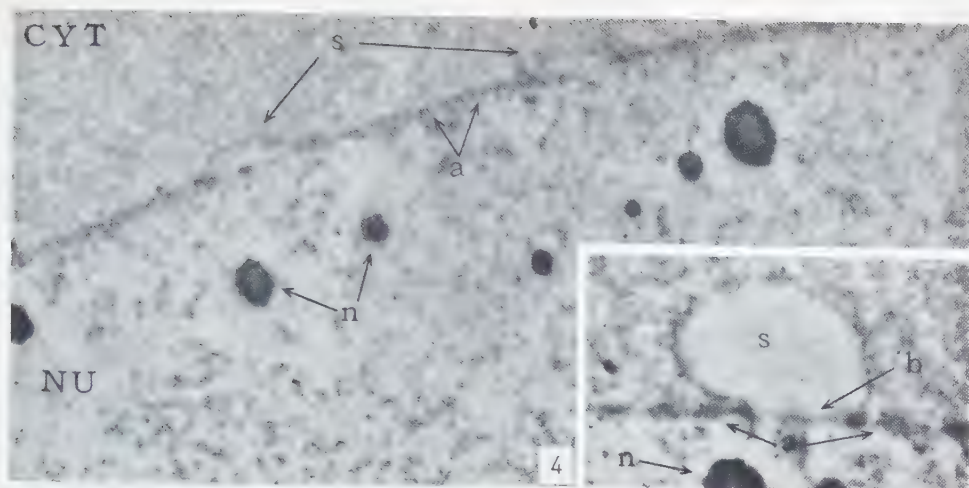
In view of the various terms used by different authors in describing the structures making up the nuclear envelope, it is considered necessary to define those to be used throughout this paper.

The structure separating the nuclear contents from the cytoplasm is called the *nuclear envelope*. It is composed of an *inner* (on the nuclear side) and an *outer* (on the cytoplasmic side) *nuclear membrane*. The region between the membranes is called the *perinuclear space*. The above terms were adopted from Watson (59).

In sections perpendicular to the nuclear envelope, the inner and outer nuclear membranes can be seen to be united at intervals, resulting in the formation of small (circular) *discontinuities*, referred to by various authors as holes, pores or fenestrae. In tangential sections *annuli* can be seen. These have also been called pores, rings, or nodes. The annuli represent, according to this investigator's findings, sections through *tubes* which lie within the discontinuities. The substructures which will be described within the walls of the tubes will be called *microcylinders* which in cross-section have the appearance of *subannuli*.

FIG. 4. An electron micrograph of a portion of an oocyte two stages prior to the onset of vitellogenesis (Stage A). The oocyte is in the very early diplotene stage of meiosis and is about 75 μ in diameter (nuclear diameter 50 μ). *CYT*, cytoplasm; *NU*, nucleus. The nuclear envelope has an even contour except for two lens-shaped sacculations (*s*). In this oblique section the annuli (*a*) are distinct. The nucleoli (*n*) are of varying sizes and are located at the periphery of the nucleus adjacent to the nuclear envelope. The mitochondria-sparse cytoplasm is densely granular, while the nucleoplasm contains small particulate clusters distributed at random. $\times 5400$. *Insert*: A lens-shaped sacculation projecting towards the cytoplasm is shown at a higher magnification. It appears as if one of the nuclear membranes encloses a structureless mass while the other membrane is present as a boundary (*b*) at the level of the nuclear envelope. Distinct annuli (*a*) are seen along the non-evaginated portion of the envelope. $\times 9000$.

FIG. 5. A portion of an oocyte, whose nucleus (*NU*) is about 150 μ in diameter, one stage before yolk formation (Stage B). The cytoplasm (*CYT*) now contains numerous mitochondria (*m*) as well as some lipochondria (*l*). Of particular significance is the onset of undulation of the nuclear envelope and shredding of the enlarged nucleolus (*n*). Cross-sections of tubes appear as annuli (*a*). $\times 19,000$.



OBSERVATIONS

Observations made on oocytes of two stages, both prior to vitellogenesis, will be reported in terms of the nuclear envelope and nucleoli.

Nuclear envelope

In amphibian oocytes the nuclear envelope is present as a distinct morphological entity. It can be seen in the transparent, yolk-free oocytes (Fig. 1) as well as in nuclei isolated from yolk-containing oocytes (Figs. 2 and 3).

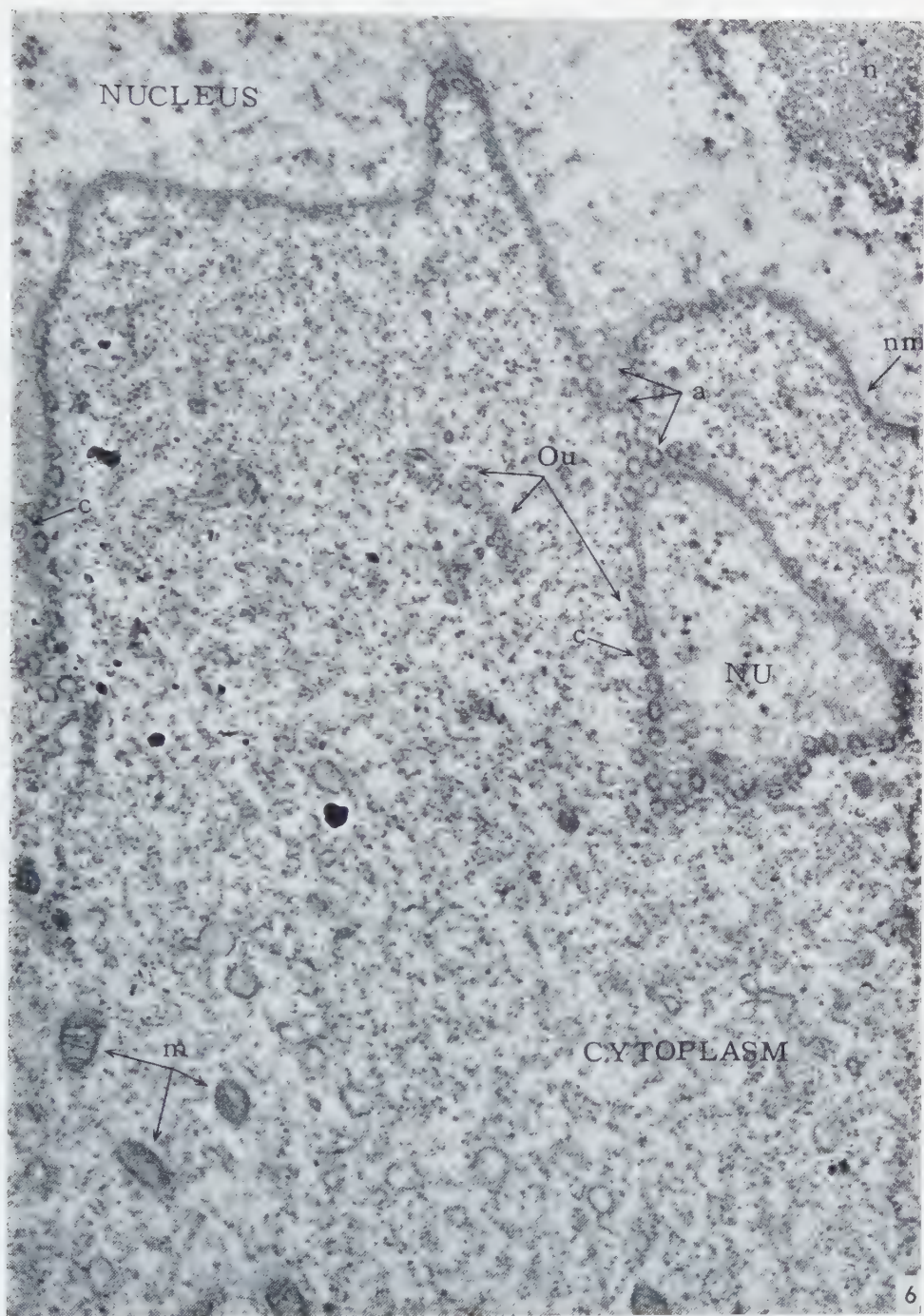
Oocytes two stages before the onset of yolk formation (referred to here as Stage A), that is, in the very early diplotene stage of meiosis, are about $75\ \mu$ in diameter (nuclear diameter $50\ \mu$). The nuclear envelope is seen as a distinct, even boundary separating the nucleus from the cytoplasm (Fig. 4). The mitochondria-sparse cytoplasm is densely granular, while the nucleoplasm contains small particulate clusters.

The even contour of the nuclear envelope is occasionally interrupted by lens-shaped sacculations projecting toward the cytoplasm. The area enclosed within these blebs is structureless. There appears to be some limiting surface between the bleb and the nucleoplasm at the level of the nuclear envelope (Fig. 4, insert) which may represent the inner nuclear membrane, while the outer membrane bounds the periphery of the sacculation. In this tangential section, as evidenced by the distinct annuli in this region, the nuclear envelope apparently is intact up to the bleb. Upon the surface of the bleb there is an apparent absence of annuli.

Still later in diplotene (to be called Stage B), when the nuclear diameter is about $150\ \mu$, the envelope is characterized by a rapid increase in surface to the point where it becomes irregular (Figs. 5, 6, 11, 13 and 14). The irregularity of the nuclear envelope may vary from simple waviness (Figs. 5 and 14) to distinct projections, the majority of which is directed into the cytoplasm for a distance of 1 to $2\ \mu$ (Figs. 6, 11 and 13).

The shape of the projections varies, although the majority are bulbous (Figs. 11 and 13). In cross-section (Fig. 7), an outpocketing often appears as an isolated segment of nuclear material separated from its surrounding cytoplasm by the nuclear envelope. Infrequently there is nuclear invagination (Fig. 11), which in cross-section is seen (Fig. 8) as cytoplasmic material enclosed by, but distinctly separated from, the nuclear contents.

FIG. 6. An electron micrograph of the irregularities in the nuclear envelope which has resulted in the formation of an outpocketing (*Ou*). Annuli (*a*) can be seen on the nuclear side (upper arrow), at the level of the nuclear envelope (middle arrow) and on the cytoplasmic side (lower arrow). Some annuli can be seen to contain a central granule (*c*). Mitochondria (*m*) are distributed within the cytoplasm. In the upper right hand corner, a portion of a nucleolus (*n*) from which peripheral strands extend towards the nuclear envelope can be seen. The granular composition of the nucleolus is also evident. $\times 28,500$.



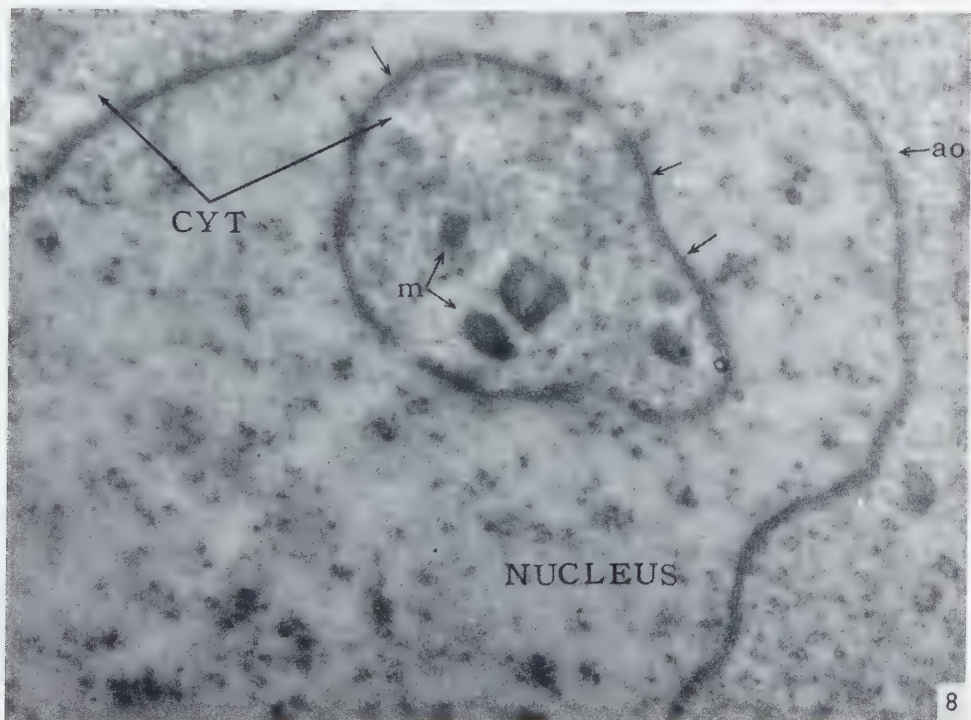
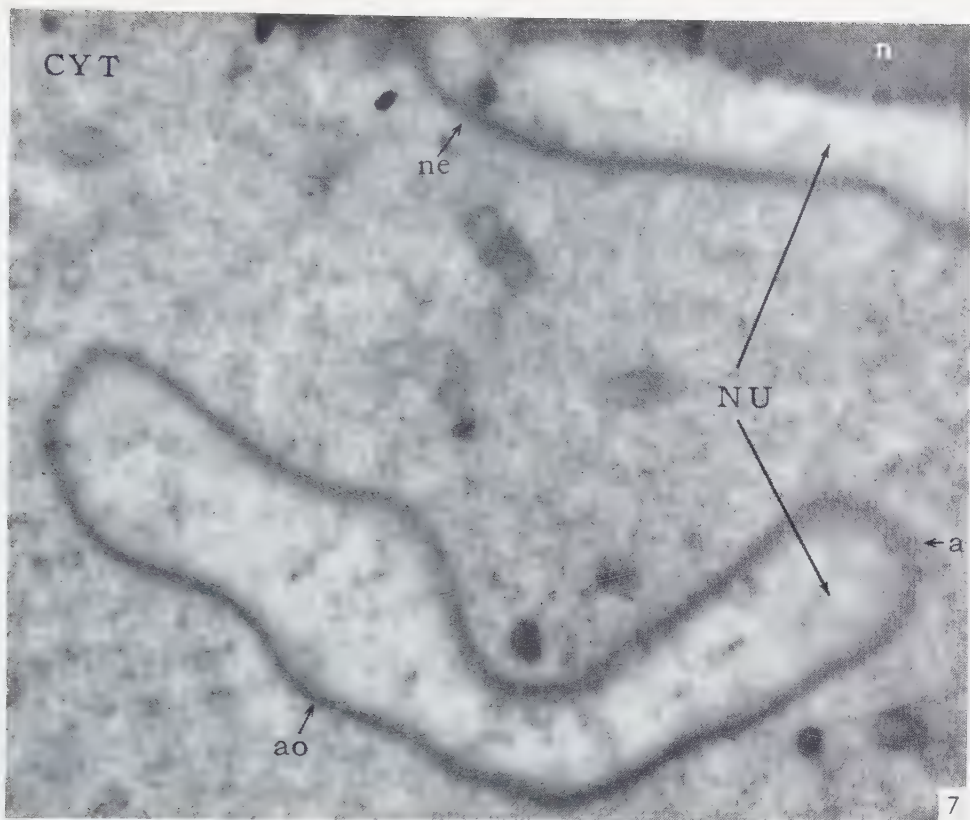
In sections perpendicular to the nucleus, the nuclear envelope is seen to be composed of two dense single membranes separated by a less dense zone (Figs. 8, 10, 13 and 14: (59)). Both membranes follow a relatively similar irregular course (Figs. 10 and 13). The contents of the perinuclear space appear to be homogeneous. The individual membranes appear to be about equally thick, that is, about 75 Å, while the zone between them is 150 Å in width, with total cross-section measurement between 250 and 350 Å.

In sections perpendicular to the nuclear envelope, the membranes which surround the nucleus are not continuous, but are interrupted by discontinuities 800–1000 Å in diameter (see below). If it can be established that the diameter of the discontinuities is relatively constant, this would confirm their circular outline. These interruptions in the nuclear envelope are due to the union of the inner and outer membranes generally in $>or\triangleright$ shaped junctions (Figs. 8, 10 and 13). Some irregular shapes can also be seen at these points (Fig. 13). Within the discontinuities and extending across their sides, that is, perpendicular to the points of union of the membranes, are rod-like structures (Figs. 8, 10 and 13). These, while having a diffuse outline, project above and below the nuclear envelope an average of near 600 Å, with some tending to project deeper into the nucleus than into the cytoplasm. Their total height is about 1500 Å.

The annuli are only seen as such in oblique or tangential sections of the nuclear envelope (Figs. 6 and 12). The majority of annuli at low magnifications (Figs. 4, 5 and 6) appear as rings having a total diameter of 750–1000 Å. This corresponds to the diameter of the discontinuities of the nuclear envelope as reflected in the width of the rod-like structures (see above). Moreover, annuli can be seen on the cytoplasmic side, at the level of the nuclear envelope, and on the nuclear side (Fig. 6, *a*). Both of these facts strongly suggest that the structures we are observing are sections through tubes, with the rod-like structures being the tube wall and the annuli representing cross-sections of the tubes. Some of the annuli tend to be elliptical in outline (Figs. 7, 9 and 12) which may be due to oblique sectioning of the tubes or compression in the process of sectioning. The tube or annular wall is 200–250 Å thick, with an inner diameter of 400–500 Å. A number of annuli contain a central granule

FIG. 7. A cross-section through a bulbous, cytoplasmically directed outpocketing is seen in this micrograph. Nuclear material (*NU*) is separated from the cytoplasm (*CYT*) by the nuclear envelope (*ne*). Both annuli (*a*) and discontinuities (*ao*) can be seen in the nuclear envelope. In the upper right hand corner is a portion of a nucleolus (*n*). $\times 26,500$.

FIG. 8. An electron micrograph of a cross-section of an outpocketing into the nucleus. The cytoplasmic material (*CYT*), which includes what are probably mitochondria (*m*), is enclosed by the two nuclear membranes (arrows). At *ao* is a representation of a section which probably includes parts of the center of the tube (see Fig. 15, *b*). The tube appears as a rectangular unit, but because of their depth, the sides appear denser than the central grooved portion. The sides of the tube wall overlap the discontinuity at the points of junction of the two nuclear membranes. $\times 30,000$.



(Figs. 9 and 12) which is 150-200 Å in diameter. At high magnifications the annuli are resolved into what appear to be 6-8 *subannuli* (usually 8) (Fig. 12 and inserts), each about 175-225 Å in total diameter. These structures appear to have a dark rim about 50 Å in diameter with a lighter center of about 100 Å (Fig. 12, upper right insert). Subannuli can be seen on the cytoplasmic side (Fig. 11), at the level of the nuclear envelope (Fig. 10) and on the nuclear side (Fig. 12). This suggests that they may represent cross-sections of *microcylinders* which are continuous throughout the length of the tube wall.

Nucleoli

The numerous nucleoli at Stage A are about 0.05-0.25 μ in diameter. They occur at the periphery of the nucleus adjacent to the nuclear envelope. At Stage B (Fig. 5) the nucleoli have enlarged to a diameter of 0.6-0.75 μ. Along with an increase in size, nucleolar shredding takes place (Figs. 5, 6 and 14). The main mass of the nucleolus appears to maintain a compact consistency, but along the periphery strands project in all directions.

At higher magnifications, the nucleoli, particularly at their periphery, are composed of granules about 150 Å in mean diameter which are embedded in a less dense matrix (Figs. 6 and 14). Because of this structure, nucleolar fragments can be recognized even when they are seen some distance from the nucleolus.

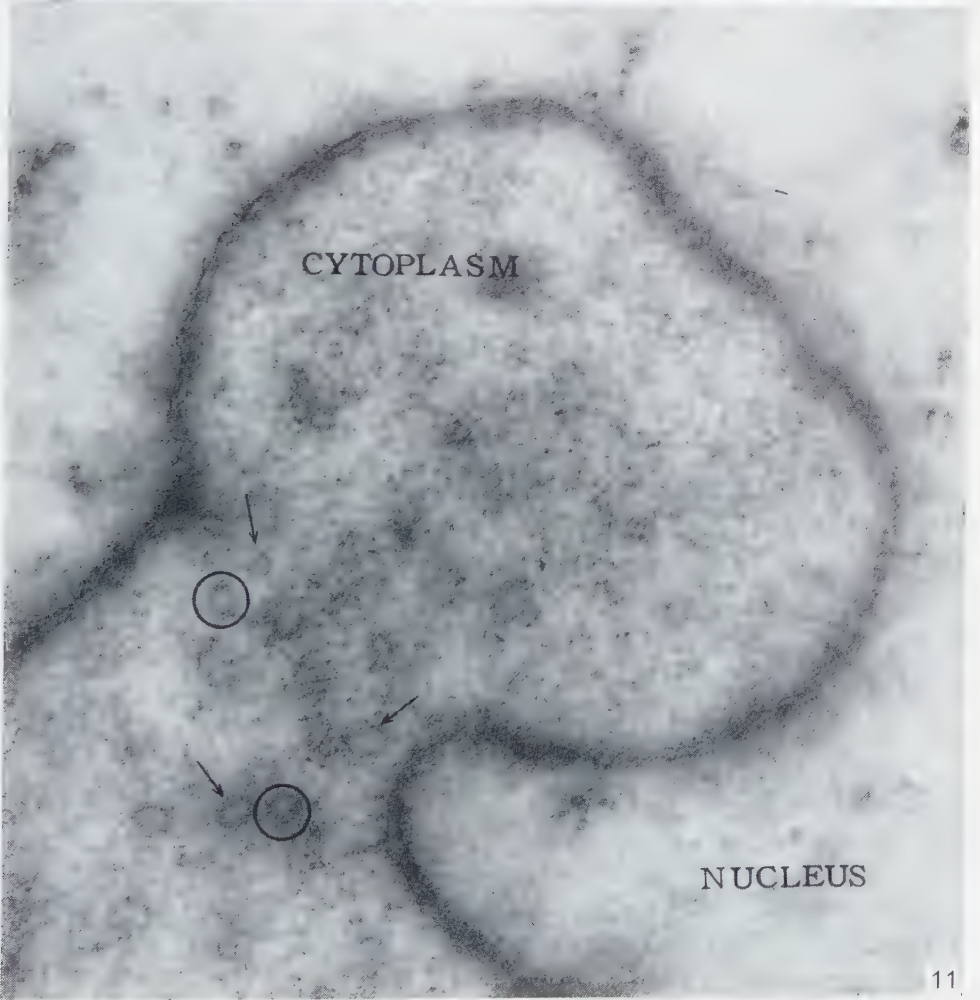
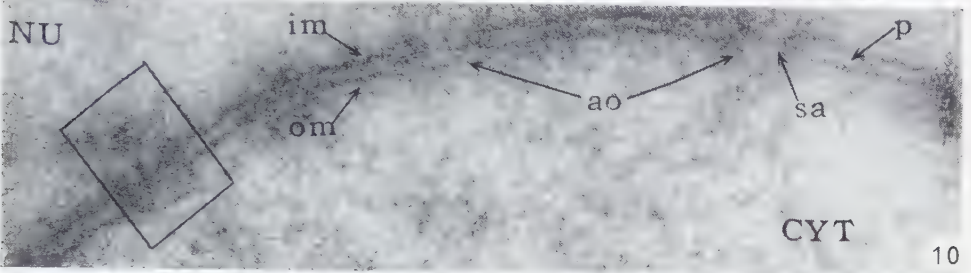
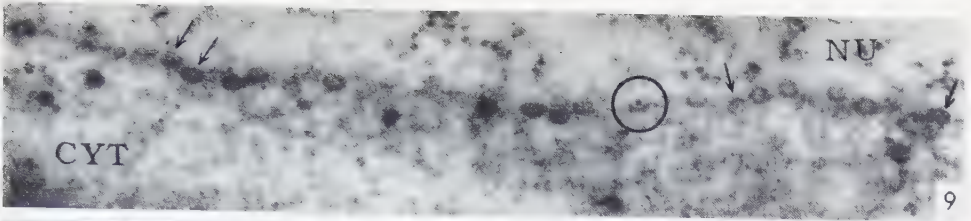
DISCUSSION

Changes in nuclear envelope contour

It has been shown that a close temporal association exists between the onset of yolk formation in the cytoplasm of the oocytes studied and the two nuclear transformations which have been observed. These were the change in contour of the

FIG. 9. A photomicrograph showing with particular clarity the central granules which are found in some of the annuli (arrows). One of the annuli has been cut so that only one half of the annulus and the central granule is visible (circle). *CYT*, cytoplasmic material; *NU*, nuclear material. $\times 32,000$.
 FIG. 10. The nuclear envelope seen at high magnification. Clearly resolved are the inner membrane (*im*), outer membrane (*om*) and perinuclear space (*p*), and the discontinuities of the nuclear envelope (*ao*). The square encloses what is probably an oblique section through a tube wall (see Fig. 15, *c* and discussion). The outline of what may be a subannulus (*sa*) is also seen near one of the discontinuities. $\times 114,000$.

FIG. 11. An electron micrograph of a cytoplasmic projection into the nucleus. In the vicinity of the "neck" of the projection the outlines of annuli are seen (arrows). The more distinct of these (circles) are resolvable into a ring of subannuli which represent cross-sections of the tubes on the cytoplasmic surface of the nuclear envelope. The presence of only a few randomly distributed annuli may be due to variations in the degree to which the tubes extend into the cytoplasm, actual differences in the position of the tubes within the discontinuities, or to minor variations in the level of the nuclear envelope. $\times 47,500$.



nuclear envelope from an even to an undulatory one, and the onset of shredding of the nucleoli.

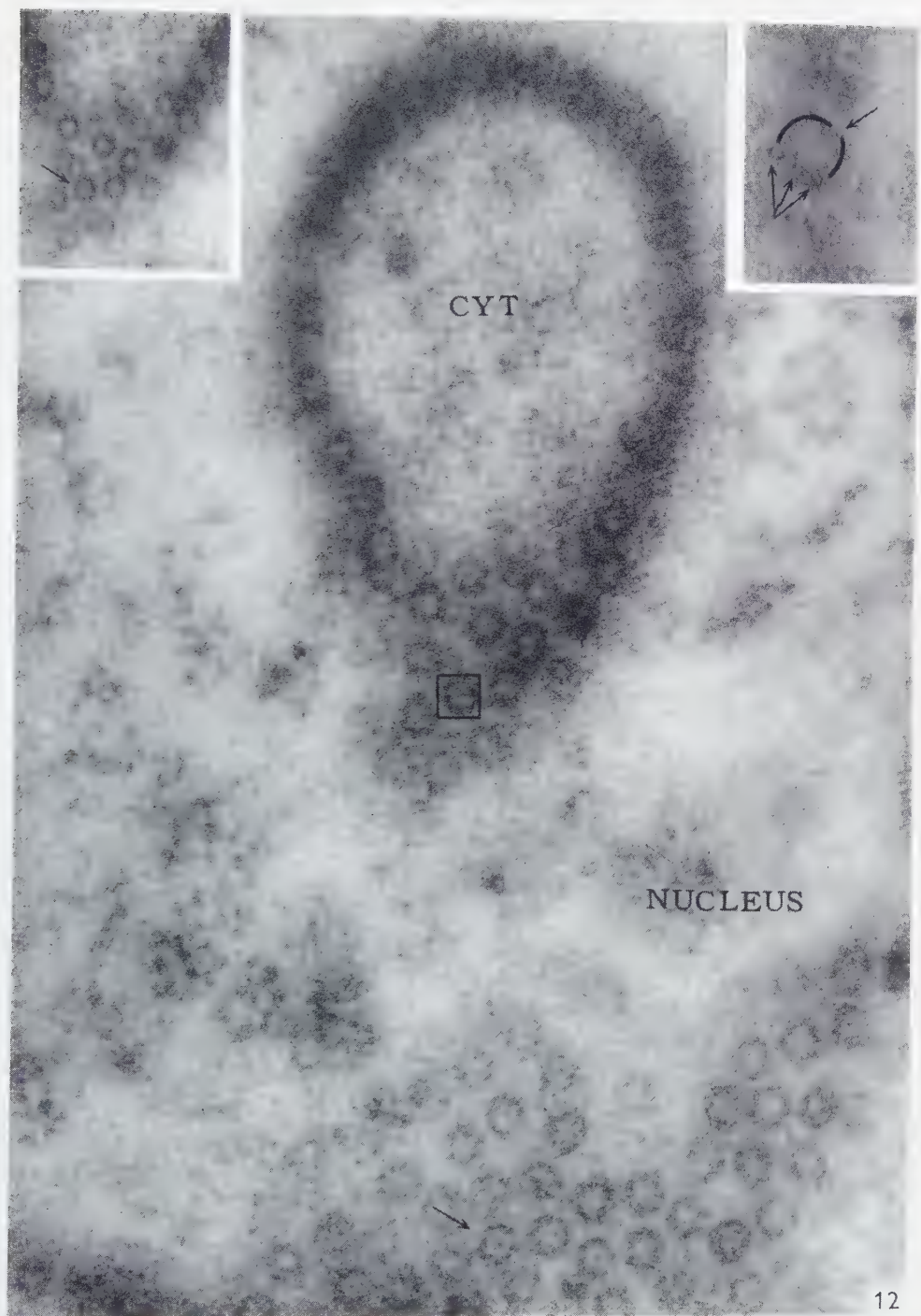
There have been a number of reports of the occurrence of undulation of the nuclear envelope in oocytes (3; 56, Fig. 1) as well as in a variety of somatic cells (35, 39, 43). The reports in which RNA appears to be enclosed within the undulated region are of particular interest (18, 31). Gay (28) has reported that an intimate relationship exists between outpocketings of the nuclear envelope and chromosomal products in embryonic salivary gland cells of *Drosophila*.

Gay (28), Swift (55) and Rebhun (53) have called attention to the similarity in the structure of the lamellae which make up the endoplasmic reticulum and the nuclear envelope, suggesting that the latter may be the source of these cytoplasmic membranes. The observation by Meves (42) that nuclear envelope fragments can be seen in the cytoplasm of *Psammechinus miliaris* appears to have been confirmed recently (2, 3). The fact that the diameter of the nucleus of mature sea urchin eggs (1) is distinctly smaller than that of the oocyte could also be reconciled with the hypothesis that the nuclear envelope may contribute to the formation of similar cytoplasmic structures. Although the endoplasmic reticulum of *Triturus* oocytes is generally similar in appearance to the nuclear envelope (unpublished data), evidences of pinching off of the outpocketings, as suggested by Gay (28), however, has not been obtained. It is possible that because of the large size of the outpocketings, numerous serial sections would have to be observed in order to establish conclusively that pinching off occurs. This is as yet technically quite difficult.

Invaginations of the nuclear envelope similar in structure to the outpocketings described above have occasionally been observed in the oocytes studied (Figs. 7 and 8) as well as in human and rat liver cells (37). Fragments resembling the nuclear envelope have not been seen within the nucleus.

During Stage A, lens-shaped sacculations (blebs) of the nuclear envelope were noted (Fig. 1 and insert). Similar observations were made by Watson (59) and Swift *et al.* (56) for mammalian tissues and *Otala* oocytes respectively. The recent observations of Policard and Bessis (49) may indicate that the sacculations are artificially induced phenomena.

FIG. 12. The annuli are shown in large numbers. A central granule is shown in an annulus (arrow) whose subannular composition, as well as central granule, is evident. The square refers to another annulus whose subannuli can be seen more distinctly in upper left insert. These subannuli apparently represent cross-sections through the microcylinders on the nuclear side of the nuclear envelope. 71,000. *Insert, upper left:* The arrow points to an annulus whose subannuli are very evident. <40,000. *Insert, upper right:* In this photograph four subannuli (arrows) are resolved. The remainder of the annulus is indicated by the ring. $\times 103,000$.



The relationship between discontinuities and annuli

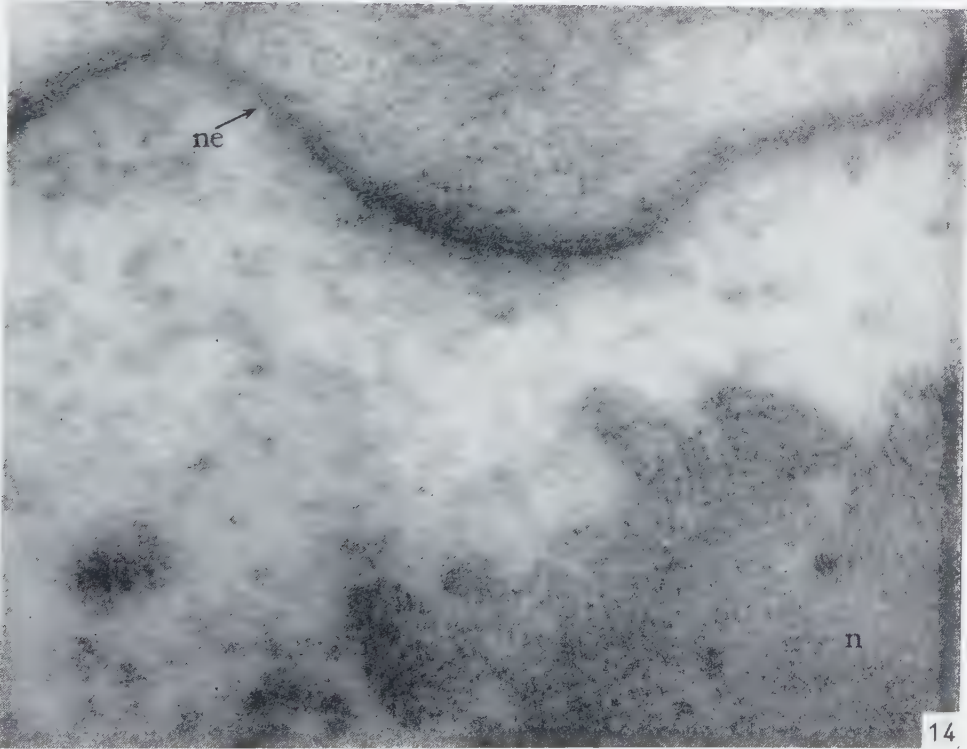
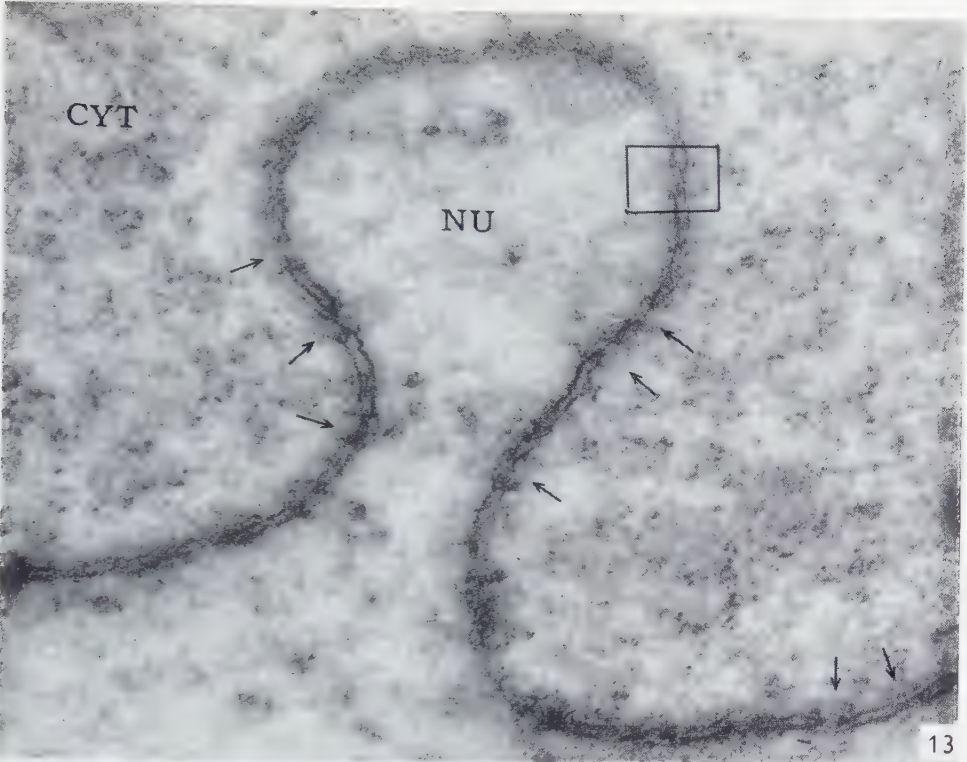
The early electron microscope studies suggested that discontinuities of the nuclear membranes could be seen. Bahr and Beermann (7), who studied the structure of the nuclear envelope in the sectioned salivary gland and midgut of *Chironomus*, observed annuli in tangential sections, while in perpendicular sections, discontinuities at identical points on both membranes were reported. Watson (59), after establishing the intimate relations between the annuli and the discontinuities, concluded, as have a number of others (15, 30, 47), that both structures are views of the same formation seen in different orientations. This is not necessarily a correct interpretation since Watson (57, 59) himself pointed out that the region within and on both sides of the discontinuities is usually denser than the cytoplasmic matrix and perinuclear space. As was suggested earlier and will be supported below, such a description can be interpreted as representing sections through the wall of tubes which are located in the discontinuities. Also from the studies reported by others (7, 11, 15, 16, 25) it can be inferred that the discontinuities may be encircled by rings of electron scattering material. Afzelius (1), using sea urchin oocytes, has suggested that at the discontinuities, tubular walls project both above and below the level of the nuclear envelope. Dawson *et al.* (15) has also presented a picture of the nuclear envelope in spinal ganglion cells in which the annuli are considered to represent cross-sections of cylinders.

The present study of sectioned yolk-free *Triturus* oocytes has confirmed the presence of a bilamellar nuclear envelope as well as of the existence of discontinuities of this envelope at the points of union of both membranes. In the next section, the existence of tubes in the discontinuities will be further supported. Moreover, high resolution electron micrographs and their interpretation may indicate a need for revision and amendment in the details of the structure of the tubes as represented by Afzelius (1) and Dawson *et al.* (15).

On the assumption that the discontinuities contain tubes it is possible to make predictions of the appearance of various parts of such a cylinder which has been sectioned longitudinally. The appearance of each of the parts will be dependent upon the place where the cylinder has been cut.

A vertical cut through the wall of the cylinder as in Fig. 15 would produce a rectangular piece. Comparable shapes apparently representing similar sections through the tube walls are seen in Fig. 13. A vertical cut which includes part of the

FIG. 13. A nuclear projection into the cytoplasm. The two nuclear membranes are seen distinctly, as are their points of union at regular intervals (arrows). Within the discontinuities can be seen the tube walls, which have various shapes reflecting the nature of the section through the tubes (see text). The square encloses an oblique section through the wall of a tube (see Fig. 15, c). $\times 62,500$.
FIG. 14. An electron micrograph showing the granular composition of the peripheral region of a nucleolus (n). $\times 57,000$.



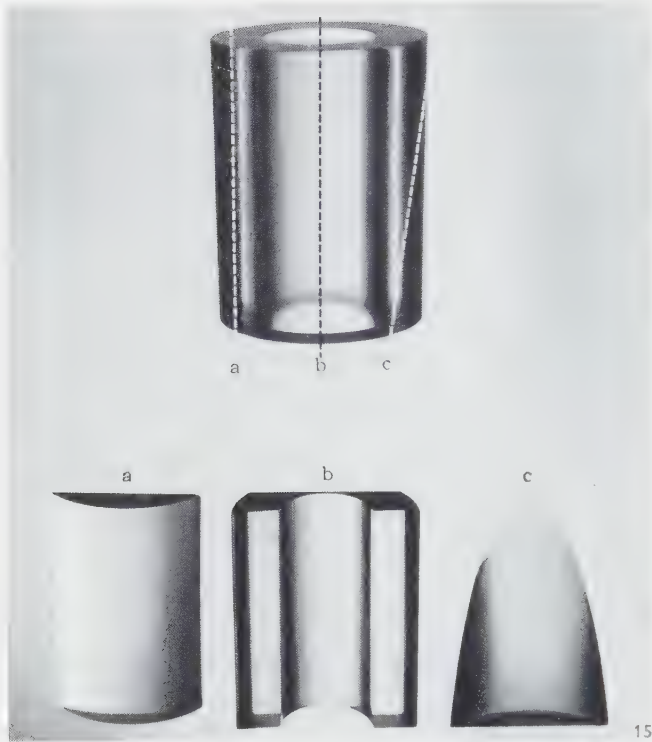
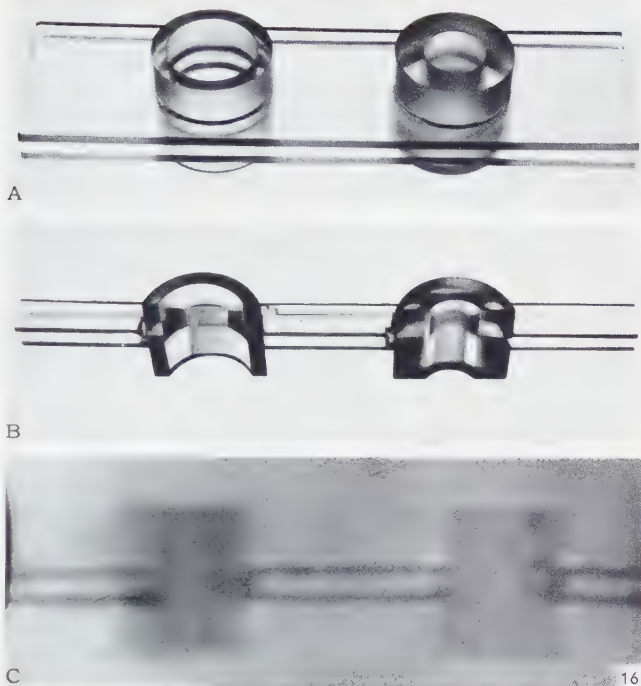


FIG. 15. This photograph illustrates the results of sectioning of a tube at three different points. The first (*a*) is rectangular in shape and results from a cut through the wall parallel to the long axis of the cylinder. The second (*b*) results from a cut parallel to the long axis, through the lumen of the cylinder; it is a rectangular piece whose sides are denser because of their increased thickness as compared with the grooved center. The third (*c*) is an oblique section through the tube wall resulting in a piece which is partly elliptical. As discussed in the text, similar figures are seen in the electron micrographs.

center of the tube (Fig. 15, *b*) also results in rectangular units, but because of their depth the sides will appear denser than the central grooved portion. Fig. 8 (at arrow *ao*) may be interpreted in this manner. Oblique sections through the wall of the cylinder (Fig. 15, *c*) result in ellipsoidal forms. Examples corresponding to such sections can be seen in Figs. 10 and 13. By finding structures in the electron micrographs comparable to those which can be postulated as resulting from sections of the model, it can be justifiably concluded that tubes exist within the discontinuities. This concept was originally suggested by the fact that annuli can be seen on the cytoplasmic side, at the level of the nuclear envelope, and on the nuclear side (Fig. 6, *a*), and that the diameter of the discontinuities (i.e. tube walls) corresponds to that of the annuli. In view of Watson's (59) observation of what apparently were tube walls in a variety of mammalian cell types (see above), it is quite possible if not probable that the nuclear envelopes of somatic cells have a comparable structure rather than simply having pore-like openings at the intervals where the two nuclear membranes are united.

FIG. 16. A lucite model, made to scale, of a portion of the nuclear envelope which contains two "tubes". *A*, complete model. *B*, a section of the model cut at a thickness proportional to that of the sections made with the microtome used in this study. The model was cut so as to allow a portion of the "nuclear envelope" partially to enclose the "tubes". *C*, a print of an X-ray of the portion of the model, embedded in paraffin, described above. The edge of the nuclear membranes *appears* to project into the tube dividing it into two portions. This, however, is an optical illusion, thereby indicating that within the discontinuities are unbroken cylinders.



Structure of tubes

Afzelius (*1*) has reported that the tube projects, from the level of the nuclear envelope, 600 Å into the nucleus and 150–200 Å into the cytoplasm. It has, in this study, been difficult to determine with certainty the height of the tube wall on both sides of the envelope. While some places (Figs. 8, 10 and 13) can be found which are in general agreement with the figures given by Afzelius, in one of the same micrographs (Fig. 13) evidence is available that the cylinders project relatively equal distances from both sides of the nuclear envelope.

Variations in the degree to which the tube extends in both directions from the level of the nuclear envelope may result from actual differences in the height of the tubes, actual differences in their position within the discontinuities, or minor variations in the position of the nuclear envelope (Fig. 11). In any case if the tube wall extends farther in one direction it is most probably in the direction of the nucleus.

According to Afzelius (*1*), the tube wall is interrupted by the bilamellar nuclear envelope, which divides it into two sections that extend from both sides of the discontinuity. This description is based on the fact that the tube walls appear in electron micrographs (Figs. 8, 10 and 13; (*1*) Fig. 3) to overlap the nuclear envelope

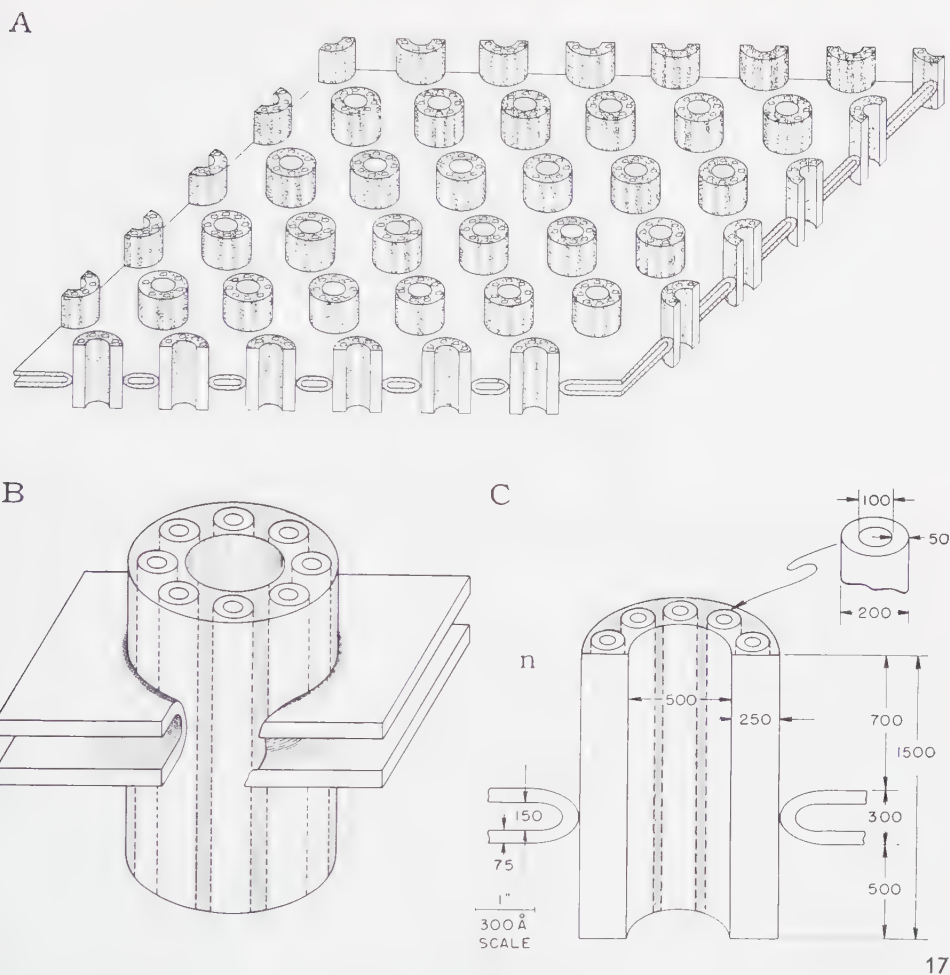
at the places where the two membranes unite. In view of evidence, to be discussed below, which suggests that a tube exists within each of the discontinuities as an unbroken cylinder, an attempt was made to determine if the interpretation of the two-dimensional image of the electron micrograph may result from an optical illusion.

To test this hypothesis, a model of the nuclear envelope, consisting of a double nuclear membrane and tubes, made to scale, was constructed out of lucite (Fig. 16, *A*). This model was then cut into sections equivalent to 300 Å in diameter, such as was the average obtained from the Porter-Blum microtome used in this research project. Each section was made up of about one third of each tube and an equivalent part of the supporting "nuclear membranes". One of the sections was cut in such a manner as to allow a small piece of the nuclear envelope to extend part of the way around each tube (Fig. 16, *B*). This section was then embedded in paraffin in order to simulate the natural environment of the nuclear envelope. To obtain a picture comparable to an electron micrograph, the model enclosed by paraffin was X-rayed. The result was a picture (Fig. 16, *C*) similar to that obtained with the electron microscope; here the nuclear envelope also *appears* to bisect the tube, but from the construction of the model we know that it does not do so. Thus the possibility is established that completely intact tubes may exist within the discontinuities of the nuclear envelope in the *in vivo* condition.

With respect to the fine structure of the tubes, Gall (26), as a result of the study of nuclear envelopes using Anderson's critical-point method, has concluded that each annulus is composed of a ring of small particles about 190 Å in diameter. Such particles, also seen by Rebhun (53), are by virtue of their size and location probably identical with the subannuli observed in this study (Fig. 12). Since these structures can be seen both on the nuclear and cytoplasmic sides as well as at the level of the nuclear envelope, it is reasonable to presume that the subannuli represent sections across different levels of microcylinders which run through the entire length of the tube wall.

In the light of the observations which have been reported, as well as those of the other investigators mentioned, and based on the interpretation of the data discussed above, a model of the nuclear envelope in three-dimensional perspective (Fig. 17, *A*), as well as of an enlarged area of a tube (Fig. 17, *B*), is presented. The dimensions of the various components of a tube are shown in Fig. 17, *C*.

Four points remain to be clarified. One is whether the subannuli have a diameter equal to that of the tube wall. From the electron micrographs examined it would appear that they may be somewhat smaller and thus lie within the wall. Secondly, it is difficult to determine if the subannuli are sections through a hollow tube or solid microcylinder. The third issue requiring further investigation is related to the observation by a number of investigators (1, 30, 59), which could not be confirmed in the



17

FIG. 17. A schematic representation of the nuclear envelope and tube. *A*, the nuclear envelope, based on the observations discussed in the text. The nuclear surface is on top. *B*, a tube and its components as well as a portion of the nuclear envelope is shown in detail. *C*, the dimensions of the various parts of the tube, based upon the average of the measurements for each of the components, are outlined in this drawing. The microcylinder is drawn as seen in electron micrographs (Fig. 12, upper right insert) and should not be interpreted as necessarily representing a microtubule. Also, the distance which the tube extends out on both sides is quite variable and the drawing was made so as to indicate that when a difference exists it tends to favor the nuclear side (*n*).

present study, that a band or diaphragm exists across the tube at the level of the nuclear envelope. The fourth problem concerns the significance of the central granule which was seen in some of the annuli (Figs. 9 and 12) and was also reported to be present in other cells (27, 55).

Nucleoli

Early workers interested in oogenesis have called attention to the fragmentation of the nucleoli during growth of the oocyte (60). This process, particularly in yolk-filled oocytes, usually was intimately associated with vacuole formation within the nucleoli. Kemp (36) in the caption of one of his electron micrographs (Fig. 2) called attention to the shredding of the nucleolus in an oocyte from *Rana pipiens* whose nuclear envelope had "begun to bulge outward". Horstmann and Knoop (35) appear to have observed the same phenomenon in some somatic cells.

The nucleolus of the typical somatic cell has been shown, both by light (17, 21, 33) and electron (8, 9, 51) microscopy to be made up of both a homogeneous mass or pars amorpha and a filamentous nucleolonema. The peripherally located nucleoli of the yolk-free oocytes have but one of these elements. The homogeneous mass, particularly at the periphery, has been shown to be made up of dense granules. This appears to be identical with the composition of the pars amorpha of a typical nucleolus as shown by electron microscopy (2, 5, 46, 51).

Nucleocytoplasmic relations

Watson (59) has suggested that two pathways exist between the nucleus and cytoplasm which would permit exchange; across the discontinuities in the nuclear envelope and by way of the perinuclear space which is continuous with the cavities of the endoplasmic reticulum. In the immature, yolk-free, amphibian oocytes the endoplasmic reticulum is only very sparingly developed and no association exists between it and the nuclear envelope; thus the annular openings are the only remaining avenue of exchange.

There is strong circumstantial evidence that RNA is in some way involved in protein synthesis (10, 12, 34, 50) which appears to be primarily, although not exclusively (4, 41), a cytoplasmic phenomenon (14). This is of particular importance in the case of yolk-synthesizing oocytes where the presence of RNA in the cytoplasm appears to be a prerequisite for vitellogenesis (19, 48).

In amphibian oocytes RNA is primarily localized in the nucleoli (24, 61). It has been shown that there is a high amino acid and RNA turnover in the nucleoli of starfish oocytes (23). Thus it is reasonable to look upon the numerous nucleoli, which undergo shredding, perhaps resulting in the liberation of their granular components, as intermediaries in the transmission of ribonucleoprotein (41) to the cytoplasm. In this regard it should be noted that in most basophilic cells studied, RNA exists predominantly as small granules whose mean diameter is 150 Å (26). Furthermore, direct evidence for nuclear synthesis of cytoplasmic RNA has recently been presented (29).

ACKNOWLEDGEMENTS

The author wishes to express his appreciation to Dr. B. R. Nebel, Dr. H. H. Swift, and Dr. F. Wassermann for their critical reading of this manuscript, and to Dr. L. E. Roth and Mr. O. T. Minick for their help and encouragement throughout the course of the investigation. The author also wishes gratefully to acknowledge the value of the discussions with Dr. H. Kubitschek pertaining to the geometrical interpretations as presented in this paper.

REFERENCES

1. AFZELIUS, B. A., *Exptl. Cell Research* **8**, 147 (1955).
2. ——— *Z. Zellforsch. u. mikroskop. Anat.* **45**, 660 (1957).
3. ——— *Electron Microscopy on Sea Urchin Gametes*, p. 10. Almqvist & Wiksell, Uppsala, 1957.
4. ALLFREY, V. G., MIRSKY, A. E. and OSAWA, S., *Nature* **176**, 1042 (1955).
5. ANDERSON, E. and BEAMS, H. W., *J. Biophys. Biochem. Cytol.* **2**, 439 (1956).
6. ANDERSON, N. G., *Science* **117**, 517 (1953).
7. BAHR, G. F. and BEERMANN, W., *Exptl. Cell Research* **6**, 519 (1954).
8. BERNHARD, W., BAUER, A., GROPP, A., HAGUENAU, F. and OBERLING, CH., *Exptl. Cell Research* **9**, 88 (1955).
9. BORYSKO, E. and BANG, F. B., *Bull. Johns Hopkins Hosp.* **89**, 468 (1951).
10. BRACHET, J., in CHARGAFF, E. and DAVIDSON, J. N. (Eds.), *The Nucleic Acids*, p. 476. Academic Press Inc., New York, 1955.
11. CALLAN, H. G. and TOMLIN, S. G., *Proc. Roy. Soc. London B* **137**, 367 (1950).
12. CASPERSON, T. O., *Cell Growth and Cell Function*. W. W. Norton and Co., New York, 1950.
13. DALQ, A. M., *Proc. Soc. Study Fertility* **7**, 113 (1955).
14. DAVIDSON, J. N., in *Structure of Nucleic Acids and Their Role in Protein Synthesis*, p. 27. Cambridge University Press, Cambridge, 1957.
15. DAWSON, I. M., HOSSACK, J. and WYBURN, G. M., *Proc. Roy. Soc. London B* **144**, 132 (1955).
16. DE, D. N., *Exptl. Cell Research* **12**, 181 (1957).
17. DENUES, A. R. T. and MOTTRAM, F. C., *J. Biophys. Biochem. Cytol.* **1**, 185 (1955).
18. DE ROBERTIS, E., *J. Histochem. Cytochem.* **2**, 341 (1954).
19. DODSON, E. O., *J. Roy. Microscop. Soc.* **72**, 177 (1953).
20. DURYEE, W. R., *Ann. N.Y. Acad. Sci.* **50**, 920 (1950).
21. ESTABLE, C. and SOTELO, J. R., in *Fine Structure of Cells*, p. 170. Interscience Publishers Inc., New York, 1955.
22. FANKHAUSER, G., in BOELL, E. J. (Ed.), *Dynamics of Growth Processes*, p. 68. Princeton University Press, Princeton, 1954.
23. FICQ, A., *Experientia* **9**, 377 (1953).
24. GALL, J. G., *J. Morphol.* **94**, 283 (1954).
25. ——— *Exptl. Cell Research* **7**, 197 (1954).
26. ——— *J. Biophys. Biochem. Cytol.* **2**, 393 (1956).
27. GAY, H., *J. Biophys. Biochem. Cytol.* **2**, No. 4, Suppl., 407 (1956).
28. ——— *Cold Spring Harbor Symposia Quant. Biol.* **21**, 257 (1956).

29. GOLDSTEIN, L. and PLAUT, W., *Proc. Nat. Acad. Sci. U.S.* **41**, 874 (1955).
30. HAGUENAU, F. and BERNHARD, W., *Bull. Cancer* **42**, 537 (1955).
31. HAYDEN, H., *Acta Physiol. Scand.* **6**, Suppl., 17, 1 (1943).
32. HENNEGUY, L. F., *Leçons sur la cellule, morphologie et reproduction*, p. 96. Georges Carre, Paris, 1896.
33. HERTWIG, G., in v. MÖLLENDORFF, W. (Ed.), *Handbuch der mikroskopischen Anatomie des Menschen*, I. Band, Teil 1, p. 175. Springer Verlag, Berlin, 1929.
34. HOAGLAND, M. B., ZAMECNIK, P. E. and STEPHENSON, M. L., *Biochim. et Biophys. Acta* **24**, 215 (1957).
35. HORSTMANN, E. and KNOOP, A., *Z. Zellforsch. u. mikroskop. Anat.* **46**, 100 (1957).
36. KEMP, N. E., *J. Biophys. Biochem. Cytol.* **2**, 281 (1956).
37. KLEINFELD, R. G., GREIDER, M. H. and FRAJOLA, W. J., *J. Biophys. Biochem. Cytol.* **2**, No. 4, Suppl., 435 (1956).
38. LATT, H. and HARTMANN, J. F., *Proc. Soc. Exptl. Biol. Med.* **74**, 436 (1950).
39. MAXIMOW, A. A. and BLOOM, W., *Textbook of Histology*, 4th Ed., p. 36. W. B. Saunders Co., Philadelphia, 1942.
40. MAZIA, D., in GUZMAN-BARRON, E. S. (Ed.), *Modern Trends in Physiology and Biochemistry*, p. 17. Academic Press Inc., New York, 1952.
41. MAZIA, D. and PRESCOTT, D. M., *Biochim. et Biophys. Acta* **17**, 23 (1955).
42. MEVES, F., *Arch. mikroskop. Anat. u. Entwicklungsmech.* **80**, 81, (1912).
43. MURRY, M. R., *Biol. Bull.* **50**, 310 (1925).
44. NEWMAN, S. B., BORYSKO, E. and SWERDLOW, M., *J. Research Nat. Bur. Standards* **43**, 183 (1949).
45. PALADE, G. E., *J. Exptl. Med.* **95**, 285 (1952).
46. PALAY, S. L. and PALADE, G. E., *J. Biophys. Biochem. Cytol.* **1**, 69 (1955).
47. PAPPAS, G. D., *J. Biophys. Biochem. Cytol.* **2**, No. 4, Suppl., 431 (1956).
48. PERKOWSKA, E., *Zoologica Poloniae* **6**, 226 (1955).
49. POLICARD, A. and BESSIS, M., *Exptl. Cell Research* **11**, 490 (1956).
50. POLLISTER, A. W., in BOELL, E. J. (Ed.), *Dynamics of Growth Processes*, p. 33. Princeton University Press, Princeton 1954.
51. PORTER, K. R., *J. Histochem. Cytochem.* **2**, 346 (1954).
52. PORTER, K. R. and BLUM, J., *Anat. Record* **117**, 685 (1953).
53. REBHUN, L. I., *J. Biophys. Biochem. Cytol.* **2**, 93 (1956).
54. SCARTH, G. W., *Protoplasma* **2**, 189 (1927).
55. SWIFT, H., *J. Biophys. Biochem. Cytol.* **2**, No. 4, Suppl., 415 (1956).
56. SWIFT, H., REBHUN, L., RASCH, E. and WOODWARD, J., in RUDNICK, D. (Ed.), *Cellular Mechanisms in Differentiation and Growth*, p. 45. Princeton University Press, Princeton, 1956.
57. WATSON, M. L., *Biochim. et Biophys. Acta* **15**, 475 (1954).
58. ———, *J. Biophys. Biochem. Cytol.* **1**, 183 (1955).
59. *ibid.* **1**, 257 (1955).
60. WILSON, E. B., *The Cell in Development and Heredity*, 3rd. Ed., p. 345. The MacMillan Co., New York, 1925.
61. WISCHNITZER, S., *Am. J. Anat.* **101**, 135 (1957)

A Filamentous Component of Protozoan Fibrillar Systems¹

L. E. ROTH

*Division of Biological and Medical Research,
Argonne National Laboratory,
Lemont, Illinois*

Received November 18, 1957

A filament, measuring $21\text{ m}\mu$ in diameter, ranging from 18 to $28\text{ m}\mu$, and having a dense outer zone and a less dense center, is proposed to occur generally in the protozoa as a fundamental filament in most protozoan fibrillar systems.

Typically, these filaments form either bundles which interconnect ciliary or flagellar bases or systems of parallel filaments arranged just beneath pellicular or vacuolar membranes.

Similar structures have been observed in studies of snail, grasshopper, toad, and cat spermatozoa.

Fibrillar structures in protozoa have received considerable attention in cytological studies for many years. Systems of varying complexity and arrangement have been described for many different organisms and numerous functions have been suggested. Although we now know that some of the structures described are membranes rather than fibrils (7), Taylor's review (29) is still good in regard to most cilium-associated fibril systems.

The findings reported here are part of a comparative electron microscope study of protozoan cilia and flagella. In all cases, the locomotor organelles were found to be structurally connected to other portions of the organism by a filamentous component. This was anticipated from the light microscope studies but the degree of interconnection often exceeded expectation. The purpose of this report is to describe the component filaments of the fibrillar systems in the protozoa thus far observed and the specific locations in which they are typically seen. Numerous other studies of protozoa and several studies of spermatozoa using the electron microscope confirm the generalized occurrence of the fundamental filament described here.

MATERIAL AND METHODS

Euglena gracilis. Organisms of the variety A 19/5 (obtained from Dr. Jack Myers, University of Texas) were cultured under sterile conditions with continuous illumination at

¹ This work was performed under the auspices of the U.S. Atomic Energy Commission.

22°C in the following fluid: 5 g proteose peptone, 2 g sodium acetate, 1 ml commercial liver extract in 1 l distilled water at pH 7.0. The organisms were fixed in 1% osmium tetroxide with MacIlvaine's buffer (pH 7.4, 0.05 M) and 0.7% sodium chloride for three hours at 22°C. A solution of 0.7% sodium chloride with 4% formalin was used as a wash-fixation step (15 minutes) followed by single changes of ethyl alcohol (50%, 75%, 95% and absolute) each for 20 minutes; each change was made by centrifuging lightly. Methacrylate (6 parts *n*-butyl and 4 parts ethyl with 1% luperco CDB) was used to embed the organisms; it was polymerized at about room temperature with radiation from two Westinghouse sun lamps placed 20 inches from the organisms.

Peranema trichophorum. Organisms grew slowly in water to which a few grains of rice had been added; the culture also contained smaller flagellates. Fixation and embedding were identical to that described above with the exceptions that the wash in saline-formalin was omitted and the methacrylate was polymerized in a 60°C oven.

Euplotes patella. The techniques used have been previously described (19); the fixation methods were similar to those used for *Euglena* but without formalin or centrifugation.

Paramecium aurelia. Organisms of strain 51 VIII S (from Prof. T. Sonneborn, Indiana University) were grown in lettuce infusion inoculated with *Aerobacter aerogenes* and concentrated with a sintered glass filter of medium porosity. They were fixed in 1% osmium tetroxide with MacIlvaine's buffer (pH 7.4, 0.05 M) for 90 minutes at 22°C followed by one 15-minute wash in distilled water. Subsequent procedures were identical to those described for *Euglena*.

Sections were cut at about $\frac{1}{40}$ μ thickness on the Porter-Blum microtome, mounted on pure carbon membranes, and viewed in the RCA EMU 3 A electron microscope using the 100-kv beam and a 25- μ objective aperture.

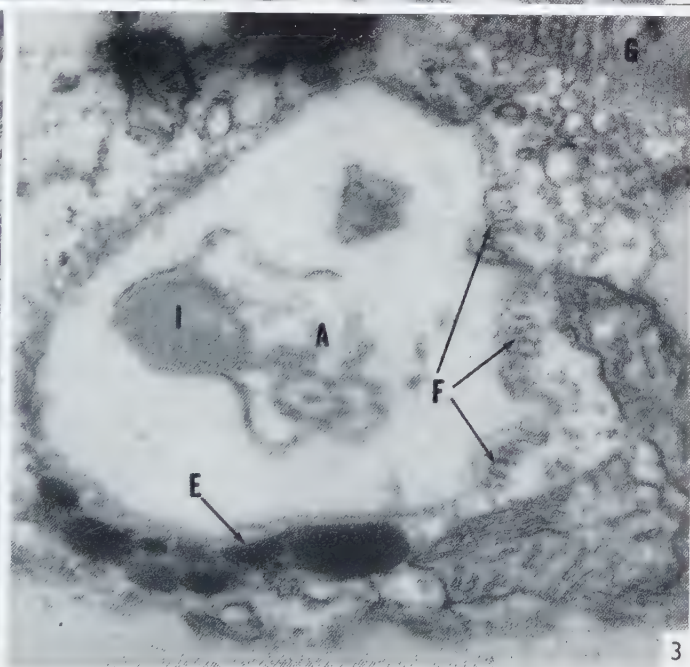
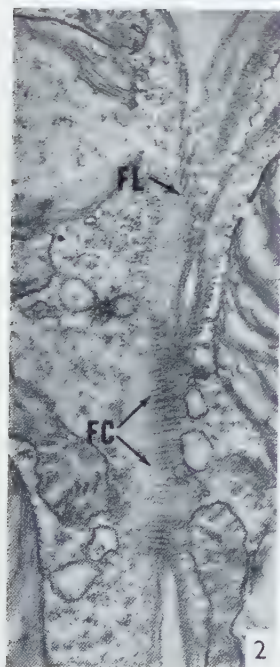
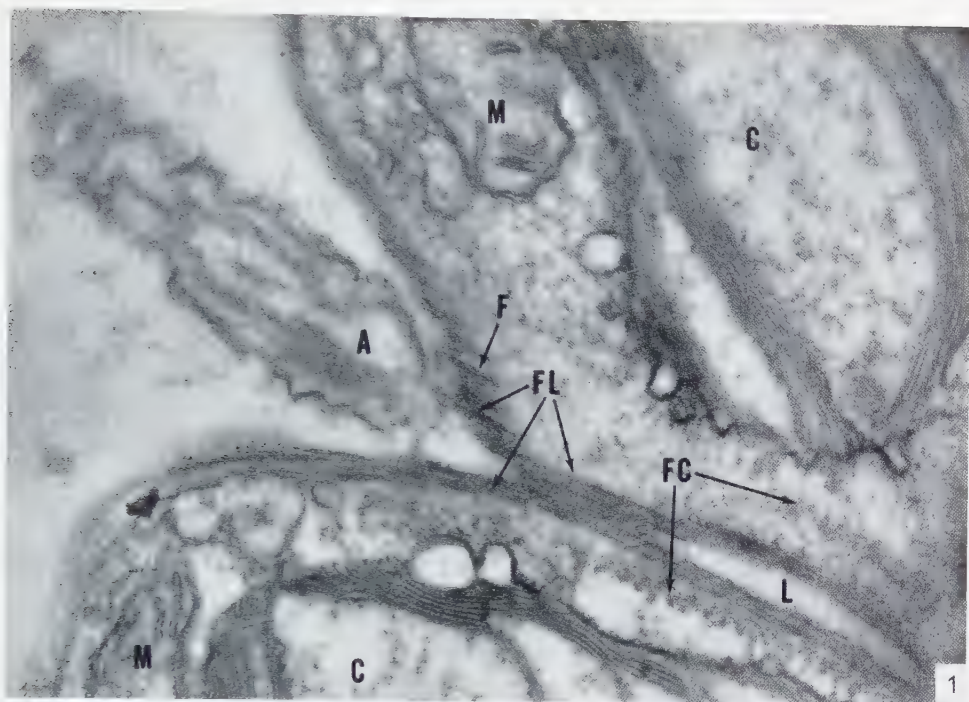
OBSERVATIONS

Euglena gracilis. The proximal portions of the two flagella in this organism are located in a pear-shaped, anterior reservoir which has a narrow neck through which one flagellum passes into the environmental fluid. Around this neck, numerous filaments closely paralleling each other have been observed oriented in both circular (Figs. 1 and 2, FC) and longitudinal directions (Figs. 1 and 2, FL); the longitudinal filaments are located just under the single-layered membrane which forms the reservoir wall, while the circular ones are slightly deeper in the cytoplasm. These filaments measure 21 m μ in diameter (ranging from 18 to 28 m μ in 57 measurements taken

FIG. 1. *Euglena gracilis*. An oblique section through the neck of the flagellar reservoir. Longitudinal (FL) and circular filaments (FC) are shown around the lumen of the neck (L). The filaments are shown to be composed of a dense outer layer surrounding a less dense central portion (F). An oblique section of the flagellum (A), some mitochondria (M), and chloroplasts (C) are also included. $\times 47,000$.

FIG. 2. *Euglena gracilis*. A longitudinal section through the neck of the flagellar reservoir showing circular (FC) and longitudinal filaments (FL). $\times 14,000$.

FIG. 3. *Euglena gracilis*. A section through the more bulbous portion of the pear-shaped reservoir. Filaments (F) are shown under the wall in a close, sheet-like array. Eyespot granules (E), the flagellum (A) with its intraflagellar swelling (I), and a portion of a Golgi-like body (G) are also shown. $\times 33,000$.



from the several organisms studied), have a dense outer zone surrounding a center of lesser density (Figs. 1, 3 and 4, *F*), and lack any periodic cross-striations. This structure is the filament which is found in numerous protozoa in rather specific locations which will be described subsequently.

Filaments also line the reservoir wall in its more bulbous portion where they closely parallel each other (Fig. 3, *F*). Filaments have not been observed under all portions of the reservoir wall in any one section since they may be oriented to the plane of section in such a way that they are not detected; however, they have been seen under several different portions of the wall including the portion by the eyespot granules (Fig. 3, *E*) where they are located between the wall and granules. Therefore, the filaments probably occur uniformly around the reservoir and those under the bulbous portion are continuous with the longitudinal filaments in the neck. No circularly arranged filaments have been observed under the bulbous portion of the reservoir.

At the bases of the flagella, filaments are seen radiating in several directions; in one case, they are seen extending from the base of a flagellum to the zone just under the reservoir wall (Fig. 5, *F*). In a serial section, located a fraction of a micron more anteriorly, this same region of the reservoir wall is shown to have typical filaments below it (Fig. 4, *F*). Thus, the flagella are connected with the filament system.

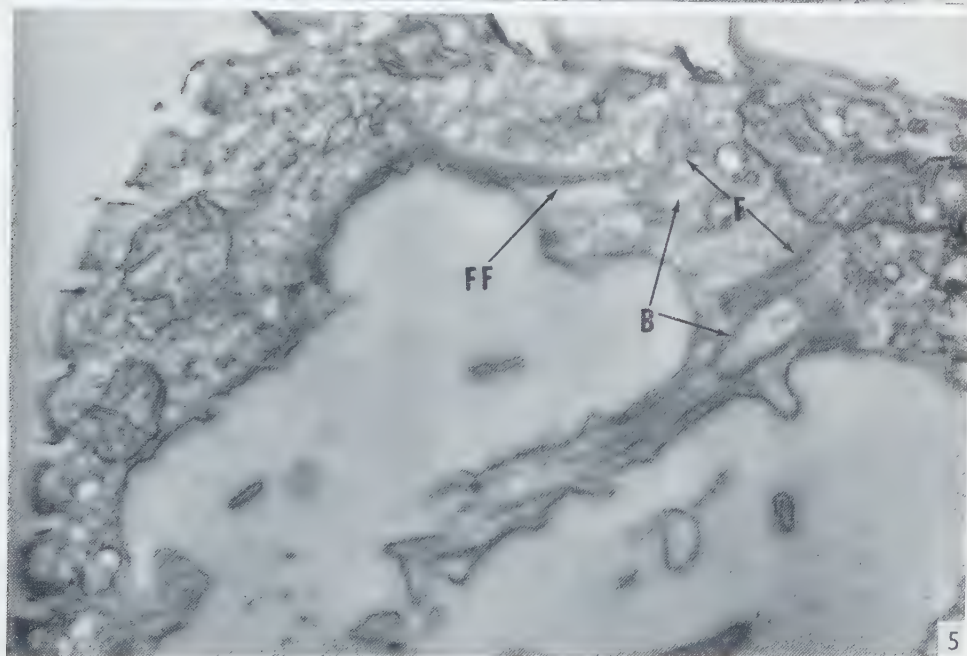
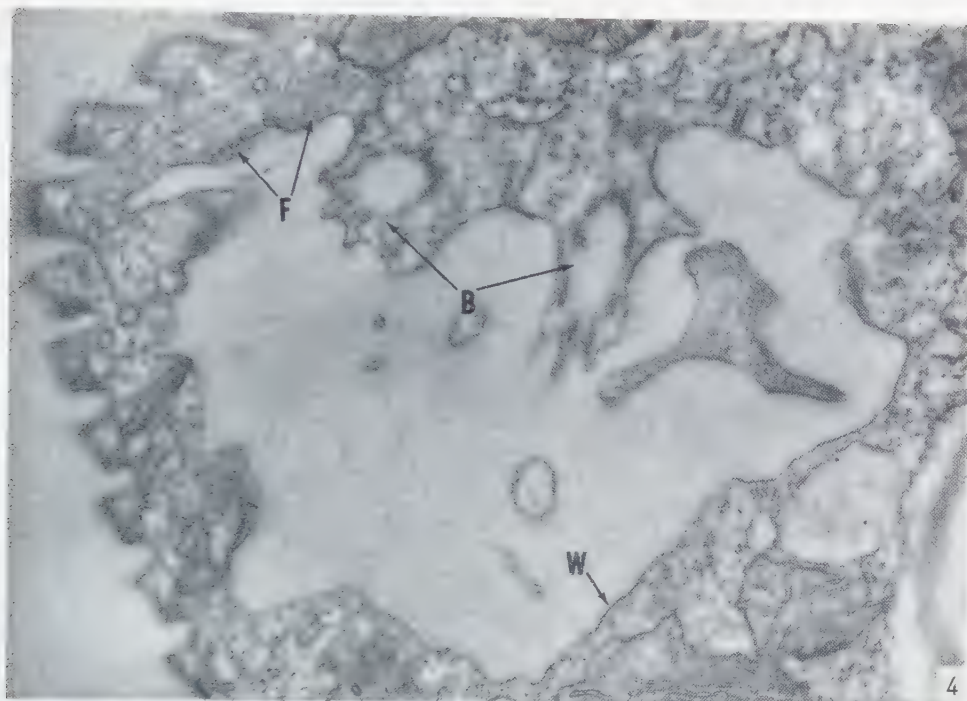
No filaments have been observed beneath the pellicle in this organism; neither has a rhizoplast been observed extending toward the nucleus as described by Kudo (11) in numerous flagellate protozoa.

Peranema trichophorum. In this organism, filaments have been observed in similar locations under the wall of the flagellar reservoir and beneath the membrane ridges of the pellicle (Fig. 6, *F*). They are rather closely spaced and parallel each other as in *Euglena*. The interconnection of flagellar base to the filaments of the wall has not yet been observed here.

A bundle of filaments has been observed extending between the flagellar bases and interconnecting the peripheral flagellar fibrils (central fibrils are lacking not only in the bases but in a proximal $1\text{-}\mu$ portion of the shaft in both *Euglena* and *Peranema*) (Fig. 7, *F*). It is evident from sections serial to this one, as well as from other sections, that this group of filaments is in contact with both flagellar bases.

Euplotes patella. Previous descriptions of the complex rootlet systems in this ciliate have been given elsewhere (18–20) and will not be repeated here. Two

FIGS. 4 and 5. *Euglena gracilis*. Serial sections through the reservoir at the level of the flagellar bases (*B*). Cross-sections of filaments (4, *F*) are seen under the reservoir wall (*W*) which is a single-layered membrane. At the most proximal tip of the base of one flagellum, filaments are shown radiating in several directions (5, *F*). Some of these (*FF*) go directly from the flagellum to the reservoir wall where they are probably continuous with those shown above (4, *F*). $\times 30,000$.



systems are present: first, a sub-pellicular filament system located just beneath the two surface membranes and consisting of longitudinal and transverse filaments and, secondly, a rootlet system which interconnects cilia and groups of cilia (Fig. 8, *F*). These two systems, which are also connected, are composed solely of filaments about $20\text{ m}\mu$ in diameter which have a dense outer zone surrounding a center of lesser density (19). The filaments are present singly or in bundles which form the fibrils observed by light microscopy. In one region there is a convergence of filaments from several directions to form an intertwining mass which is the light microscopist's motorium¹ (18).

Paramecium aurelia. In addition to the kinetodesmal fibrils (Fig. 9, *K*) described in electron microscope studies by Metz, Pitelka, and Westfall (13) and Sedar and Porter (27), filaments in small bundles are closely associated with the ciliary bases also (Fig. 9, *F*). These filaments are about one-third smaller than the average major diameter ($63\text{ m}\mu$) of the tapering kinetodesmal fibrils.

A region of convergence of filaments has also been observed underlying the organelles of the anterior portion of the gullet between the dorsal peniculus and the ribbed wall (according to the description of Ehret and Powers (8)). This region of randomly intertwining filaments corresponds to the motorium described in light microscope studies by Lund (12); it measures about 1 by $2\text{ }\mu$ (circumscribed by unlettered arrows in Fig. 10) and is similar to the mass of filaments described in *Euplotes* (19).

DISCUSSION

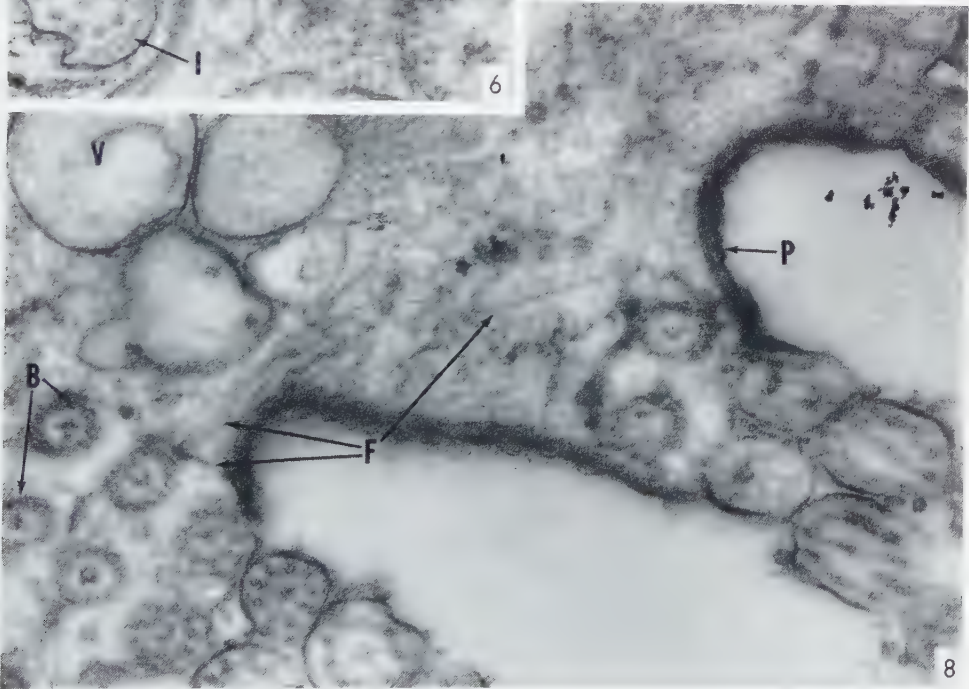
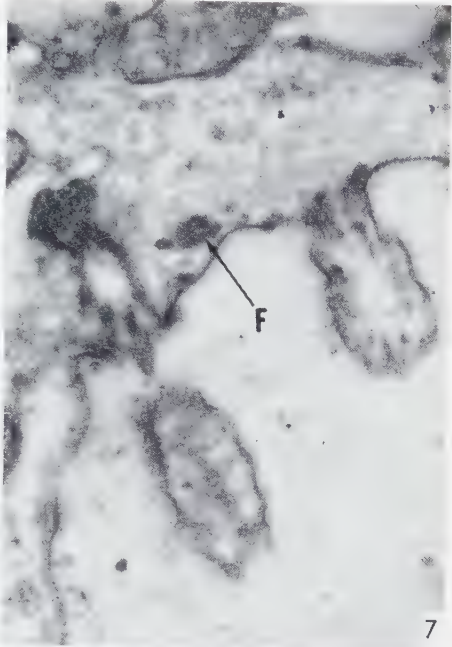
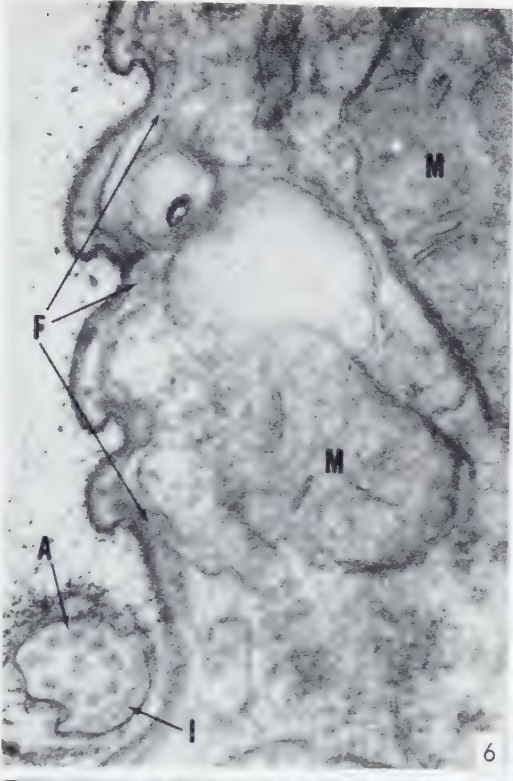
Filamentous structures of the type herein described have been observed in electron microscope studies of other protozoa. Anderson (2) describes filaments of this size in a parallel array which forms the parabasal body in *Trichomonas muris*; this structure extends from the bases of the flagella into the cytoplasm and encircles the

¹ The structure designated "motorium" by early light microscopists unfortunately has a functional connotation which has never been established and which may well be erroneous. However, the terminology is retained rather than introduce a new name and thereby cause confusion.

FIG. 6. *Peranema trichophorum*. A transverse section through the pellicle. Filaments (*F*) are shown under the pellicular membranes and correlated with the ridges of the pellicle. The shaft of the trailing flagellum is included with its flagellar fibrils (*A*) and intraflagellar material (*I*); mitochondria (*M*) are also present. $\times 50,000$.

FIG. 7. *Peranema trichophorum*. An oblique section through the bases of both flagella. A small filament bundle (*F*) extends between and interconnects the two bases. $\times 27,000$.

FIG. 8. *Euplotes patella*. Section through three membranelles. Filaments (*F*) are shown extending toward small granules which are closely related to the peripheral ciliary fibrils. These filaments form a complex rootlet system in this organism; similar filaments form a sub-pellicular system which has been described earlier in this organism (15, 16). Sections of the bases (*B*) of cilia are shown as well as ciliary vacuoles (*V*) and the two membranes composing the pellicle (*P*). $\times 46,000$.



nucleus. Randall (15) describes filaments 20 $m\mu$ in diameter with a similar appearance which interconnect the bases of cilia in *Carchesium*. Rouiller, Faure-Fremiet, and Gauchery (22) demonstrate similar filaments in the tentacles of the suctorian, *Ephelota*, and show that they extend into the cytoplasm in large bundles; this group also studied pharyngeal structures in several holotrichs (23) and observed that the fibers were bundles of parallel filaments 15 to 20 $m\mu$ in diameter. Rudzinska (24) has described a system of filaments around the neck of the contractile vacuole in the suctorian, *Tokophrya infusionum*; the arrangement is similar to the system around the neck of the flagellar reservoir described here in *Euglena*. Pitelka (14) demonstrates similar filaments in pellicular fragments of *Opalina obtrigonoidea*. In the cortex of *Paramecium multimicronucleatum*, Sedar and Porter (27) describe filaments which are probably the same as those illustrated in this report (Fig. 9, *F*).

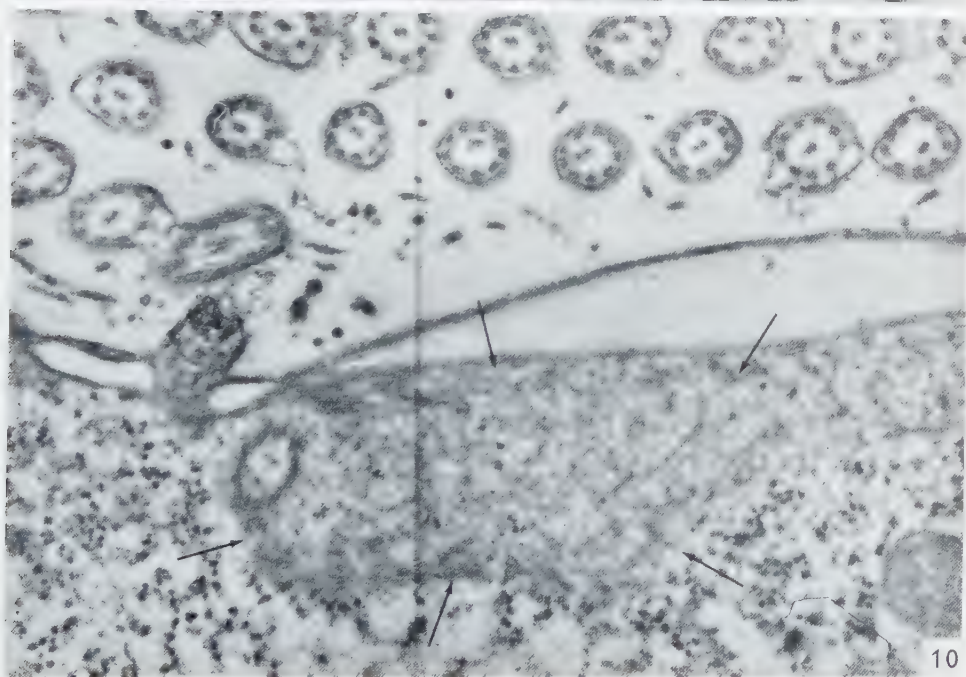
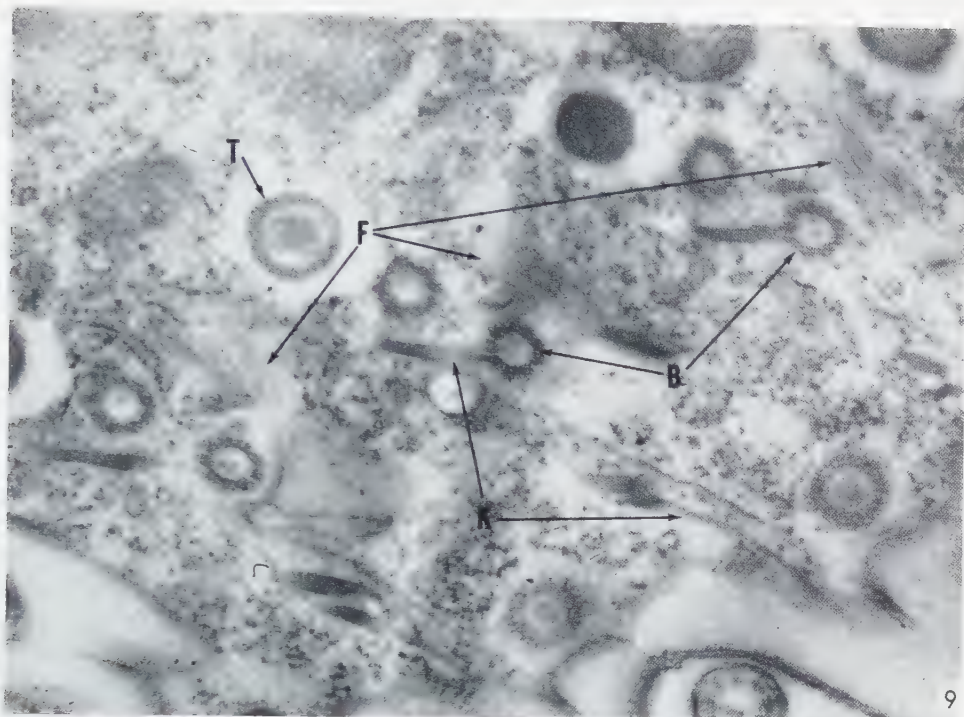
Such filaments have also been observed in several species of *Stentor* and in *Spirostomum ambiguum*. Randall (15) and Fauré-Fremiet, Rouiller, and Gauchery (9) suggest that the filaments are components of the myonemes. However, work in this laboratory (21) indicates that two structures are present in the myoneme location; one is composed of filaments which are similar to those described in this report and which are attached to the ciliary bases, while the second is composed of smaller filamentous structures. Randall (16) in his study of *Spirostomum* also reports that filaments comprise the myonemes but described, in addition, filaments arrayed in parallel sheets beneath the pellicle.

In the protozoa, therefore, the occurrence of the above described filamentous component is quite generalized; it is probable that most fibrils described in light microscope studies of protozoa will prove, as many now have, to be bundles of these basic filaments. The filaments typically occur connected to or closely associated with cilia and flagella or oriented beneath pellicular or vacuolar membranes in sheet-like arrays of parallel filaments. The only exceptions thus far observed to these typical locations are that filaments may occasionally form randomly intertwining masses and may be seen singly around nuclei (19).

In spermatozoa, filament systems of the same type are also present. In the cat, Burgos and Fawcett (4) have shown the manchette to be composed of parallel filaments of the size and morphology described here. Similarly, in the toad *Bufo*, Burgos and Fawcett (5) have observed that there is a single sheet of filaments present. In

FIG. 9. *Paramecium aurelia*. An oblique section through the pellicle. Bundles of filaments (*F*) are shown in close relationship to the ciliary bases (*B*). Kinetodesmal fibrils (*K*) are shown attached to the cilia; trichocyst heads (*T*) are seen in cross-section. $\times 45,000$.

FIG. 10. *Paramecium aurelia*. A section through the oral region. Just beneath the wall of the gullet there is a region of close intertwining of filaments (unlettered arrows). This is the size and location of the motorium described in light microscope studies. $\times 33,000$.



spermatids of the grasshopper *Chorthippus*, Sjöstrand and Afzelius (28) have also demonstrated the presence of a filament system in their figure 4. According to Grassé, Carasso, and Favard (10), there is a system of filaments in the tail of the spermatozoa of the snail *Helix pomatia*; these filaments parallel the flagellar fibrils but are located more peripherally. Rebhun (17) in spermatozoa of the snail *Otala lactea* describes a system in which 20-m μ filaments are present close to the cytoplasmic side of the nuclear membrane; from there they continue over the centriole and form the outermost layer of the tail sheath of the mature sperm. Observations in this laboratory (21) on the sperm of the snail *Helix aspersa* reveal a system similar to that described by Rebhun. In this case, the filaments average 21 m μ in diameter (ranging from 16 to 30 m μ in 16 measurements), have a dense outer layer with a less dense center, and are arranged in sheet-like, parallel arrays. Thus, the same structural filament in a similar arrangement is present in spermatozoa or spermatids of several snails, of a grasshopper, and of the toad and cat.

The structural similarity of these 21 m μ filaments to the fibrils present in the shafts of cilia is quite great. Although the cross-section of the peripheral fibrils is different, the two central fibrils do have circular cross-sections as well as a non-striated appearance like the filaments observed in this study. As for the comparison of diameters, Afzelius (1) reports average diameters of 25, 27, and 28 m μ for the central fibrils of three species of sea urchin spermatozoa. In *Helix aspersa* the central fibrils are oval-shaped with average diameters of 19 and 27 m μ (21).

Filaments which are morphologically similar to those described here have also been observed in nerve cells. Schmitt and Geren (25) first described neurofilaments 10 to 20 m μ in diameter which have either a nodose or tubular appearance in formalin- and osmium-fixed axons. Schultz, Maynard, and Pease (26) observed similar filaments in cortical neurons. (They also list numerous other observations of such structures in nerve cells.) Typically, neurofilaments parallel to the length of the axon have a tubular cross-section, and have diameters near the high end of the 10 to 20 m μ range originally given by Schmitt and Geren.

The validity of comparing filamentous components in different organisms without knowledge of chemical composition, methods of formation, or functional usage is, of course, questionable; however, such comparisons have often resulted in valuable information. Moreover, both the location and grouping of these filaments are additional similarities which argue strongly for a similarity of composition, formation, and function.

A more generalized similarity of structure in protozoan organelles is evident and has been described earlier by Ehret (6). The concepts discussed are pertinent to considerations of morphogenesis in protozoa and are particularly worthy of study in respect to cilia and cilium-associated organelles in protozoan ciliates.

The function of these filament systems is not understood. Rudzinska (24) suggests a contractile function, i.e., closure of the orifice of the contractile vacuole. However, such a function for ciliary rootlets is difficult to reconcile with current concepts of methods of ciliary function (3). Rouiller, Fauré-Fremiet, and Gauchery (23) suggest that, in the holotrichs, the pharyngeal structures which they studied serve to guide ingesta; however, it is difficult to know whether this is a primary or secondary function. A coordinative function also seems appropriate in many cases and the author has summarized the, as yet, incomplete evidence for a coordinative function of ciliary rootlets (20). In addition, it is possible that rootlets may serve as sites for chemical reactions in a way similar to that of the endoplasmic reticulum and ergastoplasm. It should be pointed out, however, that the rather restricted size range and close association with ciliary fibrils suggests that these filaments are not a part of the ergastoplasmic system. A functional explanation cannot be given but the above possibilities now seem to be the only ones worthy of serious consideration.

REFERENCES

1. AFZELIUS, B. A., *Z. Zellforsch. u. mikroskop. Anat.* **42**, 134 (1955).
2. ANDERSON, E., *J. Protozool.* **2**, 114 (1955).
3. BRADFIELD, J. R. G., *Symposia Soc. Exptl. Biol.* **9**, 306 (1955).
4. BURGOS, M. H. and FAWCETT, D. W., *J. Biophys. Biochem. Cytol.* **1**, 287 (1955).
5. ——— *ibid.* **2**, 223 (1956).
6. EHRET, C. F., Symposium on Information Theory in Health Physics and Radiobiology. Pergamon Press, London, in press.
7. EHRET, C. F. and POWERS, E. L., *J. Protozool.* **3**, Suppl., 5 (1956).
8. ——— *ibid.* **4**, 55 (1957).
9. FAURÉ-FREMIET, E., ROUILLER, C. and GAUCHERY, M., *Arch. d'anat. microsc. morphol. exp.* **45**, 139 (1956).
10. GRASSÉ, P.-P., CARASSO, N. and FAVARD, P., *Ann. sci. nat. Zool. et biol. animale* **18**, 339 (1956).
11. KUDO, R. R., Protozoology. Thomas, Springfield, Illinois, 1954.
12. LUND, E. E., *Univ. Calif. Publ. Zool.* **39**, 35 (1933).
13. METZ, C. B., PITELKA, D. R. and WESTFALL, J. A., *Biol. Bull.* **104**, 408 (1953).
14. PITELKA, D. R., *J. Biophys. Biochem. Cytol.* **2**, 423 (1956).
15. RANDALL, J. T., *Nature* **178**, 9 (1956).
16. ——— *Symposia Soc. Exptl. Biol.* **9**, 185 (1957).
17. REBHUN, L. I., *J. Biophys. Biochem. Cytol.* **3**, 509 (1957).
18. ROTH, L. E., *J. Biophys. Biochem. Cytol.* **2**, Suppl., 235 (1956).
19. ——— *ibid.* **3**, 985 (1957).
20. ——— *Exptl. Cell Research*, in press.
21. ROTH, L. E. and MINICK, O. T., unpublished observations.
22. ROUILLER, C., FAURÉ-FREMIET, E. and GAUCHERY, M., *J. Protozool.* **3**, 194 (1956).
23. ——— *Proc. Stockholm Conf. Electron Microscopy*, 1956, p. 216. Almqvist & Wiksell, Stockholm, and Academic Press, New York, 1957.

24. RUDZINSKA, M. A., *J. Protozool.* **4**, Suppl., 9 (1957).
25. SCHMITT, F. O. and GEREN, B. B., *J. Exptl. Med.* **91**, 499 (1950).
26. SCHULTZ, R. L., MAYNARD, E. A. and PEASE, D. C., *Amer. J. Anat.* **100**, 369 (1957).
27. SEDAR, A. W. and PORTER, K. R., *J. Biophys. Biochem. Cytol.* **1**, 583 (1955).
28. SJÖSTRAND, F. S. and AFZELIUS, B. A., *Proc. Stockholm Conf. Electron Microscopy*, 1956, p. 164. Almqvist & Wiksell, Stockholm, and Academic Press Inc., New York, 1957.
29. TAYLOR, C. V., in CALKINS, G. N. and SUMMERS, F.N. (Eds.), *Protozoa in Biological Research*, p. 191. Columbia University Press, New York, 1941.

A Comment on the Fine Structure of the Parathyroid Gland

J. D. LEVER

Department of Anatomy, University of Cambridge

Received November 25, 1957

In a recent paper Ekholm (1) has suggested that micrographs in an earlier work on the rat parathyroid (3) were "more applicable to the thyroid gland than the parathyroid".

At the outset of an extensive experimental study of the rat parathyroid, part of which remains to be published, some difficulty was experienced in locating these bodies since they are inconspicuous and commonly embedded in the posterior aspect of the thyroid gland. In hasty search for the parathyroid in the rat it is all too easy to remove in error a small fat body which is intimately associated with the superior pole of the thyroid. This mistake was made once but not repeated: the identity of the adipose tissue removed was unequivocally established since a study of fat tissues was the subject of another and distinct enquiry which has since been published (2, 4). The author has no doubt as to the correct identity of the rat parathyroid gland as recently described by him (3). This identity has been repeatedly confirmed by light microscopy (Fig. 1) particularly in recent work on the effects of phosphate administration and nephrectomy on the fine structure and histology of the rat parathyroid. Marked cytological and histochemical changes have been noted under these experimental conditions, changes which would not be expected to occur in any other tissue after such treatment, and this investigation is shortly to be published.

No observations have been made by the author on the *mouse* parathyroid and in consequence a direct criticism cannot be made of the recent investigation by Ekholm (1) on the gland of this animal. It is, however, extremely unfortunate that Ekholm has suggested that the recent description of fine structure in the *rat* parathyroid (3) was "more applicable to the thyroid than the parathyroid". Furthermore it is noteworthy that all the electron micrographs published by Ekholm as depicting mouse "parathyroid" provide an unmistakable demonstration of adipose tissue (2, 4), particularly as regards the large size of the mitochondria with their regular parallel internal cristae. Lipid droplets look much the same in any tissue: in the parathyroid cell they are few in number and in general small in size as compared with the fat cell in which they abound and are of various sizes. The endoplasmic reticulum of brown adipose tissue is unexpanded and vesicular and bears but slight resemblance to that

in the rat parathyroid cell in which on occasions large sacs and long double membranous outlines may be seen (Fig. 2). All the electron micrographs shown by Ekholm (1) are high magnification views of portions of cells and there is no evidence in them of the essentially epithelial nature of parathyroid tissue (Fig. 2).

Figs. 3, 4 and 5 in the present paper are micrographs of rat brown adipose cells which bear a strong resemblance to the photographs recently presented by Ekholm and purported by him to demonstrate mouse "parathyroid" cells. A full account of the fine structure of brown adipose tissue appears elsewhere (4). Figs. 1 and 2 are micrographs of the rat parathyroid.

REFERENCES

1. EKHOLM, R., *J. Ultrastructure Research* **1**, 26 (1957).
2. LEVER, J. D., *Proc. Stockholm Conf. Electron Microscopy*, 1956, p. 182. Almqvist & Wiksell, Stockholm, and Academic Press Inc., New York, 1957.
3. ——— *J. Anat.* **91**, 73 (1957).
4. ——— *Anat. Record* **128**, 361 (1957).

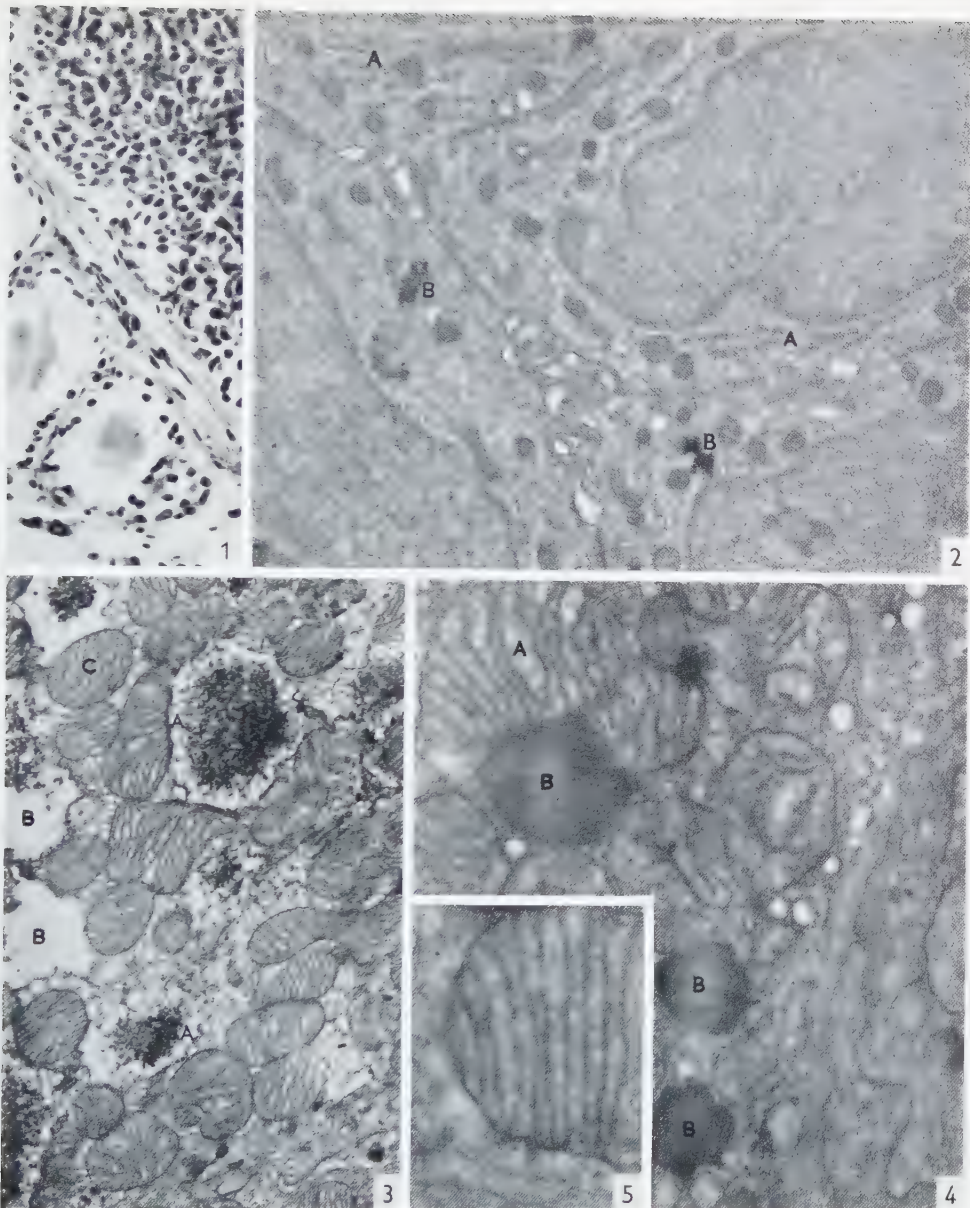


FIG. 1. Light micrograph of adjacent portions of rat thyroid and parathyroid glands. Note colloid vesicles in thyroid and the obvious epithelial nature of the parathyroid. Section taken from methacrylate embedded tissue prior to thin sectioning for electron microscopy; stained with haematoxylin and eosin after removal of plastic. $\times 290$.

FIG. 2. A low magnification electron micrograph of rat parathyroid. Note the essentially epithelial nature of the tissue with convoluted intercellular spaces. The endoplasmic reticulum commonly appears in long double-membranous outlines (A). There is variation in the cellular lipid content of the parathyroid but in general lipid droplets (B) are sparse. $\times 15,000$.

FIG. 3. Electron micrograph of rat adipose tissue. Large numbers of lipid droplets (A) of various sizes abound in this tissue: in preparation much of this lipid is extracted leaving partly filled vacuities (B). Mitochondria (C) are large and contain prominent internal cristae. $\times 17,000$.

FIGS. 4 and 5. Micrographs of rat adipose tissue. Note the prominent mitochondrial cristae (A) and numbers of lipid droplets (B). $\times 33,000$ and $42,000$ respectively.

Remark on J. D. Lever's Note "A Comment on the Fine Structure of the Parathyroid Gland"

R. EKHOLM

Department of Anatomy, University of Gothenburg

Received December 7, 1957

Since a fairly long time I have been engaged in an electron microscopic investigation on the mouse thyroid gland, part of which has already been published (2). The preparation technique used in this study is the following.

The upper part of the trachea, the larynx and the thyroid are excised in one piece and put into the fixating fluid. During the dehydration in alcohol, the thyroid is isolated under the microscope from the other parts of the specimen and divided into its two lobes. The lobes are separately embedded in methacrylate and then sectioned.

In about 20 per cent of the sections from these specimens I have met with a non-thyroid tissue. This tissue has always been found in intimate relation to the thyroid cells, separated from these by a narrow space containing no defined structures, small bundles of fibrils or a capillary. No other type of non-thyroid tissue has ever been observed in the sections.

It is known from the light microscopy that the parathyroid is intimately connected with the thyroid in the mouse. Therefore, I have felt justified to draw the conclusion that the observed tissue constitutes the parathyroid gland and so I have given a short description of my incidental observations (1).

After having acquainted myself with Lever's study on the brown adipose tissue in the rat (3) I am clear about the strong resemblance between this tissue and that which I have described as the parathyroid gland in the mouse. Consequently, I admit that my description of the mouse parathyroid is not applicable to this gland but to a body of brown adipose tissue situated in close relation to the thyroid gland.

REFERENCES

1. EKHOLM, R., *J. Ultrastructure Research* **1**, 26 (1957).
2. EKHOLM, R. and SjöSTRAND, F. S., *J. Ultrastructure Research* **1**, 178 (1957).
3. LEVER, J. D., *Anat. Rec.* **128**, 361 (1957).

Fixation by Freezing-Drying for Electron Microscopy of Tissue Cells

F. S. SJÖSTRAND and R. F. BAKER¹

*Laboratory for Biological Ultrastructure Research,
Department of Anatomy, Karolinska Institutet, Stockholm*

Received December 21, 1957

Immersion of frozen-dried tissue into methacrylate under high vacuum at a temperature below the boiling point of methacrylate at that pressure makes it possible to obtain a perfect penetration of the methacrylate. The polymerization according to Müller (3) by u.v. light in the cold gives satisfactory results. These techniques for immersion and polymerization prevent an extensive vacuolization of the tissue due to improper embedding. The vacuolization due to ice crystal formation does not interfere in a critical way with the structural organization of the pancreas cells studied so far and represents an easily recognizable artifact.

Preliminary observations on frozen-dried pancreas tissue confirm the geometrical structural pattern observed in mitochondria in osmium-fixed material. The basic membrane of the α -cytomembranes also has its counterpart in the frozen-dried material. However, the contrast conditions are such that the picture appears as the negative of that of osmium-fixed material.

The opaque 150 Å particles ("RNA particles"), or any component that would correspond to them, have not been observed.

The tissue cells which are analyzed by means of the electron microscope have to be subject to a rather drastic treatment involving fixation, dehydration, embedding, and sectioning. The complex structural patterns which appear rather uniformly after fixation in various solutions of osmium tetroxide, buffered or unbuffered, are in general considered reliable as representing the structural organization of the living cells. This seems fully justifiable in such cases where the observations are in full agreement with what could be predicted from polarization optical analysis performed on living cells as in several lipo-protein structures (for instance the myelin sheath). However, we have no means of checking the effect of the osmium fixation on the structurally less firmly organized ground substance of the cytoplasm, and the obser-

¹ Department of Medical Microbiology, School of Medicine, University of Southern California, Los Angeles, California.

vations made originally in this laboratory regarding this component of the cell were presented with reserve (11).

To check a result obtained when applying a chemical fixation by using another chemical fixative seems unsafe, as both may exert a similar effect on the components which are studied. The most satisfactory way of checking appears to involve the use of a method of fixation, which acts according to a definitely different principle as compared with the chemical fixative. The method of choice will then be preservation through freezing-drying.

Freezing-drying was applied in electron microscopy of tissue cells in the early days of electron microscopy (4-6) but the results were poor due to the primitive method used for thin sectioning and the equally primitive electron microscope used for the analysis. With improvements in both respects, the system of cytoplasmic membranes, the α -cytomembranes, in the exocrine pancreas cells could be observed in frozen-dried, unstained specimens (9, 10).

Recently Müller (3) has contributed in an important way by designing a method for freezing-drying of plant material for electron microscopy, which allowed a check of the general plan of organization of chloroplasts.

The repeated trials to apply freezing-drying in our laboratory since 1952 have given unsatisfactory results as compared to the osmium fixation. The tissue appeared mostly heavily vacuolated, a condition that for a long time was ascribed to the formation of ice crystals in connection with the freezing of the tissue. However, the freezing could not be the only cause for the vacuolization because the results were not even comparable to those obtained for light microscopy (7, 8) and it became obvious that the artifacts were to a great extent due to improper embedding.

The penetration of the hydrophobic methacrylate into the tissue is incomplete when immersing the frozen-dried tissue into the embedding medium. This difficulty could not be overcome by embedding in vacuum or by passing the tissue through some hydrophilic liquid before the immersion into the methacrylate.

The principle that was arrived at as useful involves immersion of the frozen-dried tissue into methacrylate in high vacuum at a temperature below the boiling point of methacrylate at that pressure. This prevents air from being trapped in the tissue and also obviates the formation of gas vacuoles through the boiling of the methacrylates.

METHOD

Very minute pieces of tissue measuring only a few tenths of a millimeter in thickness are quickly removed from the experimental animal and immersed into isopentane chilled to -150 to -160°C by means of liquid air. The tissue should be frozen within 60 seconds after the killing of the experimental animal (7). The frozen tissue is

dehydrated in vacuum by means of molecular distillation during 48 hours at a temperature below -40°C . The apparatus for freezing-drying is built mainly according to conventional principles (2) with an outer glass tube forming the vacuum chamber and an inner tube filled with liquid air acting as a cold finger. An oil diffusion pump and a backing mechanical pump are used to ensure a high vacuum for the molecular distillation and for the drying of the cold finger after the tissue has been dehydrated.

After drying, the tissue is removed from the vacuum chamber and kept over phosphorous pentoxide. The bottom of the vacuum chamber is covered with the methacrylate mixture and immersed into liquid air in order to solidify the methacrylate. The pieces of tissue are now placed on the surface of the solid methacrylate. These manipulations are performed in nitrogen atmosphere in order to prevent condensation of water vapour inside the vacuum chamber.

With the methacrylate still in a solid state, the apparatus is evacuated anew. The lower end of the vacuum chamber containing the solid methacrylate is kept immersed in liquid air until the high vacuum has been restored and kept for 24 hours. The liquid air is then removed and the methacrylate allowed to melt. The methacrylate immediately penetrates the tissue, and a perfect immersion of the tissue is secured. Dry air is let into the vacuum chamber before the temperature of the methacrylate has raised above its boiling point.

Following the recommendation of Müller (3), the polymerization of the methacrylate was achieved by means of u.v. light at a low temperature. The polymerization was in our case performed in a cold room at -10°C . The specimens were cooled by circulating the air by means of a fan.

The tissue was cut on a Sjöstrand ultramicrotome and the sections examined directly or after staining according to Gibbons and Bradfield (1). For staining the specimen grids were placed on the surface of a 1% solution of osmium tetroxide or of phosphotungstic acid without any previous dissolving of the methacrylate.

RESULTS

The observations made so far are of a preliminary character. As test specimen the exocrine cells of the mouse pancreas were used.

The mitochondria are easily recognized due to their characteristic structural organization (Figs. 1 and 2). The pattern represents a negative picture of that observed after osmium fixation. A less opaque zone forms a surface layer showing the outlines of the mitochondria. In the interior, a great number of less opaque layers are oriented perpendicularly to the long axis of the mitochondria. Most of these layers extend across the whole diameter of the mitochondria. The less opaque layers frequently

show indications of a triple-layered pattern with a slightly more opaque middle layer separating the lightest layers (Fig. 2, insert).

The α -cytomembranes appear as less opaque layers in the cytoplasm. These layers are arranged in pairs with a narrow space in between the layers of a pair. This space is filled with a homogeneous material. The cytoplasm between the membrane pairs appears mainly homogeneous. No opaque 150 Å particles or any components that might correspond to them have been observed.

The nucleus has a homogeneous appearance and is vacuolated.

Vacuoles lacking any content except the embedding medium are present at a varying concentration, and are interpreted as artifacts due to local ice crystal formation.

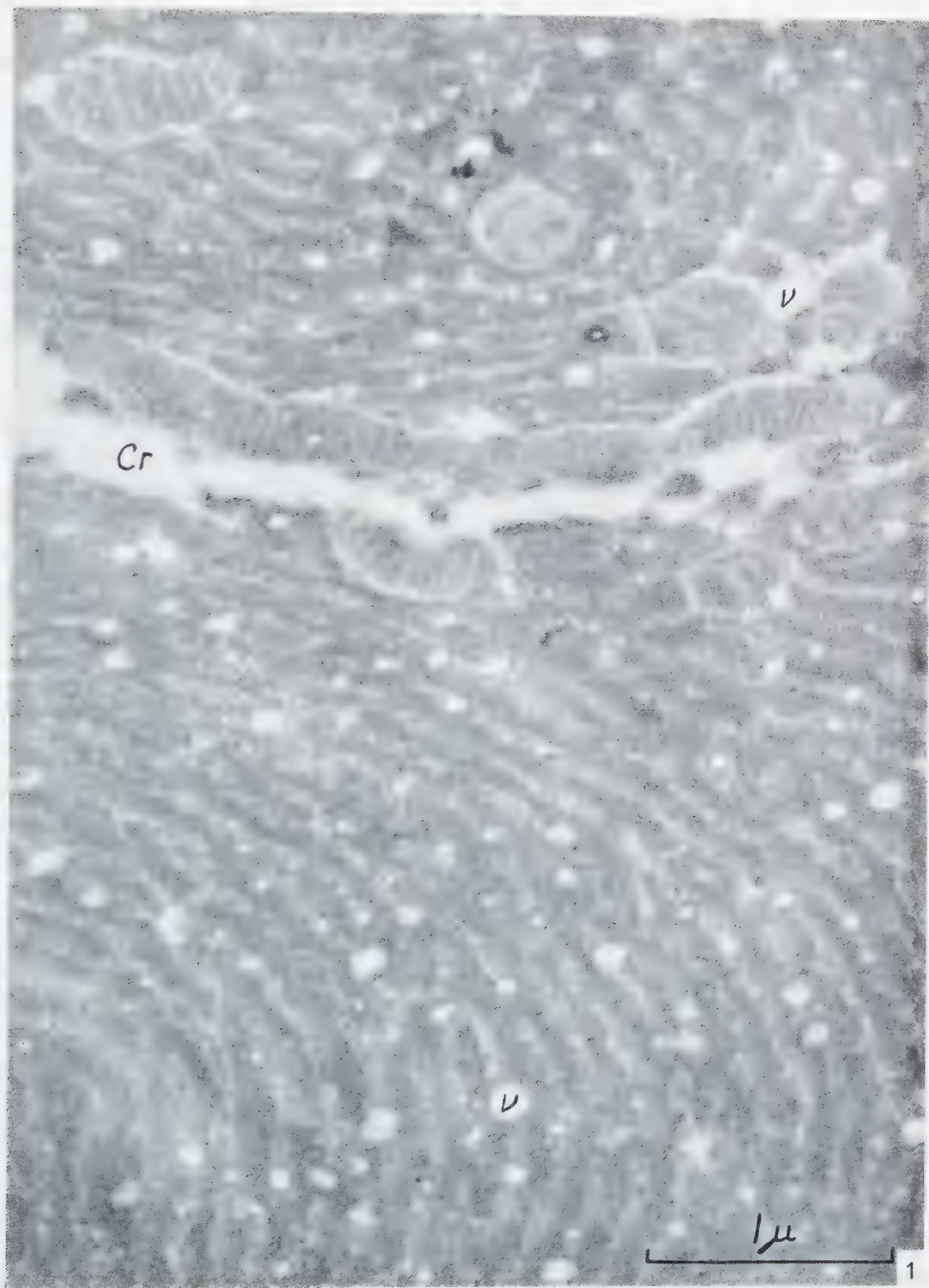
DISCUSSION

The results obtained so far have demonstrated that freezing-drying can be applied in electron microscopy of whole tissue without too severe interference from artifacts due to ice crystal formation. That the methacrylate embedding constitutes one main source of artifacts because of improper penetration has been clearly demonstrated. With the technique described here, this artifact is prevented as is obvious from the homogeneous appearance of the cytoplasm of the cells. The technique used by Müller (3) is comparable to the immersion under vacuum at a temperature above the boiling point of the methacrylate that has been tried with unsatisfactory results in previous experiments in our laboratory. When working with minute pieces of tissue, only a very narrow region at the surface of the tissue will be fairly well embedded, and these regions are difficult to localize. They represent only fractions of a cell diameter. The penetration might be better for plant material especially when such small objects are used as isolated chloroplasts. However, the technique worked out by Müller will be tried to insure that this conclusion is not premature.

With this method the tissue is subject to treatment with only one chemical, the methacrylate monomer, which, however, is a solvent for lipids. As Müller points out, an efficient cooling of the methacrylate in connection with the embedding decreases the solubility of the lipids presumably sufficiently to prevent extraction.

The observations made so far confirm the existence of certain geometrical patterns

FIG. 1. Survey picture of frozen-dried exocrine pancreas tissue showing the α -cytomembranes and mitochondria. A long mitochondrion extends across the picture and is located at the boundary between two exocrine cells. Parallel to this boundary runs a crack (Cr) representing an artifact presumably produced during the freezing of the tissue. Several small vacuoles (V) are observed and are interpreted as due to the formation of ice crystals during the freezing. The ultrathin section has been stained with phosphotungstic acid (1% aqueous solution) for 20 minutes without dissolving the plastic. $\times 34,000$.



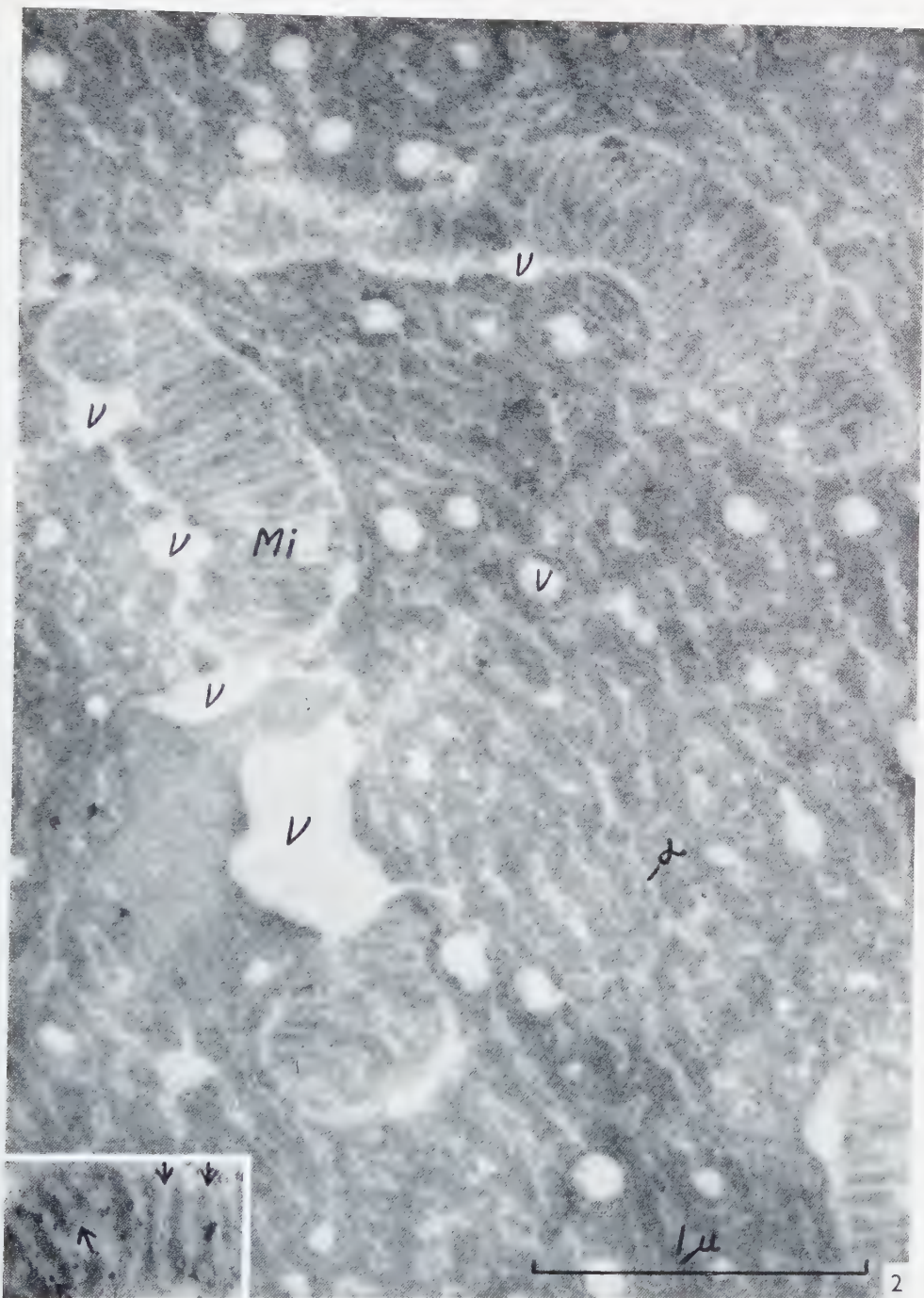
of the mitochondria and the cytoplasmic membranes. The layers of low opacity observed in the mitochondria certainly correspond to the outer and inner mitochondria membranes as observed after osmium fixation. The low opacity of the layers that are intensely stained after osmium fixation is characteristic before as well as after staining of the sections in solutions of osmium tetroxide or phosphotungstic acid. No definite explanation to this difference in contrast and osmiophilia can be given at present. The freezing-drying and embedding might radically change the reactivity of what has been assumed to represent lipo-protein components of the mitochondria. This effect might be due to an extraction of the lipids or a denaturation of the protein components. The less opaque layers might represent layers that are highly hydrated in the intact cell. Further studies with different electron stains and a more careful preventing of an extraction of lipids than was achieved in these experiments might help to solve the problem regarding the interpretation of the molecular organization of the "double membranes".

No indications of the existence of the 150 Å particles, which are so characteristic in osmium-fixed material, have been found. The regions in the cytoplasm, to which these particles are located, were uniformly stained under the conditions of staining applied so far. This seems surprising, especially when considering the statement that their opacity is not entirely due to osmium staining because they have been observed in formalin-fixed material. After osmium fixation, these regions appear rather empty except for the 150 Å particles. On frozen-dried material, on the other hand, these regions appear uniformly filled with a relatively opaque material, the opacity of which increases uniformly when increasing the time for staining.

This observation makes it uncertain whether the 150 Å particles are preformed and existing as such in the living cell. They might well be formed as artifacts through precipitation of the ground substance of the cytoplasm during the fixation. This possibility has to be tested by further experiments, which seem rather important with regard to the present development of the microsome concept.

The freezing-drying technique seems to be a prerequisite for a systematic application of more or less specific electron staining methods for localizing certain chemical components in the ultrastructural components of the tissues.

FIG. 2. Mitochondria (*Mi*) and α -cytomembranes (α) in frozen-dried exocrine pancreas cell. The mitochondria show a negative picture of what is observed after osmium fixation. Less opaque layers are observed as a surface layer and as internal septa corresponding to the outer and inner mitochondria membranes. In the insert, these septa appear as triple-layered structures (indicated by arrows) with two less opaque layers separated by a more opaque layer. Staining of the section without dissolving the plastic with a 1% aqueous solution of phosphotungstic acid for 20 minutes. Insert stained with 1% aqueous solution of osmium tetroxide for two hours. $\times 46,000$, insert $\times 77,000$.



ACKNOWLEDGEMENT

This study has been made possible through a grant from the Swedish State Medical Research Council and, for one of the authors (RFB) through a fellowship from the Commonwealth Fund.

REFERENCES

1. GIBBONS, I. R. and BRADFELD, J. R. G., *Proc. Stockholm Conf. Electron Microscopy*, 1956, p. 121. Almqvist & Wiksell, Stockholm, and Academic Press Inc., New York, 1957.
2. GLICK, D. and MALMSTRÖM, B. G., *Exptl. Cell Research* **3**, 125 (1952).
3. MÜLLER, H. R., *J. Ultrastructure Research* **1**, 109 (1957).
4. SJÖSTRAND, F. S., *Nordisk Medicin* **19**, 1207 (1943).
5. ——— *Arkiv Zool.* **35 A**, 1 (1943).
6. ——— *Nature* **151**, 725 (1943).
7. ——— *Acta Anat.*, Suppl. 1 (1944).
8. ——— *in* Freezing and Drying, *Symp.*, London, 1951, p. 177.
9. ——— *Nature* **171**, 31 (1953).
10. ——— *J. Appl. Phys.* **24**, 116 (1953).
11. SJÖSTRAND, F. S. and RHODIN, J., *Exptl. Cell Research* **4**, 426 (1953).

X-Ray Diffraction of Stopper Cork

D. R. KREGER

*Laboratory of General and Technical Biology,
X-Ray Department of the Laboratory of Technical Physics,
Technical University, Delft*

Received December 27, 1957

The observation of earlier investigators that the X-ray powder diagram of stopper cork shows a strong, diffuse diffraction ring attributable to suberin in the 5.3-3.8 Å region was confirmed.

In addition, by a slight improvement of technique, weak diffraction rings could be observed corresponding to spacings 4.15, 5.75, 6.85 and 12.5 Å. It was shown that these belong to extractable lipoid constituents containing an aliphatic fraction which produces the 4.15 Å ring and a cyclic fraction producing the other rings. The latter correspond to spacings characteristic of friedelin. These constituents are therefore present in the membranes in a crystalline condition. The aliphatic fraction is poorly crystalline, the cyclic fraction highly crystalline.

It was shown that both fractions have a preferred orientation in the cell-walls.

The orientation of the aliphatic fraction could not be determined completely from the X-ray data, but optical evidence indicates that the preferred direction of the aliphatic chains is perpendicular to the cell-walls.

The friedelin crystallites were found to be oriented with the *b*-axis perpendicular to the plane of the cell-wall. Probably the friedelin molecules are placed in the unit cell with the general plane of the carbon rings and the long axis of the molecule about parallel to the *b*-axis.

It is a well known fact that the cell-walls of cork tissue contain suberin as their main constituent and that extractable fatty and waxy substances form a considerable proportion of the other components (14). In contrast to most plant cell-walls, the cork membranes are strongly negatively birefringent with reference to tangential directions, i.e. the long axis of the refractive index ellipsoid is in the direction normal to the plane of the cell-wall.

Ambronn (2) observed that the birefringence disappears on heating and reappears on cooling. Earlier investigators had already observed its disappearance on extraction with alkali and chloroform. The optical behaviour on heating and cooling—a behaviour also observed by Ambronn in cutinised membranes—was ascribed by him to melting and recrystallisation of the membrane waxes and was regarded as con-

vincing evidence for his opinion that the waxes in the membranes are present as crystalline inclusions with a preferred orientation of crystallites, while the non-melting ground substance is amorphous.

As to cutinised membranes, Ambronn's views have been confirmed and extended by detailed optical studies of Meyer (11). This work led to the conclusion that the waxes are present in flat, tangentially oriented pores and that the aliphatic chain molecules are oriented with their long axis normal to the cell-wall. Later Roelofsen (15) and Freytag (6) extended the optical information.

As regards cork no detailed optical investigations comparable to those of Meyer and other authors on cutinised membranes have been made as yet. Mader (10) reports observations in polarised light, but these refer mainly to growth and ageing of the membranes. They yield no new data concerning the submicroscopic organisation of the waxes, neither does the thorough electron microscope study by Sitte (17).

It must be noted that Ambronn's and Meyer's conception of crystallinity of the waxes in the membranes contains an element of speculation since double refraction is no proof of crystallinity. In order to obtain more conclusive evidence in this respect and to gain data on the submicroscopic structure of these membranes along other lines, we have examined both cutinised and cork membranes by X-ray diffraction. The results obtained with cutinised membranes, which will be published later, have confirmed Ambronn's and Meyer's conclusion for this type of membranes.

The first X-ray examination of cork reported in the literature is that of Prins (13), who found that stopper cork produces only a diffuse diffraction ring which roughly covers the diffuse ring of liquid long-chain aliphatic products. This is in agreement as well with chemical evidence indicating that suberin consists of a spatial network of condensed aliphatic products as with the optical evidence that it is amorphous. However, the diffuse ring did not support the optical data suggesting the presence of waxy crystallites in cork.

When, some years ago, we made an X-ray diagram of cork our results were the same as reported by the above author and no further attention was then paid to the problem involved. Sitte (17), in his study of the fine structure of cork by the electron microscope, reports that Dr. O. Rizzoli, Vienna, who examined cork by X-ray diffraction, had not obtained any results confirming the optical data either. Rizzoli (personal communication to Sitte) observed very faint lines in addition to the diffuse ring in his diagram, which on comparison with a diagram of cotton hairs were attributed to cellulose.

Dr. H. Mader, Schwabach, again confronted me (personal correspondence) with the problem of the lack of conformity between the optical and X-ray data on cork. The old diagram then was studied again and close inspection showed that inside the diffuse ring some very faint, sharper rings could be observed which earlier had escaped

my attention because of the rather heavy background. The present paper deals mainly with an investigation into the origin of these rings and the orientation of the cell-wall component involved.



FIG. 1. Quadrants of X-ray powder diagrams of: *A*, piece of stopper cork; *B*, wax extracted from cork with chloroform; *C*, wax from cabbage leaves; *D*, cork made optically isotropic by extraction.

POWDER DIAGRAMS OF CORK AND ITS EXTRACTABLE WAX

The first aim was to obtain a diagram in which the faint rings mentioned above would stand out more clearly. For that purpose a piece of stopper cork, 2 mm thick in the beam direction, was irradiated using a pinhole collimator 0.25 mm wide and 40 mm long (Ni filtered CuK_α radiation, specimen-film distance 40 mm). The earlier diagram had been obtained with a wider pinhole, which influences the line definition and background blackening unfavourably.

The new diagram indeed showed the weak rings inside the diffuse ring more clearly (Fig. 1*A*).¹ They do not correspond with the rings which are characteristic of normal aliphatic wax constituents and which are shown in Fig. 1*C*. Nevertheless they might be ascribed to the wax in the cell-walls because cork wax contains non-aliphatic waxy constituents. These do not produce the same X-ray diffraction rings as the n-aliphatic chain compounds because their molecules have a quite different shape and packing. The terpenoids known as friedelin and cerin form the main portion of this fraction (19), and friedelin is the dominating constituent (4). It will be shown later that the rings correspond to certain friedelin spacings.

In order to investigate whether the rings are actually produced by the waxes, a piece of cork, cut into flakes on the microtome, was extracted with chloroform for 6 hours in a soxhlet. After evaporation of the chloroform a fatty substance was left.

¹ Only one of these rings is visible in the reproduction.

An X-ray diagram of this substance is shown in Fig. 1*B*. The intense rings in this diagram closely correspond in diameter to the weak rings of Fig. 1*A*. In addition, part of the rings correspond to those of aliphatic long chains, as is seen on comparison with Fig. 1*C*, showing a diagram of wax scraped from cabbage leaves, which is aliphatic (9). On close inspection of the cork diagram of Fig. 1*A* it appears that the strongest one of these aliphatic rings can also be distinguished in that diagram. It is overshadowed by the diffuse halo from the suberin and perhaps not visible in the reproduction.

After the extraction the cork cell-walls still showed some negative double refraction. Complete isotropism was attained by boiling for 24 hours in dichlorethylene and then for 12 hours in pyridine. The material then produced a diffuse diffraction ring without any traces of other rings (Fig. 1*D*).

We may conclude that the X-ray diagram of bottle cork is in agreement with the chemical evidence according to which cork contains extractable aliphatic and non-aliphatic waxy substances and that it confirms the optical data suggesting that these are embedded as micro-crystalline inclusions in an amorphous ground substance.

Some further extraction experiments may also be mentioned here.

Two different types of stopper cork, one of light colour and comparatively soft, the other darker and harder, were powdered in a mill to grains of maximum diameter of 1 mm. The powders were extracted for 6 hours with chloroform in a soxhlet. After evaporation of the chloroform, residues of rather hard, brown to yellow wax were obtained, in both cases ca. 8% in weight of the whole cork. The wax from the light cork was slightly softer and less sticky than that from the dark one. The X-ray diagrams resembled that shown in Fig. 1*B*, but the aliphatic rings were less conspicuous, and even very weak in the wax from the darker cork, whereas the non-aliphatic rings were stronger.

The sample of light cork was then extracted with pyridine in the soxhlet. On evaporation of the pyridine, a dark-brown sticky mass was obtained constituting ca. 10% of the whole cork. The X-ray diagram showed faint, broadened aliphatic rings and no indication of non-aliphatic constituents. Roughly half of this material dissolved in cold chloroform, and yielded a brownish wax after evaporation of the chloroform. The other half, the insoluble residue, looked like black, soft tar. The wax produced an X-ray diagram clearly showing the strongest and second strongest aliphatic interference rings, which were slightly broadened.

The cell-walls, after the chloroform extraction, were still strongly negatively birefringent. After the pyridine extraction some were isotropic, but many still showed a considerable double refraction.

We may conclude from the above experiments that a six hours' extraction with chloroform is sufficient to remove the non-aliphatic, crystalline constituents from the cell-walls. Furthermore, since the cell-walls after that procedure remain negatively birefringent and still contain extractable aliphatic products, evidence has been obtained indicating that the aliphatic chain molecules are oriented with their long

axis in radial directions. This will be understood from Meyer's considerations on the wax in cutinised membranes (11).

Stopper cork is reported to contain 10–20 % constituents soluble in fat solvents (for references cf. (14)), which is in agreement with our data mentioned above. Zetsche and Lüscher (19), on the basis of their detailed chemical investigations of cork wax, conclude that terpenoids constitute approx. 25 % of the wax and consist mainly of friedelin-cerin (18–19 % of the wax). The friedelin-cerin fraction, therefore, would amount to 2–4 % of the cork. This probably explains why the reflections from this fraction had not been observed so far in X-ray diagrams of whole cork. The fact that they are perceptible despite the small proportion of the material, and that they do not show any apparent broadening, leads to the assumption that the terpenoids are well crystallised.

In the non-terpenoid, major part of the wax Zetsche and Lüscher (19) have identified a number of diverse aliphatic constituents: probably this part of the wax is mainly aliphatic. Aliphatic reflections, however, do not show up clearly in the cork diagram, and those produced by the extracted waxes are neither very intense nor very sharp. The general impression therefore is that this material is of comparatively poor crystallinity in both the extracts and the cork. This corresponds with the inhomogeneity of the fraction indicated by the chemical data.

DEMONSTRATION OF ORIENTATION OF THE WAX

In order to demonstrate röntgenographically the orientation of the wax in the cell-walls a specimen with oriented cell-walls is required. This was obtained by making use of the high compressibility of cork. A piece of stopper cork, $12 \times 4 \times 2$ mm, the 12×4 -plane tangential with reference to the year rings, was clamped in a small clampscrew and compressed in the longitudinal direction to a length of 2 mm (Fig. 2). Thus the cell-walls were given a preferred orientation with their surfaces perpendicular to the direction of compression. The specimen was then irradiated with the X-ray beam parallel to the original 2 mm-side (Fig. 2).

The diagram obtained is shown in Fig. 3. It is evident in this diagram, in particular for the reflections of the non-aliphatic wax fraction, that they do not form homogeneously blackened rings, but consist of loose arcs in a symmetrical position with reference to the equator and meridian of the diagram. This indicates that there is a preferred orientation of wax crystallites.

Since the specimen was rather tightly pressed, which might effect a disturbance of the natural disposition of wax crystallites in the cell-walls, a cork specimen compressed to only $\frac{1}{3}$ of its original dimension in the direction of compression was also investigated. The arrangement of the arcs was the same as in Fig. 3, though they were

much longer as a result of less orientation in the cell-wall positions. Therefore, a rearrangement of the crystallites with reference to the cell-wall surface effected by pressure plays no role.

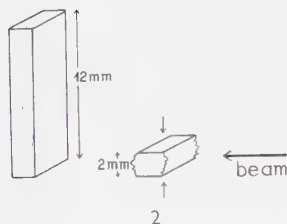


FIG. 2. Method of obtaining an X-ray diagram of oriented cork cell-walls.

FIG. 3. X-ray diagram produced by a specimen of compressed stopper cork on irradiation as indicated in Fig. 2.



The less sharp aliphatic reflection in Fig. 3 shows equatorial arcs which are overshadowed by the diffuse suberin diffraction ring. They do not show up well as separate arcs in the reproduction, so that the diffuse suberin ring itself seems to have intensified equatorial arcs. It is evident in the meridian that the diffuse ring is continuous along the whole circle. Meanwhile, it is difficult to decide whether the enhanced equatorial intensity is due only to oriented extractable aliphatic constituents.

DETERMINATION OF THE ORIENTATION OF THE WAXES

The aliphatic fraction

The aliphatic equatorial arc in the diagram of Fig. 3 corresponds to a crystal spacing of 4.15 \AA . This is the spacing of the plane (110) in the aliphatic chain lattice (12). Reflection of this plane in the equator indicates that it is oriented vertically to the equatorial plane of the specimen and, therefore, also vertically to the surface of the cell-wall since the cell-walls in the specimen are oriented in the equatorial plane. The aliphatic chains in the lattice run parallel to the plane (110) in the direction of the *c*-axis. Our X-ray diagram yields no further information on the position of this

axis, and consequently, neither on that of the aliphatic rod-shaped molecules in the cell-walls.

It has been mentioned already that the optical behaviour of the cork membranes after the chloroform extraction, indicates a vertical position of the aliphatic molecules with reference to the surface of the walls. Then all lattice planes parallel to the chain direction of the molecules will also be vertical. This was already concluded from the X-ray data above for the (110) plane. It appears therefore that the X-ray data on the orientation of this wax fraction, though scarce as a result of poor crystallinity, are consistent with the optical data.

The non-aliphatic fraction

In the preceding paragraphs a further identification of the non-aliphatic diffraction rings could be omitted. In order to determine the orientation of the crystallites of this fraction more details are required. In the first place, even though there is little reason for doubt that the rings are due to friedelin, the most prominent of the known cyclic cork wax constituents, it has to be verified whether they all belong to this substance. Furthermore, the unit cell of friedelin and the indices of the reflections have to be determined. Fortunately, X-ray crystallographic data on friedelin have been published recently by Rogers and Thomas (16), which considerably facilitates these procedures.

The unit cell of friedelin is reported to be orthorhombic with axes $a = 6.42 \text{ \AA}$, $b = 13.75 \text{ \AA}$ and $c = 28.3 \text{ \AA}$. It contains 4 molecules and the space-group is indicated as $P 2_1 2_1 2_1$.

In Table I the spacings of some important net-planes, calculated from these unit cell dimensions, are mentioned along with the three most prominent non-aliphatic spacings observed in our specimens and some other data of the diagrams. In column 1 the indices (hkl) of the important net-planes are mentioned and in column 2 the corresponding lattice spacings. The latter are calculated from the relation: $d_{(hkl)} = 1 / \sqrt{(h/a)^2 + (k/b)^2 + (l/c)^2}$ which applies to the orthorhombic system (7). In column 3 the spacings observed in our specimens are given and in column 4 the corresponding

TABLE I
DATA ON FRIEDELIN AND NON-ALIPHATIC REFLECTIONS OF FIG. 3

| (hkl) | $d_{\text{calc.}}$ | $d_{\text{obs.}}$ | $2f_{40}$ | |
|-----------|--------------------|-------------------|-----------|------|
| 110 | 5.79 | 5.75 | 22.0 | eq. |
| 101 | 6.14 | | | |
| 020 | 6.87 | 6.85 | 18.3 | mer. |
| 011 | 12.45 | 12.5 | 9.9 | mer. |

ring diameters on the film from which they have been calculated (distance from film to specimen 40 mm). Finally, in column 5 the position, either equatorial or meridional, of the reflection arcs in Fig. 3 is mentioned.

It is seen in Table I that the three non-aliphatic spacings observed in the diagrams closely correspond with the calculated friedelin spacings (110), (020) and (011). We may therefore safely assume that we are dealing with friedelin reflections in our diagrams.

The next point is what conclusions can be drawn perhaps about the orientation of the unit cell of friedelin on the basis of the above-mentioned data.

The fact that the reflection arc (020) is situated meridionally suggests that the crystallites have a preferred orientation with (020) parallel to the equatorial plane of the specimen, i.e. parallel to the cell-wall planes.

This will be understood considering that incident and reflected beam lie in a plane perpendicular to the plane of reflection. Further, it has to be borne in mind that no reflection will take place if a plane is exactly parallel to the incident beam. The reflection is due to the fact that there is a dispersion of crystallite positions around the preferred position, including positions in which the angle between (020) and the incident beam reaches the reflection angle.

This orientation would involve that the *b*-axis is preferentially oriented vertical to the equatorial plane since we are dealing with an orthorhombic unit cell. Because any further orientation is unlikely the specimen may then be regarded as a fibre specimen with *b* in the fibre direction and a great dispersion in the positions of *b*.

The suggested orientation can be checked by considering the positions of the (110) and (011) reflection arcs.

For that purpose, in Fig. 4 the unit cell is shown in its suggested orientation with respect to the X-ray beam. The surface of the cell-wall is parallel to the basal plane. The (110) and (011) planes are indicated. A view at the position of these planes shows that the normal to (110) makes a definitely smaller angle with the equatorial plane than the normal to (011). Therefore (110) will reflect more in the direction of the equator than (011). This is observed in the diagram.

A more exact check may be obtained by calculation of the positions of the (110) and (011) reflections on the film when a crystallite is rotated about the *b*-axis with the beam perpendicular to that axis.

This can be done on the basis of the layer-line relationship of the lattice planes in question. On rotation about *b* the planes (*hkl*) for which *k* = 1 reflect in the first layer-line, i.e. the angle μ between the diffracted beam and the equatorial plane is the same for any of this group of planes (cf. the textbooks on X-ray crystallography). There exists between the wave length of the radiation (λ) and the translation period (*T*) in the direction of the axis of rotation the relation $\sin \mu = \lambda/T$ (1).

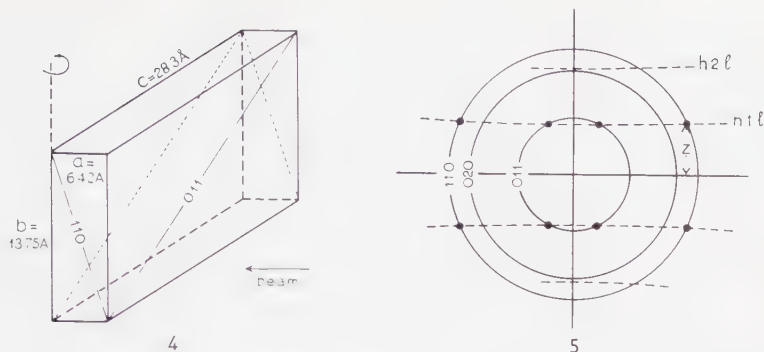


FIG. 4. Dimensions and supposed orientation of the friedelin unit cell in the cork cell-wall. Cell-wall surface parallel to a , c -plane.

FIG. 5. Calculated position of reflection spots (110) and (011) on rotation of a friedelin crystallite about its b -axis in a beam perpendicular to b .

Furthermore, if a reflection spot on the flat film is situated at a distance f from the central spot and z from the equator, while the specimen-to-film distance is r , it is easily found that $\sin \mu = z / \sqrt{f^2 + r^2}$ (2).

The relations (1) and (2) yield: $z = \lambda \sqrt{f^2 + r^2} / T$. From the numerical values $\lambda = 1.54$ Å, $T = 13.75$ Å (b -axis of unit cell), $r = 40$ mm, $f_{(110)} = 11$ mm and $f_{(011)} = 4.95$ mm (Table I), we find $z_{(110)} = 4.64$ mm and $z_{(011)} = 4.52$ mm.

In Fig. 5 the calculated positions are indicated by black dots. Naturally, their f -values correspond to those of the reflection rings (110) and (011) respectively.

On account of the dispersion of crystallite positions it cannot be expected that reflection is limited to the points indicated in Fig. 5. We must expect arcs elongated along the corresponding powder rings, with their maxima of intensity in the places indicated. If they are sufficiently elongated, adjacent arcs will overlap. It is evident from Fig. 5 that this will give rise to equatorial arcs for (110) and to meridional arcs for (011), as is actually observed in the diagram of Fig. 3. In addition the intensity distribution along the arcs (110) on the diagram suggests that they each arise from two overlapping arcs with their centres near the place calculated: there is no maximum of intensity on the equator. Probably this detail is not well perceptible in the reproduction.

In Fig. 5 we have also indicated the position of the layer-line formed by the reflections ($h2l$). Its z -value on the meridian is calculated from $\sin \mu = \lambda / 0.5 T$ as 9.26 mm. The line does not intersect with the (020) powder ring (radius 9.15 mm). This shows that (020), on rotation of a crystallite about b , does not pass through the reflection position, which is explained by the fact that (020) is parallel to the incident beam. The distance between layer-line and powder ring is very small, however. It is evident,

therefore, that broadening of the layer-line, which is caused by deviation of b from perpendicularity to the incident beam, will give rise to intersection of layer-line and ring, first on the meridian and then on either side of it, dependent on the degree of deviation of b . Therefore, if there is in the specimen a statistical distribution of deviations around the preferred position of b , which appears most probable, we

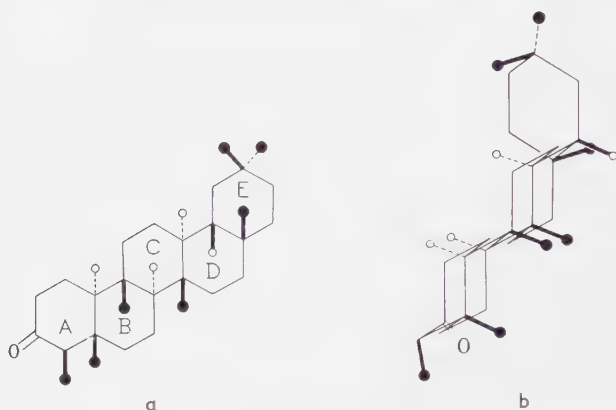


FIG. 6. Chemical structure (a) and supposed stereochemical conformation (b) of friedelin. ● = methyl, ○ = hydrogen.

may expect that the arc formed along the powder ring has its maximum of intensity on the meridian. In fact this is the case in the diagram. Therefore, also in this detail it is up to expectations.

It appears from the foregoing that all details of the diagram of the specimen with oriented cell-walls are in agreement with the assumption that the b -axis of the friedelin crystallites is oriented perpendicularly to the cell-walls. The assumption is therefore considered to be correct.

THE ORIENTATION OF THE FRIEDELIN MOLECULES

The question arises what the result from the preceding section means in terms of the orientation of the friedelin molecules. A detailed analysis of the unit cell pattern is not available in the literature, so that the position of the molecules is not at once clear from that of the unit cell. Nevertheless we might derive some data in this respect by combining the dimensions of the unit cell with those of the molecule and taking into account what is known of related compounds.

The skeleton of the molecule consists of five condensed carbon six-rings (Fig. 6a). It is a pentacyclic ketone, and the details of the chemical structure shown in Fig. 6a have been assessed recently by several investigators (3, 5, 18).

For the stereochemistry of similar pentacyclic structures we refer to Klyne (8). Two-dimensional X-ray analysis has so far been applied in the study of these structures only in the case of the iodo acetate of oleanolic acid by Abd El Rahim and Carlisle (1). The results appear to support a structure with parallel carbon rings *A*, *B*, *C* and *D*, whereas ring *E* is rotated out of the plane of the other rings. This is



FIG. 7. Chemical structure (a) and stereochemical conformation (b) of 18 β -oleanane (8).

explained from the *cis*-configuration in the junctions with ring *D*. The principle is illustrated in Fig. 7b for a member of the oleanane group with a figure from Klyne (8).

If, on the basis of the same principles, we try to develop a space model for friedelin we come to a result as shown in Fig. 6b. The skeleton differs from that of oleanolic acid in that the *A*-*B*-*C*-*D* rings are the mirror images of those in oleanolic acid and that the *E* ring has a different position.

The unit cell of the iodo acetate of oleanolic acid resembles that of friedelin. It is orthorhombic with axes $a = 7.70 \text{ \AA}$, $b = 16.11 \text{ \AA}$ and $c = 25.14 \text{ \AA}$. The space group is the same as that of friedelin. The position of the molecules in this cell is such that the general plane of the four parallel carbon rings is about parallel to the b , c -plane and that its greatest length is in a direction similar to that of the b -axis (1). The fact that this axis is longer than the same one in friedelin is explained by the presence of the iodine atoms.

The correspondences of the above-mentioned compound with friedelin as regards molecular structure, cell dimensions and space group suggest that in friedelin the position of the molecules in the unit cell is about the same. It is therefore most

probable that the friedelin molecules in the cell-walls are placed with the planes of the carbon rings and the long axis of the molecule in about radial positions.

The author is indebted to Dr. E. Nicolaï, Leiden, for corrections of the English text and to Miss H. J. M. Poot for technical assistance. The work has been supported by the Netherlands Organisation for Pure Research (Z.W.O.).

REFERENCES

1. ABD EL RAHIM, A. M. and CARLISLE, C. H., *Chemistry & Industry*, 279 (1954).
2. AMBRONN, H., *Ber. deut. botan. Ges.* **6**, 226 (1888).
3. BROWNLIE, G., SPRING, F. S., STEVENSON, R. S. and STRACHAN, W. S., *J. Chem. Soc.*, 2419 (1956).
4. DRAKE, N. L. and JACOBSEN, R. P., *J. Am. Chem. Soc.* **57**, 1570 (1935).
5. DUTLER, H., JEGER, O. and RUZICKA, L., *Helv. Chim. Acta* **38**, 1268 (1955).
6. FREYTAG, K., *Ber. oberhess. Ges. Natur- u. Heilk. Giessen* **26**, 21 (1956).
7. International Tables for the Determination of Crystal Structure. Borntraeger, Berlin, 1935.
8. KLYNE, W., *Progress in Stereochemistry I*, p. 57. Butterworth, London, 1954.
9. KREGER, D. R., *Rec. trav. botan. néerl.* **41**, 603 (1948).
10. MADER, H., *Planta* **43**, 163 (1954).
11. MEYER, M., *Protoplasma* **29**, 552 (1938).
12. MÜLLER, A., *Proc. Roy. Soc. London A* **120**, 437 (1928).
13. PRINS, J. A., *Physica* **1**, 752 (1934).
14. RIBAS-MARQUÈS, I., *Chimie & industrie* **68**, 333 (1952).
15. ROELOFSEN, P. A., *Acta Bot. Neerl.* **1**, 99 (1952).
16. ROGERS, D. and THOMAS, D. V., *Bull. soc. chim. France*, 361 (1956).
17. SITTE, P., *Mikroskopie* **10**, 178 (1956).
18. TAKAHASHI, T. and OURISSON, G., *Bull. soc. chim. France*, 353 (1956).
19. ZETSCHKE, F. and LÜSCHER, E., *J. Prakt. Chem.* **150**, 68 (1938).

Submicroscopic Structure of the Compound Eye as Revealed by Electron Microscopy

G. YASUZUMI and N. DEGUCHI

*Laboratory for Electron Microscope Research,
Department of Anatomy, Nara Medical College, Kashihara, Nara-Pref.*

Received January 10, 1958

The submicroscopic structure of the ommatidium and periophticon of the adult *Drosophila virilis* has been studied in thin tissue sections by electron microscopy.

The rhabdomere of the compound eye is composed of two segments, a distal segment with a homogeneous structure and a proximal segment with a lamellar or polygonally reticular structure. The submicroscopic structure of the rhabdomere is compared with that of the vertebrate retinal rod cell. The present observations lend support to the idea that the proximal segment of the rhabdomere consists of tightly packed tubules or rods which are arranged perpendicularly or obliquely to the long axis of the rhabdomere.

The ommatidium comes in close contact with the non-medullated nerve fibers through discontinuities in the basement membrane. The periophticon, which consists of ganglion cells and a complex synaptic apparatus, is demonstrated at a low magnification.

The study of the submicroscopical organization of the compound eye is of particular importance in view of the genetics and physiology of vision. Much of our recent knowledge of the structure of the compound eye has been derived from light microscopic studies (16, 25). The compound eye of *Drosophila* is constructed of a number of units called ommatidia. Each consists of seven elongated retinula cells which are radially arranged to form a cylinder. Each retinula cell has, extended along its inner edge, a highly differentiated structure called the rhabdomere. In cross-section, the rhabdomeres make a rosette within the ommatidium. The proximal end of each ommatidium rests on a basement membrane below which lie the ganglion cells of the periophticon. Nerve fibers and branches of the tracheal system penetrate the basement membrane. In the wild-type of *Drosophila*, pigment cells surround the retinula cells.

During the course of this work, Fernández-Morán (11) reported on the fine structure of the rhabdomeres of the house fly, *Musca domestica*, and described it as being composed of fenestrated discs. Nearing the completion of this work, three excellent reports appeared by Miller (18), Goldsmith and Philpott (13), and Wolken *et al.* (41) describing detailed observations on the fine structure of the arthropod

compound eye. The primary interest of these workers has been with the rhabdomeres. Miller (18) working with *Limulus*, Goldsmith and Philpott (13) with *Sacrophaga bullata* and *Anax junius*, and Wolken *et al.* (41) with *Drosophila melanogaster* have reported that the rhabdomere consists of tubes or rods oriented perpendicularly to the long axis of the rhabdomere. This gives the rhabdomeres a lamellar or reticular appearance. It has been assumed that the analysis of polarized light within the insect eye is probably related to the radial arrangement of the radially unsymmetrical rhabdomeres within the ommatidium (13, 41).

The present communication concerns additional findings, obtained at high resolution, regarding the fine structure of the ommatidium of the wild-type of *Drosophila virilis*.

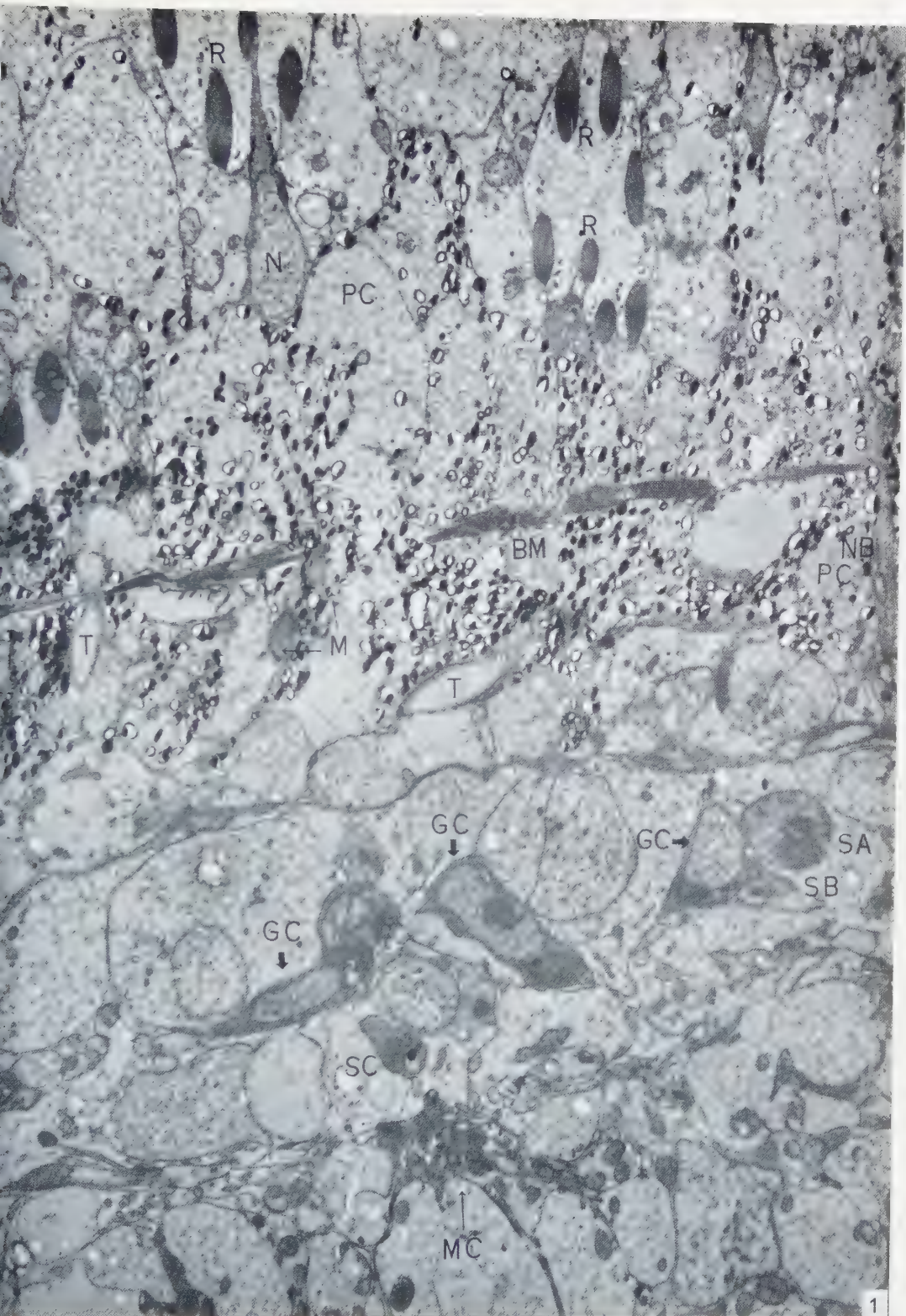
MATERIAL AND METHODS

Wild-type, red-eyed, adult *Drosophila virilis* were used in the present study. The flies were decapitated with a fine scapel under a binocular microscope and the heads immediately fixed in 1% osmium tetroxide buffered (pH 7.3) with acetate-veronal (20). Fixation was carried out for one week at 10°C. Thereafter, the specimens were dehydrated directly, without washing in distilled water (42), in 70% ethyl alcohol for 4 hours or overnight, 96% ethyl alcohol for one hour and absolute alcohol for 30 minutes. They were impregnated with a 1 to 4 mixture of methyl and *n*-butyl methacrylate for at least one hour and finally embedded in the same mixture by polymerization with 2,6-dichlorobenzoyl peroxide at 46°C (19). Sections were cut with glass knives on a Shimadzu microtome. Their thickness ranged from 200 to 500 Å as determined by light interference colors. All sections were examined, without removing the embedding plastic, in an Akashi electron microscope model TRS-50.

RESULTS

Fig. 1 demonstrates, at a low magnification, a section through the ommatidia and outer ganglion cell layer (periopticon) of the wild-type of *Drosophila virilis*. Seven rhabdomeres, slightly obliquely cross-sectioned, form a rosette in the rhabdom, which is surrounded by seven retinula cells. Pigment cells encircle this entire composite. One of the rhabdomeres is displaced toward the center of the rhabdom.

FIG. 1. A slightly oblique longitudinal section through several ommatidia, basement membrane and periopticon. Elliptical profiles of rhabdomeres (*R*) can be seen forming a rosette. The nucleus of the retinula cell is marked by *N*. The pigment cells (*PC*) with pigment granules are found surrounding the retinula cells. The pigment cells (*PC*) appear also in the outer ganglion layer (periopticon). Below the basement membrane (*BM*) and seldom upon it, branches of the tracheal system (*T*) appear showing spindle-shaped profiles with lacerated inner edge. A nerve fiber can be seen at the point marked by *NB*. Swollen mitochondria (*M*) are found attached to the nerve fiber. Apposed to the margin of the ganglion cell (*GC*) is a broad, rounded (*SA*), triangular (*SB*) or irregular shaped profile (*SC*) of an axo-somatic synaptic terminal. The axo-dendritic synaptic apparatus contains a collection of mitochondria (*MC*). $\times 5000$.



Most of the retinula cells have only a small amount of electron scattering material. The one, however, which belongs to the displaced rhabdomere, contains homogeneous masses of a material with an intermediate electron density. This may suggest a different visual activity. The pigment granules are situated, in many cases, in the periphery of the pigment cell. The basement membrane is not always continuous and varies in thickness. It has no definite structure. Below the basement membrane, one or two layers of pigment cells appear along with branches of the tracheal system.

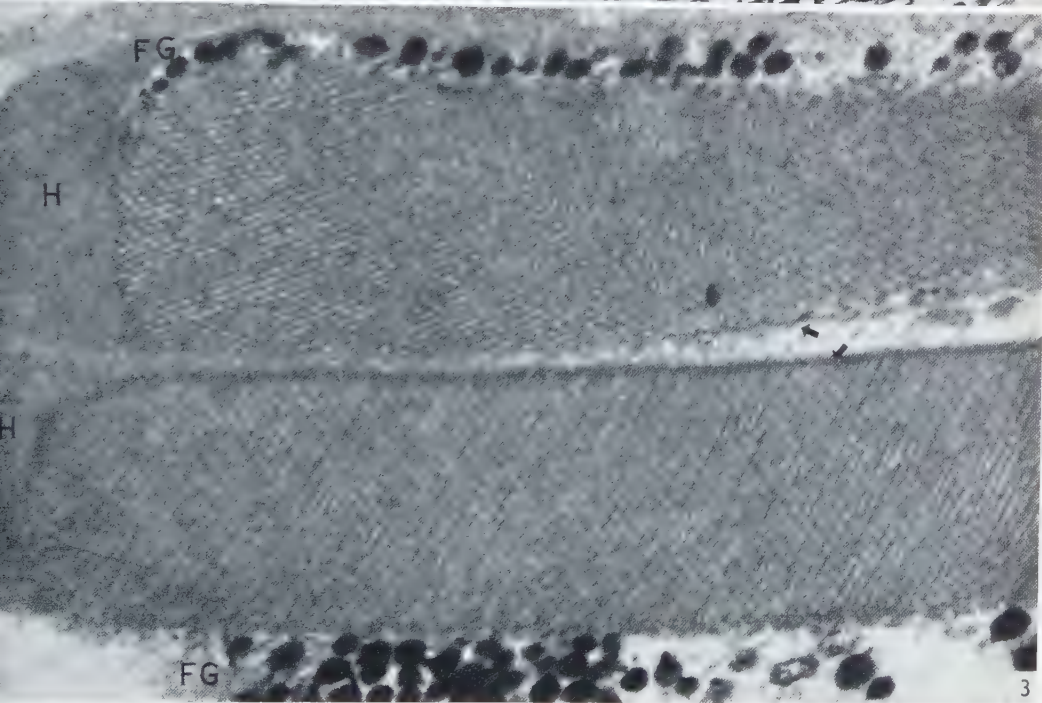
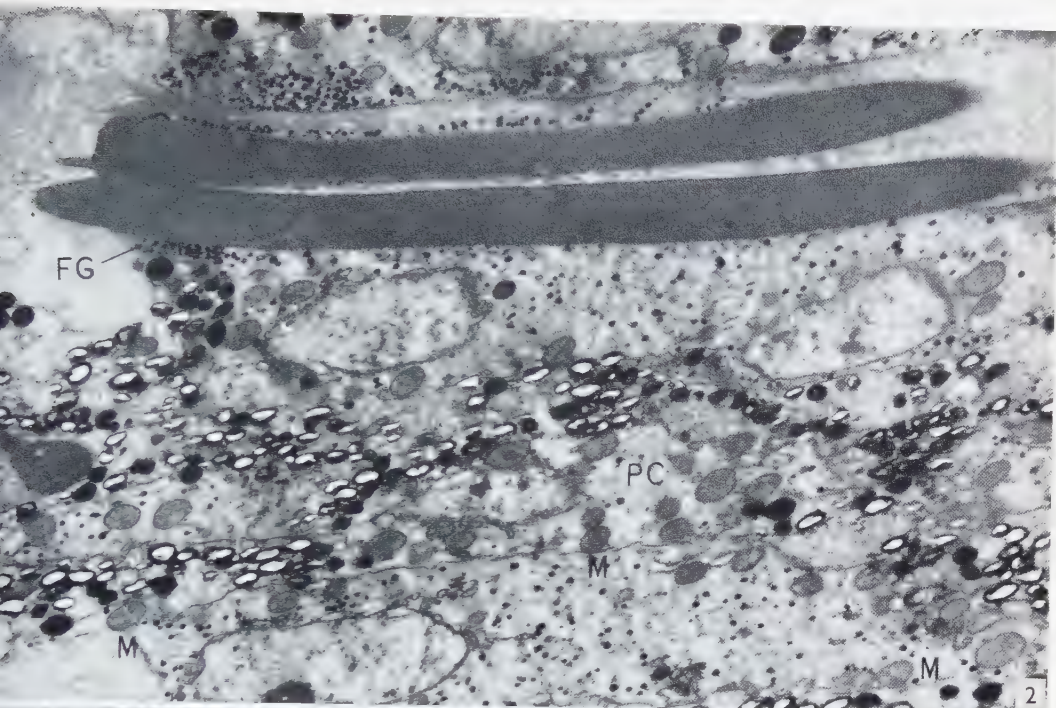
The retinula cell is elongated through gaps in the basement membrane to attach to non-medullated nerve fibers (Fig. 1). Swollen mitochondria can be found in this region. In longitudinal sections through the outer ganglion cell layer (periopticon), some ganglion cells appear to have a dense cytoplasm, a less dense karyoplasm and a dense nucleolus. The complex synaptic axo-dendritic apparatus consists of a broad, branching axon terminal and associated small dendrites. These contain a dense collection of mitochondria. The axo-somatic synaptic terminal can be found apposed to the margin of the ganglion cells. It is characterized by a broad, rounded triangular or irregularly shaped profile which contains mitochondria and granular or synaptic vesicles. The latter was observed for the first time by Sjöstrand (33, 35, 36) and by de Robertis and Bennett (27). A detailed description of the synapsis will be reported elsewhere.

In longitudinal section, the rhabdomere appears as a rod-shaped, dense body with a tapering end distally. A small projection on the distal end may often be seen. Fine dense granules, 90–180 $m\mu$ in diameter, are found scattered throughout the retinula and pigment cells. These granules cluster around and surround the distal portion of the rhabdomere (Figs. 2, 3 and 4). The rounded or oval-shaped, large dense pigment granules, 0.44–0.60 μ in diameter, are often shrunken as a result of fixation or dehydration. Mitochondria with *cristae mitochondriales* (Fig. 4) and matrix with intermediate density (Fig. 2) appear in the retinula and pigment cells.

In higher magnification (Figs. 3, 4 and 7), it is clearly visible that the rhabdomere is composed of two segments: a distal portion with a homogeneous structure and a proximal portion with a lamellar or reticular structure. Fig. 3 shows an obscure limiting membrane between the distal and proximal segments but in other cases (Figs. 4 and 7) no such limiting membrane can be visualized. A few granules are

FIG. 2. A slightly oblique longitudinal section through the ommatidia, showing two rhabdomeres in the retinula cells and the pigment cells (PC) with pigment granules and mitochondria (M). The fine, dense granules (FG) are found in the retinula cell, especially clustered surrounding the distal part of the rhabdomere. A few mitochondria (M) are found in the retinula cell. $\times 5300$.

FIG. 3. Two rhabdomeres from Fig. 2 at higher magnification showing a closely packed polygonal structure and a lamellar pattern. The distal end of the rhabdomere is of a homogeneous structure (H). The limiting membrane (arrows) is visible around the rhabdomere. The clusters of fine granules (FG) can be seen. $\times 26,000$.



often found between the distal and proximal segments (Fig. 3). The proximal segment is a long, rod-shaped body. It has two distinctive patterns of internal structure even in similarly sectioned ommatidia. In one pattern it appears to have a closely packed polygonal structure while in the other it appears to have a lamellar structure. These lamellae are inclined at 60 degrees or may be perpendicular to the longitudinal axis of the rhabdomere (Figs. 3 and 4).

In a slightly oblique cross-section through an ommatidium (Fig. 5), the seven retinula cells appear radially arranged. Each has a medial portion which extends toward the center of the ommatidium and terminates in an elliptical rhabdomere. Here (Fig. 5) the rhabdomeres show the characteristic lamellar or reticular internal structure. The reticular pattern is seen as a polygonal or roughly hexagonal framework of dense lines about 100 Å in thickness (Figs. 6 and 7). The light areas inside the lines measure about 200 Å in diameter. The dimension of these light areas changes from place to place. This may be due to slight changes in the angle of sectioning or compression during sectioning.

In a higher magnification of a rhabdomere (Fig. 8), parallelly arranged, dense lines, averaging 100 Å in thickness, with less dense interspaces, 170–220 Å, can be seen which run parallel with the long axis of the rhabdomere. A limiting membrane around the rhabdomere is visible here. In another profile (Fig. 9) a lamellar structure is seen. Here the lamellae are inclined at a 50 degree angle to the longitudinal axis of rhabdomere. The lamellae are 100 Å thick and have the typical average separation of 200 Å. There can be found circular appearances, multiple splittings and disruptions of the parallel dense lines.

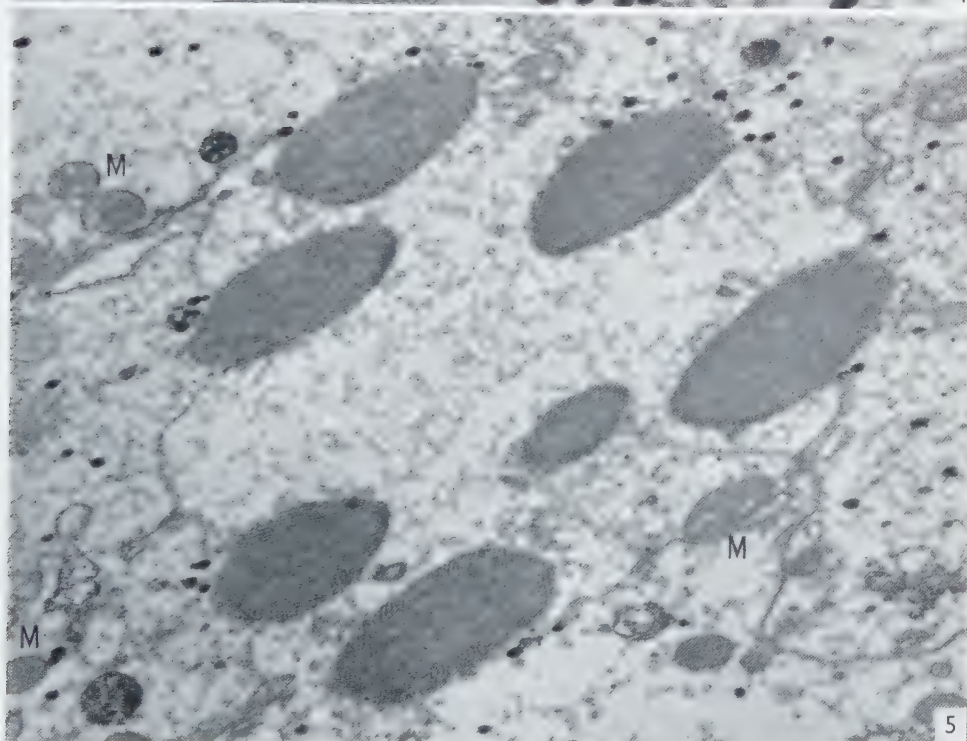
DISCUSSION

The insect compound eye is separated from the brain by a basement membrane. Here the latter has been observed for the first time by the electron microscope. It is discontinuous and through its discontinuities the ommatidia come in close contact with the non-medullated nerve fibers. Rhabdomeres can never be found below the basement membrane.

Goldsmith and Philpott (13) demonstrated, with respect to size, two types of pigment granules in the ommatidium. The present paper confirms this. Charac-

FIG. 4. A longitudinal section of three pieces of rhabdomeres, showing lamellar and reticular patterns. A fine granular homogeneous mass (*H*) can be seen in the upper right-hand corner and fine dense pigment granules (*FG*) in the lower right-hand corner. The limiting membrane surrounding the rhabdomere can be seen at the point marked by the arrow. $\times 27,000$.

FIG. 5. A slightly oblique cross-section through seven retinula cells, showing seven rhabdomere profiles with a reticular or lamellar internal structure. The mitochondria (*M*) provided with cristae mitochondriales are found in the retinula cells. $\times 13,000$.



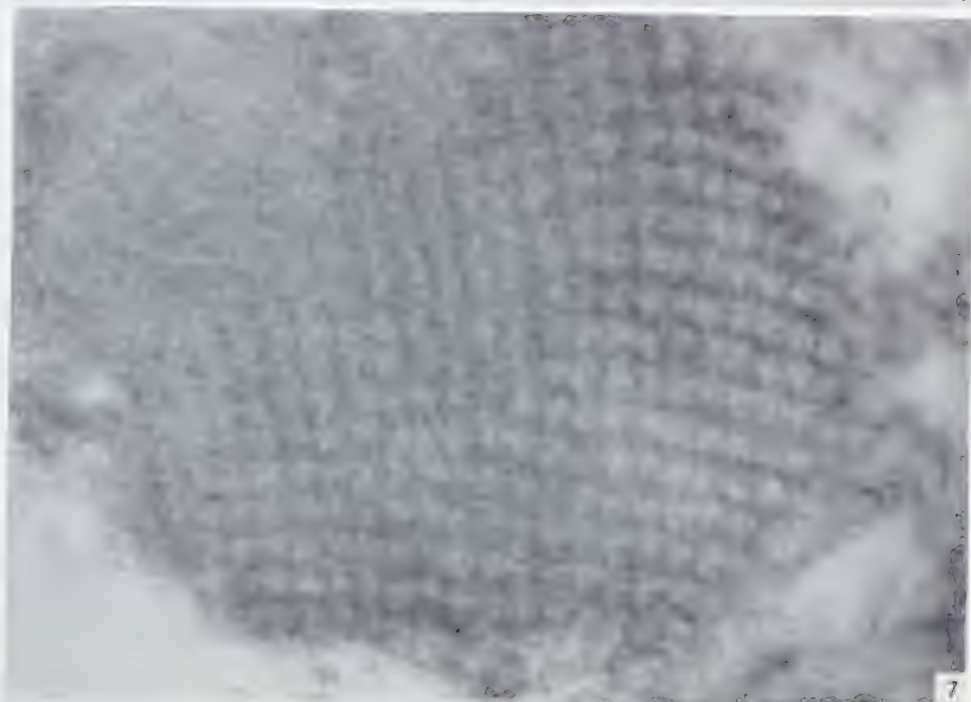
teristically the fine granules are found clustered about the distal portion of the rhabdomere. As suggested by Goldsmith and Philpott (13), the chemical composition of the pigment granules is related probably to the ommochromes described by Butenandt (6) and Butenandt and his co-workers (7).

The synaptic junction described in this paper belongs to the two categories listed by Ramón y Cajal (24) as axo-somatic and axo-dendritic junctions. They have not been studied with the electron microscope, as yet, in the central nervous system of *Drosophila*. The present study has been done at a low magnification and shows only the relationship between ommatidium and periopticon. It has been revealed here that the synaptic apparatus consists of a broad branching axon terminal, i.e. a presynaptic expansion of the axon with a collection of mitochondria and synaptic vesicles. A similar finding has been obtained already in other materials (8-10, 21-23, 27-29, 30, 31, 33, 38-40). The correlation between the concentration of mitochondria in synaptic areas (1-6, 14, 15, 23) and the activity of enzymes involved in oxidative phosphorylation (17) in such regions is too well known to require comment here. A detailed observation of the synapsis will be reported in the near future.

In the vertebrate eye, each retinal rod proper consists of an outer and inner segment. The outer rod segment is composed of plate-like elements oriented perpendicularly to the long axis of the rod (12, 26, 32, 34). In the compound eye of *Drosophila virilis* the rhabdomere is composed of outer and inner segments. The outer segment is homogeneous and has an intermediate density. It has not been described in previous communications (11, 13, 18, 41). The inner segment is laminated and resembles superficially the outer segment of the vertebrate retinal rod. The vertebrate eye has a distinctly red color due to the presence in the outer segment of the rods of visual purple (37). The homogeneous mass at the distal end of the rhabdomere may be homologous to the vertebrate rhodopsin. Since the fine dense pigment granules seem to be associated so closely with the distal portion of the rhabdomere, a study of the rhabdomere under light and dark conditions will be undertaken in an attempt to elucidate any relationship which may exist between these structures.

The lamellar and reticular patterns, as visualized within the rhabdomeres, might suggest two different internal structures. However, the fact, that the dense lines and less dense interspaces are of the same width in both the lamellar and reticular configurations, more strongly suggests a single structural form (13, 18, 41). Thus Goldsmith and Philpott (13) and Wolken *et al.* (41) demonstrated almost similar diagrams. The results of the re-examination of the present study concur with their conclusions.

FIG. 6. A longitudinal section through the rhabdomere, showing a polygonal structure. $\times 67,000$.
FIG. 7. A segment of the distal portion of a rhabdomere slightly obliquely cross-sectioned. Notice the transition between the reticular system and the homogeneous system. $\times 136,000$.



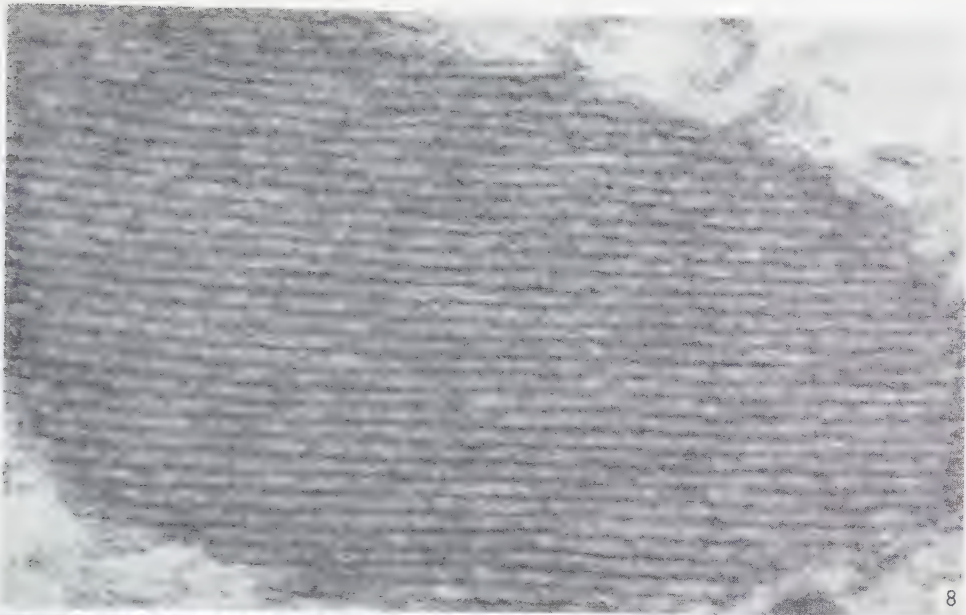
Each rhabdomere, as indicated by their observations and the observations of this work, consists of tightly packed tubules or rods which pile up perpendicularly or obliquely along the long axis of the rhabdomere. The number of dense lines limiting the tubules or rods is estimated to be thirty to forty-two in a slightly oblique cross-section of the rhabdomere. Each tubule or rod shows a polygon or roughly hexagonal cross-section as shown by Fernández-Morán (11), Miller (18), Goldsmith and Philpott (13) and Wolken *et al.* (41). Circular appearances, multiple splitting and disruption of the parallel lines have been observed but they may be due to the fixing or sectioning procedures.

REFERENCES

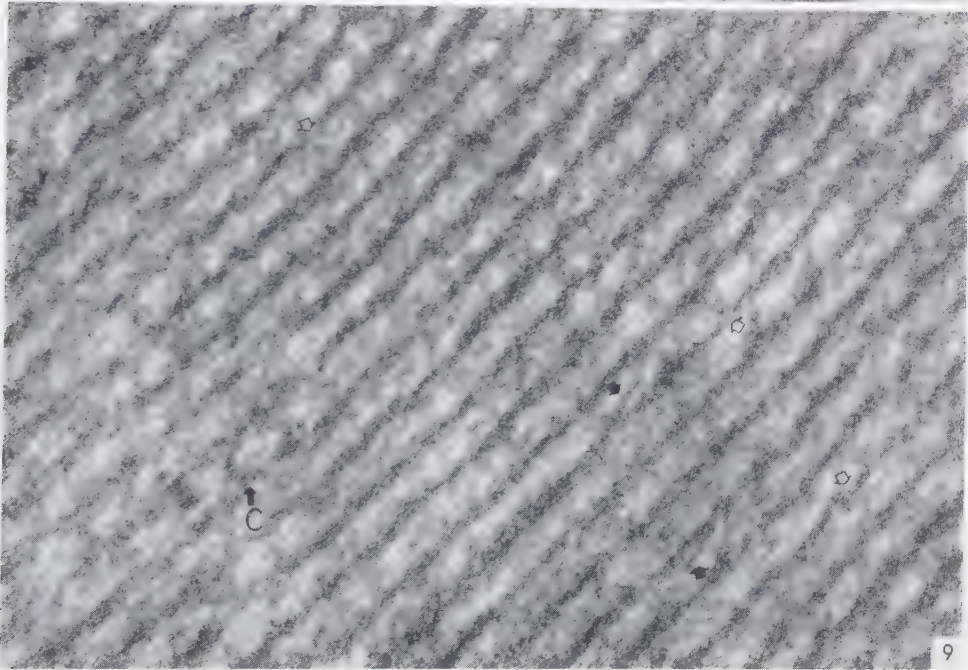
1. AUERBACH, L., *Neurol. Centr.* **17**, 445 (1898).
2. BARTELMIZ, G. W. and HOERR, N. L., *J. Comp. Neurol.* **57**, 401 (1933).
3. BODIAN, D., *J. Comp. Neurol.* **68**, 117 (1937).
4. — *ibid.* **73**, 323 (1940).
5. — *Physiol. Rev.* **22**, 146 (1942).
6. BUTENANDT, A., *XIV. Japan. Med. Kong., Tokyo*, 1956, p. 2, 15.
7. BUTENANDT, A., SCHIEDT, U., BIEKERT, E. and CROMARTIE, R. J. I., *Ann. Chem. (Leipzig)* **590**, 75 (1954).
8. ENGSTRÖM, H. and SJÖSTRAND, F. S., *Acta Oto-Laryngol.* **44**, 490 (1954).
9. ENGSTRÖM, H. and WERSÄLL, J., *Acta Oto-Laryngol.* **43**, 323 (1953).
10. FERNÁNDEZ-MORÁN, H., *VI Congr. Latinoamer. Neurocir., Montevideo*, 1955, p. 599.
11. — *Nature* **117**, 742 (1956).
12. FINEAN, J. B., SJÖSTRAND, F. S. and STEINMANN, E., *Exptl. Cell Research* **5**, 557 (1953).
13. GOLDSMITH, T. H. and PHILPOTT, D. E., *J. Biophys. Biochem. Cytol.* **3**, 429 (1957).
14. HELD, H., *Arch. Anat. u. Physiol. Anat. Abt.*, 1897, p. 204.
15. — *ibid.*, Suppl., p. 273.
16. KRAJKA, J., *Biol. Bull.* **47**, 143 (1924).
17. LOWRY, O. H., ROBERTS, N. R., LEINER, K. Y., WU, M.-L., FARR, A. L. and ALBERS, R. W., *J. Biol. Chem.* **207**, 39 (1957).
18. MILLER, W. H., *J. Biophys. Biochem. Cytol.* **3**, 421 (1957).
19. NEWMAN, S. B., BORYSKO, E. and SWERDLOW, M., *J. Research Nat. Bur. Standards* **43**, 183 (1949).
20. PALADE, G. E., *Anat. Record* **114**, 427 (1952).
21. — *ibid.* **118**, 335 (1954).
22. PALADE, G. E. and PALAY, S. L., *Anat. Record* **118**, 336 (1954).
23. PALAY, S. L., *J. Biophys. Biochem. Cytol.* **2**, No. 4, Suppl. 193 (1956).

FIG. 8. A cross-section through a rhabdomere, showing a lamellar pattern consisting of osmium fixed dense bands averaging 100 Å in thickness, and less dense interspaces 170–220 Å. No limiting membrane can be found around the rhabdomere. $\times 83,000$.

FIG. 9. High power, rhabdomere segment transversely sectioned, showing a lamellar structure at fifty degrees to the longitudinal axis of the oval-shaped profile. Multiple splitting (black arrows), circular appearance (C) and disruption (white arrows) of the dense lines can be seen. $\times 171,000$.



8



9

24. RAMÓN Y CAJAL, S., *Histologie du système nerveux de l'homme et des vertébrés I. A.* Maloine, Paris, 1911.
25. RICHARDS, M. H. and FURROW, E. Y., *Biol. Bull.* **48**, 243 (1925).
26. DE ROBERTIS, E., *J. Biophys. Biochem. Cytol.* **2**, No. 4, Suppl. 209 (1956).
27. DE ROBERTIS, E. D. P. and BENNETT, H. S., *J. Biophys. Biochem. Cytol.* **1**, 47 (1955).
28. DE ROBERTIS, E. and FERREIRA, A. V., *J. Biophys. Biochem. Cytol.* **3**, 611 (1957).
29. DE ROBERTIS, E. and FRANCHI, C. M., *J. Biophys. Biochem. Cytol.* **2**, 307 (1956).
30. ROBERTSON, J. D., *Proc. Soc. Exp. Biol. Med.* **82**, 219 (1953).
31. ——— *Anat. Record* **118**, 346 (1954).
32. SJÖSTRAND, F. S., *J. Cellular Comp. Physiol.* **33**, 383 (1949).
33. ——— *J. Appl. Phys.* **24**, 1422 (1953).
34. ——— *J. Cellular Comp. Physiol.* **42**, 15 (1953).
35. ——— *Z. wiss. Mikroskop.* **62**, 65 (1954).
36. ——— *3rd Internat. Conf. Electron Microscopy, London, 1954*, p. 428. Royal Microscopical Society, London, 1956.
37. WALD, G. and HUBBARD, R., *J. Gen. Physiol.* **32**, 367 (1948–49).
38. WERSÄLL, J., *Acta Oto-Laryngol.* **44**, 359 (1954).
39. ——— *ibid.*, Suppl. 126 (1956).
40. WERSÄLL, J., ENGSTRÖM, H. and HJORTH, S., *Acta Oto-Laryngol.*, Suppl. 116, 298 (1954).
41. WOLKEN, J. J., CAPENOS, J. and TURANO, A., *J. Biophys. Biochem. Cytol.* **3**, 441 (1957).
42. YASUZUMI, G. and ISHIDA, H., *J. Biophys. Biochem. Cytol.* **3**, 663 (1957).

The Ultrastructure of the Intercalated Discs of Frog, Mouse and Guinea Pig Cardiac Muscle

F. S. SJÖSTRAND, EBBA ANDERSSON-CEDERGREN and M. M. DEWEY¹

*Laboratory for Biological Ultrastructure Research,
Department of Anatomy, Karolinska Institutet, Stockholm*

Received March 7, 1958

The intercalated discs of cardiac muscle of the frog, mouse and guinea pig consist of transversally oriented cell boundaries and of about $0.1\ \mu$ broad zones of dense cytoplasm associated with the plasma membranes at these boundaries.

The plasma membranes are represented by an opaque osmiophilic layer, the o-layer, which in certain regions appears triple-layered. The two o-layers of the two cells at the boundary are separated by a less osmiophilic interspace, the l-space. This space varies in thickness in different parts of the boundary and in different species. It is interpreted as representing the lipid layers of the two plasma membranes in close contact. This arrangement is assumed to ensure a mechanically firm contact between the cells.

It is possible structurally to distinguish between interfibrillar and intersarcomeric regions along the disc. The density of the cytoplasm in the interfibrillar regions is due to a dense network that connects the I-band part of the myofilaments with the o-layer of the plasma membrane. In the intersarcomeric regions, zones of dense cytoplasm contribute to the differentiation of specialized regions of cellular contact, the S-regions according to the terminology used here.

The interpretation of the significance of the intercalated discs of heart muscle tissue has been the subject of much controversy in light microscopical studies. The main debate has focussed on whether they represented cell boundaries or not. The concept of a syncytial arrangement (8-11, 30) gained a rather general acceptance. This is especially obvious when reading the extensive monograph on the intercalated discs published by Aurell (2). The idea of a syncytial arrangement has been helpful to physiologists in understanding the physiological characteristics of the heart muscle.

The earliest electron microscopical studies did not show a sufficient high resolution to allow any definite conclusions. This applies, for instance, to the study by van Breemen (4) who concluded "that the intercalated discs are structures produced by collagenous invasion at cell wall junctions". He interpreted the opaque dense

¹ National Research Foundation Fellow, Division of Medical Sciences.

zones, which are in fact located in the cytoplasm at the cell boundaries, as representing this extracellular collagenous invasion. He thus claimed that "the disc is not intracellular". This description clearly shows that the information gained by low resolution electron microscopy hardly surpassed that collected from light microscopical studies.

For any judgement whether the intercalated discs are associated with cell boundaries or not, a prerequisite must be that at least some component of the plasma membrane itself has been observed and analyzed in this region. In a preliminary report (27) the arrangement of the opaque osmiophilic layer of the plasma membrane had been analyzed at the intercalated disc and found to traverse the cardiac muscle branches through the intercalated disc region. Two such opaque layers belonging to two plasma membranes of two separate cell territories were found to be completely separated by a 150-200 Å wide, less opaque interspace. Most of the material responsible for the appearance of the intercalated discs in the light microscope was found to consist of a zone of dense, osmiophilic cytoplasm located at the cell boundary.

These observations have been confirmed by Poche and Lindner (17), Price *et al.* (18), Lindner (13), Muir (15) and by Moore and Ruska (14).

The present study reports in a more detailed way the ultrastructural organization of the intercalated discs and their subdivision into regions of different structural arrangement.

MATERIAL AND METHODS

Cardiac muscle tissue from mouse, guinea pig, frog and toad has been studied after fixation in a buffered, isotonic 1% solution of osmium tetroxide, dehydration in ethyl alcohol or isopropyl alcohol and embedding in a mixture of *n*-butyl and methyl methacrylate. The hearts from mouse, narcotized with nembutal, were fixed *in vivo* by injection of the osmium tetroxide solution into the pericardial cavity from the abdominal cavity through the diaphragm. After about 15 minutes the heart was removed from the body and fixed *in toto* another 30-45 minutes. Injections into the pericardial cavity were made on frogs after cooling of the animal at -5°C. In this case the time for fixation *in situ* was 5-15 minutes. After dehydration and transfer to methacrylate, the outer layers of the ventricular wall were cut off and embedded in gelatin capsules. From the heart of the guinea pigs, the papillary muscles were selected and were attached to glass forks before removal from the heart. They were fixed and embedded when attached to the glass fork. Some of the mouse cardiac tissue was stained in 0.5% phosphotungstic acid dissolved in the alcohols used for dehydration. Sections were cut on Sjöstrand ultramicrotomes and examined in an RCA EMU 3A electron microscope at 100 kV and electron optical magnifications of mostly 21,000 to 36,000 times.

FIG. 1. Section through an intercalated disc of mouse cardiac muscle. *IF*, interfibrillar region; *IL*, longitudinal connection between two steps; *IS*, intersarcoplasmic region; *M*, mitochondrion; *S*, S-region. Arrows point to the edges of the intercalated disc. Phosphotungstic staining after osmium fixation. $\times 55,000$.



OBSERVATIONS

The intercalated discs consist of the two plasma membranes of the joining cell territories and a zone of dense osmiophilic cytoplasm located at each plasma membrane. The cell boundary shows in sections a more or less wavy course. This description has a general application. When going into details, there are considerable structural differences between several regions along the intercalated disc.

The region where the myofibrils reach the cell surface appears different from that part of the disc which is interposed between the interfibrillar spaces where frequently the mitochondria are lined up. Those parts of the cell boundary which extend between two steps of an intercalated disc over a distance of one or two sarcomeres are structurally organized according to still another pattern. These three regions will be referred to as the *interfibrillar*, the *intersarcoplasmic* regions and the *longitudinally connecting surfaces*.

The wavy course of the cell boundary which is characteristic when observing longitudinal sections through cardiac muscle shows great variation with species. The amplitude of these waves is larger in mouse and guinea pig (Figs. 1 and 2) than in frog cardiac muscle (Fig. 3). In the two first-mentioned cases, the waviness is very irregular and shows narrow peaks within the interfibrillar regions. The orientation of the cell boundary will therefore be at a rather acute angle to the orientation of the myofibrils.

This waviness has been interpreted by light microscopists as rods or pores (for literature, see (2)).

The plasma membrane at the intercalated discs appears as an opaque, osmiophilic layer which is continuous with that covering the lateral surfaces of the muscle cell branches (Figs. 4 and 5). This opaque layer will here be called the *o-layer* of the plasma membrane. The two opaque layers of the two joining cells are separated by a less opaque interspace which shows a rather constant width within the different regions. The widths differ in various species and measure, for instance, in the interfibrillar region 120–130 Å in the mouse and frog and 70 Å in the guinea pig. Further figures are presented in Table I. This less opaque, light interspace will here be referred to as the *l-space*.

In the mouse the *o-layer* of the plasma membrane appears as a triple-layered structure at the intercalated disc. Two strongly osmiophilic layers are separated by a less osmiophilic layer. The thickness of each layer is about 25 Å and the total thickness of the triple-layered structure is about 75 Å (Figs. 4 and 5).

FIG. 2. Survey picture of section through intercalated disc of guinea pig cardiac muscle. *IF*, interfibrillar region; *IS*, intersarcoplasmic region; *M*, mitochondrion; *S*, S-region. Arrow points to the edges of the intercalated disc. Fixation in isotonic buffered osmium solution. $\times 60,000$.

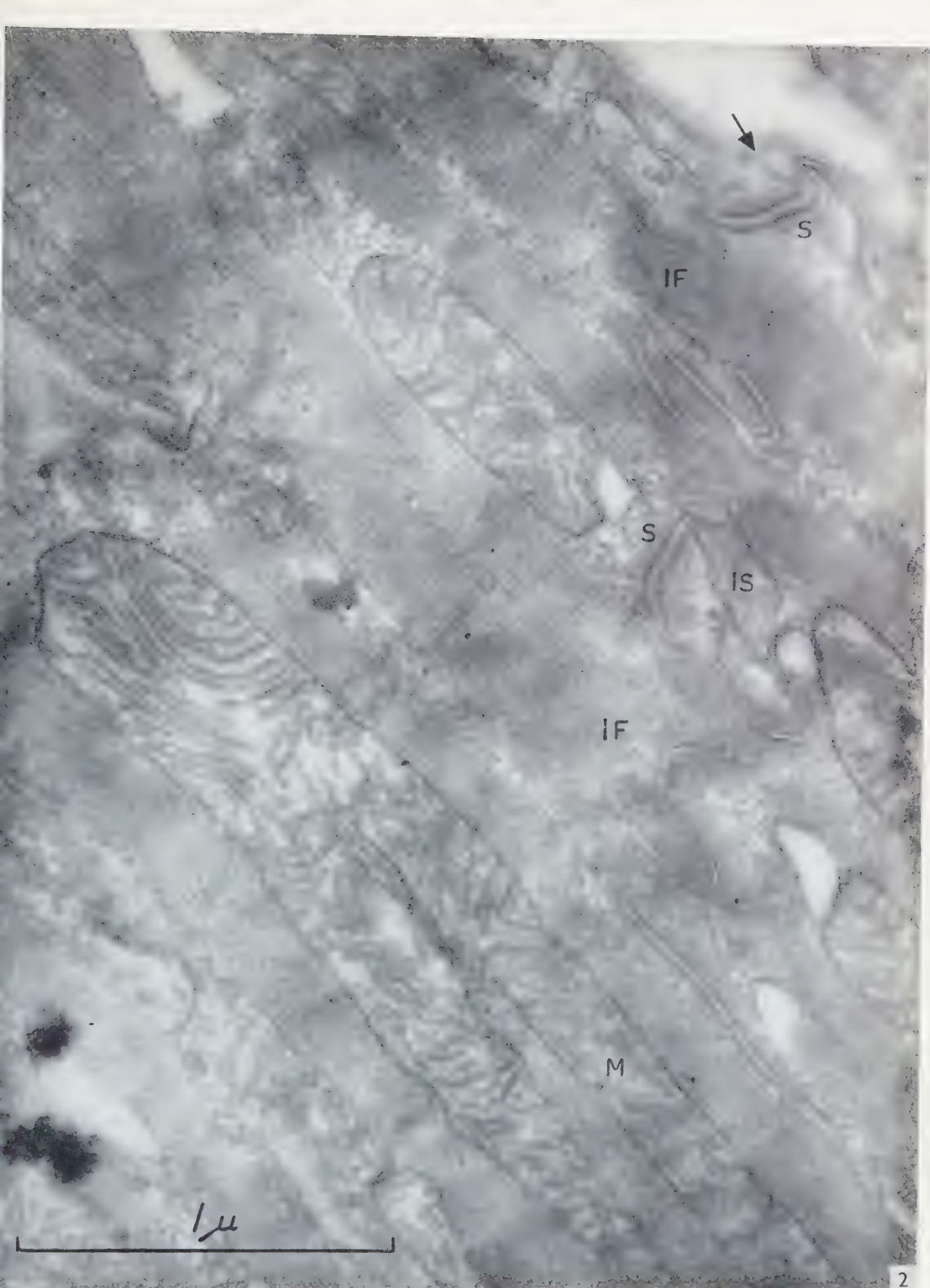


TABLE I
THE WIDTH IN Å OF THE L-SPACE AT THE INTERCALATED DISC

| Species | Interfibrillar region | Intersarcoplasmic region | Specialized region | Longitudinal connecting surfaces |
|------------|-----------------------|--------------------------|--------------------|----------------------------------|
| Mouse | 130 | 130 | 95 | 90 |
| Guinea pig | 70 | — | 130 | 50 |
| Frog | 120 | 120 | — | — |

In the guinea pig a similar triple-layered arrangement has so far been observed only in the specially differentiated zones described below in the intersarcoplasmic regions (Fig. 6). The inner opaque sublayer is frequently diffusely outlined towards the adjacent, rather dense cytoplasm of these zones. The total thickness of the plasma membrane is 80 Å and the thickness of the sublayers is about 20 Å for the opaque layer and 40 Å for the interposed, less opaque layer. In the interfibrillar regions the o-layer of the plasma membrane appears as a single layer measuring 40 Å in thickness.

A similar subdivision into three layers has been observed within certain regions of the plasma membrane in the toad intercalated discs.

In the electron micrographs the cell boundaries are observed running across the branches of the muscle tissue network completely, frequently in a step-wise manner.

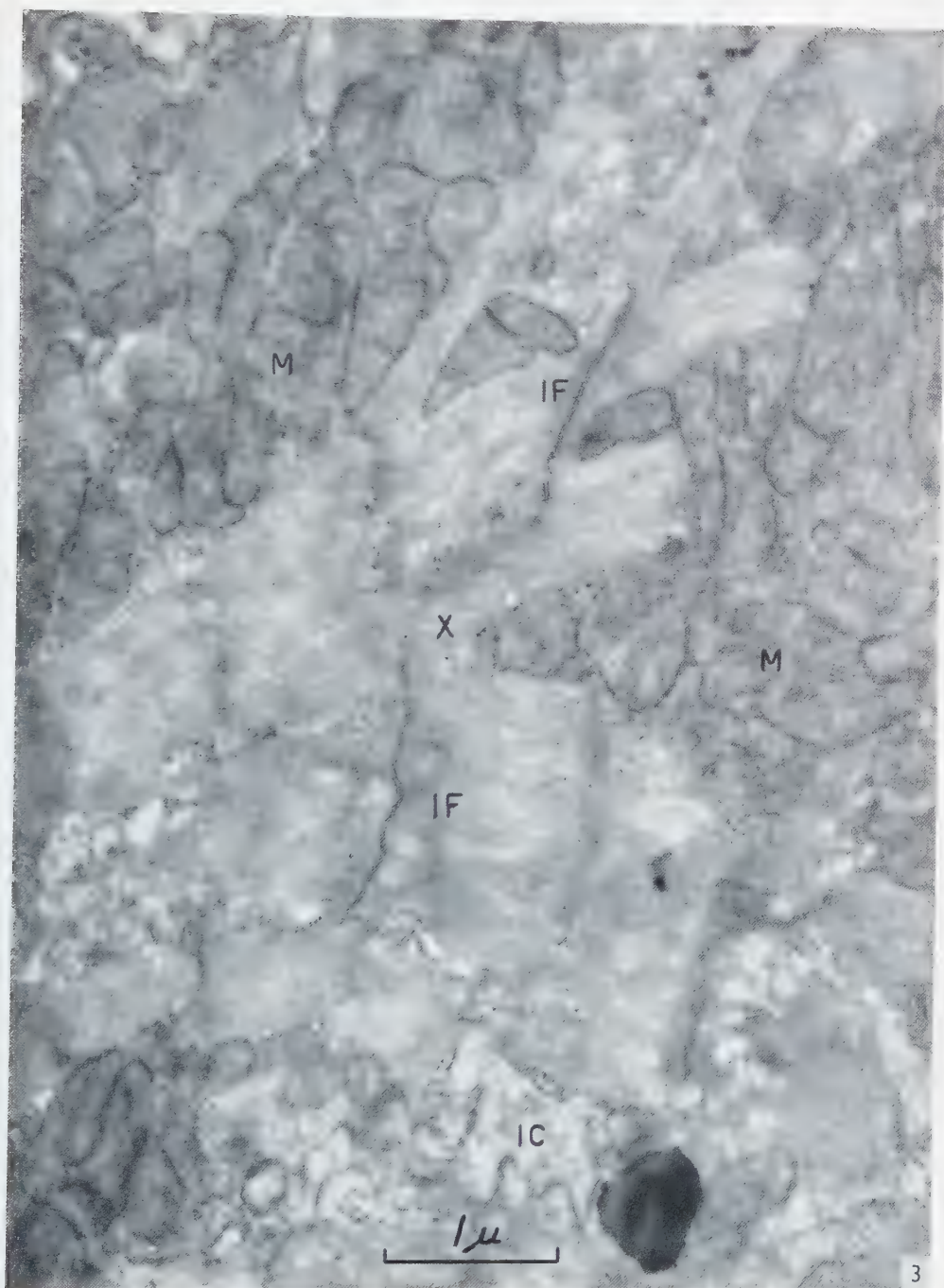
At the edge of the intercalated disc, there is a gap between the o-layers of the plasma membranes corresponding to the l-space which extends across the disc (Figs. 4 and 5). The basement membrane, which bounds the intercellular connective tissue space, bridges this gap as was pointed out by Lindner (13) (Fig. 4).

The cytoplasm at the intercalated discs is particularly dense and differentiated differently in the interfibrillar and the intersarcoplasmic regions. The density varies with the species. It is well pronounced in, for instance, the mouse and the guinea pig but not particularly obvious in the frog. This appears to explain the fact that intercalated discs have been reported as missing in frog cardiac muscle.

In the *interfibrillar regions* of the intercalated disc the cytoplasm contains an irregular network of fine filaments which extends from the o-layer of the plasma membrane to a distance of about 0.1 μ from the boundary (Fig. 4).

The I-band part of the myofilaments merges with this network and appears to be continuous with the filaments of the network.

FIG. 3. Survey picture of section through intercalated disc of frog cardiac muscle. The parallel course of the two plasma membranes of the cell junction can be followed over long distances. IC, intercellular space; IF, interfibrillar region; M, mitochondrion; A, cell boundary oriented obliquely to the plane of the section. Fixation in buffered osmium tetroxide solution. $\times 24,000$.



No filaments bridge the I-space at the boundary. There is therefore no continuity of the myofibrils of adjacent cardiac muscle cells.

The intercalated discs are located at the end of a sarcomere.

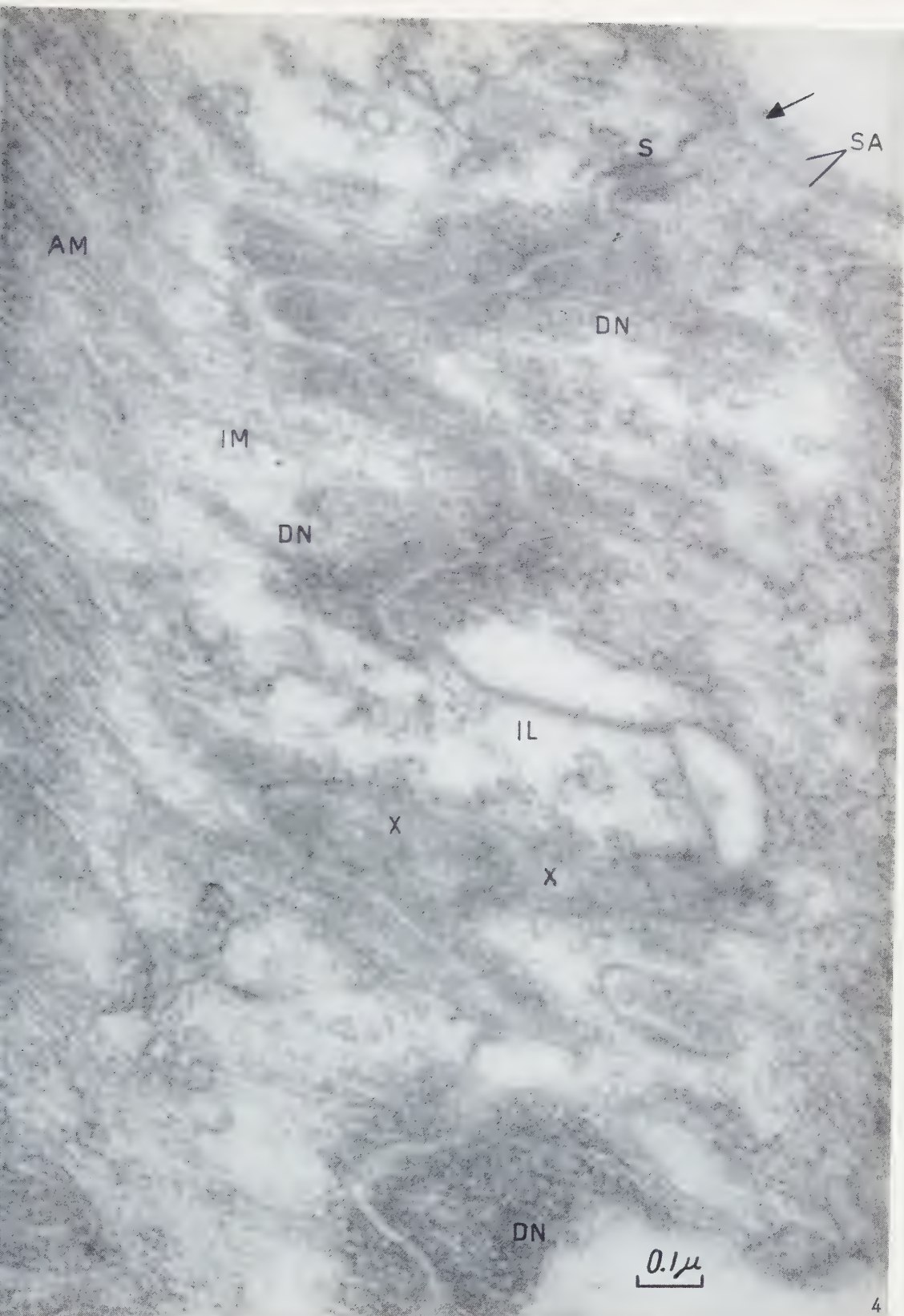
In the *intersarcoplasmic regions* of the intercalated discs, there are rather sharply outlined places where the cytoplasm forms very dense, osmiophilic zones. As to details, there are considerable differences between species regarding the appearance of these specialized regions which here will be referred to as the *S-region*.

In the mouse these dense zones are very sharply outlined and appear in sections, which are cut perpendicularly to the cell boundary, as a rectangularly shaped zone (Fig. 5). The opacity varies periodically in a direction normal to the cell surface. Therefore, the opaque zone appears as multilayered with at least two about 100 Å broad, diffusely outlined, opaque layers. The most peripheral layer is in direct contact with the adjacent opaque sublayer of the plasma membrane. The two opaque layers of the cytoplasm are separated by a slightly less opaque and roughly equally thick zone. The opaque layers appear to consist of densely packed osmiophilic filaments. The I-space, which is interposed between the o-layers of the plasma membrane, appears in these regions particularly opaque, partially due to fine opaque irregular lines crossing this interspace. The width of this interspace is here 95 Å. The rest of the intersarcoplasmic regions appears similar to any ordinary boundary between densely packed cells. The I-space measures here 130 Å. No dense zone is observed in the adjacent cytoplasm in these regions.

In the guinea pig there are numerous areas along the intersarcoplasmic regions which show a specialized structure resembling the one described for the mouse cardiac muscle. These areas are characterized by the triple-layered appearance (Fig. 6) of the o-layer of the plasma membrane and a zone of opaque cytoplasm extending from the inner opaque sublayer and gradually fading towards the interior of the cell. The width of this zone is about 0.1 μ . Within these areas the cell boundary shows a fairly straight or slightly curved course in contrast to the irregular course within the interfibrillar regions. Such especially differentiated areas, S-regions, appear to form units of a fairly regular size. Between these closely arrayed areas, the cell junction appears as consisting of only the o-layers of the two plasma membranes separated by a less opaque interspace.

At the *longitudinal connecting surfaces* of the cell boundary, the two plasma membranes can be in what is interpreted as close contact or they can be separated by an intercellular space (Figs. 1 and 4). In the former case, the o-layers in the guinea pig

FIG. 4. Section through intercalated disc of mouse cardiac muscle showing relations between the myofilaments and the disc network. *A* and *I*, A- and I-bands of the myofibril; *DN*, disc network; *IL*, longitudinal connection; *S*, S-region; *SA*, sarcolemma. Arrow points to the edge of the intercalated disc. Phosphotungstic staining after osmium tetroxide fixation. $\times 106,000$.



cardiac muscle (Fig. 6) are separated by an about 50 Å wide l-space. The intercellular space is common when the separation of the steps of the intercalated disc is larger than the length of one sarcomere. In the guinea pig, S-regions can extend along the longitudinal connecting surfaces.

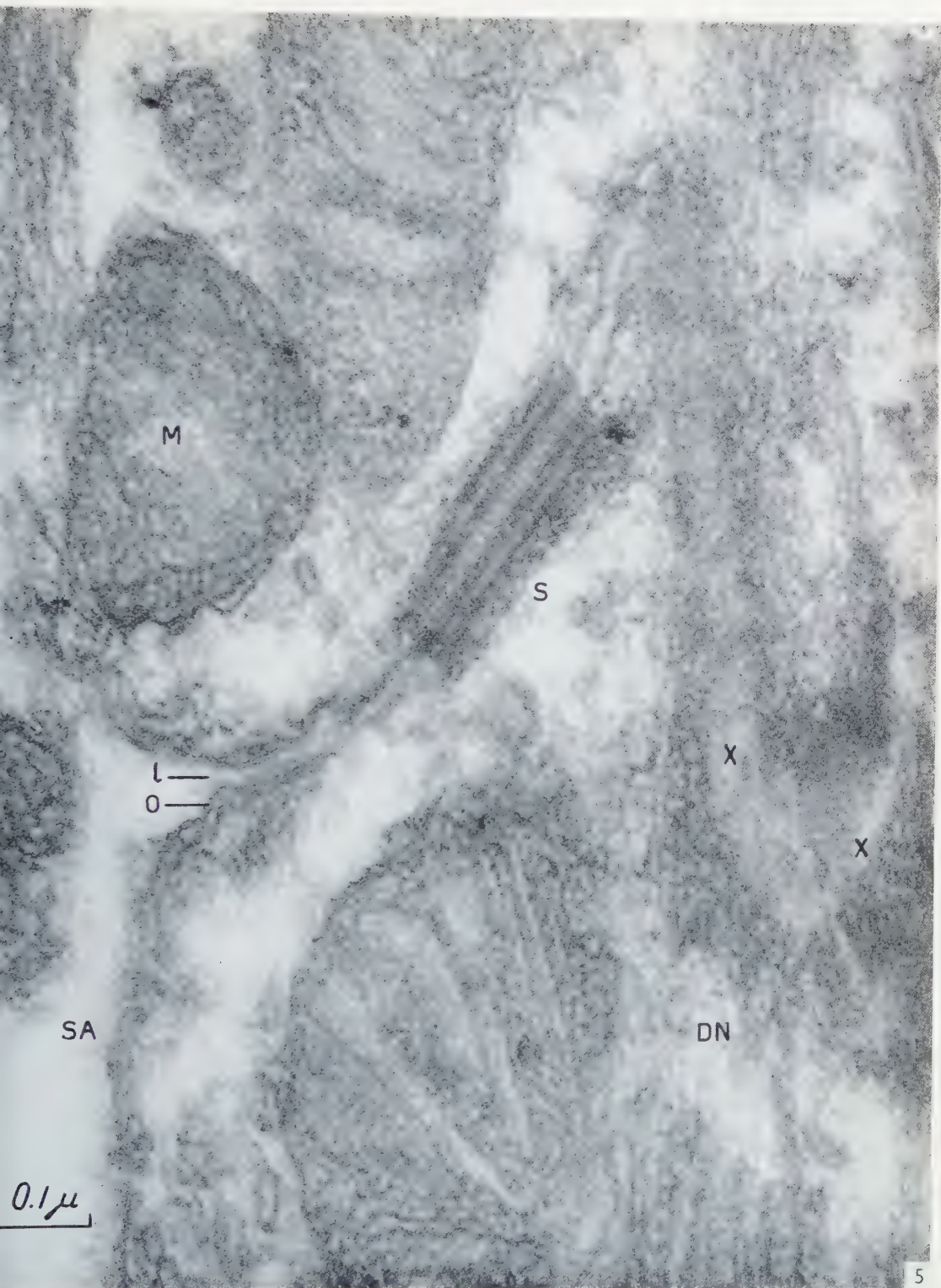
In the mouse cardiac muscle, the two plasma membranes in close contact give rise to a layered structure with five layers, three opaque layers and two less opaque interposed layers. The middle opaque layer is thinner than the two others, which measure 40 Å in thickness. It divides the 90 Å wide interspace between the other two opaque layers into two equal halves. There is no opaque cytoplasm associated with this type of junction between the cardiac muscle cells.

DISCUSSION

That the intercalated discs are located at cell boundaries that are oriented transversally is obvious from the fact that the easily osmium stained, opaque layer of the plasma membrane, the o-layer, which covers the lateral surfaces of the cardiac muscle branches, is continuous with the o-layer observed at the intercalated disc. Furthermore, a less opaque interspace, the l-space, definitely separated the o-layers at the intercalated disc in a similar way as in other cases where two cells are in close contact, for example as in epithelial cells. There is no continuity between the o-layers of two cell territories along the lateral surfaces. The l-space is thus not bridged over by the o-layer of the plasma membrane at the edge of the disc. Fig. 7 gives a schematic presentation of mouse cardiac muscle.

It could be questioned whether these transversally oriented cell boundaries represented complete boundaries or mere folds of the plasma membrane. A complete separation would require that the cell boundary could be followed all the way across the branches of the cardiac muscle tissue. No incomplete separations have been observed. On structural grounds this would exclude that we are dealing with folds. The careful three-dimensional reconstruction made by Aurell (2) from light microscopical pictures also showed that the various areas of intercalated discs cover the whole cross-section of a muscle fiber. The reasonable conclusion must be that the cardiac muscle is divided into discrete cell territories. This is in agreement with the original light microscopical studies by, for instance, Eberth (7). This interpretation was also presented by Tawara (29), v. Palczewska (16), Werner (31) and

FIG. 5. Section through an S-region and the lateral edge of an intercalated disc (mouse) where the plasma membrane changes orientation from covering the lateral surface of a cardiac muscle cell to pass into the intercalated disc area. *DN*, disc network; *L*, l-layer; *M*, mitochondrion; *O*, o-layer; *S*, S-region; *SA*, sarcolemma; *X*, cell boundary oriented obliquely to the plane of the section. $\times 145,000$. (Higher magnification of an area of the electron micrograph shown in Fig. 1.)



Schäfer (21). To this we can add the microdissection experiments of de Rényi (19), the observations of Lewis (12) on heart muscle in tissue cultures and of d'Ancona (1) on the difference in state of contraction on both sides of the disc which all in an indirect way point to the intercalated discs representing zones of discontinuity in the cardiac muscle.

What makes the intercalated discs so easy to observe in light microscopy is the zone of opaque cytoplasm that is associated with the cell boundary. This study has revealed that this zone of cytoplasm is structurally organized in a different way in regions where the cell boundary intercepts the myofibrils and where it is interposed between sarcoplasmic regions.

The wavy course of the cell boundary that is obvious when observing longitudinal sections through the muscle cell branches corresponds to interdigitating processes of the cell surfaces as proposed by Poche and Lindner (17). This interpretation, as illustrated in Fig. 8, is supported by the appearance of the intercalated discs in tangential sections where the plasma membranes form a net-like pattern due to the cross-sections through densely arranged cell processes.

The interruption of the myofilaments at the cell boundary means that we face a mechanical problem which demands a sufficient mechanical strength of the connection between myofilaments and the plasma membrane as well as between the two plasma membranes.

The dense network that has been revealed in this study of the interfibrillar regions means a broadening of the insert at the plasma membrane of the individual myofilaments. The irregular form of the cell surface at the intercalated disc means that the surface area available for this insert is increased and that the direction of the pull of the myofilaments is mainly at a rather oblique angle to the plane of the plasma membrane.

The mechanical requirements at the cell boundary make it justifiable to assume that the space separating the layers of the two plasma membranes is filled with some cementing material. This is also obvious from the fact that this interspace is by far more opaque than the opacity of pure methacrylate. It is proposed that this material consists of the lipid components of the two plasma membranes which are assumed to be in mutual contact. The width of the I-space is about right to accommodate one to two double layers of lipid molecules. This would easily explain the rather marked constancy of the width of this space. It seems, on the other hand, rather unlikely that the I-space would correspond to a water phase containing salt ions.

FIG. 6. Section through intercalated disc of guinea pig cardiac muscle. The difference of the structure of the cell boundary in the interfibrillar (*IF*) and intersarcoplasmic (*IS*) regions is observed. Several S-regions (*S*). *IL*, longitudinal connecting surfaces; *M*, mitochondrion. Fixation in isotonic buffered osmium tetroxide solution. $\times 130,000$.



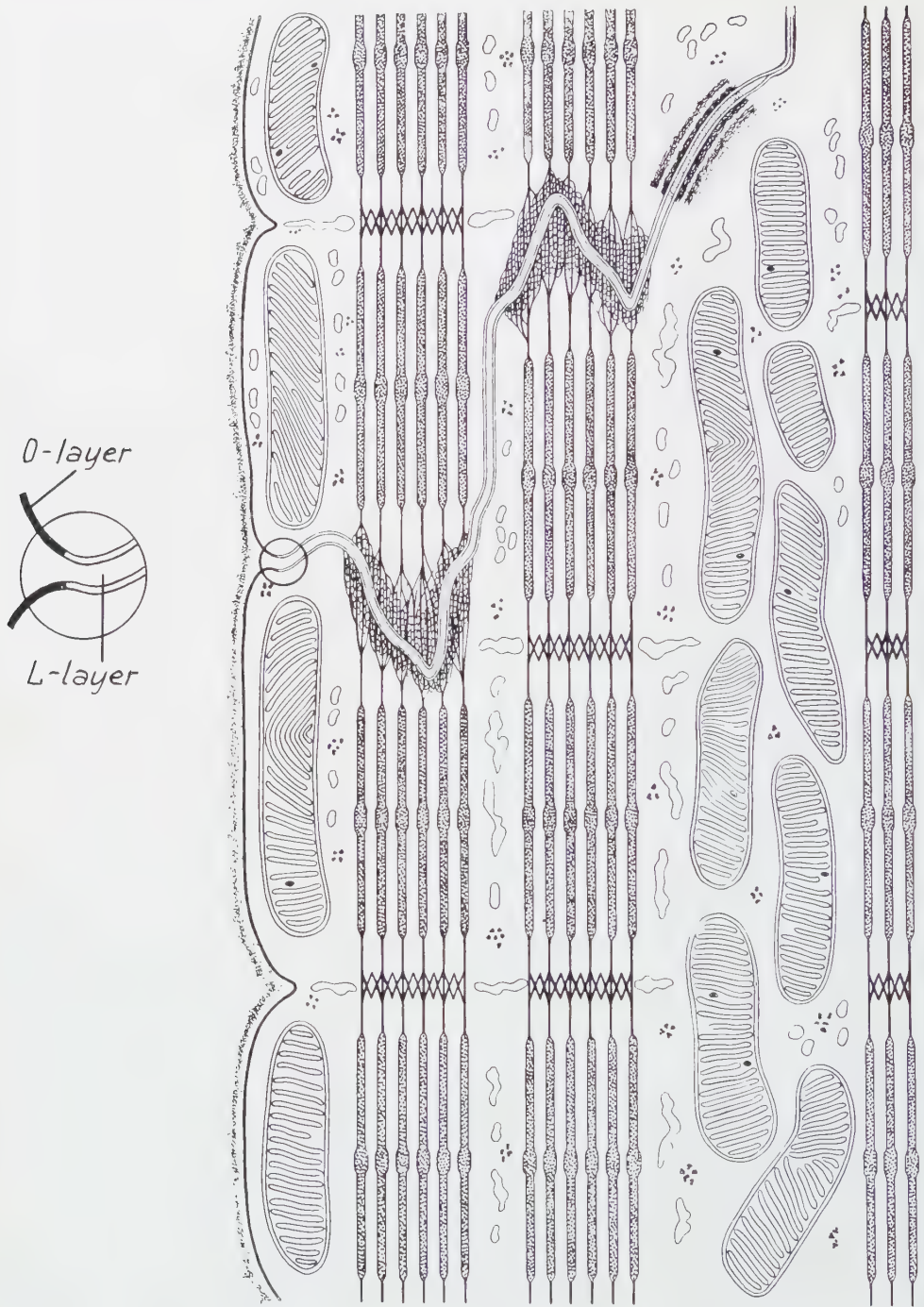


FIG. 7. Schematic drawing of intercalated disc of mouse cardiac muscle.

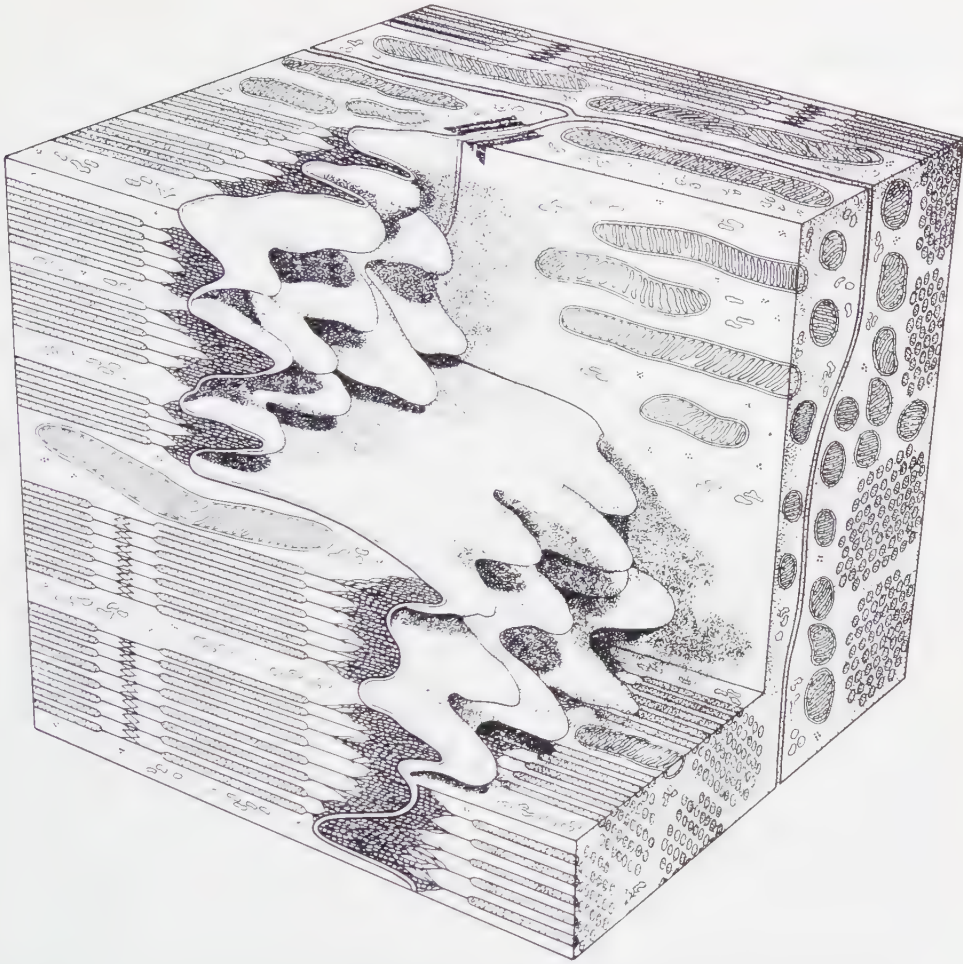


FIG. 8. Three-dimensional presentation of intercalated disc of mouse cardiac muscle. Free reconstruction based on observations made on sections; model has not been reconstructed from serial sections.

The drastic treatment that the old light microscopists used (35–40 % KOH) in order to separate the heart muscle cells at the intercalated discs indicates that the junction is rather firm.

The subdivision of the o-layer of the plasma membrane into two about 25 Å thick, osmiophilic layers and one interposed, less osmiophilic layer can be explained in several ways. It has repeatedly been proposed that the opaque layers observed in electron micrographs indicate the localization of the protein components of the plasma membrane (22–26, 28). The triple-layered appearance might be explained as

due to a preferential staining of the two surfaces of the protein layer where the side chains of the protein molecules are more accessible for the electron stain. A similar subdivision of the 75 Å thick, opaque layer of the plasma membrane was observed by Zetterqvist (32) in the intestinal epithelium and by Robertson (20) in the Schwann cell plasma membrane. Robertson interpreted the triple-layered component as representing the whole plasma membrane including lipids as well as proteins.

In the mouse cardiac muscle, the cell boundary at the longitudinal connecting surfaces showed an arrangement which is similar to the identity period of the nerve myelin sheath with five layers. The intermediate opaque layer can be interpreted to correspond to a layer of proteins. We would then deal with two tightly packed plasma membranes organized according to the scheme proposed by Danielli and Dawson (5, 6) with two protein layers sandwiching a lipid layer. The intermediate layer would represent the fused peripheral protein layers of the two plasma membranes.

Regarding the propagation of excitation through the cardiac muscle the concept of this being a syncytium has fitted well with physiological observations. The propagation of the excitation proceeds thus without noticable synaptic delay.

This would, however, be possible also in the case of a subdivision of the cardiac muscle into cell territories if we assume that the conduction from cell to cell would be due to the action of local currents. The plasma membrane at the cell junction appears structurally organized in a similar way as the plasma membrane covering the rest of the cell surface. This would mean that the cell junction would represent a high ohmic resistance in the local current circuit which would result in a low safety factor for conduction across the cell junction. An additional attenuation of the local excitatory currents would be brought about if the I-space would consist of a water phase containing salt ions. A rather free, unsupported speculation is that the S-regions would represent areas with a lower ohmic resistance and would form paths with a greater safety factor for conduction across the cell junction.

The less opaque interspaces, which are frequently observed in connection with various types of membranes, have been interpreted as representing the lipid component of the membranes (22-26). Regarding the intercalated discs, this interpretation makes it easier to understand functional problems than the assumption that these spaces represent discontinuities filled with an ionic water milieu.

Bourne (3) has proposed that the intercalated discs might act as boosters of the contraction wave spreading through the cardiac muscle. This would give a rôle to his demonstration of a high concentration in the discs of certain enzymes.

REFERENCES

1. D'ANCONA, U., *Protoplasma* **10**, 177 (1929).
2. AURELL, G., Die Glanzscheiben des Herzmuskelgewebes und ihre Verbindungen. Thesis. Almqvist & Wiksell, Uppsala, 1945.
3. BOURNE, G. H., *Nature* **172**, 588 (1953).
4. VAN BREEMEN, V. L., *Anat. Record* **117**, 49 (1953).
5. DANIELLI, J. F., *J. Cellular Comp. Physiol.* **7**, 393 (1936).
6. DANIELLI, J. F. and DAWSON, I. M., *J. Cellular Comp. Physiol.* **5**, 495 (1934).
7. EBERTH, C. J., *Virchow's Arch. pathol. Anat. u. Physiol.* **37**, 100 (1866).
8. VON EBNER, V., *Sitz.ber. Akad. Wiss. Wien, Math.-naturw. Kl., Abt. III* **109**, 700 (1900).
9. ——— *Verh. Morph.-physiol. Ges., Wien*, 1902. *Centralblatt. Physiol.* **16**, 566 (1902).
10. ——— *Köllikers Handbuch der Gewebelehre des Menschen*, Bd. III. Wilhelm Engelmann, Leipzig, 1902.
11. HEIDENHAIN, M., *Anat. Anz.* **20**, 33 (1901).
12. LEWIS, W. H., *Carnegie Inst. Wash., Contrib. Embryol.* **18**, 1 (1926).
13. LINDNER, E., *Z. Zellforsch. u. mikroskop. Anat.* **45**, 702 (1957).
14. MOORE, D. H. and RUSKA, H., *J. Biophys. Biochem. Cytol.* **3**, 261 (1957).
15. MUIR, A. R., *J. Biophys. Biochem. Cytol.* **3**, 193 (1957).
16. VON PALCZEWSKA, I., *Arch. mikroskop. Anat. u. Entwicklungsmech.* **75**, 41 (1910).
17. POCHE, R. and LINDNER, E., *Z. Zellforsch. u. mikroskop. Anat.* **43**, 104 (1955).
18. PRICE, K. C., WEISS, J. M., DAIKICHI, H. and SMITH, J. R., *J. Exptl. Med.* **101**, 687 (1955).
19. DE RENYI, G. S., *Am. J. Med. Sci.* **209**, 270 (1945).
20. ROBERTSON, J. D., *J. Biophys. Biochem. Cytol.* **3**, 1043 (1957).
21. SCHÄFER, E. A., *The Essentials of Histology*, 8th ed. Philadelphia and New York, 1910.
22. SJÖSTRAND, F. S., *J. Cellular Comp. Physiol.* **42**, 15 (1953).
23. ——— *ibid.* **42**, 45 (1953).
24. ——— *Nature* **171**, 31 (1953).
25. ——— *Experientia* **9**, 68 (1953).
26. ——— *International Review of Cytology*, Vol. V, p. 455. Academic Press Inc., New York, 1956.
27. SJÖSTRAND, F. S. and ANDERSSON, E., *Experientia* **10**, 369 (1954).
28. SJÖSTRAND, F. S. and RHODIN, J., *Exptl. Cell Research* **4**, 426 (1953).
29. TAWARA S., *Das Reizleitungssystem des Säugetierherzens*. Gustav Fischer, Jena, 1906.
30. WAGENER G. R., *Sitz.ber. Ges. Beförder. ges. Naturw., Marburg* **7**, 141 (1872).
31. WERNER, M., *Arch. mikroskop. Anat. u. Entwicklungsmech.* **75**, 101 (1910).
32. ZETTERQVIST, H., *The Ultrastructural Organization of the Columnar Absorbing Cells of the Mouse Jejunum*. Thesis. Stockholm, 1956.

Experimental Cell Research SUPPLEMENT 4

CYTOCHEMICAL METHODS WITH QUANTITATIVE AIMS

BIOPHYSICAL AND BIOCHEMICAL APPROACHES

Proceedings of the Symposium held September 27–29, 1956, by the Institute
for Medical Cell Research and Genetics, Karolinska Institutet, Stockholm, Sweden

Edited by *BO LINDSTRÖM, Karolinska Institutet, Stockholm, Sweden*
and *R. BROWN, Oxford University, Oxford, England*

1957, 296 pp., illus., \$9.50

CONTENTS:

The Biophysical Approach

Optical Absorption Methods (pp. 3–102)

Contributions by *L. Åkerman, G. Attardi, T. Caspersson, G. Lomakka, G. Pillat, B. M. Richards, F. Ruch, W. Sandritter, G. Svensson, E. Theiss, B. Thorell, and P. M. B. Walker.*

Methods Involving Interference Microscopy (pp. 103–171)

Contributions by *R. Barer, H. G. Davies, E. M. Deeley, E. F. Denby, D. A. T. Dick, E. Ingelstam, L. P. Johansson, and G. Svensson.*

X-Ray Absorption Methods (pp. 172–237)

Contributions by *L. Carlson, J. G. Clemmons, J. E. Gullberg, O. Hallén, H. Hydén, H. Levi, and S. R. Pelc.*

The Biochemical Approach (pp. 241–293)

Contributions by *E. Berne, S.-O. Brattgård, J. N. Davidson, J.-E. Edström, A. Knobloch, T. Lindqvist, S. Lovtrup, E. Robins, K. Roos, K. Sigroth, C. Vendrely, R. Vendrely, and M. Vialli.*

Author Index–Subject Index.

Experimental Cell Research SUPPLEMENT 5

SUBMICROSCOPIC ORGANIZATION AND FUNCTION OF NERVE CELLS

Proceedings of the Symposium held March 15–22, 1957,
by the Institute of Neurology and Brain Research, Caracas, Venezuela

Edited by *H. FERNÁNDEZ-MORÁN* and *R. BROWN*

Spring 1958, in preparation



ACADEMIC PRESS INC., Publishers

111 Fifth Avenue, New York 3, New York, U.S.A.

Ultrastructure des cinétosomes à l'état de repos et à l'état ciliifère chez un Cilié péritriche

CH. ROUILLER ET E. FAURÉ-FREMIET

*Laboratoires de Médecine expérimentale et d'Embryologie expérimentale
du Collège de France, Paris*

Reçu le 19 mars 1958

La frange ciliaire aborale des Péritriches, définie par Chatton et Lwoff comme « périodiquement récessive et génétiquement continue », permet de démontrer que l'ultrastructure d'un cinétosome au repos est exactement comparable à celle d'un centriole.

On sait que, chez quelques Ciliés, tout ou partie du revêtement ciliaire peut disparaître à certains stades et se reconstituer ultérieurement; dans de tels cas Chatton, Lwoff et leurs collaborateurs (5) ont constaté que les corpuscules basaux ou cinétosomes mis en évidence par les imprégnations argentiques persistent après résorption partielle ou totale des cils vibratiles; la permanence des cinétosomes et leur pouvoir de multiplication assurent la continuité génétique de l'infraciliature.

Chez les Ciliés péritriches, les individus ordinairement fixés par un pédoncule, peuvent se détacher et nager librement grâce au développement temporaire d'une frange ciliaire dite aborale. Chez les individus sédentaires, la place de cette frange est marquée par un léger sillon circulaire transversal portant des cinétosomes; lorsque ces mêmes individus se transforment en migrants, leurs ceinture aborale devient rapidement plus haute par la multiplication des cinétosomes qui se disposent en courtes rangées obliques régulières et serrées; sitôt après on observe la poussée des cils vibratiles qui atteignent, en moins de 10 à 15 minutes, leur taille normale et leur motilité.

Nous avons examiné au microscope électronique l'infraciliature aborale de l'*Ophrydium versatile* chez des individus sédentaires coloniaux et chez des individus migrants libérés.

Chez les sédentaires coloniaux, les cinétosomes apparaissent sous l'aspect de tubes hauts de $450\text{ m}\mu$, larges de $120\text{ m}\mu$ environ (fig. 1). Ils sont formés par une paroi épaisse, très absorbante; à l'intérieur on observe la présence de quelques granules sombres. Les deux extrémités distale ou antérieure et proximale ou postérieure sont apparemment ouvertes; la paroi de l'extrémité postérieure est épaissie sur une hauteur

de 100 $m\mu$ environ et semble entourée à ce niveau par un manchon diffus, peut-être filamenteux, qui la relie à celle des cinétosomes voisins. Les sections transversales de ces cinétosomes montrent nettement dans l'épaisseur de leur paroi 9 épaississements annulaires correspondant à 9 fibrilles longitudinales. Cette structure des cinétosomes cilières décrite ici chez *Ophrydium* est étroitement comparable à celle déjà observée chez d'autres espèces par Sedar et Porter (14), Roth (12), Fauré-Fremiet et collaborateurs (6), etc.

La pellicule périplasmique, séparée de la cuticule par une série d'espaces annulaires transversaux, recouvre l'extrémité antérieure des cinétosomes tubulaires dont elle est parfois séparée par une faible épaisseur cytoplasmique. Au-dessous de l'extrémité postérieure des corpuscules tubulaires, on peut observer la présence de l'un des myonèmes longitudinaux.

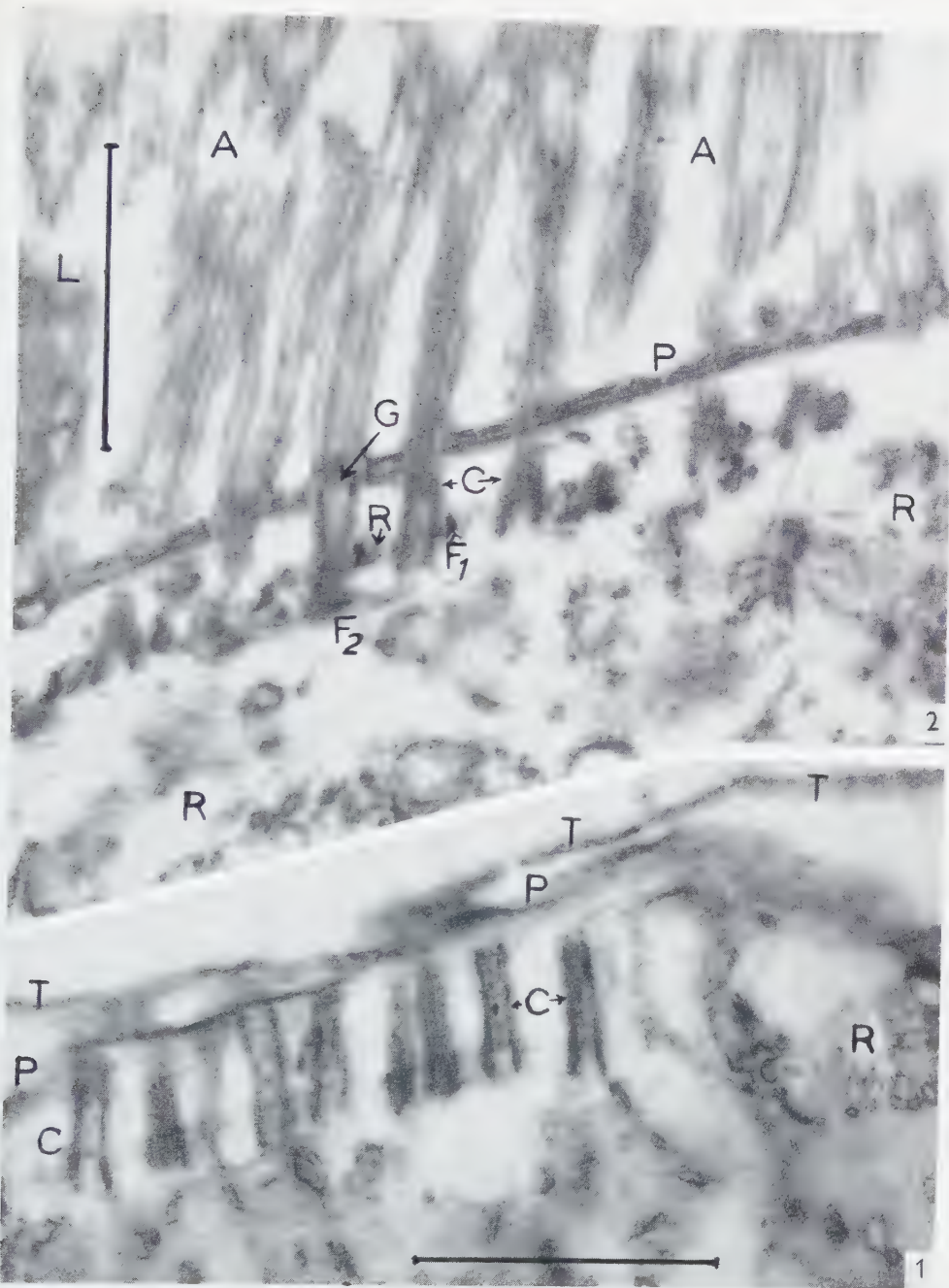
Chez les individus migrants (fig. 2), la cuticule se trouve repoussée de part et d'autre de la ceinture devenue ciliée, en formant de chaque côté une mince lèvre circulaire; la pellicule périplasmique paraît dédoublée, la lame superficielle se soulevant pour former la membrane de chaque cil; les 9 fibrilles pariétales se sont allongées distalement de manière à former le faisceau périphérique du cil; la double fibrille centrale s'est constituée, et commence à l'extrémité antérieure du tube cinétosomien, au niveau d'un corpuscule dense. La question de savoir quelle est l'origine de ce corpuscule apical et de la double fibre qui le prolonge reste ouverte, mais on remarquera que les granulations internes des cinétosomes au repos ont disparu.

La hauteur des tubes cinétosomiens ne s'est pas modifiée, mais peut-être se sont-ils légèrement épaissis; de toute manière, leur nombre s'est accru et ils sont disposés en séries coupant obliquement la hauteur de cette ceinture (fig. 3). Sur chaque série les cinétosomes sont espacés — d'axe en axe — de 200 à 220 $m\mu$, ce qui ne laisse entre leurs parois qu'une faible distance voisine de 50 à 60 $m\mu$. Entre deux séries obliques, l'écartement est plus grand et atteint — d'axe en axe — environ 900 $m\mu$.

Ces cinétosomes cilières sont reliés les uns aux autres par un double système de fibrille croisées à angle droit. Le long de chaque série oblique court, à mi-hauteur des

FIG. 1. Infraciliature de la frange aborale au repos chez *Ophrydium versatile*. Les cinétosomes *C* sont dressés au-dessous de la pellicule épiplasmique *P* surmontée par la cuticule *T*. La forme tubulaire des cinétosomes au repos est comparable à celle d'un centriole; la seule marque d'une différenciation est donnée par le léger renforcement de leur extrémité interne ou proximale. Présence irrégulière de granules denses dans la cavité centrale des cinétosomes. *R*, reticulum endoplasmique. 41.000

FIG. 2. Frange aborale après formation des cils *A*. La cuticule est repoussée sur la lèvre bordante *L*; la pellicule épiplasmique est dédoublée et son feuillet externe, lui-même dédoublé, est en continuité avec la paroi du cil. La double fibrille centrale se termine sur un corpuscule apical *G*. A mi-hauteur des cinétosomes, section transversale des fibres *F*₁ et des canalicules du reticulum endoplasmique *R*; à la base, section oblique des fibres *F*₂. 41.000



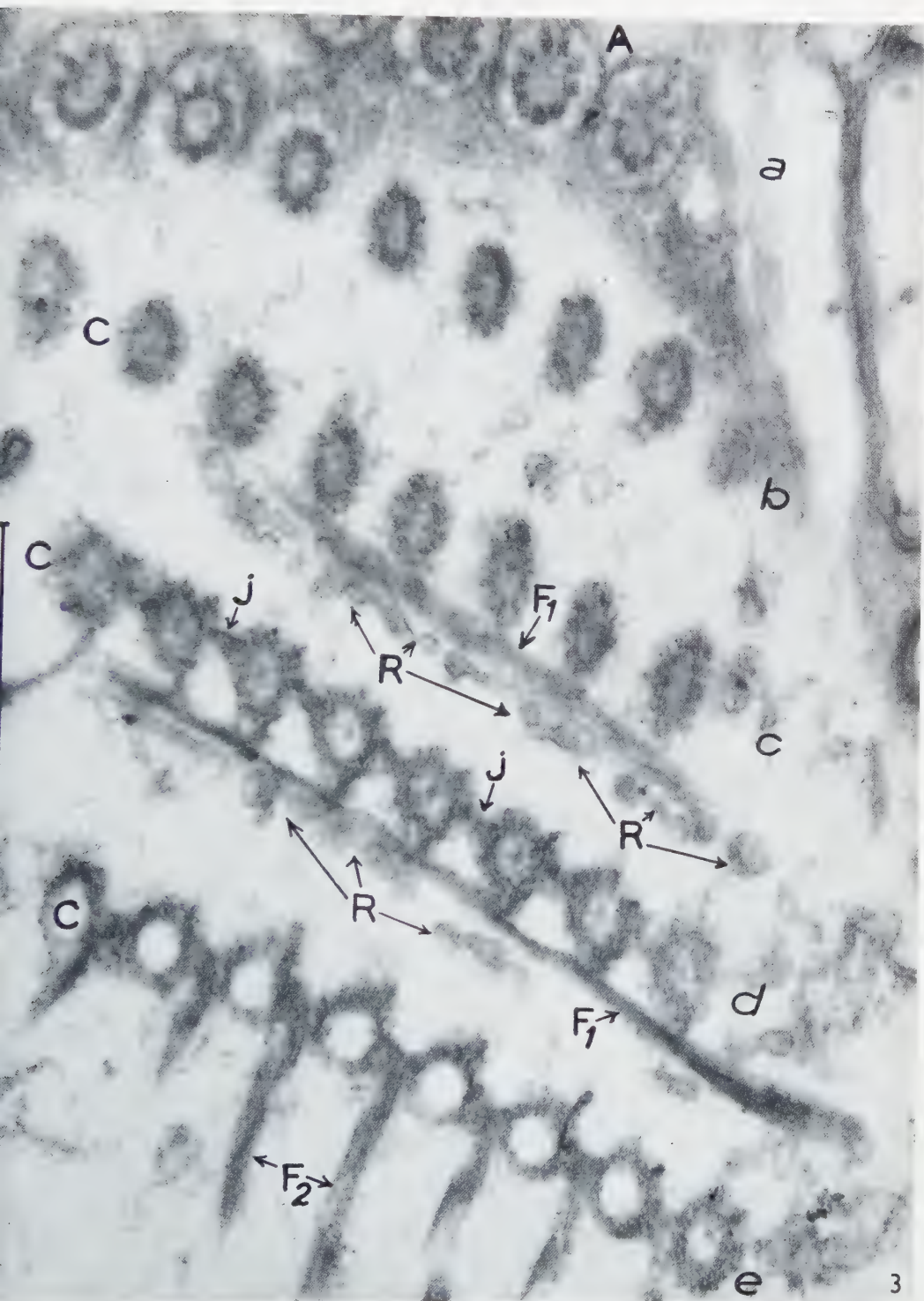
cinétosomes auxquels un épaississement la relie étroitement, une fibre apparemment plate, large de 80 à 90 m μ , épaisse de 30 à 40 m μ (fig. 2 et 3, F_1). Des canalicules à paroi mince et lisse, larges de 200 à 600 Å, variqueux et irrégulièrement contournés, sont accolés à cette fibre oblique, et se rattachent probablement au reticulum endoplasmique de Porter et Palade (fig. 2 et 3, R).

Le second système, à peu près perpendiculaire au premier, se situe sur un plan plus profond car les fibres qui le constituent sont reliées par un épaississement latéral à la base de chaque cinétosome (fig. 2 et 3, F_2). Il est possible que les fibres basales F_2 correspondent au cinétodesme et leur aspect composite (fig. 3, F_2) évoque la structure constatée chez d'autres espèces par Metz et ses collaborateurs (9, 10).

La comparaison des cinétosomes à l'état de repos et à l'état ciliifère montre que la formation du cil comporte 1° la continuité des 9 fibrilles périphériques du faisceau ciliaire avec les 9 fibrilles pariétales du cinétosome; 2° la néoformation de la double fibrille centrale et de son corpuscule basilaire; 3° l'apparition d'un double système de fibres en rapport avec les régions moyenne et basale des cinétosomes.

On constate d'autre part que le cinétosome au repos est étroitement comparable aux centrioles décrits dans diverses cellules animales par Bernhard et de Harven (3, 7), par Bessis et Breton-Gorius (4) et par Amano et Tanaka (1, 2). Cette conclusion n'est pas nouvelle puisque l'identité de nature des centrioles et des corpuscules ciliaires était postulée des 1897 par Henneguy (8) et que l'identité de leur ultrastructure est aujourd'hui démontrée par de Harven et Bernhard (7) et par Porter (11). De Harven et Bernhard insistent sur le rôle de ces corpuscules dans la synthèse et la morphogénèse des protéines fibreuses. Nos observations chez *Ophrydium* sont en faveur de cette hypothèse qui semble trouver une confirmation expérimentale dans les recherches biochimiques récemment résumées par Seaman et Gottlieb (13). Ces auteurs, en effet, auraient isolé de *Tetrahymena*, lysés aseptiquement par la digitonine, des cinétosomes à l'état pur. Ceux-ci, mis en présence d'un mélange d'acides aminés, auraient provoqué la formation d'une substance donnant la réaction du biuret.

FIG. 3. Section presque tangente à l'infraciliature aborale, dont les différents niveaux apparaissent successivement, grâce à une légère obliquité. *a*, sections transversales des bases ciliaires montrant la membrane et le faisceau fibrillaire. *b*, idem à gauche; à droite, section de la partie supérieure ou distale des cinétosomes; noter les épaississements pariétaux correspondant aux 9 fibrilles périphériques. *c*, sections des parties supérieure et moyenne des cinétosomes *C*; en étroit contact avec leur paroi, on voit la fibre F_1 et, au long de celle-ci, le réseau canaliculaire R . *d*, niveau immédiatement inférieur montrant encore les mêmes structures; noter les interconnexions *J*. *e*, niveau inférieur ou proximal des cinétosomes montrant les interconnexions et les fibres F_2 du système basal. Leur aspect irrégulier traduit peut-être une structure composite due à la superposition de segments fibrillaires parallèles. Le grand axe du Cilié est à peu près parallèle à la largeur de la figure, mais le sens antéro-postérieur correspondant est indéterminé. 72.000



BIBLIOGRAPHIE

1. AMANO, S., *Cytologia (Tokyo)* **22**, 193 (1957).
2. AMANO, S. et TANAKA, H., *Acta Haem. Jap.* **20**, 319 (1957).
3. BERNHARD, W. et de HARVEN, E., *Compt. rend.* **242**, 288 (1956).
4. BESSIS, M. et BRETON-GORIUS, J., *Bull. microscop. appl.* **7**, 54 (1957).
5. CHATTON, E., LWOFF, A. et LWOFF, M., *Compt. rend.* **188**, 1190 (1929).
6. FAURÉ-FREMIET, E., ROUILLER, CH. et GAUCHERY, M., *Bull. Soc. Zool. France* **81**, 168 (1956).
7. DE HARVEN, E. et BERNHARD, W., *Z. Zellforsch. u. mikroskop. Anat.* **45**, 378 (1956).
8. HENNEGUY, L. F., *Arch anat. Microsc.* **1**, 481 (1897).
9. METZ, CH. B., PITELKA, D. R. et WESTFALL, J. A., *Biol. Bull.* **104**, 408 (1953).
10. METZ, CH. B. et WESTFALL, J. A., *Biol. Bull.* **107**, 106 (1954).
11. PORTER, K. R., *Harvey Lectures Ser.* **51**, 175 (1957).
12. ROTH, L. E., *J. Biophys. Biochem. Cytol.* **3**, 985 (1957).
13. SEAMAN, G. R. et GOTTLIEB, S. H., *J. Protozool.* **4**, Suppl., 11 (1957).
14. SEDAR, A. W. et PORTER, K. R., *J. Biophys. Biochem. Cytol.* **1**, 583 (1955).

The Submicroscopic Structure of the Inner Segments of the Rods and Cones in the Retina of *Uroloncha Striata* Var. *Domestica* Flower

G. YASUZUMI, O. TEZUKA AND T. IKEDA

Laboratory for Electron Microscope Research, Department of Anatomy, Nara Medical College, Kashihara, Nara Pref.

Received March 20, 1958

The membranes surrounding the proximal portion of the inner segments of the rods and cones of an *Uroloncha* eye, previously thought to be needle-like fibrillar baskets, are the limiting membranes themselves. They are characterized by duplicated pecten-like margins. So far as is known, such structure has never been observed with the light microscope or with the electron microscope. The average distance between each projection, in transverse section, was about $0.24\ \mu$; the width of the projection, $40\text{--}70\ m\mu$; the length of the projection, $0.35\text{--}0.67\ \mu$. However, the projections become shorter distally until at the most distal portion of the inner segment they are totally lacking. The rod is always surrounded by a regular or an irregular semilunar profile. The inner segment of the rod is a bulge of cytoplasm containing mitochondria, rough-surfaced endoplasmic reticulum (α -cytomembranes), numerous fine vesicles and an intermediate electron dense body without a limiting membrane. These cytoplasmic elements are characteristically defined. The intermediate electron dense body is composed of small circular or elongated vesicles embedded in a homogeneous substance. This body is discussed in comparison with previous histochemical studies.

The fine structure of glia fibers in the retina of various animals has long been a subject of particular interest in ophthalmology and cytology. In the period from 1851 through 1900, Müller (14–16), Kölliker and Müller (9–10), Remak (22), Schultze (24–29), etc. made conspicuous contributions to our understanding of the glia fibers in the retina of several vertebrate species. After a gap of nearly two decades, distinguished by an almost complete absence of active interest in the finer morphology of the retina, a period of research reopened (6–8, 11–13, 20, 37–40), which attempted to apply to the retina Río-Hortega's concept of the neuroglia of the central nervous system (23).

Polyak, in a summary statement on glia fibers (20), records that the top-most portion of Müller's radial fiber has been considered to be a fibrillar basket (Faserkorb) as termed by Schwalbe (30). The fibers resemble short, thick needles with slightly bulging

sides. They are broad at their bases and taper into long, thin points which seem gradually to become lost in the thin membranes stretching farther up toward the pigment epithelium. The fibers also appear to be merely the ribs of the fibrillar baskets or cups, between which membranes of extreme thinness are expanded like the web stretched between the toes of aquatic birds. These membranes, together with the fibers, accordingly form molds where the bases of the rods and cones are accommodated.

Recently, the submicroscopic structure of the visual cells of the retina of such vertebrates as guinea pig and perch (5, 31-35), albino rat and mouse (1-3) and frog (41) has been studied intensively by electron microscopy and their characteristic internal structure well defined. However, the peculiarities of the inner segments of the rod and cone of the avian retina have so far attracted little attention. The present study attempts to define their structure, as revealed by electron microscopy.

MATERIAL AND METHOD

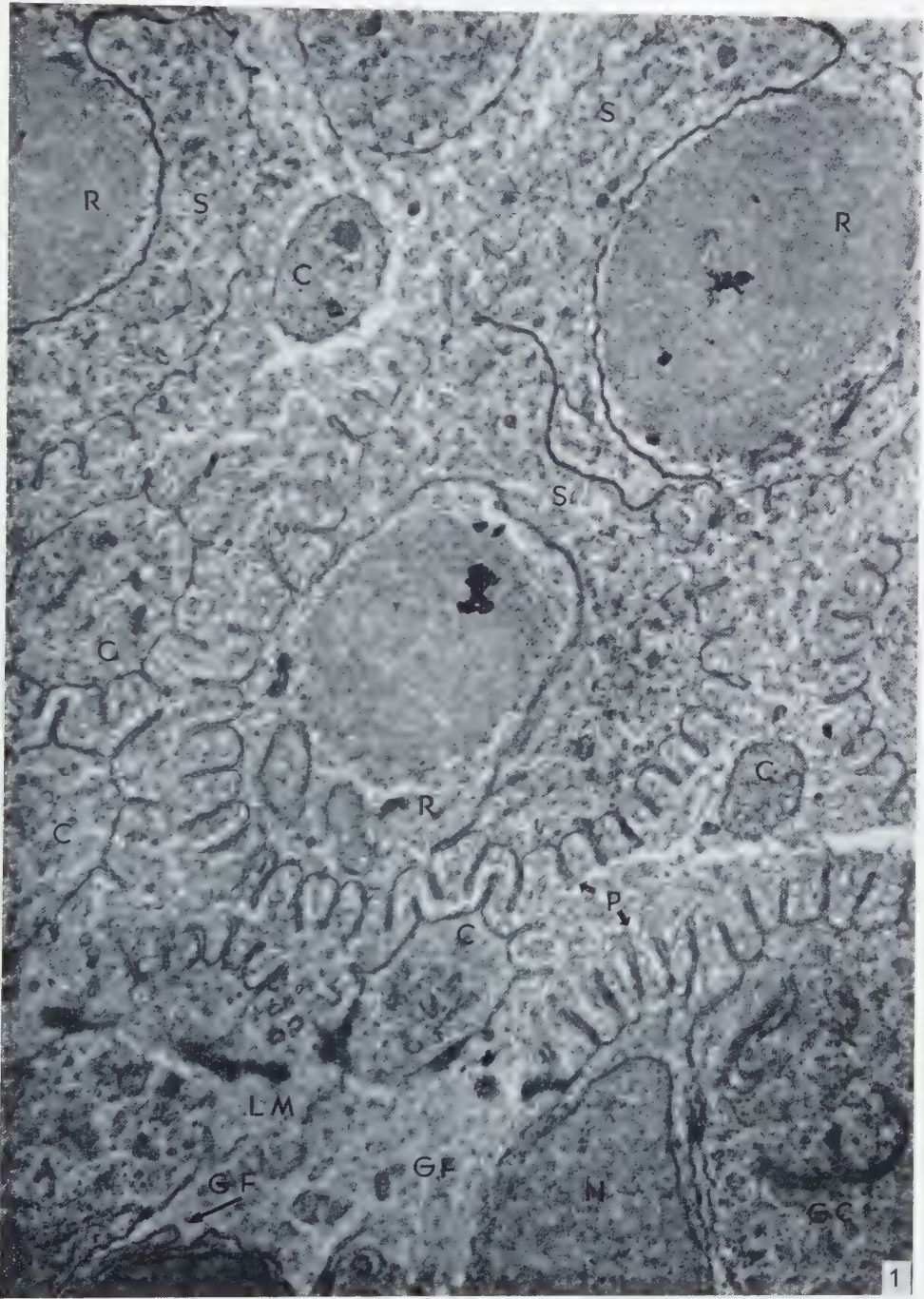
Adult *Uroloncha striata* var. *domestica* Flower were used in the present study. Whole eyes were fixed for 2 hours in 1% osmium tetroxide buffered (pH 7.3) with veronal-acetate and then pieces of retina were removed and fixed for an additional 1 hour (18). After fixation, the tissue was dehydrated directly, without washing in distilled water, in a graded series of ethyl alcohol. The tissue, embedded in a mixture of *n*-butyl and methyl methacrylate, was cut with glass knives on a Shimadzu microtome. All sections were examined, without removing the embedding plastic, in an Akashi electron microscope, model TRS-50.

RESULTS

The receptors of the *Uroloncha* retina consist of rods and cones. The rod of *Uroloncha* measures, in the light microscope, about $4.5\ \mu$ in width and the cone 1.0-1.5 μ .

The inner segments of rods is shown in slightly oblique cross-sections in Figs. 1 and 2. The rods, surrounded by a thin membrane with toothed, wheel-like projections, can be observed outside the dense, discontinuous outer limiting membrane. Nuclei, cytoplasm and twisted glia fibers are observed in the lower part of the figures, which show slightly oblique cross-sections through the outer nuclear layer. It is interesting that a part of the inner segment of the rod is surrounded by a regular or an irregular navicular profile, which is provided with long projections. These projections become

FIG. 1. A slightly oblique cross-section through the *Uroloncha* retina, showing a dense outer limiting membrane (LM), and profiles of rods (R) and cones (C) surrounded by a membrane with pecten-like margins (P). The rod is surrounded by a regular or irregular semilunar profile (S). The rod is composed of fine circular profiles embedded in an intermediate electron dense substance. In a lower portion of the figure, the outer nuclear layer can be seen in a narrow space where nuclei (N) of rods, Golgi complex (GC) in the rod cell and twisted glia fibers (GF) are demonstrated. $\times 15,000$.



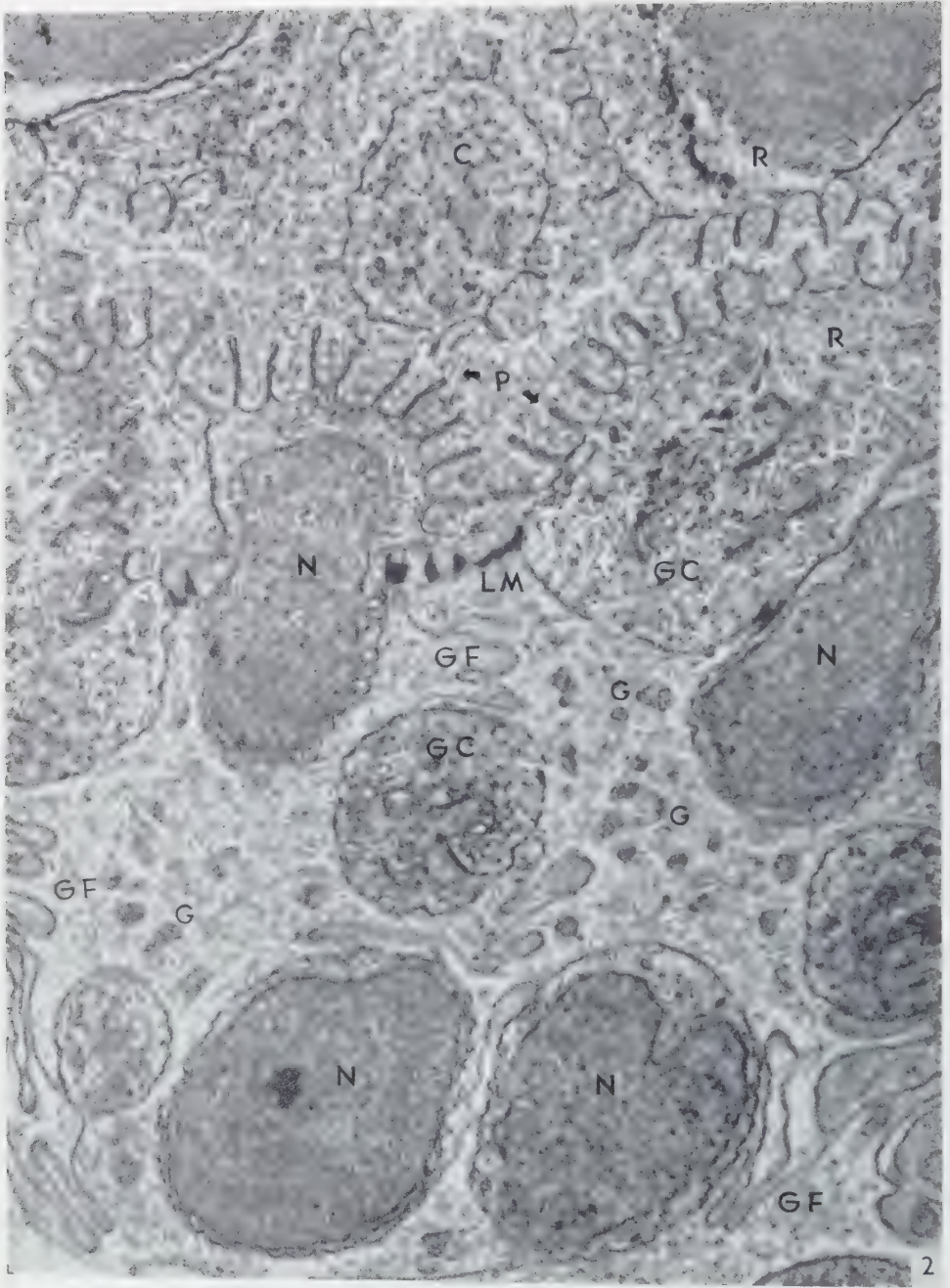


FIG. 2. In the upper part of the figure can be seen clearly the tooth-like projections (*P*), in the middle part the Golgi complex (*GC*) in the rod and cone cell, and in the lower part the rod cell nuclei (*N*) and twisted glia fibers (*GF*). The intermediate electron dense granules (*G*) can be seen in the fine granulated intercellular substance of the outer nuclear layer. $\times 15,000$.

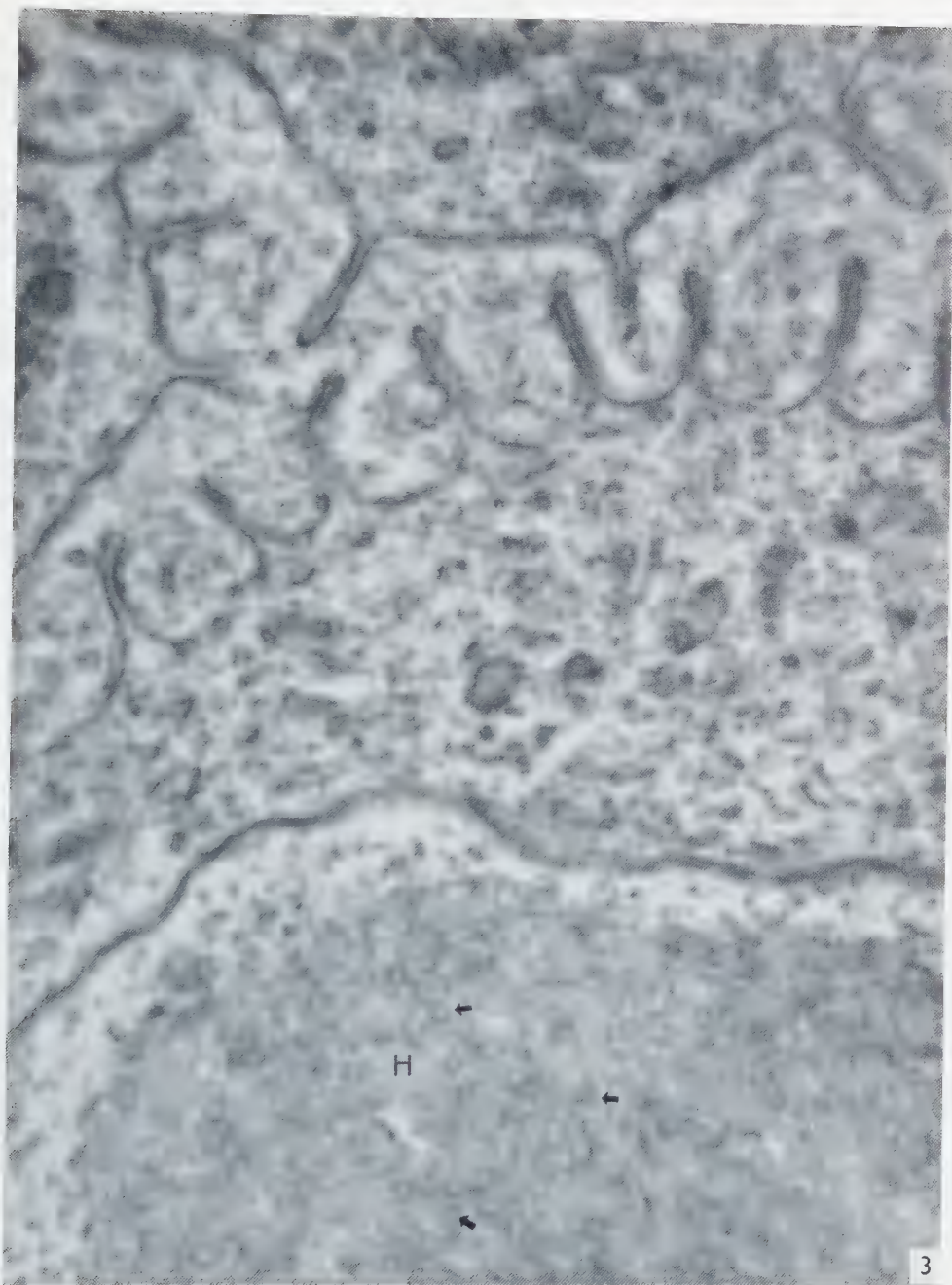


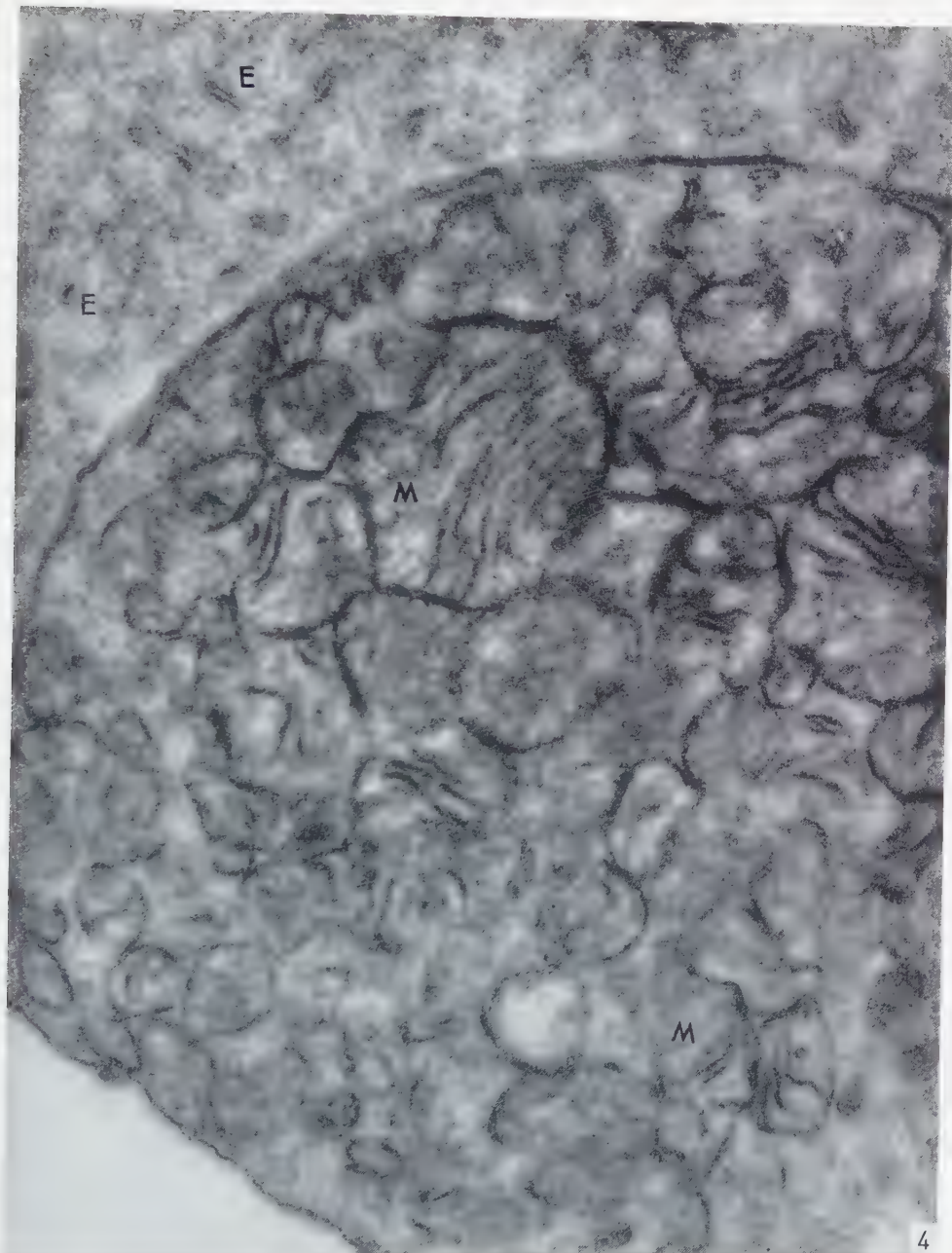
FIG. 3. Two projections are wedged into a single, corresponding space. Fine circular profiles (arrows) embedded in an intermediate electron dense, homogeneous substance (*H*) can be seen in the inner segment of the rod. $\times 39,500$.

progressively shorter toward the distal portion of the inner segments until they are totally lacking at its most peripheral portion (Figs. 1 and 6). The projection of the membrane in the proximal portion of the inner segment measures $0.33\text{--}0.67\ \mu$ in length and $40\text{--}70\ \mu$ in width. It consists of a double membrane; each member of the pair measures about $80\text{--}150\ \text{\AA}$ thick. The projections are spaced at intervals of $0.17\text{--}0.50\ \mu$. Cross-sections through the proximal part of the rod demonstrate 40 to 50 projections. In general, the projections between the adjacent membranes are observed to mesh with each other like gears, with an exception where two or three projections are wedged into a single, corresponding space (Figs. 1–3). The inner segment of the cone is also surrounded by the pecten-like margin at its proximal portion. The space between the rods and cones in their inner segment layer is filled with fine vesicular elements (Figs. 1–3).

The visual cells in the outer nuclear layer are connected by twisted glia fibers which occasionally cover the visual cells (Fig. 2). The intercellular area is filled with a homogeneously granulated substance, as well as with regularly or irregularly round masses, $0.17\text{--}0.28\ \mu$, with an intermediate density. In profile, the nucleus of the rod cell occupies most of the cell and leaves only a narrow area of cytoplasm. The cytoplasm of the cone contains the Golgi complex and circular profiles of the endoplasmic reticulum (21). The Golgi complex consists of a few pairs of membranes in a more or less parallel arrangement and with a wavy course which have been called the γ -cytomembranes by Sjöstrand (36). In association with these membranes a number of vacuolar spaces of varying size are found. No membrane with pecten-like margins is observed in the outer nuclear layer.

The inner segment of the rod is characterized by definite regional differences in the cytoplasm. This is demonstrated, in detail, in cross-sections of the rods (Figs. 3–6). The proximal portion presents an appearance of fine vesicles packed in a homogeneous substance of an intermediate electron density. In the distal portion of the inner segment of the rod, the portion without the pecten-like margins, the cytoplasm is filled with mitochondria, rough-surfaced endoplasmic reticulum (19) or α -cytomembranes (36) and fine circular profiles. In the half-moon-shaped area attached to the inner segment of the rods, a number of fine circular profiles and a small amount of endoplasmic reticulum can be found. No mitochondria are present here (Figs. 4 and 5). The inner segment of the rod and the semilunar portion attached to it are separated by double membranes. Each membrane measures $40\ \text{\AA}$ in width and the intervening space measures $80\ \text{\AA}$ in width (Fig. 5).

FIG. 4. The inner segment of the rod is occupied with compressed mitochondria (*M*) of varying sizes. The semilunar profile consists of a small amount of rough-surfaced endoplasmic reticulum (*E*) and fine vesicular elements. $\times 41,000$.



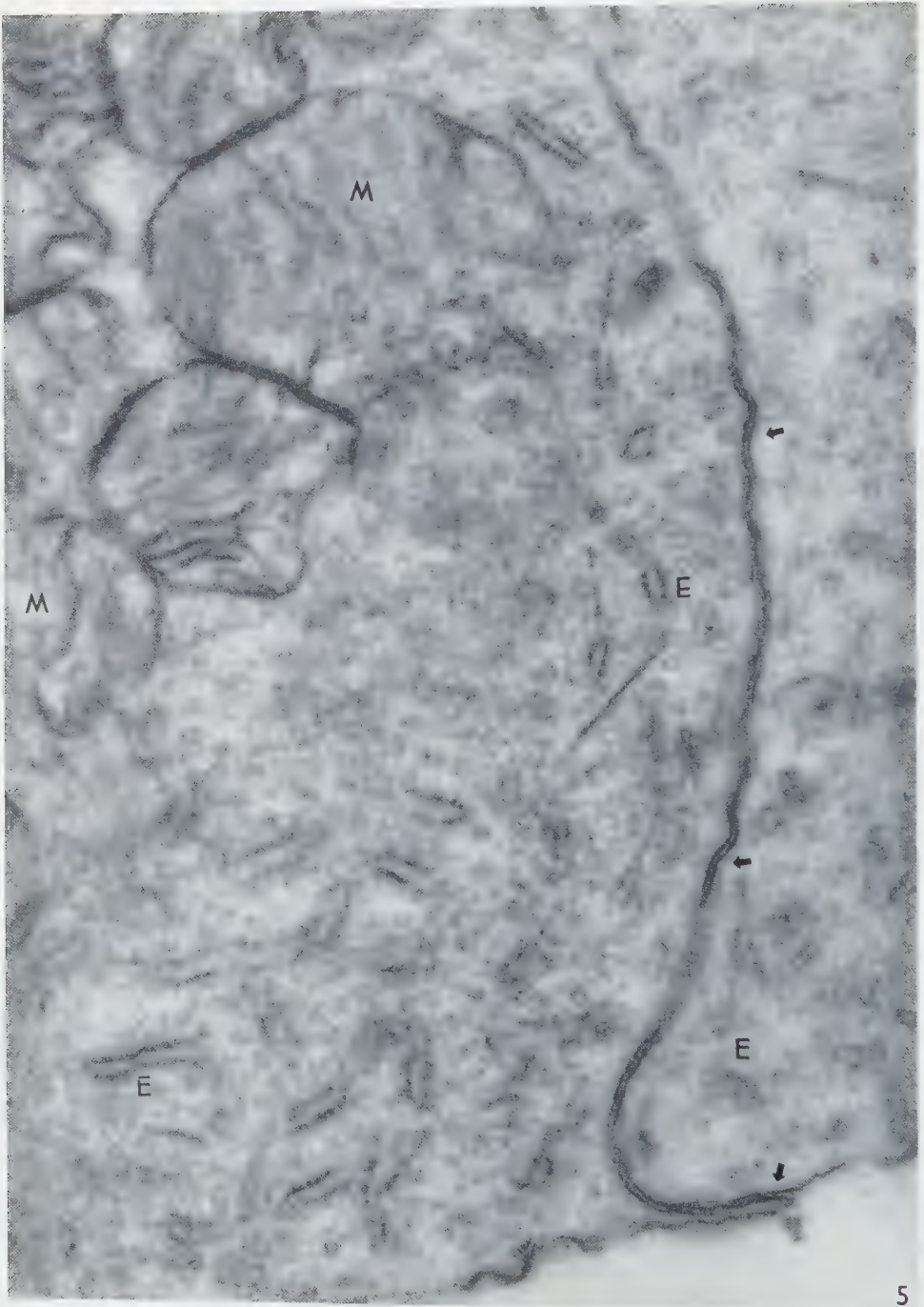


FIG. 5. The internal substance of the inner segment of the rod is characterized by two separated structures, mitochondria (*M*) and rough-surfaced endoplasmic reticulum (*E*). The rod and the semi-lunar profile are separated by a space 80 Å in width (arrows). $\times 63,000$.

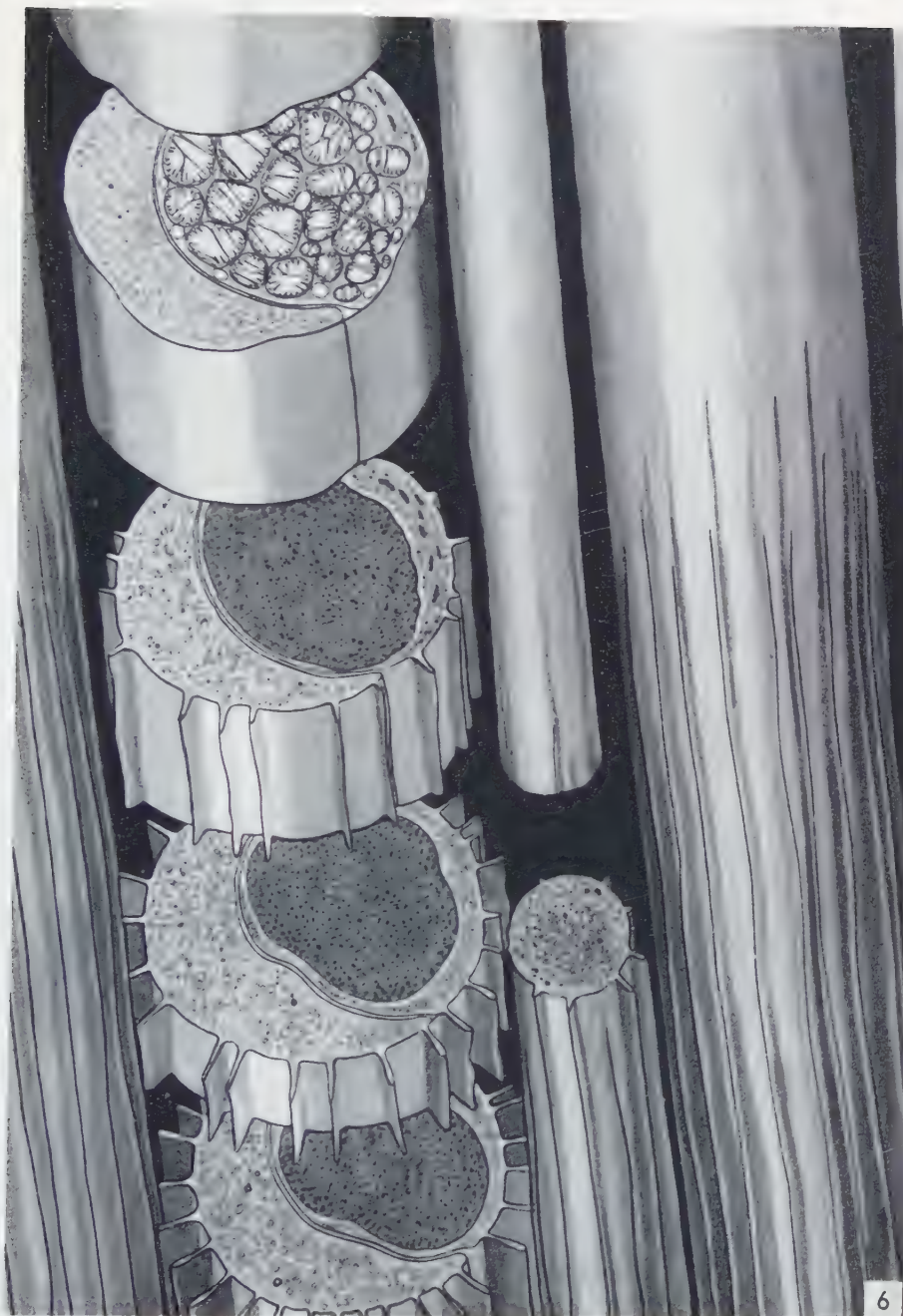


FIG. 6. Schematic drawing of a three-dimensional reconstruction of the structure of the inner segment of the rod and cone layer in the retina of the *Urolophora*.

In the present study, many longitudinal sections through the inner segment layer were obtained. However, they have not been illustrated here because they have shown only cylindrical profiles with no pecten-like margins.

DISCUSSION

Kolmer (11) has shown a schematic illustration of rods and cones of various vertebrates; the rods and the cones of *Alauda* measure about 4μ and 1μ in width respectively, and the relationship between the width of the rods and the cones in *Uroloncha striata* var. *domestica* Flower is similar.

A peculiar structure has been demonstrated in cross-sections through the inner segment layer of the rod. About one-third or one-half of the rod profiles is enveloped with a membrane with pecten-like margins; the remaining rod profiles have a smooth surface and are surrounded by a regular or irregular semilunar profile with tooth-like projections. It is interesting that the projections between the adjacent membranes mesh with each other like gears, with an occasional exception where two or three projections are wedged into a single, corresponding space. The cones, which have a smaller size in width than that of the rods, are provided with pecten-like margins at their basal portions. Characteristically, the projections become shorter as the distal portion of the inner segments of the rods and cones is approached until at their most distal portion the projections are totally lacking.

The limiting membrane with pecten-like margins, depicted here, seems to be referable to the fibrillar baskets (Faserkorb) observed previously with the light microscope (4, 6-16, 22, 24-30, 37-39). What was observed following silver and gold impregnation procedures does not coincide in general feature with what is described above because of limited resolving power of the ordinary light microscope. The outer limiting membrane, according to Schultze (24-29), consists of the broadened upper ends of Müller's fibers, which give off at the top a great number (forty or fifty) of fine, stiff fibrils. These fibrils form baskets surrounding the inner and probably the outer segment of the rods and cones. The projections surrounding the inner segment of the rods and cones, observed here, seem to correspond to these fibrils.

It is evident that the thin membrane with pecten-like margins should not be considered a simple supporting cell membrane but rather a complex system in which expansion and reduction of the inner segment of the rods and cones can occur easily.

Within the inner segment of the rods and cones, the following components can be observed: a homogeneous, intermediate electron dense body, which has no limiting membrane, involving small, circular or elongated profiles; rough-surfaced endoplasmic reticulum scattered in a fine vesicular ground substance; mitochondria with the typical internal structure. Mitochondria have never been found between the inner

segment of the rods and cones and the outer nuclear layer, or in the semilunar profile attached to the rod inner segment. The inner segments of the rods and cones of *Uroloncha* seem to show a more or less different structure from that reported for other animals (1-3, 5, 31-35, 41). Mitochondria with the typical internal structure are found compressed, showing varying sizes. The endoplasmic reticulum with its associated granules is disposed in a fine vesicular matrix without showing a regular array. The mitochondria and the endoplasmic reticulum are distributed in different areas and never intermingled.

The relationship between the ultrastructure observed here and its possible chemical make-up deserves special consideration. So far as is known, this type of fine structure has not been previously described. The electron microscopic pattern seems to show that the tubular system is embedded in lipid-like, homogeneous masses. A similar region has been observed histochemically in other birds by previous workers. Kolmer (12) has revealed oil-spheres in *Uria aalge* and Ohashi (17) has described glycogen and pyronine-positive, Nissl body-like basophilia in *Passer montanus saturatus* Stejneger. It is difficult to decide whether all of these components or only some of them are responsible for the electron microscopic pattern observed here. The final proof for this correlation can be expected in the near future with the establishment of electron staining and by comparison with histochemically defined materials.

REFERENCES

1. DE ROBERTIS, E., *J. Biophys. Biochem. Cytol.* **2**, 329 (1956).
2. — *ibid.* **2**, No. 4, Suppl., 209 (1956).
3. DE ROBERTIS, E. and FRANCHI, C. M., *J. Biophys. Biochem. Cytol.* **2**, 307 (1956).
4. DOGIEL, A. S., *Arch. mikroskop. Anat.* **41**, 612 (1893).
5. FINEAN, J. B., SJÖSTRAND, F. S. and STEINMANN, E., *Exptl. Cell Research* **5**, 557 (1953).
6. FORTIN, E. P., *Compt. rend.* **183**, 452 (1926).
7. — *Arch. oftalm., Buenos Aires* **5**, 301 (1930).
8. KAJIKAWA, K., *Albrecht von Graefes Arch. Ophthalmol.* **112**, 260 (1923).
9. KÖLLIKER, A. and MÜLLER, H., *Verhandl. Physik.-Med. Gesells., Würzburg* **3**, 316 (1852).
10. — *ibid.* **3**, 336 (1852).
11. KOLMER, W., in v. MÖLLENDORF, W. (Ed.), *Handbuch der mikroskopischen Anatomie des Menschen*, Bd. III, Teil 2, p. 318. Springer, Berlin, 1936.
12. — *ibid.* Bd. III, Teil 2, p. 431.
13. MENNER, E., *Z. Zellforsch. u. mikroskop. Anat.* **11**, 414 (1930).
14. MÜLLER, H., *Verhandl. Physik.-Med. Gesells., Würzburg* **2**, 216 (1851).
15. — *Z. wiss. Zool.* **3**, 234 (1851).
16. — *ibid.* **8**, 1 (1856/57).
17. OHASHI, Y., *Hokuetsu-Igakuzasshi* (in Japanese) **41**, 119 (1926).
18. PALADE, G. E., *J. Exptl. Med.* **95**, 285 (1952).
19. — *J. Biophys. Biochem. Cytol.* **1**, 59 (1955).
- 20 — 583562 *J. Ultrastructure Research*

20. POLYAK, S. L., *The Retina*. The University of Chicago Press, Chicago, 1941.
21. PORTER, K. R., *J. Exptl. Med.* **97**, 727 (1953).
22. REMAK, R., *Deut. Klin.* **6**, 177 (1854).
23. RÍO-HORTEGA, P. D., *Trabajos lab. invest. biol., Madrid* **14**, 269 (1916).
24. SCHULTZE, M., *Arch. mikroskop. Anat.* **2**, 165 (1866).
25. — *ibid.* **2**, 175 (1866).
26. — *ibid.* **3**, 215 (1867).
27. — *ibid.* **3**, 371 (1867).
28. — *ibid.* **3**, 404 (1867).
29. — *ibid.* **5**, 379 (1869).
30. SCHWALBE, G., in GRAEFKE, A. and SAEMISCH, E. T. (Eds.), *Handbuch der gesamten Augenheilkunde*, Bd. I, p. 321. Engelmann, Leipzig and Springer, Berlin, 1874.
31. SJÖSTRAND, F. S., *J. Cellular Comp. Physiol.* **33**, 383 (1949).
32. — *ibid.* **42**, 15 (1953).
33. — *ibid.* **42**, 45 (1953).
34. — *J. Appl. Phys.* **24**, 117 (1953).
35. — *Proc. Stockholm Conf. Electron Microscopy*, 1956, p. 194. Almqvist & Wiksell, Stockholm, and Academic Press Inc., New York, 1957.
36. — *Physical Techniques in Biological Research*, Vol. III, p. 241. Academic Press Inc., New York, 1956.
37. STRICHT, O., *Arch. Biol., Liège* **32**, 173 (1922).
38. — *ibid.* **32**, 345 (1922).
39. — *Compt. rend. soc. biol.* **74**, 266 (1922).
40. UYAMA, Y., *Folia Anat. Japonica* **4**, 389 (1926).
41. YAMADA, E., *Acta Anat. Nipponica* (in Japanese) **32**, 77 (1957).

A Method for Preparing Individual Cells for Electron Microscopy

K. DEUTSCH and A. E. G. DUNN

Department of Zoology, University of Edinburgh

Received March 28, 1958

In the course of an investigation into the mitotic apparatus, we wished to cut electron microscope thin sections of cells of a known stage in the mitotic cycle. We therefore developed a method which permits the embedding and sectioning of single cells and we have used it successfully on *Paramecium aurelia* and a small soil amoeba, *Hartmannella astronyxis*.

The organism was dehydrated and transferred into a drop of methyl methacrylate on a cavity slide. The end of a glass tube (diameter about 5 mm) was drawn into a short capillary (diameter 0.1–0.2 mm), and the end of the capillary was sealed off. It was then filled with a prepolymerised standard mixture of methacrylate and spun on a centrifuge with a swing-out head to remove any air bubbles. The organism was then transferred with a braking micropipette into the capillary under a dissecting microscope. Two micromanipulators, one for the capillary, the other for the pipette, were used for this purpose. The capillaries were again spun on a centrifuge to ensure that the organism moved to the tip of the capillary. The samples were fully polymerised at a temperature of about 45°C. The polymerised cylinder with the organism in it could be easily removed by breaking off the capillary after scratching slightly with a diamond. A hole (diameter about 0.2 mm) was drilled into the conically shaped end of a short Perspex rod (diameter of rod about 7.5 mm, length about 12 mm). The cylinder was inserted into the hole and firmly cemented by adding a small drop of monomer. Only the tip of the cylinder (about 0.3–0.5 mm) containing the specimen protruded from the hole, and the sample was now ready for sectioning.

For sectioning, a Porter–Blum ultramicrotome was used, but any good ultramicrotome would presumably be suitable for this purpose. The tip of the specimen block was brought as near as possible to the edge of the knife, using the fine adjustment. The distance of the specimen from the edge of the knife was then measured using a stereoscopic microscope (magnification about 100×) with a micrometer eyepiece. The advance of the microtome was set at 0.5 μ , and the appropriate number of sections were cut off until the specimen was reached, e.g. if the distance was 15 μ , 30

sections were taken off. The knife was drawn back, and another part of the edge selected for producing thin sections. The knife edge was again brought as near as possible to the specimen by the same procedure. The specimen advance was then set to cut sections of suitable thickness. When the top layer of the specimen had been studied, a number of thick sections were taken off, and a deeper layer was ready for further investigation. In this way we proceeded until all strata of the specimen which were of interest had been explored.

Another method which might also be useful is very similar to one designed by Borysko (1). A small drop of a prepolymerised standard methacrylate mixture was deposited on a cavity slide. The drop spread somewhat, and the organism was transferred into the drop. The cavity was covered with a coverslip, and polymerisation was finished at a temperature of about 48°C. After polymerisation the thin sheet of polymer containing the organism could easily be removed from the slide, and prepared for sectioning as described by Borysko.

The authors would like to express their gratitude to the Melville Trust for Cancer Research, who provided the electron microscopy laboratory in which the work was carried out.

REFERENCE

1. BORYSKO, E., *J. Biophys. Biochem. Cytol.* **2**, Suppl., 15 (1956).

Recherches ultrastructurales sur le virus de la leucémie érythroblastique du poulet

E. L. BENEDETTI ET W. BERNHARD

Institut de Recherches sur le Cancer, Villejuif (Seine). Directeur : Prof. Ch. Oberling

Reçu le 28 mars 1958

Cette étude porte sur l'examen au microscope électronique de 47 cas d'érythroblastose aviaire et sur de nombreux témoins normaux. Dans la moelle de 37 de ces poulets et dans la rate de 21 d'entre eux, des particules virales de 80 μ de diamètre environ ont pu être mises en évidence. Dans les cas de leucémie avancée avec un fort pourcentage de cellules paraérythroblastiques, 90 % des animaux ont été trouvés positifs.

Les particules virales sont situées soit dans les espaces intercellulaires, soit dans des vacuoles intracytoplasmiques des cellules réticulaires, des macrophages et des paraérythroblastiques.

Certaines des vacuoles contenant ces particules sont d'origine *mitochondriale*. Les inclusions vacuolaires sont moins fréquentes dans les paraérythroblastiques que dans les cellules réticulaires. D'autres vacuoles intracellulaires contenant à la fois des particules virales et des débris de globules rouges (lipides, substance ferrugineuse), semblent révéler un *processus de phagocytose* qui intéresse également les particules virus.

En plus, on peut montrer l'existence, au niveau de la membrane cellulaire, d'un phénomène de bourgeonnement, probablement en rapport avec la production de virus.

Les mêmes particules ont été retrouvées en grand nombre, intactes ou partiellement désintégrées dans le plasma des poulets leucémiques.

Par ailleurs, elles sont morphologiquement identiques aux virus mis en évidence dans d'autres affections néoplasiques du poule.

Enfin, elles ont également été mises en évidence dans les tissus de 12,5 % des cas témoins considérés comme normaux. La signification de cette observation est discutée. Les auteurs admettent qu'il s'agit là soit d'un virus du groupe lymphomatose cliniquement latent, soit d'un autre virus inactif, et qu'il existe chez le poulet une vaste famille d'agents filtrables d'aspect morphologique identique, mais biologiquement distincts les uns des autres. L'importance d'une telle constatation d'un point de vue doctrinal est soulignée.

La nature virale de la leucose aviaire a été démontrée déjà en 1908 par Ellermann et Bang (27) qui l'ont reproduite expérimentalement par injection intraveineuse d'ultrafiltrats de tissu ou plasma leucémique.

Aussitôt après l'injection, le virus disparaît du sang et ne peut réapparaître qu'après une période de latence (46) dont la durée est en rapport avec la dose infectieuse initiale (22). L'apparition des cellules leucémiques dans le sang va de pair avec une forte virémie. En même temps, la moelle et les autres tissus deviennent également très infectieux (28).

En accord avec la démonstration biologique de l'étiologie virale de la leucose confirmée par de nombreux travaux, Beard, Sharp et coll. (4, 49) ont isolé et purifié par ultra-centrifugation du plasma leucémique, l'agent infectieux dont ils ont décrit pour la première fois l'aspect au microscope électronique. Ces auteurs ont employé la méthode de l'ombrage métallique.

Se basant sur la même technique, Harel et Vigier (37) sont ensuite arrivés à des résultats semblables. Les virus apparaissent sous forme de particules sphéroïdes mais aplaties après le séchage, dont le diamètre varie de 80 à 120 m μ .

Grâce à la technique de coupes ultra-fines, il a été possible de décrire avec plus de détails la structure interne des particules virales dans les tissus hématopoïétiques (8) et dans le plasma leucémique (10).

Dans la myéloblastose et l'érythroblastose, le plasma contient des particules dont l'aspect morphologique est identique (10); cependant, les deux virus diffèrent entre eux par leurs caractères biochimiques et immunologiques ainsi que par leur cytotropisme (3, 14).

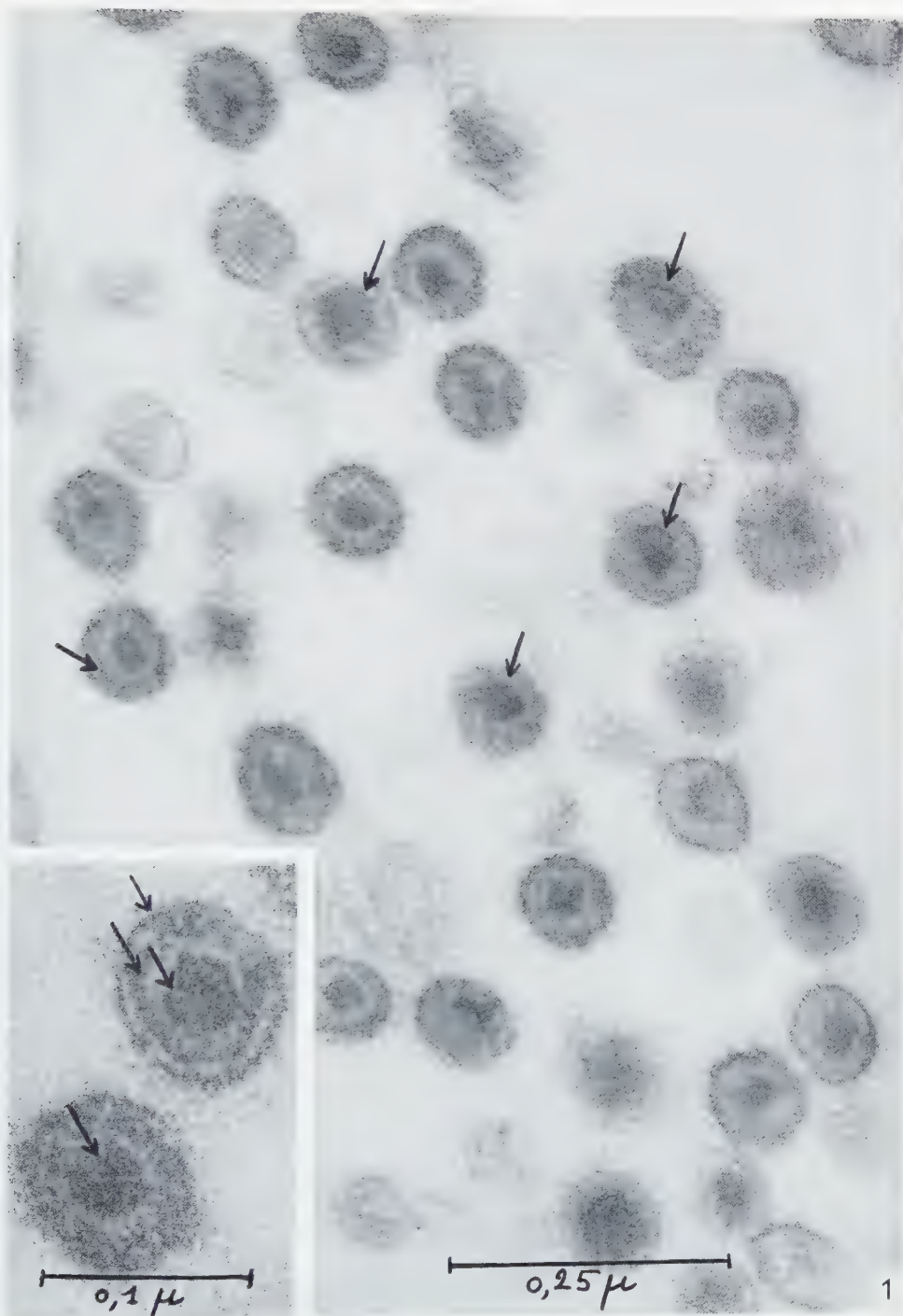
Dans une observation préliminaire qui a porté sur la rate et la moelle d'animaux érythroleucémiques, nous avons signalé que des particules virales sont localisées surtout dans les cellules réticulaires et histiocytaires du tissu splénique ou médullaire (8).

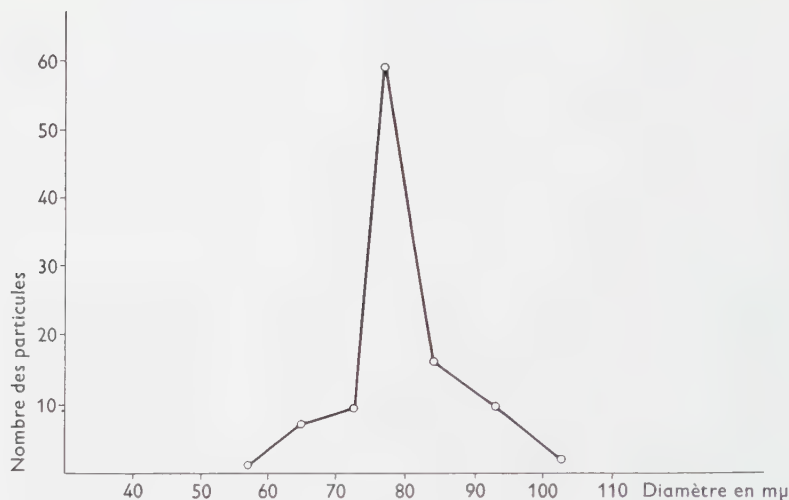
Le but de la présente étude est d'apporter plus de détails sur la morphologie du cycle évolutif de l'agent infectieux dans les tissus hématopoïétiques. L'histogénèse et la description de l'ultrastructure des cellules leucémiques est rapportée ailleurs (9).

MATERIEL ET TECHNIQUE

Nos recherches concernent la moelle, la rate, les cellules leucémiques du sang circulant ainsi que le plasma de poulets de différents âges atteints d'érythroblastose. Le tableau I indique le nombre d'animaux leucémiques de souches variées, ayant été examinés au microscope électronique.

FIG. 1. Aspect typique des particules virus mises en évidence dans l'érythroblastose et vues à un fort grossissement. Les flèches (\rightarrow) indiquent la présence d'une ou de deux membranes internes cernant le nucléoïde central. 159.000 et 290.000





GRAPHIQUE 1. Distribution de la taille des particules.

TABLEAU I

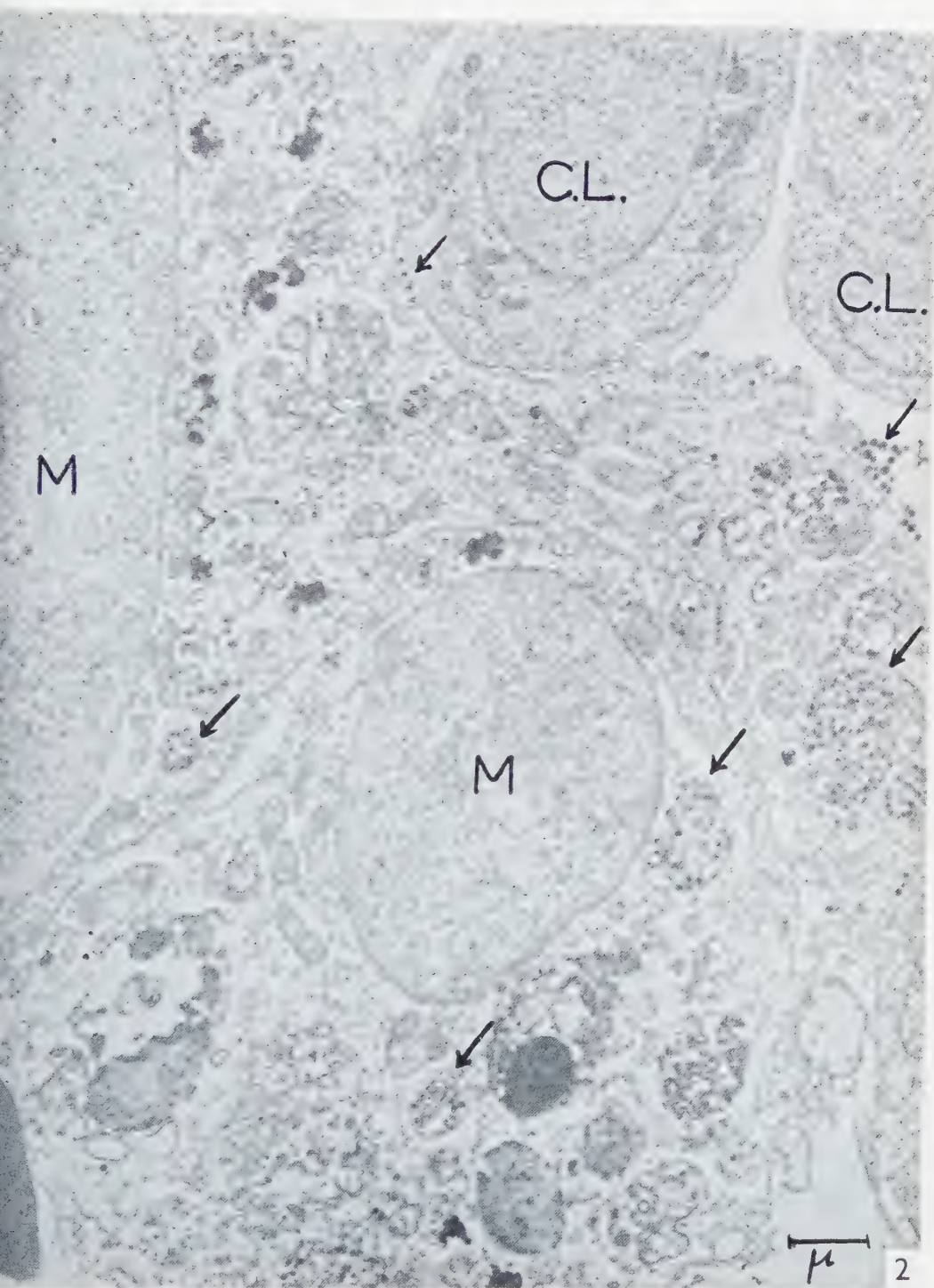
| Souche | Nombre d'animaux leucémiques examinés | Age (jours) | Matériel soumis à l'examen |
|----------------|---------------------------------------|-------------|--|
| Sussex | 22 | 22 | rate et moelle |
| Leghorn Blancs | 14 | 50 | rate, moelle, plasma et cellules sanguines |
| Leghorn Bruns | 11 | 19 | rate, moelle et plasma |
| Total | 47 | | |

En plus, de nombreux témoins normaux ont servi de contrôle, dont 21 poulets de la race Sussex, 18 Leghorn Blancs et 20 Leghorn Bruns. 12 embryons et 5 rates de poussins cultivés *in vitro*, et 12 plasmas de poulets normaux ont également été étudiés.

La transmission de l'érythroblastose fut effectuée par la technique indiquée dans un précédent travail (9)¹. Les animaux, avant d'être sacrifiés par décapitation, furent saignés par ponction cardiaque. Le sang héparinisé fut centrifugé une première fois à 700 t/m pendant 10' pour éliminer les globules rouges. Le surnageant fut repris et centrifugé à 1000 t/m pendant 10' pour recueillir les *cellules érythroblastiques*. Le culot adhérent au fond du tube fut fixé à l'acide osmique à 2 %, pH 7,3, pendant 1 heure. Après un rapide lavage

¹ Nous tenons à exprimer notre gratitude au Dr. Atanasiu, de l'Institut Pasteur, qui a bien voulu mettre à notre disposition la souche E. H. du virus de l'érythroblastose.

FIG. 2. Moelle érythroblastique : de nombreux foyers de virus intra- et extracellulaires (→). C.L., érythroblastes; M, macrophages. 11.500



à l'eau distillée, le centrifugat fut coupé en petits fragments et, après déshydratation à l'alcool éthylique, inclus au méthacrylate de butyle selon la méthode usuelle. Enfin, le *plasma* fut centrifugé une nouvelle fois, d'abord à 4000 t/m pendant 30', et ensuite à 50.000 g (Spinco) pendant une heure et demie. Le pellet ainsi obtenu fut fixé pendant 1 heure à l'acide osmique à 2 % et inclus au méthacrylate. De petits morceaux de la *moelle* et de la *rate* furent fixés et enrobés selon la même technique. Les coupes furent effectuées à l'ultramicrotome Servall et examinées ensuite au microscope RCA EMU 2E. Quelques micrographies ont également été faites au microscope Siemens Elmiskop I.

RESULTATS

Rapports des particules virus avec les structures cellulaires des tissus leucémiques

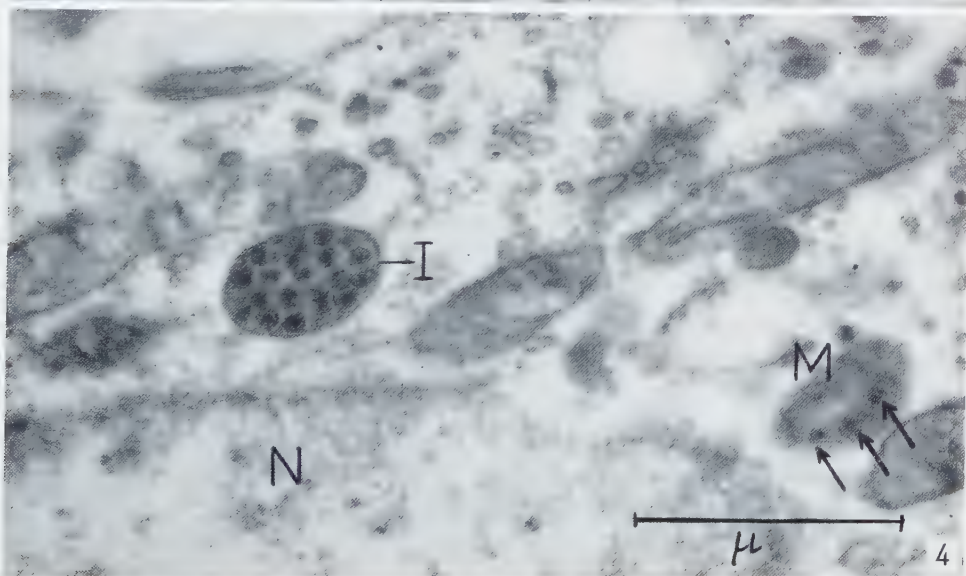
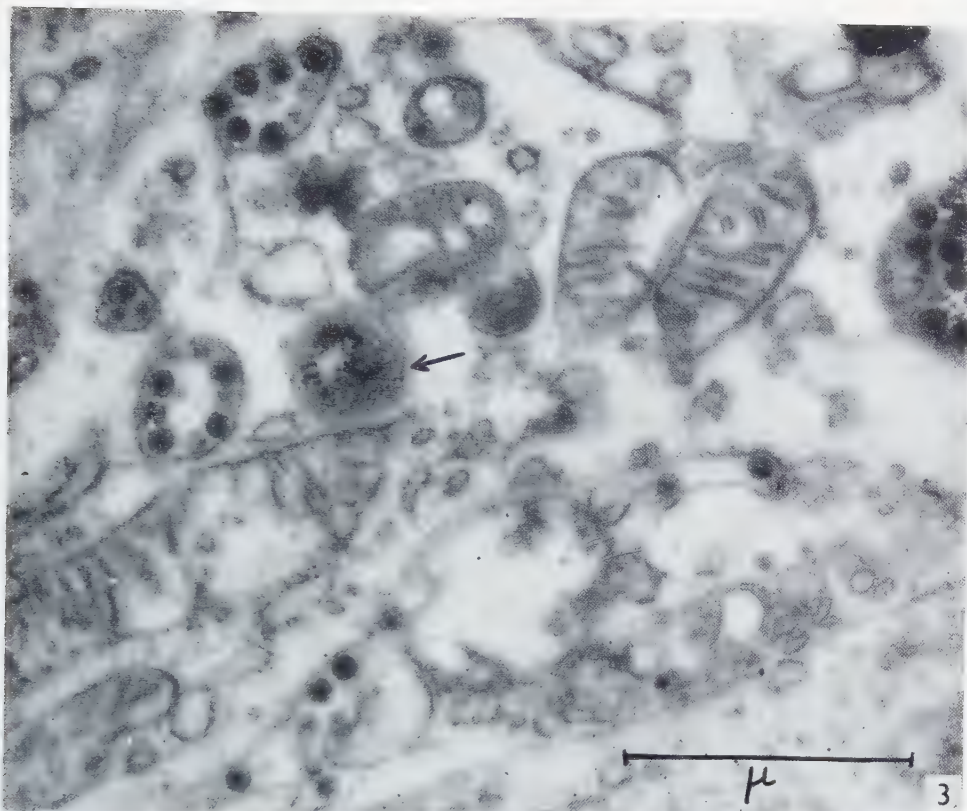
Comme il a déjà été signalé (8), il est relativement aisé de mettre en évidence dans les tissus hématopoïétiques d'animaux atteints de leucémies, des particules d'aspect viral, ayant un diamètre de 80 m μ environ. Cernées d'une membrane externe, elles contiennent un nucléoïde central très dense, dont le diamètre oscille entre 30 et 40 m μ . Sur des micrographies de haute résolution, on peut reconnaître l'existence d'une deuxième et peut-être même d'une troisième membrane, interposées entre le corps central et la membrane externe (fig. 1).

Le graphique 1 indique que la *taille des particules* peut varier considérablement à l'intérieur d'un seul échantillon de tissu. Cette variation n'est certainement due que partiellement à l'incidence de la coupe intéressant des portions plus ou moins étendues de la sphère du corpuscule virus. La conservation plus ou moins bonne des particules peut jouer un rôle dans la variation de leur diamètre, étant donné que certains éléments paraissent souvent plus clairs et gonflés. Mais on doit certainement tenir compte d'une variation réelle de leur taille qui peut osciller entre 58 et 102 m μ , alors que le sommet de la courbe de distribution correspond à 78 m μ . Des mesures effectuées sur des micrographies variées de tissus leucémiques ou normaux contenant des particules peuvent donner des courbes à sommets légèrement différents de ceux-ci. Il est alors important de vérifier l'étalonnage des grossissements du microscope avant de conclure à une présence de souches de virus morphologiquement distinctes les unes des autres.

La *localisation des particules* dans les tissus leucémiques spléniques et médullaires peut être à la fois intra- et extracellulaire. On les trouve plus facilement dans les cellules du système réticulo-endothélial (macrophages et cellules histiocytaires en transformation érythroblastique), tandis que les cellules leucémiques (paraérythroblastes) ne

FIG. 3. Erythroblastose. Cellule histiocytaire de la moelle. Vacuoles avec particules virus (→). « Microbody » avec un dépôt ferrugineux. 38.000 \times .

FIG. 4. Erythroblastose. Cellule endothéliale de la moelle. N, noyau; I, inclusion virale; M, mitochondrie remplie d'une substance dense et contenant quelques virus (→). 35.000 \times .



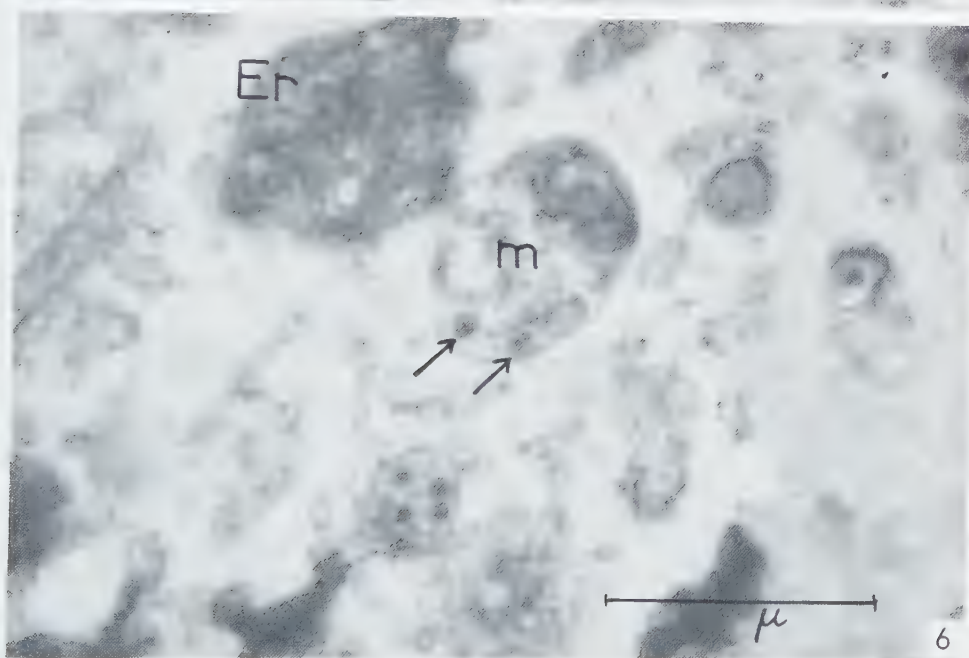
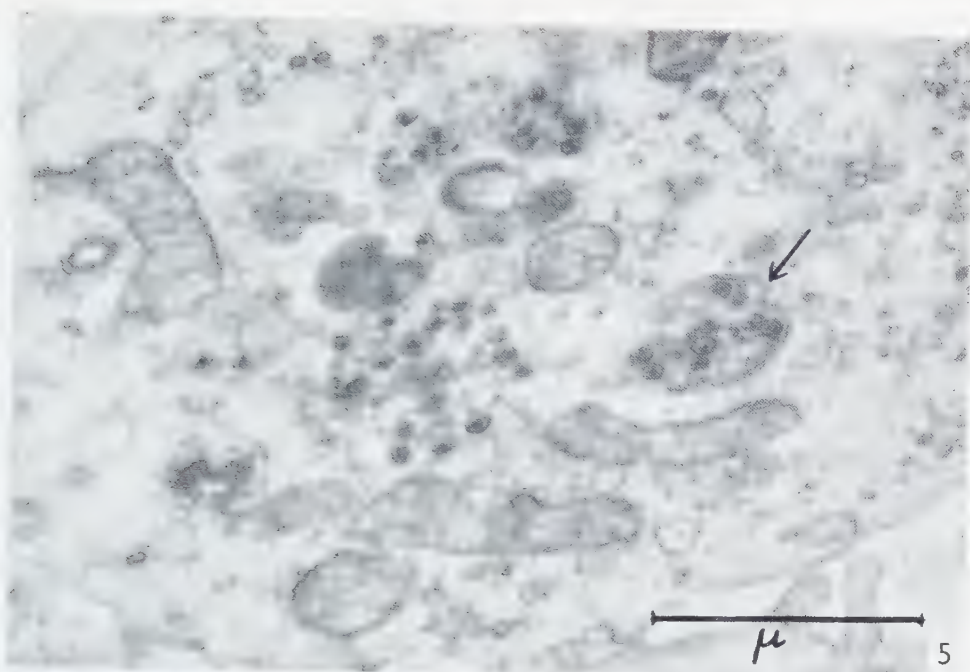
contiennent en général que peu d'inclusions virales. Fig. 2 représente un aspect typique de la répartition des particules dans une région médullaire particulièrement riche en virus.

En étudiant d'abord les rapports de ceux-ci avec les cellules du *système réticulo-endothélial* (S.R.E.), on est surtout frappé par la présence dans le cytoplasme d'*inclusions vacuolaires* dont la taille est de l'ordre de celle des mitochondries, mais pouvant atteindre quelques μ de diamètre. Celles-ci renferment un nombre généralement élevé de particules (fig. 2-7). Entourées le plus souvent d'une membrane simple, ces inclusions se trouvent dans n'importe quelle région du cytoplasme, mais sont souvent observées sous-jacentes à la membrane cellulaire. Les particules virus peuvent être le seul contenu visible des vacuoles. Mais parfois, celles-ci renferment également une substance finement grenue et dense au sein de laquelle on arrive à distinguer avec quelque difficulté les corpuscules viraux (fig. 4 et 5). Il est indéniable qu'au moins certaines de ces inclusions ont un rapport avec les *mitochondries*. En effet, on arrive à observer dans des cellules réticulaires des mitochondries dont les crêtes ne sont visibles que sous forme de fragments. Tuméfié à l'extrême ou, au contraire, densifié, le corps mitochondrial est délimité par une double membrane fréquemment incomplète. Mais si celle-ci persiste au moins à certains endroits, elle peut être le seul critère permettant l'identification de l'organe cytoplasmique. Or, à l'intérieur de mitochondries ainsi modifiées, on retrouve les mêmes particules virus présentes dans des vacuoles cernées d'une membrane simple (fig. 4-6). S'il existe des cas intermédiaires qui suggèrent une transition entre mitochondries et vacuoles contenant des virus, rien ne permet de conclure que toutes les inclusions soient d'origine mitochondriale. Il paraît même hautement probable que certaines cellules du type macrophagique absorbent par *phagocytose des particules virus* du milieu environnant. En effet, dans de nombreuses vacuoles, les particules virus sont mélangées à des dépôts amorphes de densité variable, répondant sans doute à des débris de globules rouges et à des pigments ferrugineux (fig. 6 et 7). Parfois, la membrane entourant ces inclusions est interrompue et le matériel amorphe ainsi que les particules apparaissent libres dans le cytoplasme. Les particules n'ont jamais été vues dans les petites cellules d'aspect lymphoïde, fréquemment rencontrées dans la moelle et la rate leucémiques, et dont la signification est discutée ailleurs (9).

La cytoplasme des *cellules paraérythroblastiques* contient rarement des particules virales. On peut y trouver de petites vacuoles cernées d'une simple membrane et

FIG. 5. Erythroblastose de la rate. Histiocyte. Plusieurs inclusions virales dont l'une de nature mitochondriale (\rightarrow). 35.000 \times .

FIG. 6. Même préparation. Macrophage avec débris érythrocytaires (*Er*) et mitochondrie altérée (*m*) contenant 2 particules virus (\rightarrow). 35.000 \times .



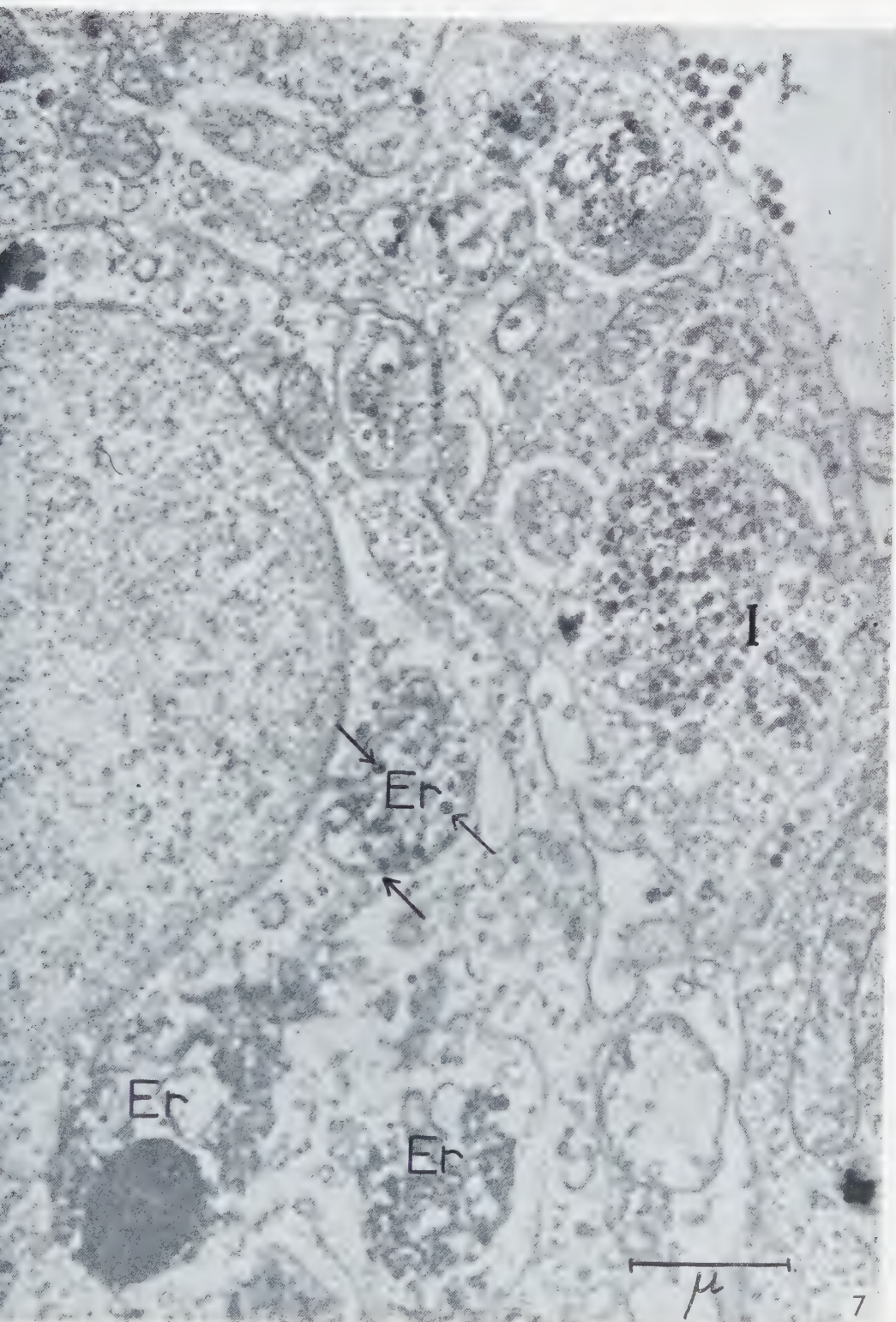
contenant des virus (fig. 8). Mais jusqu'ici, aucune mitochondrie renfermant ces particules n'y a été mise en évidence. Les virus sont le plus souvent en dehors de la cellule, juxtaposés à la membrane, ou dispersés librement dans les espaces intercellulaires (fig. 9).

La question se pose de savoir à quel endroit de la cellule les particules virus prennent naissance. Il est probable que dans certains cas elles se forment à l'intérieur des mitochondries. Mais les images qui peuvent suggérer une telle origine sont relativement rares (fig. 4-6). Par contre, un autre phénomène semble jouer un rôle important dans l'évolution morphologique du virus. On peut trouver dans les paraérythroblastes de petites vésicules à proximité de la surface cellulaire, dont la taille est identique ou légèrement inférieure aux particules virus. Elles sont cernées d'une membrane épaisse et très contrastée, voire même double, ce qui les distingue nettement des microvésicules golgiennes (fig. 10-12). La signification exacte de ces anneaux n'est pas encore connue. S'il paraît probable qu'ils interviennent dans le processus de formation de l'agent, le mécanisme de leur transformation en particules virus complètes reste à déceler.

Le passage des virus à travers la membrane cellulaire semble pouvoir s'effectuer selon deux modes différents: d'une part, des vacuoles intracytoplasmiques, remplies d'un grand nombre de virus peuvent sans doute se coller à la membrane cellulaire (fig. 3), et si celle-ci est percée, déverser leur contenu vers l'extérieur; d'autre part un phénomène de *bourgeonnement* a été mis en évidence dans les paraérythroblastes, qui n'est pas sans analogie avec des observations sur l'évolution d'autres virus (fig. 13-16). Des bourgeons fortement osmiophiles apparaissent isolés à quelques endroits de la membrane cellulaire (fig. 13), et y forment une petite saillie arrondie. On peut parfois y reconnaître une membrane double renfermant un centre très osmiophile (fig. 14 et 16). Ces bourgeons peuvent être associés à des vésicules qui sont situées à leur base (fig. 14 et 16). On peut supposer que les petites vésicules à membranes très épaissies ou doubles décrites ci-dessus, peuvent déclencher ce processus de bourgeonnement dès qu'elles entrent en contact avec la membrane cellulaire, lieu de leur transformation en particules virus complètes. Mais il faudra encore trouver des documents supplémentaires pour prouver cette hypothèse.

Notons encore que les virus qui sont entièrement détachés des cellules et disséminés dans les espaces intercellulaires semblent avoir une certaine affinité pour des fibres réticulaires ou collagènes, ou pour la substance amorphe remplissant l'espace de ce qui a été classiquement appelé « membrane basale » (fig. 18). Quoiqu'il en soit, on peut les voir accumulés dans ces régions.

FIG. 7. Erythroblastose de la moelle. Cellules macrophagiques avec inclusions de débris érythrocytaires (*Er*) dont l'une contient également des virus (\rightarrow). *I*, inclusion virale volumineuse. 24.000 \times .



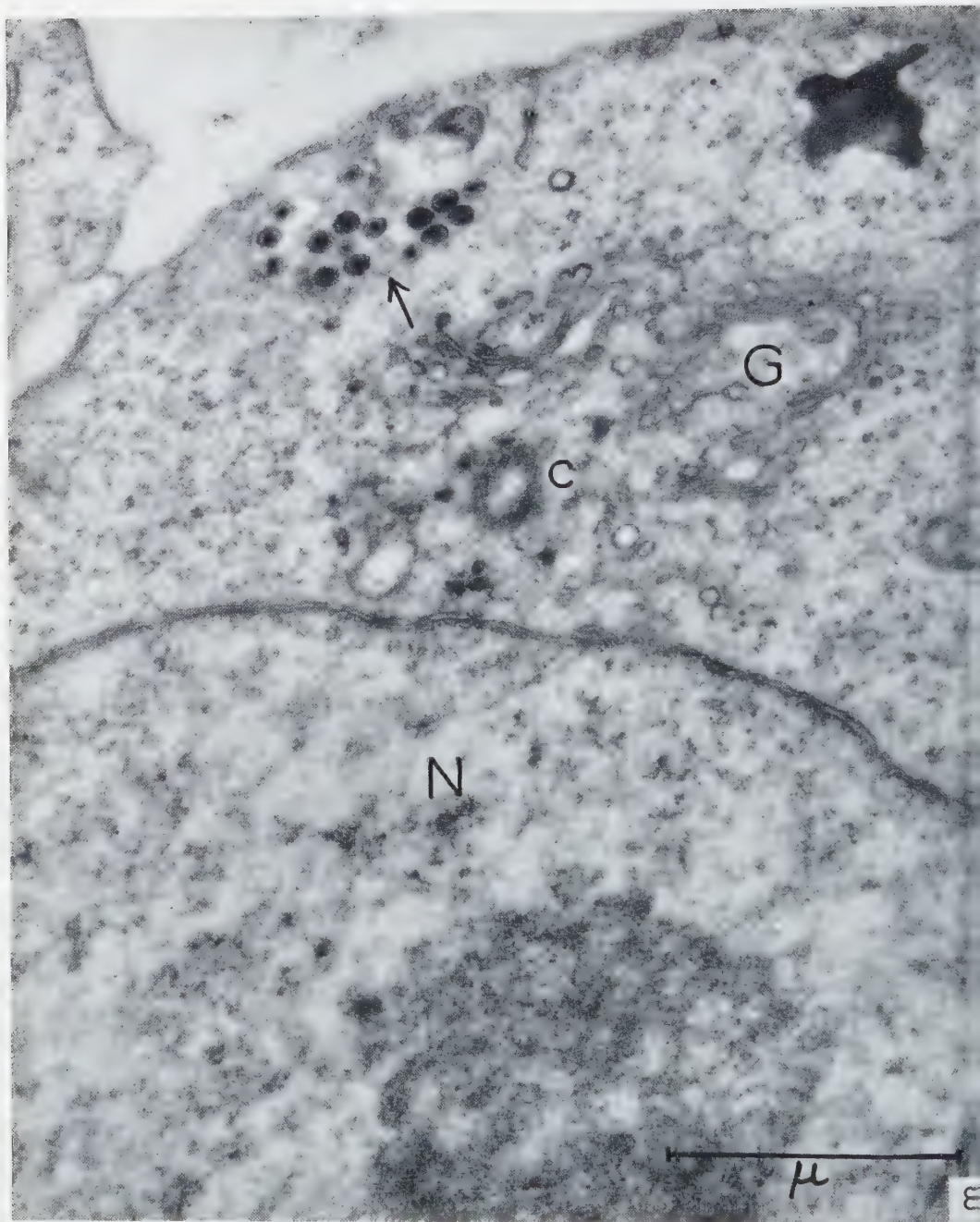


FIG. 8. Erythroblastose. Portion de cellule paraérythroblastique avec un noyau (N) et un cytoplasme contenant une zone de Golgi (G), un centriole (c) et une vacuole remplie de virus (→). 40.000

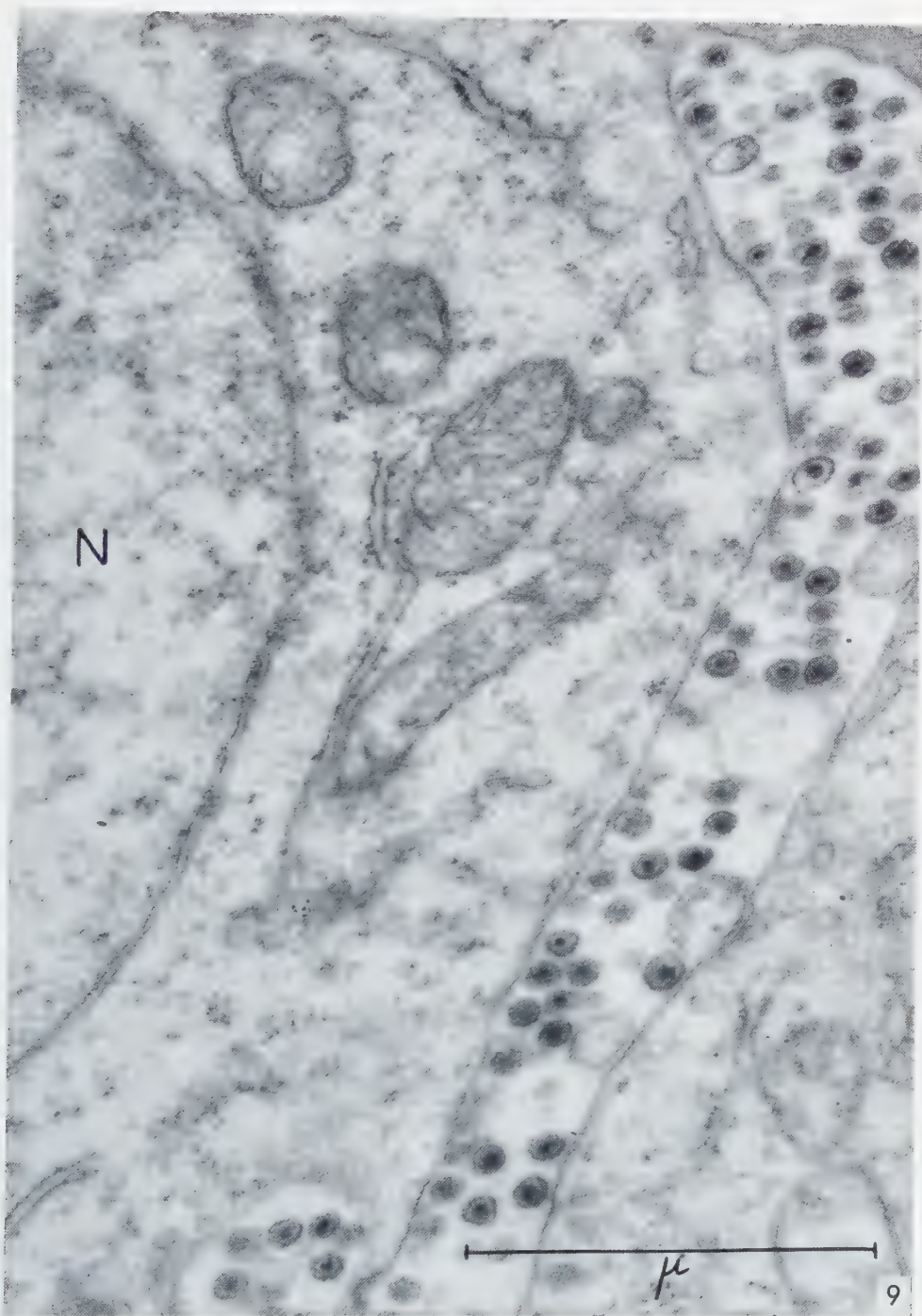


FIG. 9. Erythroblastose de la moelle. De nombreuses particules extracellulaires à la surface d'un paraérythroblaste. N, noyau. 56.000

Le nombre total des particules intra- ou extracytoplasmiques varie considérablement d'un cas à l'autre; cependant, il est à peu près constant pour un échantillon de tissu donné. *La quantité des particules visibles* dépend nettement du stade de la maladie. En effet, il existe un rapport entre la richesse d'un myélogramme en paraérythroblastos et le nombre de cas trouvés positifs au microscope électronique. Sur 32 cas leucémiques avancés dont 70 % des cellules médullaires étaient formées par des paraérythroblastos, 29 cas (90,6 %) furent trouvés positifs, c'est à dire contenaient des particules visibles. Par contre, sur 15 cas de leucémie peu avancée dont la population cellulaire de la moelle ne contenait qu'un faible pourcentage de cellules leucémiques, 7 cas (46,6 %) seulement présentaient des virus (voir graphique 2). Cette observation fut confirmée sur la rate des mêmes animaux.

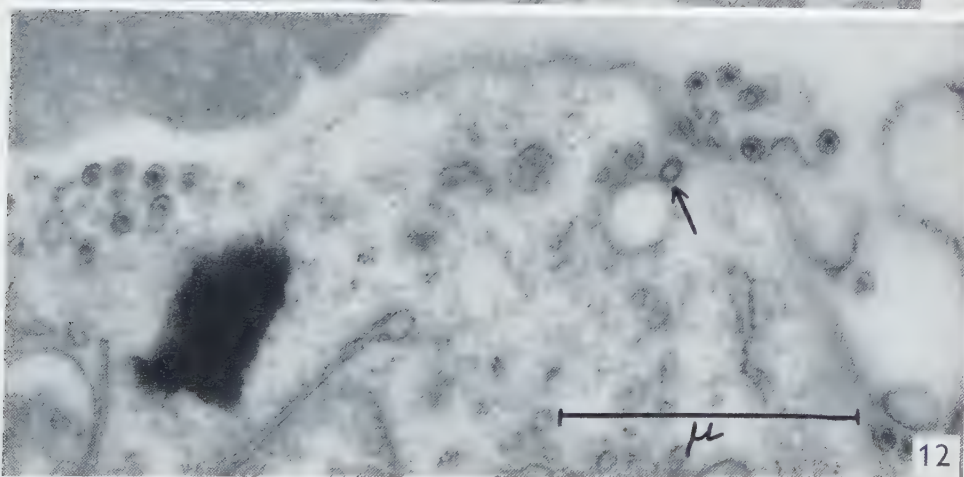
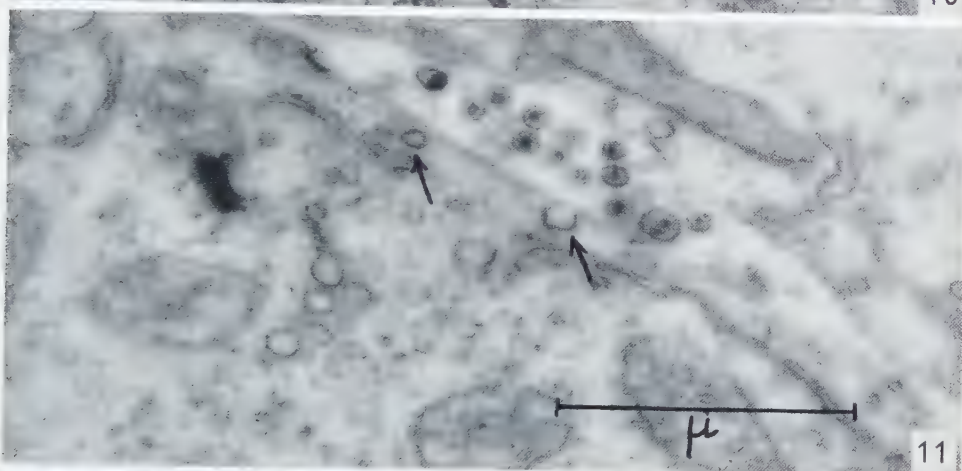
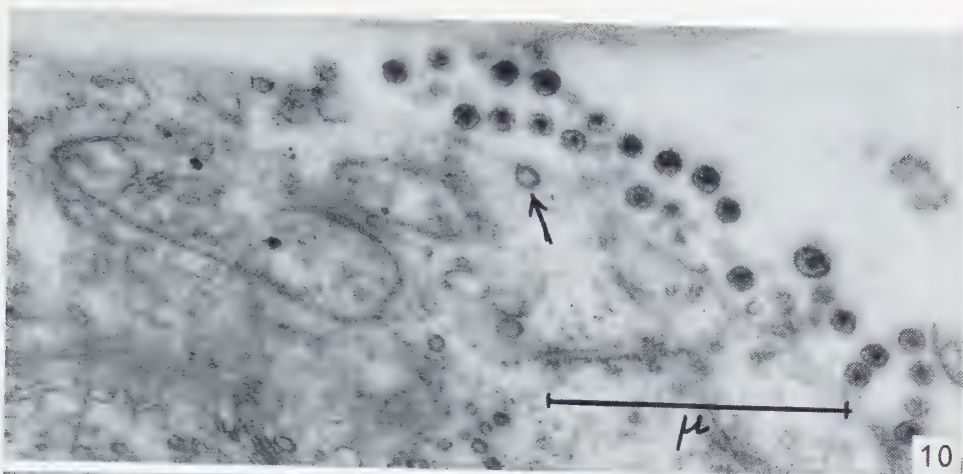
Recherche des particules dans le sang périphérique

Il a été plus difficile de mettre en évidence les mêmes particules dans les cellules du *sang périphérique*. Comme il a été dit plus haut, les *paraérythroblastos* présents dans les tissus ne contiennent que rarement des inclusions virales et les particules extracellulaires ne semblent pas rester collées longtemps sur leur membrane cellulaire. Les cellules érythroblastiques du sang circulant sont un objet encore moins favorable pour la mise en évidence de virus intra- ou extracytoplasmiques. Cependant, quelques examens du « buffy coat » leucémique ont révélé de rares particules intra- ou extracellulaires.

Quant à la détection de virus dans le *plasma leucémique* qui est en général, comme on sait, hautement infectieux, il a été possible de retrouver des corpuscules identiques dans les culots de centrifugation purifiés dans 11 cas sur 21 échantillons en tout (fig. 17). Les cas apparemment négatifs ont présenté de nombreux profils vésiculaires vides ou contenant plusieurs granules osmiophiles comparables aux grains R.N.A. La taille de ces vésicules oscillait entre 80 et 180 m μ , et leur identification n'était plus possible. Mais il s'agissait probablement en grande partie de virus en désintégration.

Les résultats concernant l'enrichissement de l'agent pathogène dans le plasma ont été dans l'ensemble peu satisfaisants, malgré les précautions prises pour la centrifugation et la fixation du plasma. Le plasma de 12 poulets témoins n'a jamais révélé la présence de virus identiques à ceux observés dans les cas d'érythroblastose, et les profils vésiculaires suspects de représenter des virus en désintégration étaient également absents.

FIG. 10 12. Erythroblastose de la moelle. Paraérythroblastos. Virus extracellulaires. Les flèches (→) indiquent la présence de profils vésiculaires, délimités par une membrane osmiophile épaisse ou double. (Stades évolutifs du virus?) 39.000



Présence des mêmes particules virales dans les tissus de témoins considérés comme normaux

Comme il a déjà été signalé à plusieurs reprises, on peut mettre en évidence les mêmes particules, présentes dans les leucémies, dans les contrôles normaux (6-8). Leur diamètre est le même et leur structure interne ne montre aucun signe distinct à la limite de la résolution actuellement atteinte en microscopie électronique.

Ces particules ont surtout été recherchées dans la *rate de poussins*. Parmi 59 cas, 6 ont été trouvés positifs. On trouve les corpuscules à nouveau, soit dans des vacuoles cytoplasmiques des cellules réticulaires, soit dans les espaces intercellulaires (fig. 18). Leur localisation ne diffère donc pas des cas leucémiques. Rarement, ces éléments ont également été observés à l'intérieur des formations identifiables à des « microbodies » ou des mitochondries. Cependant, les lésions virales sont moins étendues dans les contrôles que dans les leucémies et les cas trouvés positifs sont plus rares (voir graphique 3).

Les mêmes particules ont pu être mises en évidence dans la *rate de 3 embryons* sur 25, considérés comme entièrement normaux. La localisation intra- et extracellulaire des virus était à nouveau retrouvée.

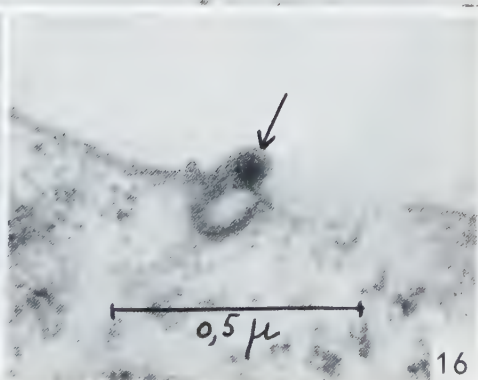
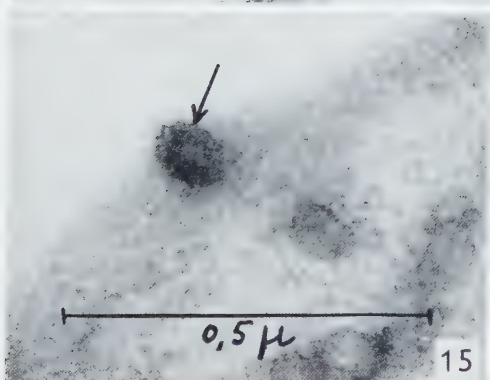
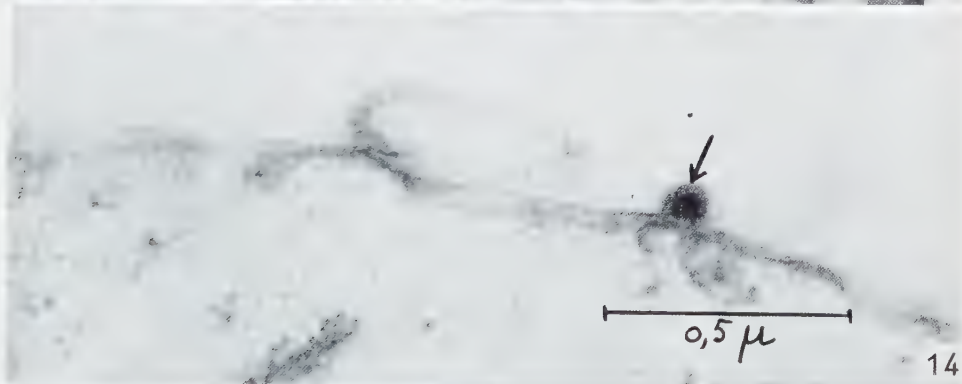
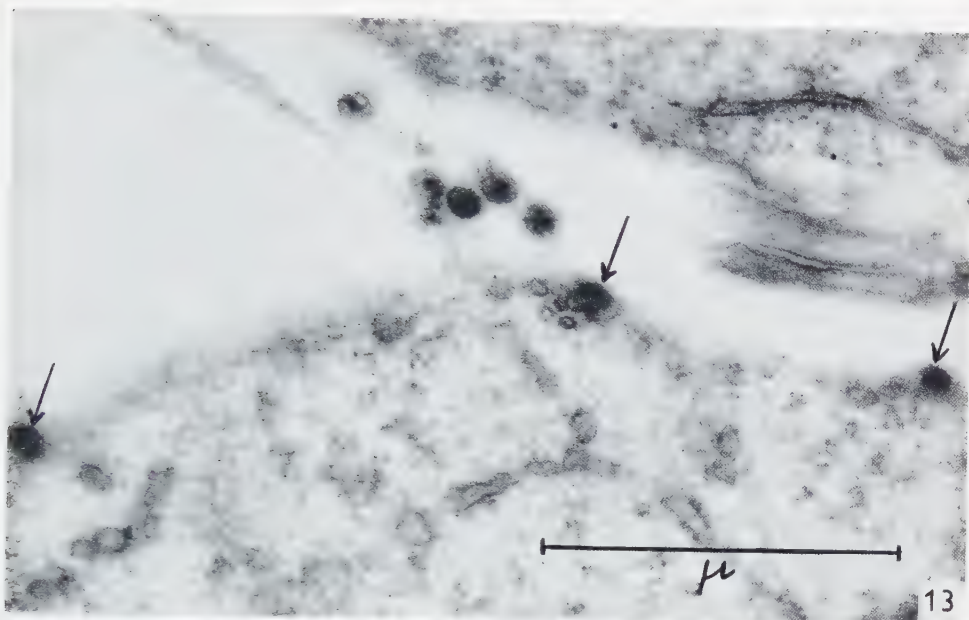
Enfin, dans 12 *cultures in vitro de fibroblastes d'embryons de poulets* normaux, les éléments viraux ont été observés, dans 3 cas, dans des vacuoles intracytoplasmiques (fig. 19) et en-dehors des cellules, entourés de débris amorphes ou mélangés à des fibres collagènes.

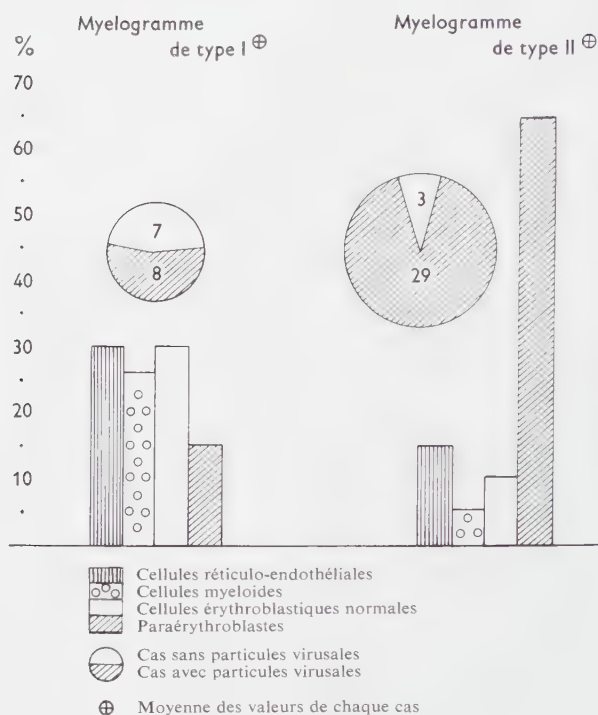
Dans l'ensemble de nos contrôles (96 cas différents), des particules ont donc pu être observées 12 fois, soit dans 12,5 % des cas du tissu témoin.

Fréquence des particules dans différentes souches de poulets normaux ou atteints d'érythroblastose

Le graphique 3 résume la situation telle qu'elle résulte de notre matériel d'expérience provenant de 3 souches de poulets distinctes : les Sussex, les Leghorn Blancs et les Leghorn Bruns. Les cas furent appelés positifs à cause de la présence de particules dans les tissus soumis à l'examen au microscope électronique. Ils furent considérés comme négatifs quand des recherches prolongées, d'une durée de plusieurs heures et intéressant plusieurs blocs du même tissu n'ont pas permis la mise en évidence de tels éléments, ce qui ne veut évidemment pas dire que les virus étaient effectivement absents chez ces animaux. Mais ce critère assez grossier a permis de juger la fréquence

FIG. 13-16. Erythroblastose. Portions de paraérythroblastes de la moelle. Processus de bourgeonnement sur la surface cellulaire, révélant peut-être le passage de particules virus, à travers la membrane cellulaire (→). 47.000 × (fig. 13); 66.000 × (fig. 14 et 16); 96.000 × (fig. 15).





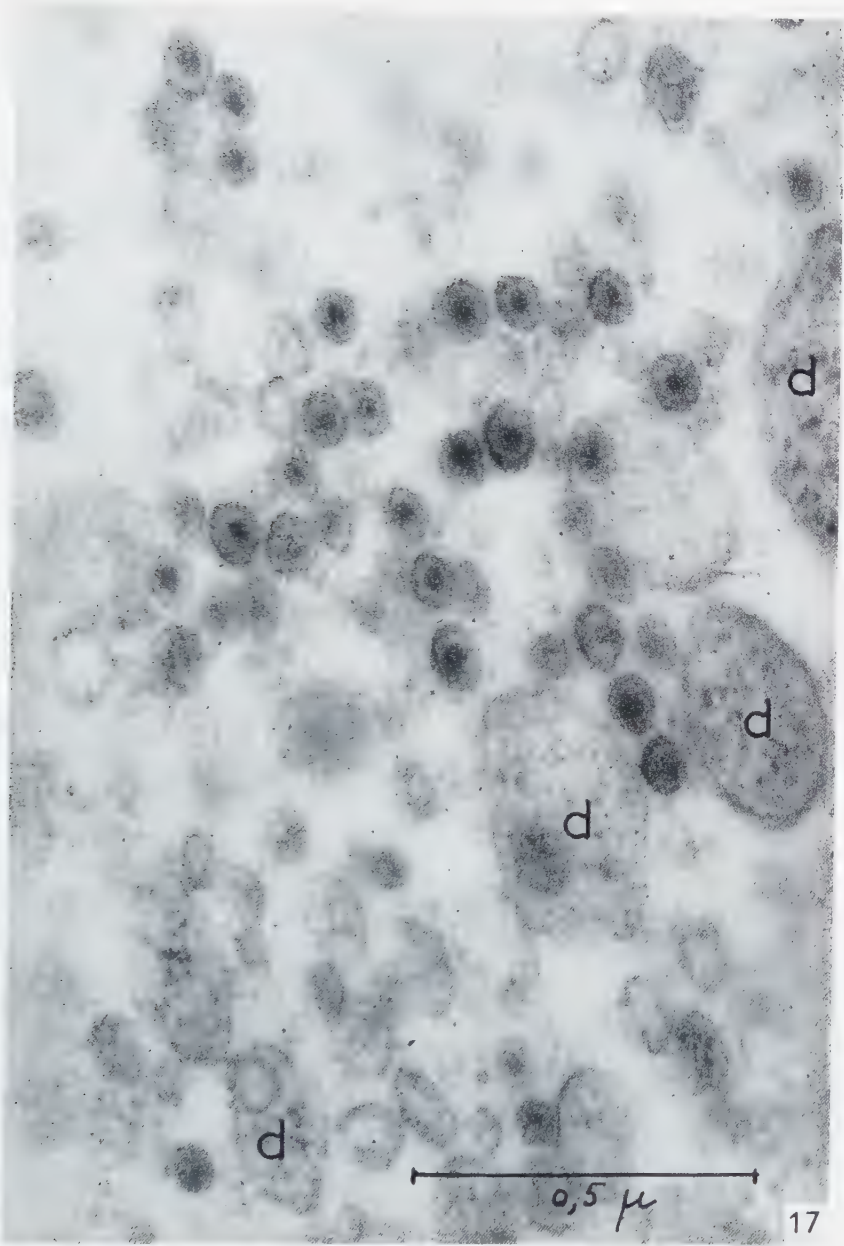
GRAPHIQUE 2

relative des particules dans les différents tissus. Le schéma ne tient pas compte des variations numériques des particules dans les cas appelés positifs.

On note une différence considérable entre le nombre de cas positifs dans les témoins et dans l'érythroblastose pour chaque race examinée. Le pourcentage de cas positifs dans les témoins de race Leghorn Blanche et Sussex est semblable, alors que dans les témoins de race Leghorn Brune, le même examen est resté négatif ainsi que dans les cinq rates prélevées sur les animaux de même souche et cultivées *in vitro*.

Le nombre des animaux positifs, atteints d'érythroblastose, s'est montré élevé dans toutes les races examinées; ceci suggère qu'il n'existe pas de rapport décelable entre la présence de particules dans les tissus des animaux avant et après la transmission de l'érythroblastose. En effet, les animaux de la race Leghorn Brune dépourvus de particules virales au départ, sont positifs en très grand nombre après l'infection par l'agent érythroblastique.

FIG. 17. Erythroblastose. Plasma « purifié » contenant de nombreuses particules identiques à celles trouvées dans les tissus leucémiques. d, débris cellulaires. 90.000 ×.



DISCUSSION

Les questions les plus importantes qui se posent d'abord concernent l'*identification des particules* décrites dans ce travail. Etant donné que des éléments morphologiquement identiques ont également été mis en évidence non seulement dans divers sarcomes aviaires (12, 29, 34, 36, 38, 41, 45, 48), mais aussi dans les tissus normaux (6, 8, 46), voire même chez l'embryon normal (7), on doit se demander :

- 1) si ces particules peuvent être considérées comme des virus;
- 2) s'il s'agit bien dans la présente étude de l'agent spécifique de la maladie;
- 3) quelle signification ces formations peuvent avoir dans les témoins normaux.

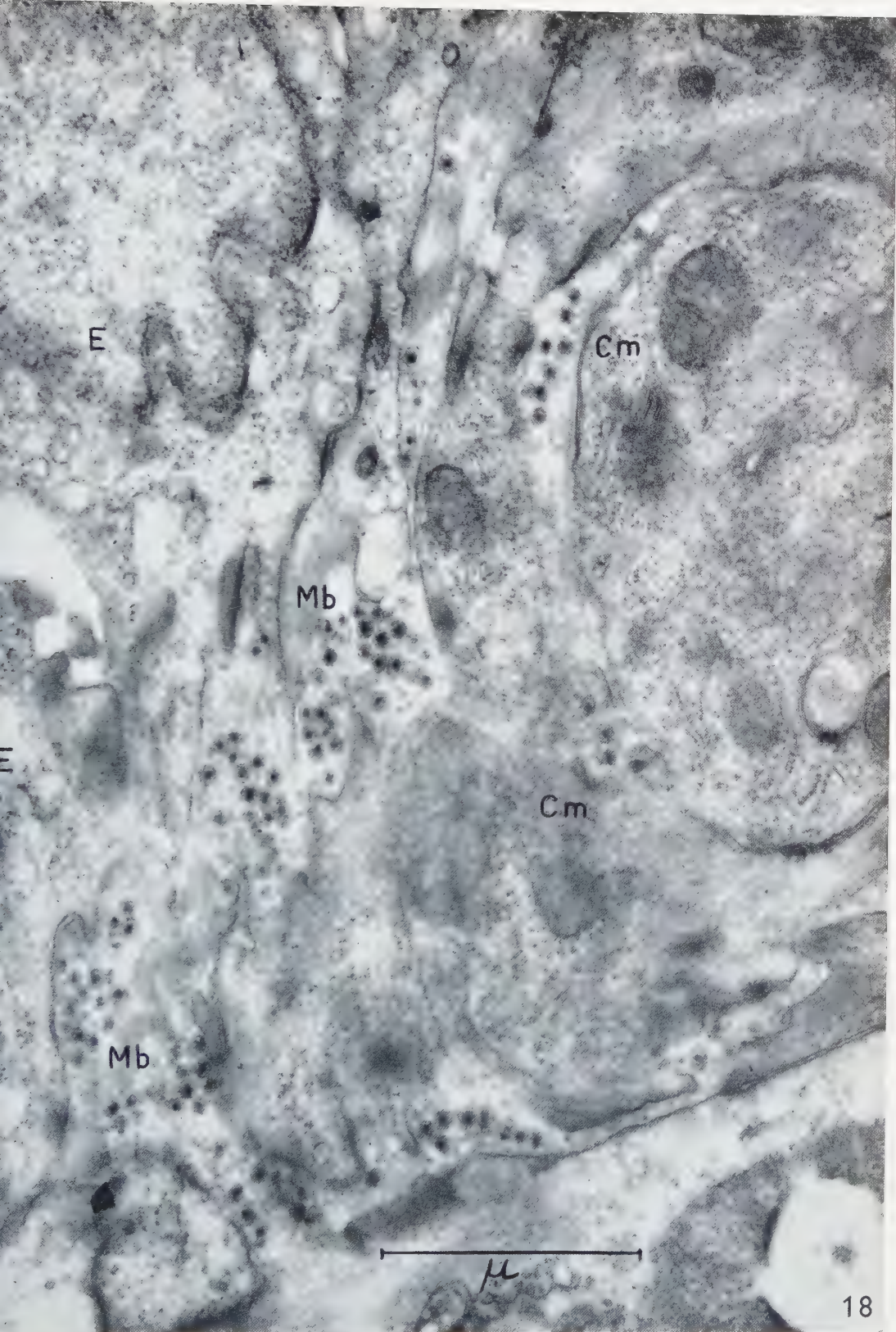
En réponse à la première question, on peut d'abord exclure que les particules soient des constituants normaux du tissu hématopoïétique. Elles n'ont été vues nulle part ailleurs que chez le poulet. Encore y sont-elles beaucoup plus rares dans les tissus normaux que dans les tissus leucémiques. Il existe même une race de poulet dont les témoins semblent en être dépourvus : on les y trouve seulement après l'infection des animaux par l'agent de l'érythroblastose. Enfin, s'il est impossible d'identifier un virus par les seuls critères morphologiques, ceux-ci plaident néanmoins fortement en faveur de l'hypothèse de la nature virale de ces particules : leur nombre, leur taille relativement homogène et leur ultrastructure ressemblent de très près aux éléments décrits dans d'autres affections virales. En plus, elles sont surtout trouvées dans les tissus dont on sait qu'ils sont infectieux.

Quant à la deuxième question de savoir si l'on est bien en présence du virus de l'érythroblastose, on peut donner une réponse affirmative pour les raisons suivantes :

Le tissu érythroblastique infecté par un agent spécifique et transmissible par filtrat acellulaire, ne contient aucun autre élément corpusculaire du type viral que les particules décrites dans ce travail. Celles-ci sont beaucoup plus nombreuses chez des animaux leucémiques que chez certains contrôles qui, provenant de la souche Leghorn Brune, sont restés jusqu'ici entièrement négatifs.

Si cette observation est importante, elle ne suffit pas à prouver la spécificité des particules dans cette maladie, car on pourrait bien admettre qu'un virus non spécifique et étranger à cette affection trouve un terrain favorable pour sa multiplication dans les cellules néoplasiques. La preuve décisive ne peut être donnée que par l'expérimentation biologique et elle est apportée par les travaux de Beard et coll. (3-5, 14, 22-26, 49) qui sont arrivés à purifier les virus de l'érythroblastose et de la myéloblastose à un degré très élevé, en centrifugeant le plasma des animaux leucémiques. Les micro-

FIG. 18. Rate d'un poulet témoin. Amas de particules virus dans les espaces intercellulaires de la paroi d'une artériole. *E*, endothèle; *Mb*, membrane basale; *Cm*, cellule musculaire. 42.000 \times .



graphies électroniques des préparations ombrées révèlent un très grand nombre de particules sphéroïdes, de taille homogène, quand le plasma est hautement infectieux, tandis que ces éléments font défaut dans le plasma normal. Les particules purifiées provoquent des anticorps capables de précipiter les particules dans le plasma et de faire disparaître son infectiosité (25). Bang, appréciant l'ensemble des recherches de Beard *et al.*, conclut que l'identification des particules présentes dans ce plasma infectieux des deux types de leucémie aviaire avec les agents spécifiques de ces maladies a été faite de la manière la plus complète (1). Or, l'un de nous a eu l'occasion de faire des coupes ultrafines des préparations de plasma leucémique purifié par Beard. Qu'il s'agisse d'érythro- ou de myéloblastose, on y trouve une abondance de particules ayant toutes une ultrastructure identique à celle des éléments mis en évidence dans nos tissus. Dans tous les cas, le plasma contenant une quantité énorme de particules était encore infectieux et transmettait la maladie spécifique à une dilution extrêmement élevée (10).

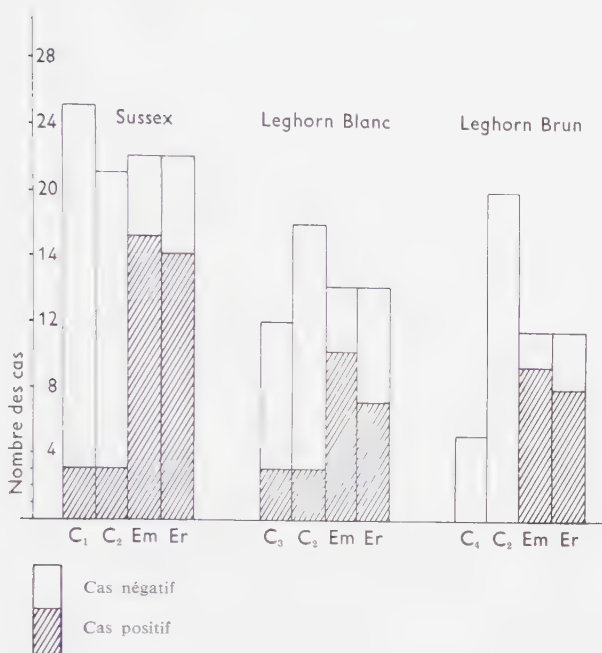
Enfin, les mêmes formations ont également été retrouvées en abondance dans le plasma érythroleucémique de nos propres poulets (fig. 17).

Il reste à expliquer les cas d'érythroblastose dans lesquels aucune particule virus n'a été vue. C'est sans doute l'imperfection de la méthode qui peut être en partie responsable des échecs. En effet, la masse de tissus effectivement explorée au microscope électronique reste infime. Si la « masse physique » du virus (5) est petite, et la sensibilité de la méthode de détection faible, les résultats, restent négatifs; il est alors dangereux de conclure à un « masquage ». Des faits semblables ont pu être signalés à plusieurs reprises pour d'autres tumeurs à virus, examinées au microscope électronique. Ainsi, dans la tumeur de Lucké de la grenouille, Fawcett (31) n'observe de particules d'aspect viral que dans les deux tiers des cas et le même pourcentage de cas positifs est signalé pour le sarcome de Rous (12). Il est évidemment possible que dans ces cas le virus existe réellement sous une forme invisible, « masquée », (21) et qu'il n'est pas possible de le mettre en évidence par des moyens morphologiques.

L'identification du virus de l'érythroblastose étant donc admise, on peut se demander pourquoi des particules morphologiquement identiques à celui-ci se trouvent également dans les contrôles.

Ces faits ont déjà été discutés ailleurs (6, 7, 32); deux principales hypothèses peuvent être envisagées pour expliquer l'apparition de telles particules chez certains animaux considérés comme entièrement normaux. D'une part, il pourrait s'agir d'un virus pathogène latent, d'une autre maladie que celle de la leucémie, mais étant causée par un agent qui ne se distingue pas morphologiquement de celui de l'érythroblastose. D'autre part, on pourrait admettre l'existence d'un virus saprophyte, appartenant morphologiquement à la famille des virus oncogènes aviaires, mais ne déclenchant jamais un processus morbide.

A l'appui de la première possibilité, on peut citer le fait que la *lymphomatose* est



GRAPHIQUE 3. Répartition des cas positifs dans les différentes souches de poulets. Contrôles: C₁, rates, embryons normaux; C₂, rates, poulets normaux; C₃, cultures fibroplastes, embryons normaux; C₄, cultures rates, poussins normaux. E_m, moelles, érythroblastose; E_r, rates, érythroblastose.

une maladie très répandue chez les poulets et que son agent causal peut être présent chez ces animaux sans se manifester cliniquement, mais en donnant lieu à la formation d'anticorps (15). Ce virus peut également être transmis par l'œuf (18). Or, les tissus de poulet atteints de neurolymphomatose (38) ou de lymphomatose viscérale (20), examinés au microscope électronique, révèlent des particules morphologiquement identiques aux nôtres. Etant donné que de rares cas de neurolymphomatose ont été enregistrés de temps à autre dans notre élevage de poulets Sussex et Leghorn Blancs, mais jamais dans l'élevage de la souche Leghorn Bruns (17, 35), dont les tissus témoins ont été trouvés dépourvus de particules, on est tenté de voir dans les cas témoins positifs, des animaux infectés par un agent latent de la lymphomatose. Mais l'apparition d'anticorps antiviral chez des animaux normaux en contact avec des poulets porteurs du sarcome de Rous suggère également l'existence d'un état latent de ce dernier virus (16, 21). Vigier (50), de son côté, a retrouvé ce virus dans le sang d'animaux infectés par voie intraveineuse, plus d'un mois après l'infection et en l'absence de tout sarcome. Or le virus de Rous est morphologiquement indiscernable, à son tour, de celui de l'érythroblastose (12, 34, 36, 45).

La deuxième hypothèse, à savoir l'existence d'un virus saprophyte et ubiquitaire dans les tissus de poulets normaux appartenant morphologiquement à la famille des virus oncogènes aviaires, mais restant biologiquement distinct de ceux-ci, est également possible, mais les faits actuellement connus parlent plutôt en faveur de la première interprétation.

La seconde partie de cette discussion a trait aux *rapports existant entre le virus et les cellules infectées*. L'infection virale du tissu hématopoïétique entraîne la prolifération des cellules réticulo-endothéliales, la différenciation de celles-ci vers les éléments de la lignée rouge, et surtout la multiplication de ces derniers dont la différenciation est pratiquement arrêtée (9).

Si le mécanisme de cette infection dépend de la *pinocytose* et de la *phagocytose*, il est probable que les premières cellules infectées sont les cellules du S.R.E., ou ces phénomènes sont particulièrement prononcés. La transmission du matériel génétique du virus aux cellules érythroblastiques pourrait s'effectuer pendant la phase où les cellules du système R.E. infectées se multiplient et se différencient en cellules de la série rouge.

En effet, les cellules histiocytaires et macrophagiques renferment des inclusions contenant à la fois des particules virales et un matériel hétérogène certainement phagocyté (débris de globules rouges, dépôt ferrugineux). Des observations comparables aux nôtres ont été faites par Hotz et Bang (39) sur des macrophages de poulets cultivés *in vitro* et infectés avec le virus de Newcastle. Ces auteurs suggèrent également que l'agent peut pénétrer dans les cellules par la voie de la pinocytose et de la phagocytose.

Ce mécanisme pourrait permettre l'absorption du virus en l'absence d'un système récepteur spécifique.

La présence de particules virales dans les mitochondries est plus difficile à expliquer, toutefois on sait que ces organites peuvent accumuler des substances variées d'origine extracellulaire introduites dans le cytoplasme par pinocytose ou phagocytose (13, 19, 33, 47). Dans le cas présent, deux hypothèses peuvent être envisagées : 1) les particules pénètrent comme telles dans les mitochondries et provoquent ainsi les altérations morphologiques décrites; 2) les particules virales sont formées au niveau des structures mitochondriales après leur éclipse. Quoiqu'il en soit, le lieu de formation des virus paraît être cytoplasmique et non pas nucléaire, observation qui vient à l'appui de celle de Fagraeus et Thorell (30). Selon ces auteurs, la fraction cytoplasmique des cellules leucémiques centrifugées est relativement plus infectieuse que l'ensemble des cellules.

Certains aspects morphologiques décrits dans les cellules du S.R.E. et dans les para-érythroblastes peuvent illustrer le *mécanisme de libération* des virus corpusculaires dans les cellules, phénomène qui ne semble pas être différent dans le cas des témoins et de l'érythroblastose.

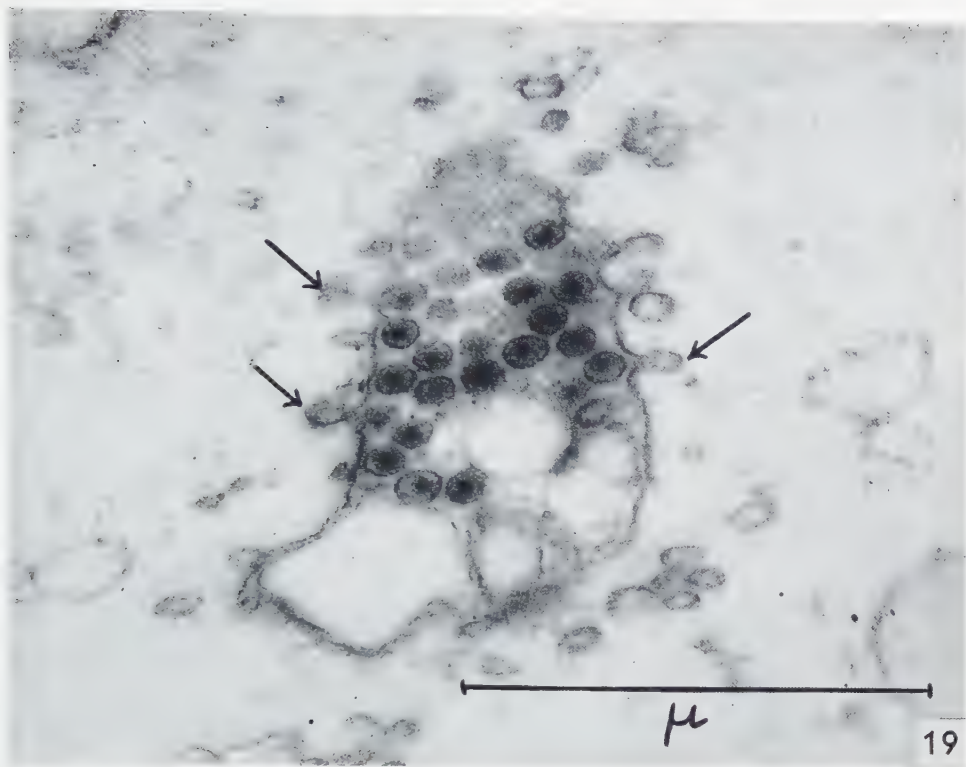


FIG. 19. Culture de fibroblastes d'embryon de poulet normal. Vacuole intracytoplasmique renfermant de nombreuses particules virus. A noter profils vésiculaires attachés à la membrane de la vacuole (\rightarrow). 61.000

Le *bourgeonnement* au niveau de la membrane cellulaire est comparable aux observations faites par Hotz et Schäfer (40) sur le virus de la peste aviaire; par Morgan *et al.* (42) sur le virus de l'influenza, et ressemble au passage des particules intracytoplasmiques à travers la membrane cellulaire dans les tumeurs mammaires de la souris (2, 11).

Mais la libération des particules vers l'extérieur peut probablement aussi s'effectuer par l'éclatement à la surface cellulaire de *vacuoles* cytoplasmiques, bourrées de virus. Ainsi on peut admettre que les cellules réticulaires aussi bien que les paraérythroblastes sont producteurs de virus, mais il est impossible de savoir lequel de tous ces types cellulaires en produit le plus. Retenons toutefois que l'apparition du plus grand nombre de particules coïncide avec une forte prédominance de cellules leucémiques dans les populations cellulaires examinées.

On peut conclure que les recherches ultrastructurales sur les tumeurs aviaires en général et sur la leucémie érythroblastique en particulier ont montré l'existence d'une *seule famille morphologique* de particules virus dans les tissus néoplasiques du poulet. Le microscope électronique n'a pu jusqu'ici distinguer les unes des autres, et la preuve de leur action spécifique dans un néoplasme donné n'est apportée que par l'*expérimentation biologique*. En outre, l'existence dans des tissus normaux de particules morphologiquement identiques à celles qui peuvent dans certaines circonstances déclencher un processus cancéreux est du plus haut intérêt théorique (43, 44).

Nous exprimons nos plus vifs remerciements à M^{mes} Jacqueline Arnoult et Andrée Pissier et à M^{lle} Simone Paillet pour leur précieuse aide technique. Ce travail a pu être réalisé grâce à l'aide substantielle de la Mutuelle de l'Education Nationale.

SUMMARY

This study deals with the electron microscopic examination of 47 cases of fowl erythroblastosis and of numerous normal controls. In the leukemic chickens, virus particles, approximately 80 m μ in diameter, were demonstrated in the bone marrow in 37 cases and in the spleen in 21 cases. In cases of advanced leukemia, in which a high percentage of paraerythroblastic cells were found in the hematopoietic tissue, 90 % of the animals were positive.

The virus particles were found either in the intercellular spaces or in intracytoplasmic vacuoles of reticulum cells, of macrophages or of paraerythroblasts. A peculiar process of budding from the cell membrane, possibly related to virus formation, has been demonstrated.

Some of the vacuoles containing particles were of mitochondrial origin. These inclusions were less frequent in the paraerythroblasts than in the reticulum cells. Other intracellular vacuoles, containing both virus particles and red cell debris (lipids, hemoglobine derivatives), seemed to involve a process of phagocytosis of virus particles as well.

The same particles, intact or partly disintegrated, were found in the plasma of the leukemic chickens.

The particles were morphologically identical to those demonstrated in other neoplastic diseases of the chicken. They were also demonstrated in the tissues of 12.5 % of the control cases considered to be normal. The significance of these findings is discussed.

BIBLIOGRAPHIE

1. BANG, F. B., *Ann. Rev. Microbiol.* **11**, 21 (1955).
2. — *Federation Proc.* **14**, 619 (1955).
3. BEARD, D. et BEARD, J. W., *J. Nat. Cancer Inst.* **19**, 923 (1957).
4. BEARD, D., ECKERT, E. A., CSAKY, T. Z., SHARP, D. G. et BEARD, J. W., *Proc. Soc. Exptl. Biol. Med.* **75**, 533 (1950).
5. BEARD, J. W., *Cancer Research* **16**, 279 (1956).
6. BENEDETTI, E. L., *Bull. Cancer* **44**, 473 (1957).

7. BENEDETTI, E. L. et BERNHARD, W., *Compt. rend.* **244**, 2204 (1957).
8. BENEDETTI, E. L., BERNHARD, W. et OBERLING, CH., *Compt. rend.* **242**, 289 (1956).
9. BENEDETTI, E. L. et LEPLUS, R., *Rev. hématol.* **13**, 2, 199 (1958).
10. BERNHARD, W., BONAR, R. A., BEARD, D. et BEARD, J. W., *Proc. Soc. Exptl. Biol. Med.* **97**, 48 (1958).
11. BERNHARD, W., GUÉRIN, M. et OBERLING, CH., *Acta Unio Intern. contra Cancrum* **12**, 544 (1956).
12. BERNHARD, W., OBERLING, CH. et VIGIER, PH., *Bull. Cancer* **43**, 407 (1956).
13. BESSIS, M. M. et BRETON-GORIUS, J., *Compt. rend.* **244**, 2846 (1957).
14. BONAR, R. A., BEAUDREAU, G. S., SHARP, D., BEARD, D. et BEARD, J. W., *J. Natl. Cancer Inst.* **19**, 909 (1957).
15. BURMESTER, B. R., *Proc. Soc. Exptl. Biol. Med.* **88**, 153 (1955).
16. CARR, J. G., *Symposium on Interaction of Viruses and Cells*, Rome, 1953.
17. ——— communication personnelle, 1957.
18. COTTRAL, G. E., BURMESTER, B. R. et WATERS, N. F., *Poultry Sci.* **33**, 1174 (1954).
19. DEMPSEY, E. W. et WISLOCKI, G. B., *J. Biophys. Biochem. Cytol.* **1**, 111 (1955).
20. DMOCHOWSKI, L. et GREY, C. E., *Texas Repts. Biol. and Med.* **15**, 704 (1957).
21. DURAN-REYNALS, F., *Bull. Cancer* **38**, 114 (1951).
22. ECKERT, E. A., BEARD, D. et BEARD, J. W., *J. Natl. Cancer Inst.* **14**, 1055 (1954).
23. ECKERT, E. A., BEARD, D., BEARD, J. W. et BURMESTER, B. R., *J. Natl. Cancer Inst.* **13**, 1167 (1953).
24. ECKERT, E. A., SHARP, D. G., BEARD, D. et BEARD, J. W., *J. Natl. Cancer Inst.* **13**, 533 (1952).
25. ECKERT, E. A., SHARP, D. G., BEARD, D., GREEN, I. et BEARD, J. W., *Proc. Soc. Exptl. Biol. Med.* **88**, 181 (1955).
26. ECKERT, E. A., SHARP, D. G., MOMMAERTS, E. B., REEVES, R. H., BEARD, D. et BEARD, J. W., *J. Natl. Cancer Inst.* **14**, 1039 (1954).
27. ELLERMAN, V. et BANG, O., *Zentr. Bakteriolog. Parasitenk.* **46**, 595 (1908).
28. ENGELBRETH-HOLM, J., dans *Spontaneous and Experimental Leukaemia in Animals*, p. 245. Oliver & Boyd, Edinburgh, 1942.
29. EPSTEIN, M. A., *Brit. J. Cancer* **11**, 268 (1957).
30. FAGRAEUS, A. et THORELL, B., *Exptl. Cell Research* **10**, 515 (1956).
31. FAWCETT, D. W., *J. Biophys. Biochem. Cytol.* **2**, 725 (1956).
32. FEBVRE, H., GOLDÉ, A. et BENEDETTI, E. L., *Compt. rend.* (1958), sous presse.
33. GANSLER, H. et ROUILLER, CH., *Schweiz. Z. allgem. Pathol. u. Bakteriolog.* **19**, 217 (1956).
34. GAYLORD, W. H., *Cancer Research* **15**, 80 (1955).
35. GREENWOOD, A. W. et CARR, J. G., *World's Poultry Science Ass. Conference, Paris*, 1951.
36. HAGUENAU, F., MOLONEY, J. et DALTON, A., *Compt. rend.* **245**, 2230 (1957).
37. HAREL, J. et VIGIER, PH., *Bull. Cancer* **40**, 186 (1953).
38. HOLLMANN, K. H., communication personnelle.
39. HOTZ, G. et BANG, F. B., *J. Pathol. Bacteriol.* **73**, 331 (1957).
40. HOTZ, G. et SCHÄFER, W., *Z. f. Naturf.* **106**, 1 (1955).
41. MANNWEILER, K. L. et BERNHARD, W., *Bull. Cancer* (1958), sous presse.
42. MORGAN, C., ROSE, H. M. et MOORE, D. H., *J. Exptl. Med.* **104**, 171 (1956).
43. OBERLING, CH., *Le Cancer*, 381 p. Gallimard, Paris, 1954.
44. ——— *Oncologia* **7**, 2, 178, 1954.

45. OBERLING, CH., BERNHARD, W. et VIGIER, PH., *Nature* **180**, 386 (1957).
46. OBERLING, CH. et GUÉRIN, M., *Bull. Cancer* **23**, 38, 1934.
47. RHODIN, J., Correlation of Ultrastructural Organization and Function in Normal and Experimentally Changed Proximal Convoluted Tubule Cells of the Mouse Kidney. Stockholm, 1954.
48. ROUILLER, CH., HAGUENAU, F., GOLDÉ, A. et LACOUR, F., *Bull. Cancer* **43**, 10 (1956).
49. SHARP, D. G., ECKERT, E. A., BEARD, D. et BEARD, J. W., *J. Bacteriol.* **63**, 151 (1952).
50. VIGIER, PH., communication personnelle, 1958.

Microradiography for Absorption Analysis

V. M. MOSLEY AND R. W. G. WYCKOFF

*National Institute of Arthritis and Metabolic Diseases, National Institutes of Health,
Public Health Service,*

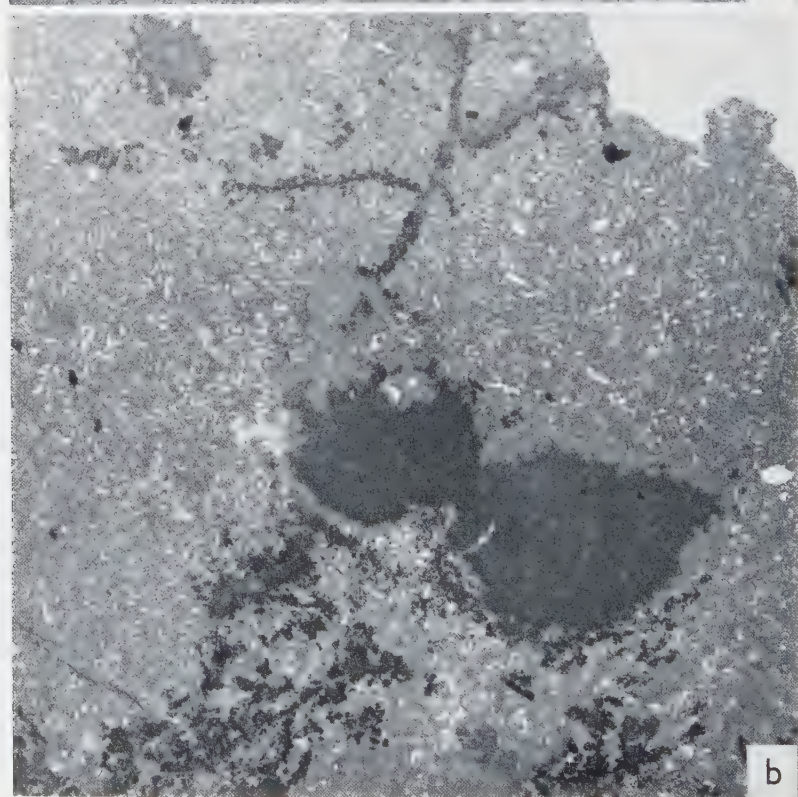
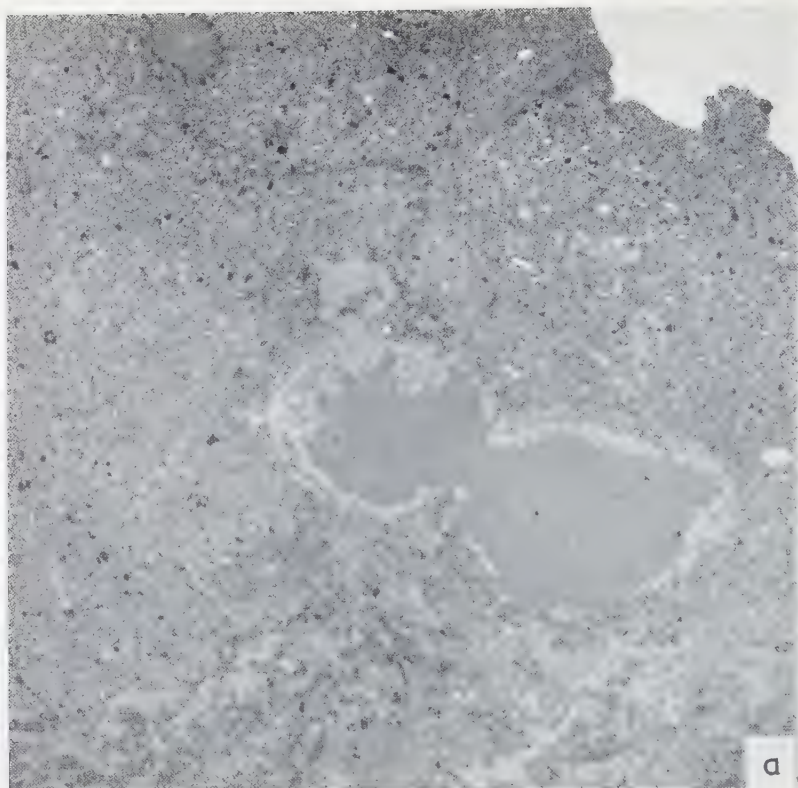
Department of Health, Education, and Welfare, Bethesda 14, Maryland

Received April 2, 1958

The projection X-ray microscope modified for vacuum microradiography can be used in absorption X-ray microanalysis for several of the lighter elements. When suitable targets are not available for it, the characteristic *K* radiation from other elements (at least down through magnesium) can be excited fluorescently with an intensity sufficient for rapid microradiography. This can be done with X-rays generated either in the microscope or in commercially available tubes having beryllium windows. The unquestionable identification of chemical elements present in microregions of a sample that thus becomes feasible is illustrated by microradiographs of several sectioned rocks.

Both the fluorescent X-rays emitted by a specimen and its X-ray absorption have long been used to identify some of the chemical elements it contains. In recent years fluorescent emission has been coming into steadily wider use due to the great sensitivity and speed possible when particle counters replace photographic registration but absorption analysis has not yet had a similarly broad acceptance.

Identification of an element can be made through its very different absorption for X-rays having wave lengths on either side of one of its critical excitation wave lengths: under favorable circumstances the amount of this element can also be determined from quantitative measurements of the change in absorption (4, 5). Such observations can be made on bulk samples but are most instructive when through microradiography they give information about the composition of microregions of a specimen. They involve radiography with a very wide selection of characteristic X-rays. Though its principles are all well-known (see for instance 1, 2, 8, 9), absorption analysis has been little used in the past through lack of adequate sources of such X-rays and because, in spite of work with calcium (3, 6 and others), it has generally been thought inapplicable to the lighter elements. This situation has been radically changed by the development of projection microradiography (X-ray microscopy) and by the introduction of water-cooled X-ray tubes having thin beryllium windows. With the X-ray microscope high resolution micrographs of both thick and thin specimens can be



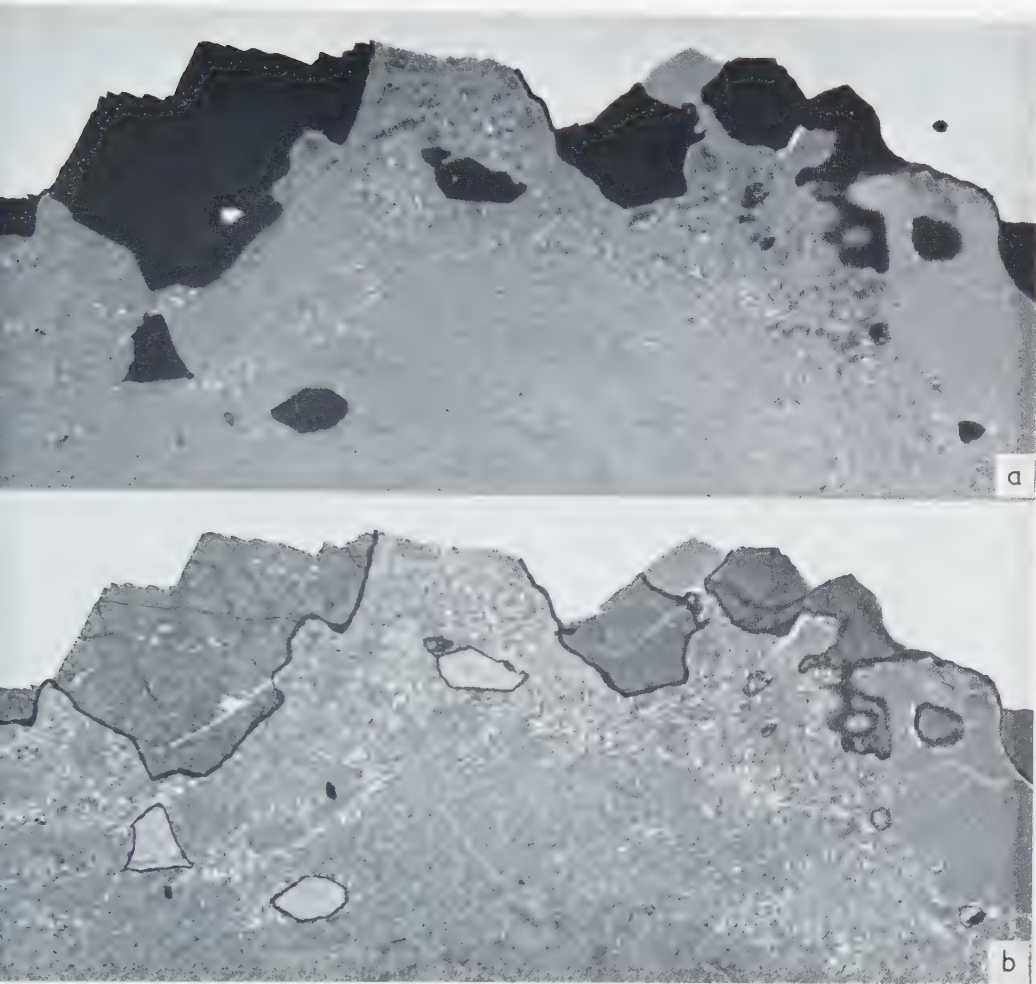


FIG. 2. *a*: A projection micrograph of another section of rock made with filtered copper *K* radiation. *b*: The same section of Fig. 2*a* photographed with titanium radiation. The increase in transparency of the two grains on the left of center is particularly striking; they must contain much titanium. $\times 15$.

FIG. 1. *a*: A projection micrograph of a 50 micra rock section made with copper *K* radiation (1 micron Cu foil as target, 15 micra Ni filter, 14 kV). The small opaque spots are rich in iron, the large relatively transparent region and several narrow veins leading to it are of a calcium mineral. *b*: A projection micrograph of the same specimen made with titanium *K* radiation (6 micra Ti foil as target, no filter, 8 kV). The calcium-rich areas have become relatively opaque owing to their high absorption of titanium radiation. In other radiographs made with calcium radiation they have again become transparent. $\times 12$.

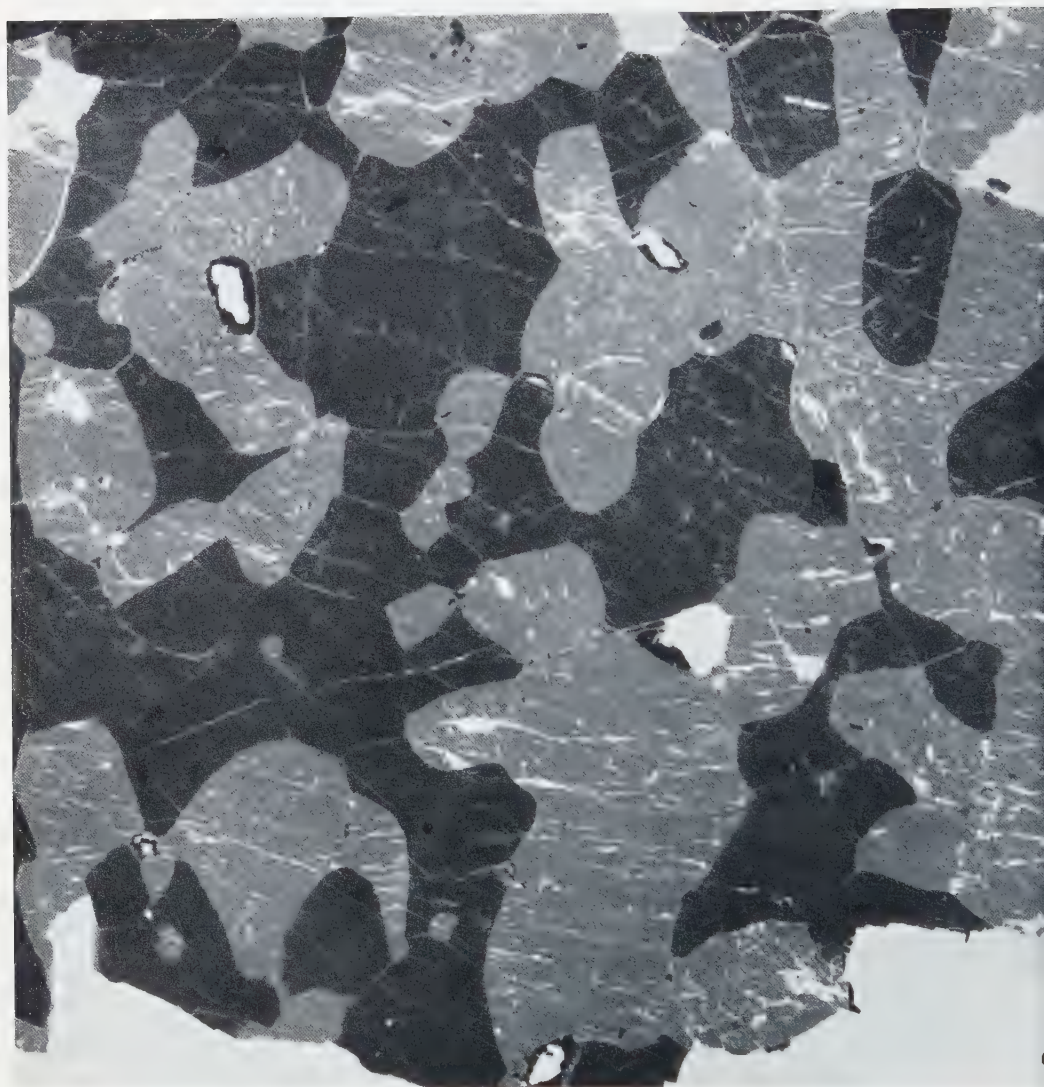


FIG. 3 *a*. A projection micrograph made with filtered copper *K* rays of another rock specimen. Here the transparent calcium-rich and the more opaque areas containing iron and titanium are of approximately equal areas. $\times 18$.

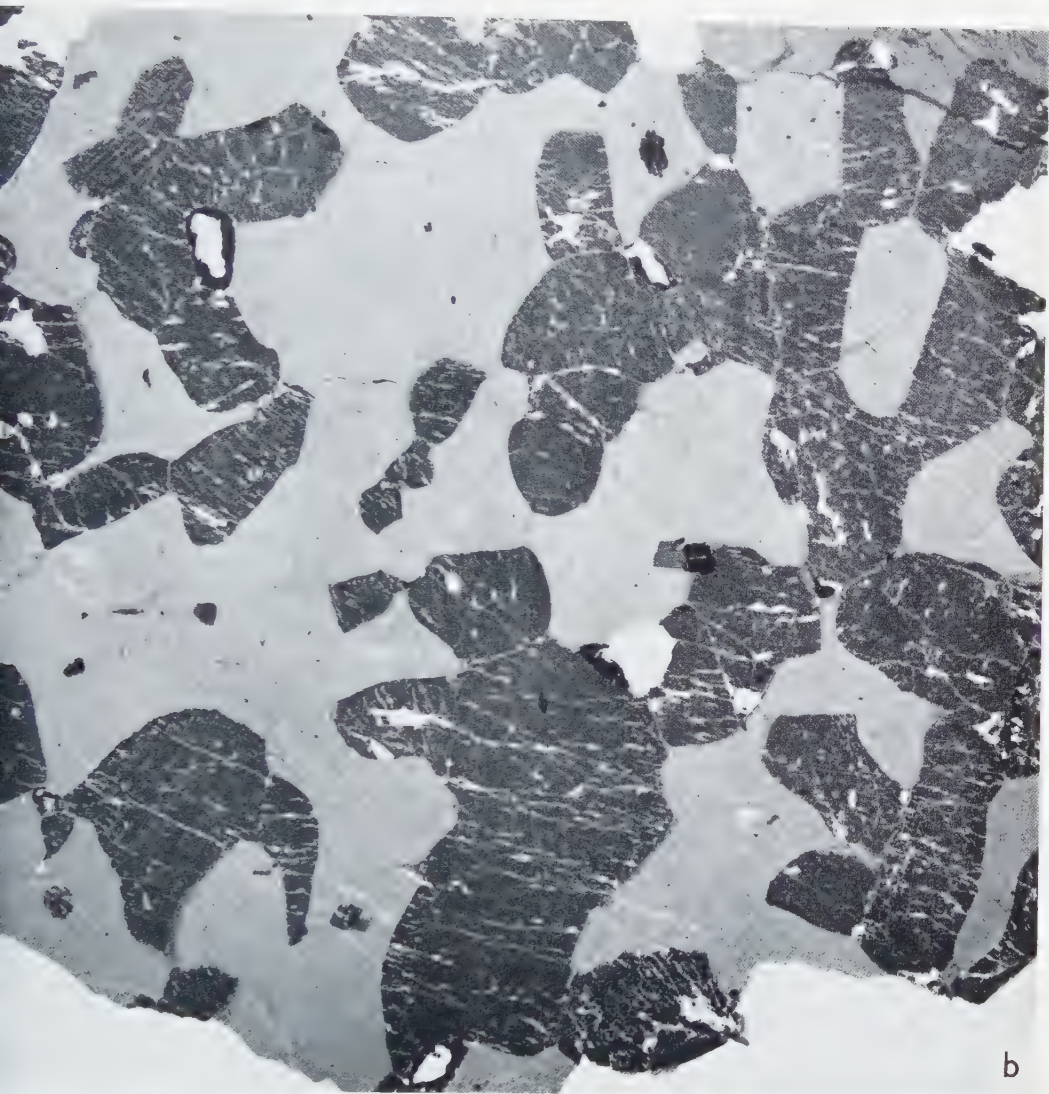


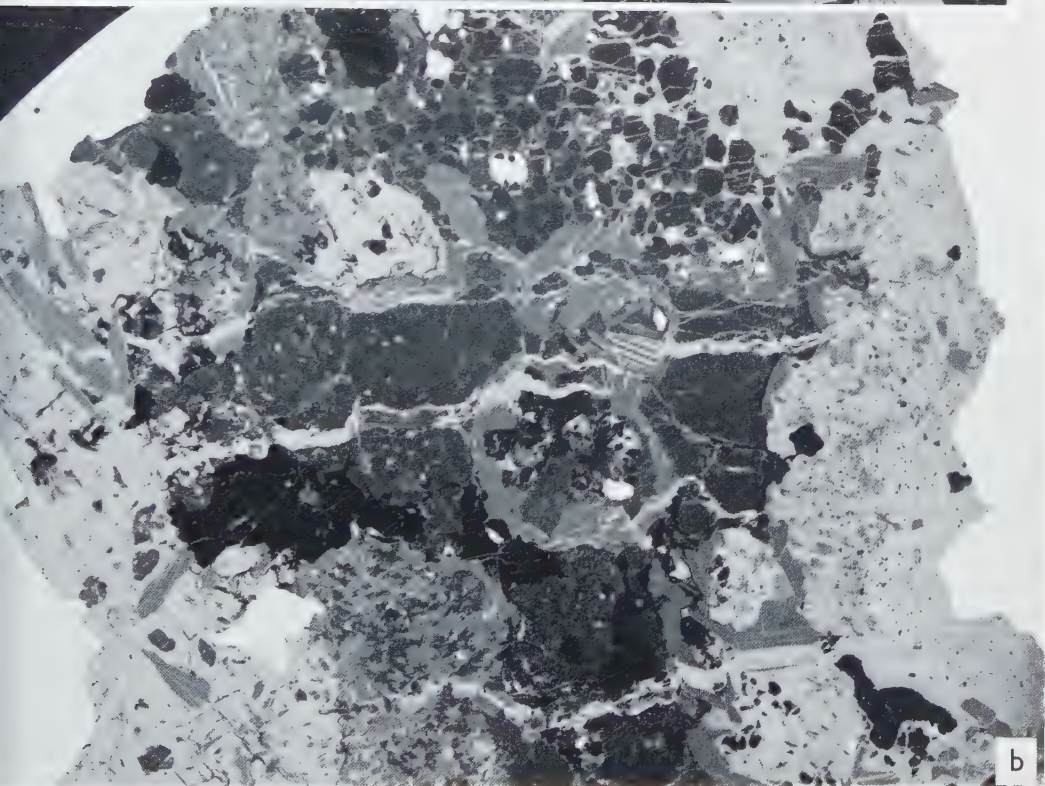
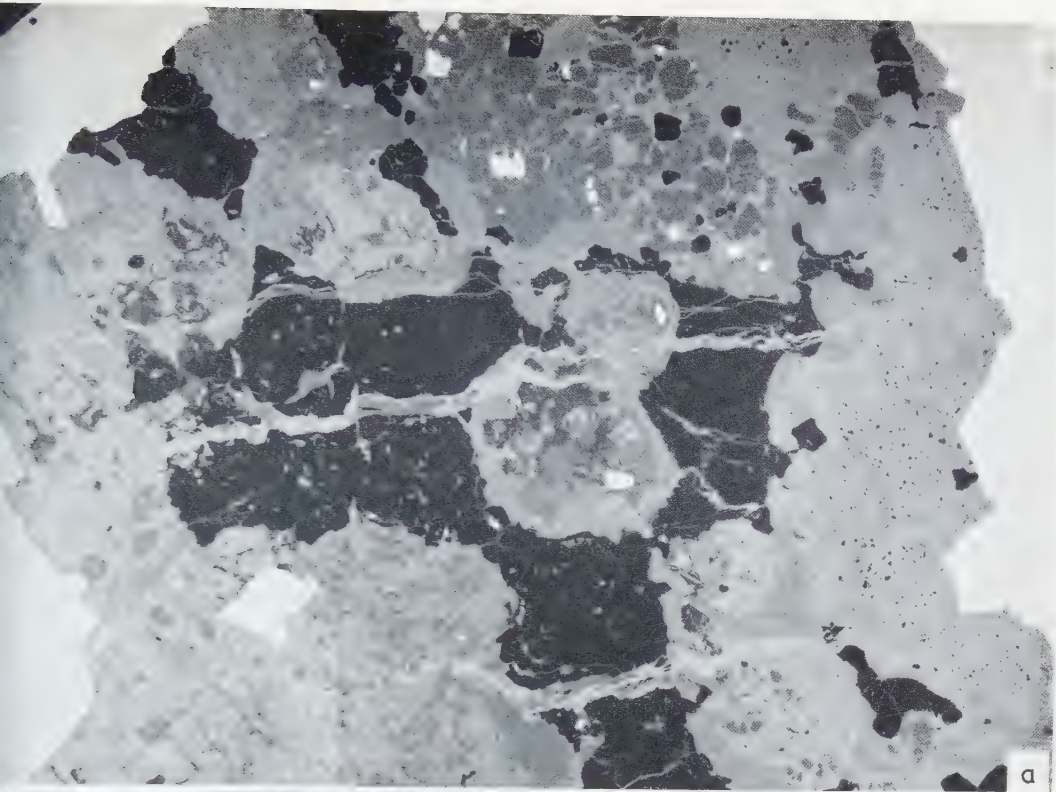
Fig. 3 *b*. The section of Fig. 3 *a* photographed with titanium radiation. The evident reversal in contrast is due to both the greater transparency of the titanium-rich areas and the enhanced absorption of calcium. $\times 18$.

made using the *K* radiation from a number of the lighter elements; beryllium-windowed tubes yield the soft X-rays needed for the intense fluorescent excitation of characteristic X-rays that cannot be directly produced. The present experiments were undertaken to evaluate the extended methods of absorption analysis that thus seem possible. In biology this analysis would have wide use as applied to the lighter elements but its immediate applications are to such inorganic materials as minerals and the light metal alloys. Specimens of rocks have proved to be especially convenient objects to use in evaluating and developing these absorption techniques. The accompanying micrographs have been made for this purpose and not to answer problems of mineralogical importance.

With the X-ray microscope of Cosslett and Nixon (7) modified for vacuum photography microradiographs can conveniently be made with both the harder X-rays and those softer radiations that are stopped in air. Its minute source gives a high resolution with samples too thick for the best contact microradiography; several targets can be made from commercially available light metal foils and these sources of characteristic X-rays can be supplemented by targets consisting of other metals evaporated on thin magnesium or aluminium foil. White radiation also is emitted by these light metal targets but if their thicknesses are properly chosen the characteristic radiation predominates.

The paired photographs of Figs. 1 through 4 are typical of the projection micrographs to be obtained with rock sections of the thickness routinely required for petrographic examination (50–100 micra). These micrographs were made with Cu *K* and Ti *K* radiations of four different rocks found by fluorescent emission to contain considerable amounts of iron and calcium. The areas relatively more opaque in Fig. 1 *b* (Ti *K*) than in Fig. 1 *a* (Cu *K*) are rich in calcium; the small especially opaque regions of Fig. 1 *a* are rich in iron. The specimens responsible for Figs. 2, 3 and 4 also gave strong fluorescent peaks for titanium. The photographs of Fig. 2, and others made with different radiations, show that the opaque iron-rich regions of Fig. 2 *a* are of three sorts: (1) small isolated areas rich in titanium which are as a consequence very transparent to the titanium *K* radiation of Fig. 2 *b*, (2) larger areas that remain moderately opaque in Fig. 2 *b*, and (3) narrow bands around both (1) and (2) which, remaining very opaque in Fig. 2 *b*, are rich in calcium. Fig. 3, reinforced by the contact microradiographs of Fig. 6 (to be discussed later), demonstrates that the more transparent areas of Fig. 3 *a* are calcium-rich while those of Fig. 3 *b* contain both iron and titanium. Fig. 4 provides an example of the discrimination between components that is possible with a morphologically more complicated rock.

FIG. 4. *a*: A projection micrograph of a portion of another rock made with filtered copper X-rays. *b*: The section of Fig. 4 *a* photographed with titanium radiation. The different iron content of different mineral grains leads to well-marked changes in their opacities compared with Fig. 4 *a*. $\times 16$.



The foil-targets of the X-ray microscope do not give enough different radiations for the positive identification of many elements. The characteristic radiations of all elements (except the rare gases) can, however, be obtained by fluorescent excitation in compounds of suitable composition. This can be done in the X-ray microscope if a foil-target is available to give primary X-rays close enough in wave length to the

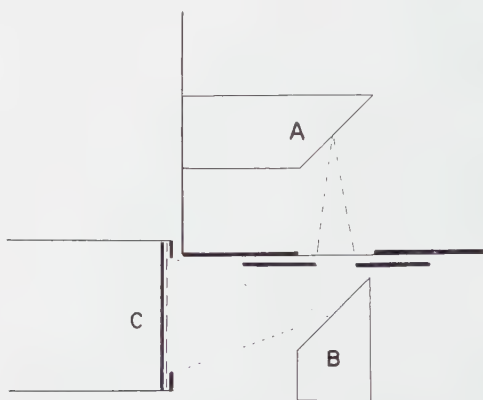
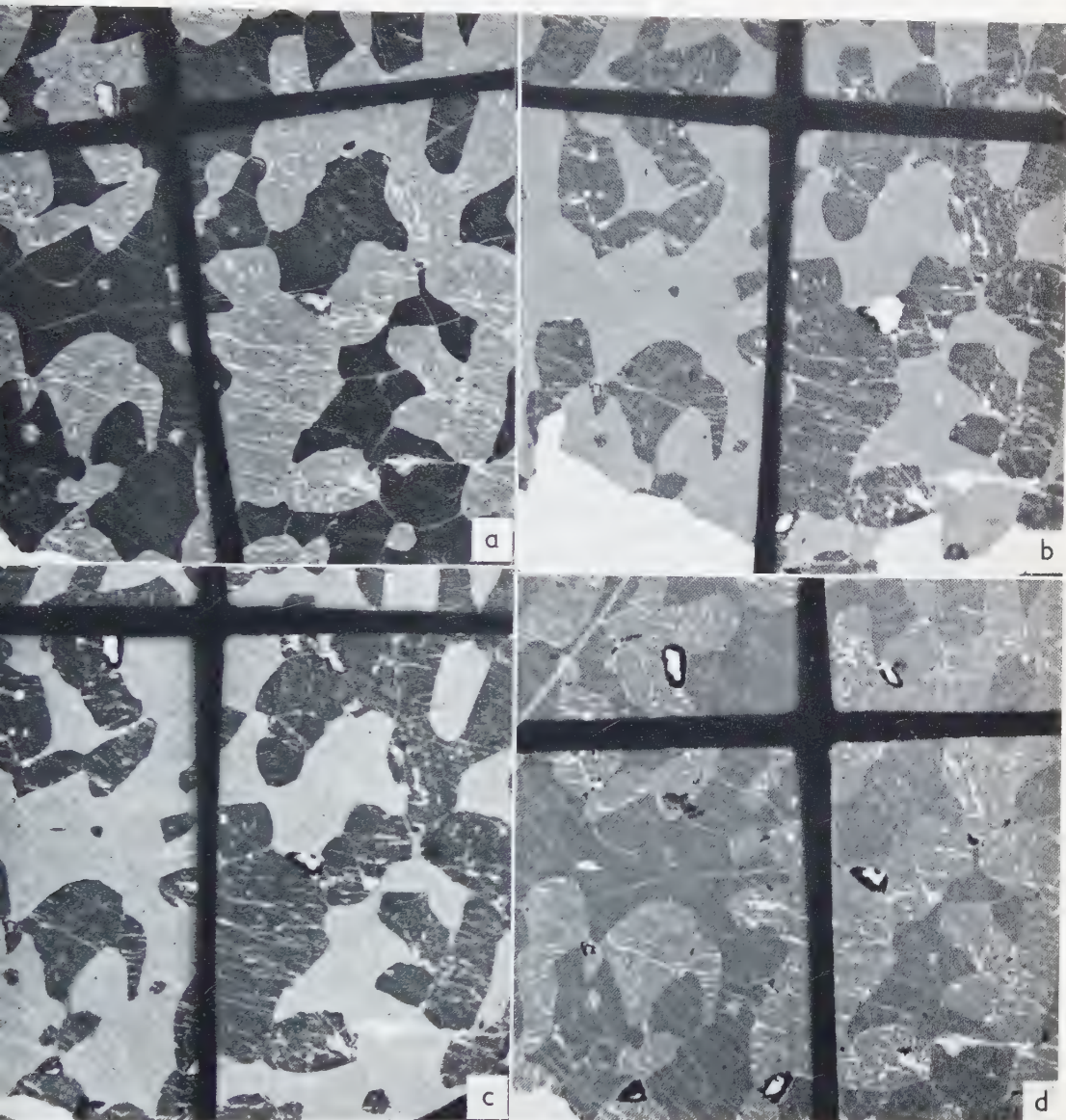


FIG. 5. The relative positions of X-ray tube (A), fluorescent radiator (B), specimen and photographic plate (C) for "reflection" fluorescent micrography

desired radiation to excite it with especial efficiency. The fluorescent radiator will then be a sheet placed upon the foil-target; it must be thick enough to absorb most of the primary X-rays but thin enough to pass most of the characteristic radiation they generate in it. For example, when a titanium foil ca. 12 micra thick is placed on a chromium target the fluorescent *K* radiation originating in it will yield a projection microradiograph of the sample of Fig. 3 showing the same detail and relative opacities as one made with a target of titanium (Fig. 3 *b*); the requisite exposure time is increased by only 50%. Similarly micrographs have been made with calcium radiation by placing a thin slab of calcite over a titanium foil-target. There is necessarily a loss of resolution due to the larger dimensions of these fluorescent sources but with good contact between target and secondary radiator it will not be apparent at the magnifications used here.

This "transmission" technique for generating the fluorescent X-rays needed for micrography can only be used when a thin homogeneous slab of the desired fluorescent material can be prepared and when primary radiation near its critical excitation wave length is available. In other instances contact must replace projection micrography and the fluorescent X-rays must be taken by "reflection" from the face of a thick secondary radiator placed close to the beryllium window of a sufficiently power-



a: A contact micrograph of the specimen of Fig. 3 made with fluorescent chromium *K* radiation generated by the element of Fig. 5, the radiator being powdered metallic chromium. The primary X-rays for this and the other contact micrographs reproduced here were the output of a tungsten-target tube operated at 40 kV, 10 mA. Exposure was 10 minutes with Eastman contrast lantern slide emulsion. The cross interrupting this and the other contact micrographs reproduced here was a frame to insure good contact between specimen and photographic plate. *b*: A similar contact micrograph made with V_2O_5 as fluorescent radiator. *c*: The contact micrograph made with metallic titanium as fluorescent radiator. The detail is seen here with the same contrast as in the projection micrograph of Fig. 3 *b* made with primary titanium radiation. *d*: The contact micrograph made when a crystal of calcite, chosen to give essentially calcium *K* radiation, served as fluorescent radiator. $\times 9$.

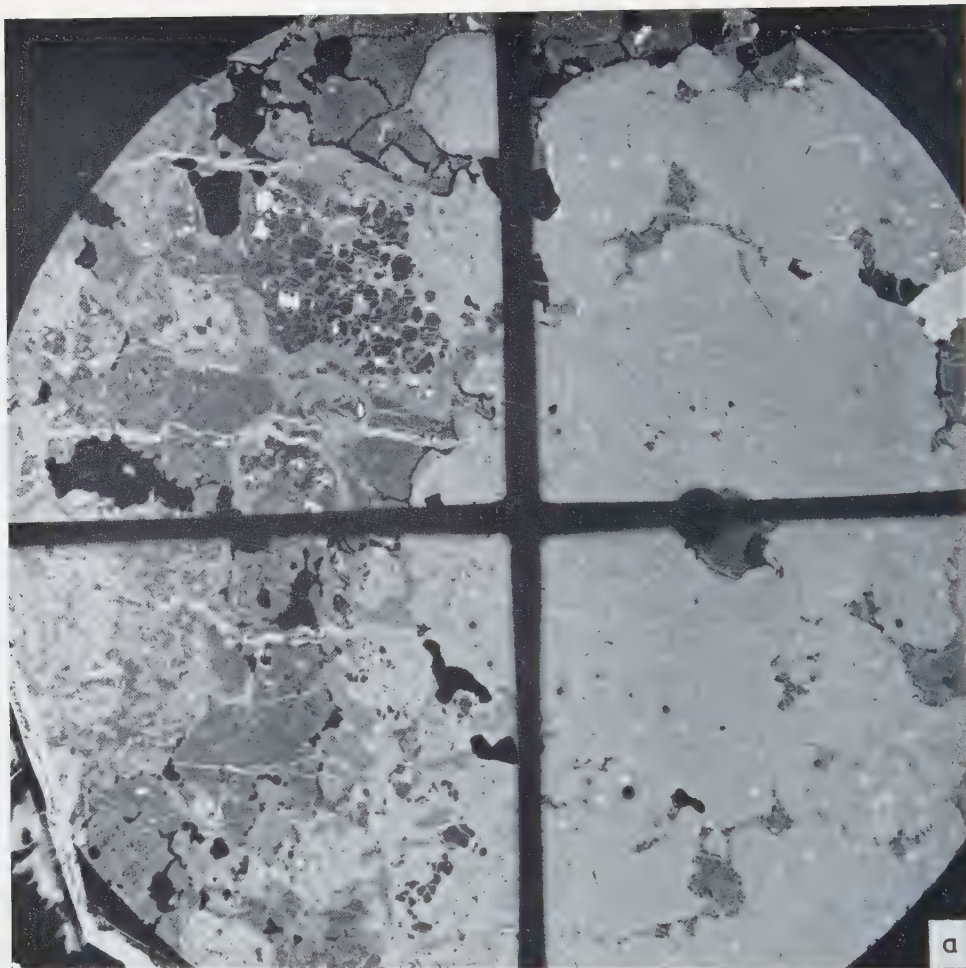


FIG. 7 *a*. A contact micrograph of a larger area of the mineral sample of Fig. 4 made with powdered metallic chromium as fluorescent radiator. The details common to this and Fig. 4 are readily recognized. $\times 9$.

ful X-ray tube (Fig. 5). When a water-cooled tungsten target tube has been used, exposures of no more than a very few minutes are required for contact micrographs with the fluorescent radiations of all the lighter elements (except argon) down through magnesium. In view of strong scattering of tungsten radiation by the lighter elements and its inefficiency as exciter of their characteristic X-rays, it is to be expected that still better and more rapid results would be obtained with X-ray tubes having light metal targets.

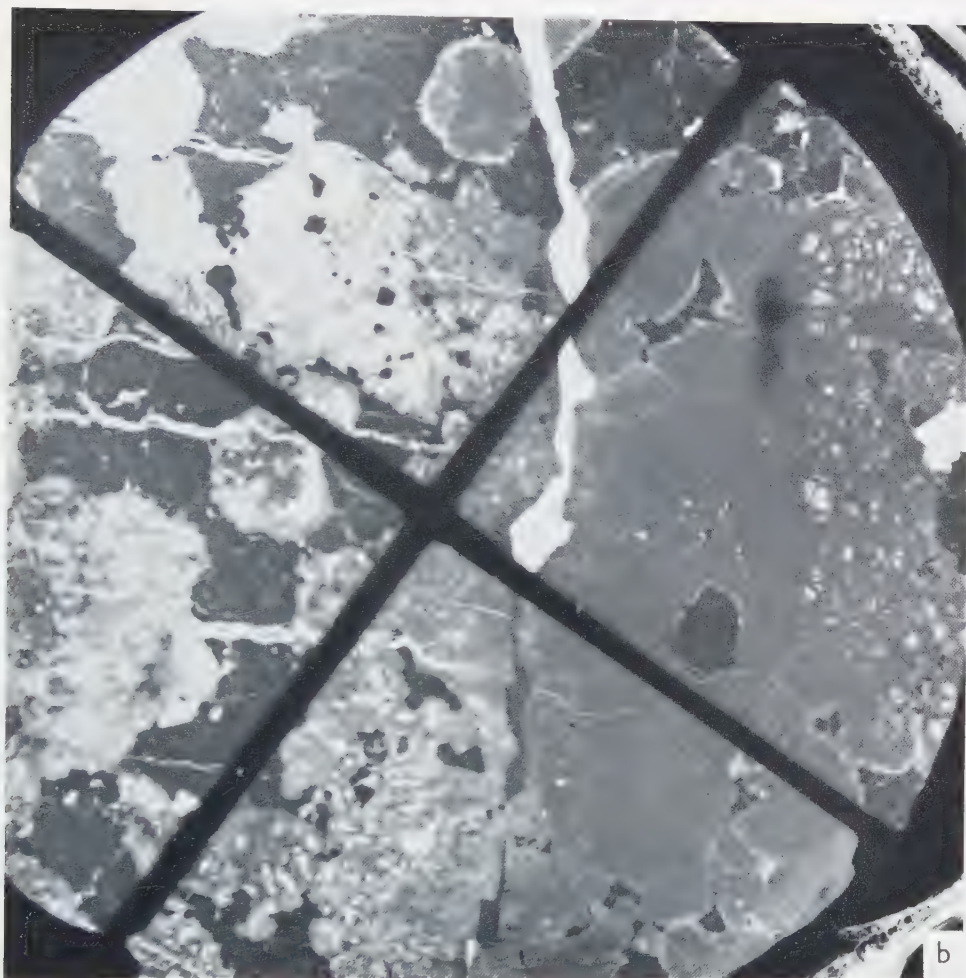


FIG. 7 *b*. A contact radiograph of the sample of Fig. 7 *a* made with a crystal of NaCl as fluorescent radiator. Note the many new details, including the otherwise invisible fibers at the right, which are brought out by this softer radiation. $\times 9$.

The good quality of the contact micrographs to be obtained with “reflected” fluorescent radiations and the certainty in identification that results from being able to use the radiations from a series of neighboring elements is illustrated by Fig. 6. These micrographs show the sample of Fig. 3 photographed with radiations of the four neighboring elements: Cr ($n\ 24$), V ($n\ 23$), Ti ($n\ 22$) and Ca ($n\ 20$). There is an evident reversal of contrast in passing from chromium to vanadium *K* radiations due to the fact that the chromium *K*, but not the vanadium *K*, X-rays excite (and hence are

strongly absorbed in) the titanium of the specimen while at the same time the vanadium *K* is more strongly absorbed than the chromium *K* radiations in the calcium that is present. As would be expected the photograph made with titanium radiation (Fig. 6 *c*) shows the same relative absorption as that made with vanadium (Fig. 6 *b*); but with calcium *K* radiation (Fig. 6 *d*), there is again a reversal of contrast due to the transparency of calcium to its own radiation.

Fig. 7 reproduces at a lower magnification two contact micrographs of larger areas of the sample of Fig. 4. The detail brought out by the chromium *K* radiation of Fig. 7 *a* is recognizably similar to that in the projection micrograph of Fig. 4 *a* made with titanium radiation. The remarkably different detail that is apparent throughout Fig. 7 *b*, made with a crystal of NaCl as fluorescent radiator, is a good illustration of how much information about microcomposition is contained in photographs made with long characteristic X-rays.

In view of their obvious value it is important to establish the best conditions for making these contact radiographs. This involves (1) having a source of primary radiation more efficient than that supplied by a tube with a tungsten target, (2) arranging the geometrical conditions of Fig. 5 so that a minimum of primary radiation scattered by the sample and apparatus reaches the photographic plate and (3) reducing as much as possible the area of fluorescent emission. The contact micrographs of Figs. 6 and 7, and about 100 more using a variety of radiators of low atomic number, have been made with very preliminary equipment giving fluorescent sources about a square centimeter in area. With so big a source the slightest lack of good contact between specimen and plate leads to the kind of diffuseness of image noticeable in Figs. 6 *c* and 7 *b*.

Work is now being carried out to design apparatus that will give the improved results the experience gained in these early experiments indicates as possible.

REFERENCES

1. CLARK, G. L., *Applied X-rays*, p. 180. New York, 1940.
2. CLARK, G. L. and GROSS, S. T., *Ind. Eng. Chem., Anal. Ed.* **14**, 676 (1942).
3. DERSHEM, E., *J. Opt. Soc. Am.* **29**, 41 (1939).
4. ENGSTRÖM, A., *Acta Radiol.* **63**, Suppl. (1946).
5. ENGSTRÖM, A. and LINDSTRÖM, B., *Biochim. Biophys. Acta* **4**, 351 (1950).
6. ENGSTRÖM, A. and WEGSTEDT, L., *Acta Radiol.* **35**, 345 (1951).
7. NIXON, W. C. and COSSLETT, V. E., *Brit. J. Radiol.* **28**, 532 (1955).
8. SPROULL, W. T., *X-rays in Practice*, p. 289. New York, 1946.
9. TRILLAT, J. J., *Bull. soc. franç. élec.* **3**, No. 25 (1943).

The Use of Gelatin for Embedding Biological Specimens in Preparation of Ultrathin Sections for Electron Microscopy¹

V. P. GIL'EV

Laboratory of Electron Microscopy, Department of Biology, Academy of Sciences of the U.S.S.R., Moscow

Received April 21, 1958

A method is described for embedding tissues in gelatin which makes it possible to cut thin sections for electron microscopy. With this method it is possible to embed the tissue without passing it through organic solvents extracting the lipid soluble components. Observations made on muscle tissue embedded with this technique have revealed structural components which do not appear after embedding in methacrylate.

The majority of investigators working in the field of electron microscopic cytology and histology apply the technique of embedding biological objects in methacrylates which was described by Newman *et al.* (8).

This method as most of the other less widely used methods (embedding in esterwax, Mixture "211", celloidin-paraffin, etc.) includes treatment of the specimens with organic solvents (alcohol, benzine, methacrylic acid aethers, etc.). Treatment with such substances changes the specimen itself and leads to a washing out of the adipic substances which are fixed badly or not at all by osmium tetroxide.

In this connection, it was proposed to embed biological objects in polyethylene-glycols of high molecular weight, which are soluble in water (2, 5, 11 and others). But, as it was difficult to make ultrathin sections of the specimens embedded in these substances, this method did not become wide-spread in electron microscopy.

The technique of gelatin embedding, proposed by the author, enables one to obtain sections as thin as 200 Å without treating the specimens with organic solvents. The latter affords a preservation of some details of the tissues which are changed to a lesser degree than when other embedding techniques are employed.

Tissues do not undergo such shrinkage with this method as when treated with alcohols. Certain details are detectable more easily than is the case in methacrylate embedding. Fat- and lipid-containing structures are well preserved. Recently Fer-

¹ The results of the work presented, with the exception of some new material, were reported at the Stockholm Conference on Electron Microscopy, held in September 1956, and published in the Proceedings of this conference.

nández-Morán and Finean (4) have applied a similar technique to that described earlier by the author (6). They state that gelatin embedding produces fewer alterations in the laminated structure of the myelin sheath than does methacrylate embedding. Sections as thick as $1-2\ \mu$ and thicker can readily be prepared from gelatin embedded specimens to be studied in the light microscope.

The technique includes the following procedures: (1) Purification of gelatin and preparation of its solutions for embedding. (2) Impregnation of fixed specimens and embedding. (3) Preparation of blocks. (4) Cutting in a microtome, flattening of the sections and mounting on the grids. (5) Further treatment of the specimens.

Purification of gelatin and preparation of its solutions for embedding

A 10% water solution of food gelatin is boiled for several minutes together with beaten-up hen egg albumen and activated charcoal. Per 300 cm³ of gelatin solution the albumen of one hen egg and 3 g of activated charcoal are taken. Then the solution, while warm, is filtered with vacuum, through a paper and then through an asbestos bacterial filter. One portion of the solution is evaporated to half its volume in a thermostat at a temperature of 45°C. The remaining portion is evaporated to three fourths of its initial volume. Thus 20% and 40% solutions are obtained which are used for impregnation and embedding.¹

20% and 40% solutions of refined gelatin in Ringer's solution can also be prepared.

The solutions must be absolutely transparent. For preparation thymol is added.

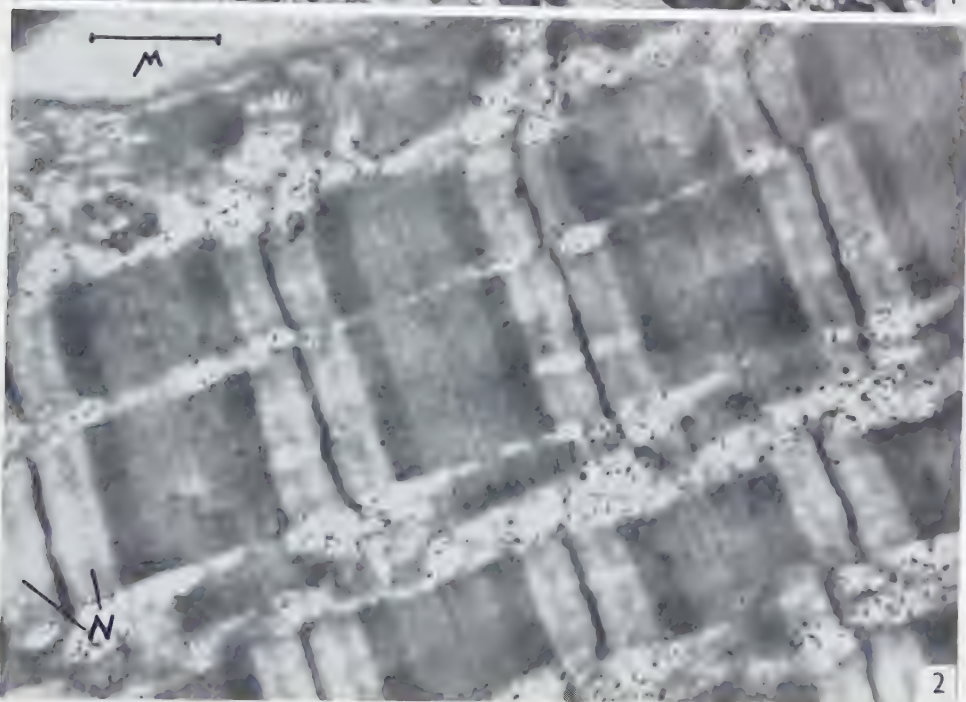
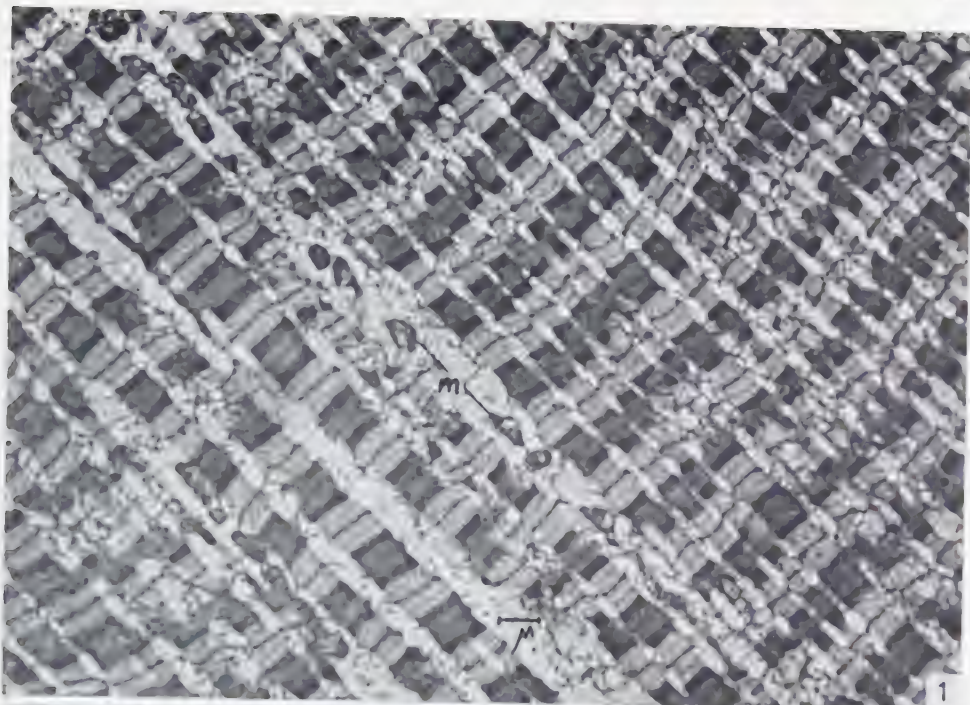
Impregnation of fixed specimens and embedding

The specimens (striated muscle tissue of the axolotl, *Amblistoma punctatum*) were fixed with osmium tetroxide according to Palade's method (9) at pH 7.4–7.5 for 20 hours at +1°C.² After being washed under tap water or in Ringer's solution (1–4 hours), the specimens were immersed for 4 hours in a 20% solution of purified gelatin at 37°C. They were then placed in a 40% solution for 15 hours. In this time pieces of muscle tissue, $1 \cdot 0.3 \cdot 0.3$ mm, are well impregnated with gelatin. Further investigations showed the specimens to be well impregnated with gelatin after a shorter period of time (2 hours in the 20% and 1 hour in the 40% solution).

¹ Gelatin solution sold in ampules (10% *gelatina sterilisata pro injectione*) may also be used.

² At present we fix (at pH 7.2) at the temperature of 4°C for 4 hours (10, 12).

FIGS. 1 and 2. Sections treated with 4% warm (37°C) acetic acid. In the myofibrils not only the A- and I-bands and Z- and M-lines are to be seen, but the N-band as well, which is badly or not at all revealed in the myofibrils of the axolotl when embedded in methacrylate. Myofilaments are to be seen, but not so distinctly, as in the case of methacrylate embedding. *m*, mitochondria. $\times 5000$ and $16,500$ respectively.



The 40% solutions containing the specimens are then poured out on oil cloth and dried slowly at 37°C until the gelatin is hard but not brittle. In order to obtain a uniform concentration of the gelatin, the drying is slowed down by covering it with a bell jar. Only a narrow gap between the edge of the bell jar and the oil cloth is left open for a slow escape of water vapour. Such gradual increase of gelatin concentration prevents uneven shrinkage of the object. In the process of hardening the specimens decrease in size, but to a lesser degree than with the case of dehydration by alcohols.

In the description of gelatin embedding presented by Fernández-Morán and Finean we do not understand quite clearly how the further impregnation of the specimen with gelatin proceeds after the cooling and solidifying of the block. It still contains about 70% of water when transferred into the vacuum. It would seem possible that the gelatin surrounding the specimen will deformate it strongly when drying.

Preparation of blocks

The hardened plate of gelatin containing the specimens is separated from the oil-cloth and cut into rectangular blocks. The blocks are glued with a 60–70% gelatin solution to an old methacrylate block sharpened in the form of a truncated pyramid. To strengthen the connection between the gelatin block and the pyramid, one makes some notches on the latter. The blocks are then placed for several hours into a thermostat (37°C) for complete drying.

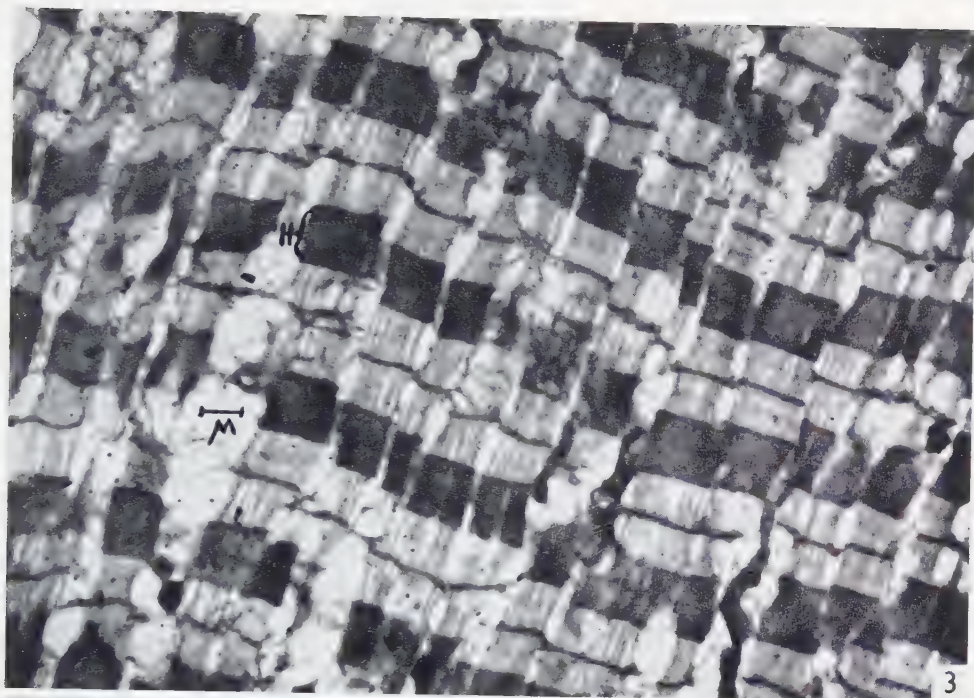
Immediately before cutting in a microtome, the blocks are sharpened in such a way that the square of the forthcoming first section does not exceed 0.1 mm². At present, we sharpen blocks in the form of a pyramid, as it is recommended in the instruction for the Sjöstrand ultramicrotome. The blocks are kept in cans with tight caps.

Cutting in a microtome, flattening of sections and their mounting on grids

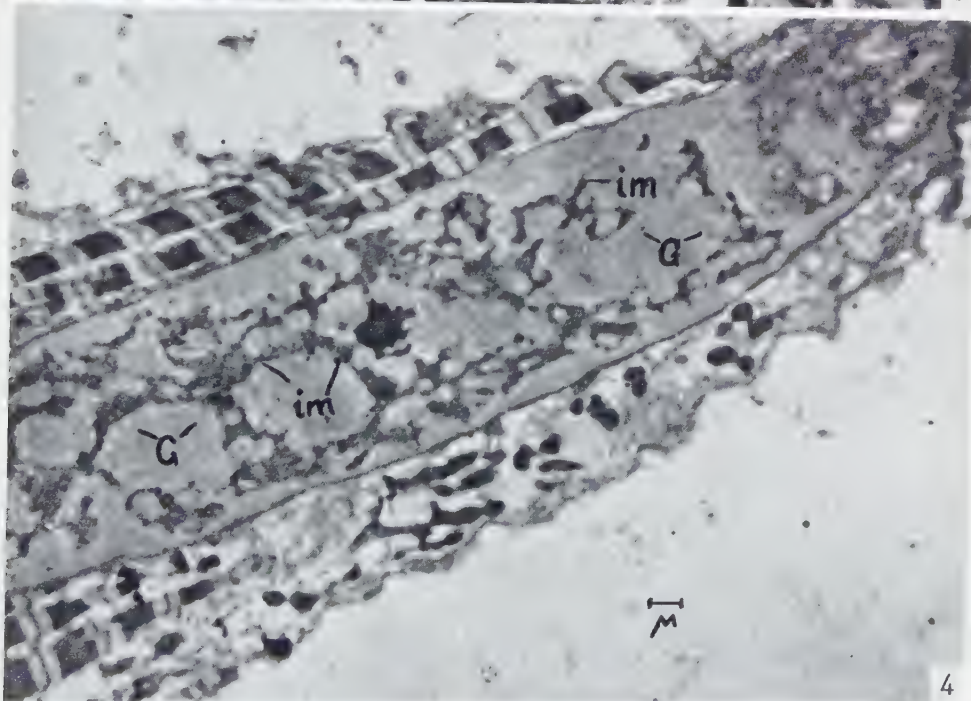
One has to cut with a glass knife (3, 7) without fluid. In our work, we used mainly a microtome of Danon and Kellenberger with a rocking block. At present we use a Sjöstrand ultramicrotome. The long side of the block or, respectively, the base of the pyramid should be parallel to the knife edge. Blocks, just dried, cut badly in

FIG. 3. Gelatin partially eliminated from the section by 2% acetic acid. The H-band strongly widened. Myofibrils in the I-bands somewhat narrowed. $\times 5000$.

FIG. 4. Among the small granules (G) in the interkinetic nuclei of the striated muscle tissue of the axolotl, peculiar small irregular masses are to be seen, which form rods and loops (*im*). Judging by the high affinity to osmium one may suppose these structures to be of lipoprotein character. These structures are not found in sections of tissues embedded in methacrylate. This fact is, presumably, connected with the nature of the treatment. However, somewhat similar structures may be seen, sometimes, in methacrylate-embedded sections (cf. Fig. 9). $\times 4000$.



3



4

dry weather. In this case, it is better to cut them not earlier than 24 hours after they were exposed to air.

In the case of considerable humidity of both the air and the blocks, it is recommended to dry the blocks some time before cutting. The position of the knife in cutting gelatin blocks is usually, to some extent, steeper than in cutting methacrylate blocks. The rate of cutting is approximately 1 section per 1 sec. It is not very difficult to obtain sections of 300–400 Å (Danon and Kellenberger's microtome). Usually the sections are formed in the shape of endurable, undisintegrating ribbons. These ribbons are separated in sections or groups of sections and transferred with a thin filament into drops of water (or better a drop of 2% acetic acid) lying on a Parlodion film floating on the surface of water (temperature of about 37–40°C) filling a Koch dish. However, better results are obtained if the sections are placed into water at room temperature, which is subsequently heated up to 37–40°C.

When flattening, the connections between the sections are destroyed, so that a series of sections is not always obtained. Then the film is punctured under each drop with a thin needle and the sections sink to the intact part of the film. The copper grids are placed on the film in such a way that the centre of the grid is above the sections. Thereafter, from above, a slide is placed on the surface and with the film and grids.¹ After drying, the specimens are ready for the examination in an electron microscope.

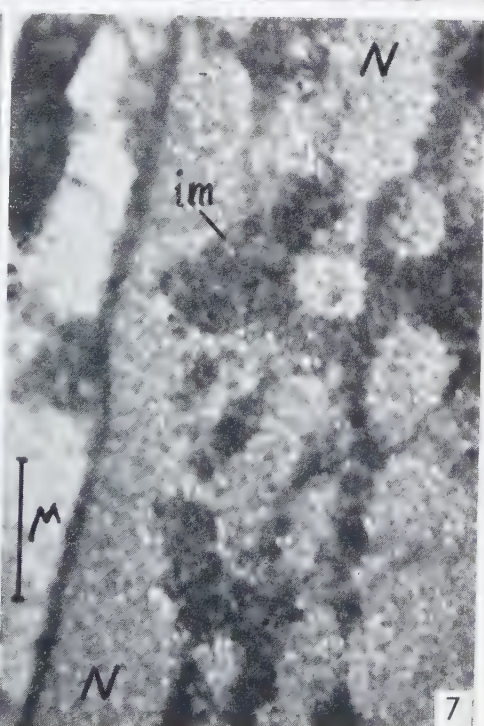
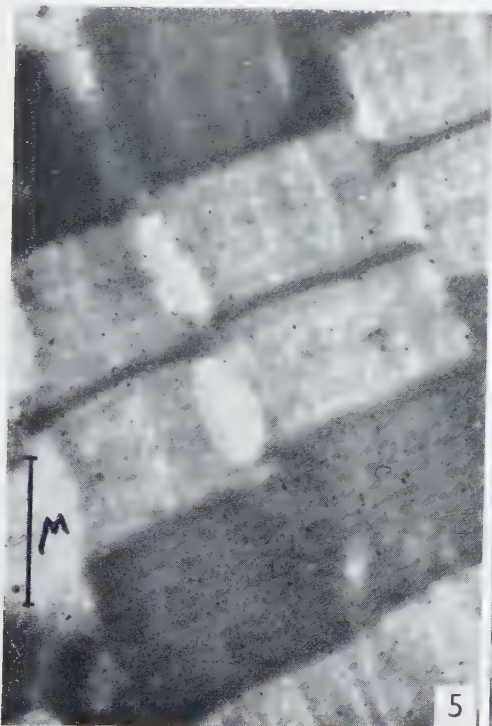
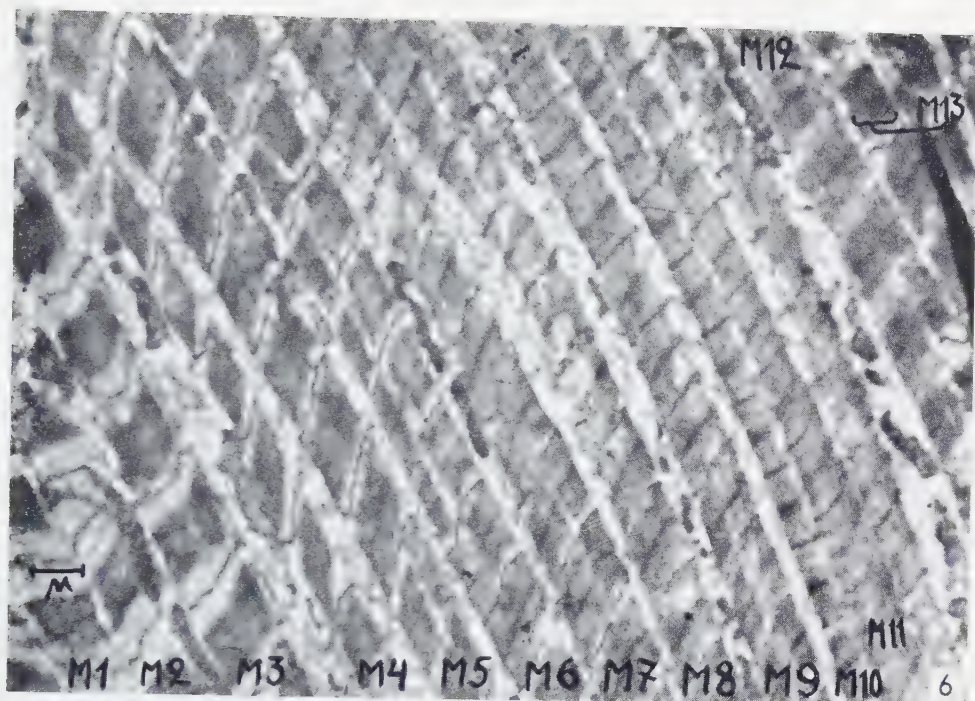
If rotary microtomes are used, the sections, when cut, are collected in a trough attached to the knife. Water or, better, an 0.5% solution of potassium chrome-alum,

¹ This method of mounting sections was elaborated together with V. I. Birjuzova, one of the collaborators of our laboratory.

FIG. 5. Higher magnification of a portion of the section shown in Fig. 3. In the I-bands, the "secondary striations" ("bridges") are to be seen. The H-band strongly widened. $\times 18,000$.

FIG. 6. The relative ease, with which large gelatin sections may be obtained, permits observation of large tissue areas in one field. In this micrograph, for example, all the stages of myofibril contraction are represented in one field. Myofibrils in the left, lower corner (*M1* and *M2*) are stretched. The A-, I- and Z-bands are well demonstrated; the M-line is almost invisible. In the middle portion (*M3-11*) are pictured a series of changes taking place in the sarcomere structure of myofibrils in the process of contraction: the heights of the I-bands rapidly decrease, the M-lines become more and more distinct and the A-bands, though barely decreasing in length, absorb osmium more feebly. At the end of the series, the I-bands disappear completely whereas the "stainable substance" of the A-band is evenly distributed over the sarcomere. Myofibrils in the right upper corner (*M12* and *M13*) are, presumably, in the state of transition from the contracted to the stretched stage: "stainable substance" is concentrated at both sides of the M-band, which at this stage is more apparent than the Z-band; the A- and I-bands appear. The Z-bands appear or become more evident only at stages that exhibit greater stretching (*M13*). It is also characteristic that the process of contraction involves many fibrils in different stages of contraction at any one time (*M3-11*) whereas the process of relaxation proceeds more "abruptly" (*M12* and *M13*). $\times 6600$.

FIG. 7. Higher magnification of a portion of the muscle fiber shown in Fig. 4. *N*, nucleus; *im*, "irregular masses". $\times 17,500$.



$K_2SO_4 \cdot Cr_2(SO_4)_3 \cdot 24H_2O$, are poured into the trough. The alum prevents the sections from sticking and from adhering to the knife edge when cutting. The sections are obtained in the form of ribbons and are readily flattened without special treatment, so they are caught on the grids directly from the trough. To remove the alum, the grid is for a few seconds put on the surface of the distilled water. On the Sjöstrand ultramicrotome good ribbons with sections of about 200 Å thick were easily obtained.

Further treatment of specimens

For a more complete elimination of gelatin from the sections, if necessary, the grids with the sections are immersed for 2–4 hours into warm water (37–40°C) or into a weak acetic acid solution.

GENERAL REMARKS

The osmium tetroxide remaining in the specimen after fixation and washing (especially if a short-termed one) interacts¹ with the gelatin to a certain degree after which the latter becomes less transparent and forms a rather strong background that makes some fine details of the tissue structure less visible.

Therefore, a shorter-termed fixation before gelatin embedding and a longer-termed washing of objects is recommended. One may suppose, however, that the presence of such a background is connected with the preservation of substances which are eliminated or precipitated by treatment with alcohol or methacrylate.

To preserve embedding material in the sections, there is no use of flattening them in cold (+1°, +2°C) water, as we thought earlier (6). There is also no need of accessory water heating for flattening the sections. The sections are readily flattened and the gelatin preserves long enough if held in water at room temperature, especially, if 0.5% alum is added to the water.

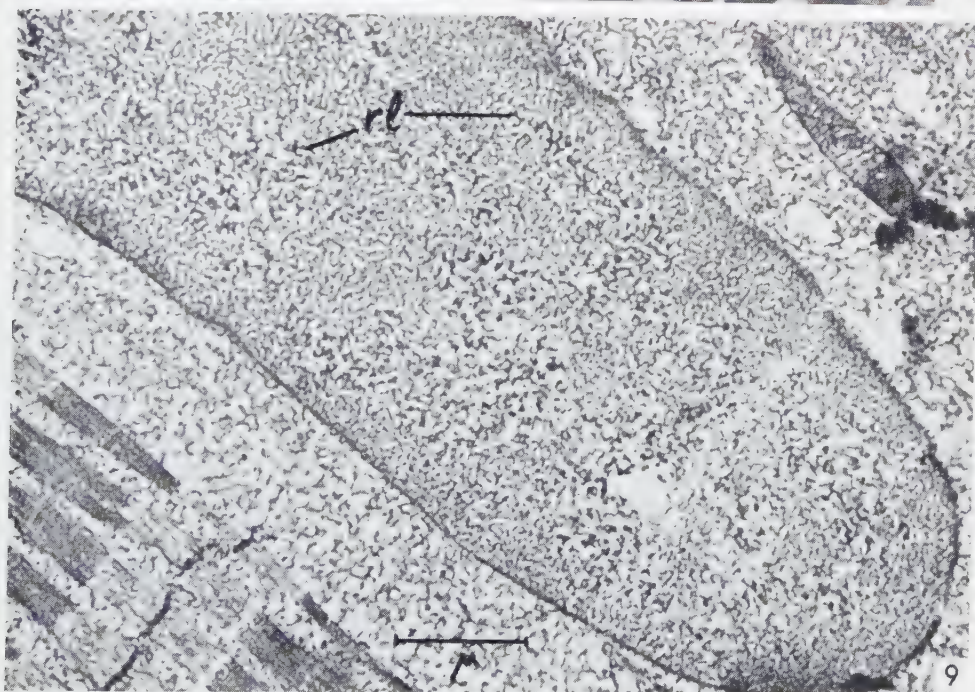
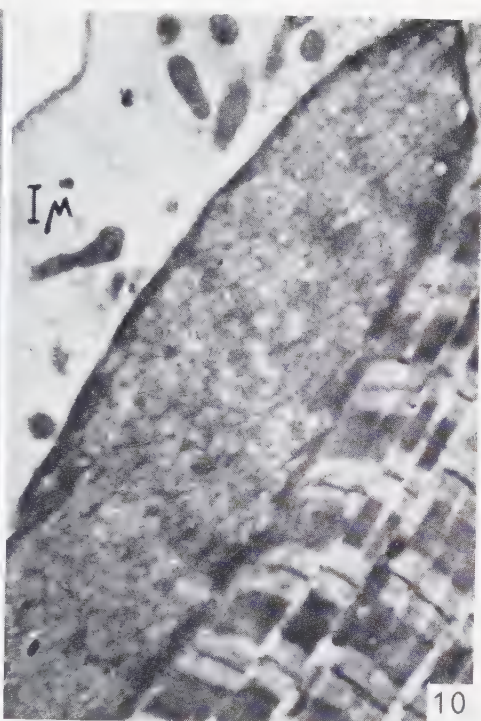
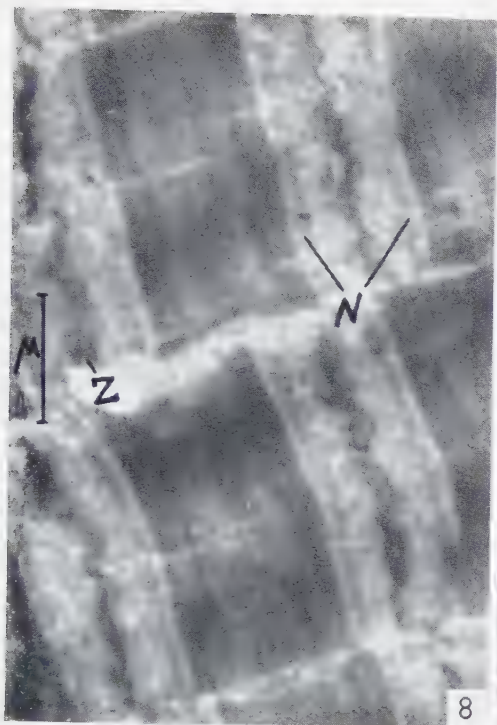
Embedding objects in gelatin relieves accessory treatment of sections with heavy metal salts for accessive contrasting, their treatment with the enzymes etc.

¹ The possibility of the interaction between osmium tetroxide and gelatin, under the given conditions, may be admitted if taking in account Bahr's data (1).

FIG. 8. The H- and N-bands and light areas at both sides of the M-line are distinctly seen. The Z-line is strongly bent. The impression is given that this line is split into two layers. $\times 15,500$.

FIG. 9. Striated muscle tissue of the axolotl, embedded in a mixture of butyl and methyl methacrylate (4:1). Embedding material was eliminated from the section by xylol. In the nucleus, among small granules, more coarse granules (rl) are to be seen. Their arrangement imitates the form of the structures shown in Figs. 4 and 7. $\times 16,500$.

FIG. 10. Before embedding this tissue in gelatin, it was passed through alcohols of increasing strength, into the butyl methacrylate monomere, and then, back through the alcohols down to water. The structures mentioned in Fig. 9 are not to be found in the nucleus pictured here. $\times 4300$.



Gelatin sections can well withstand the electron beam.

1 μ thick sections with a block face of up to 2 mm² can easily be cut from tissue embedded in gelatin. Such sections are useful for examination by means of light microscopy. In this case the blocks should not be too dry and, therefore, are kept in open vessels. The sections are adfixed to the slides with albumen to which some glycerin has been added. The gelatin is removed by dissolving in warm water.

Gelatin embedding certainly does not replace methacrylate embedding. However, the data obtained show this technique to be able to reveal new details in the tissue structure which are concealed in the case of methacrylate embedding.

Some examples of the application of this method on muscle tissue are illustrated in Figs. 1-10.

All the micrographs, with the exception of Fig. 9, are made from the sections of a gelatin-embedded striated muscle tissue of the axolotl (*Amblistoma punctatum*). The sections are 300-400 Å thick. They were studied in a UEM-100 electron microscope, accelerating voltage of 60 kV. Attention is to be paid to the fact that almost all the tissue details are of larger size than in the case of methacrylate embedding.

ACKNOWLEDGEMENTS

The author would like to thank Prof. A. E. Kriss, Chief of our Laboratory, and Prof. A. N. Studitsky for their interest and careful criticism of this manuscript. Thanks are also due to Mrs. A. A. Kashljunova for much photographic assistance willingly given.

REFERENCES

1. BAHR, G. F., *Exptl. Cell Research* **7**, 457 (1954).
2. BRANDES, C. H., *Mikrokosmos* **44**, 167 (1955).
3. CAMERON, D. A., *J. Biophys. Biochem. Cytol.* **2**, No. 4, Suppl., 57 (1956).
4. FERNÁNDEZ-MORÁN, H. and FINEAN, J. B., *J. Biophys. Biochem. Cytol.* **3**, 725 (1957).
5. FIRMINGER, H. I., *Stain Technol.* **25**, 121 (1950).
6. GILĚV, V. P., *Proc. Stockholm Conf. Electron Microscopy*, 1956, p. 113. Almqvist & Wiksell, Stockholm, and Academic Press Inc., New York, 1957.
7. LATTA, H. and HARTMANN, J. F., *Proc. Soc. Exptl. Biol. Med.* **74**, 436 (1950).
8. NEWMAN, S. B., BORYSKO, E. and SWERDLOW, M., *J. Research Natl. Bur. Standards* **43**, 183 (1949).
9. PALADE, G. E., *J. Exptl. Med.* **95**, 285 (1952).
10. RHODIN, J., Correlation of Ultrastructural Organization and Function in Normal and Experimentally Changed Proximal Convoluted Tubule Cells of the Mouse Kidney. Thesis. Stockholm, 1954.
11. RICHARDS, A. G., ANDERSON, T. F. and HANCE, R. T., *Proc. Soc. Exptl. Biol. Med.* **51**, 148 (1942).
12. SJÖSTRAND, F. S. and HANZON, V., *Exptl. Cell Research* **7**, 393 (1954).

The Fine Structure of the Tapetum of the Kitten Eye as Revealed by the Electron Microscope

E. YAMADA

Department of Anatomy, School of Medicine, Kurume University, Kurume

Received April 29, 1958

The cell of the tapetum of the kitten eye was observed with the electron microscope. Within the cell body, characteristic fibrous structures or filaments were observed. Each filament shows a cross-striation with a 45 Å periodicity and is enclosed within a capsule.

During a study of the kitten eye retina, cells of the tapetum were recognized in the choroid and their fine structure was observed with the electron microscope. In the case of the cat and carnivores in general, the tapetum is composed mainly of a mass of cellular elements i.e., the tapetal cells, and is located on the inner side of the choroid facing the *stratum pigmenti* of the retina. The tapetum of these animals is called *tapetum cellulosum* in comparison with *tapetum fibrosum* and *guanin tapetum* as found in other types of vertebrates. The tapetum is considered as a kind of reflecting plate and as a structure which increases photoreception of the retina. A special kind of structure within the cytoplasm of the tapetal cells would be anticipated, and in this paper a characteristic fibrous structure, which has not been revealed thus far in other cell types, is described.

MATERIAL AND METHODS

Kitten eyes were fixed with a modified Palade's buffered osmium tetroxide solution for 30 to 60 minutes. After dehydration with ethanol, the tissues were embedded in *n*-butyl methacrylate. Sections were cut with a JCM microtome and were observed with a JEM-4c electron microscope.

OBSERVATIONS

The cells of the tapetum of the kitten eye are large ovoid to round cells and their round nuclei with prominent nucleoli are usually located in the center of the cell body. Within the cell body, one can observe the usual cell organelles: mitochondria, Golgi apparatus, rough-surfaced endoplasmic reticulum with its associated particles

(4). The mitochondria have slender rod- or filament-like shapes and show *cristae mitochondriales* (3). The Golgi apparatus is found near the nucleus and shows a structure similar to that described in other cell types (Fig. 2). The rough-surfaced endoplasmic reticulum is observable in considerable amounts mainly around the mitochondria (Figs. 1 and 3–6).

The most conspicuous and characteristic feature of the tapetal cell of the kitten eye is the presence of numerous fibrous or filamentous structures within the cell body. Each filament appears to be almost straight and more than $2\ \mu$ long as judged from single sections. It is ovoid or round in cross-section and about $300\text{--}370\ \text{\AA}$ in diameter. The filaments occupy the majority of the cell body except for a small area where mitochondria and the Golgi apparatus usually can be observed. They show some tendency to gather in groups and, while each group runs in a different direction to each other, most groups are disposed parallel with the plane of retina, as shown in Fig. 1.

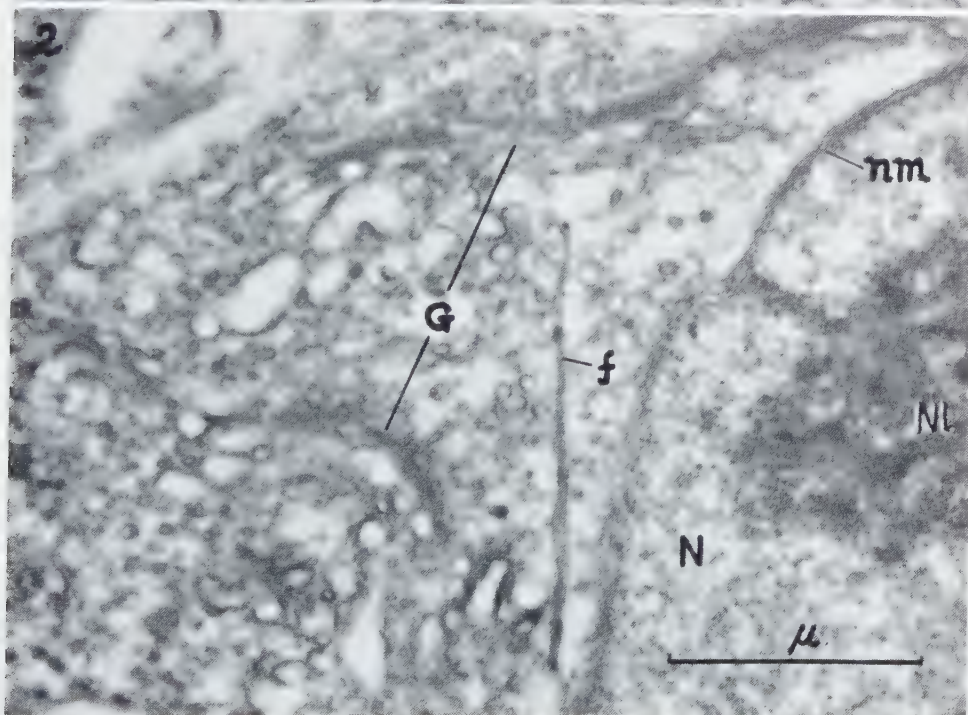
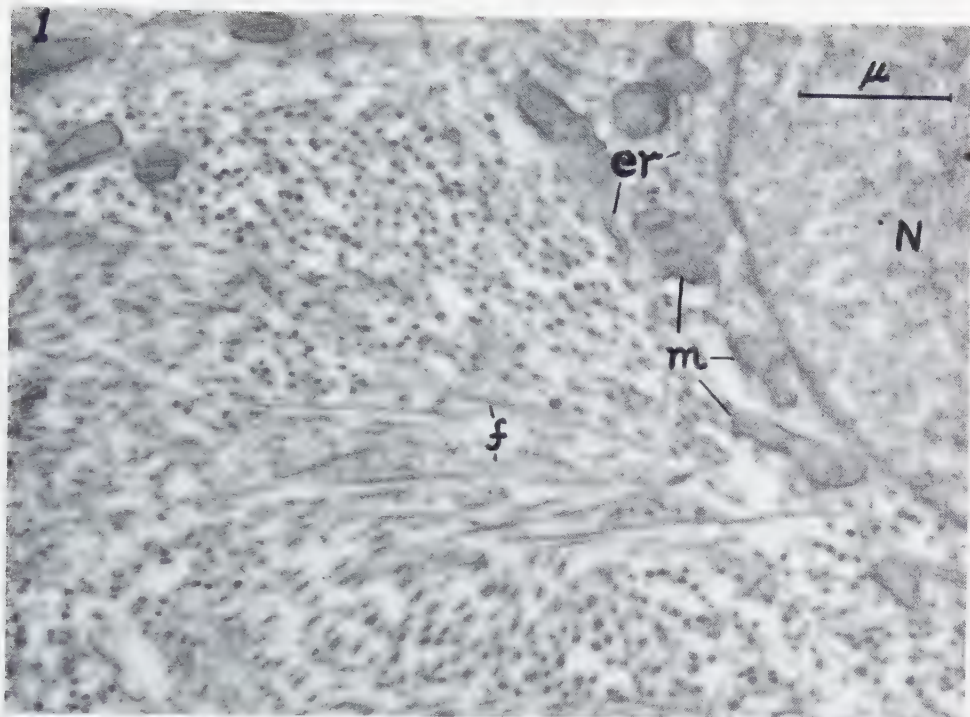
Closer observation (Figs. 3–6) reveals that each filament is encapsulated by a thin single membrane. The membrane or the capsule of the filament shows dilatations or folds at certain places along the filament. The matrix limited by this membrane has a density which differs from that of the surrounding cytoplasm and the filament within it. The filament, itself, is much denser than the matrix. These findings are shown most clearly where dilatation of the capsule is observed.

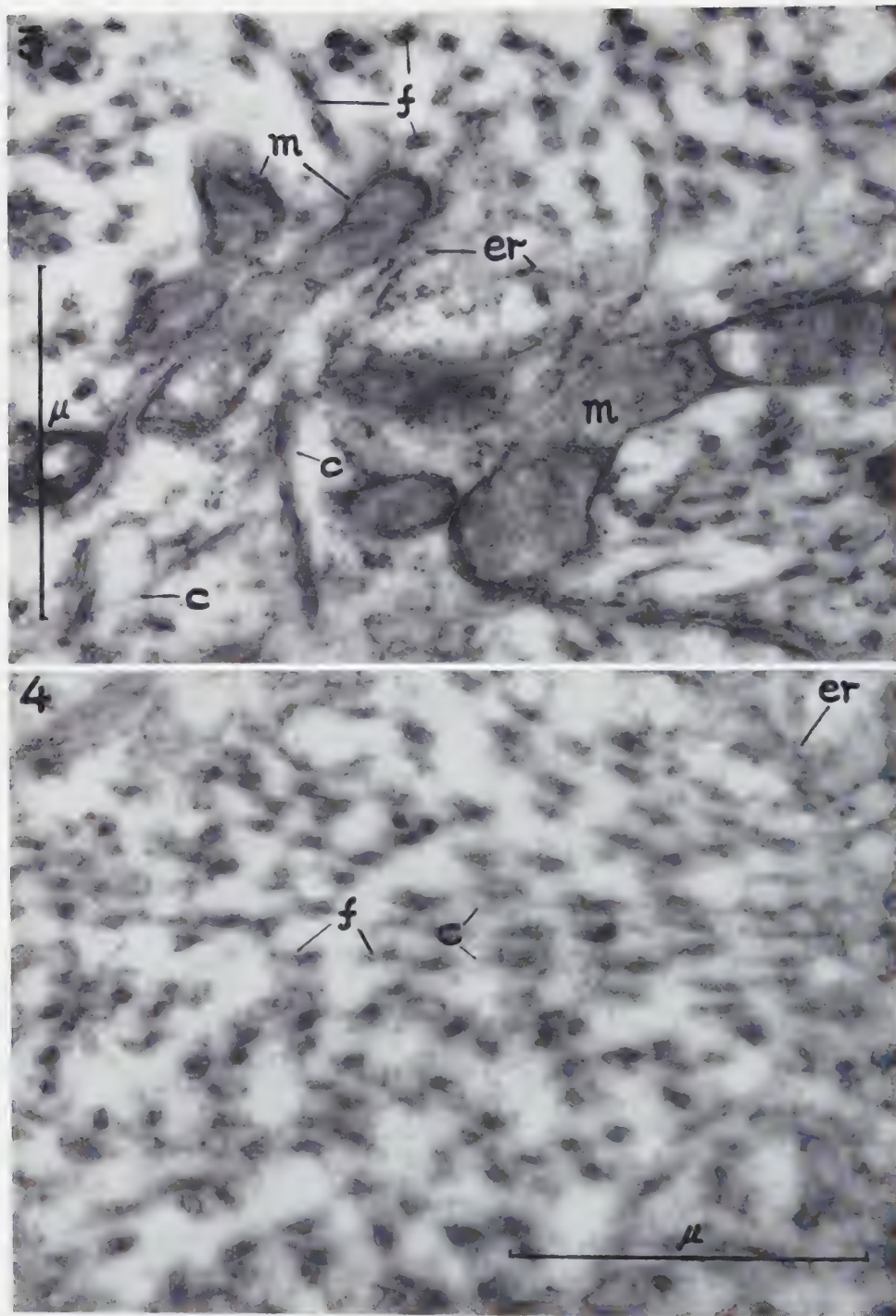
Another feature of the fine structure of the filament is a cross-striation or the axial periodicity along its length. The narrow cross-band, of high electron density, and the less dense interspace are almost the same width, measuring about $45\ \text{\AA}$ wide (Figs. 5 and 6).

DISCUSSION

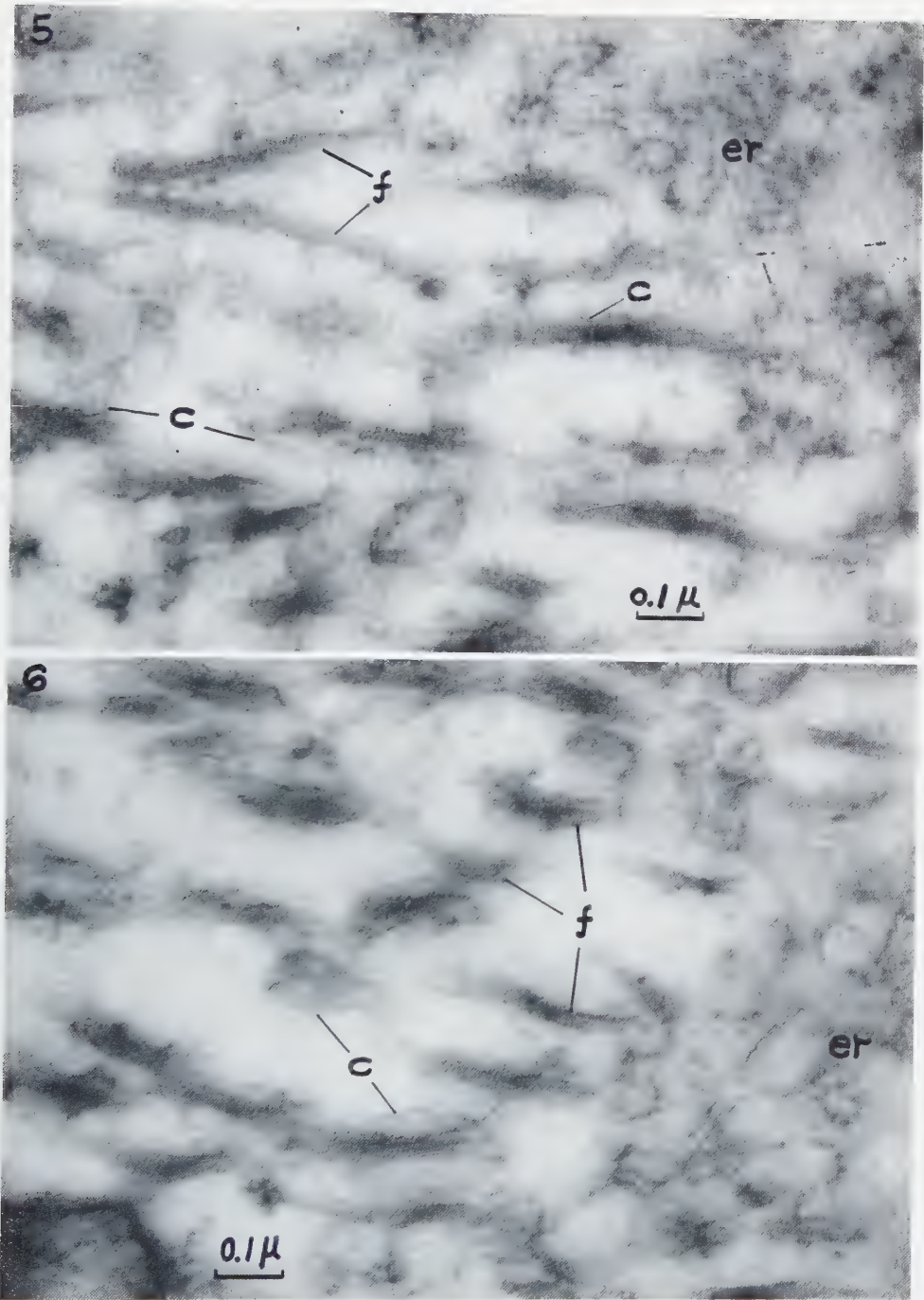
The most eminent example of fibrous structures within a cell body are the myofibrils of striated muscle. Recent electron microscopy has revealed filamentous structures within other cell types. For example, Porter (5) has described keratin filaments, which have a characteristic periodicity, within epidermal cells. The fibrous rootlet associated with the basal body of the cilium often shows cross-striation (1, 6). The findings presented here represent another example. However, the filaments of the

FIGS. 1 and 2. General surveys of the tapetal cell of the kitten eye. In Fig. 1, the majority of the cell body is seen to be full of filaments (*f*). They are running as groups in different directions but, in general, seem to be parallel to the plane of the retina. Well-developed Golgi bodies (*G*) in Fig. 2 near the vicinity of the nucleus (*N*) consist of the usual components. A part of the nucleolus (*NI*) extends towards the nuclear membrane (*nm*). Rough-surfaced endoplasmic reticulum (*er*) is found surrounding the mitochondria (*m*). $\times 20,000$ and $33,000$ respectively.





FIGS. 3 and 4. Parts of the cytoplasm of the tapetal cell. The rod-shaped mitochondria (*m*) and the rough-surfaced endoplasmic reticulum (*er*) are clearly shown. Each filament (*f*) is encapsulated by a thin membrane (*c*) which sometimes shows dilatations or folds. Some of the filaments are cross-sectioned. Note the difference of density between the matrix limited by the membrane and the cytoplasm. $\times 50,000$.



FIGS. 5 and 6. The longitudinal profiles of filaments (*f*) are shown at high magnification, and the axial periodicity of about 45 Å is observable in most of the filaments. The capsule (*c*) or membrane which encloses the filament is also demonstrated. The capsule seems to be continuous with the membranes of the rough-surfaced endoplasmic reticulum (*er*) to the right of both figures. $\times 90,000$.

tapetal cells have features which distinguish them from the others. Firstly, the filament of the tapetal cell shows a striation with the periodicity of 45 Å and secondly, the filament is enclosed within a membrane or capsule. From these findings, one can imagine that the filamentous structure might be differentiated from the substance or the matrix limited by the membrane within the cytoplasm of the cell of the tapetum.

The fact that frame-works of filaments which run in different directions as a whole are parallel to the retinal plane seems to explain the reflecting nature which has been considered the characteristic function of the tapetal cell layer.

Kolmer (2) described with the light microscope a net-like apparatus in the tapetal cell of cat. This may correspond to the filaments described here. The exact chemical nature and the morphogenesis of the filaments are not known and await elucidation by further investigations.

REFERENCES

1. BRADFIELD, J. R. G., *Symposia Soc. Exptl. Biol.* **9**, 306 (1955).
2. KOLMER, W., in v. MÖLLENDORFF, W. (Ed.) *Handbuch der mikroskopischen Anatomie des Menschen*, Bd. 3, Teil 2 (1936).
3. PALADE, G. E., *Anat. Record* **114**, 427 (1952).
4. ——— *J. Biophys. Biochem. Cytol.* **2**, No. 4, Suppl., 85 (1956).
5. PORTER, K. R., *Anat. Record* **118**, 433 (1954).
6. SJÖSTRAND, F. S., *J. Cellular Comp. Physiol.* **42**, 45 (1953).

Macrocrystalline Patterns of Closely Packed Poliovirus Particles in Ultrathin Sections

F. S. SJÖSTRAND and A. POLSON¹

Laboratory for Biological Ultrastructure Research, Department of Anatomy, Karolinska Institutet, and State Bacteriological Laboratory, Stockholm

Received May 2, 1958

Purified preparations of poliovirus MEF₁ (Type II) were spun down into a pellet by means of ultracentrifugation. The virus particles became closely packed and showed macrocrystalline patterns on sectioning. At least two well differentiated patterns were observed. The average spacing was 200–220 Å and the virus particles consisted of osmiophilic, opaque centres which have average diameters of 160 Å. These centres are surrounded by approximately 30 Å thick, less osmiophilic zones.

Poliovirus particles have been shown by Schwerdt and Schaffer (5) to contain 20–30% ribonucleic acid. From this it follows that if all the nucleic acid is confined to a nucleus in the particles, it should be possible to distinguish a central core approximately 200 Å in diameter in electron micrographs of the virus particles. Direct evidence for the existence of a nucleus of this order of magnitude in the virus particle was obtained from electron micrographs by Taylor and McCormick (8).

In the present work the presence of an osmiophilic core of the same order of magnitude was observed in the centre of the poliovirus particle. This was demonstrated by electron microscopy of ultrathin sections of pellets of purified virus obtained by ultracentrifugation and which had been fixed in osmium tetroxide. It was further noticed that the virus preparations of highest purity formed macrocrystalline patterns in the pellets.

MATERIAL AND METHODS

Two of the type strains incorporated in the Swedish poliomyelitis vaccine were used. These were MEF₁ (Type II) and Saukett (Type III). The crystalline patterns have so far been observed in preparations of the MEF₁ (Type II) virus. They were purified by the method of Polson and Hampton (4) from relatively large volumes of infective tissue culture fluid.

¹ Permanent address: C.S.I.R. and U.C.T. Virus Research Unit, University of Cape Town, South Africa.

The method of purification involved preliminary concentration of the infective agents by pervaporation in "cellophane" bags, removal of undesired proteins by chloroform treatment and final concentration into a pellet by ultracentrifugation. The last step was carried out in the preparative Spinco ultracentrifuge head run at 30,000 rpm for 90 minutes. The pellet was resuspended in 1% sodium chloride solution and the homogeneity of the virus suspension assessed by electron microscopy and analytical ultracentrifugation. After a satisfactory degree of purity had been established in this way, the virus was spun down once more into a pellet and then subjected to fixation in a 1% buffered osmium tetroxide solution dehydrated in ethyl alcohol and embedded in a mixture of *n*-butyl and methyl methacrylate. Sections through the pellet were cut with a Sjöstrand ultramicrotome and examined in an RCA EMU 3A electron microscope.

OBSERVATIONS

In the electron micrographs (Figs. 1–3), through large, closely packed regions, the various particles are packed according to at least two different patterns. The transition from one pattern into the other occurs abruptly along well defined lines. One pattern appears to represent a fairly regular, hexagonal type of close packing, and the other shows, where most regular, a rectangular arrangement of the virus particles.

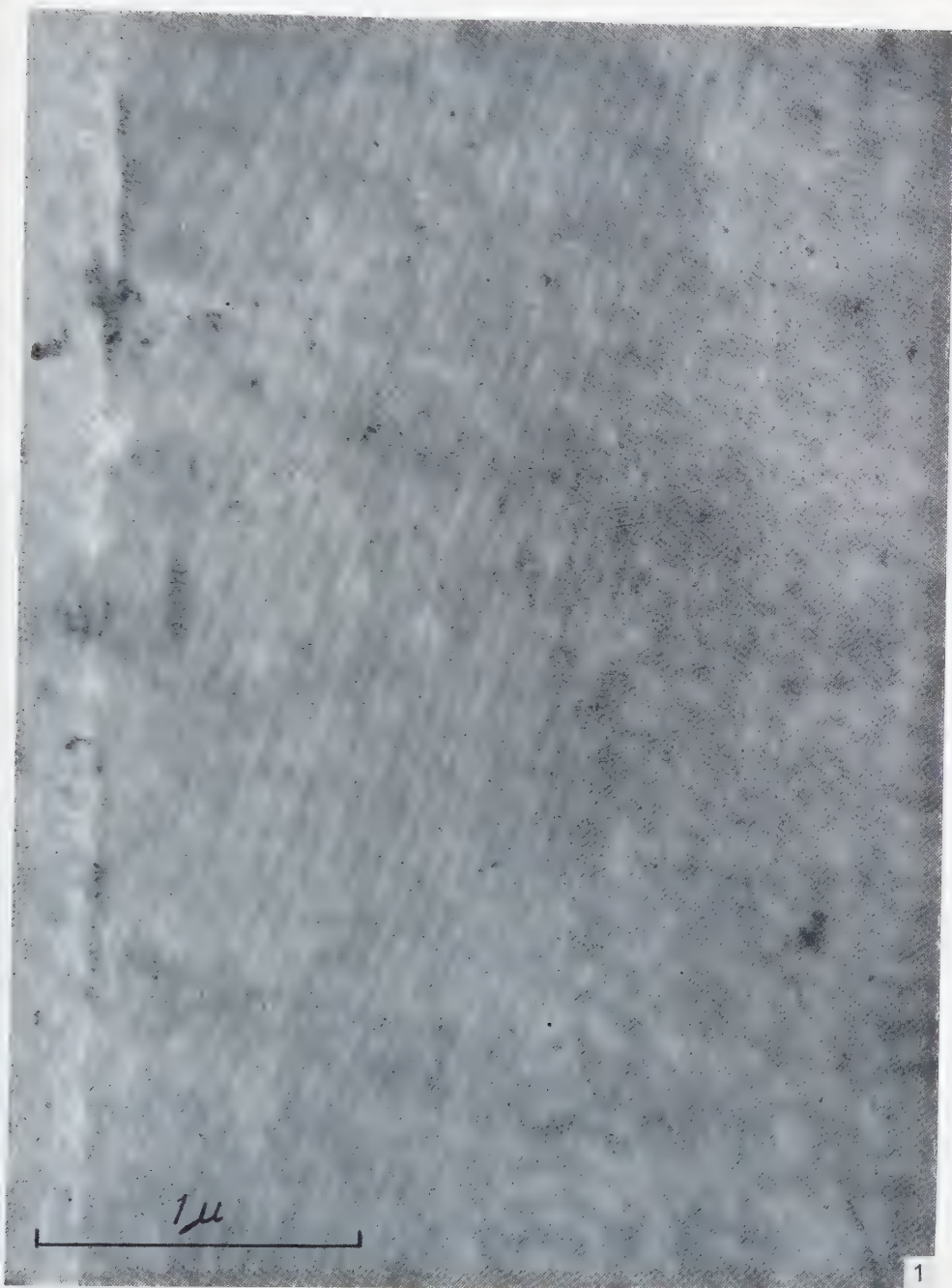
In regions showing the hexagonal type of close packing, the average spacing of the various particles was measured and found to be 200–220 Å. The average long spacing, in the regions of rectangular packing, was found to be 250 Å and the average short spacing was 195 Å.

The virus particle appears as an opaque body surrounded by or embedded in a homogeneous material of fairly high opacity. The opaque portion is interpreted as representing a central osmiophilic region of the virus particle. This central region is assumed to be surrounded by a less opaque or less osmiophilic periphery. This interpretation is supported by the observations made on the size and form of the virus particles in drop preparations of virus suspensions. These observations indicate that a well defined central region is present.

The average diameter of the opaque central region of the virus particles was 160 Å. The average width of the less opaque peripheral zone would be about 30 Å, and the total diameter of closely packed virus particles 220 Å.

All these measurements are subject to a certain error caused by the "compression" of the sections during sectioning. The compression also introduces a certain deformity of the macrocrystalline patterns. It seems improbable that this factor can be respon-

FIG. 1. Survey picture of poliovirus particles forming a macrocrystalline pattern in the pellet formed after ultracentrifugation. Moiré effects are observed on sections of this thickness. Along the left edge of the picture a part of a thinner section is included. The type of packing differs in different regions of the pellet. A cubic type of packing is observed in the largest part of the section. At the right, lower corner the packing approaches a hexagonal type. $\times 43,000$.



sible for the difference in appearance of the two packing patterns as these patterns appear side by side independently of the direction of movement of the block relative to the knife edge.

The shapes of the virus particles vary considerably. Rounded, squared and triangular forms can be observed. In thin sections the sizes vary considerably due to the fact that certain areas contain fragments of the virus particles that have been cut off. This occurs when the section is oriented somewhat obliquely to the plane of the layers of the virus particles (Fig. 3). It then passes through the less opaque layer between the opaque centres of the particles. Taking the width of the less opaque layer forming the outer shell of the particles into consideration and which was estimated at 30 Å, the thickness of these thin sections is probably of the order of 50–100 Å.

The small virus fragments do not show any characteristic form. An irregular filamentous structure observed in these fragments could not be differentiated with certainty from accidental lining up of groups of photographic grain. In thin sections of virus particles that were mounted on formvar nets (7), a certain frequency of particles showing square outlines was observed (Fig. 4). In some cases these particles appeared to consist of two parallel rods. The significance of these observations cannot be evaluated at present.

In addition to the 220 Å particles, a varying number of smaller particles, which are well defined in size and opacity, is observed. These very opaque particles measure 70 Å in diameter and appear mixed with the 220 Å particles in regions where the latter are not closely packed (Fig. 5).

DISCUSSION

The bodies that have been observed in the closely packed macrocrystalline patterns have been assumed to represent the MEF₁ (Type II) poliovirus particles. This assumption is based on the fact that these represent the largest particles observed in these preparations. Infectivity tests have revealed that the greatest virus activity is associated with the heaviest fraction of particles, the sedimentation constant of which was estimated at 156 S in ultracentrifugation experiments (3). This sedimentation constant is in good agreement with the figure of 154 S found by Schwerdt and Schaffer (5) for MEF₁ (Type II) virus.

The figure for the diameter, 220 Å, is considerably smaller than the 270 Å obtained by Williams *et al.* (10) on drop preparations including frozen-dried specimens. From the sedimentation data and an estimation of the average density of the particles, Schwerdt and Schaffer (5) estimated the diameter at 220 Å. The average diameter

FIG. 2. Higher magnification of a thin section through a pellet. The opaque central cores show a certain variation in form. $\times 118,000$.



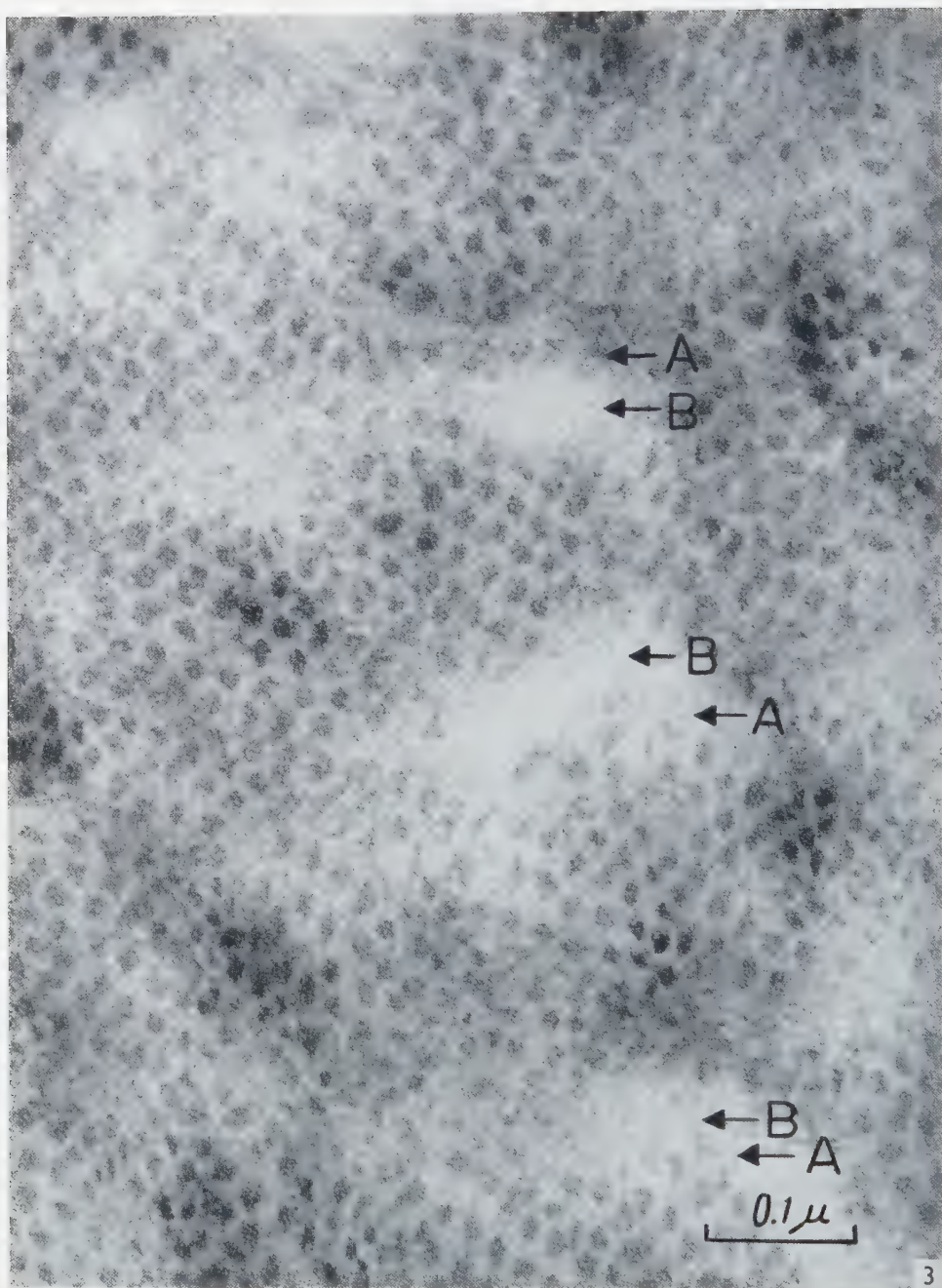


FIG. 3. High magnification of a very thin section through a pellet. The section passes through adjacent layers of particles. Within certain areas (*A*) the section contains only minute fragments of the dense core of the particles and within other areas (*B*) only the less dense matrix. $\times 200,000$.



FIG. 4. Ultrathin section through a pellet containing poliovirus particles mounted on a formvar net. Some particles showing a square form are enclosed by circles. $\times 200,000$.

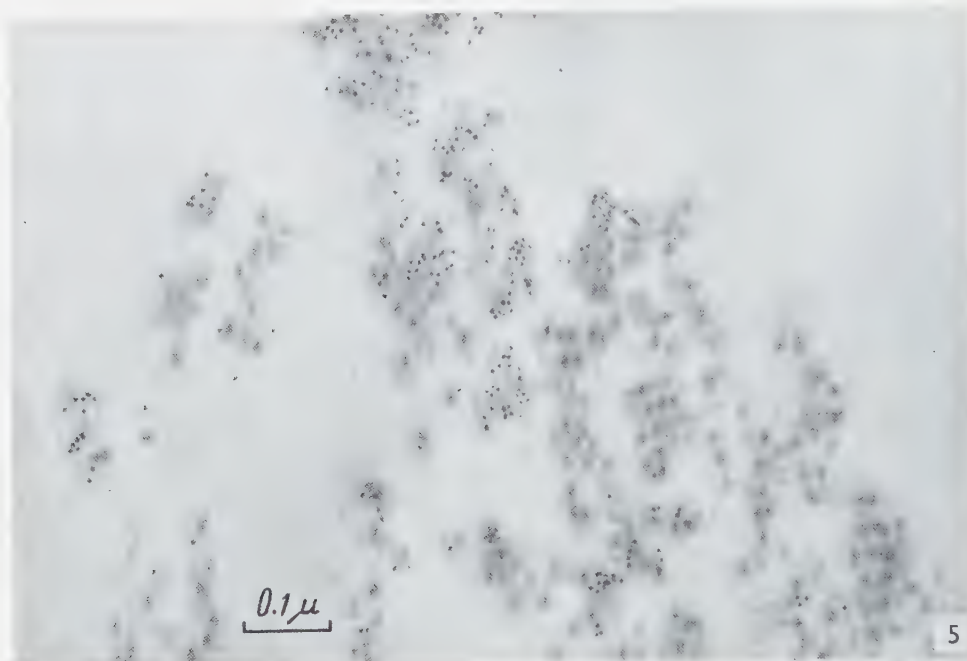


FIG. 5. Section through a pellet containing poliovirus particles and a second type of particles of a smaller size. $\times 101,000$.

found in the present study therefore falls within the 220 to 270 Å range within which the poliovirus particles were assumed to fall according to Schwerdt and Schaffer. That the mean diameter would approach the lower limit of this range has to be expected because the true dimensions are reduced by the fixation and embedding technique used, which is known to produce considerable shrinkage. The reduction of the volume of the methacrylate during polymerization is generally estimated at 10–20%. The shrinkage during the dehydration is dependent on the water content of the material which can be assumed to be less for the present specimens than for tissue cells. Another source of error is ascribed to the so-called compression of the sections during the cutting of ultrathin sections. The diameters of the particles are reduced in the direction of the movement of the knife edge relative to the block face. This “compression” results in a corresponding increase of the thickness of the section or an increase in both the width and thickness of the section. We do not know to what extent the last-named factor produces an actual increase in the diameter of the particles in a direction perpendicular to that of the movement of the knife edge. We cannot, therefore, state whether the maximum distances measured between the centres of the particles should be considered more reliable than the average distance.

The diameter of the MEF₁ (Type II) poliomyelitis virus was estimated by Bachrach and Schwerdt (1) at 350 Å when the virus particles appeared as isolated single units on the supporting film. In packed arrays in drop preparations they found a diameter of 280 Å. In our drop preparations, the mean diameter of the virus particles in a packed array was 290 Å, a figure which agrees well with Bachrach and Schwerdt's value when the errors in the method of measurement are taken into consideration.

It seems likely that the value for the diameter obtained on drop preparations is too large even if we only consider measurements performed on packed arrays in single layers. On the other hand, the sectioning of virus particles in close packing, which involves fixation, dehydration and embedding, introduces shrinkage effects which certainly give unduly low values. The difference in the values for the diameters of these particles can be explained by the difference in techniques used for preparation.

The nature of the 70 Å particles is uncertain but the possibility cannot be excluded that they are identical with the specific non-infective particles of sedimentation constant 20–26 S found in purified preparations of poliovirus (3, 6). This appears to be likely if we assume that they were reduced in volume to the same degree as the large virus particles.

When the structure of poliovirus, as revealed by electron microscopy of ultrathin sections, is compared with the structure of other viruses obtained by similar techniques, certain similarities and differences are evident. The virus particles of myeloblastosis and erythroblastosis isolated from leukaemic chickens have diameters ranging from 600–800 Å, are encased in a single or double membrane and have dense cores of approximately 350–400 Å in diameter. These particles, however, show no regular packing arrangement in the pellet (2). The packing arrangement of poliovirus particles is very similar to that of the virus of the larvae of *Tipula paludosa* examined by Williams and Smith (9). This virus is considerably larger in particle size than the poliovirus and also appears to consist of an electron dense core surrounded by a less opaque matrix.

It has not been possible to draw any conclusion regarding the crystal form of the closely packed regions from a study of the patterns observed in the sections. X-ray scattering diagrams might throw additional light on this problem.

ACKNOWLEDGEMENTS

The authors are grateful to Drs. Melén and Wrange for the generous supply of infective tissue culture fluid used in this work. Grateful acknowledgements are also made to Mrs. Kajland for technical assistance. One of us (A. P.) is specially indebted to Professor S. Gard and to the C.S.I.R., South Africa, for financial aid during the course of this work.

REFERENCES

1. BACHRACH, H. L. and SCHWERDT, C. E., *J. Immunol.* **72**, 30 (1954).
2. BERNHARD, W., BONAR, R. A., BEARD, D. and BEARD, J. W., *Proc. Soc. Exptl. Biol. Med.* **97**, 48 (1958).
3. POLSON, A., EHRENBERG, A. and CRAMER, R., in preparation.
4. POLSON, A. and HAMPTON, J. W. F., *J. Hyg.* **55**, 344 (1957).
5. SCHWERDT, C. and SCHAFER, F. L., *Ann. N.Y. Acad. Sci.* **61**, 740 (1955).
6. SELZER, G. and POLSON, A., *Biochim. Biophys. Acta* **15**, 251 (1954).
7. SJÖSTRAND, F. S., *Proc. Stockholm Conf. Electron Microscopy*, 1956, p. 120. Almqvist & Wiksell, Stockholm and Academic Press Inc., New York, 1957.
8. TAYLOR, A. R. and MCCORMICK, M. J., *Yale J. Biol. and Med.* **28**, 589 (1956).
9. WILLIAMS, R. C. and SMITH, K. M., *Nature* **179**, 119 (1957).
10. WILLIAMS, R. C., STANLEY, W. M., SCHAFER, F. L. and MCCLAIN, M. E., *Proc. Soc. Exptl. Biol. Med.* **86**, 310 (1954).

Ultrastructure of Mouse Uterine Surface Epithelium under Different Estrogenic Influences

1. Spayed Animals and Oestrous Animals

O. NILSSON

*Department of Histology and Laboratory for Biological Ultrastructure Research, Department
of Anatomy, Karolinska Institutet, Stockholm*

Received May 16, 1958

The differences in the appearance of the uterine epithelium from spayed mice and from oestrous mice comprised, in particular, an increase of the cell height and of some membrane structures in the cell, a change in the amount of lipid granules, and a change in the appearance of the mitochondria.

The cell height was increased from 7-10 μ to 18-22 μ ; the cell width remained at 4-5 μ . The luminal cell surface possessed longer microvilli and the lateral cell surface ran in a more folded manner in the epithelium of oestrous animals. There was an absolute increase in the area of the cell membrane and also a relative one in relation to the cell volume. The system of α -cytomembranes and the Golgi membranes also showed an absolute increase in amount. Large vacuoles appeared both in the Golgi apparatus and in intercellular spaces.

The uterine epithelium of spayed animals contained many lipid granules, but in the epithelium of oestrous animals, there were only a few. The epithelial cells also contained granules, which were accompanied by different kinds of membrane structures.

The mitochondria of the uterine epithelium from oestrous animals were longer than in the cells from spayed animals, and there sometimes appeared dense, homogeneous, spherical, intramitochondrial bodies with a diameter of about 0.15 μ .

Comprehensive light microscopical studies of the uterine changes during the oestrous cycle of the mouse were made by Allen (2), Clauberg (6), and Parkes (26). The uterus of the rat is regarded to show the same variations, and these were described, in particular, by Alden (1) and Long and Evans (18). Many other investigators also contributed to our knowledge of this organ (see, for instance, 5, 29 (mouse), 3, 14, 15, 21, 27 (rat)). The results have been summarized in several monographs (4, 8-10, 13, 38, 40).

The studies showed that spayed mice and rats possessed thin uterine cornua with low epithelial cells, which contained many lipid granules. In oestrus, the uterine

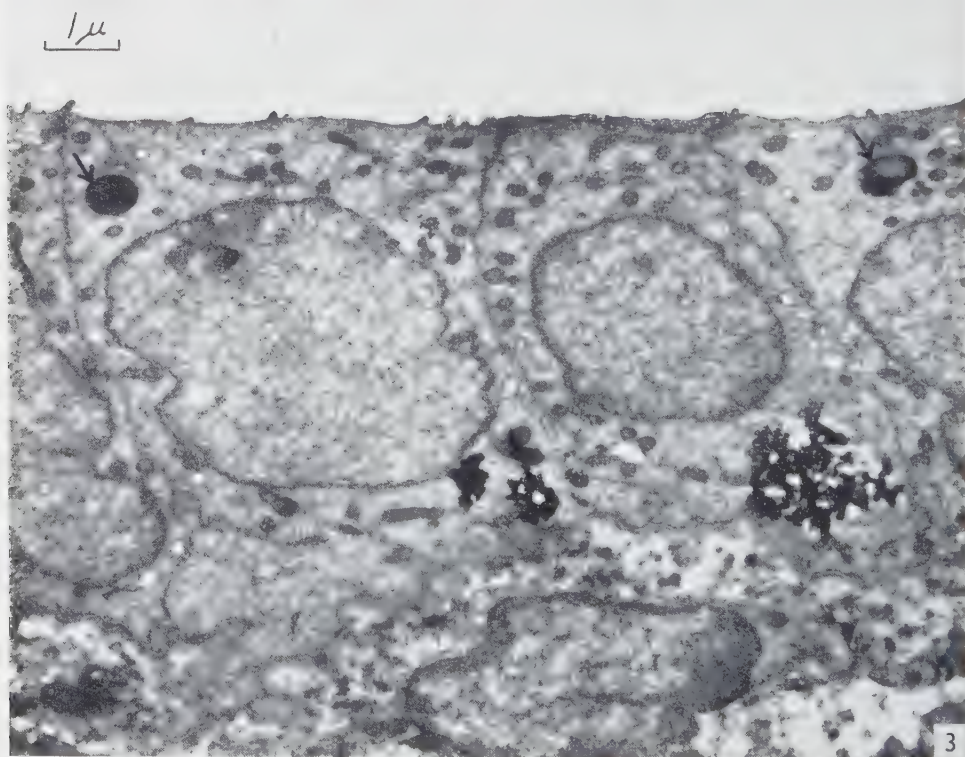
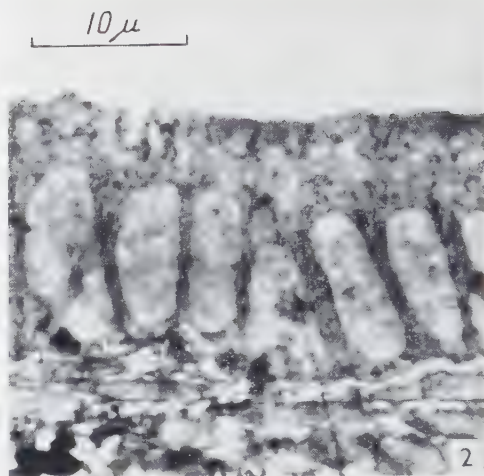
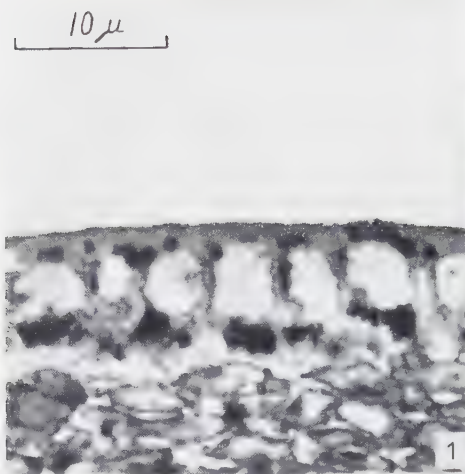
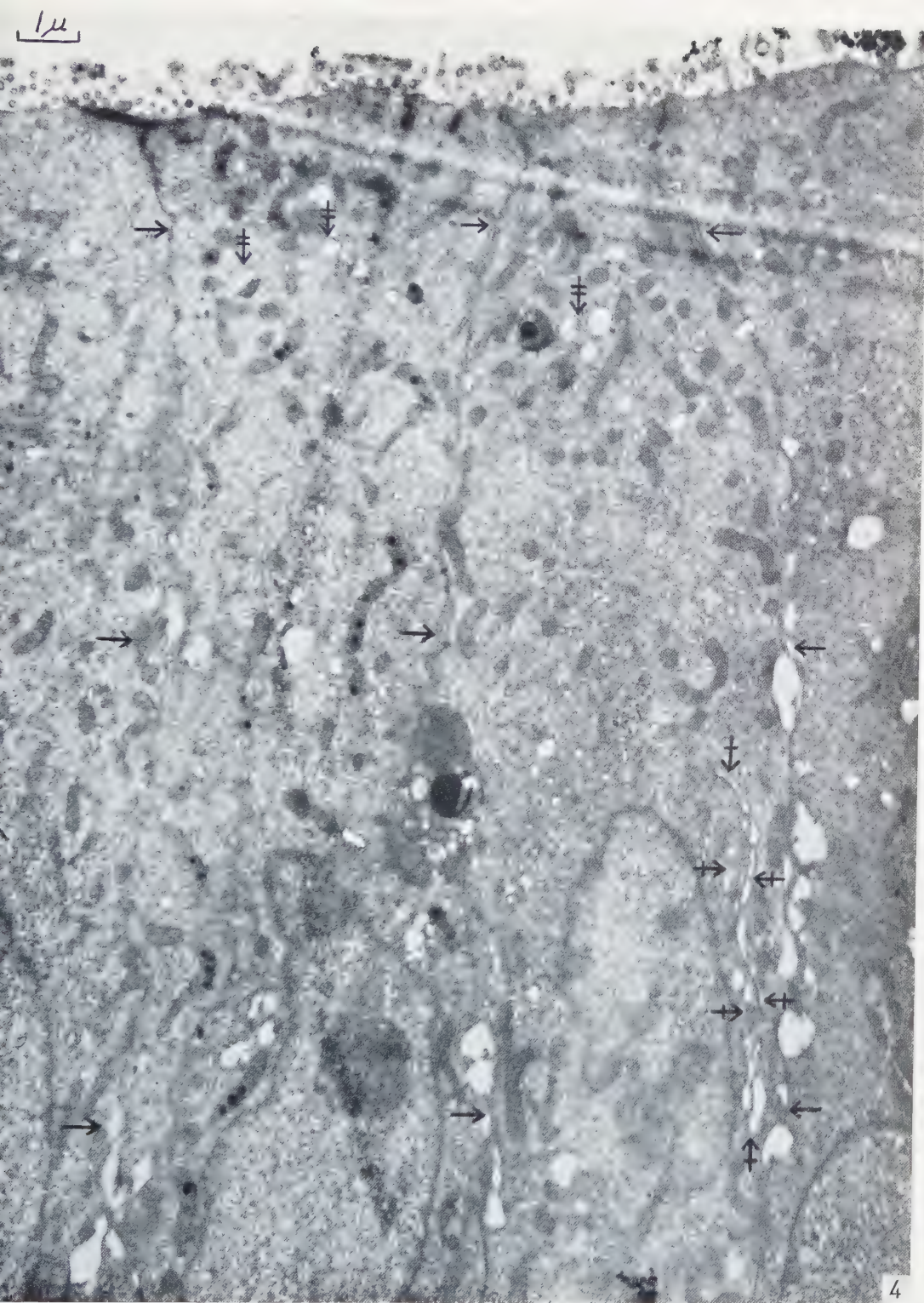


FIG. 1. Uterine surface epithelium from spayed animal. Phase contrast micrograph. $\times 2000$.

FIG. 2. Uterine surface epithelium from oestrous animal. Phase contrast micrograph. $\times 2000$.

FIG. 3. Survey picture of uterine epithelium from spayed animal. The epithelial cells are low and rest on a folded basement membrane. The nuclei occupy the main part of the cells. The luminal cell surface possesses a few, short microvilli; the lateral, adjacent cell surfaces run parallel and are slightly folded. In the cytoplasm, there appear mitochondria, some granules with a smooth outline (\rightarrow) and, basally, many irregular lipid granules. $\times 9500$.



Survey picture of uterine epithelium from oestrous animal. The epithelial cells are high and have basally located nuclei. The luminal cell surface possesses rather long microvilli with a luminal substance; the lateral, adjacent cell borders run parallel and folded (↔). Many intercellular vacuoles are demonstrated. A Golgi apparatus lies between the nucleus and the lower, left side of the cell border in the right-hand part of the figure (→). In the cytoplasm, there appear mitochondria, some of which contain dense bodies and vesicles with an irregular, amorphous material (x9500).

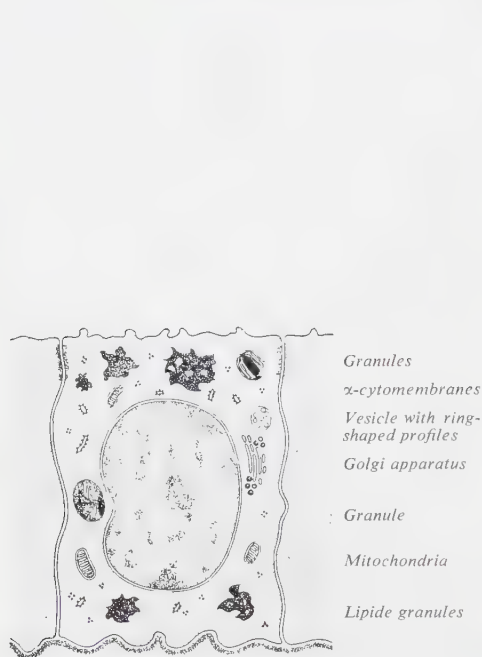


FIG. 5. Schematic drawing showing some of the structures found in uterine epithelial cells from spayed animals.

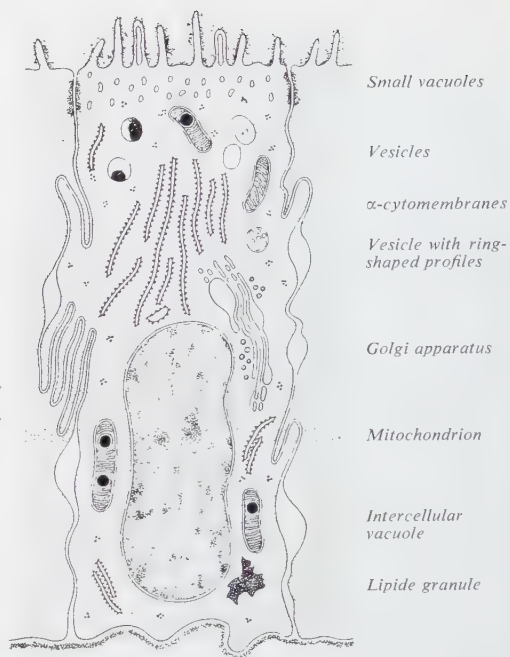


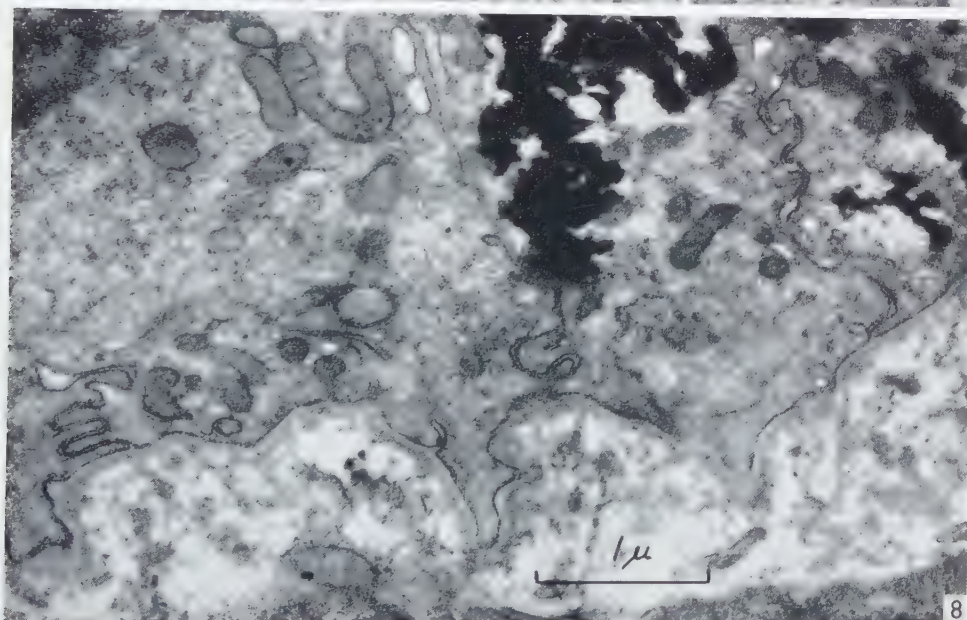
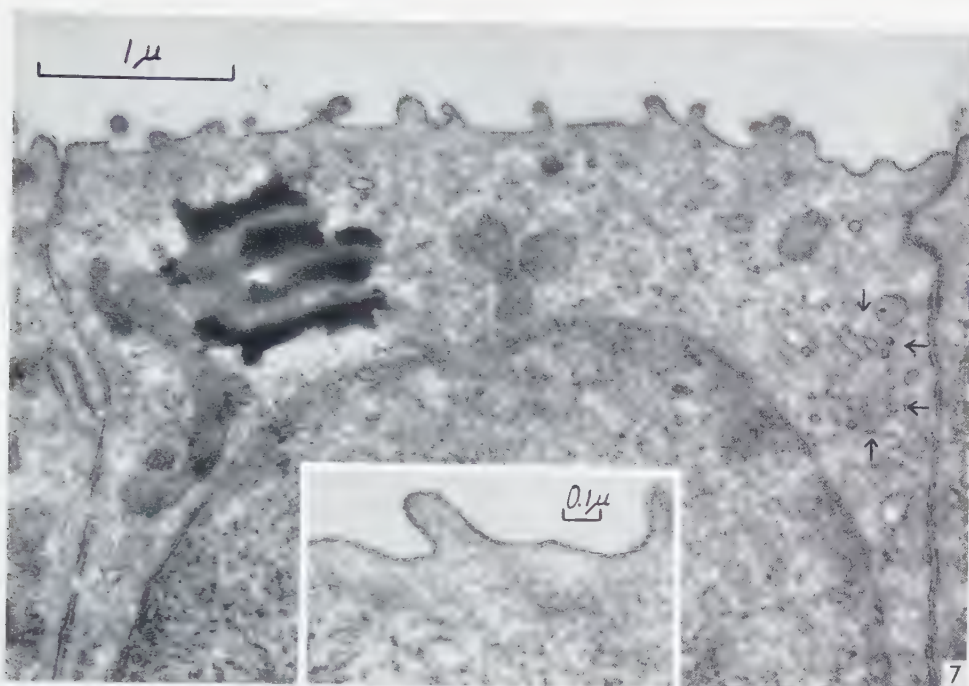
FIG. 6. Schematic drawing showing some of the structures found in uterine epithelial cells from oestrous animals.

cornua were distended with a watery fluid, and the epithelium was increased in height and had lost most of its lipid granules. Estrogen, administered to spayed animals, caused somewhat the same changes in the uterus as were present in the oestrous phase. Prolonged administration, however, induced a hyperplasia, which sometimes was followed by a squamous metaplasia of the endometrium.

The electron microscopical studies of the uterine epithelium are few (7, 44), and the purpose of this series of investigations is to follow those ultrastructural changes in the mouse uterine epithelium that might be correlated to the effect of estrogen.

FIG. 7. Luminal part of uterine epithelium from spayed animal. The surface membrane possesses short microvilli. A few mitochondria appear in the cytoplasm. A lipid granule lies at the upper, left-hand side of the nucleus, the Golgi apparatus at the upper, right-hand side (→). Cell borders showing terminal bars run to the right and left in the figure. $\times 25,000$. *Insert*: Microvilli projecting from luminal surface membrane of uterine epithelium from spayed animal. $\times 49,000$.

FIG. 8. Basal part of uterine epithelium from spayed animal. The irregular basement membrane runs in the lower part of the figure. Lipid granules and mitochondria lie in the cytoplasm. $\times 23,000$.



MATERIAL AND METHODS

Eight spayed and 8 oestrous, virgin mice from a subline of C3H mice were employed in this study. The strain is maintained by strict single-line brother×sister mating. The colony is isolated in a room where precautions are taken to obtain uniformity of conditions. The mice are kept on a standard checker diet which, with drinking water, is available *ad libitum*.

The females devoted to the experiments lived in individual cages. When the animals were three months old, daily vaginal smears were taken for about two weeks to assure a normal oestrous cycle. The last few days of the period, smears were taken both in the morning and in the afternoon to obtain a more exact assessment of the cycle. The smears were taken carefully from the lower part of the back wall of the vagina with a small metal spatula.

Animals for the spayed group were castrated, controlled by daily smears, and sacrificed two weeks after the operation. Animals for the oestrous group were sacrificed in the morning the day after the appearance of cornified smears. Only those animals were used in the investigation where fluid was expelled from the cornua upon the incision that preceded the injection of the fixative.

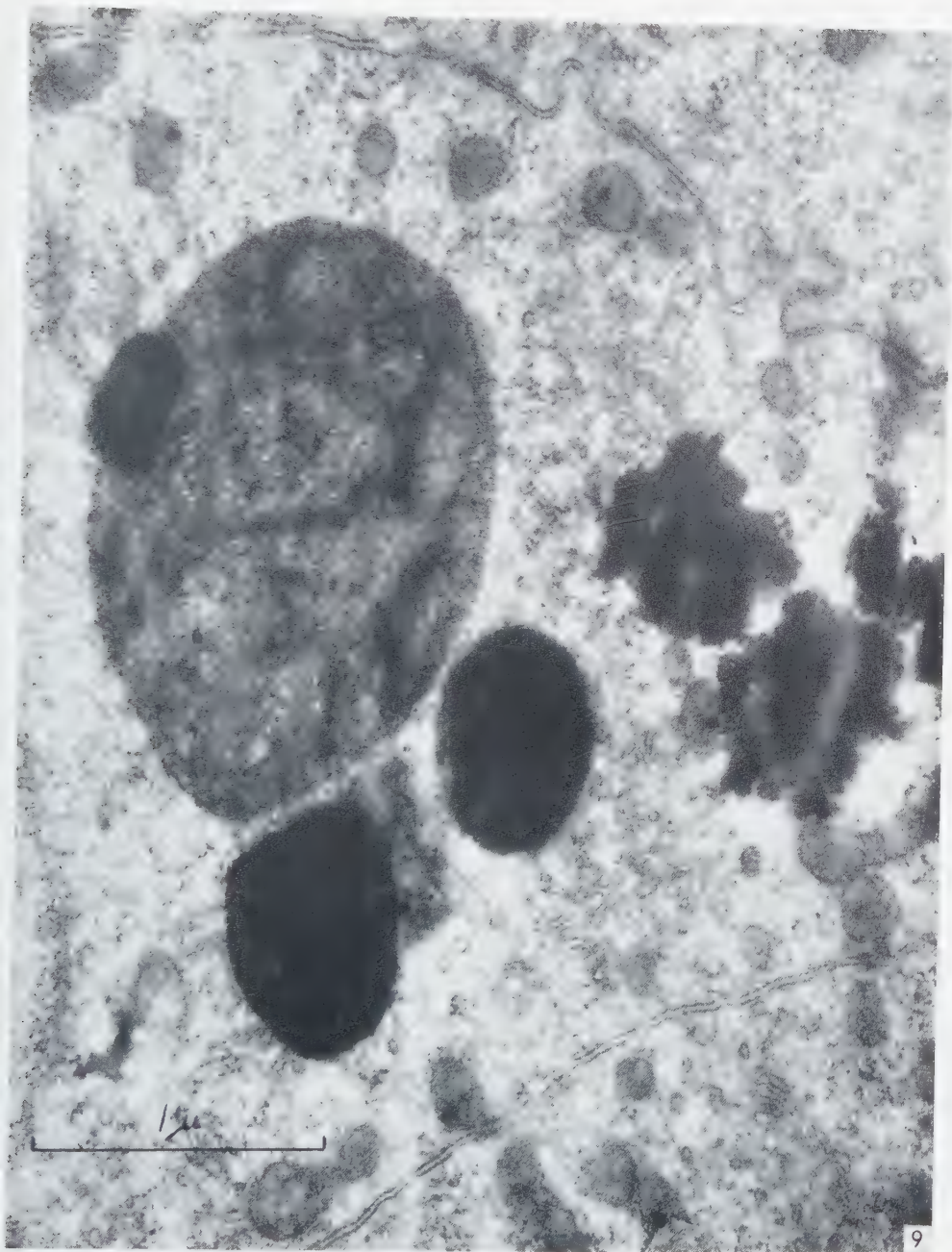
The fixative was a 1% osmium tetroxide solution of pH 7.2–7.3 in a veronal acetate buffer (24, 28) at room temperature. The animals were anesthetized by an intraperitoneal injection of about 1 cc of a 0.1% Nembutal solution. The uterus was exposed, and a thin glass rod was inserted through each distal mesometrium. This was made carefully to keep the blood circulation intact. Pins outside the body kept the rod with the uterine cornua in place. An incision was made in the extreme upper part of each cornu to prevent a high intra-uterine pressure, when the fixative was injected. Injections were made with a thin glass cannula inserted into each cervical canal through an incision made in the anterior wall of the vagina.

Five minutes after the injection of the fixative, the uterine cornua were carefully dissected free, the middle third was placed in osmium solution, and cut into small pieces with razor blades. The fixation was performed at room temperature for three hours and was followed by rinsing in Ringer solution for 15 minutes. Dehydration and embedding (22) were made according to the following schedule.

| | | |
|--|-----------|-------|
| Ethyl alcohol, 70 % | | ½ hr |
| 90 % | | ¼ hr |
| abs. | | ½ hr |
| Butyl methacrylate | | 2 hrs |
| Butyl methacrylate with 0.1 % benzoyl peroxide | | 1 hr |

Prepolymerization of the embedding plastic preceded a final polymerization at 45°C. The preparations were studied first with the phase contrast microscope to control the homogeneity in the appearance of the epithelium. Material then was taken for further

FIG. 9. Part of uterine epithelium from spayed animal demonstrating the three types of granules: one large, slightly dense granule (*left*), two dark granules with smooth outlines (*bottom*), and dark granules with irregular outlines (*right*). Cell borders run in the upper and lower part of the figure. Mitochondria containing dark areas lie in the upper part and two Golgi apparatus are situated in the lower, right-hand part of the figure. ×39,000.



studies with the electron microscope. For phase contrast microscopy, the preparations were sectioned with a Spencer Rotary Microtome type no. 621 with specially polished razor blades (34). The sections were caught on a cover-glass and then floated in amyl acetate for about one minute to remove the plastic. The sections were cut $0.05\ \mu$ thick and mounted in air (41). The phase contrast microscopy was made with a Leitz "Ortholux" microscope with a $90\times$, A 1.15 objective. For electron microscopy, the sections were made with glass knives (16) on an ultramicrotome designed by Sjöstrand (33). The sections were examined in an RCA EMU-2C electron microscope. Equipment and method of calibration have been communicated earlier (34).

RESULTS

The epithelium that coated the inner surface of the mouse uterus consisted of a single layer of cells, which rested on a folded basement membrane. The epithelium also formed tubules down into the connective tissue. The appearance of the surface epithelial cells varied with the changes in the hormonal state of the animal.

Spayed mice

Spayed mice had a low uterine surface epithelium with cells about $7\text{--}10\ \mu$ in height and $4\text{--}5\ \mu$ in width. They contained dark granules in both the apical and basal parts (Figs. 1, 3, 5, 7 and 8).

The cell membrane possessed, at the luminal cell surface, microvilli with a maximum length of about $0.2\ \mu$ (Figs. 3 and 7). Lateral, adjacent cell surfaces were parallel and had, in the sections, a slightly wavy course (Figs. 3 and 7). The lateral cell membrane and the surrounding cytoplasm had in the upper part of the epithelium the appearance that is known to be characteristic of terminal bars (Fig. 7).

The mitochondria appeared mostly as small rods. They possessed the triple-layered outer and inner membranes. A few small, dark granules with a size of about $200\text{--}600\ \text{\AA}$ often were seen in the mitochondria (Figs. 7–9).

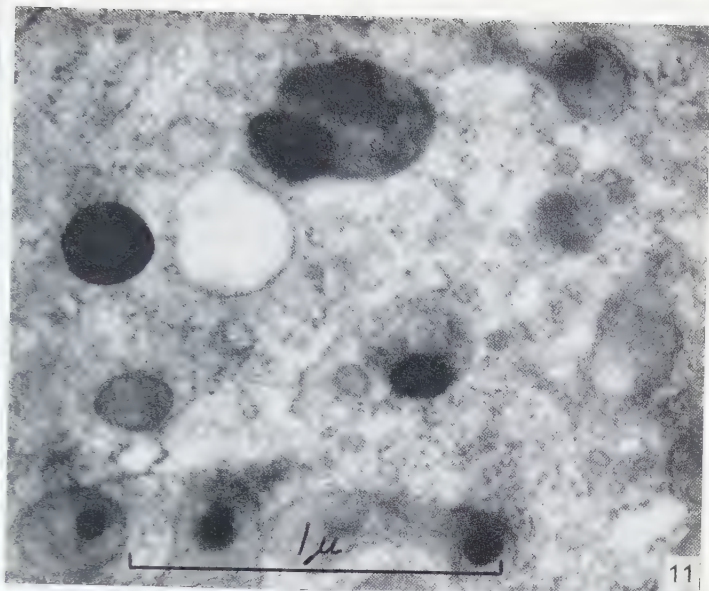
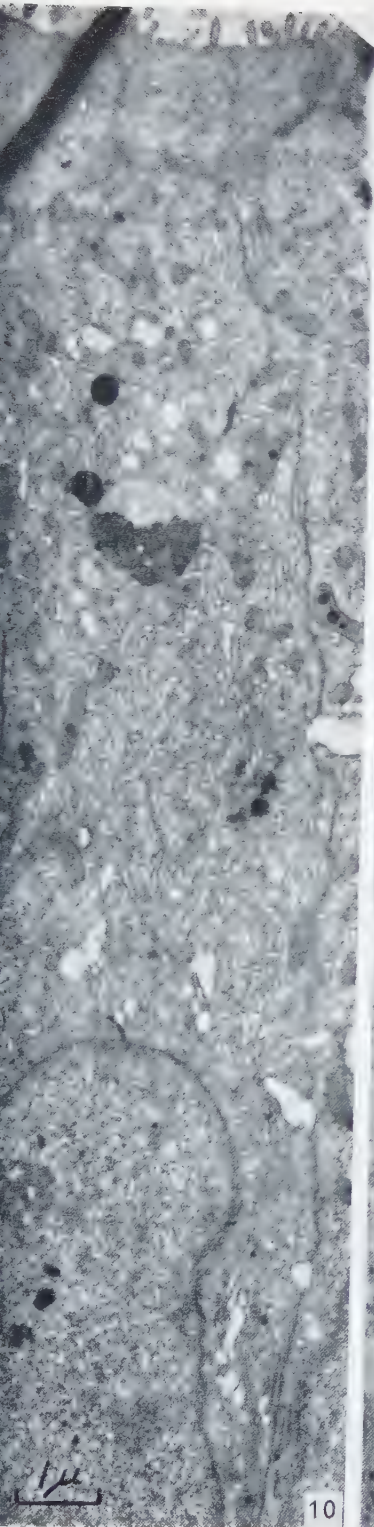
The small particles of the cytoplasm occurred in groups or attached to cytomembranes. The system of α -cytomembranes (35) was developed poorly, and was observed as small vesicles scattered in the cytoplasm.

The Golgi apparatus was situated at the upper pole of the nucleus (Fig. 7). The smooth membranes ran fairly parallel, and among them, small vacuoles sometimes

FIG. 10. Survey figure showing upper part of uterine epithelium from oestrous animal. Mitochondria containing dense bodies, α -cytomembranes, Golgi apparatus, granules, vesicles, and intercellular vacuoles are demonstrated. $\times 11,000$.

FIG. 11. Part of uterine epithelial cell from oestrous animal. In the cytoplasm, there are vesicles, dark granules, and some mitochondria, which contain dense bodies. $\times 49,500$.

FIG. 12. Part of uterine epithelial cell from oestrous animal. A nucleus lies in the lower part of the figure. Mitochondria and α -cytomembranes are situated above the nucleus. $\times 49,500$.



appeared (Fig. 9). The Golgi granules were scanty. Structures, very similar to the granules, were enclosed in some vesicles which appeared in the Golgi region.

Dark granules, with a maximum size of about $2\ \mu$, were noted in the cytoplasm. They showed different structures (Figs. 3 and 5): (1) Slightly dense granules with a smooth outline (Fig. 9). They had an ovoid shape. Their interior showed an amorphous substance of varying density, groups of parallel membranes, and, sometimes, a dark granule. In Fig. 9, the membranes were about $65\ \text{\AA}$ thick, and the distance between adjacent membranes was about $85\ \text{\AA}$. (2) Dark granules with a smooth outline (Fig. 9). They had an ovoid shape and were homogeneous. Sometimes they were surrounded by membranes. (3) Dark granules with an irregular outline (Figs. 7-9). They were homogeneous, and no border membrane could be demonstrated. These granules were observed most frequently. Furthermore, some granulated bodies, measuring about $0.5\ \mu$, were marked.

Vesicles, which contained small, ring-shaped profiles, were seen in the cells. The vesicles were bordered by a single membrane and had a varying size.

Small membrane-bounded vacuoles sometimes appeared under the luminal cell surface.

The nuclear membrane was composed of two dense layers surrounding a less dense layer, and the nucleoplasm was visualized as a varying amount of small granules (Figs. 3 and 7).

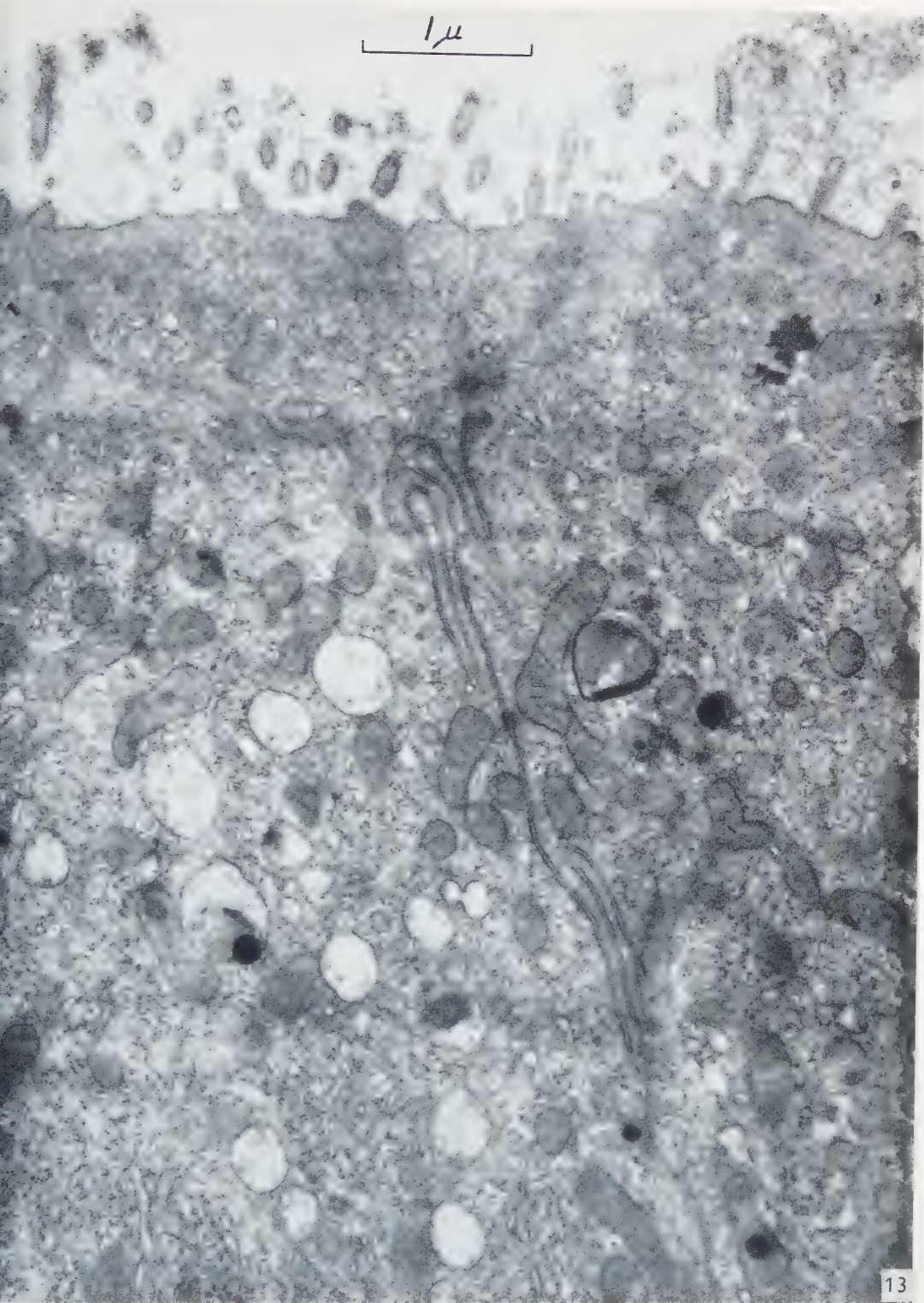
Oestrous mice

Oestrous animals showed uterine epithelial cells, about $18-22\ \mu$ high, with basally located nuclei. No definite change of the cell width was observed. Most of the dark granules had disappeared, but a few of them were yet visible in the lower part of the epithelium (Figs. 2 and 6).

The cell membrane possessed, at the luminal cell surface, microvilli with a maximum length of $0.6-0.7\ \mu$ (Figs. 4, 13 and 14). These sometimes contained a vacuolar space (Figs. 15 and 16). A luminal substance, consisting of an irregular network of thin, dense strands, was noted at the cell surface (Figs. 13-16). Lateral, adjacent cell surfaces ran parallel and were folded (Figs. 10, 13 and 17). Intercellular vacuoles often were observed (Figs. 4, 10 and 17).

The mitochondria mostly were formed as bent rods (Figs. 4, 13 and 17), which sometimes were found to branch. Their limiting membrane was triple-layered, and among the internal membranes, small dark granules and, in some animals, spherical,

FIG. 13. Luminal part of uterine epithelium from oestrous animal. Microvilli with luminal substance, mitochondria, α -cytomembranes, and vesicles are demonstrated. Folded cell borders run in the middle of the figure. $\times 26,000$.



homogeneous bodies appeared. The granules varied between 200–500 Å in size (Fig. 19). The bodies had a maximum diameter of about $0.15\ \mu$. They lay along the central line of the mitochondria and displaced the inner membranes. A single membrane closely surrounded the outline of the bodies (Figs. 19 and 20).

The small particles of the cytoplasm occurred in groups or appeared in the x-cytomembranes. These constituted a system, which was well developed and noted as rounded or elongated profiles in the cytoplasm (Figs. 10, 12, 19–21).

The Golgi apparatus was extensive (Fig. 4). In the micrographs, it sometimes appeared both at the upper pole and at the lateral sides of the nucleus (Fig. 10). The Golgi apparatus showed large vacuoles interspaced among the smooth membranes of the region. The vacuolar spaces varied in form and size. The Golgi granules, which had a diameter of about 300 Å, appeared scattered in the Golgi zone (Figs. 18 and 19). Structures, very similar to the granules, were enclosed in some vesicles that appeared in the region (Fig. 19).

Vesicles, containing small, ring-shaped profiles with a diameter of about 300 Å, were observed in the cells (Fig. 15). They showed the same characteristics as did the vesicular structures that were noted in the epithelium of spayed animals.

Vesicles, which appeared empty or contained an irregularly distributed, amorphous material of varying density, lay in the upper part of the cell (Figs. 4, 10, 11 and 13). These profiles had a maximum size of about $0.5\ \mu$.

Small vacuoles, with a size of about $0.1\ \mu$ and bordered by a membrane, were observed in the cytoplasm adjacent to the luminal cell surface. They also were seen lying elongated in the cell projections (Figs. 15 and 16).

Dark granules with an irregular outline, similar to those demonstrated in spayed animals, were observed in oestrous animals but fewer in number (Fig. 22). Furthermore, there were encountered granules of different size and structure in the cytoplasm (Fig. 22).

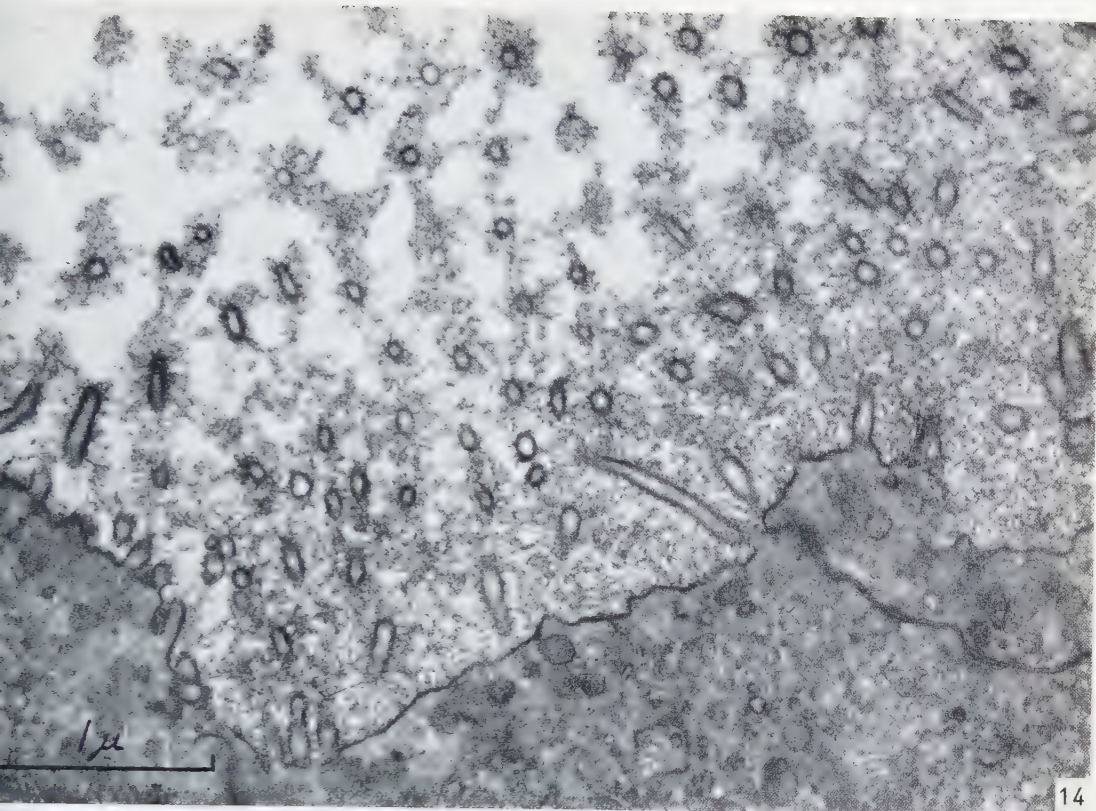
Structures, $2\text{--}3\ \mu$ large and composed of an irregular system of membranes, lay in the cytoplasm, often in an indentation of the nucleus (Fig. 23). A part of their interior sometimes was occupied by dark, irregular granules.

The nuclear membrane and the nucleoplasm were no different from those in the epithelium of spayed animals (Figs. 12 and 23).

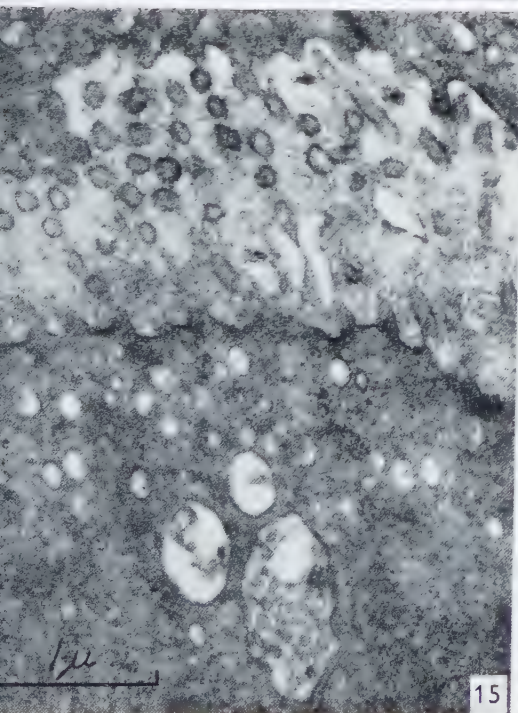
FIG. 14. Luminal part of uterine epithelium from oestrous animal showing microvilli and luminal substance. Cell borders with terminal bars to the right and left in the figure. $\times 30,000$.

FIG. 15. Luminal part of uterine epithelium from oestrous animal showing microvilli and luminal substance. Vacuoles lie under the cell membrane and inside some of the microvilli. A vesicle containing small, ring-shaped profiles is situated in the lower part of the figure. $\times 25,000$.

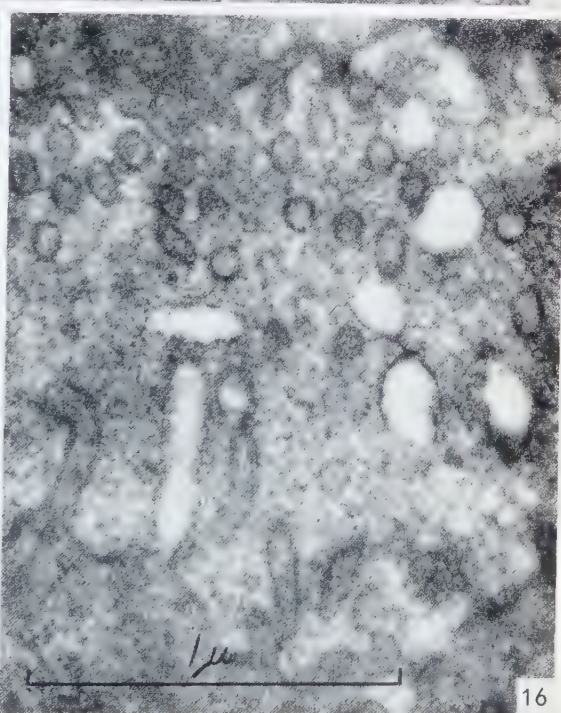
FIG. 16. Luminal part of uterine epithelium from oestrous animal showing microvilli and luminal substance. Some microvilli contain vacuoles. $\times 50,000$.



14



15



16

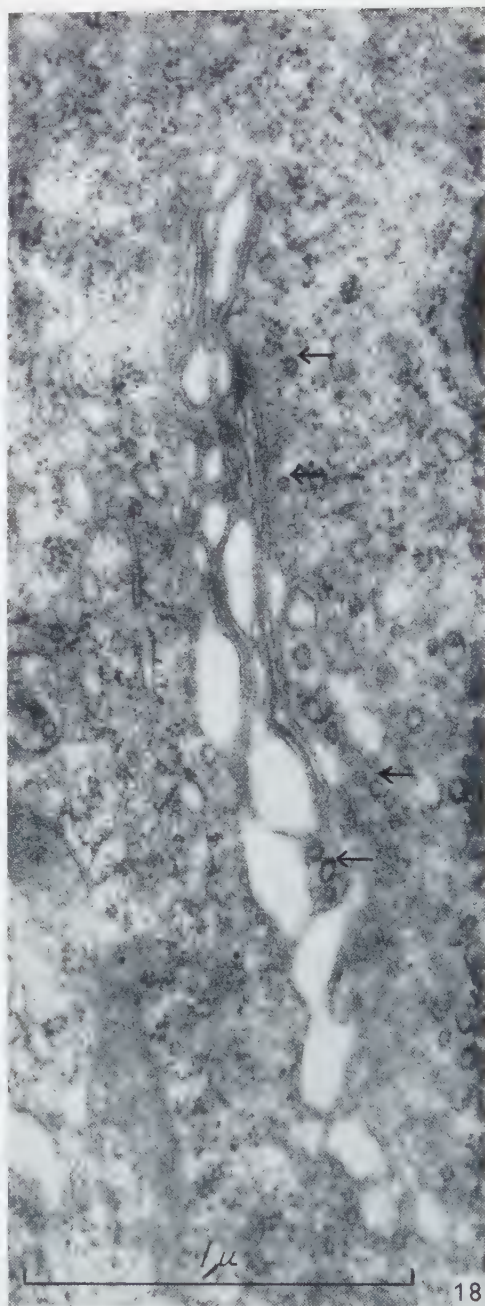
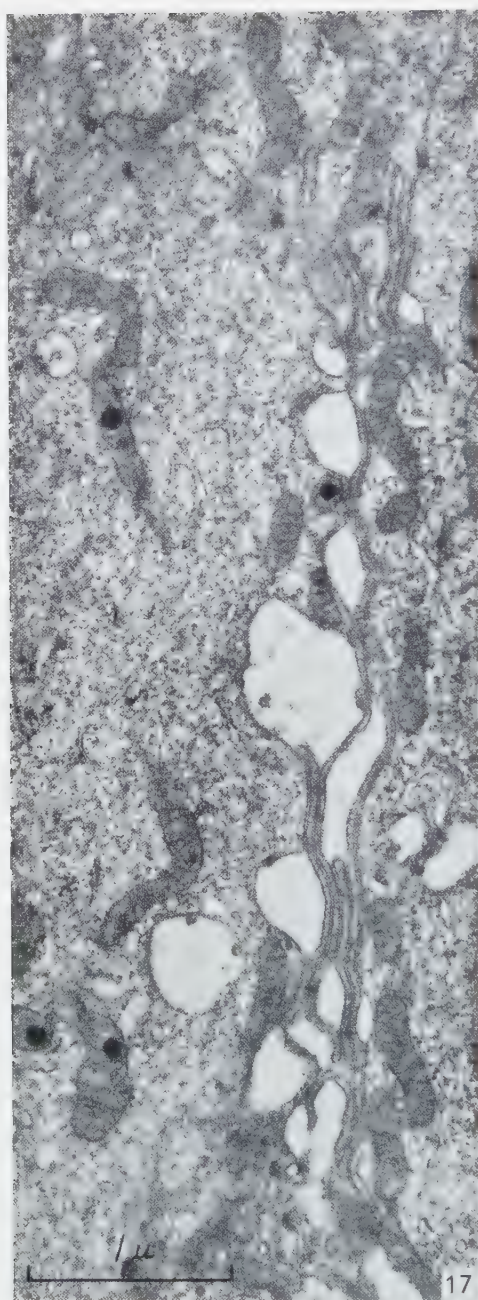


FIG. 17. Folded cell borders in uterine epithelium from oestrous animal. There appear many inter-cellular vacuoles. $\times 27,000$.

FIG. 18. Golgi apparatus in uterine epithelial cell from oestrous animal showing smooth membranes, vacuolar spaces, and Golgi granules (\rightarrow). Some α -cytomembranes also are recognized. $\times 51,000$.

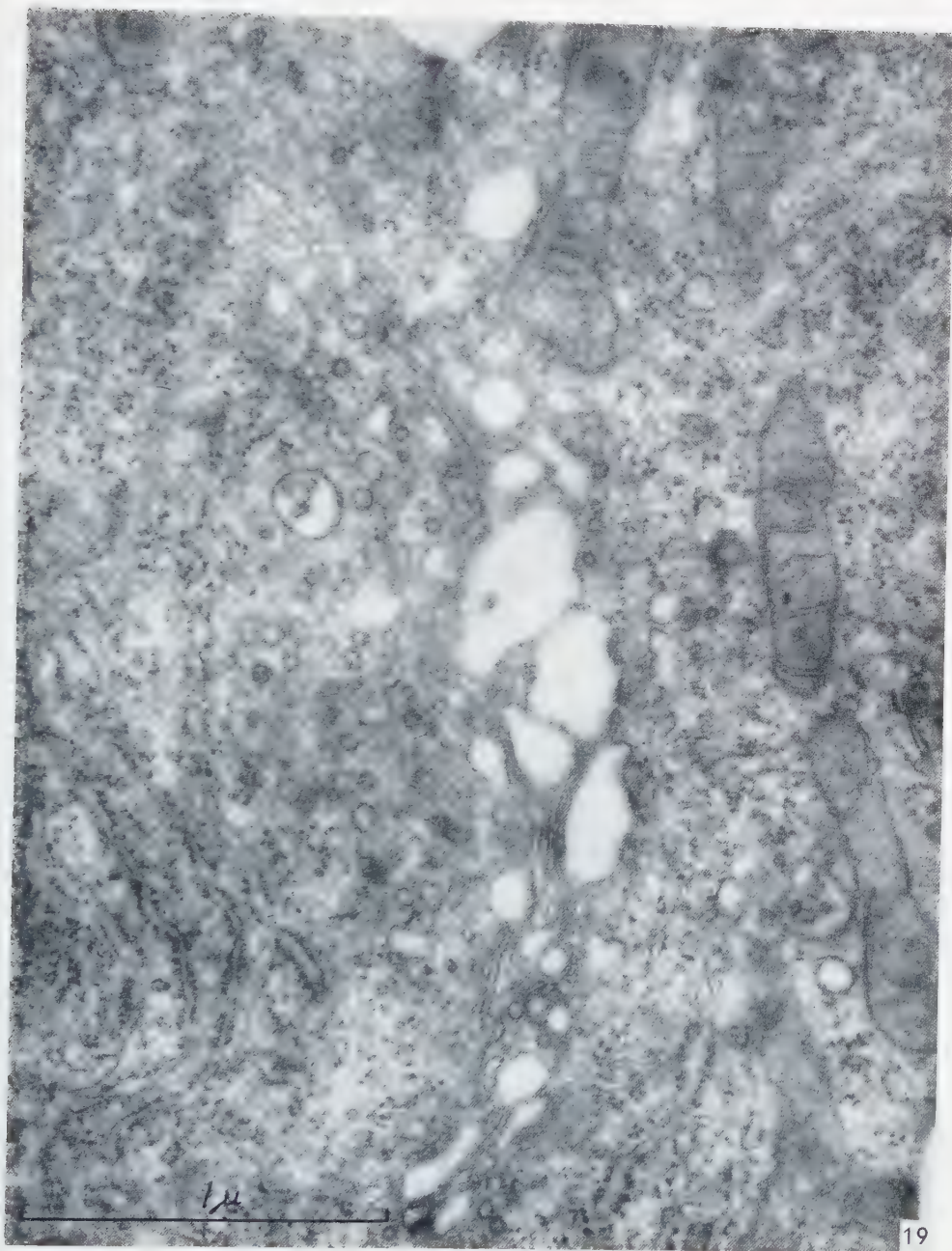


FIG. 19. Golgi apparatus in uterine epithelial cell from oestrous animal showing smooth membranes, vacuolar spaces, and Golgi granules. A vesicle containing small, ring-shaped profiles lies in the left-hand part of the region. A system of α -cytomembranes is seen to the left and mitochondria with dense bodies to the right in the figure. $\times 49,000$.

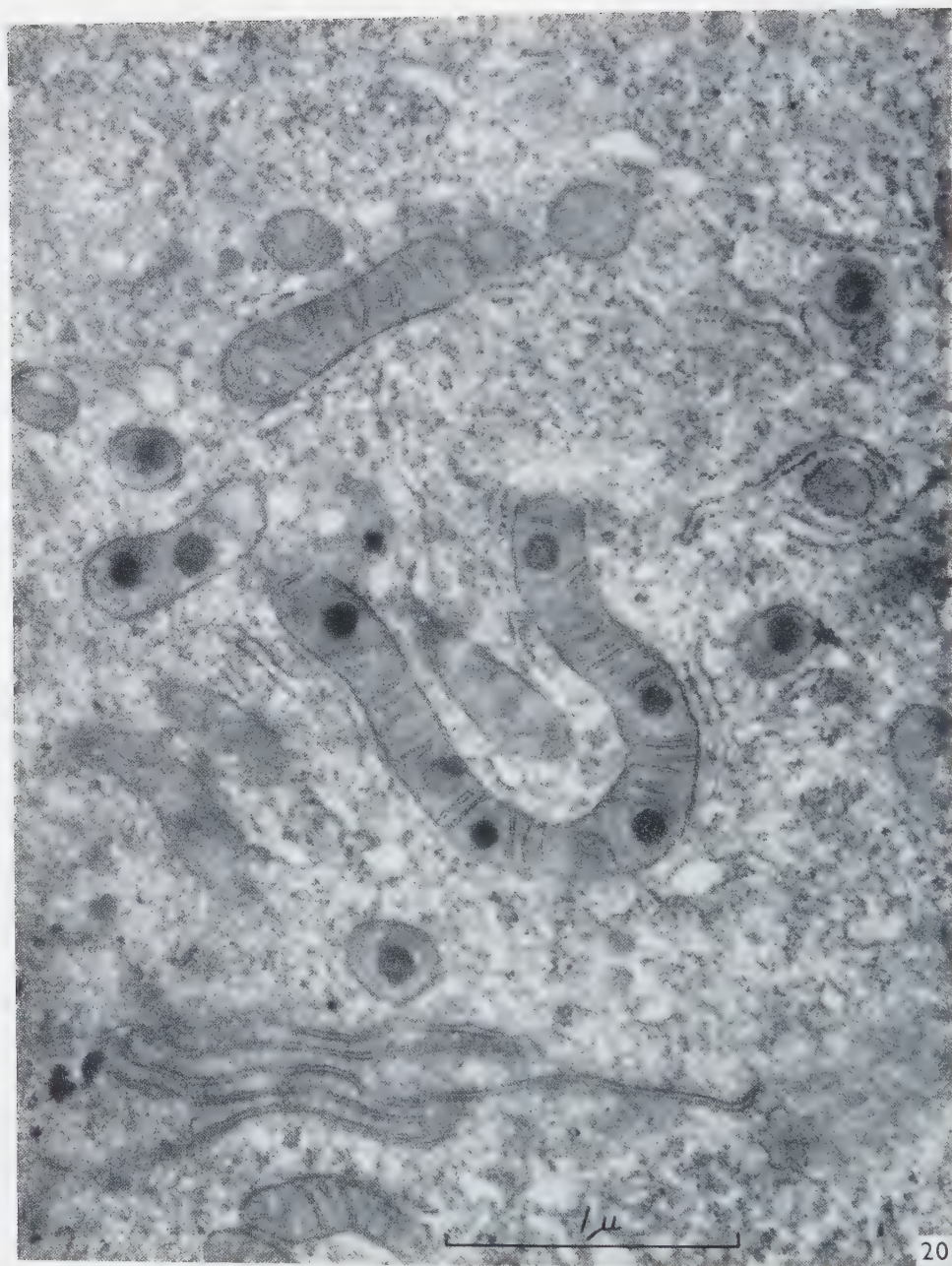


FIG. 20. Mitochondria and α -cytomembranes in uterine epithelium from oestrous animal. Mitochondrial bodies are visible. Cell borders are seen in the lower part of the figure. $\times 39,000$.

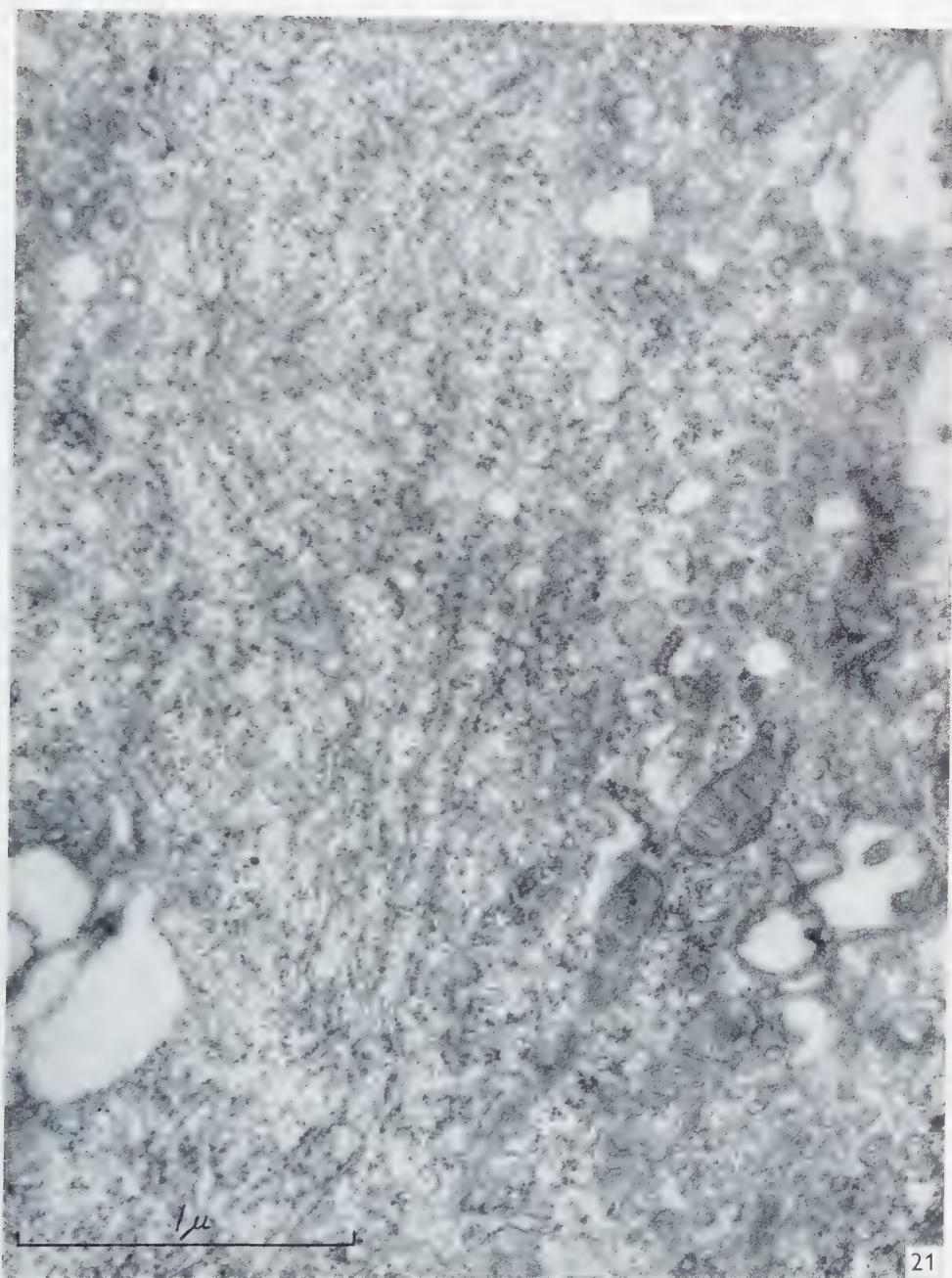


FIG. 21. System of α -cytomembranes in uterine epithelial cell from oestrous animal. $\times 44,000$.

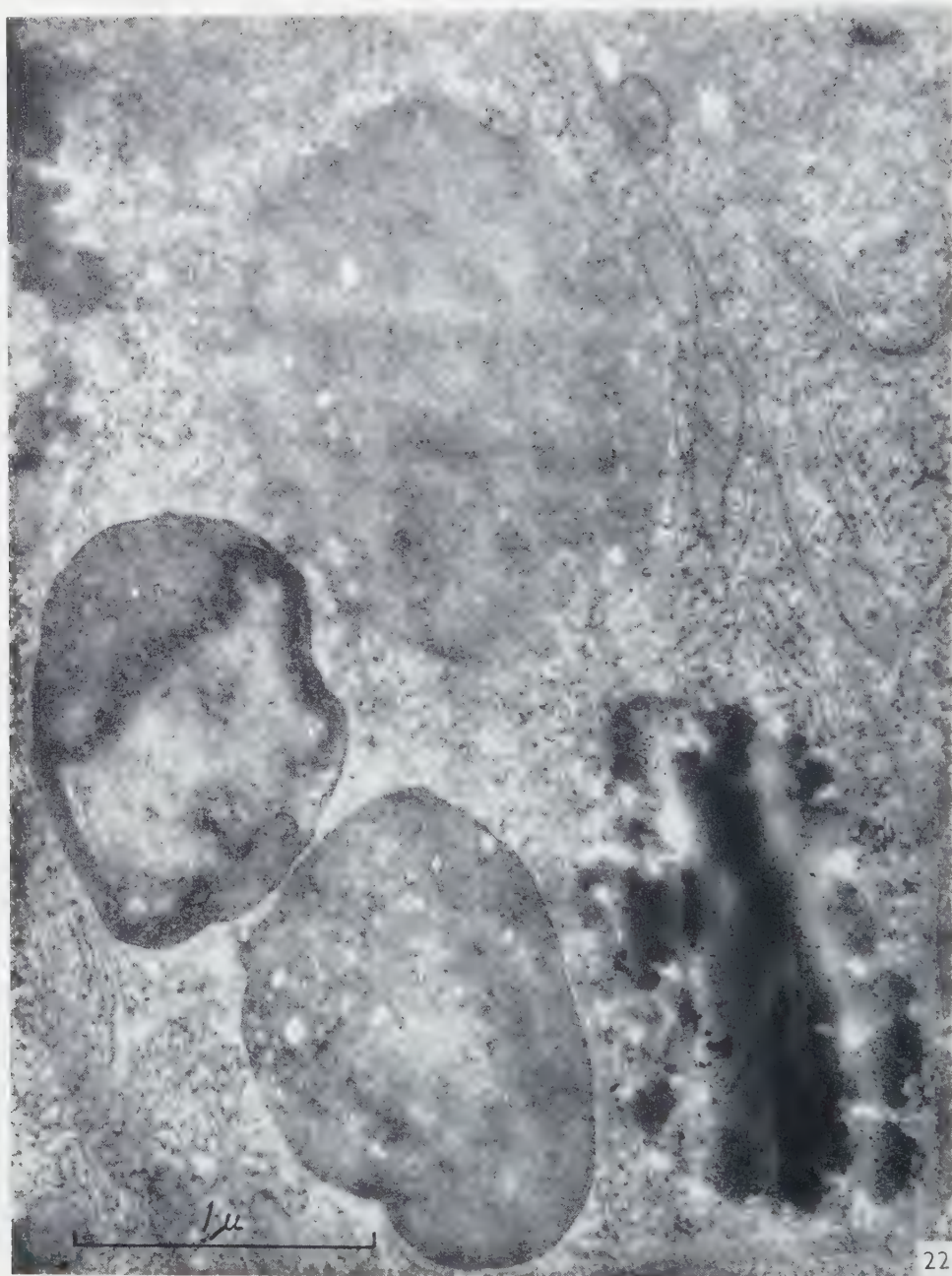


FIG. 22. Several types of granules in uterine epithelial cell of oestrous animal. $\times 40,000$.

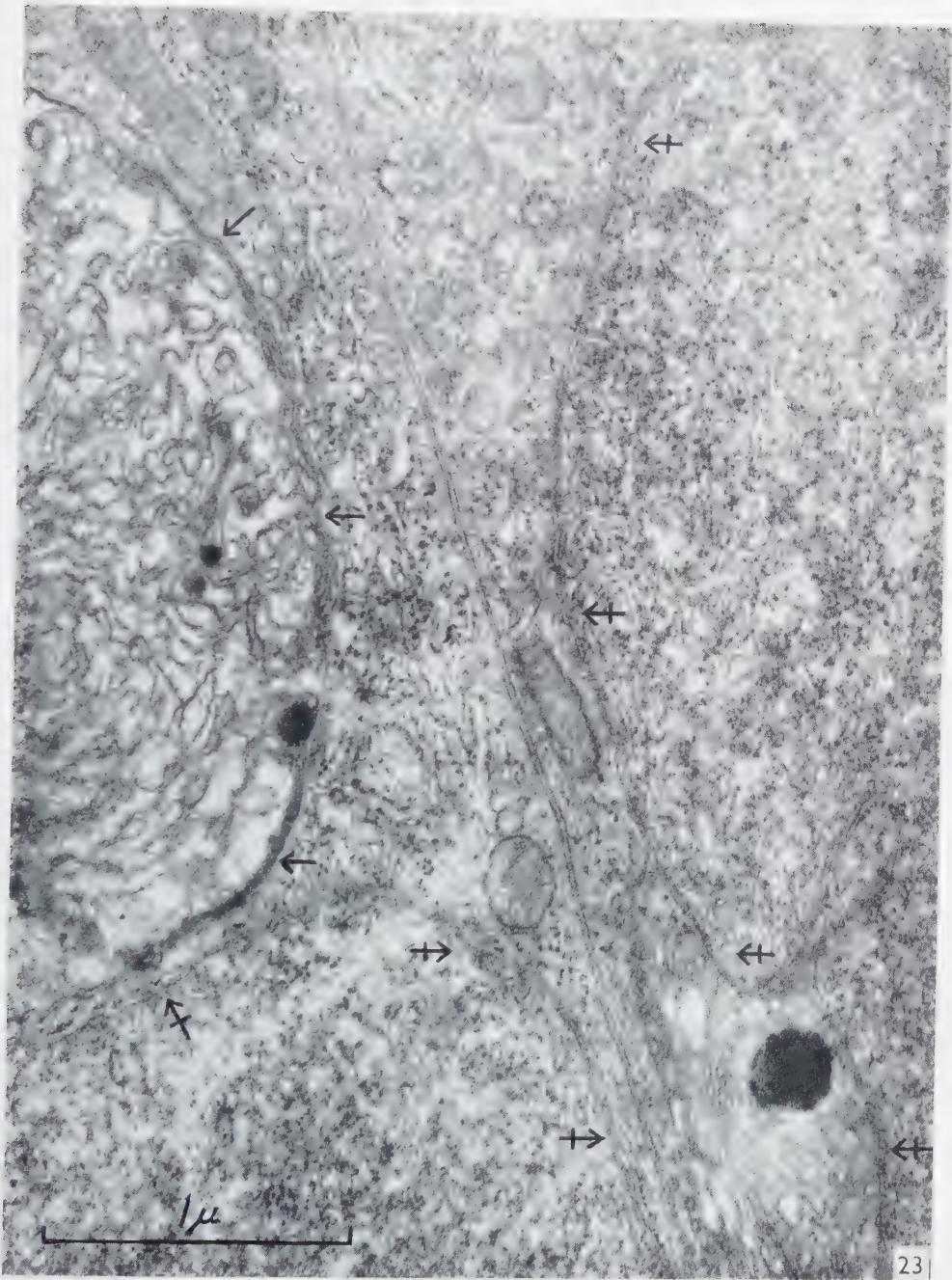


FIG. 23. Membrane structure in uterine epithelial cell from oestrous animal (>). Cell borders run in the middle of the picture. Nuclear membranes appear to the lower left and to the right in the picture (↔). $\times 41,000$.

DISCUSSION

The light microscopy of the uterine epithelium from spayed and from oestrous animals gave results, which were in accordance with earlier findings. The appearance of the several oestrous epithelia in this investigation was homogeneous, but as the methods available to time the different stages of the oestrus are not exact (12, 20, 31, 39, 43), the animals might not have represented the same oestrous development. Thus, this paper is a survey of some structural changes that appeared in the uterine epithelium. A possible way to get a more exact timing of such changes is to induce them by injections of estrogen. A quantitative analysis of ultrastructural changes can then be made, and the result of such a study will be presented in sequent reports (23).

In the light microscope, the most obvious differences between the uterine epithelium from spayed animals and that from oestrous animals were an increase in cell height and a decrease in amount of dark granules in the latter. In the electron microscope, several other differences also were observed.

The cell membrane demonstrated an irregular course in sectioned material from oestrous animals. The luminal cell surface showed longer microvilli and the lateral cell surfaces were folded much more than in the uterine epithelium from spayed animals. This implies an absolute increase in the surface area and, as the cell width was rather constant, also an increase relative to the cell volume. The appearance of the microvilli of oestrous animals coincided with earlier observations (44).

The system of α -cytomembranes was more developed in the uterine epithelium from oestrous animals, but it is not known if this increase was also relative. The Golgi apparatus had grown in size, and the smooth membranes occupied in oestrous animals a larger space than in the epithelium of spayed animals.

This general increase in amount of membranes in oestrous animals seems to run parallel with the decrease in amount of dark granules with an irregular outline. These granules might be lipid granules, and it seems probable that material from lipid granules of spayed animals was used to synthesize the lipoproteins of the different membranes in oestrous animals. Furthermore, some of the granules in the epithelial cells of both spayed and oestrous animals were connected to complicated membrane systems. Conclusions about their significance, however, have to await further knowledge of their structural variations.

The mitochondria in the uterine epithelium of spayed animals contained small, dark granules, but in some oestrous animals there also were noted dense, homogeneous, rather large bodies. Many authors described mitochondrial inclusions (25, 30, 36, 37 and others), and their significance was much discussed. They were regarded, for example, as visualizations of a changing functional process (19), as segregations of

cations (42), and as steps in the production of different cytoplasmic granules (17, 32). However, those mitochondrial inclusions did not seem to have the appearance of the distinctly outlined bodies of the uterine epithelium. Nothing can, as yet, be said about the significance of these bodies.

One task of the uterine endometrium in oestrous mice is to produce the uterine fluid, and it has been shown that estrogen favors endometrial secretion (11). Probably, some of the structures observed in this study of the uterine epithelium from oestrous animals were signs of a secretion. As this process is influenced by estrogen, the uterine epithelium also seems to be suitable for an experimental study of the secretion process. Further investigations might show the structural changes in details.

"Professor Erik Ahlströms fond för obstetrisk-gynekologisk forskning", the foundation "Therese och Johan Anderssons minne", and the Swedish State made grants toward the expenses of the investigation. Mrs. Dorrit Lindahl and Miss Maud Hoffstedt provided much able technical assistance. Miss Maj Berghman made the prints and drawings.

REFERENCES

1. ALDEN, R. H., *Anat. Record* **97**, 1 (1947).
2. ALLEN, E., *Am. J. Anat.* **30**, 297 (1922).
3. ALLEN, W. M., *Anat. Record* **48**, 65 (1931).
4. ASDELL, S. A., *Patterns of Mammalian Reproduction*. Comstock Publ., New York, 1946.
5. BUSSE, O., *Über den Genitalcyklus und die Schwangerschaft bei der weissen Maus*. Thesis. H. Lüdtke, Kiel, 1931.
6. CLAUBERG, C., *Arch. Gynäkol.* **147**, 550 (1931).
7. DEMPSEY, B. W. and WISLOCKI, G. B., *J. Biophys. Biochem. Cytol.* **2**, 743 (1956).
8. ECKSTEIN, P. and ZUCKERMAN, S., in PARKES, A. S. (Ed.), *Marshall's Physiology of Reproduction*, Vol. I, Part 1, p. 543. Longmans, Green and Co., London, 1956.
9. FARRIS, E. J. and GRIFFITH, J. Q., *The Rat in Laboratory Investigation*. J. B. Lippincott Co., London, 1949.
10. GREENE, E. C., *The Anatomy of the Rat*. Hafner Publ. Co., New York, 1955.
11. HOMBURGER, F. and TREGIER, A., *Endocrinology* **61**, 627 (1957).
12. ISHII, O., *Anat. Record* **23**, 311 (1922).
13. JUNQUEIRA, L. C. U. and MARTINS, E. O., *Atlas de anatomia microscópica do rato*. Publicação da universidade de São Paulo, 1947.
14. LANGE, K. H., *Z. Zellforsch. u. mikroskop. Anat.* **29**, 115 (1939).
15. LANGSTON, W. C. and ROBINSON, B. L., *Endocrinology* **19**, 51 (1935).
16. LATTI, H. and HARTMANN, J. F., *Proc. Soc. Exptl. Biol. Med.* **74**, 436 (1950).
17. LEVER, J. D., *Anat. Record* **128**, 361 (1957).
18. LONG, J. A. and EVANS, H. M., *Mem. Univ. Calif.* **6**, 1 (1922).
19. LOW, F. N., *J. Biophys. Biochem. Cytol.* **2**, No. 4, Suppl., 337 (1956).
20. MANDL, A. M., *J. Exptl. Biol.* **28**, 576 (1951).
21. MASSON, G. and SELYE, H., *Federation Proc.* **1**, 59 (1942).

22. NEWMAN, S. B., BORYSKO, E. and SWERDLOW, M., *J. Research Natl. Bur. Standards* **43**, 183 (1949).
23. NILSSON, O., in preparation.
24. PALADE, G. E., *J. Exptl. Med.* **95**, 285 (1952).
25. ——— *J. Histochem. Cytochem.* **1**, 188 (1953).
26. PARKES, A. S., *Proc. Roy. Soc., London* **100**, 151 (1926).
27. REESE, J. D., *Anat. Record* **48**, 55 (1931).
28. RHODIN, J., Correlation of Ultrastructural Organization and Function in Normal and Experimentally Changed Proximal Convoluted Tubule Cells of the Mouse Kidney. Thesis. Stockholm, 1954.
29. RIETSCHEL, P. E., *Z. wiss. Zool.* **135**, 428 (1929).
30. ROGERS, G. E., *Exptl. Cell Research* **13**, 517 (1957).
31. ROGERS, P. V. and ALLEN, E., *Endocrinology* **21**, 629 (1937).
32. SHELDON, H. and ZETTERQVIST, H., *Bull. Johns Hopkins Hosp.* **98**, 372 (1956).
33. SJÖSTRAND, F. S., *Experientia* **9**, 114 (1953).
34. ——— *J. Cellular Comp. Physiol.* **42**, 15 (1953).
35. ——— *Intern. Rev. Cytol.* **5**, 455 (1956).
36. SJÖSTRAND, F. S. and HANZON, V., *Exptl. Cell Research* **7**, 393 (1954).
37. SJÖSTRAND, F. S. and RHODIN, J., *Exptl. Cell Research* **4**, 426 (1953).
38. SNELL, G. D., *Biology of the Laboratory Mouse*. Dover Publications, New York, 1956.
39. SNELL, G. D., FEKETE, E., HUMMEL, K. P. and LAW, L. W., *Anat. Record* **76**, 39 (1940).
40. STRONG, L. C., in FARRIS, E. J. (Ed.), *The Care and Breeding of Laboratory Animals*, p. 79. J. Wiley & Sons, New York, 1950.
41. SWANBECK, G., *Mikroskopie* **11**, 398 (1956).
42. WEISS, J. M., *J. Exptl. Med.* **102**, 783 (1955).
43. YOUNG, W. C., BOLING, J. L. and BLANDAU, R. J., *Anat. Record* **80**, 37 (1941).
44. ZELANDER, T., in preparation.

The Submicroscopic Development of Chromoplasts in the Fruit of *Capsicum annuum* L.

A. FREY-WYSSLING and EMILIA KREUTZER

Department of General Botany, Swiss Federal Institute of Technology, Zürich

Received May 3, 1958

From a structural point of view, there are three different types of chromoplasts in carotinoid pigmented plant organs (8): plastids which contain (1) microscopic crystals of carotinoids, (2) microscopic and submicroscopic yellow globuli, and (3) bundles of orange-red pigmented submicroscopic filaments.

After having studied the development of the globuli in the second case (8), an investigation of the transformation of chloroplasts into the spindle-shaped chromoplasts containing submicroscopic filaments (23) has been undertaken. While the ultrastructure of the chloroplast, as well as that of the transformed chromoplast, are fairly stable and can be satisfactorily fixed, the stages of transition appear to be very unstable so that it is difficult to avoid swelling and artifacts even with osmic acid or permanganate.

The filaments appear as bundles during and directly after the disintegration of the grana in the chloroplastic structure. But there is no direct transformation of the grana into the bundles of long filaments because only a few (3 or 4) such bundles are formed, while the grana are numerous (Fig. 2). Apart from their shape, the filaments display a similar ultrastructure to the grana discs in the active chloroplast because they show a denser osmophilic rind measuring 50 Å in width and a less dense colorless core (Figs. 15 and 16). The origin and development of these filaments, which present some morphological resemblance to filamentous virus particles, is discussed.

The submicroscopic development and structure of chromoplasts has recently been shown to be closely related to that of green chloroplasts (8, 9, 18). These observations assume increased significance when it is remembered that chromoplasts are undoubtedly the final products of plastid development. Thus the photosynthetizing green plastid, the most important physiological stage, is so much the center of interest. The question of where they come from and what further potentialities for producing new forms they possess becomes most important then.

The grouping of the yellow and red chromoplasts into three types with respect to shape and submicroscopic structure (8, 24) depends in the last analysis on the manner in which the large amounts of carotenoid pigments are accommodated in the plastid.

At present, neither the alternative avenues of development (from proplastids, leuco-

or chloroplasts (8, 9)), nor the distribution of the related but chemically slightly different pigments occurring in various species offer an explanation of why one or the other of these three different structures should be formed.

In the first group, e.g. carrot plastids, the pigments seem to be unbound and crystallize out on their own, while in the second group, the globular type, e.g. *Ranunculus repens* (8) or *Aloe plicatilis* (24), they are dissolved most probably in the lipid component of the broken-down plastid structures. Finally in the spindle-shaped filamentous type or third group, the carotenoids appear to be bound chemically to filamentous protein structures as found in some solanaceous fruits and rose hips (23, 24).

The question of whether these forms are the result of degeneration or of ontogenetic development is at present a disputed one. However, formation of new structures from any of these forms has never been observed and a reversion to the original, highly organized lamellar structure seems to be most unlikely.

In the present paper, the structure of the third type of colored chromoplasts, namely, the filamentous chromatophores, will be discussed. This type occurs in fruits and some flowers of angiosperms (15, 22-24, 26) and in most cases contains, in addition to the yellow pigments, a large amount of red and orange colored carotenoid pigments.

Capsicum annuum appeared to be a suitable object for study as it has a large number of these typical spindle-shaped, red chromoplasts in the fruit flesh.

MATERIAL AND METHODS

Fruits of *Capsicum annuum* L., the red pepper, were observed in the fresh state or fixed and embedded for electron microscopic observation.

Three varieties, Marktgärtner, Friesdorfer gelb and Roter Zwerg, were grown in a greenhouse. No difference in the plastids of these could be observed. Hand sections were made through the fruit wall of different developmental stages as judged by their color. (A single fruit occasionally may possess differently colored regions.)

Fresh sections were observed in isotonic sucrose solution or glycerine.

For observation in the electron microscope, tissue slices were fixed in a 1% OsO_4 solution in acetate-veronal buffer pH 7.4 (19) or in a similarly buffered 2% KMnO_4 solution (16). To speed-up penetration of the fixative at the beginning of fixation, the sections in the fixative were placed in a vacuum desiccator and evacuated with a water pump for 30 minutes after which they were placed in the refrigerator (2-4°C) for two to four hours. This method was found to be satisfactory for thin tissue slices. A large number of other fixatives, mainly those recommended by Strugger (25) and their variations, were tried. None of them, however, gave an acceptable preservation of cytoplasmic structures. Tissues were dehydrated in an acetone series and embedded in araldite in the usual manner (10).

The thin sections were mounted on a formvar film on a wire specimen grid and examined in the Philips or Siemens Elmiskop I electron microscopes.

OBSERVATIONS

Fresh material

A great variety of shapes and sizes of chromoplasts can be observed in the fruit wall, similar to those found in other solanaceous fruits (15, 22-24), in *Sorbus* (22, 26) and in rose hips (22, 23). In the outermost cells, which have thick cell walls and small lumena, the plastids are more or less oval in shape and have an overall distribution of pigments with a hardly discernible striation. Toward the inner cavity of the fruit, the cells become gradually larger and the plastids more and more drawn out into spindle, crescent or triangular shapes with the striated, colored portion arranged in various ways, distinct from the completely colorless portions that appear to be optically empty.

The striations always follow the longitudinal axis or the direction in which the plastid appears to have been drawn out and not infrequently show as many as three directions in the case of triangular plastids. A number of these forms is represented diagrammatically in Fig. 1. The striation is confined to the orange-red portion of the mature plastids.

The chromoplasts vary greatly in size from 3-5 μ wide and 4-6 μ long oval forms to spindles which may be up to 15-20 μ in length and only 2-3 μ in width at the broadest point.

Between crossed nicols, the plastids show a strong birefringence. This is particularly remarkable in plastids where the colored portion is of the crescent-type with curved striations. When the stage is rotated, a different portion lights up, indicating a

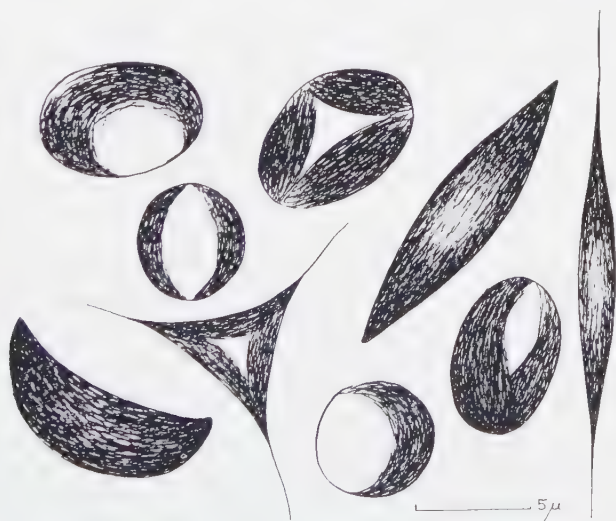


FIG. 1. Drawing of mature chromoplasts.

circular texture. With a red, first-order platelet the pigmented bundles appear lemon yellow and dark greenish-blue when perpendicular to and parallel with the major axis of the platelet respectively. Thus they are optically positive with respect to the direction of the striations.

Development of the chromoplasts

Soon after fertilization, young green fruits contain typical chloroplasts with numerous green grana in all layers. The plastids develop normally until, when the fruit has almost reached its full size, those in the inner cell rows begin to store starch in the form of numerous small granules. Parallel with this, the chloroplasts become paler green in color and the grana less distinct until they are no longer discernible in the homogeneous, pale yellowish-green plastids. Starch and chlorophyll gradually disappear with an increase in the intensity of the yellow coloration. The colored mass of the slowly elongating plastid often gets drawn to the side and is concentrated into striated, elongated shapes or crescents which leave the rest of the plastid colorless (Fig. 2). This is accompanied by a change in color from a pale yellow to an increasingly intense orange-red along with an ever greater distortion of the originally oval plastid to the characteristically pointed shapes of the mature fruit. The yellow coloration appears simultaneously with the striation which would indicate that the pigment is deposited in this manner. Intermediate stages are very labile and swell or burst easily or become completely disorganized into colored droplets and pieces of membrane



FIG. 2. Drawing of young, yellow plastids. The spindle-shaped bodies contain the pigments. Starch granules (*st*) are present in some cases.

FIG. 3. Plastid from young, green fruit. $\times 12,000$.

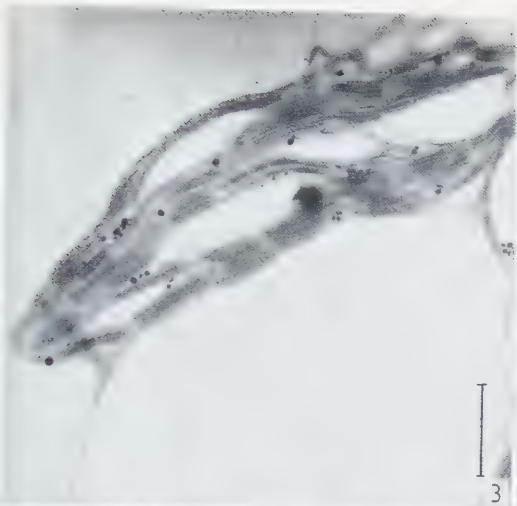
FIG. 4. Chloroplast from young fruit with starch granules. Note the different directions of the lamellar layers. $\times 13,000$.

FIG. 5. Very slightly swollen chloroplast from pale-green fruit. $\times 13,000$.

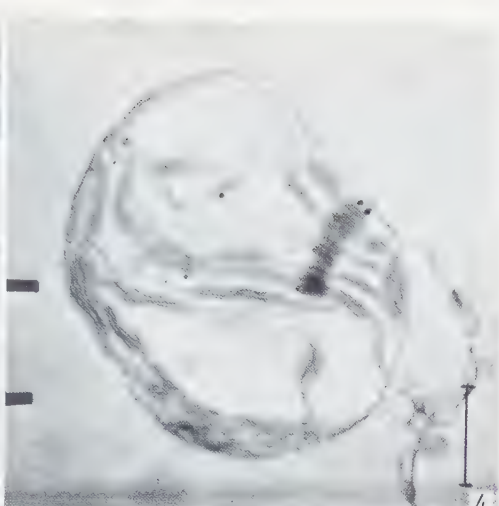
FIG. 6. Intermediate stage from pale-green fruit. Note the small osmophilic globuli in rows at the edges of the grana (*g*), cut transversely; *sl*, stroma lamellae. $\times 13,000$.

FIG. 7. Same stage as Fig. 6; grana cut almost parallel to the lamellae. *g*, granum; *sl*, stroma lamellae. $\times 13,000$.

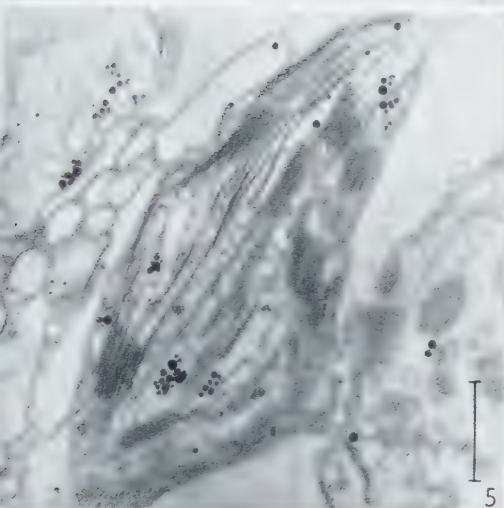
FIG. 8. Intermediate stage from orange-red fruit. $\times 13,000$.



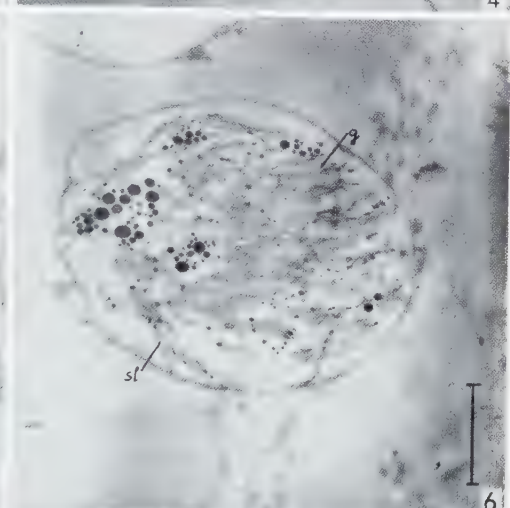
3



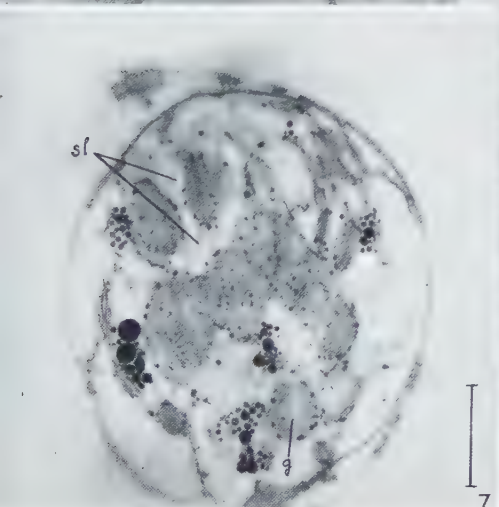
4



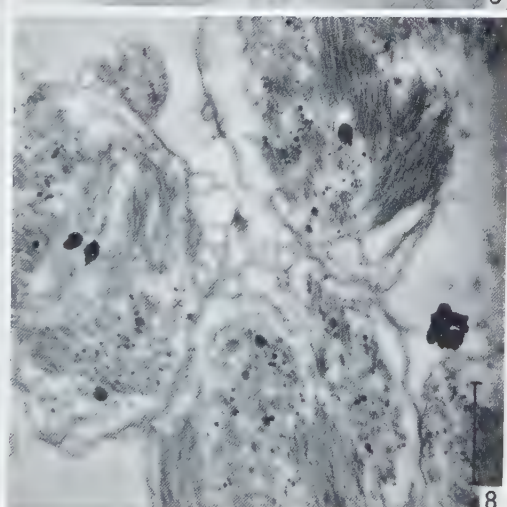
5



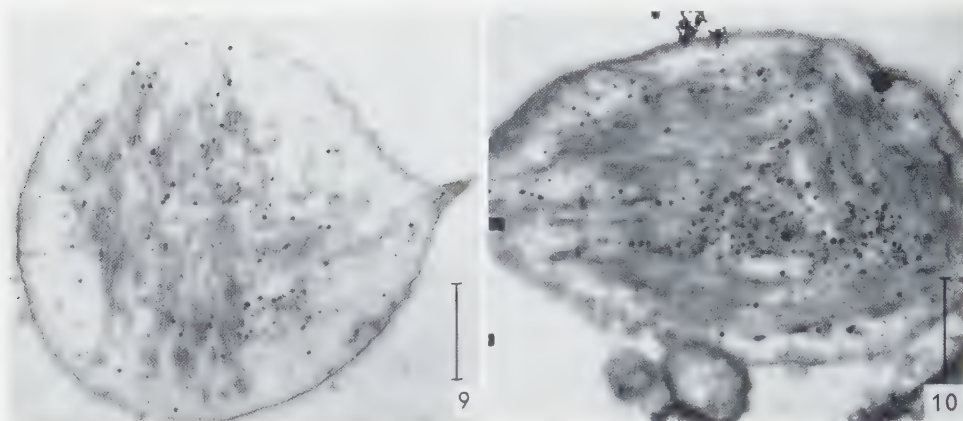
6



7



8



FIGS. 9 and 10. Plastids from mature, dark-red fruits. Note the different grouping of the filaments. $\times 12,500$ and $14,000$ respectively.

residues. This lability may be responsible for the large variety of intermediate forms encountered. In the same cell, the long spindle-shaped plastids remain intact; as mature forms, they are difficult to cause to swell or to squash.

The striated, colored portion of the chromoplasts does not give reactions with lipid stains. It is not destroyed by lipid solvents. The latter, however, cause damage to the rest of the plastid whereby the colored bundles become liberated into the cell cavity.

Experiments were also performed with lipase prior to fixation, by incubating sections in various aqueous, isotonic buffers of different pH which contained crystalline pancreatic lipase. The spindles remained intact even after a prolonged incubation which destroyed other structures. Thus the striated bundles are not lipochrome structures.

Extraction of the pigments with various lipophilic solvents was never complete even after prolonged periods. This confirms the suggestion that they are bound structurally, at least in part, to some non-lipid component of the plastid.

Electron microscopic observations

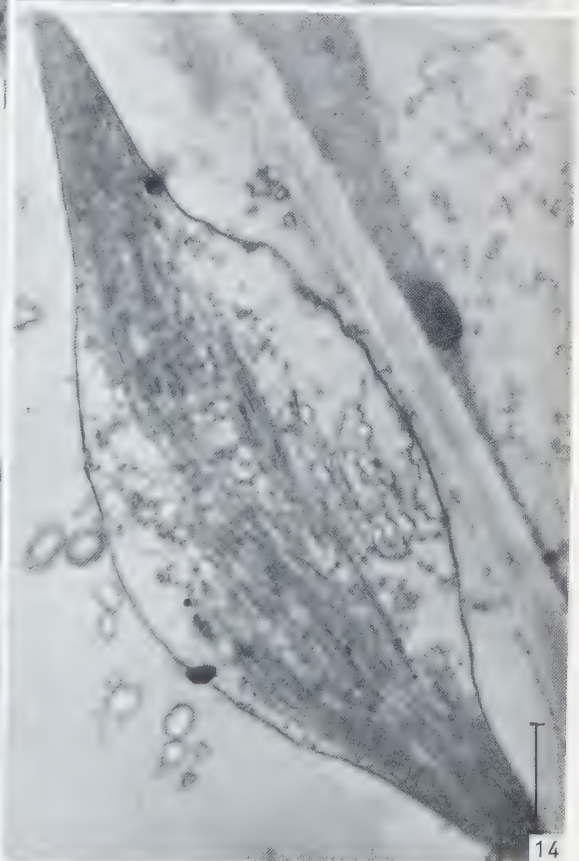
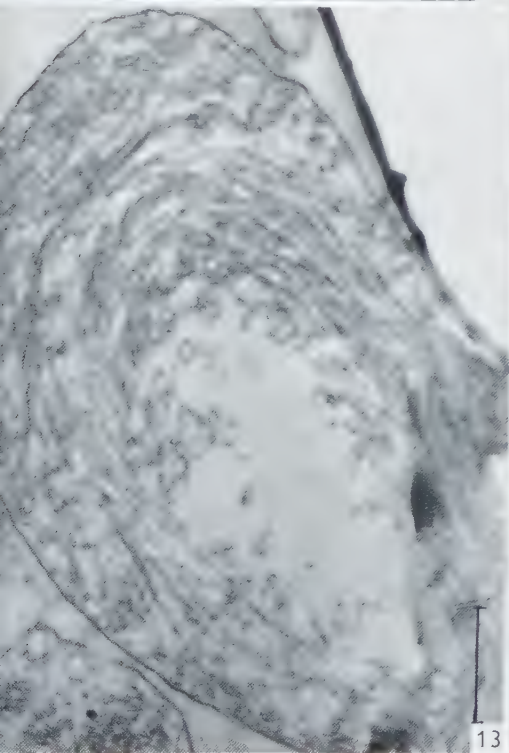
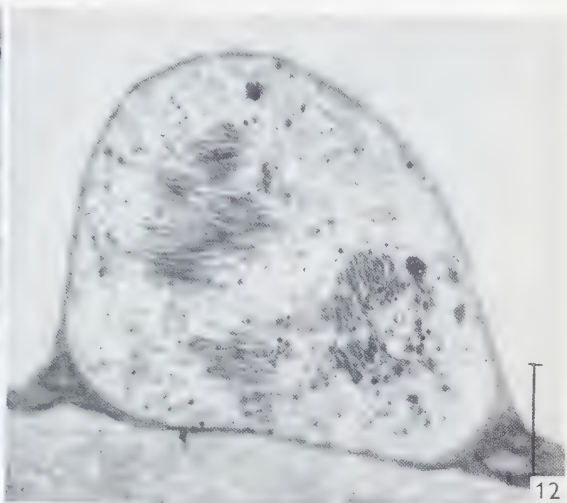
Sections of young green fruits revealed the presence of plastids with a typical chloroplastidic structure, i.e., with lamellated stroma, grana, starch and a few groups

FIG. 11. Detail from Fig. 9. Note the filaments crossing over $\times 36,000$.

FIG. 12. Chromoplast from red fruit. Note the bundles of filaments running in various directions and cut obliquely. $\times 14,000$.

FIG. 13. Oval chromoplast. Filaments arranged in crescent shape. KMnO_4 fixation. $\times 15,000$.

FIG. 14. Spindle-shaped mature chromoplast cut longitudinally. KMnO_4 fixation. $\times 14,000$.



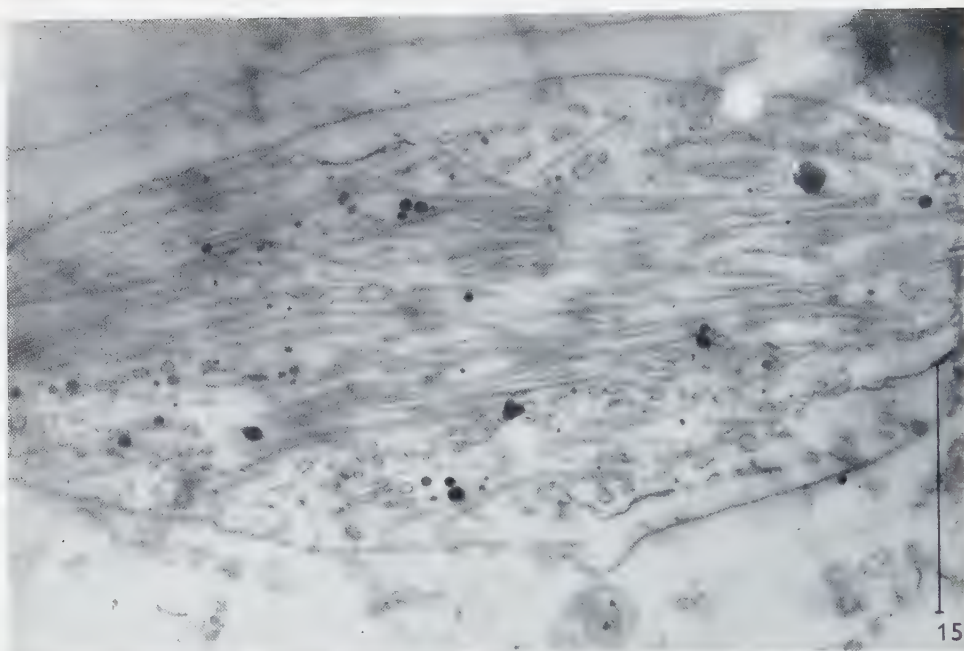


FIG. 15. Longitudinal section through oval chromoplast. Note the denser outer layer of the filaments. (With Siemens Elmiskop I.) $\times 42,000$.

of small osmophilic globuli (Fig. 3). In some cases, the amount of stored starch was very large and displaced the lamellae so that they ran at an angle to one another (Fig. 4). The first noticeable change is a general increase in lability which results in swelling. This is probably the cause of the many swollen plastids encountered in certain preparations next to well-preserved chloroplasts and fully developed chromoplasts. A slight loosening of structures is the first step in the transformation. It reveals the arrangement of the lamellae (Fig. 5) and shows the closed, characteristic bags of the grana discs. The substance inside these discs possesses a great swelling power which causes this unit to be inflated very easily (7). The loosening of attachments is carried further and results in the granum piles being pushed aside. This causes the individual grana to become indistinct. Small, strongly absorbing globuli appear at the edges of the grana discs at the same time (Fig. 6). These droplets form a regular ring around the outside of the granum as observed in a surface view (Fig. 7), while in grana cut longitudinally they appear to lie more or less in a straight row (Fig. 8). (Also compare (24), Figs. 8*a* and *b*.)

However, because of the lateral displacement of the grana, the rows are no longer quite straight. Note that the stroma lamellae persist. These forms give the impression

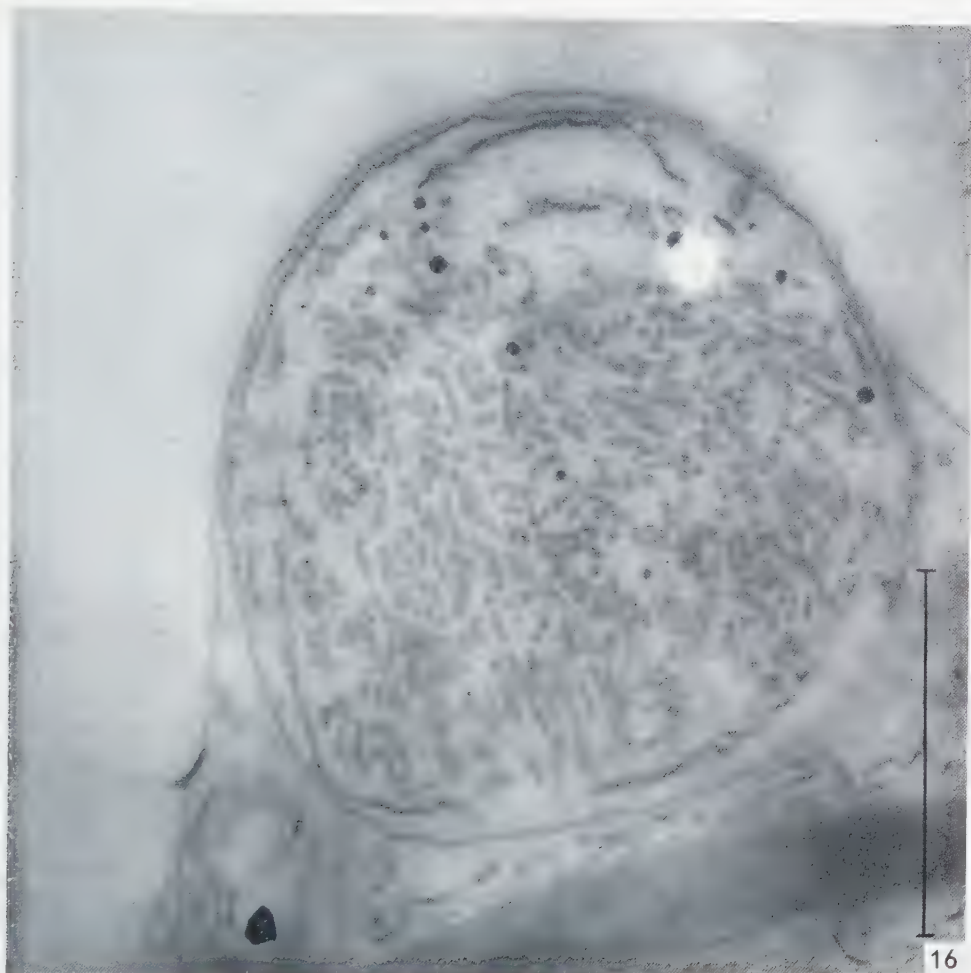


FIG. 16. Transverse section through similar plastid. (With Siemens Elmiskop I.) $\times 58,000$.

that the grana lamellae are capable of splitting into narrow strips, each of a different length depending on its position in the disc. This is followed again by a very unstable stage which is difficult to fix. Fig. 10 shows a section of such a stage. The stroma and grana lamellae are no longer distinguishable from each other and seem to be replaced by long *filaments* whose length exceeds the diameter of the former granum discs. Finally, the intact outer membrane envelops bundles of such filaments and globuli in various arrangements (see Figs. 9, 10 and 12–14). The bundles clearly correspond to the colored spindle bodies as they appear in the light microscope. The

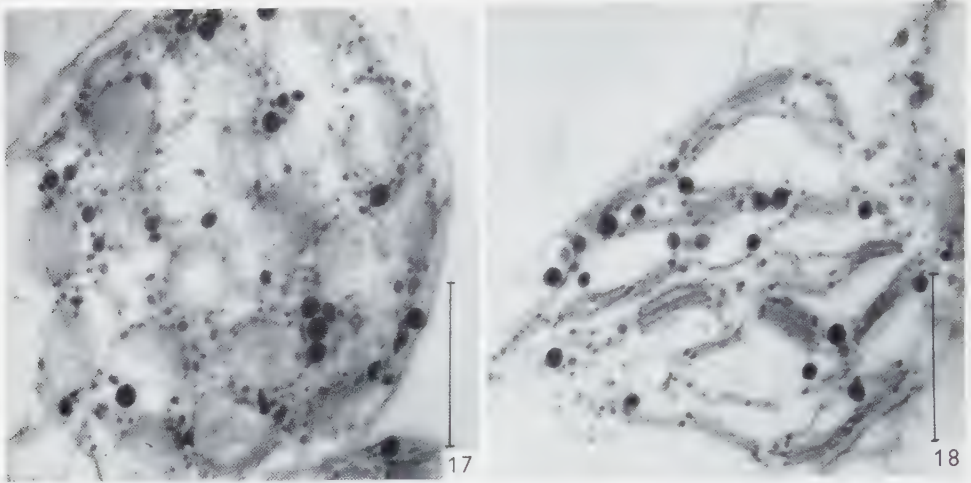


FIG. 17. Yellow chromoplast from petals of *Tropaeolum majus*. Note the falling apart of the grana cut almost parallel to the lamellae into filamentous threads, and the ring of globuli around the edges. $\times 22,000$.

FIG. 18. Same as Fig. 17; cut perpendicularly to the grana lamellae; vertical rows of globuli at the edges of the grana. $\times 22,000$.

striations, therefore, must be caused by these colored filaments which are, individually, of submicroscopic thickness. Their diameter increases during the maturing process.

Fig. 15 shows an enlarged portion of a mature plastid. The higher resolution permits us to distinguish between a denser outer portion, 40–50 Å thick, and an inner portion which is less dense though slightly more so than the stroma background. The thickness of this less dense core varies greatly (between 50–150 Å) as shown in transverse section (Fig. 16). Note the great difference in density between these filaments and the few osmophilic globuli. The large rings, toward the outside, correspond to the vesicles seen in longitudinal section which are probably residues of peristromium material (Figs. 15 and 16 were taken with the Siemens Elmiskop, which gives better resolution but, unfortunately, poorer contrast).

Figs. 17 and 18 show two pictures of chromoplasts from the petals of *Tropaeolum majus*. The development of the chromoplasts seems to be similar at first to that of *Capsicum annuum*, but it never gets beyond the pale yellow stage corresponding to the submicroscopic disorganization of the grana as shown in Figs. 17 and 18.

DISCUSSION

As already observed by Schimper in 1885 (22) and others (15, 23, 24, 26), it appears from the above observations that the elements characteristic of the spindle-shaped

and angular chromoplast type are bundles of the colored filaments, which were described as "protein crystals" by Schimper (22). Zurzycki (26) also suggests that the proteins, not the pigments, are responsible for the remarkable shapes.

Our experiments also confirm the findings that the filaments contain mainly proteins. They are resistant to lipase and lipid solvents, in general, and show no properties characteristic of lipids. Of course, this does not exclude the possibility of built-in lipidic components, but these are probably incorporated in a stable lipoprotein structure.

It has been suggested by Steffen and Walter (24) that the filaments originate from the osmophilic globuli, the dissociation products of intermediate stages. This is unlikely as the density of the filaments in osmium stained preparations is different from that of the globuli, and they are not homogeneous. Nor can it be explained by postulating that it is due to a fixation artifact, namely, that only the peripheral part is stained, preventing the further penetration of the fixative, for in transverse sections globuli of the same diameter are stained throughout. Therefore, the filaments must consist of a different substance. We would like to suggest that the globuli present in Figs. 6, 10, 17 and 18 are the structures so often encountered in many green plastids. In chromoplasts in our material they appear in a significantly greater number only as a result of bad fixation. According to observations of Professor Mühlethaler (verbal communication) their number may even increase under the influence of the electron beam during examination of the preparations in the electron microscope. The globuli probably contain a large proportion of lipids while the protein component predominates in the filaments. For this reason, it is doubtful whether the pigmented filaments have their origin in these globuli. It is difficult to visualize how the completely homogeneous globuli could be drawn out into filaments with a distinctly differentiated outer and inner layer that differ so much in stainability or density from their precursors. There is a possibility that elongated globuli are fixation artifacts. Unfortunately, it is difficult to determine if this is true from the pictures of Steffen and Walter (24) as only small portions of plastids are shown and the state of preservation of other structures cannot be compared. Of course, it may also happen that, during the great stretching which occurs in the maturing process, the globuli are drawn out. But as to the origin of the filaments, it is more likely that their formation is connected with the disintegration of the lamellae.

As far as the composition of the filaments is concerned, it is not necessary to consider the denser contours of these tubular filaments to be a lipid sheath as it has been disclosed (3, 4), in the light of more recent studies on the specificity of OsO_4 toward biological compounds, that neither proteins nor lipids have a significant preference for OsO_4 . Therefore, characterization by their osmophilic behavior is not justified. It is true that conjugated double-bond systems, as they occur in un-

saturated fatty acids and carotenoids, react readily with osmic acid, but so do some functional groups which are often encountered in proteins such as: free $-\text{NH}_2$, $-\text{SH}-$ and $-\text{S}-$, terminal $-\text{OH}$, etc. Thus, the possibility of whether the carotenoids are concentrated in the rind of the filaments remains questionable.

Numerous indications of the existence of such chromoproteins are known, e.g., in chloroplasts. Menke (17), Granick and Porter (12) and Borsdorff (5) have found carotenoids associated with the chlorophyll-protein complex and, therefore, most likely bound to the lamellae. Saperstein and Starr (21) met with polyene pigments in the protein fraction of bacteria, as well. Capsanthin, the chief pigment in *Capsicum annuum*, is found esterified in fruit flesh (14). Most carotenoids, with the possible exception of α - and β -carotene and lycopin, which have no hydroxyl groups, can occur both in the free and in the bound state. These examples demonstrate the possibility of such an association. On the other hand, examples of carotenoids occurring as lipochromes in both plants and animals are not uncommon.

The anisotropic properties of the submicroscopic filaments raise the question of how the pigment molecules are orientated in them. It is known that the major absorption direction of the carotenoid molecules is parallel with their longitudinal axis, i.e., in the direction of the double bonds, which are the oscillating systems responsible for the pronounced optical anisotropy (11). As the filaments are positively birefringent, it is most likely that the polyene molecules run more or less parallel with their length as, otherwise, the positive birefringence would be neutralized by a strong negative one, due to the perpendicularly arranged pigment molecules.

A possible hypothesis explaining the origin of the filaments would be the assumption that the few carotenoid molecules present in a normal granum are arranged on the surfaces or edges of the lamellae and are bound to a relatively small number of available functional groups of the globular proteins forming the grana discs. During chromoplast formation, a larger amount of carotenoids is produced which can be no longer accommodated in the available free groups. Some of them may simply be dissolved in the droplets appearing at the edges of the discs, which are produced during the disruption of the grana and are comparable to the chromoplasts of the globular type (8). A further disintegration of the lamellae into filamentous structures, which would have its cause in the originally linear aggregation of the protein macromolecules of the grana discs, would provide a greatly increased number of functional groups available for pigment coupling. This stage, however, which would be a state of transition between two stable structures, a lamellar and a filamentous one, is extremely labile and can very easily be destroyed through a dissociation of its components. This may be the reason why a clear transition stage could never be observed. The variability of the length of the filaments might be explained by their position in the disc and whether they were originally continuous with a stroma

lamella or not. The increase in thickness during development may be caused by the addition of pigment material.

It is not likely that the pigments or a lipochrome form a simple sheath around the protein filaments, but rather that they are incorporated into a chromoprotein or a chromo-lipoprotein. Recent evidence does not justify the postulation of pure layers of the lipid or protein fractions in protoplasmic structures, but rather the presence of lipoprotein complexes containing various proportions of the two fractions (6, 7).

The carotenoid molecules could exercise a similar stabilizing action on the filaments as chlorophyll does on the granum structure.

While the development of the globuli in yellow chromoplasts can be interpreted as a phenomenon of lipophanerosis (8), such an explanation is impossible for the formation of the bundles of submicroscopic filaments in the chromoplasts under investigation. Here, not only a complete break-down of the ultrastructure of the chloroplast, but at the same time the neo-formation of a new structure is observed. Therefore, some kind of morphogenetic force must be involved. It transforms the material of the disintegrated grana and stroma lamellae into submicroscopic filaments and molds the originally ellipsoidal plastid into a spindle-shaped chromoplast (Fig. 14). Such a metamorphosis requires energy and an organizer. Since starch is present in the plastids at the beginning of the transformation (Figs. 3, 4 and 18), a possible source of energy is available.

As to the presence of an organizer, a comparison with the formation of filiform virus particles may be suggested. The appearance of the filamentous bundles in the chromoplasts has a certain similarity with the microscopic spindles of agglomerated virus threads in the epidermal cells of certain cacti (1, 2). In both cases, the classic cytologists called those bodies "protein spindles". Also the submicroscopic aspect of the chromoplastidic filaments (Fig. 11) recalls the pictures of certain virus infections, although apparently no contamination is necessary for the transformation under consideration. Nevertheless, there might be an analogy concerning the organizer. In virology, it is admitted that nucleic acids catalyze the synthesis of virus proteins. There is some probability that the nucleic acids of the chloroplast assume such a function when its ultrastructure breaks down and they become liberated. Since Ruch and Stäubli (20) prove that all of the detectable nucleic acid is located in the grana (9), the hypothesis advanced could explain why the synthesis of the filaments starts in the place of disappearing grana. Since there are many more disintegrating grana than resulting "protein bundles" (Fig. 12), several such localities must coöperate in the formation of one filamentous bundle.

This activity of the nucleic acids would not be a new manifestation of its function in the plastid because it behaves similarly when the proplastids differentiate into

chloroplasts. There, a nucleic acid containing "prolamellar body" (13, 18), with a lattice structure, synthesizes submicroscopic lamellae which grow out of its surface much in the same way as the filaments grow out of the locality where the grana have disappeared. It is true that, in one case, planary grana discs and, in the other, linear filaments result as final differentiations. But both these formations have a denser rind, which is osmophilic, and an "empty" core.

In concluding this discussion, a comparison with the chromoplasts containing carotenoid crystals or globuli is indicated. The common feature of all three types of chromoplasts seems to be an increased production of carotenoids. This excess crystallizes, dissolves in lipophilic globuli or is incorporated into lipoprotein filaments. Most likely, the globuli are the result of a lipophaneroze. In the third case, there is a transformation into filaments of lipoproteins originally arranged in a lamellar ultrastructure. It is difficult to say whether there is a synthesis of additional lipoproteins, as well, by an afflux of additional metabolites. It may be tentatively inferred, that in the chromoplasts with carotenoid crystals, there is a minimum of transformation in the plastid. In those with globuli, a stage of disintegration becomes stable while in those with filaments, a profound transformation of the available structural plastidic material takes place. Therefore, the three different aspects of the chromoplast seem to be caused by as many different types of metabolisms of the plastids which are quite arbitrarily named by one and the same term, chromoplast.

REFERENCES

1. AMELUNXEN, F., *Protoplasma* **45**, 228 (1955).
2. ——— *ibid.* **49**, 140 (1958).
3. BAHR, G. F., *Exptl. Cell Research* **7**, 457 (1954).
4. ——— *ibid.* **9**, 277 (1955).
5. BORSDORFF, R., Die Lipoproteine der Chloroplasten. Diploma-Thesis. Eidg. Techn. Hochschule, Zürich, 1956, unpublished.
6. FREY-WYSSLING, A., Die submikroskopische Struktur des Cytoplasmas. Protoplasmatologia, Vol. II, A 2. Verlag Springer, Wien, 1955.
7. ——— Macromolecules in Cell Structure. Harvard University Press, Cambridge, Mass., 1957.
8. FREY-WYSSLING, A. and KREUTZER, Emilia, *Planta* **50**, 104 (1958).
9. FREY-WYSSLING, A., RUCH, F. and BERGER, X., *Protoplasma* **45**, 97 (1955).
10. GLAUERT, A. M., ROGERS, G. E. and GLAUERT, R. H., *Nature* **178**, 803 (1956).
11. GOEDHEER, J. C., *Biochim. Biophys. Acta* **16**, 471 (1955).
12. GRANICK, S. and PORTER, K. R., *Am. J. Botany* **34**, 545 (1947).
13. HODGE, A. J., McLEAN, J. D. and MERCER, F. V., *J. Biophys. Biochem. Cytol.* **2**, 597 (1956).
14. KARRER, P. and JUCKER, E., Carotenoids. Elsevier Publ. Co., Amsterdam, 1950.
15. KRAUS, G., *Jahrb. wiss. Botan.* **8**, 136 (1872).

16. LUFT, J. H., *J. Biophys. Biochem. Cytol.* **2**, 799 (1956).
17. MENKE, W., *Naturwissenschaften* **28**, 31 (1940).
18. MÜHLETHALER, K., *Fortschr. Botan.* **19**, 40 (1957).
19. PALADE, G. E., *J. Exptl. Med.* **95**, 285 (1952).
20. RUCH, F. and STÄUBLI, W., in press.
21. SAPERSTEIN, S. and STARR, M. P., *Biochim. Biophys. Acta* **16**, 482 (1955).
22. SCHIMPER, A. F. W., *Jahrb. wiss. Botan.* **16**, 1 (1885).
23. STEFFEN, K. and WALTER, F., *Naturwissenschaften* **42**, 395 (1955).
24. ——— *Planta* **50**, 640 (1958).
25. STRUGGER, S., *Naturwissenschaften* **44**, 543 (1957).
26. ZURZYCKI, J., *Acta Soc. Botan. Polon., Krakau* **23**, 161 (1954).

Studies on the Structure of Bacterial L Forms, Protoplasts and Protoplast-like Bodies

K. G. THORSSON and C. WEIBULL

Central Bacteriological Laboratory of Stockholm City, Stockholm

Received May 22, 1958

Protoplasts of *Bacillus megaterium*, protoplast-like bodies prepared from *Escherichia coli* cells by means of penicillin treatment and a stable L form of *Proteus vulgaris* have been studied electron microscopically. Sectioned specimens were investigated.

Although no cell wall surrounded *B. megaterium* protoplasts, a thin, single membrane could be seen around some of the specimens, closely adhering to the cytoplasmic ground material. This structure probably represents a cytoplasmic membrane.

A double envelope surrounded many of the penicillin-treated *E. coli* cells. Moreover, large vacuoles were frequently present in such cells. The cell wall seemed to expand rather than to break during the conversion of the cells into spherical, protoplast-like bodies.

Morphological elements of varying complexity could be seen in sectioned specimens of the *Proteus* L form. Complex structures consisting of large vesicles enclosing smaller, spherical bodies were sometimes seen and are especially noteworthy. These structures could be interpreted as stages of a complicated life-cycle of the L form.

A granular, cytoplasmic ground material and threads of nuclear material were observed in the protoplasts as well as in the penicillin-treated cells and in many of the L bodies.

The existence of a well-defined, rigid cell wall in most bacteria has been demonstrated by a number of cytological and chemical investigations (16, 35, 57). However, the bacterial L forms, which may arise when normal bacteria (mainly Gram negative species) are subjected to an unfavorable environment, seem to lack a rigid wall. These forms (reviewed by Klieneberger-Nobel (14), Dienes and Weinberger (7), Tulasne (45) and Schellenberg (37)) are highly pleomorphic; they may consist of granular, vesicular and branched structures. The L forms, moreover, are characterized by plasticity and by sensitivity toward osmotic changes in the medium. These facts are most easily explained by assuming that the L forms lack the rigid envelope that normal bacterial cells possess. However, it is likely that L forms differ from normal bacteria in other

respects as well. Thus several workers (7, 37, 45) have described compound structures in L forms consisting of granular elements located inside larger vesicles. Klieneberger-Nobel (14) has reported the fusion of these granules and she suggests that the fusion may represent a sexual reproductive process. Tulasne (45) assumes that the various morphological structures found in cultures of bacterial L forms represent stages of a life cycle; this has, however, been denied by Kellenberger, Liebermeister and Bonifas (13).

Osmotically fragile structures may be obtained from certain Gram positive bacteria by dissolving the wall of living cells with lysozyme at pH 7 (25, 27, 42, 48, 56). It has been established that, at least in the case of *Bacillus megaterium*, this treatment removes the entire cell wall from the cells (21, 34, 42, 43, 47, 49, 52, 55). Provided that the osmotic pressure of the surrounding medium is maintained at a high level by means of suitable solutes the wall-less protoplasts obtained by lysozyme treatment are rather stable structurally. Moreover, they retain most of the physiological and biochemical capabilities of intact cells (21). Under appropriate conditions they may increase in dry weight by several hundred per cent and initiate a division process (20). However, it has yet to be shown that wall-less bacterial protoplasts are able to form colonies and to resynthesize cell walls. In spite of this, striking similarities exist between bacterial protoplasts, prepared by lysozyme treatment, and bacterial L forms.

The cell walls of Gram negative bacteria cannot be degraded to any great extent by lysozyme alone at pH 7. Methods have been devised, however, to produce spherical, osmotically fragile cells of such bacteria by treating the bacteria with lysozyme at pH 9 or 5 (58), by a combined treatment with lysozyme and a chelating agent (19) or by other means (2, 17, 23, 24). One of these methods (17) consists of penicillin treatment of growing cells in a medium of high osmotic pressure. Penicillin treatment has also been widely used for the production of L forms. Thus the osmotically fragile structures described by Lederberg (17) and others can be regarded as more or less identical with the first stages in the conversion process of normal bacterial cells into L forms.

It has been pointed out above that wall-less protoplasts have been prepared from *B. megaterium* cells. It remains to be proven, however, that the osmotically fragile structures that have been obtained from various Gram negative bacteria are also deprived of their walls. As yet, the possibility cannot be excluded that some partly degraded cell wall material surrounds the protoplasm of these bacteria, even when the cells have become osmotically fragile (22, 24, 36, 53). Thus it seems advisable not to use the term protoplast in connection with osmotically fragile cells of Gram negative bacteria, even if these cells have assumed a spherical shape. Therefore, in this study these structures will be referred to as protoplast-like bodies. The term

protoplast should be used only when it has been established that the entire cell wall structure has been removed from the cells (22, 26, 36).

The present study deals with electron microscopical investigations of bacterial L forms, protoplasts and protoplast-like bodies. L forms have been studied repeatedly by electron microscopy (5, 6, 11, 15, 30, 31, 33, 40, 46). To the authors' knowledge no reports of sectioned L bodies have, however, been published. The sectioning technique has been used exclusively in the present study. Some preliminary results from this study have been published elsewhere (41, 52).

MATERIALS AND METHODS

Organisms and growth conditions

Proteus vulgaris. The L form used was obtained from Dr. E. Klieneberger-Nobel, the Lister Institute, London. It was originally produced by penicillin treatment of *Proteus vulgaris*, strain 9, and has not shown any sign of reversion to the bacillary form during its history. It has been designated as strain L9 (15).

Generally, the synthetic, liquid medium described by Abrams (1) was used as the growth medium for both the normal *P. vulgaris* cells and the L form. The bacteria were grown in 250 ml Erlenmeyer flasks, each containing 50 ml of medium. The cultures were incubated at 30°C on a rotary shaker. The speed of the shaker was 100 r.p.m. The L forms were incubated for 24 hours, the normal bacteria for 16 hours. The organisms were then in the stationary growth phase.

In a few experiments the L form was grown in meat broth supplemented with 10% of horse serum. These cultures were incubated for 3–4 days at 37°C without aeration or agitation.

Escherichia coli. The American strain B was used in all experiments. The bacteria were grown in Difco Penassay broth. The growth conditions were the same as those pertaining to *P. vulgaris*, strain 9.

B. megaterium. The strain M (3) was grown in the medium described by Gladstone and Fildes (8). The cultures were incubated for 16 hours at 30°C on the rotary shaker.

Preparation of protoplasts, protoplast-like bodies and "ghosts"

The method of Lederberg (17) was used for the preparation of protoplast-like bodies from *E. coli*.

In order to obtain protoplasts of *B. megaterium* cultures of this bacterium were centrifuged and the cells were resuspended in 0.5 M sucrose containing phosphate buffer (pH 7) at a

FIGS. 1 and 2. Protoplasts of *Bacillus megaterium*, strain M. The protoplasts consist of a granular, cytoplasmic ground substance in which vacuoles, containing threads of nuclear material, are embedded. A thin membrane can be discerned, in part, at the periphery of the protoplasts. $\times 58,000$ (Fig. 1) and $\times 102,000$ (Fig. 2).

FIGS. 3 and 4. "Ghosts" of *B. megaterium* protoplasts. The vesicular "ghosts" contain some granular elements and sometimes (Fig. 4) smaller vesicles inside the limiting membrane of the "ghosts". The small vesicles may be artefacts, due to sectioning of deformed "ghosts". $\times 61,000$.



final concentration of 0.02 *M*. Lysozyme was then added at a final concentration of 0.2 mg/ml. Spherical protoplasts were formed within 15 min. "Ghosts" were prepared by centrifuging the protoplasts and resuspending these bodies in 0.02 phosphate of pH 7. The protoplasts were almost instantaneously converted into transparent "ghosts". The "ghosts" were centrifuged and washed with distilled water by centrifugation at 20,000 *g*.

"Ghosts" of L forms were prepared essentially in the same way as "ghosts" of *B. megaterium* protoplasts. However, distilled water was used instead of phosphate buffer in order to shock the L bodies osmotically.

Electron microscopy

Fixation. In spite of numerous trials with various fixatives, no fixation method was found which consistently stabilized the osmotically fragile forms under investigation satisfactorily, and which simultaneously preserved their fine structure well. Thus protoplasts and L forms sometimes burst even when the osmotic pressure of the medium was maintained at a high level. Most consistent results were obtained when the bacterial material was fixed directly in the growth medium for 2 hours at 37°C with the vapors from a 1% osmium tetroxide solution. Fixation by immersing specimens in buffered osmium tetroxide solution (28) more frequently caused a disintegration of osmotically fragile forms. Provided that the bacterial forms were satisfactorily stabilized by the fixing process the cell structures were preserved equally well by the two fixation methods just mentioned. Figs. 6, 8-10 and 13-16 represent specimens fixed by osmium tetroxide vapors; Figs. 1-5, 7, 11, 12, 17 and 18 show specimens fixed in 1% osmium tetroxide solution.

Protoplasts of *B. megaterium* were markedly stabilized by the addition of magnesium chloride at a final concentration of 0.01 *M* to the surrounding medium (50). Serum albumin at a final concentration of 2% was added to media containing L forms and penicillin-treated bacteria, since Zinder and Arndt (58) reported that osmotically fragile *E. coli* cells are stabilized by such an addition.

Embedding, sectioning and investigation of the sectioned specimens. The fixed bacterial material was dehydrated in alcohol and transferred into a mixture of 9 parts of *n*-butyl and 1 part of methyl methacrylate, containing 0.1% of benzoyl peroxide. Polymerization took place at 60°C (4). The methacrylate blocks were sectioned in a microtome of the Sjöstrand design (39). The sectioned specimens were investigated with an RCA model EMU 2D electron microscope. Pictures were taken at an electron optical magnification of *c.* 20,000 diameters.

RESULTS

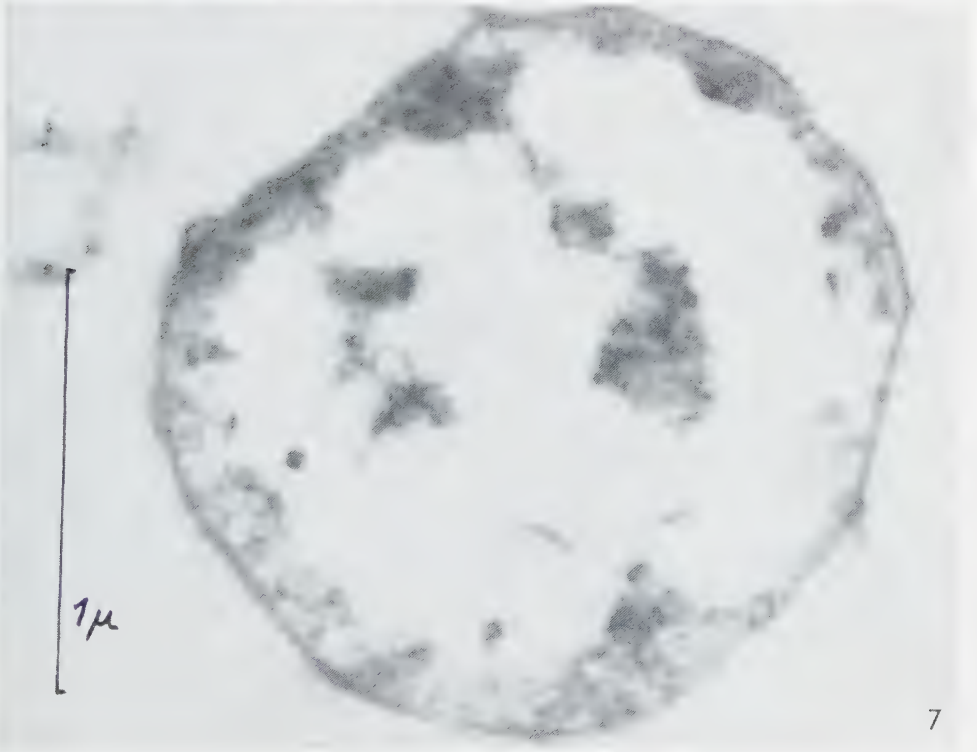
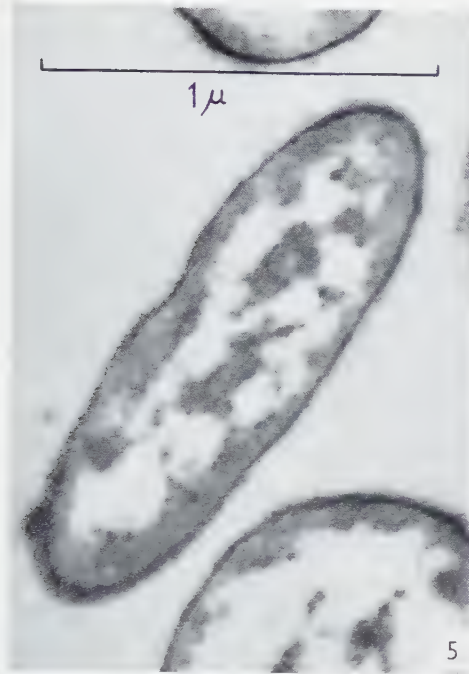
Protoplasts and "ghosts" of B. megaterium, strain M

From pictures published elsewhere (52) it can be concluded that intact cells of *B. megaterium*, strain M, are surrounded by a cell wall, *c.* 250 Å thick in the de-

FIG. 5. Cells of *Escherichia coli*, strain B, before treatment with penicillin. The figure shows the cell wall, the cytoplasmic ground substance and the nuclear equivalents of the bacteria. $\times 51,000$.

FIG. 6. Penicillin-treated *E. coli* cells. The large extra-nuclear vacuoles are noteworthy. At least the upper cell is surrounded by a continuous envelope, probably the expanded cell wall. $\times 41,000$.

FIG. 7. Penicillin-treated *E. coli* cell. The double structure of the cell envelope is shown. $\times 55,000$.



hydrated state. An open space, probably an artefact, was generally observed between the wall and the cytoplasm. Such a cell wall structure was not found in protoplasts prepared by lysozyme treatment of whole cells of this organism. Otherwise the structural organization of intact cells and protoplasts was much the same.

In pictures published in the present report (Figs. 1 and 2) a thin membrane (thickness *c.* 80 Å) can be seen, in part, at the periphery of the protoplasts. This membrane adheres closely to the granular basic material of the cytoplasm. Vacuoles containing threads of nuclear material are found embedded in the cytoplasm.

Bacterial protoplasts are spherical when viewed in the light microscope, even after fixation. Therefore the ellipsoidal shape of the protoplasts shown in Figs. 1 and 2 must be due to deformations during the embedding or sectioning procedures. The same is true for the L bodies shown below in Figs. 12–16.

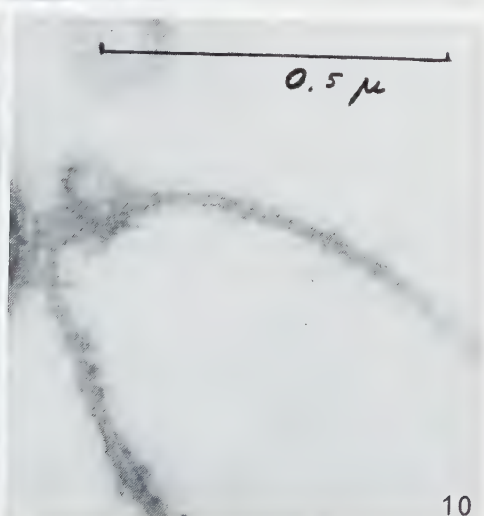
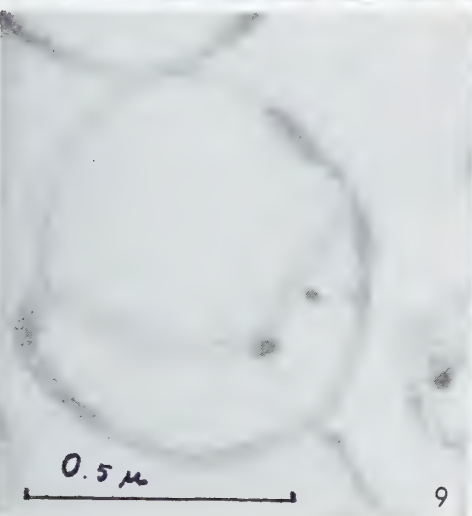
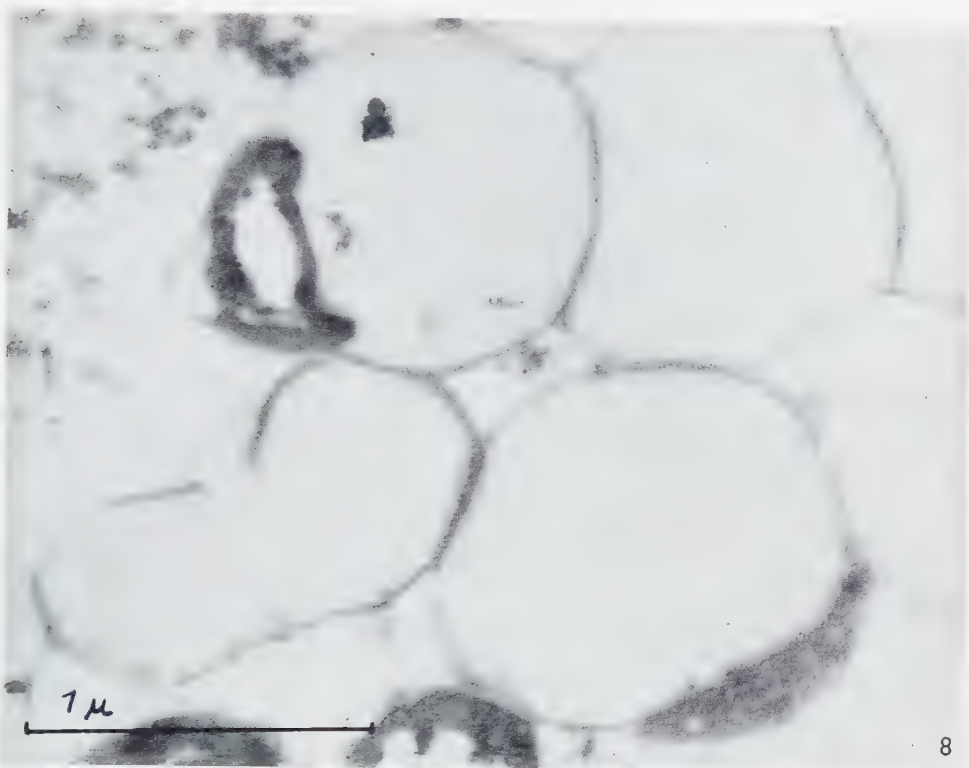
Light microscopic studies have revealed fewer granules in the “ghosts” of *B. megaterium* described in this report than in those previously investigated (52). This may be the result of altered cultural conditions; the medium described by Gladstone and Fildes (8) has replaced the peptone water medium used earlier. The light microscopical observations are borne out by electron microscopy (Figs. 3 and 4). Granular elements are, however, not altogether missing. Moreover, small vesicles are sometimes found inside the “ghost” membranes. These vesicles may, however, represent artefacts due to sectioning of deformed “ghosts”. The “ghost” membranes seem to be *c.* 150 Å thick, but a correct estimation of their thickness is rendered difficult by the somewhat diffuse appearance of the membrane structure.

Protoplast-like bodies obtained from E. coli, strain B

The conversion of *E. coli* cells to spherical, protoplast-like bodies was followed in the phase contrast microscope. Samples for electron microscopy were taken at various intervals from the beginning of the process until most of the transiently formed protoplast-like bodies had been converted into “ghosts”. Fig. 5 shows the appearance of intact bacteria immediately before the addition of penicillin to the culture medium. Since the various stages of the conversion process in no way occurred synchronously in the bacterial population it was not possible to map in detail the sequence of events that followed after the addition of penicillin to the medium. The

FIG. 8. Penicillin-treated *E. coli* cells. Late stage of the conversion process. Crescent-formed protoplasmic structures are seen in some of the degraded cells. Other cells are converted into empty vesicles (“ghosts”). $\times 45,000$.

FIGS. 9 and 10. “Ghosts” of *E. coli* cells, formed by prolonged treatment of the cells with penicillin. At least part of each “ghost” membrane has a double structure. The structure shown in Fig. 9 could be interpreted as a crescent-shaped cytoplasmic membrane located inside the (partly degraded) cell wall. $\times 69,000$ (Fig. 9) and $\times 91,000$ (Fig. 10).



cells, however, either developed vacuoles or underwent an apparent general swelling (Figs. 6 and 7). The cell wall seemed to expand rather than to break under these circumstances (Figs. 6 and 7). During the conversion process the vacuoles of the protoplast-like bodies enlarged continuously (Fig. 8) and finally empty "ghosts" were formed (Figs. 8–10).

In electron micrographs of the "ghosts", a double structure of the cell envelope appears still more clearly than in the protoplast-like bodies (cf. Figs. 7, 9 and 10). Fig. 9 is of especial interest in this respect. The "ghost", shown here, evidently represents a vacuolated protoplasmic crescent inside an outer envelope. This suggests that the inner layer of the double envelope that is seen around part of the "ghost" represents a cytoplasmic membrane, whereas the outer layer is formed by the (partly degraded) cell wall of the original cell.

Nuclear equivalents and a granular cytoplasm are seen in intact cells as well as in penicillin-treated ones (Figs. 5–8).

Bacterial L forms

Sections of normal *P. vulgaris* cells (strain 9) are shown in Fig. 11. The sections reveal structures that are found in most bacteria: a cell wall, a granular cytoplasm and nuclear equivalents. The cell wall has a thickness of *c.* 150 Å.

Sections of the stable L form of *P. vulgaris*, strain 9 (*Proteus* L9), reveal spherical or ellipsoidal bodies of varying sizes. The smallest bodies were most often found free in the medium (Figs. 13 and 14) but sometimes they were observed inside larger structures (Figs. 13–16). These small bodies are generally rather compact. Minute granules can be seen inside them.

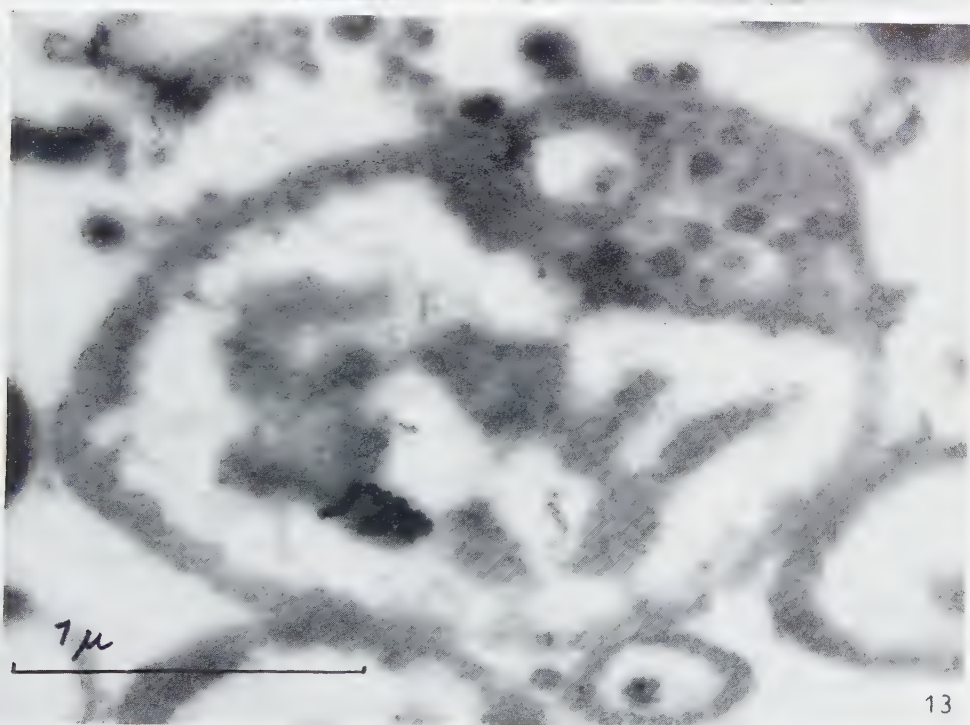
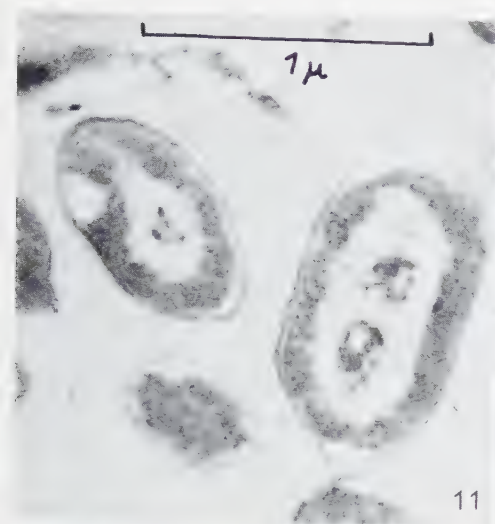
The larger forms (bodies having a diameter of *c.* 0.5 μ or more) show a rather complex organization. In some of them (Figs. 12–14), a granular basic material can be seen, similar to that found in normal bacteria. Moreover, threadlike structures, probably nuclear material, can sometimes be discerned (Figs. 12 and 13). A thin outer membrane (thickness *c.* 80 Å), closely adhering to the cytoplasmic ground material of the L bodies, may also be visible (Fig. 12).

Some large forms contain as an additional substructure the small bodies described

FIG. 11. Normal cells of *Proteus vulgaris*, strain 9. The figure shows the cell wall, the cytoplasmic ground substance and the nuclear equivalents of the bacteria. $\times 37,000$.

FIG. 12. The stable L form of *P. vulgaris*, strain 9. The L form (*Proteus* L9) was grown in meat broth supplemented with 10% horse serum. A thin membrane is discernible around the cytoplasmic ground substance. A thread of nuclear material is seen in the vacuolated region of the L body. $\times 49,000$.

FIG. 13. The L specimens (*Proteus* L9) shown in this and following figures were grown on synthetic medium. Small, compact bodies are seen inside and outside the large, central structure. Threads of nuclear material are seen inside the large structure. $\times 45,000$.



in the preceding section. The small bodies may be found either in a limited area of the large forms (Figs. 13, 14 and 16) or they may be scattered anywhere inside of this structure (Fig. 15). In the latter case the large form looks like a vesicle, containing nothing but the small bodies. In these vesicles an envelope consisting of two layers is observed, each layer having a granular fine structure (Fig. 15).

"Ghosts" of large L forms were seldom completely empty. The smaller forms were very resistant to osmotic shocking but once disintegrated they yielded quite empty "ghosts" (Figs. 17 and 18).

DISCUSSION

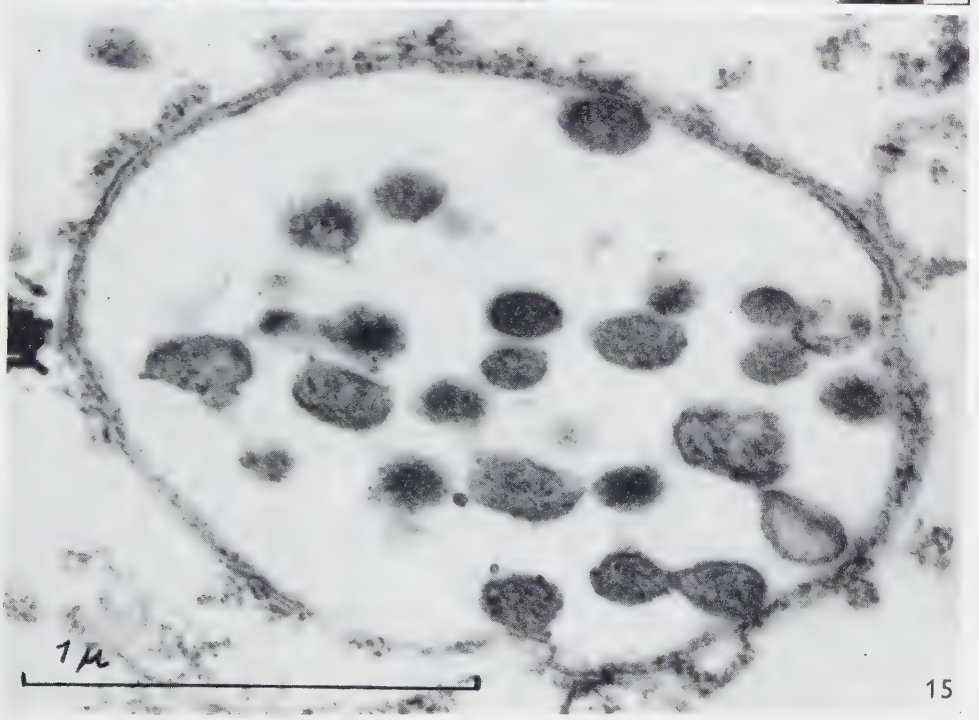
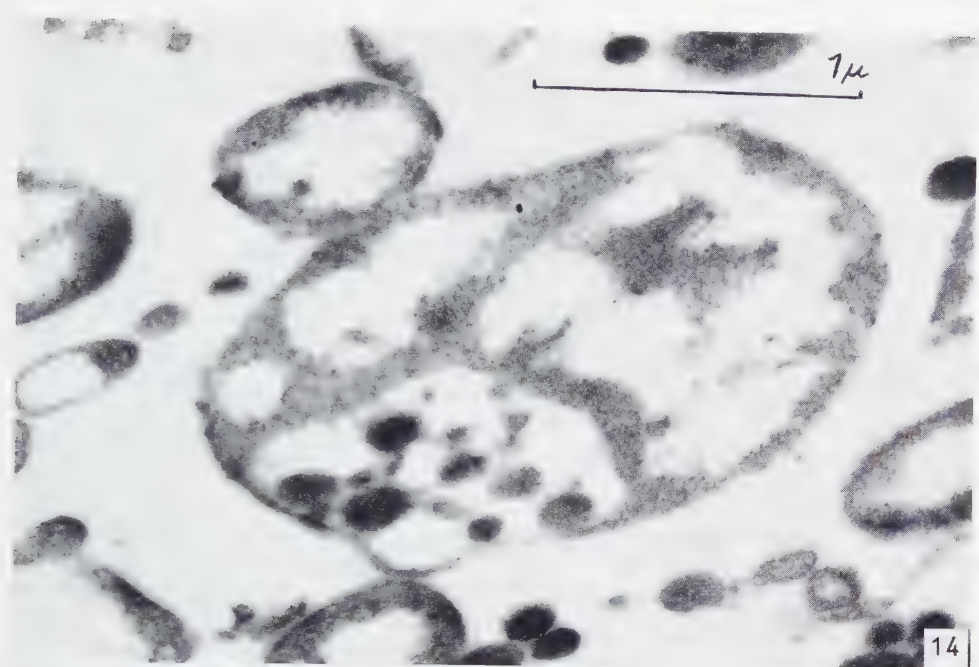
Light microscopical, chemical and immunological observations (21, 34, 42, 43, 47, 49, 55) indicate that the cell wall structure of intact cells of *B. megaterium* is completely missing in protoplasts of this organism. The electron microscopical observations reported by us in a preliminary note (52) confirmed these findings. Furthermore we reported that the outer border of the cytoplasm appeared slightly darker than the rest of it, suggesting the presence of a cytoplasmic membrane. The observations made during the present study confirm this suggestion, showing that a thin membrane surrounds the protoplasts. The fact that this membrane closely adheres to the cytoplasmic ground material makes it highly improbable that it represents remnants of a degraded cell wall, since the cell wall of *B. megaterium* becomes distinctly separated from the interior of the organisms when the fixed specimens are embedded in methacrylate (52).

The "ghosts" that are obtained when protoplasts of *B. megaterium* are shocked osmotically consist of a membrane, which encloses some granular (and perhaps also some vesicular) structures. It was pointed out under *Results* that an estimation of the thickness of the "ghost" membrane could not be made easily because of the somewhat diffuse appearance of this structure. However, the "ghost" membrane seemed to be thicker than the cytoplasmic membrane of the protoplasts. This might imply that small amounts of material from the interior of the cells become adsorbed to the "ghost" membrane when the protoplasts disintegrate.

Light microscopic observations have shown that *E. coli* cells generally swell and lyse after penicillin has been added to the culture medium (17). When a stabilizing agent (e.g. sucrose) is present, lysis is prevented or retarded and the cells are converted into spherical, protoplast-like bodies (9, 17, 18). Vacuoles often arise in these bodies. Lederberg and St. Clair (18) have reported that the protoplast-like bodies are sur-

FIG. 14. *Proteus* L9. Similar structures as those shown in Fig. 13. $\times 43,000$.

FIG. 15. *Proteus* L9. A complex structure consisting of small bodies inside a vesicle. $\times 59,000$.



rounded by a double envelope, judging from light microscopical observations on specimens suspended in India ink.

The light microscopical findings just mentioned are confirmed by our electron microscopical observations. Thus large extra-nuclear vacuoles are seen in most sections of penicillin-treated cells. Furthermore double envelopes surround several protoplast-like bodies. Also "ghost" membranes often have a double structure.

Weidel and Primosigh (53, 54) have reported that the cell wall of *E. coli* cells is composed of two layers. The outer layer is reported to consist of lipoprotein, the inner one of lipopolysaccharide material and a few amino acids. According to Weidel and Primosigh the lipopolysaccharide layer is destroyed by the action of penicillin and bacteriophages. As mentioned previously one of the two membranes found by us around penicillin-treated *E. coli* cells most probably represents a cytoplasmic membrane. The outer membrane might correspond to the lipoprotein layer described by Weidel and Primosigh.

According to some workers (9, 17, 18, 29) penicillin causes an inhibition of cell wall synthesis in sensitive bacteria. Pardee and collaborators (32, 44) are of the opinion, however, that the primary effect of penicillin may instead consist of damage to the osmotic barrier (cytoplasmic membrane) of the susceptible organism. The electron micrographic material studied by us does not favor any of these views. However, the cell wall seems to expand rather than to rupture when the cells are converted into protoplast-like bodies. Trucco and Pardee (44) have drawn the same conclusion from the appearance of isolated walls of penicillin-treated *E. coli* cells.

The multiformity of the L specimens investigated by us suggests that bacterial L forms are distinctly different from the protoplasts and protoplast-like bodies just discussed. The complex L structures that consist of large bodies or vesicles enclosing smaller, spherical elements are of especial interest in this connection. Similar structures have been described by Dienes and Weinberger (7) and Tulasne (45), using the light microscope. Tulasne assumes that they represent a stage of a complicated life cycle characteristic of bacterial L forms. Kellenberger, Liebermeister and Bonifas (13) are of the opinion, however, that the granular elements inside larger L structures represent protoplasmic debris. Our findings hardly favor the latter view. The granules or small bodies shown in Figs. 13-16 are morphologically and structurally well-defined. Whether or not they represent stages in the life-cycle of the L form investigated cannot, however, be ascertained by electron microscopy alone.

Attempts have recently been made to investigate the nature of bacterial L forms by means of chemical analyses (10, 12, 38, 51). It has been found that typical cell wall constituents such as diaminopimelic acid (DAP) and hexosamines are found in smaller amounts in L forms than in normal bacteria. However, the results of the different investigations do not agree completely. Thus Kandler and collaborators (10, 12) did

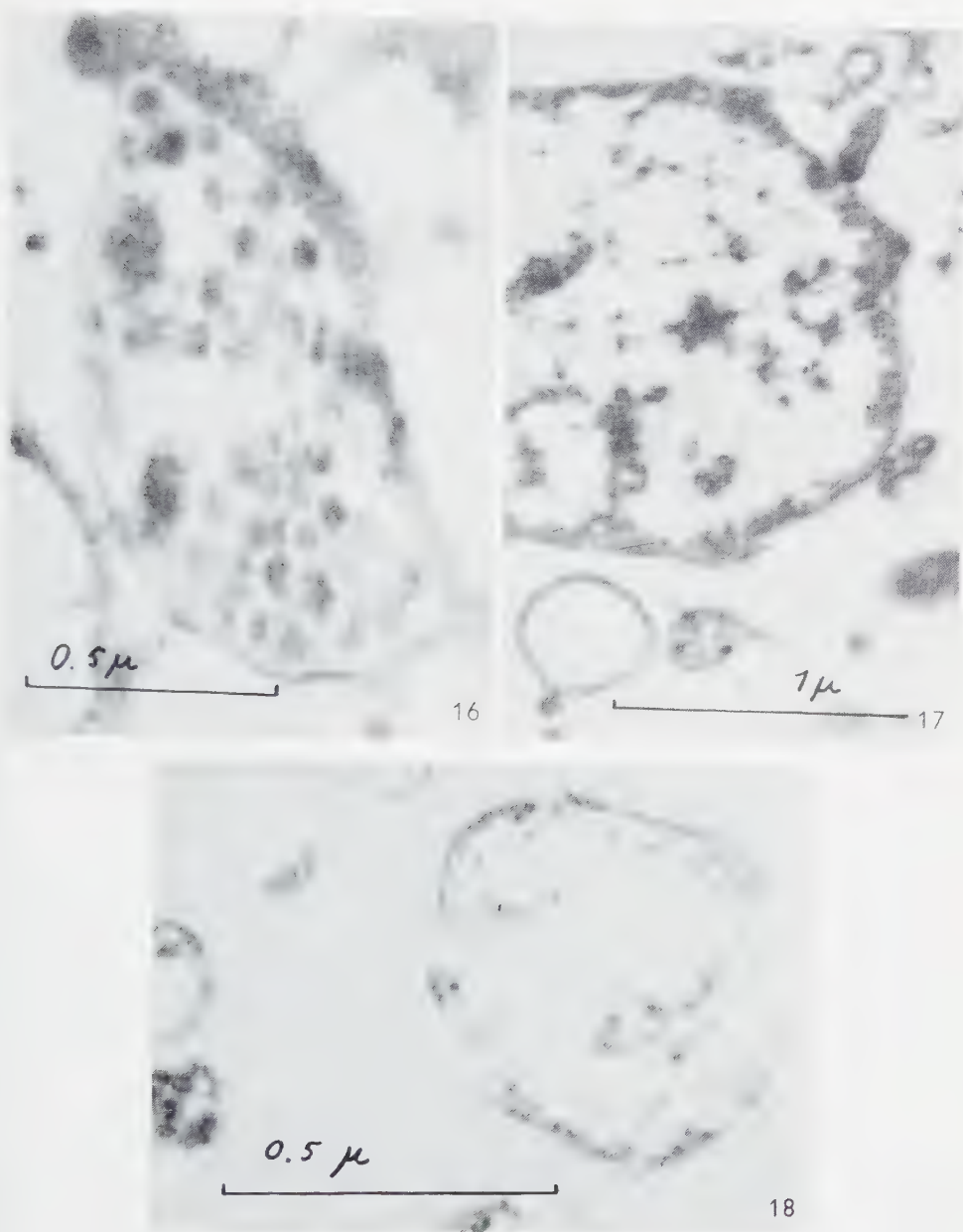


FIG. 16. *Proteus* L9. Similar structures as those shown in Fig. 13. $\times 64,000$.

FIGS. 17 and 18. "Ghosts" of *Proteus* L9. Considerable amounts of material are seen inside most of the "ghost" membranes. $\times 38,000$ (Fig. 17) and $\times 95,000$ (Fig. 18).

not detect any DAP in ten stable L strains of *Proteus vulgaris*, whereas Weibull (51) detected noticeable amounts of this substance in the stable L9 strain of the same bacterium. Perhaps an L form may develop structural elements that contain DAP only under certain conditions. The electron microscopical findings reported here, showing a remarkable inhomogeneity of the L form studied, are not inconsistent with such a view.

ACKNOWLEDGEMENTS

The authors wish to thank Miss A. Laakko and Mrs. C. Hornstrand for skillful technical assistance. Thanks are also due to Dr. E. H. Cota-Robles for the preparation of "ghosts" of the L form studied and for linguistic revision of the manuscript.

This investigation was financially supported by The Swedish Medical Research Council and The Swedish Natural Science Research Council.

REFERENCES

1. ABRAMS, R. Y., *J. Bacteriol.* **70**, 251 (1955).
2. BAUMAN, N. and DAVIS, B. D., *Science* **126**, 170 (1957).
3. BAUMANN-GRACE, J. B. and TOMCSIK, J., *Gen. Microbiol.* **17**, 227 (1957).
4. BORYSKO, E., *J. Biophys. Biochem. Cytol.* **2**, Suppl., 1 (1956).
5. BRINGMANN, G., *Zentr. Bakteriolog. Parasitenk., Abt. I, Orig.* **160**, 507 (1953).
6. DIENES, L., *J. Bacteriol.* **66**, 280 (1953).
7. DIENES, L. and WEINBERGER, H. J., *Bacteriol. Revs.* **15**, 245 (1951).
8. GLADSTONE, G. P. and FILDES, P., *Brit. J. Exptl. Pathol.* **21**, 161 (1940).
9. HAHN, F. E. and CIAK, J., *Science* **125**, 119 (1957).
10. KANDLER, O., HUND, A. and ZEHENDER, C., *Nature* **181**, 572 (1958).
11. KANDLER, G., KANDLER, O. and HUBER, O., *Arch. Mikrobiol.* **21**, 202 (1954).
12. KANDLER, O. and ZEHENDER, C., *Z. Naturforsch.* **12b**, 725 (1957).
13. KELLENBERGER, E., LIEBERMEISTER, K. and BONIFAS, V., *Z. Naturforsch.* **11b**, 206 (1956).
14. KLIENEBERGER-NOBEL, E., *Bacteriol. Revs.* **15**, 77 (1951).
15. — *Zentr. Bakteriolog. Parasitenk., Abt. I, Orig.* **165**, 329 (1956).
16. KNAYSI, G., *Elements of Bacterial Cytology*, 2nd Ed., p. 114. Comstock Publishing Company, Inc., Ithaca, N.Y., 1951.
17. LEDERBERG, J., *Proc. Natl. Acad. Sci. U.S.* **42**, 574 (1956).
18. LEDERBERG, J. and ST. CLAIR, J., *J. Bacteriol.* **75**, 143 (1958).
19. MAHLER, H. R. and FRASER, D., *Biochim. et Biophys. Acta* **22**, 197 (1956).
20. MCQUILLEN, K., *Biochim. et Biophys. Acta* **18**, 458 (1955).
21. — *in* SPOONER, E. T. C. and STOCKER, B. A. D. (Eds.), *Bacterial Anatomy*, p. 127. The University Press, Cambridge, 1956.
22. — *Biochim. et Biophys. Acta* **27**, 410 (1958).
23. MEADOW, P., HOARE, D. S. and WORK, E., *Biochem. J.* **66**, 270 (1957).
24. MITCHELL, P. and MOYLE, J., *Nature* **178**, 993 (1956).
25. — *J. Gen. Microbiol.* **15**, 512 (1956).
26. — *ibid.* **16**, 184 (1957).

27. OPARIN, A. I., GELMAN, N. S. and ZHUKOVA, I. G., *Compt. rend. acad. sci. U.R.S.S.* **105**, 1036 (1955).
28. PALADE, G. E., *J. Exptl. Med.* **95**, 285 (1952).
29. PARK, J. T. and STROMINGER, J. L., *Science* **125**, 99 (1957).
30. PEASE, P., *J. Gen. Microbiol.* **17**, 64 (1957).
31. — *Giorn. microbiol.* **3**, 44 (1957).
32. PRESTIDGE, L. S. and PARDEE, A. B., *J. Bacteriol.* **74**, 48 (1957).
33. RUBIO HUERTOS, M. and DESJARDINS, P. R., *Microbiol. Española* **9**, 375 (1956).
34. SALTON, M. R. J., *J. Gen. Microbiol.* **11**, ix (1954).
35. — *in* SPOONER, E. T. C. and STOCKER, B. A. D. (Eds.), *Bacterial Anatomy*, p. 81. The University Press, Cambridge, 1956.
36. — *Bacteriol. Revs.* **21**, 82 (1957).
37. SCHELLENBERG, H., *Zentr. Bakteriell. Parasitenk., Abt. I, Orig.* **161**, 433 (1954).
38. SHARP, J. T., HUMANS, W. and DIENES, L., *J. Exptl. Med.* **105**, 153 (1957).
39. SJÖSTRAND, F. S., *Experientia* **9**, 114 (1953).
40. SMITH, W. E., MUDD, S. and HILLIER, J., *J. Bacteriol.* **56**, 603 (1948).
41. THORSSON, K. G. and WEIBULL, C., *Nature* **181**, 1348 (1958).
42. TOMCSIK, J. and GUÉX-HOLZER, S., *Schweiz. Z. Pathol. u. Bakteriell.* **15**, 517 (1952).
43. — *Experientia* **10**, 484 (1954).
44. TRUCCO, R. E. and PARDEE, A. B., *J. Biol. Chem.* **230**, 435 (1958).
45. TULASNE, R., *Rend. ist. super. sanità, Suppl.* **I**, 144 (1953).
46. TULASNE, R. and BRINGMANN, G., *Rev. immunol.* **16**, 325 (1952).
47. VENNES, J. W. and GERHARDT, P., *Science* **124**, 535 (1956).
48. WEIBULL, C., *J. Bacteriol.*, **66**, 688 (1953).
49. — *Exptl. Cell Research* **9**, 139 (1955).
50. — *ibid.* **10**, 214 (1956).
51. — *Acta Pathol. Microbiol. Scand.* **42**, 324 (1958).
52. WEIBULL, C. and THORSSON, K. G., *Proc. Stockholm Conference Electron Microscopy*, 1956, p. 266. Almqvist & Wiksell, Stockholm, and Academic Press Inc., New York, 1957.
53. WEIDEL, W. and PRIMOSIGH, J., *Z. Naturforsch.* **12b**, 421 (1957).
54. — *J. Gen. Microbiol.* **18**, 513 (1958).
55. WELSHIMER, H. J., *J. Bacteriol.* **66**, 112 (1953).
56. WIAME, J., STORCK, R. and VANDERWINKEL, E., *Biochim. et Biophys. Acta* **18**, 353 (1955).
57. WORK, E. *Nature* **179**, 841 (1957).
58. ZINDER, N. and ARNDT, W. F., *Proc. Natl. Acad. Sci. U.S.* **42**, 586 (1956).

The Ultrastructure of Unmyelinated Fibers in the Splenic Nerve of the Cat

L.-G. ELFVIN

*Laboratory for Biological Ultrastructure Research, Department of Anatomy,
Karolinska Institutet, Stockholm*

Received May 24, 1958

The unmyelinated fibers in the splenic nerve of the cat are usually enveloped by the Schwann cell plasma membrane. Sometimes they have a small surface in contact with the basement membrane. The axolemma and plasma membrane of the Schwann cell contain an opaque layer with a thickness of about 60 Å. Here and there the membrane is triple-layered and has a total thickness of approximately 75 Å. Between the membranes of the axon and of the cell there is a lighter interspace around 90 Å thick.

The axoplasm contains neurofibrils approximately 60 Å in diameter, long slender mitochondria about 0.1 μ thick and vesicular structures about 450 Å in diameter. Intra-axonal granular structures are present. These granules have a diameter of about 0.28 μ and are of somewhat varying appearance.

The Schwann sheath consists of cells linked in series. The sheath is separated from the connective tissue space by a basement membrane about 450 Å thick.

The nucleus of the Schwann cell is enclosed by a double membrane. There appears to be no specific nucleolar structure.

The ground cytoplasm exhibits no structures specific for the Schwann cell. No equivalents of the Golgi apparatus were observed.

Mitochondria about 0.18 μ thick and of varying length are relatively sparse in the cell. The outer and inner membranes are triple-layered and show the conventional arrangement.

The cytoplasm contains granular structures varying in diameter between 0.2 and 1.1 μ .

In recent years the unmyelinated nerve fibers have been the subject of numerous electron microscopic studies. Both the internal structure of the axon and the relation between the axon and Schwann sheath have been analyzed on an ultrastructural level.

Fernández-Morán (15) described fibrillar structures in isolated unmyelinated nerve fibers from spinal cord of frog and rat. The fibrils had a diameter of approxi-

mately 100 Å, and he regarded them as being neurofibrils. The plasma membrane of the nerve fiber had a thickness of 60–100 Å.

Gasser's investigations (16, 17) on dorsal root fibers from cat have served to elucidate the morphologic relationship between the axons and Schwann cell. He demonstrated that the axons, two or more, are insheathed in the plasma membrane of the cell. In this way the nerve fibers have a mesaxon formed by the membrane of the Schwann cell. In the axons are neurofibrils, mitochondria and vesicular structures. Gasser referred to the vesicular structures as the endoplasmic reticulum. The Schwann cell contains, mainly around the nucleus, mitochondria and structures belonging to the endoplasmic reticulum.

In the olfactory nerve, Gasser (18) found the same relationship, in principle, between the axons and the Schwann cell, though in that nerve each plasma membrane sheath contained a number of axons.

Hess (20) made similar observations in unmyelinated fibers from the autonomic nervous system. Each axon runs in a pocket in the Schwann cell plasma membrane. The nucleus of this cell is enclosed by a double membrane.

Robertson (37) recently reported that the opaque lamella in the plasma membrane of the axons and Schwann cells of unmyelinated nerve fibers had three layers. According to him the lamella, with a thickness of about 75 Å, consists of two opaque layers, each 25 Å thick, separated by a less osmiophilic interspace also about 25 Å thick. His material, derived from sciatic nerves of frogs, was fixed in potassium permanganate.

The aim of the present investigation was to analyze the ultrastructure of the unmyelinated sympathetic nerve fibers. It seemed important from the functional standpoint to elucidate the morphology of these fibers since, among other things, they form a part of the peripheral nervous system which is of special interest by virtue of its specific transmission behavior.

Unmyelinated fibers of the splenic nerve were chosen for this investigation because there is conclusive evidence that the majority of them belong to the sympathetic nervous system. This finding is based on both light microscopic and physiologic criteria (1, 33, 45).

MATERIAL AND METHODS

The splenic nerves used in this investigation were taken from cats. Animals weighing between 2 and 3 kg were anesthetized with nembutal intraperitoneally in a dose of 30–50 mg per kg body weight. The splenic nerves, accompanying the large vessels to the spleen, were dissected free as carefully as possible. Small pieces, 1–3 mm long, were cut from the nerve and immediately placed in the fixing solution, i.e., 1% osmium tetroxide solution isotonic with blood and buffered to pH 7.2–7.4. The temperature of the fixation fluid was about 2° to 5°C.

| | |
|--|-----------|
| Fixation time | 2 hours |
| Rinsing in Tyrode's solution | 1 hour |
| Dehydration | |
| 70 % ethyl alcohol | Overnight |
| 95 % ethyl alcohol | 1 hour |
| absolute alcohol | 2-3 hours |

Embedding was done in a mixture of *n*-butyl and methyl methacrylate *ad modum* Newman, Borysko and Swerdlow (27).

Sections were cut with glass knives on a Sjöstrand ultramicrotome (39). They were floated on a 20% ethyl alcohol solution and transferred to specimen grids covered with a thin formvar film. The methacrylate was not removed prior to examination of the slices in the electron microscope. The microscope, RCA EMU-2C, had a standard compensated objective pole piece having an objective aperture of 50 μ , with three apertures in the projector lens and a reduced condensor lens aperture.

The measured values of the dimensions of various structures as detailed in Tables I, II and III were subjected to analysis of variance. For the plasma membrane, the analysis disclosed a significant difference between animals, but for the other structures there were no significant differences between animals.

RESULTS

The unmyelinated fibers of the splenic nerve are insheathed in the Schwann cell plasma membrane similarly to those of the dorsal root fibers as described by Gasser (17). Each Schwann cell contains more than one nerve fiber (Figs. 1-3). Usually, the total varies between 5 and 15 per cell, though both greater and smaller numbers have been found. Most of the axons have a well developed mesaxon that is formed by the plasma membrane of the Schwann cell (Figs. 1*b*, 4 and 13).

Each Schwann cell, including the axons lying within it, is separated from the endoneurial connective tissue space by a basement membrane. The predominant structures in this space are collagen fibers with irregular courses. Occasional connective tissue cells are observed also.

The splenic nerve contains a few, single myelinated nerve fibers which exhibited, in this study, no specific components or otherwise noteworthy features.

The unmyelinated nerve fibers

The diameter of the nerve fibers varies between 0.3 and 1.3 μ but most of them are less than 1 μ .

The axon is bounded by a continuous plasma membrane in which an opaque layer about 60 Å thick is discernible. Where the axon adjoins the Schwann cell, this opaque layer is separated from one of equal thickness, belonging to the plasma membrane of the Schwann cell, by a less osmiphilic space approximately 90 Å in thickness (Table I).

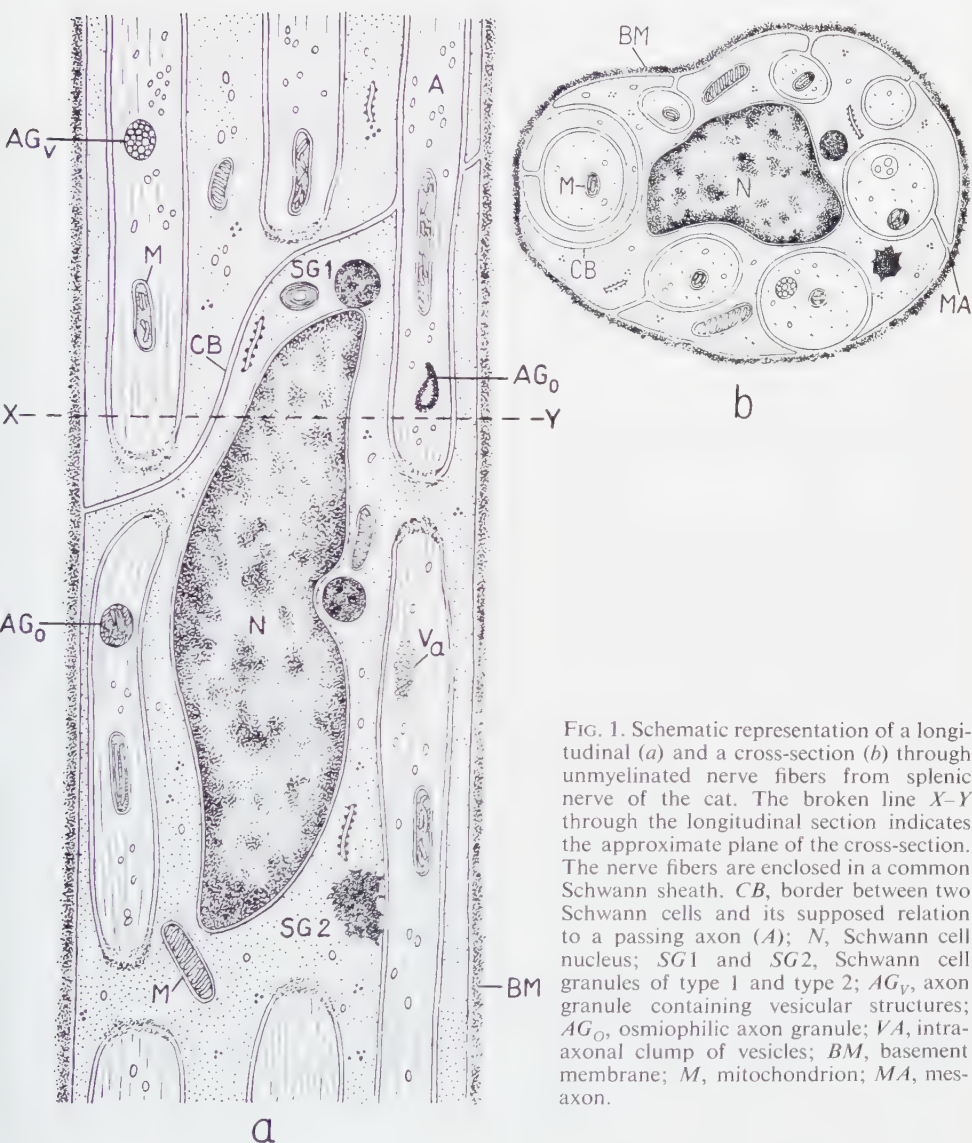


FIG. 1. Schematic representation of a longitudinal (a) and a cross-section (b) through unmyelinated nerve fibers from splenic nerve of the cat. The broken line X-Y through the longitudinal section indicates the approximate plane of the cross-section. The nerve fibers are enclosed in a common Schwann sheath. CB, border between two Schwann cells and its supposed relation to a passing axon (A); N, Schwann cell nucleus; SG1 and SG2, Schwann cell granules of type 1 and type 2; AG_v, axon granule containing vesicular structures; AG_o, osmiophilic axon granule; VA, intra-axonal clump of vesicles; BM, basement membrane; M, mitochondrion; MA, mesaxon.

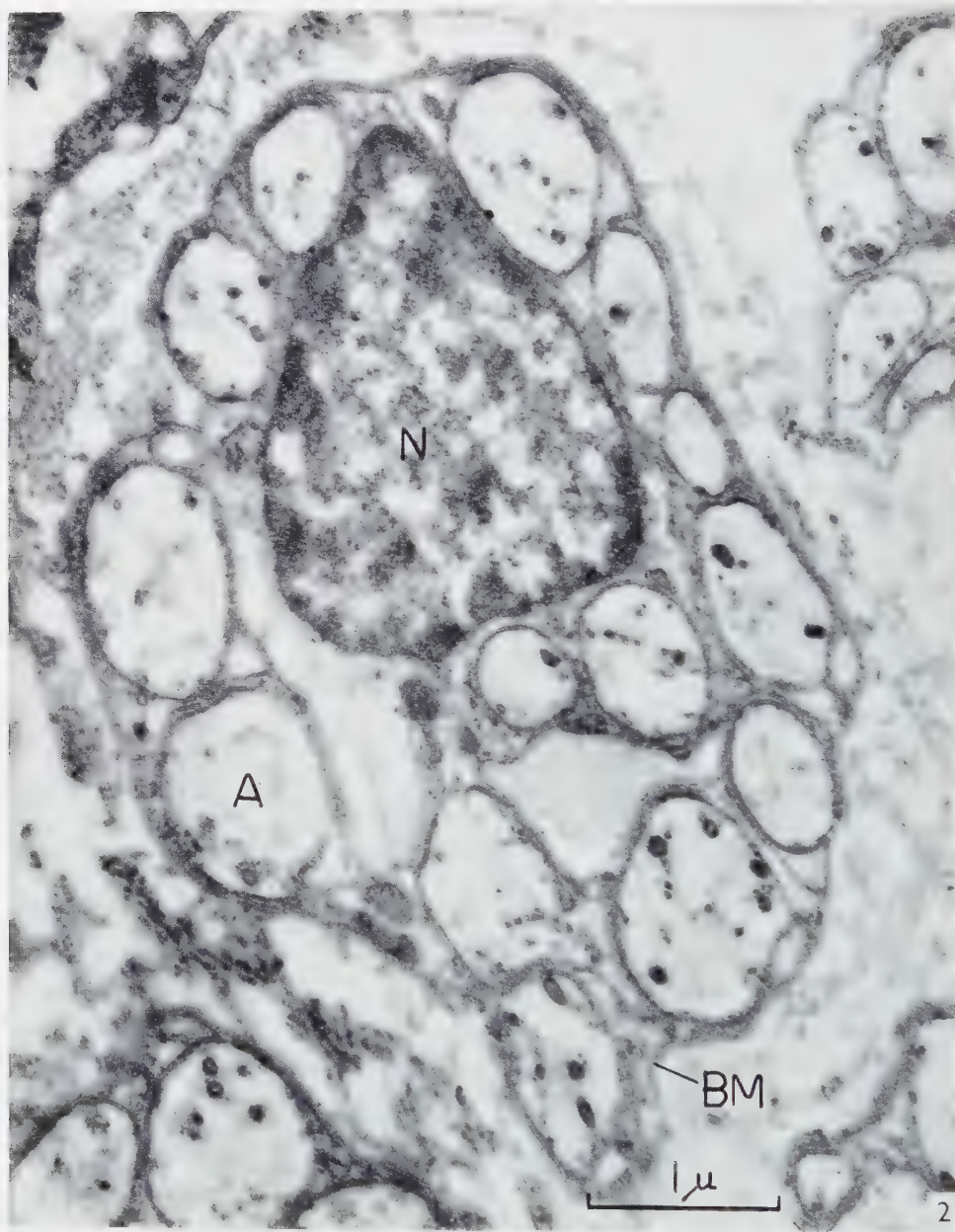


FIG. 2. Electron micrograph showing a cross-section through unmyelinated fibers from splenic nerve of the cat. The central nerve fibers are enclosed in the same Schwann cell, which is separated from the connective tissue space by a basement membrane (BM). A, unmyelinated axon; N, Schwann cell nucleus. In the axons are mitochondria and vesicular structures. $\times 25,000$.

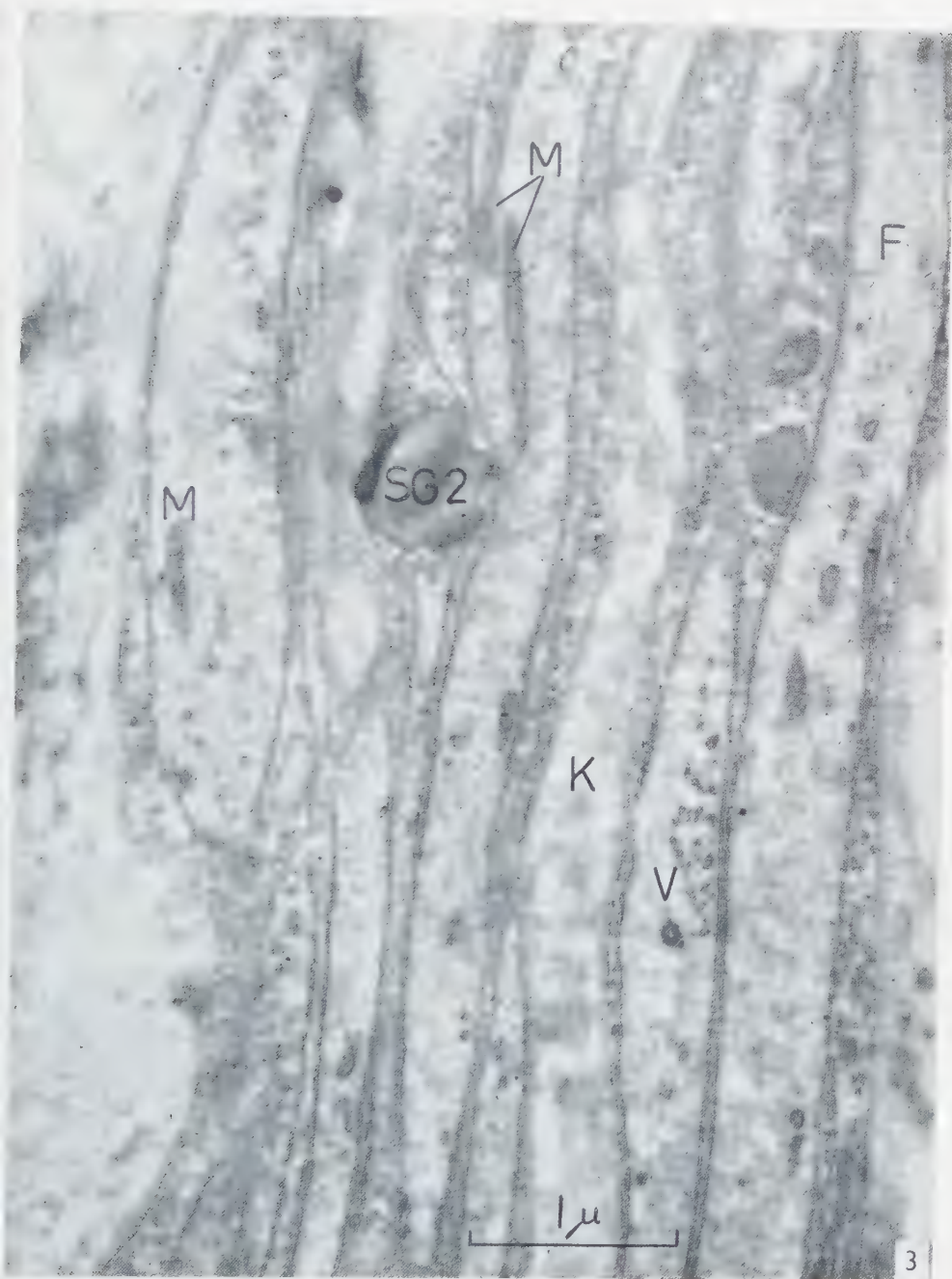


FIG. 3. Longitudinal section through unmyelinated nerve fibers located in two separate Schwann sheaths. The nerve fiber bundles are separated by connective tissue, largely consisting of collagen (*K*). In the axons are mitochondria (*M*), vesicular structures (*V*) and neurofibrils (*F*). *SG2*, Schwann cell granule, type 2. $\times 28,000$.

TABLE I

DIMENSIONS OF THE PLASMA MEMBRANES SEPARATING THE AXON FROM THE SCHWANN CELL
Ten measurements recorded for each nerve fiber.

| Animal No. | Number of nerve fibers | Mean thickness of the opaque layer in A | Mean thickness of the light space between opaque layers in A |
|------------|------------------------|---|--|
| 1 | 10 | 50 | 83 |
| 2 | 3 | 47 | 73 |
| 3 | 5 | 54 | 89 |
| 4 | 3 | 60 | 113 |
| 5 | 5 | 62 | 111 |

Here and there, the opaque layer of the plasma membrane is composed of three lamellae (Fig. 4). In these zones it is divided into two opaque lamellae, about 25 Å thick, separated by a less dense layer of similar thickness. The opaque layer accordingly has, in these areas, a total thickness of around 75 Å.

This stratification of the membrane may be found, it would appear, at any point along the axon. If it is to be detectable on the electron micrograph, the section must be virtually perpendicular to the membrane.

The cytoplasm of the axons includes clearly differentiated cell organelles. There are neurofibrils, mitochondria and vesicular structures. This finding is consistent with earlier investigations. In the present study, moreover, it was possible to analyze granular elements with a specific ultrastructure.

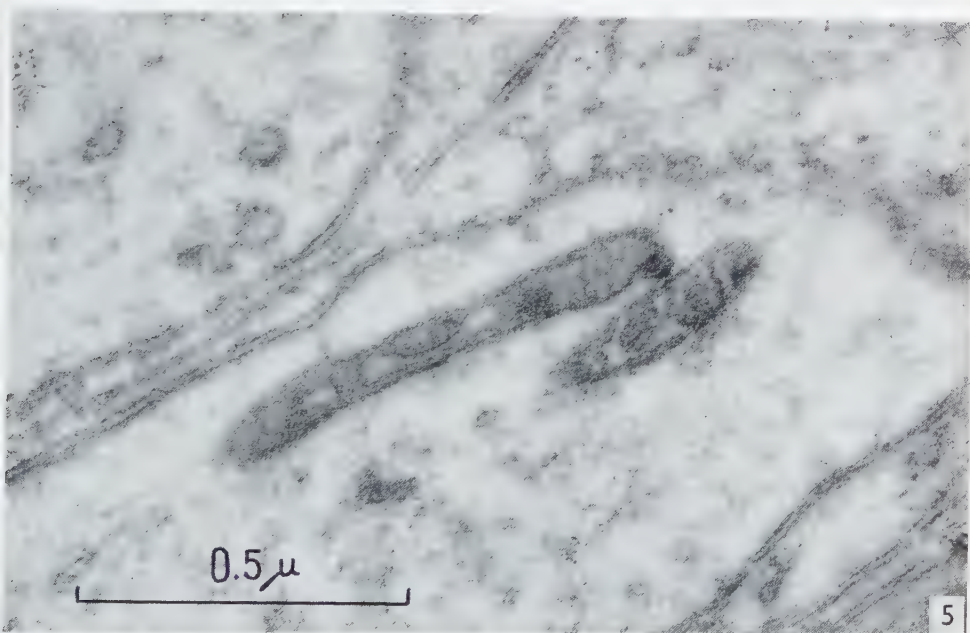
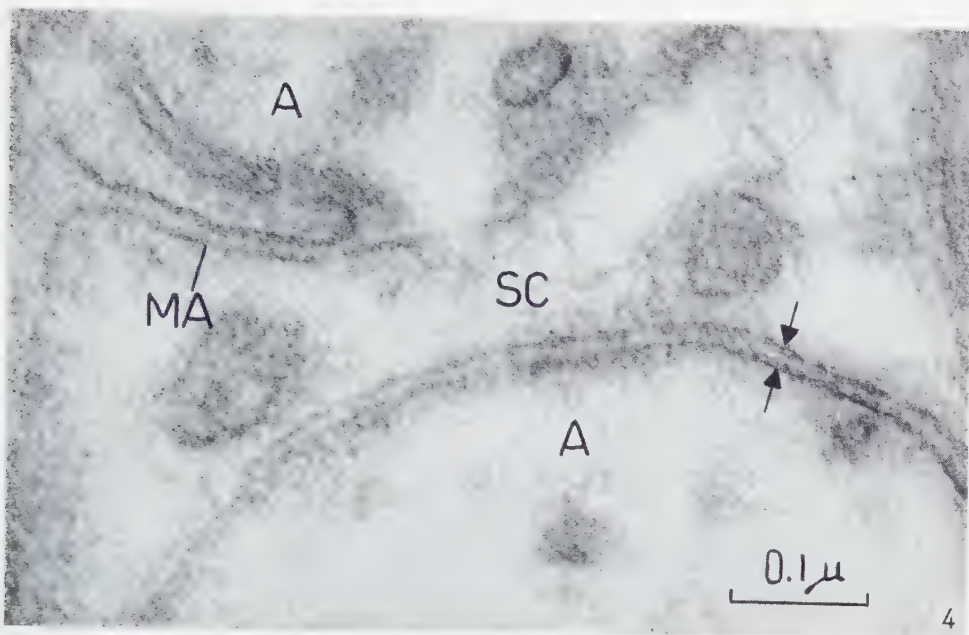
The diameter of the *neurofibrils* measured about 60 Å (Table II); their length naturally could not be estimated with this method. However, the neurofibrils appear to run independently, like those described in myelinated nerve fibers.

Long *mitochondria*, with the shape of sausages, are common throughout the axoplasm (Figs. 5 and 17). Their long axes are usually parallel with those of the nerve fibers. Here, too, it was impossible to determine their length, though in some longitudinal sections a length of about 1 μ was measured. The width is constant at around 0.10 μ (Table II).

The mitochondria are bounded by a triple-layered membrane, like those in other tissues. This membrane has a thickness of about 140 Å, the opaque layers being approximately 40 Å and the lighter intermediate layer about 60 Å thick (Fig. 17).

FIG. 4. Cross-section through parts of two axons (A) localized in the same Schwann cell (SC). At the arrows, the opaque layers of the plasma membranes are seen to be triple. MA, mesaxon of the upper axon. $\times 181,000$.

FIG. 5. Oblique section through two mitochondria situated in the same axon. The interior of the mitochondria is divided by the inner membranes into lighter and denser areas. The outer membranes are indistinct. $\times 87,000$.



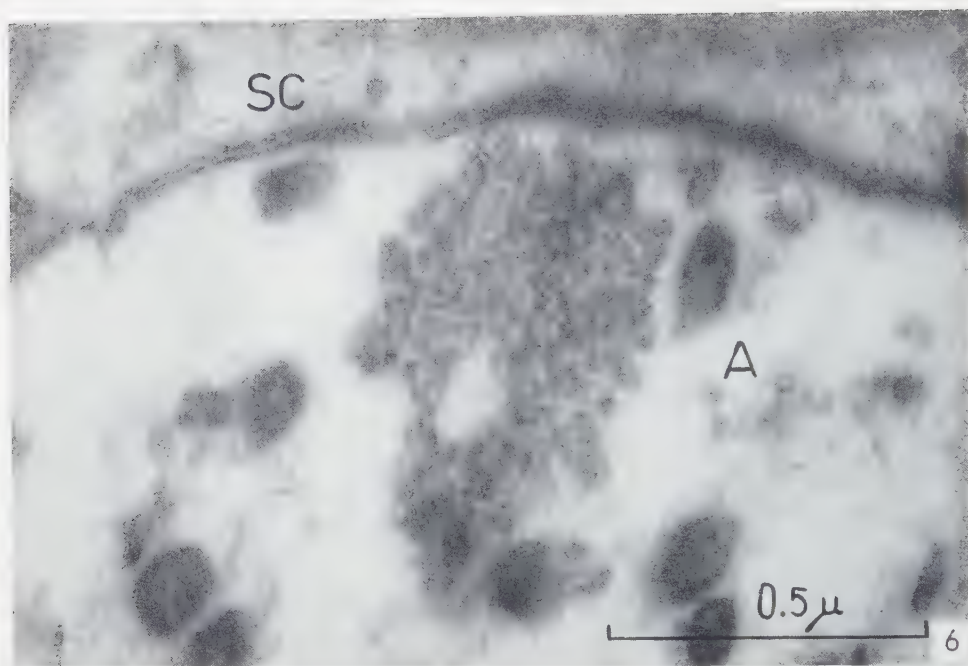


FIG. 6. Intra-axonal aggregation of vesicular structures. The clump is in close proximity to the cell membrane. A, axon; SC, Schwann cell. $\times 83,000$.

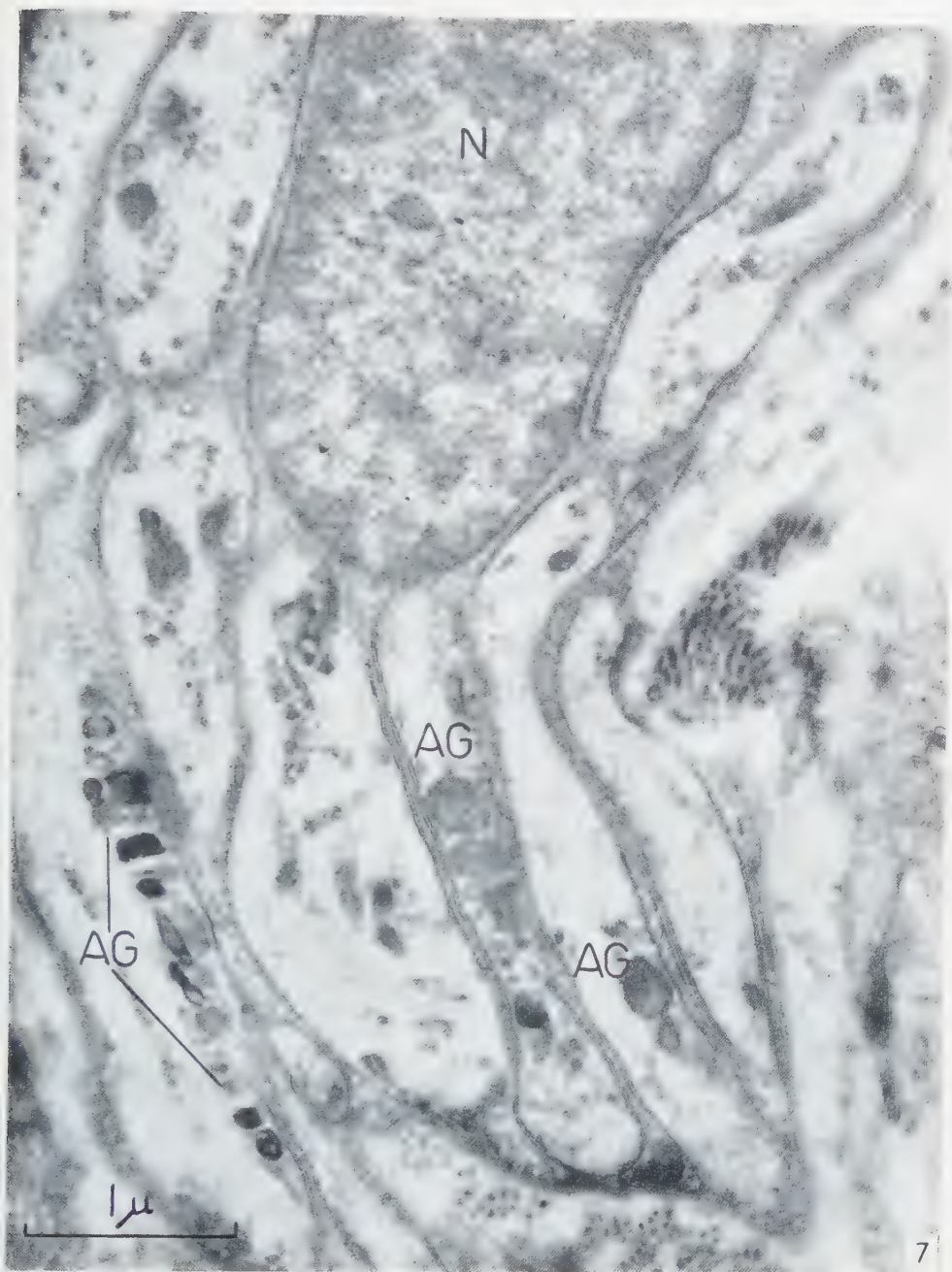
The interior of the mitochondrion consists of zones characterized by their opacity and separated from less dense areas by inner membranes. The course of the inner membranes is irregular, though, in general, it is parallel with the long axis of the mitochondrion. The membrane thickness is approximately 40 Å.

Frequently, the inner membranes are disposed in pairs, and thus form opaque double membranes separated by a lighter interspace which is sometimes quite broad. In the latter case, the distance between the midlines of the two membranes may amount to as much as 300 Å (Fig. 5).

The mitochondria, in general, are strongly osmiophilic with the exception of the aforementioned interspace, and the inner membranes are often difficult to differentiate.

The *vesicular structures* are common in the unmyelinated nerve fibers studied here. They may occur in any part of the axoplasm, usually either singly or in small groups.

FIG. 7. Oblique section through a number of axons located in the same Schwann cell. Some of the axons contain numerous granules (AG). Intra-axonal mitochondria and vesicular structures are also discernible. N, Schwann cell nucleus. $\times 28,000$.



The single vesicles are circular or oval in shape and have a mean diameter of around 450 Å (Table II), though diameters of up to about 800 Å are found. The central portion is generally homogeneous and only slightly osmiophilic. The peripheral zone consists of osmiophilic material arranged in a layer approximately 60 Å thick (Table II). Some vesicles contain small opaque particles about 85 Å in diameter.

More rarely, there are dense aggregations of vesicles, often situated quite close to the plasma membrane. Such vesicles generally have a diameter of about 200–400 Å (Fig. 6).

In places, the axoplasm contains *granular* elements, termed axon granules. They vary in appearance but are of roughly uniform size, usually circular or oval, and have diameters of approximately 0.28 μ (Table II). Sometimes these granules are

TABLE II
DIMENSIONS OF THE INTRA-AXONAL STRUCTURES
Measurements made on five animals.

| Structure | Number of nerve fibers | Number of measurements | Mean width (\pm S.E.) |
|--------------|---------------------------|---------------------------|-----------------------------|
| Neurofibrils | 12 | 120 | 60 ± 2 Å |
| Mitochondria | 19 | 95 | 0.101 ± 0.004 μ |
| Granules | 35 | 84 | 0.28 ± 0.02 μ |
| Vesicles | | | |
| (a) diameter | 12 | 120 | 442 ± 22 Å |
| (b) membrane | 11 | 110 | 61 ± 3 Å |

found in clumps occupying a large part of the nerve fiber (Fig. 7), but in the main they are isolated and have an apparently irregular distribution. It was possible, on the basis of the morphologic picture, to differentiate three main types of axon granules: those containing vesicular structures, and two types of granules being more osmiophilic. The latter have been classified as type 1 and type 2.

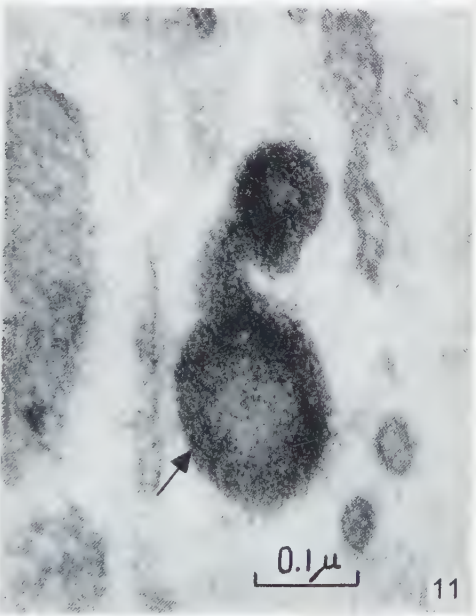
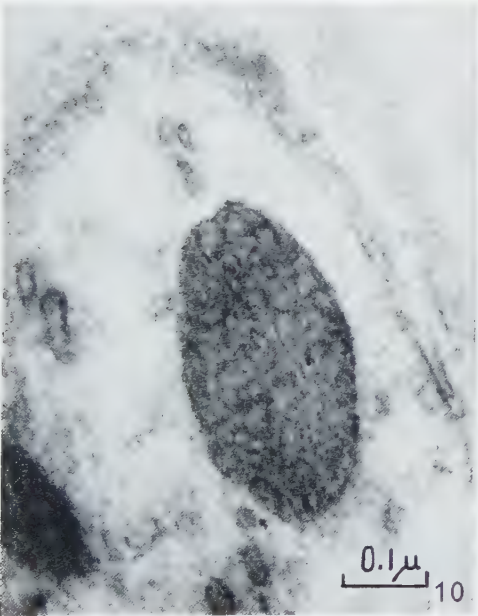
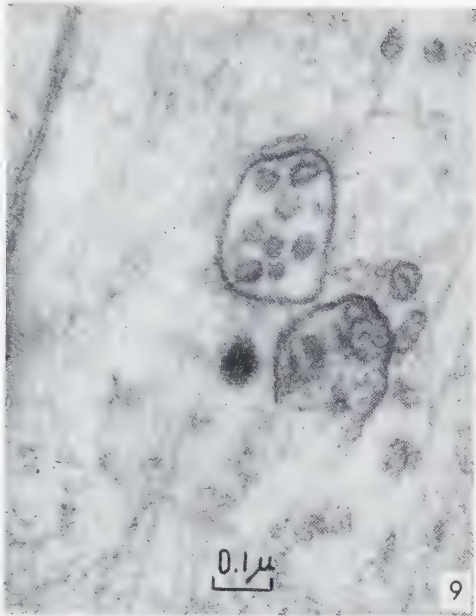
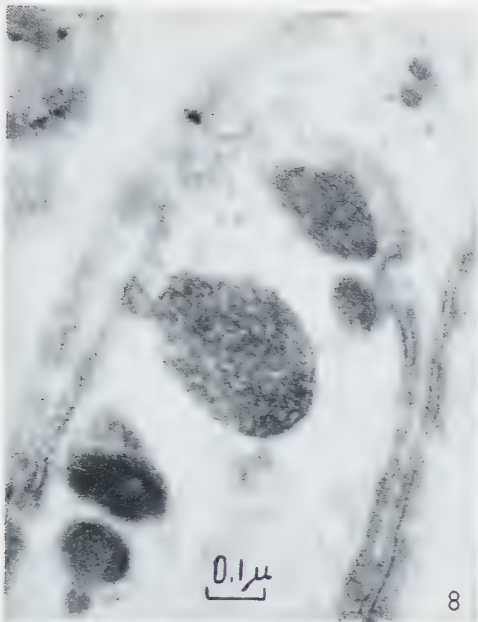
The *vesiculated axon granule* is the most common form. It is oval, sac-like and more or less filled with vesicular structures. It is bounded by a membrane which

FIG. 8. Vesiculated axon granule completely filled with vesicular structures and separated from the surrounding axoplasm by a distinct osmiophilic layer. $\times 75,000$.

FIG. 9. Two vesiculated axon granules, one of which is only partly filled by the vesicular structures. $\times 75,000$.

FIG. 10. Osmiophilic axon granule, type 1. The osmiophilic material inside the granular structure is clearly stratified and thus gives rise to lighter and denser areas. In places, the osmiophilic layers form circular structures. $\times 106,000$.

FIG. 11. Osmiophilic axon granule, type 2. The osmiophilia is not so pronounced centrally as at the periphery. The arrow indicates an area in which the osmiophilic material shows slight signs of stratification $\times 134,000$.



varies in thickness from 60 to 100 Å. The vesicles are approximately 400 Å in diameter: their periphery is more osmiophilic than their central portion and has a thickness of around 60 Å (Figs. 8 and 9).

The *osmiophilic type 1* axon granule is similar in shape to that described above. It is enveloped by an outer membrane, about 60 Å thick, and has a heterogeneous internal structure. The osmiophilic material is generally arranged in layers, about 70 Å thick, and the opaque layers are separated by less dense zones approximately 100 Å in thickness. Sometimes the layers have a circular arrangement (Fig. 10).

The third and less common form of axon granule is the *osmiophilic type 2*. Morphologically it is less differentiated. It is frequently elongated and semilunar, and has a very dense inner structure. Sometimes, however, there is a central part characterized by weaker osmiophilia. A tendency to stratification of the osmiophilic material is occasionally discernible (Fig. 11).

The Schwann cell

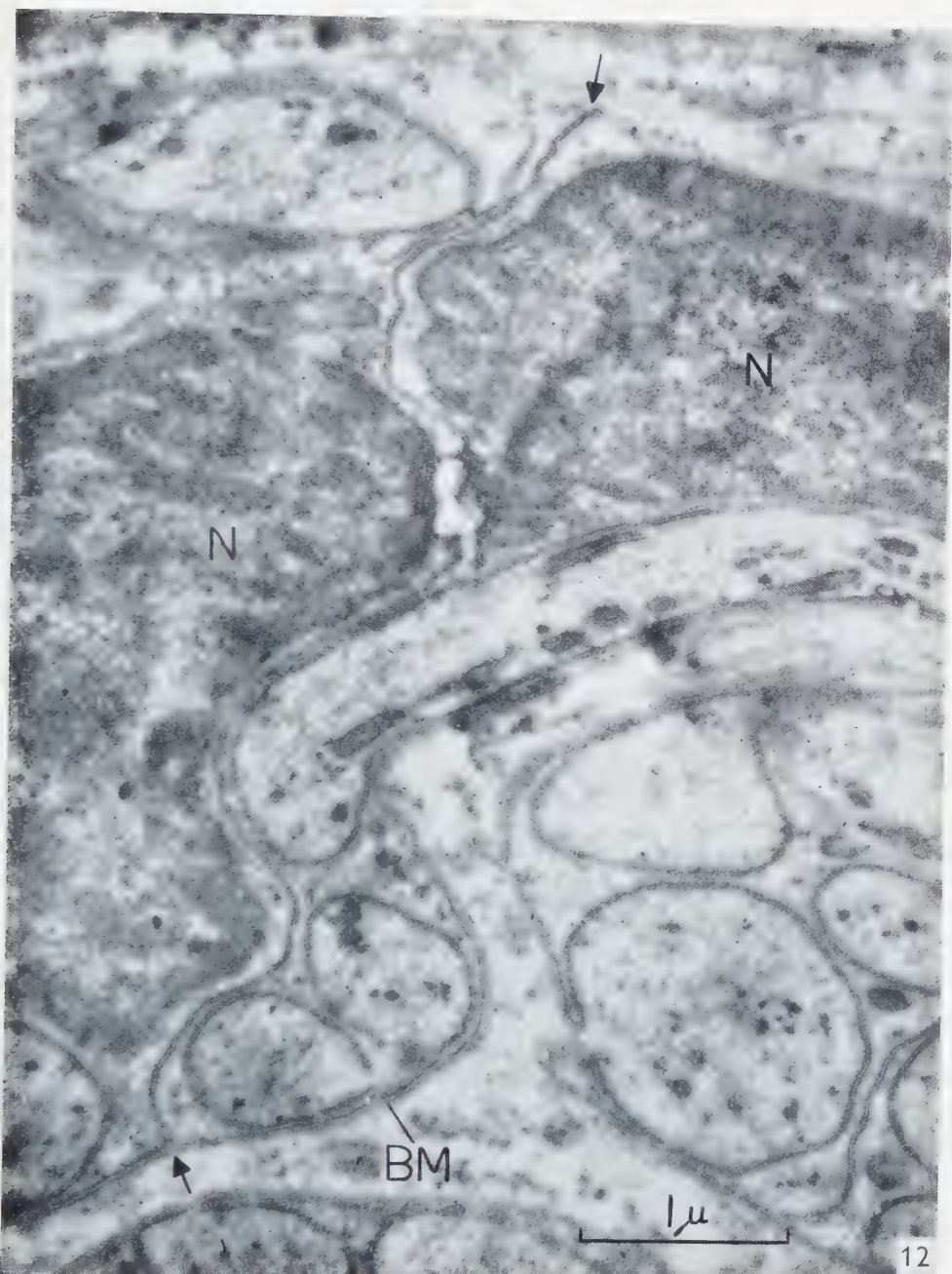
A number of Schwann cells occur along one and the same axon bundle. They are disposed in series like those described for myelinated nerve fibers (46).

The border between two Schwann cells generally has varying levels in relation to the individual axons in the nerve fiber bundles (Figs. 1 and 12). A cytoplasm protrusion from one Schwann cell may accompany an axon some distance into the the next cell. A cross-section of a nerve in such a zone is shown in Figs. 1*b* and 13. The plasma membrane of the Schwann cell completely envelops the axons, except where the latter are bounded by the basement membrane. The pocket which the Schwann cell forms round an individual nerve fiber apparently continues directly, at its termination, into a sheath formed by the plasma membrane of the contiguous cell.

The opaque lamellae of the plasma membranes show the same thickness of about 60 Å in both the peripheral and central parts of the cell (Table I). Here and there, as in the axolemma, a division of the plasma membrane into two opaque layers is seen. These are around 25 Å thick and are separated by a lighter space of similar thickness. At the border between two Schwann cells, the opaque layers of the plasma membranes are separated by a less dense layer approximately 100 Å thick.

The Schwann cell, and hence the intracellular nerve fiber bundle, are enclosed by a basement membrane about 450 Å thick (Table III) outside of which the connective tissue, largely consisting of collagen fibers, begins. The basement membrane is continuous and passes unbroken from the outer surface of one Schwann cell to the

FIG. 12. Irregular border between two Schwann cells which passes close to their nuclei (*N*). At the arrows, the border reaches the basement membrane. $\times 28,000$.



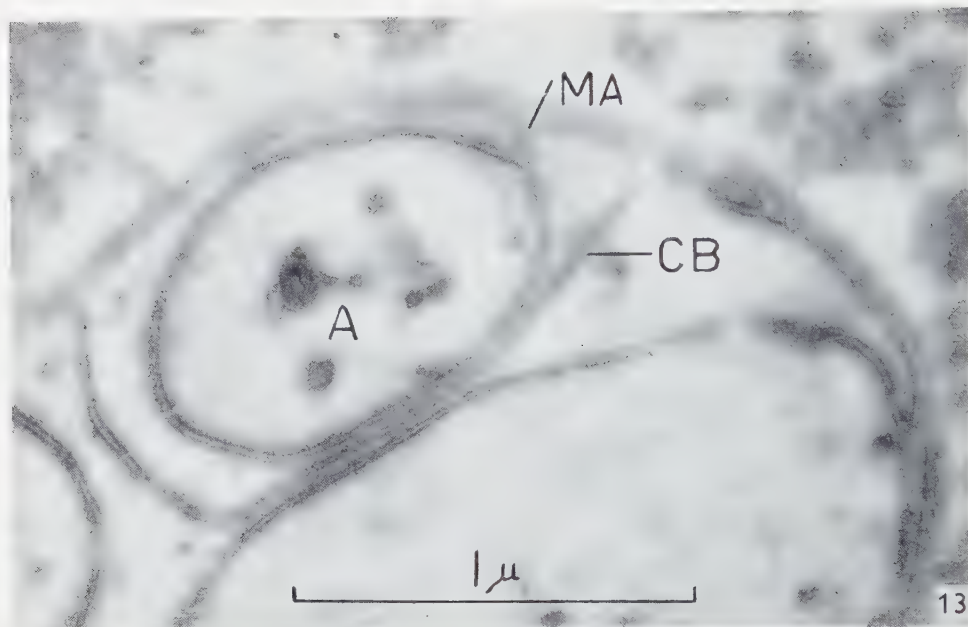


FIG. 13. Cross-section through a cytoplasmic protuberance from one Schwann cell located in the contiguous cell. The protuberance contains an axon (*A*). *MA*, mesaxon; *CB*, cell border between the two Schwann cells. $\times 52,000$.

next. No inner structure was observed in the basement membrane, which is not particularly dense. In places, a zone about 100–150 Å thick, close to the Schwann cell plasma membrane, is characterized by its weaker osmiophilia.

The *nucleus* is fusiform and usually localized to the center of the cell; it is about 1.5μ thick and 5μ long. Axons passing close to the nucleus sometimes produce impressions in it and thus make it have an irregular contour. Often the axons are in very close proximity to the nucleus. The nuclear membrane consists of two opaque layers with a lighter interspace varying from 90 to 150 Å in thickness. The outer of the two, which, in this study, was not observed to continue unbroken across any major part of the nuclear surface, is approximately 40 Å thick, and the inner one about 50 Å.

Within the nucleus are round or irregular osmiophilic particles with a relatively constant diameter of approximately 200 Å. They are assembled densely at the nuclear membrane but are also abundant throughout the nucleus, frequently in aggregations (Fig. 14). The center of these particles is less compact than their peripheral parts. The rest of the intranuclear material is lighter and without any specific structure.

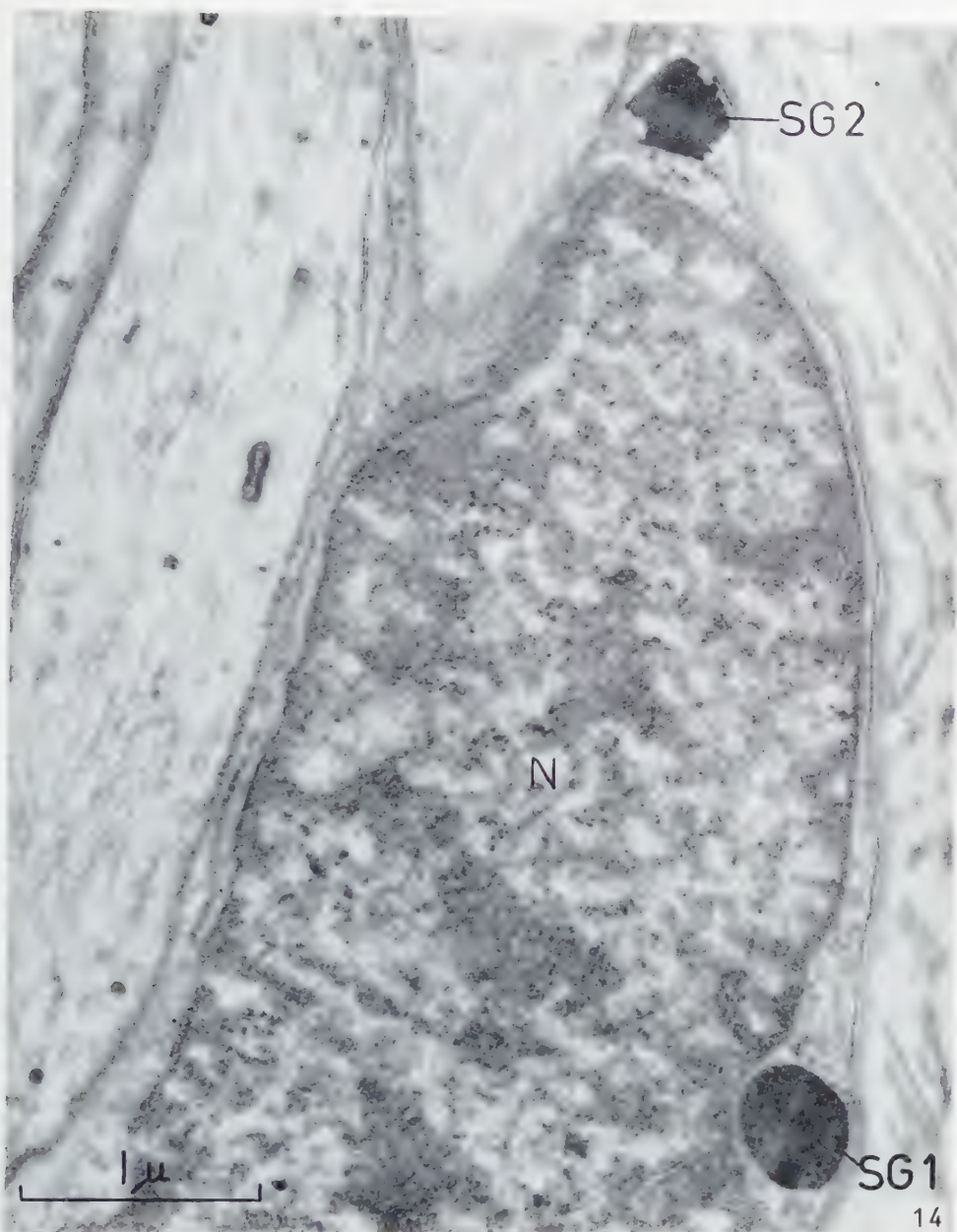


FIG. 14. Detail of longitudinal section through Schwann cell, showing nucleus (*N*), granules of types 1 and 2 (*SG1* and *SG2*) and a few axons. *SG1* shows regular borders and an inhomogeneous distribution of the osmiophilic material; *SG2* shows irregular borders and a homogeneous inner structure. $\times 31,000$.

The *cytoplasm* is most profuse in the nuclear zone. It consists of granular formations about 100 Å in size, mostly in groups, and a few vesicular structures varying in diameter from 200 to 500 Å. In occasional cells, moreover, corpuscles are observed which contain vesicle-like formations. Morphologically, they resemble the vesiculated granules that have been described in the axon. Only a few such structures were detected, however.

Very seldom there are found intracellular membranes disposed in pairs. Generally, they are only about 0.3–0.4 μ long. On one side of the approximately 50 Å thick membrane are attached opaque particles around 125 Å in diameter. The distance between the membranes is usually about 250 Å.

In addition to these elements of the ground cytoplasm, the cytoplasm contains mitochondria and osmiophilic granular structures.

TABLE III
WIDTH OF THE BASEMENT MEMBRANE AND MITOCHONDRIA IN THE SCHWANN CELL
Measurements made on five animals.

| Structure | Number of cells | Number of measurements | Mean (\pm S.E.) |
|-------------------|-----------------|------------------------|-------------------------|
| Basement membrane | 20 | 200 | 447 \pm 13 Å |
| Mitochondria | 26 | 52 | 0.183 \pm 0.012 μ |

Mitochondria are sparse in the Schwann cell. They mostly have a perinuclear localization, and are oval or elongated in shape. Their width is relatively constant at about 0.18 μ (Table III), but their length varies considerably. They are bounded by a triple-layered outer membrane around 175 Å thick. The opaque layers in this membrane have a thickness of about 50 Å and are separated by a lighter interspace approximately 75 Å thick. The inner membranes, also triple-layered, often have an irregular course in the mitochondria but are usually disposed perpendicular to its long axis. The thickness of these inner membranes is about 190 Å. The opaque layers are around 50 Å thick, and the lighter intermediate layer about 90 Å.

The number and size of the *granular structures* vary substantially from one cell and from one animal to another. There are two different types of granules, and in diameter they vary within the same limits, i.e., 0.2–1.1 μ . They are designated here as types SG 1 and SG 2 (Figs. 14 and 15).

SG type 1 is circular to oval in shape and is usually localized at the nuclear poles (Fig. 15). They often occur in groups of two or more and are bounded by a membrane

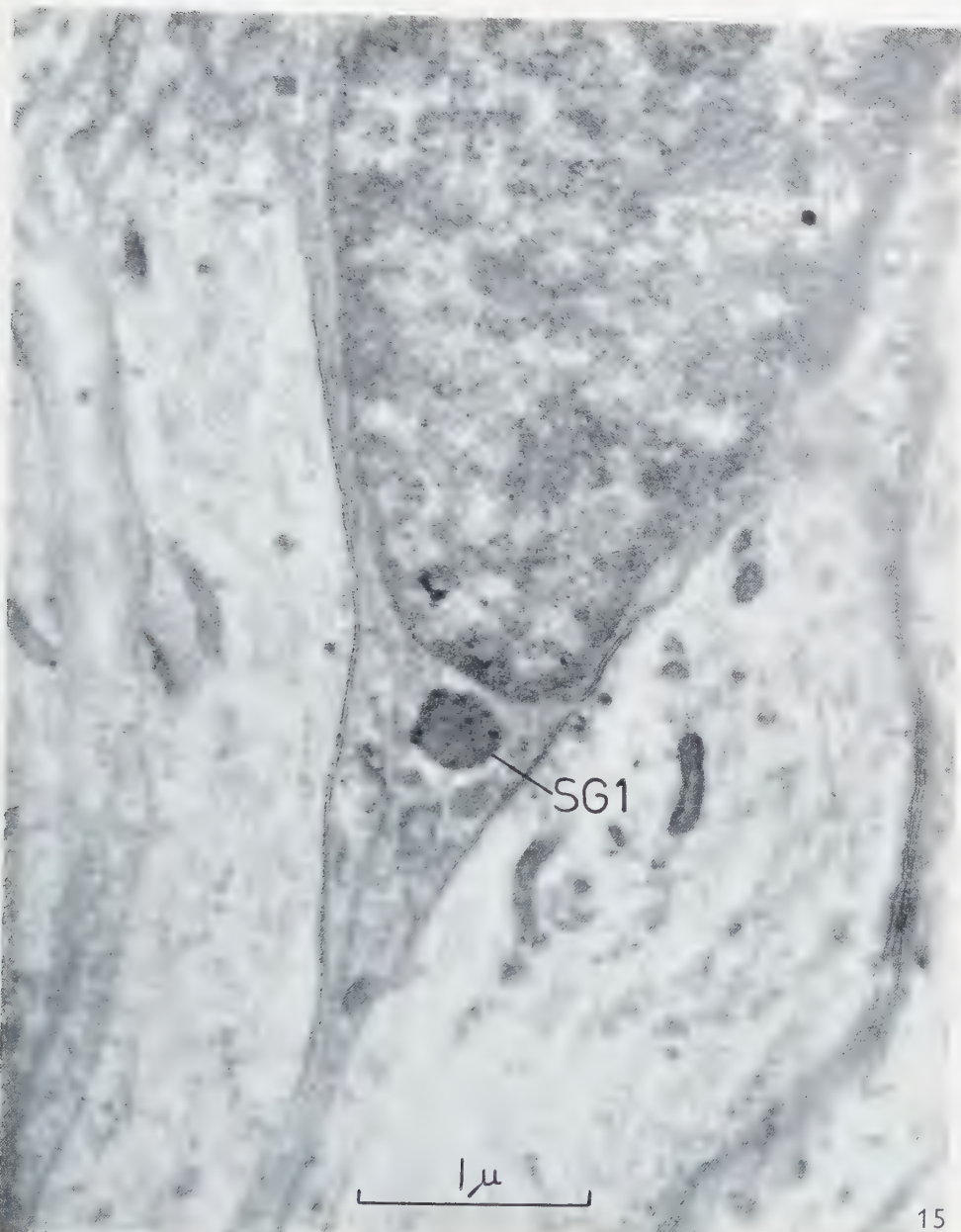


FIG. 15. The same Schwann cell as in Fig. 14, but showing the opposite pole of its nucleus at which there is a type 1 granule. In the axons are mitochondria, vesicular structures, and neurofibrils. $\times 31,000$.

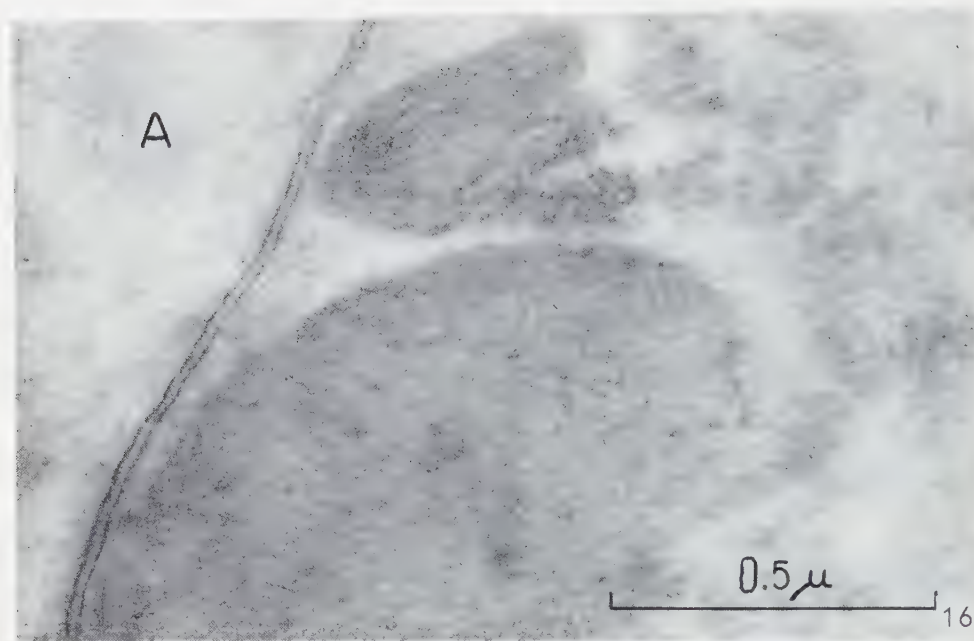
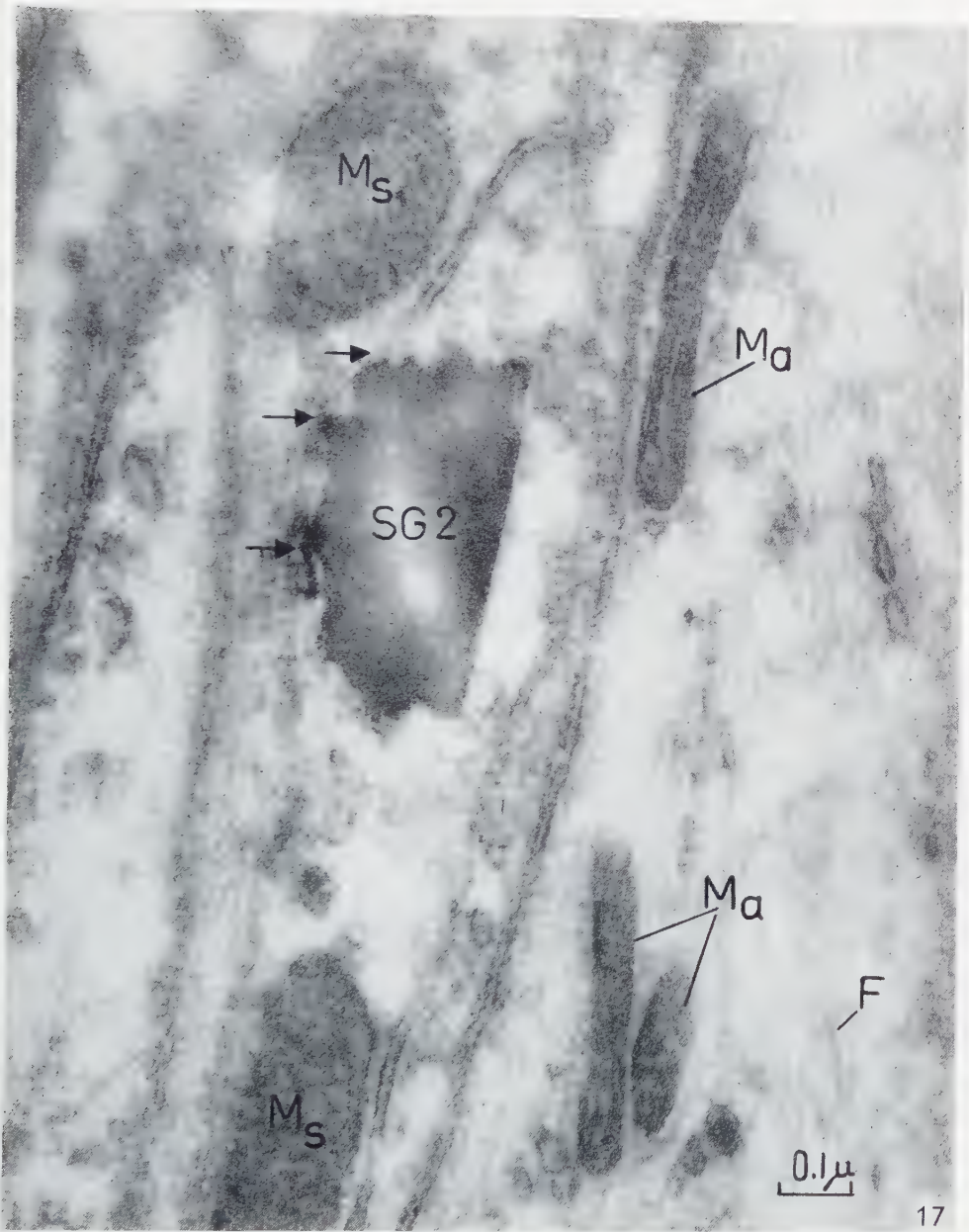


FIG. 16. Two Schwann cell granules of type 1, the smaller of which shows concentric stratification of the osmiophilic material. *A*, axon. $\times 84,000$.

approximately 60 Å thick. The inner structure consists of more or less strongly osmiophilic particles about 60 Å in diameter. The more osmiophilic of them sometimes occur in clumps and thus give rise to denser areas. These zones vary in size but commonly have diameters of 200–300 Å. In some of these granules, the osmiophilic material forms layers, occasionally with a concentric arrangement (Fig. 16).

The localization of SG type 2 varies but it is very often contiguous with the plasma membrane of the cell (Figs. 3 and 17). Indeed, the two may be in very close contact, in which case the plasma membrane is difficult to differentiate in the electron micrograph. The granule has an irregular contour and, for the most part, a jagged edge. The inner structure is homogeneous and consists of strongly osmiophilic particles with diameters of about 40 Å. In this study, no stratification or lack of uniformity in the disposition of the osmiophilic substance was observed.

FIG. 17. Longitudinal section through unmyelinated nerve with Schwann cell granule, type 2 (SG2), the close contact of which with the cell membrane is marked by arrows. *M_S*, mitochondria in the Schwann cell; *M_A*, intra-axonal mitochondria. The outer membranes of the axon mitochondria have a distinct double contour. *F*, neurofibril. $\times 93,000$.



DISCUSSION

The unmyelinated nerve fibers

In principle, the structure of the unmyelinated axon in the splenic nerve of the cat is in accord with the findings reported by Gasser (17) for dorsal root fibers from the cat, and by Hess (20) for autonomic nerves from the rabbit. However, the present analysis also disclosed some details that have not previously been described.

The axon is enveloped by a plasma membrane containing an osmiophilic component which generally has a thickness of about 60 Å. The individual axon, nevertheless, shows zones, here and there, in which the opaque membrane appears as a triple-layered structure with a total thickness of approximately 75 Å. Rhodin (34) described a triple-layered structure of similar dimensions in restricted regions of the cell membrane of proximal tubular cells from mouse kidney. Robertson (37) reported that the cell membrane in unmyelinated axons from frog nerve had three layers. The individual lamellae had the same dimensions as those observed in the present study. Robertson did not mention any structural heterogeneity in different parts of the membrane.

Earlier electron microscopic investigations have, nevertheless, shown that the thickness and structure of the plasma membrane may vary in one and the same cell. Zetterqvist (48) analyzed in detail the plasma membrane of the columnar epithelium in the mouse jejunum. He showed that the membrane, where it is in contact with an adjacent cell, reveals one osmiophilic layer which is about 50 Å thick; but, where it faces an intercellular space or runs along the basement membrane, it shows three layers, each approximately 25 Å in thickness.

Ekholm and Sjöstrand (9) demonstrated structural variations in the plasma membrane of epithelial cells from the mouse thyroid gland. In the area of contact with a contiguous cell, the osmiophilic layer is about 80 Å thick. Where the plasma membrane encloses the apical part of the cell and the microvilli, however, it has a triple-layered structure with a total thickness of 60 Å.

A conceivable explanation of the observed variation in the ultrastructure of the axon membrane is that the latter was affected during preparation. We may be concerned here either with an artificial splitting of the membrane or, on the contrary, with a fusion of membrane layers. Since, therefore, the chances that alterations of the membrane occurred during preparation seem to have been appreciable, no conclusions can be drawn regarding functional aspects of the above findings. The possibility of a false layering due to overfocussing was ruled out by taking through-focus series of the membrane at high magnification.

The opaque membrane is separated from the corresponding layer of the Schwann cell plasma membrane by a less dense interspace approximately 90 Å thick.

The lighter space observed between the opaque layers in the plasma membranes of adjoining cells consists, according to one hypothesis, of organized lipid layers (42, 43). In the opinion of Robertson (37), however, it is very uncertain whether the less dense layer between the opaque cell membranes of the axon and the Schwann cell and in mesaxons contains macromolecular components. He assumes that this space represents the extracellular space. He agrees on interpreting the opaque layers as indicating the location of the protein components of the plasma membrane, but assumes that the lipids of the plasma membrane are located in the less opaque inter-space of the 75 Å thick, triple-layered structure which, after osmium fixation, mostly appears as a uniform osmiophilic layer.

Other studies of unmyelinated nerves include an analysis of the intestinal nerve from *Helix pomatia* that was reported by Schlote (38). In the nerve from this invertebrate, the plasma membrane was stated to be 40 Å thick.

There is an abundance of mitochondria in the axon, and they are long and slender in shape. Indeed, this form seems to be the most common in both myelinated and unmyelinated nerve fibers. The inner structure presents features hitherto not described, which conceivably are specific for this tissue. Aside from irregularities in the inner membranes, which have also been described in the myelinated nerve fiber (47), there are appreciable variations of density in one and the same mitochondrion. Inconsistencies of the mitochondrial structure are found in different tissues and species of animals, and they have been attributed, among other things, to differences in enzymatic activity (28).

The neurofibrils have a diameter of approximately 60 Å. For myelinated nerves Hess and Lansing (21) reported a figure of 70 Å for the neurofibrils of the sciatic nerve of the guinea pig and the rabbit, and Wersäll (47) recorded 100 Å for those of the vestibular nerve of the guinea pig. Fernández-Morán (15) reported that in the unmyelinated nerve fibers of the spinal cord of frog and rat the neurofibrils had a diameter of around 100 Å. Palay and Palade (31) gave diameters of 60–100 Å for the neurofibrils in nerve cells of rat. The present analysis has not revealed any further details specific for this structure.

Vesicular structures about 450 Å in diameter were very numerous in the nerve fibers analyzed here. Usually they occurred singly but sometimes in aggregations, mostly close to the plasma membrane. Vesicles of a non-characteristic type are found in myelinated nerve fibers (47). However, no intra-axonal vesicular clumps of the type observed above have been described thus far, either in myelinated or unmyelinated nerves.

Sjöstrand has reported vesicular aggregations of a characteristic type in receptor cells of the retinal synapse of the guinea pig eye (40, 41). They have also been detected in some nerve terminals in the organ of Corti (11), in the vestibular apparatus (47),

the adrenal medulla (8), and in the motor end plate (36). These "synaptic vesicles", are abundant, too, on the presynaptic side of interneuron synapses (3-5, 29, 30).

The structures appear to be characteristic components of the synaptic cytoplasm. It has been suggested that their function is associated with the transmission of nerve impulses. A hypothesis is that transmitter substances such as acetylcholine or catechols may be contained in the vesicles (2, 5).

The nerve fibers contain granular elements having a diameter of about 0.28μ and somewhat varying inner structures. It is, naturally, impossible from this investigation to ascertain whether any common denominator exists for the different types of granules. If one does exist, the discrepancies in the morphologic picture might represent different stages in function.

The form in which these granules usually occur resembles a sac, more or less filled with vesicular structures. Similar cell components have been described in a number of epithelial cells and in nerve cells. Palay and Palade (31) observed a vesicular structure containing circular profiles in nerve cells from the rat. Zetterqvist (48) reported a vacuole-containing body of similar appearance in the columnar epithelium of the mouse jejunum. Structures having a corresponding electron microscopic picture have been reported in tracheal epithelium (35), sensory epithelium of the cristae ampullares (47), and ciliary epithelium (23).

In some cells from the adrenal medulla of rabbits, De Robertis and Vaz Ferreira (7) observed vesiculated corpuscles that had diameters of $0.5-2 \mu$ and generally were enveloped by a double membrane. The vesicles in this structure averaged 590 \AA in diameter and sometimes contained osmiophilic zones. These formations were assumed to represent catechol depots.

Schlote (38), in his analysis of the unmyelinated intestinal nerve from *Helix pomatia*, described intra-axonal corpuscular structures which he termed "Einschlusskörper" and for which he recorded diameters of between 0.1 and 0.25μ . They were round and had a dense, homogeneous inner structure. In his opinion, they morphologically resembled viruses, but their significance was obscure.

The Schwann cell

In 1922, Nageotte (26, p. 255) described the Schwann sheath in Remak nerves as a multitubular system in which a nerve fiber filled each tubule. He regarded the Schwann sheath protoplasm as a syncytium directly enveloping the axons. Following the investigations of Gasser (16, 17) we now know that the nerve fibers are located outside the Schwann cell cytoplasm, though insheathed in the latter's plasma membrane.

In the unmyelinated splenic nerve, the Schwann sheath is built up of a series of

cells. The plasma membranes of the cells form distinct borders. The cell border, itself, is irregular and often can be traced along an individual nerve fiber some distance into one of two contiguous Schwann cells. In this way, the cells project into each other with relatively long cytoplasmic protuberances. The axons appear to be enclosed throughout by the Schwann cell plasma membranes, except where they are bounded by the basement membrane.

This investigation accordingly shows that the Schwann sheath of unmyelinated nerves has, in principle, the same organization as that in myelinated ones. It cannot be regarded as a syncytium, but rather as built up of a series of cells.

The basement membrane forms a continuous envelope round the Schwann sheath. Occasionally, a part of it nearest to the plasma membrane is less dense than the rest. Whether these differences in osmiophilia coincide with a membrane differentiation *in vivo* cannot be decided on the basis of this study. A plausible explanation of the electron microscopic picture is that the membrane was altered during preparation, for instance, by shrinkage. The latter phenomenon has been found in the basement membrane of renal glomeruli (19).

The cell nucleus is enveloped by a double membrane, but the present study failed to reveal whether its outer layer runs continuously across the nuclear surface. The intranuclear structure largely consists of round opaque particles that are relatively densely packed. This opaque material usually forms discrete areas, chiefly at the nuclear membrane but also inside the nucleus. In the present study no specific nucleolar structures were detected.

The ground substance of the cytoplasm is on the whole sparse and mainly localized to the nuclear zone. No structures specific for the Schwann cell were observed.

The mitochondria, which mostly have a perinuclear localization, are of conventional type with a double outer membrane and inner membranes usually disposed perpendicular to the long axes of the mitochondria. The latter membranes, too, are triple-layered. The mitochondria are remarkably few in number, which fact may suggest a comparatively low cell metabolism.

Key and Retzius demonstrated, as early as 1873, granular structures in the Schwann sheath of myelinated nerve fibers (24) and, in 1876, also in the neurilemma of unmyelinated fibers (25). Hess and Lansing (21) observed osmiophilic granules in Schwann cells on electron microscopic analysis of myelinated nerves. They were inclined to regard them as counterparts of the Elzholz granules (10) and, in part, of the μ -granules described by Reich (32). In their opinion, Reich's π -granules possibly corresponded to certain intracellular membranes that were interpreted as endoplasmic reticulum. In the present analysis of the Schwann cell, intracellular membranes were observed. The morphologic picture suggests that they are of the type which Sjöstrand (42) designated as α -cytomembranes. Possibly they coincide with the mem-

branes described by Hess and Lansing. According to Reich, μ -granules contained lecithin. π -granules exhibited metachromatic characteristics.

In unmyelinated fibers of the splenic nerve, the Schwann cells contain osmiophilic granular structures, 0.2–1.1 μ in diameter, which apparently vary in number from one animal to another. It seems probable that a large proportion of these granules are composed of lipids, in view of their pronounced osmiophilia. Possibly they are counterparts of what have been described as Reich's μ -granules in light microscopic studies.

In the present investigation of unmyelinated fibers in splenic nerve from cats, granular structures were found in the axons and in the associated Schwann cells. The morphologic picture does not yet allow any conclusions regarding the biologic significance of these structures. We do know, however, that the splenic nerve has a relatively high noradrenaline content (13). According to the studies of von Euler and Hillarp (14) on centrifugate of homogenized splenic nerve, part of the noradrenaline is attached to corpuscular structures less than 1 μ in diameter. It is known, moreover, that catechols may be liberated from granular structures isolated from adrenal medullary cells (22). These granules vary in size from 0.1 to 0.6 μ . So-called catechol-containing granules of similar magnitude also have been described *in situ* in adrenal medullary cells, on electron microscopic study (6, 44).

Hence the possibility cannot be ruled out that noradrenaline may occur attached to granular elements in the splenic nerve, too. Far more data on the mechanism whereby noradrenaline is stored in adrenergic nerves are required, nevertheless, before any corollaries can be drawn as to the present findings in relation to the transmitter substance. However, experiments have been instituted which may conceivably throw light on the localization of noradrenaline in this nerve.

The splenic nerve also has a relatively high histamine content (12). According to von Euler and Hillarp's investigation (14), this substance was not attached to the corpuscular elements isolated from homogenized splenic nerve on the same scale as was noradrenaline. No conclusions can be drawn from the above results with regard to the localization of histamine in the splenic nerve.

ACKNOWLEDGEMENTS

The author wishes to express his sincere gratitude to Dr. Fritiof S. Sjöstrand, Associate Professor of Anatomy, Karolinska Institutet, for valuable discussions regarding this work and for the privilege of working in his laboratory. The author is also indebted to Professor Ture Petrén, head of the Department of Anatomy, for placing the resources of the department at his disposal. Thanks are also due to Miss Maud Hoffstedt for technical assistance, to Miss Maj Berghman for making the schematic drawings and to Dr. B. Vincent Hall

and Dr. Maynard M. Dewey for criticism of the manuscript. Statistical advice was given by Mr. Staffan Ekblom, member of the Statistical Research Group at Stockholm's Högskola. Mr. Stanley Vernon translated the paper into English.

REFERENCES

1. BACQ, Z. M. and FREDERICQ, H., *Arch. intern. physiol.* **41**, 322 (1935).
2. CASTILLO, J. DEL and KATZ, B., *Progr. in Biophys. and Biophys. Chem.* **6**, 137 (1956).
3. DE ROBERTIS, E., *Acta Neurol. Latinoamer.* **1**, 3 (1955).
4. DE ROBERTIS, E. and BENNETT, H. S., *Federation Proc.* **13**, 35 (1954).
5. ——— *J. Biophys. Biochem. Cytol.* **1**, 47 (1955).
6. DE ROBERTIS, E. and VAZ FERREIRA, A., *Exptl. Cell Research* **12**, 568 (1957).
7. ——— *ibid.* **12**, 575 (1957).
8. ——— *J. Biophys. Biochem. Cytol.* **3**, 611 (1957).
9. EKHOLM, R. and SJÖSTRAND, F. S., *J. Ultrastructure Research* **1**, 178 (1957).
10. ELZHOZ, A., *Jahrb. Psychiat. u. Neurol.* **17**, 323 (1898).
11. ENGSTRÖM, H. and SJÖSTRAND, F. S., *Acta Oto-Laryngol.* **44**, 490 (1954).
12. EULER, U. S. VON, *Acta Physiol. Scand.* **19**, 85 (1949).
13. ——— *ibid.* **19**, 207 (1949).
14. EULER, U. S. VON and HILLARP, N.-Å., *Nature* **177**, 44 (1956).
15. FERNÁNDEZ-MORÁN, H., *Exptl. Cell Research* **3**, 282 (1952).
16. GASSER, H., *Cold Spring Harbor Symposia Quant. Biol.* **17**, 32 (1952).
17. ——— *J. Gen. Physiol.* **38**, 709 (1955).
18. ——— *ibid.* **39**, 473 (1956).
19. HALL, B. V., *J. Histochem. and Cytochem.* **3**, 310 (1955).
20. HESS, A., *Proc. Roy. Soc. London* **B144**, 496 (1956).
21. HESS, A. and LANSING, A., *Anat. Record* **117**, 75 (1953).
22. HILLARP, N.-Å., LAGERSTEDT, S. and NILSSON, B., *Acta Physiol. Scand.* **29**, 251 (1953).
23. HOLMBERG, Å., Ultrastructural Changes in the Ciliary Epithelium Following Inhibition of Secretion of Aqueous Humour in the Rabbit Eye. Thesis. Stockholm, 1957.
24. KEY, A. and RETZIUS, G., *Arch. mikroskop. Anat. u. Entwicklungsmech.* **9**, 308 (1873).
25. ——— Studien in der Anatomie des Nervensystemes und des Bindegewebes. Samson-Wallin, Stockholm, 1876.
26. NAGEOTTE, J., L'organisation de la matière. Felix Alcan, Paris, 1922.
27. NEWMAN, S. B., BORYSKO, E. and SWERDLOW, M., *Science* **110**, 66 (1949).
28. PALADE, G. E., *Anat. Record* **114**, 427 (1952).
29. PALADE, G. E. and PALAY, S. L., *Anat. Record* **118**, 335 (1954).
30. PALAY, S. L., *J. Biophys. Biochem. Cytol.* **2**, No. 4, Suppl., 193 (1956).
31. PALAY, S. L. and PALADE, G. E., *J. Biophys. Biochem. Cytol.* **1**, 69 (1955).
32. REICH, F., *J. Psychol. u. Neurol.* **8**, 244 (1907).
33. REXED, B. and EULER, U. S. VON, *Acta Psychiat. Neurol. Scand.* **26**, 61 (1951).
34. RHODIN, J., Correlation of Ultrastructural Organization and Function in Normal and Experimentally Changed Proximal Convolute Tubule Cells of the Mouse Kidney. Thesis. Stockholm, 1954.
35. RHODIN, J. and DALHAMN, T., *Z. Zellforsch. u. mikroskop. Anat.* **44**, 345 (1956).

36. ROBERTSON, D., *J. Biophys. Biochem. Cytol.* **2**, 381 (1956).
37. ——— *ibid.* **3**, 1043 (1957).
38. SCHLOTE, F. W., *Z. Zellforsch. u. mikroskop. Anat.* **45**, 543 (1957).
39. SJÖSTRAND, F. S., *Experientia* **9**, 114 (1953).
40. ——— *J. Appl. Phys.* **24**, 1422 (1953).
41. ——— *Proc. 3rd Intern. Conf. Electron Microscopy, London*, 1954, p. 424. Royal Microscopical Society, London, 1956.
42. ——— *Intern. Rev. Cytol.* **5**, 455 (1956).
43. SJÖSTRAND, F. S. and RHODIN, J., *Exptl. Cell Research* **4**, 426 (1953).
44. SJÖSTRAND, F. S. and WETZSTEIN, R., *Experientia* **12**, 196 (1956).
45. UTTERBACK, R., *J. Comp. Neurol.* **81**, 55 (1944).
46. UZMAN, B. and NOGUERIA-GRAF, G., *J. Biophys. Biochem. Cytol.* **3**, 589 (1957).
47. WERSÄLL, J., Studies on the Structure and Innervation of the Sensory Epithelium of the Cristae Ampullares in the Guinea Pig. Thesis. Stockholm, 1956.
48. ZETTERQVIST, H., The Ultrastructural Organization of the Columnar Absorbing Cells of the Mouse Jejunum. Thesis. Stockholm 1956.

Author Index

ANDERSSON-CEDERGREN, Ebba, 74, 271

BAKER, R. F., 239

BANG, B. G., 138

BANG, F. B., 138

BENEDETTI, E. L., 309

BERGENDAHL, GUDRUN, 147

BERNHARD, W., 158, 309

DALTON, A. J., 62

DEGUCHI, N., 259

DEUTSCH, K., 307

DEWEY, M. M., 271

DUNN, A. E. G., 307

EKHOLM, R., 26, 178, 238

ELFVIN, L.-G., 428

ENGSTRÖM, A., 147

FAURÉ-FREMIET, E., 1, 289

FERREIRA, D., 14

FREY-WYSSLING, A., 38, 397

GILĚV, V. P., 349

IKEDA, T., 295

KREGER, D. R., 247

KREUTZER, EMILIA, 397

KUFF, E. L., 62

LEVER, J. D., 235

LINDBERG, B., 147

MANNWEILER, K. L., 158

MENEFEFEE, M. G., 49

MOSLEY, V. M., 337

MÜLLER, H. R., 38, 109

NILSSON, O., 170, 375

POLSON, A., 365

ROTH, L. E., 223

ROUILLER, CH., 1, 289

SJÖSTRAND, F. S., 74, 178, 239, 271, 365

TEZUKA, O., 295

THORSSON, K. G., 412

WEIBULL, C., 412

WISCHNITZER, S., 201

WYCKOFF, R. W. G., 337

YAMADA, E., 359

YASUZUMI, G., 259, 295

Subject Index

- Absorption analysis, microradiography for, MOSLEY and WYCKOFF, 337
- Amphibian oocytes, electron microscope study of the nuclear envelope of, WISCHNITZER, 201
- Bacterial L forms, protoplasts and protoplast-like bodies, studies on the structure of, THORSSON and WEIBULL, 412
- Basal corpuscle, ultrastructure of, in a peritrichous *Ciliata*, ROUILLER and FAURÉ-FREMIET, 289
- Capsicum annuum* L., submicroscopic development of chromoplasts in the fruit of, FREY-WYSSLING and KREUTZER, 397
- Cat, ultrastructure of unmyelinated fibers in the splenic nerve of, ELFVIN, 428
- Chicken, ultrastructural investigations on virus of the erythroblastic leukemia of, BENEDETTI and BERNHARD, 309
- Chromoplasts, submicroscopic development of, in the fruit of *Capsicum annuum* L., FREY-WYSSLING and KREUTZER, 397
- Cilia, observations on a type of, in rat oviduct, NILSSON, 170
- Ciliata*, reticular ultrastructure of a skeletal fiber of, ROUILLER and FAURÉ-FREMIET, 1; peritrichous, ultrastructure of the basal corpuscle in, ROUILLER and FAURÉ-FREMIET, 289
- Cucurbita*, submicroscopic differentiation of plasmodesmata and sieve plates in, FREY-WYSSLING and MÜLLER, 38
- Embedding biological specimens, use of gelatin for, in preparation of ultrathin sections for electron microscopy, GILĚV, 349
- Embryo—mice, structure changes occurring in the epidermis of, during differentiation, MENEFEE, 49; and new-born rat, ultrastructure of the endocrine pancreas cells in, FERREIRA, 14
- Epidermis of embryo mice, structure changes occurring in, during differentiation, MENEFEE, 49
- Eye, compound, submicroscopic structure of, as revealed by electron microscopy, YASUZUMI and DEGUCHI, 259; kitten, fine structure of the tapetum of, as revealed by the electron microscope, YAMADA, 359
- Ferritin, molecular, identification of, in homogenates and sections of rat liver, KUFF and DALTON, 62
- Filamentous component of protozoan fibrillar systems, ROTH, 223
- Fixation by freezing-drying for electron microscopy of tissue cells, SJÖSTRAND and BAKER, 239; freezing-drying as a method of, of plant cells, MÜLLER, 109
- Freezing-drying, fixation by, for electron microscopy of tissue cells, SJÖSTRAND and BAKER, 239; as a method of fixation of plant cells, MÜLLER, 109
- Frog, mouse and guinea pig cardiac muscle, ultrastructure of the intercalated discs of, SJÖSTRAND *et al.*, 271
- Gelatin, use of, for embedding biological specimens in preparation of ultrathin sections for electron microscopy, GILĚV, 349
- Graphic reconstruction of the third dimension from serial electron microphotographs, BANG and BANG, 138
- Guinea pig, cardiac muscle, ultrastructure of the intercalated discs of, SJÖSTRAND *et al.*, 271
- Hamster, ultrastructural investigations on an experimental renal tumour of, MANNWEILER and BERNHARD, 158
- Intercalated discs of frog, mouse and guinea pig cardiac muscle, ultrastructure of, SJÖSTRAND *et al.*, 271
- Kitten eye, fine structure of the tapetum of, as

revealed by the electron microscope, YAMADA, 359

Leukemia, erythroblastic, of chicken, ultrastructural investigations on virus of, BENEDETTI and BERNHARD, 309

Liver, rat, molecular ferritin in homogenates and sections of, KUFF and DALTON, 62

Macrocrystalline patterns of closely packed poliovirus particles in ultrathin sections, SJÖSTRAND and POLSON, 365

Microradiography for absorption analysis, MOSLEY and WYCKOFF, 337; high resolution, with ultrasoft X-rays, ENGSTRÖM *et al.*, 147

Mouse, cardiac muscle, ultrastructure of the intercalated discs of, SJÖSTRAND *et al.*, 271; parathyroid gland, observations on the ultrastructure of, EKHOLM, 26; thyroid gland, ultrastructural organization of, EKHOLM and SJÖSTRAND, 178; uterine surface epithelium, ultrastructure of, under different estrogenic influences, NILSSON, 375

Muscle, cardiac, frog, mouse and guinea pig, ultrastructure of the intercalated discs of, SJÖSTRAND *et al.*, 271; skeletal, myofilaments, ultrastructure of, at various states of shortening, SJÖSTRAND and ANDERSSON-CEDERGREN, 74

Myofilaments, skeletal muscle, ultrastructure of, at various states of shortening, SJÖSTRAND and ANDERSSON-CEDERGREN, 74

Nerve, splenic, ultrastructure of unmyelinated fibers in, of the cat, ELFVIN, 428

Nuclear envelope of amphibian oocytes, electron microscope study of, WISCHNITZER, 201

Oestrous animals, NILSSON, 375

Oocytes, amphibian, electron microscope study of the nuclear envelope of, WISCHNITZER, 201

Oviduct, rat, observations on a type of cilia in, NILSSON, 170

Pancreas cells, endocrine, ultrastructure of, in embryo and new-born rat, FERREIRA, 14

Parathyroid gland, mouse, observations on the

ultrastructure of, EKHOLM, 26; comment on the fine structure of, LEVER, 235; remark on J. D. Lever's note, EKHOLM, 238

Plant cells, freezing-drying as a method of fixation of, MÜLLER, 109

Plasmodesmata and sieve plates in *Cucurbita*, submicroscopic differentiation of, FREY-WYSSLING and MÜLLER, 38

Poliovirus particles in ultrathin sections, macrocrystalline patterns of, SJÖSTRAND and POLSON, 365

Preparing individual cells for electron microscopy, DEUTSCH and DUNN, 307

Protoplasts and protoplast-like bodies, studies on the structure of, THORSSON and WEIBULL, 412

Protozoan fibrillar systems, a filamentous component of, ROTH, 223

Rat, new-born and embryo, ultrastructure of the endocrine pancreas cells in, FERREIRA, 14; liver, identification of molecular ferritin in homogenates and sections of, KUFF and DALTON, 62; oviduct, observations on a type of cilia in, NILSSON, 170

Renal tumour of hamster, ultrastructural investigations on, MANNWEILER and BERNHARD, 158

Retina of *Uroloncha striata* var. *domestica* Flower, submicroscopic structure of the inner segments of the rods and cones in, YASUZUMI *et al.*, 295

Rods and cones, inner segments of, in the retina of *Uroloncha striata* var. *domestica* Flower, YASUZUMI *et al.*, 295

Serial electron microphotographs, graphic reconstruction of the third dimension from, BANG and BANG, 138

Sieve plates in *Cucurbita*, submicroscopic differentiation of, FREY-WYSSLING and MÜLLER, 38

Skeletal fiber of a *Ciliata*, reticular ultrastructure of, ROUILLER and FAURÉ-FREMIET, 1

Spayed animals and oestrous animals, NILSSON, 375

- Splenic nerve, ultrastructure of unmyelinated fibers in, of the cat, ELFVIN, 428
- Stopper cork, X-ray diffraction of, KREGER, 247
- Tapetum of the kitten eye, fine structure of, as revealed by the electron microscope, YAMADA, 359
- Third dimension from serial electron microphotographs, graphic reconstruction of, BANG and BANG, 138
- Thyroid gland, mouse, ultrastructural organization of, EKHOLM and SJÖSTRAND, 178
- Tumour, experimental renal, ultrastructural investigations on, of hamster, MANNWEILER et BERNHARD, 158
- Unmyelinated fibers, ultrastructure of, in splenic nerve of the cat, ELFVIN, 428
- Uroloncha striata* var. *domestica* Flower, submicroscopic structure of the inner segments of the rods and cones in the retina of, YASUZUMI *et al.*, 295
- Uterine surface epithelium, mouse, ultrastructure of, under different estrogenic influences, NILSSON, 375
- Virus—of the erythroblastic leukemia of chicken, ultrastructural investigations on, BENEDETTI and BERNHARD, 309; polio, macrocrystalline patterns of, in ultrathin sections, SJÖSTRAND and POLSON, 365
- X-Ray—diffraction of stopper cork, KREGER, 247; ultrasoft, high resolution microradiography with, ENGSTRÖM *et al.*, 147